Unravelling the deformation history of the Northern Hastings Block, southern New England Orogen

Author:
Yan, Jie

Publication Date:
2016

DOI:
https://doi.org/10.26190/unsworks/18792

Unravelling the deformation history of the Northern Hastings Block, southern New England Orogen

Jie Yan

BEng- Central South University, China

A thesis in fulfilment of the requirements for the degree of

Doctor of Philosophy

School of Biological, Earth and Environmental Sciences

Faculty of Science

March 2016

PLEASE TYPE

THE UNIVERSITY OF NEW SOUTH WALES
Thesis/Dissertation Sheet

Surname or Family name: Yan

First name: Jie Other name/s:

Abbreviation for degree as given in the University calendar: PhD

School: Biological, Earth and Environmental Sciences Faculty: Science

Title: Unravelling the deformation history of the Northern Hastings Block, southern New England Orogen.

Abstract 350 words maximum: (PLEASE TYPE)

The Northern Hastings Block (NHB) consists of Carboniferous, complexly folded, weakly cleaved, extensively faulted, fore-arc sequences out of position in the New England Orogen. It shares part of deformation history with the adjacent Nambucca Block (NB) and Southern Hastings Block (SHB). It was subjected to prolonged N-S and later E-W shortening.

Four generations of macroscopic and mesoscopic folds and associated cleavage have formed within the NHB region according to their cross-cutting relationships. Fault analysis shows faults of a similar orientation in the NHB did not form at the same time. Some fault movement is related to Late Carboniferous emplacement of Hastings Block, but most faults formed and moved after cleavage and fold formation. Limited fault movement occurred after Triassic granite emplacement.

The extreme variability in the orientation of bedding from fault block to fault block recognized in this study, highlights the shuffling of fault blocks between the NHB and SHB post-Parrabel Dome formation. The extreme disruption of sequences between the NHB and SHB, are considered to be due to the rotation and translation or because of a fault network produced in a restraining fault-bend along strike-slip faults. Gravity and magnetic worm analysis revealed a possible new boundary between the NHB and SHB.

Four cross sections across the NHB based on field data are presented and have been 2D restored following the principles of structural balance. Based on these sections, the Parrabel Dome is a NW and SE-plunging dome which is box-like in the core and more open towards the north and south. The total horizontal shortening suggests only moderate cleavage development could occur consistent with field observations.

A 3D structural model is created from a comprehensive field dataset which shows a gross picture of the shape of the NHB. This model has aided fault block reconstruction and provided information on the direction and movement of fault blocks.

The formation of the Hastings Block was not due to large-scale 'oroclinal' folding in the Manning and Hastings area as suggested by previous authors but has been transported northward between two major fault systems. The NHB at this time underwent counterclockwise rotation.

Declaration relating to disposition of project thesis/dissertation

I hereby grant to the University of New South Wales or its agents the right to archive and to make available my thesis or dissertation in whole or in part in the University libraries in all forms of media, now or here after known, subject to the provisions of the Copyright Act 1968. I retain all property rights, such as patent rights. I also retain the right to use in future works (such as articles or books) all or part of this thesis or dissertation.

I also authorise University Microfilms to use the 350 word abstract of my thesis in Dissertation Abstracts International (this is applicable to doctoral theses only).

Signature Dr Paul Lennox Witness 26/8/15 Date

The University recognises that there may be exceptional circumstances requiring restrictions on copying or conditions on use. Requests for restriction for a period of up to 2 years must be made in writing. Requests for a longer period of restriction may be considered in exceptional circumstances and require the approval of the Dean of Graduate Research.

FOR OFFICE USE ONLY Date of completion of requirements for Award:

THIS SHEET IS TO BE GLUED TO THE INSIDE FRONT COVER OF THE THESIS

Originality Statement

'I hereby declare that this submission is my own work and to the best of my knowledge it contains no materials previously published or written by another person, or substantial proportions of material which have been accepted for the award of any other degree or diploma at UNSW or any other educational institution, except where due acknowledgement is made in the thesis. Any contribution made to the research by others, with whom I have worked at UNSW or elsewhere, is explicitly acknowledged in the thesis. I also declare that the intellectual content of this thesis is the product of my own work, except to the extent that assistance from others in the project's design and conception or in style, presentation and linguistic expression is acknowledged.'

Signed .....

Date 26/08/2015

Acknowledgements

I would like to express appreciation to many people who have supported me throughout the course of this research.

First of all, my thanks go to my supervisor Dr. Paul Lennox. I could not have asked for a more engaged, patient, practical and encouraging supervisor to guide me through the very first stage of formulating the research proposal to the final stage of compiling this thesis. I would also like to thank my co-supervisors A/Prof. Bryce Kelly for his guidance in 3D geological modelling, his practical and emotional help in addressing the research questions, and A/Prof. Robin Offler who provided much valued guidance through this project. His ongoing priceless comments and ideas on the research area inspired me a lot.

It has been a great privilege to learn from A/Prof Shawn Laffan on the use of Arcgis and Dr Derecke Palmer on the Petroleum Geophysics.

Thanks to the staff at the School of BEES including Firoza Cooper, Jonathan Russell, Jonathan Pritchard, Francine Gregory and Kate Stuart and anyone else who have supported and encouraged me. Thank you for your kind assistance in times of need. Thanks to Sichong Chen for your company though my PhD years.

This research could not have started without financial support from the Chinese Scholarship Council-UNSW Scholarship program. Midland Valley Exploration Ltd. and ARANZ Geo Limited generously supported this research with the use of their software packages 3D Move™ and Leapfrog Geothermal™ respectively. Thanks to the Graduate Research School and School of BEES, UNSW for the funding on field work and conferences. Thanks to PESA who provided me the 2013 Tertiary Institution Study Grant.

My final thanks go to my family. Thanks for supporting me from the beginning of my study. I would like to dedicate my thesis to them for their endless love!!! I love you so much, my father, mother and little brother. Thank you!

Abstract

The Northern Hastings Block (NHB) consists of Carboniferous, complexly folded, weakly cleaved, extensively faulted, fore-arc sequences out of position in the New England Orogen. It shares part of deformation history with the adjacent Nambucca Block (NB) and Southern Hastings Block (SHB). It was subjected to prolonged N-S and later E-W shortening.

Four generations of macroscopic and mesoscopic folds and associated cleavage have formed within the NHB region according to their cross-cutting relationships. Fault analysis shows faults of a similar orientation in the NHB did not form at the same time. Some fault movement is related to Late Carboniferous emplacement of Hastings Block, but most faults formed and moved after cleavage and fold formation. Limited fault movement occurred after Triassic granite emplacement.

The extreme variability in the orientation of bedding from fault block to fault block recognized in this study, highlights the shuffling of fault blocks between the NHB and SHB post-Parrabel Dome formation. The extreme disruption of sequences between the NHB and SHB, are considered to be due to the rotation and translation or because of a fault network produced in a restraining fault-bend along strike-slip faults. Gravity and magnetic worm analysis revealed a possible new boundary between the NHB and SHB.

Four cross sections across the NHB based on field data are presented and have been 2D restored following the principles of structural balance. Based on these sections, the Parrabel Dome is a NW and SE-plunging dome which is box-like in the core and more open towards the north and south. The total horizontal shortening suggests only moderate cleavage development could occur consistent with field observations.

A 3D structural model is created from a comprehensive field dataset which shows a

gross picture of the shape of the NHB. This model has aided fault block reconstruction and provided information on the direction and movement of fault blocks.

The formation of the Hastings Block was not due to large-scale ‘oroclinal’ folding in the Manning and Hastings area as suggested by previous authors but has been transported northward between two major fault systems. The NHB at this time underwent anticlockwise rotation.

Table of Contents

List of Figures

List of Tables

List of Appendices

Abbreviations

2D	two-dimensional
3D	three-dimensional
AF	Arizona Fault
BF	Bagnoo Fault
BFC	Birdwood Fault Complex
BWF	Beechwood Fault
CF	Cowarral Fault
CHB	Coffs Harbour Block
CWF	Cowarra Fault
DDG	downslope distance gradient
DEM	digital elevation model
HB	Hastings Block
HF	Hastings Fault
K	Kunderang Brook
Km	kilometres
m	metres
MF	Mingaletta Fault
MIVBF	multiresolution index of valley bottom flatness
NB	Nambucca Block
NEO	New England Orogen
NHB	Northern Hastings Block
PAF	Pappinbarra Fault
PD	Parrabel Dome
PMB	Port Macquarie Block
PMFS	Peel-Manning Fault System
RRF	Rollans Road Fault
SHB	Southern Hastings Block
SNEO	southern New England Orogen
SRI	shaded relief images
SS	strike-slip fault
TAFS	Taylors Arm Fault System
TB	Tamworth Belt
TC	Tablelands Complex
TCF	Taylors Creek Fault
TFC	Threadneedle Fault Complex
T_{OR}	over thrust fault
TPF	Telegraph Point Fault
T_R	thrust fault
TRI	terrain ruggedness index
VTR	vector terrain ruggedness
W.V.	Werrikimbe Volcanics
Y	Yarras area

Chapter 1 Introduction

1.1 Overview

The aim of this thesis is to unravel the deformation history of the Northern Hastings Block (NHB), southern New England Orogen. It reviews existing studies of this area, presents a new structural dataset, re-interprets a variety of geological data and builds a 3D model of the NHB in order to better understand this comprehensively mapped, complexly folded, extensively faulted Northern Hastings Block.

The Hastings Block is an enigmatic region, located on the outboard margin of a subduction complex (Tablelands Complex) and on the northern margin of the fore-arc Tamworth Belt of the southern New England Orogen (Figure 1.1). It consists of Devonian to Carboniferous arc-derived sedimentary rocks disconformally overlain by the Early Permian sediments of the Nambucca Block. It is structurally complex and has been placed in a unique crustal position where it is subjected to prolonged almost N-S shortening as a result of southward push of the indenter (Coffs Harbour Block) (Lennox *et al*. 1999; Johnston *et al*. 2002). The Hastings Block is divided into two parts: a northern part dominated by the northwesterly-trending Parrabel Dome and a southern part with mainly meridional folds that is structurally similar to the Tamworth Belt west of the Peel-Manning Fault System. Previous studies indicated that the northern Hastings Block (NHB) has undergone two or possibly three phases of folding, three episodes of faulting and has been rotated clockwise 130° or anticlockwise 230° (Schmidt *et al*. 1994; Lennox *et al*. 1999). Lennox *et al*. (1999) showed that the NHB contains both macroscopic and mesoscopic folds but little cleavage. In contrast, the southern Hastings Block (SHB) is not as structurally complex as the NHB. It is characterized by the meridional-trending, macroscopic folds overprinted by northwest-trending folds and was subjected to three episodes of faulting (Lennox *et al*. 1999).

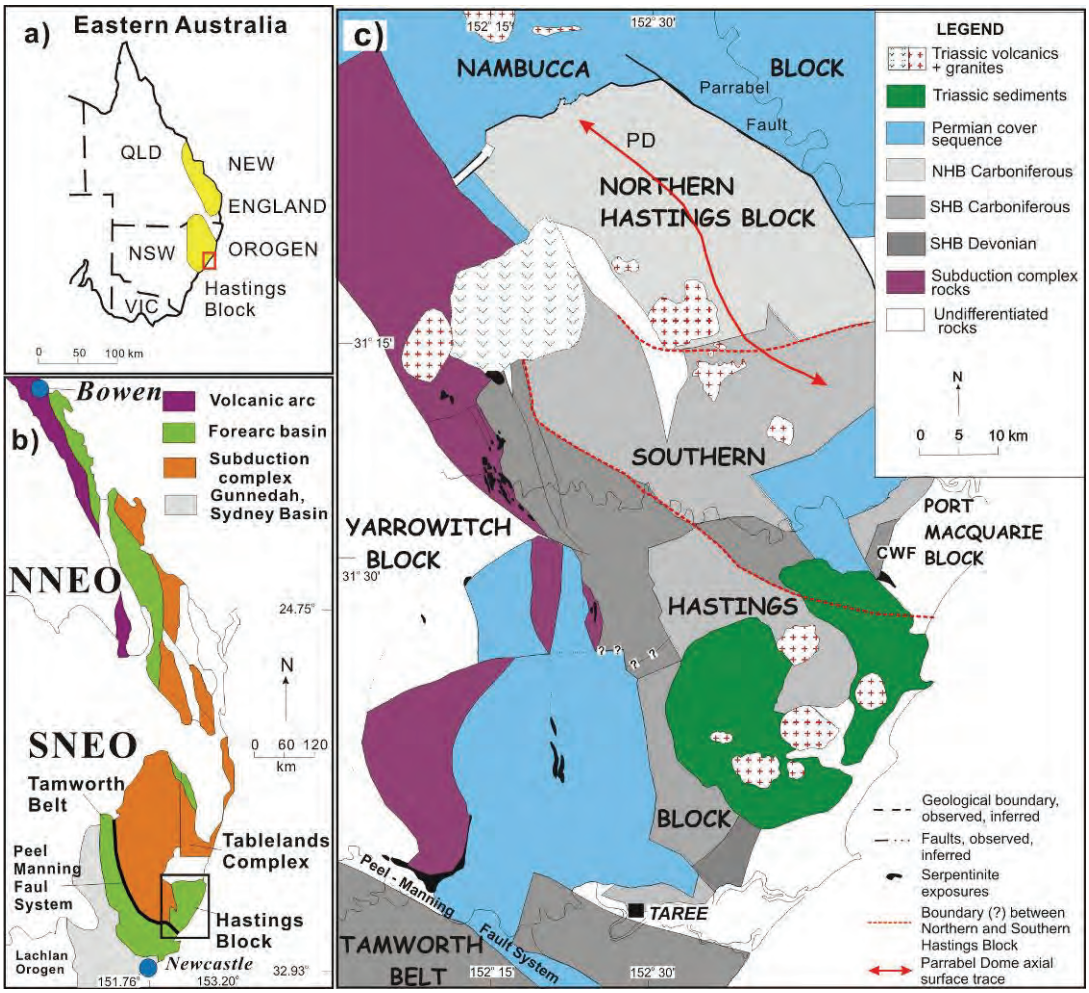

Figure 1.1: Location and tectonic setting of the Hastings Block, within eastern Australia (a), and within the southern New England Orogen (b). (c) Major tectonic units and faults within and adjacent to the Hastings Block (simplified from Roberts *et al*. 1995). CWF = Cowarra Fault; PD = Parrabel Dome.

A number of models have been used to explain the structural and tectonic development of the Hasting Block including: (i) an allochthonous origin (Leitch 1980; Lennox & Roberts 1988); (ii) a result of transcurrent motion (sinistral strike-slip transport) from a position southeast of the present eastern termination of the Tamworth Belt (Cawood & Leitch 1985; Roberts *et al*. 1993; Collins 1991; Johnston *et al*. 2002); (iii) oroclinal bending of the southern part of the orogen (Korsch & Harrington 1987; Cawood *et al*. 2011; Rosenbaum *et al*. 2012; Glen & Roberts 2012 and Li *et al*. 2014); and (iv) transcurrent displacement with 130° clockwise or 230° anticlockwise rotation of the Northern Hastings Block from outboard of the Tamworth Belt (Schmidt *et al*. 1994).

Which of these tectonic models are more likely to be consistent with the structures observed in the Hastings Block? This thesis will provide some important constraints on the validity of the existing models and better explain the geological history including the different deformation phases, the timing of fault development, leading to a better model of the structural and tectonic development of the Northern Hasting Block. The SHB is far less complex than the NHB hence this project has concentrated on the NHB.

1.2 Research Objectives and Methodology

The following five objectives were undertaken in order to accomplish the aims of this study.

1. To identify and separate the different deformation phases (cleavage and fold episodes) in the Northern Hastings Block.

The methodology to achieve objective one includes:-

- Prepare maps of the overall orientation of the bedding and the derived fold axes from these bedding readings in major subareas within the NHB–Nambucca Block regions and analyze the map patterns.
- Determine the order of events from overprinting relationships shown by cleavages, possible fold-bent faults, refolded folds and disrupted, already cleaved fault blocks (i.e. 1-5 km^2 blocks of coherent geology bounded by faults) and faults displacing cleaved and folded rocks.
- Analyze the map pattern of the limited cleavage data and the mesoscopic fold axes orientation. Further, to compare the map pattern of macroscopic folding described by Lennox *et al*. (1999) with the mesoscopic fold pattern.
- Compare the orientation, intensity and map pattern of cleavage and fold data in the NHB with that in the adjoining Nambucca Block (NB). Document the similarties and differences between structures in these blocks.

2. To unravel the fault history in the Northern Hastings Block, including estimating the timing, type and extent of apparent movement on all faults.

The methodology to achieve objective two includes:-

- Analyze and summarize the main characteristics of each fault including the length, shape and orientation, timing and apparent movement using data from Honour theses and the existing literature.
- The timing of fault formation by determining the earliest time faulting could have begun and the latest time it could have stopped using a number of techniques (Bykerk-Kauffman 1987; Bykerk-Kauffman 1989; Nieto-Samaniego and Alaniz-Alvarez, 1997; Tsutsumi *et al*. 2001; Van der Pluijm *et al*. 2004). These include using conventional fault analysis (e.g. repetition of stratigraphy and fault drag) and examining cross-cutting relationships between faults to determine the order of faulting.
- Identify whether faults of similar orientation formed or have been active at the same time or not.
- Establish the relationship between the timing of faults and fold/cleavage development in the NHB.

3. To analyze all the fault blocks within the Northern Hastings Block to see whether the bedding in the fault block is consistent with their position within the Parrabel Dome. This objective underpins the computer modeling of the NHB.

The methodology to achieve objective three includes:-

- Analyze and re-interpret a variety of geological data, including bedding data, cleavage and folds within key fault blocks in the NHB as delineated by Lennox *et al*. (1999) and Roberts *et al* (1995). Compare the orientation of bedding in the fault blocks with what would be expected if the block formed a part of a dome. The fault block-by-fault block analysis enables determination

as to whether the faults on the Roberts *et al*. (1995) map are correctly positioned.

- Establish the presence or not of a geological boundary between the NHB and Southern Hastings Block (SHB) and its position based on evidence from the gravity and magnetic worms for this region.
- Use QFL analysis of the sandstones from key formations to try to establish possible links between fault blocks containing the same formation.
- Undertake computer modelling of fault blocks and computer visualisation of the results to better understand the bedding pattern within different fault blocks.
- Restoration of the fault blocks to their possible position prior to bending of the northeast limb of the dome and fault disruption of the formations after folding and cleavage development.

4. To better understand the geological history of the dome by preparing three cross sections at right angles to the Parrabel Dome trend and one parallel to the dome axis using existing field data.

The methodology to achieve objective four includes:-

- Construct and then analyze four geometrically constrained (balanced), vertical cross sections across the Northern Hastings Block (A-B, C-D, E-F and X-Y).
- Perform 2D reconstruction on the completed cross-sections following the principles of structural balance (line length balancing).
- Calculate the shortening from each cross section during the deformation responsible for dome formation.
- Provide support for the validity of the 3D modeling and constraints on the formation of the NHB (e.g. Parrabel Dome) and its deformation history.

5. To construct a three dimensional structural surface model of the NHB under a new workflow without well-log data, to visualize the geology of the NHB in three

dimension, to aid fault block reconstruction, to test the validity of the existing tectonic models and provide insights into the geological history.

The methodology to achieve objective five includes:-

- Undertake data preparation, data structuring and interpretation for 3D Visualization.
- Use different types of processing of the digital elevation model (DEM) to find major structures such as faults, igneous bodies or other types of geological boundaries already mapped or unmapped in this area.
- Construct a 3D fault model based on the interpretation of the geological map of Roberts *et al*. (1995).
- Horizon (bottom surfaces of each formation) construction fault block-by-fault block using the comprehensive strike and dip structural dataset available across the block.
- Compare and contrast the cross-sections constructed using this 3D model with those constructed from the fieldwork studies.

1.3 Thesis framework

This thesis seeks to address the five research objectives about the deformation history of the NHB posed in section 1.2.

Chapter Two is a review of the current literature relating to the regional setting of the study area, structural history of the Hastings Block with adjoining Nambucca Block, Port Macquarie Block and Tamworth Belt. It includes a review the Hunter-Bowen Orogeny and its affects on the southern New England Orogen (NEO).

Chapter Three includes an analysis of the map pattern of the bedding, cleavage and of the mesoscopic fold axes. The cleavage and mesoscopic folds are subdivided according to their orientation in the NHB – NB region. Evidence of overprinting of cleavages and

refolding of folds in the NB and NHB are used to separate different deformation phases.

Chapter Four includes a detailed structural analysis of faults in the Northern Hastings Block using conventional fault analysis including estimating the earliest time faulting could have begun and the latest time faulting could have stopped. The evidence from cross-cutting relationships helps to constrain the relative timing between faults and in identifying different fault types. This analysis provides important information related to the brittle deformation history of the Northern Hastings Block and the adjacent Nambucca Block. Evidence is presented for some faults having a movement history related to the Late Carboniferous emplacement of Hastings Block, movement after cleavage and fold formation and movement post Triassic granite emplacement.

Chapters Five examines the variability in the orientation of bedding within fault blocks, between adjacent fault blocks, and around significant sections of the dome to enable a re-interpretation of the Northern Hastings Block geology. It highlights the shortcomings of the geological map of the Northern Hastings Block presented by Roberts *et al.* (1995). It offers alternative geological models to explain the map pattern of the current arrangement of fault blocks within the Northern Hastings Block prior to possible clockwise rotation of the northeastern limb of the Parrabel Dome. This analysis provide new constraints on the history recorded in the rocks of the NHB.

Chapters Six presents four balanced and restored cross-sections across the Northern Hastings Block based on field data. From these cross sections the three dimensional shape of the dome prior to fault disruption can be derived. These cross section help to constrain the structural and stratigraphic history (some units such as Boonanghi Beds in the NHB are time equivalent to the Nevann Siltstone, Pappinbarra and Hyndmans Creek Formations in the SHB according to the Roberts et al. 1995 boundary). They provide insights into the geometry of earlier stages in the geological development of the NHB.

Chapter Seven outlines a new workflow (progress and methods in work being done) for the construction of a 3D geological structural model of the Northern Hastings Block from comprehensive field datasets (bedding, geological maps, cross sections, digital elevation models and other geological information). Preliminary fault models, horizon (bottom surface of formations) construction, the digital elevation model (DEM) analysis and the virtual cross sections have been discussed in this chapter.

Chapter Eight presents concluding remarks on the current knowledge and summarizes the geological history of the Northern Hastings Block based on this study. The limitation of the current study are outlined and some suggestions of areas for future research are also discussed.

Chapter 2 Literature Review

2.1 Tectonic Setting

The New England Orogen is the easternmost and youngest component of the Tasmanide orogenic collage of eastern Australia (Glen 2005; Offler and Murray 2011), which comprises various terranes that interacted, accreted or amalgamated with each other. It is a major north-trending, Palaeozoic structure that extends over approximately 1300 km from Bowen (20° S) in Queensland to Newcastle (33° S) in New South Wales (Figure 2.1). Further, it developed over a period of approximately 300 million years along the East Gondwana margin and underwent pulses of contraction and extension resulting in folding, oroclinal bending, metamorphism, and basin formation. In the latter part of its history, a Carboniferous volcanic arc, forearc basin and accretionary wedge terranes formed (Leitch 1975; Cawood & Leitch 1985; Flood & Aitchison 1988). The arc, particularly in the south, is largely buried under the Sydney, Gunnedah and Bowen basins. The forearc and subduction complex are separated by a major fault, the Peel-Manning-Yarrol Fault System which is marked by serpentinite bodies that may represent a disrupted, early Cambrian ophiolite succession (Aitchison *et al*. 1992). The orogen can be subdivided into a northern segment and a southern segment, separated by Mesozoic sedimentary rocks of the Clarence-Moreton Basin (Figure 2.2). Further, the Northern New England Orogen can be subdivided into: 1) a northern region within which deformation is characterised by open folds and variable, but generally minor, thrusting; 2) a central region of thin-skinned, fold-thrust deformation with cross-orogen tear faults, and within which strain is strongly partitioned and cleavage development is variable (Gogango Thrust Belt and more eastern terranes) (Figure 2.1, Cawood *et al.* 2011), and 3) a southern region of thick-skinned deformation within which basement appears to have been involved in deformation. The southern New England Orogen constitutes a weakly deformed forearc basin in the west (Tamworth Belt) and accretionary wedge of metasedimentary rocks in the east (Tablelands Complex) (Figure

2.2). These are separated by the Peel-Manning Fault System (Leitch 1974; Korsch 1977).

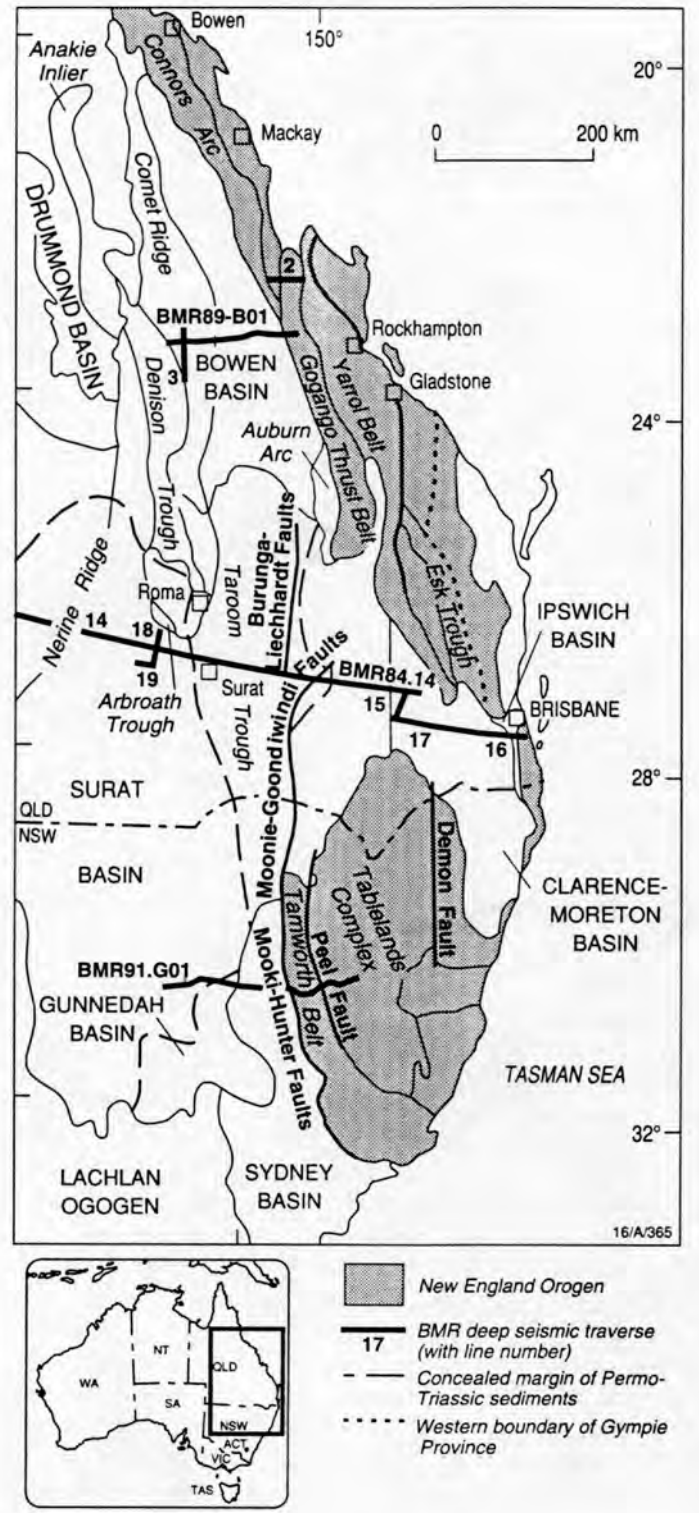

Figure 2.1: Map showing the locations of the New England Orogen (from Korsch *et al*. 1997).

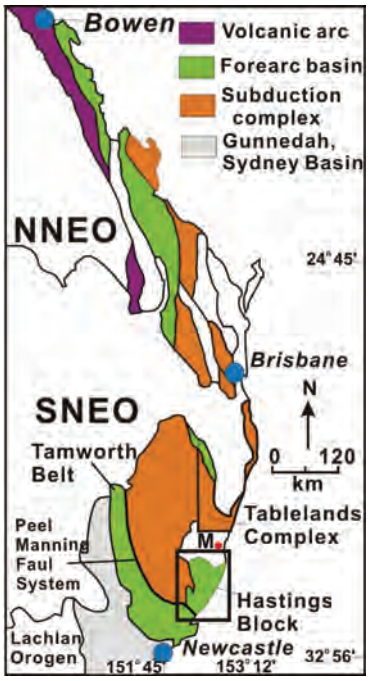

Figure 2.2: Location of the New England Orogen (from Cawood *et al*. 2011). Abbreviations (geologic terms): SNEO – Southern New England Orogen; NNEO – Northern New England Orogen; SB – Sydney Basin; BB – Bowen Basin.

Numerous tectonic models have been proposed for the development of the New England Orogen (Scheibner 1973; Leitch 1974; Cawood 1982; Murray *et al.* 1987). Most infer a long-lived, east-facing convergent plate margin configuration with progressive accretion of younger rocks at the eastern margin of Gondwana. Offler and Murray (2011) showed that intra-oceanic island arc and back arc basin (BAB) settings dominate throughout the Devonian and that basalt compositions in the Late Devonian sequences of the southern New England Orogen and the northern New England Orogen become more arc-like to the west suggesting that the subduction zone dipped to the east beneath intra oceanic arcs at this time. Buckman *et al*. (2014) proposed that the NEO contains a large, far-travelled oceanic and island arc terrane that was emplaced over the Gondwanan margin during the latest Devonian to Early Carboniferous.

2.2 Local Setting

The Southern New England Orogen (SNEO) buried volcanic arc, concave to the east

forearc (Tamworth Belt) and a accretion-subduction complex (Tablelands Complex) associated with a west-dipping subduction zone consists of Cambrian to Carboniferous buried volcanic arc, a forearc basin sequences of the Tamworth Belt and a Silurian to Early Carboniferous accretion-subduction complex rocks of the Tablelands Complex (Figure 2.3). The Tamworth Belt is separated from the Tablelands Complex by the Peel-Manning Fault System. The Tamworth Belt is faulted against the Sydney Basin, along the Hunter-Mooki Thrust System. To the southeast, near Maitland, sediments of the Sydney basin overlap those of the Tamworth Belt (Figure 2.3).

Assemblages in the southern New England Orogen are predominantly Devonian and Carboniferous volcanic and sedimentary units intruded by younger S- and I-type granite plutons, with several major occurrences of ultramafic rocks and serpentinite-matrix melange which have 'ophiolitic' affinities (Aitchison & Ireland, 1995). In the Tamworth Belt, the rocks record burial metamorphism with diagenetic to sub-greenschist facies assemblages (Offler *et al.* 1997; Offler 2005) while in the Tablelands Complex, subgreenschist to greenschist facies rocks occur as well as high P - low T (Phillips *et al.* 2010) and higher grade high T - low P metamorphic rocks (Dirks *et al.* 1992). The geothermal gradient was moderately low during subduction that produced the high P - low T assemblages (Phillips *et al.* 2010).

The sequences in the southern New England Orogen experienced oroclinal bending (Flood & Fergusson 1982) in the north (Texas-Coffs Harbour oroclines) and possibly bending or faulting in the south of the SNEO (Korsch & Harrington 1987, Glen & Roberts 2012, Li and Rosenbaum 2014, Lennox *et al*. 2013). The major uncertainties are in regard to the exact number, geometry and the tectonic evolution of the oroclines in the SNEO. Lucas (1960) and Korsch (1981) recognized oroclinal bends in the northern part of the SNEO that are now referred to as the Texas-Coffs Harbour oroclines. These have been incorporated in models proposed for the development of the SNEO (Korsch and Harrington, 1987; Lennox and Flood, 1997; Cawood *et al*. 2011;

Rosenbaum *et al.* 2012; Li *et al*. 2012a; Hoy *et al*. 2014; Rosenbaum *et al.* 2015). A less well defined orocline, the Manning Orocline, was proposed in the south (Cawood 1982; Korsch & Harrington 1987; Cawood *et al*. 2011). Recently, an additional orocline, the Nambucca/Hastings Orocline has been suggested by Rosenbaum (2010) and Glen and Roberts (2012). Oroclinal bending in the Texas and Coffs Harbour area is well established as a result of detailed mapping (Korsch *et al*. 1993; Flood & Fergusson 1982; Murray *et al*. 1987; Fergusson 1988; Lennox & Flood 1997), and aeromagnetic and gravity studies (Wellman 1990). Many authors (Cawood 1982; Glen 2005; Cawood & Leitch 2006; Glen & Roberts 2012; Li and Rosenbaum 2014; Mochales *et al*. 2014; Shaanan *et al*. 2015) maintained that the Manning Orocline exists, although they propose very different positions for the axial surface trace. For example, Li and Rosenbaum (2014), on the basis of the map-view curvature of early Permian granitoids and the Palaeozoic serpentinite belt, believed there was strong evidence for the Manning Orocline. Mochales *et al.* (2014) presented anisotropy of magnetic susceptibility (AMS) data in support of the existence of this orocline except for the Gresford and west Hastings areas. Others, such as Roberts *et al*. (1993), considered the bend in the forearc basin sequences to be a primary structure present prior to the tectonic event that Cawood (1982) believed was responsible for the bending of the forearc – accretion complex sequences. Detailed mapping by Lennox *et al*. (2013) and Offler *et al*. (2014) showed geological evidences for such oroclines was poor. The position of the hinge zone of the Manning orocline relies on the correct identification of the fabrics in the Walcha district (Li & Rosenbaum 2014; Offler *et al.* 2014). Rosenbaum *et al.* (2012) assume the serpentinites are all the same age and are present in the same fault. They also assume that granites of the same age were originally arranged in a linear north-south belt prior to the orocline formation. The aeromagnetic signature of the Manning and Nambucca (Hastings) oroclines is very poor compared with the signature of the Texas-Coffs Harbour oroclines.

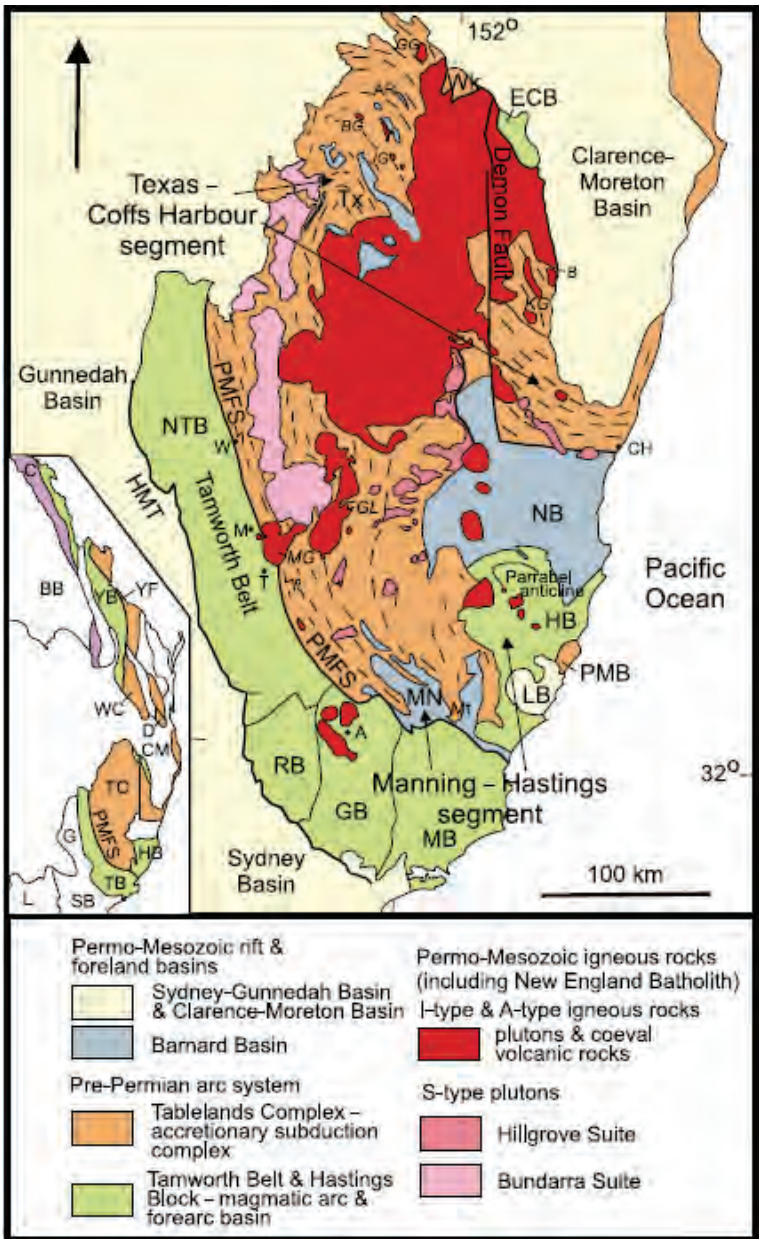

Figure 2.3: Location of the Southern New England Orogen (from Cawood *et al*. 2011). Abbreviations (geologic terms): AR, Alum Rock; BG, Bullaganang Granite; ECB, Emu Creek Block; GB, Gresford Block; GG, Greymare Granodiorite; GL, Glenburnie Leucoadamellite; HB, Hastings Block; HMT, Hunter Mooki Thrust; JG, Jibbinbar Granite; KG, Kaloe Granite; LB, Lorne Basin;MB, Myall Block;MG, Moonbi Granite;MN, Manning Block; NB, Nambucca Block; NTB, Northern Tamworth Block; PMB, Port Macquarie Block; PMFS, PeelManning Fault System; RB, Rouchel Block; TB, Tamworth Belt; Tx, Texas; Wk, Warwick; Abbreviations (geographic terms): A, Alyn River; B, Baryulgil; CH, Coffs Harbour; M, Manila; T, Tamworth; W, Woodsreef; Abbreviations (inset): BB, Bowen Basin; C, Connors Arc; CM, Clarence Moreton Basin; D, D'Aguilar Block; HB, Hastings Block; G, Gunnedah Basin; L, Lachlan Fold Belt; Mt,

Mt.George; SB, Sydney Basin; TB, Tamworth Belt; TC, TablelandsComplex;WC, Wandilla Complex; YB, Yarrol Belt; YF, Yarrol Fault.

Cawood *et al*. (2011) constrained the final stage of the timing of the Texas-Coffs Harbour and the southern Manning and Hastings oroclines formation to around 270-265 Ma (Middle Permian). Li *et al.* (2014) suggested that the main phase of oroclinal bending occurred during the Early Permian, and terminated at 271–266 Ma. Geeve *et al*. (2002) demonstrated that rotation of part of the Manning Orocline was completed prior to the late Asselian (Early Permian, about 300 Ma) .

Buckman *et al.* (2014) correlated parts of the Port Macquarie Block with the Hastings Block, and suggested a slab-rollback beneath the evolving Gamilaroi terrane and proposed that the New England Orogen, involving vertical displacement, contains a large, far-travelled oceanic and island arc terrane that was emplaced over the Gondwanan margin during the latest Devonian to Early Carboniferous without large-scale ‘oroclinal’ folding and or significant sinistral faulting.

2.3 Structural History

The southern New England Orogen (SNEO) from west to east, consists of a buried volcanic arc, concave to the east forearc (Tamworth Belt) and a accretion-subduction complex (Tablelands Complex) associated with a west-dipping subduction zone. The Nambucca and Hastings Blocks are the fault-bound blocks in the eastern part of the southern New England Orogen. The detailed geological histories of various parts in the SNEO will be discussed below.

2.3.1 Nambucca Block

The Nambucca Block (NB) is one of several fault-bound Permian blocks that make up the eastern part of the southern New England Orogen, eastern Australia. It is

characterized by the coincidence of thick marine sedimentation, polyphase deformation, and regional metamorphism. Rapid faulted-controlled subsidence commenced initially and ended with intense compressive deformation (Leitch 1988; Johnston *et al*. 2002). In the Nambucca Block, early Permian clastic and silicic volcanic rocks, tholeiitic and slightly alkaline basalts, and minor limestones have been found (Leitch 1978; Asthana and Leitch 1985). These rocks were deformed under low grade metamorphic conditions (prehnite-pumpellyite to greenschist facies), ca. 260 Ma ago (Leitch 1978; Offler & Foster 2008). A feature of the NB is that the structures within it trend east-west in contrast to the meridional trends recorded elsewhere in the Palaeozoic rocks of the forearc and accretion-subduction complex of the southern New England Orogen and rocks in other Early Permian rift basins. Several models have been proposed for the formation of this basin (Leitch 1978; Offler & Brime 1994; Adams *et al*. 2013; Shaanan *et al*. 2015; Li *et al*. 2015). However, there is disagreement concerning the timing of formation of the NB, the Texas-Coffs Harbour (TCH) megafold and the Hastings Block (HB) and whether the TCH and HB are involved in the deformation of the sediments in the NB. One model involves the movement towards the north of the HB, and the Coffs Harbour orocline towards the south, causing the young, soft sediments of the Nambucca Block to be squeezed between the two more rigid blocks, causing intense deformation, crustal thickening and low-grade metamorphism. This led to the symmetrical pattern of isograds and deformational intensity, both of which increase towards a centre of the Nambucca Block (Leitch 1978; Offler & Brime 1994).

In terms of folding and cleavage history in the Nambucca Block, according to Leitch (1978), there are five fold episodes in the Nambucca Block. The first generation, D1, consists of the E-W folds, which are rounded, open, upright with S_1 parallel to their axial surfaces. During D2, new E-W folds develop with gentle to moderately inclined axial surfaces which are parallel to crenulation cleavage S_2 that deforms S_1. S_2 dips north and fold axes of this generation are horizontal. During D3, new E-W folds, vary from broad open flexures to tight rounded structures and have axial surface crenulation

cleavage S_3. D4 folds are similar to those of D3 but are even less regular and less axially continuous. Both D3 and D4 structures are restricted to the center of the Nambucca Block more than ten kilometers from the edges of the NHB. No large-scale D4 folds have been recognized. D5 structures have NNW-SSE to NW-SE orientated folds which profoundly affect the whole slate belt including adjacent to the NHB mapped coastal exposures and between Grassy Head and Nambucca Heads (Figure 2.5). Johnston *et al*. (2002) confirmed that folds and cleavage formed during D1 and D2 trend E-W (Figure 2.5), with S_2 and S_3 being folded about E-W axes (Table 2.1). S_3 varies in strike from northwest-southeast in the hinterland to northeast-southwest on the central coast to east–west on the north-northeast coast. S_4 has a northeast-southwest strike and moderate southeast dip to the west, while in the Taylors Arm Fault System (Figure 2.5) it trends east–west and dips shallowly to moderately north, which defined east-northeast- trending, open folds in this area. In contrast, Shaanan *et al*. (2014) recognized four phases of folding and associated structural fabrics ($S_{1–4}$) in the Nambucca Block from examination of coastal exposures from Crescent Head to Bundagen Headlands (Figure 2.6). The first generation of folding, is E-W trending, and the folds are asymmetric, rounded, and open, with wavelengths of ~10 m (Table 2.1, Figure 2.6). The second phase of folds, trend NE-SW, are subhorizontal to gently inclined with slaty to spaced cleavage (S_2) axial surface. The rounded, upright F_3 folds are oriented NW-SE and are characterized by steeply inclined axial surfaces and associated crenulation cleavage planes (S_3) that strike NNW-SSE (Table 2.1, Figure 2.6). The fourth generation of folds (F_4) forms NE-SW striking, moderately inclined axial surfaces. Crenulation cleavage planes (S_4) vary spatially in intensity and orientation within this block (Table 2.1).

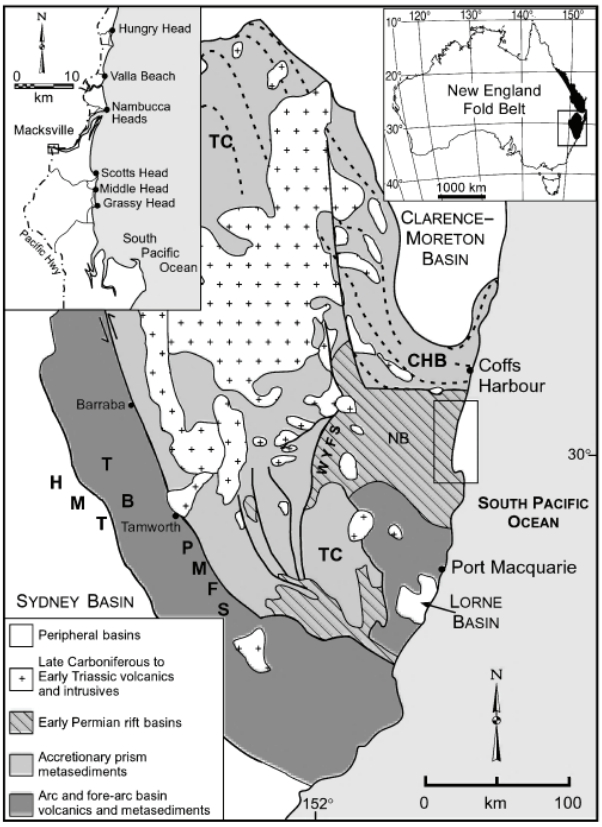

Figure 2.4: Location of Nambucca Block (NB) in the southern New England Orogen (SNEO) adjacent to the Coffs Harbour Block (CHB) to the north and bounded by the Wongwabinda Yarrol Fault system (WYFS) and Tablelands Complex (TC) to the west (From Johnston *et al*. 2002). HMT = Hunter Mooki Thrust, TB = Tamworth Belt. PMFS = Peel-Manning Fault System.

Table 2.1: Comparison of the orientation of different fold phase in the Nambucca Block (NB) and the proposed ages of these phases.

	Nambucca Block		
Deformation	Leitch (1978)	Johnston *et al*. (2002)	Shaanan *et al*. (2014)
D1	E-W (250 Ma)	E-W	E-W
D2	E-W	E-W (264-260 Ma)	NE-SW (275–265 Ma)
D3	?E- W	NNE-SSW	NNW-SSE to NW-SE (268–265Ma)
D4	?	NNE-SSW	NE-SW
D5	NNW-SSE to NW-SE (244 Ma)		

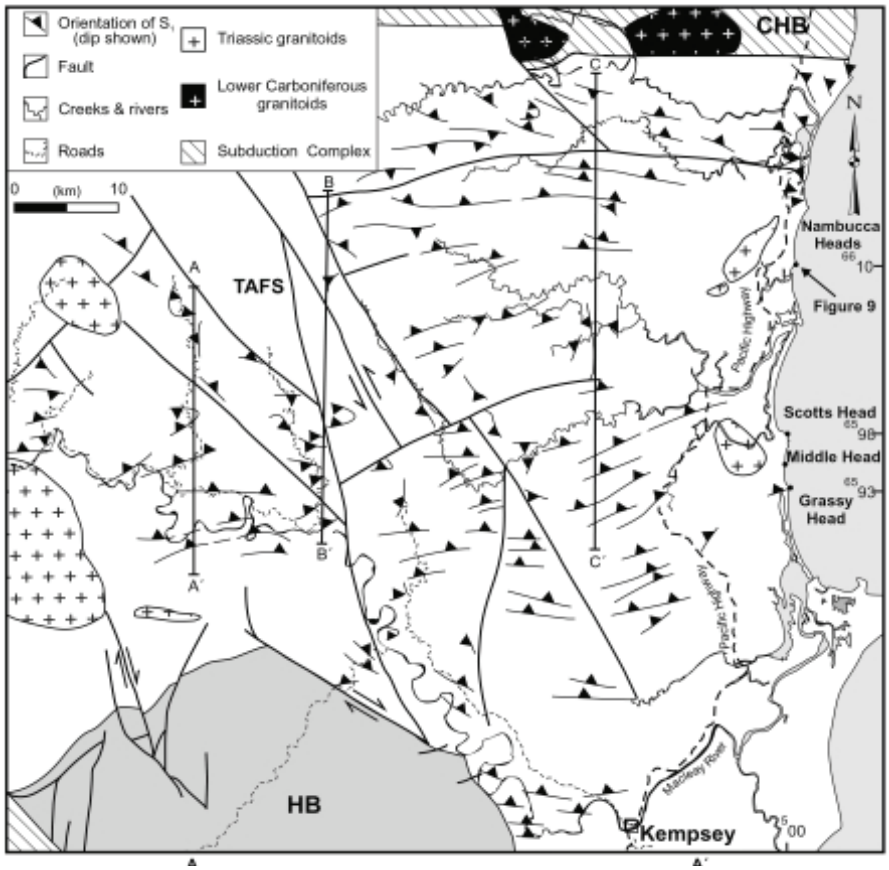

Figure 2.5: Trend of S_1 in the Nambucca Block with the teeth indicating dip direction. Faults are from Leitch (1978) and boundaries of Hastings Block (HB) from Roberts *et al*. (1993). Note S_1 is folded about E-W axes. TAFS is Taylors Arm Fault System; CHB is Coffs Harbour Block (Johnston *et al*. 2002).

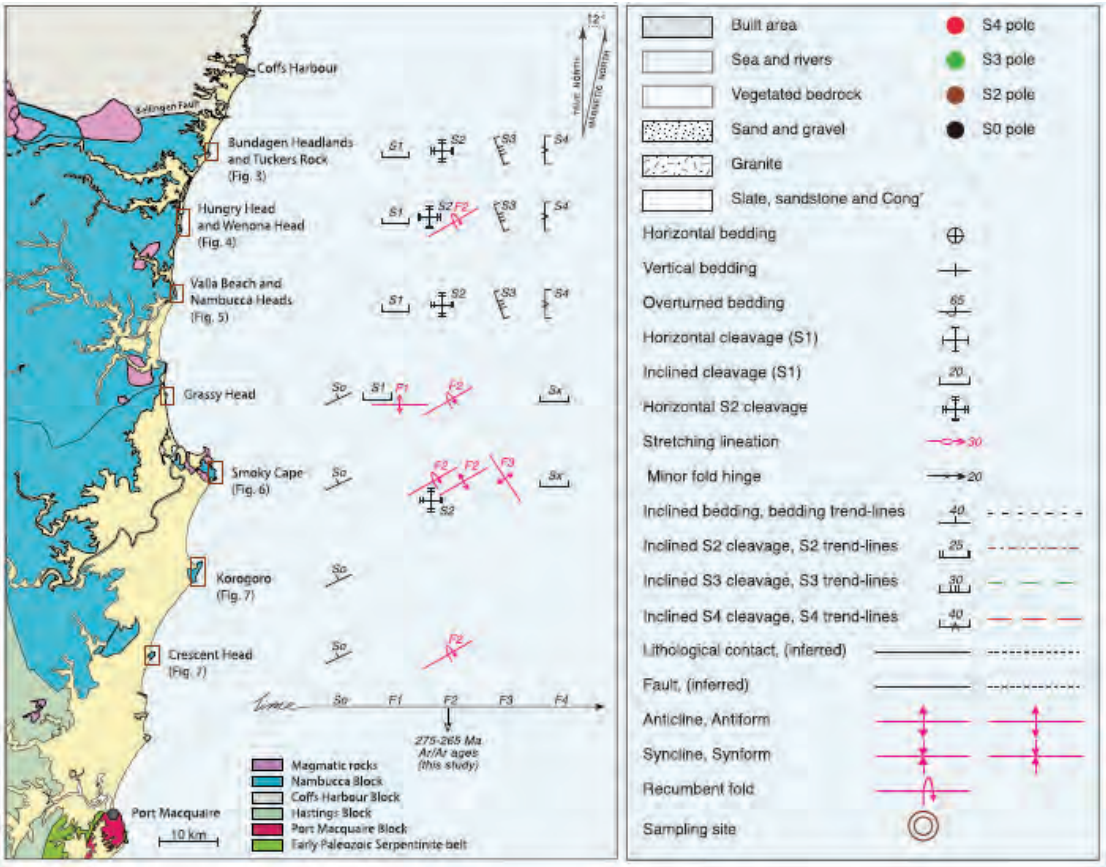

Figure 2.6: Simplified geologic map of the coastline of the Nambucca Block showing the strikes of different cleavage phases (from Shaanan *et al*. 2014).

Whole rock dating on biotite using K/Ar on slate and phyllite in the NB from Leitch (1978) and Leitch and MacDougall (1979) implies that orogenesis occurred at about 250-255 Ma. All folding was accomplished in a period of about 5 m.y. Offler and Foster (2008) dated whole rock chips dominated by mica from S_1 and S_2 cleavage domains in the slate and phyllite using $^{40}Ar/^{39}Ar$ analysis which constrained timing at between 264-260 Ma, which is similar to the recalibrated Leitch and MacDougall (1979) dates. In contrast, Shaanan *et al.* (2014) using $^{40}Ar/^{39}Ar$ on muscovite dated the second phase (S_2) at 275–265 Ma.

Johnston *et al.* (2002) suggested that the D1 and D2 structures in the Nambucca Block are the result of the south-directed movement of the Coffs Harbour Block. They implied that the HB was in its current position prior to Early Permian sedimentation in the NB. Some of the macroscopic folds in the southern NB are similar in orientation to the

macroscopic and mesoscopic folds in the Northern Hastings Block (NHB). The pattern of some of cleavages from Nambucca Block and NHB data are also similar suggesting they may have formed at the same time. Rosenbaum *et al.* (2012) implies that the emplacement of S-type granitoids in the SNEO occurred simultaneously with the development of rift basins filled with clastic sedimentary rocks (Nambucca Block). And then deformation during the Hunter-Bowen Orogeny (265Ma – 228Ma, Holcombe *et al.* 1997) affected early Permian sedimentary rocks of the Nambucca Block (Johnston *et al.* 2002; Offler and Foster, 2008; Rosenbaum *et al.* 2012). Shaanan *et al*. (2014) argued that the development of the Nambucca Block was accompanied by the initial oroclinal bending and it was possibly associated with trench retreat. The N-S contraction between the Coffs Harbour Block and the Hastings Block is possibly in response to the dextral transpression, and the subsequent NW-SE contraction was responsible for tightening the oroclinal structure.

The detrital zircon ages from early Permian sandstones in the southern part of the Nambucca Block were reported in Adams *et al*. (2013). They suggested the following tectonic history with: (1) Accretionary wedge development during the Devonian to Carboniferous in the New England Orogen; (2) Outward translocation of the arc in the latest Carboniferous time resulting in a more local provenance for early Permian sediments deposited in the Nambucca Block; and (3) Early Permian outboard repositioning of the primary, magmatic arc allowing formation of extensional basins throughout the New England Orogen.

2.3.2 Hastings Block

The Hastings Block (HB) is a large faulted-bounded block, consisting of mainly Devonian to Carboniferous rock sequences, and an Early Permian cover sedimentary sequence. It is located on the eastern side of the subduction complex, northern margin of the fore-arc Tamworth Belt of the southern New England Orogen and southern margin of the Nambucca Block (Figure 2.7, Roberts *et al.* 1995). It is thought to be an

along strike continuation of the fore-arc sequences in the Tamworth Belt before being emplaced into its current position (Cawood *et al*. 2011). Major faults on the margins juxtapose the Hastings Block with the Early Permian successor sediments against the Parrabel Fault in the northeast. Further, they juxtapose the accretion-subduction complex rocks of the Yarrowitch Block (Leitch *et al.* 1990) to the west, and Devonian-Carboniferous sediments of the Myall Block of the Tamworth Belt (Roberts & Engel 1987; Roberts *et al.* 1991) against the Manning Fault in the south (Figure 2.7c). The Port Macquarie Block (Leitch 1980) is divided from the Hastings Block by the Cowarra Fault as a composite block (Figure 2.7c). Some units of the Port Macquarie Block have a close affinity with sequences in the Hastings Block (Pickett *et al.* 2009).For example, parts of the Walibree Formation in the Hastings Block resemble sedimentary rocks and tuffs within the Touchwood Formation of the Port Macquarie Block (Roberts *et al.* 1995).

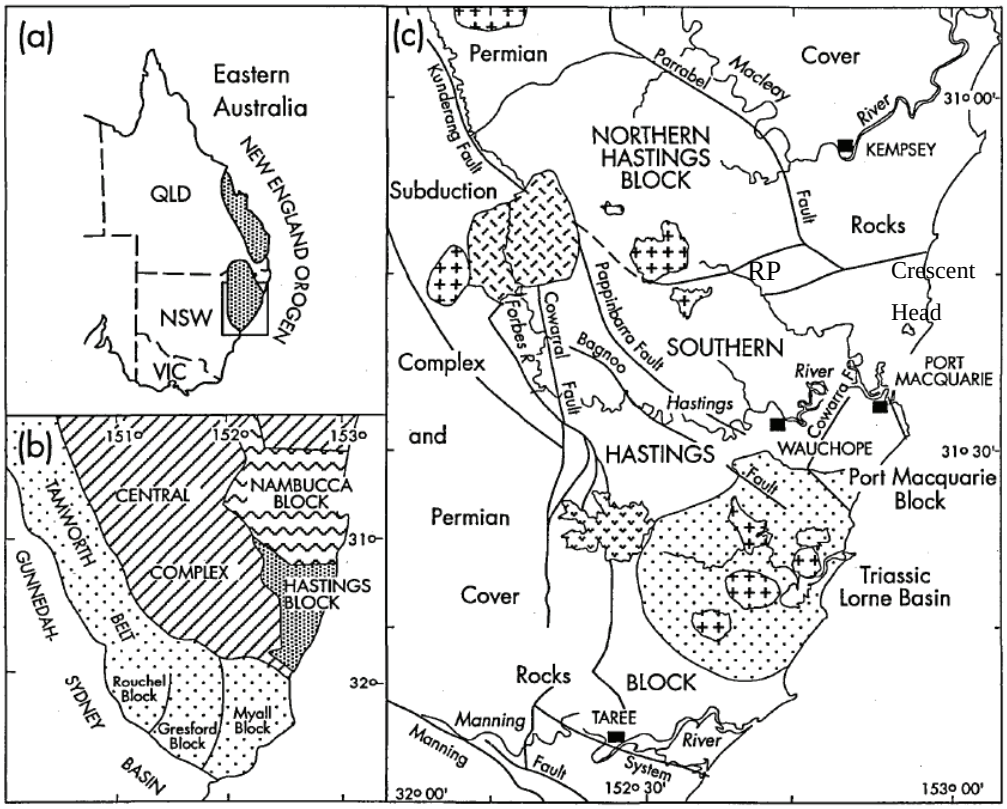

Figure 2.7: Location and tectonic setting of the Hastings Block, (a) within eastern Australia, (b) within the southern New England Orogen. (c) Major tectonic units and faults within and adjacent to the Hastings Block (From Roberts *et al*. 1995).

The Hastings Block can be subdivided into two sections the northern (NHB) and southern Hastings Block (SHB), which are distinguished by the differences in structural style, structural history and pre-Permian stratigraphy (Lennox & Roberts 1988). The NHB contains a sequence of Early to Late Carboniferous rocks, while the SHB consists of Devonian to Carboniferous rocks disconformably overlain by Early Permian successor sediments. The NHB includes the shallowly northwesterly-plunging Parrabel Dome which has a northwest-southeast structural grain. In contrast, the SHB is characterized by a north-south structural grain.The NHB is characterised by four phases of folding as opposed to two phases of folding in the SHB. Lennox & Roberts (1988), Schmidt et al. (1994) and Roberts et al. (1995) suggested that the NHB and the SHB are separated by an arcuate line possibly related to a fault system extending from the northwestern edge of the HB near Kunderang Fault (Figure 2.7), southeasterly through Rollands Plains (RP on Figure 2.7) and east-northeasterly towards Crescent Head (Figure 2.7). The boundary is faulted in the west and east, but in the central part the boundary is obscured by younger volcanics and granitoids (Figure 2.7).

Lennox & Roberts (1988), Schmidt *et al.* (1994) and Roberts *et al.* (1995) suggested that the NHB and the SHB are separated by an arcuate line possibly related to a fault system extending from the northwestern edge of the HB near Kunderang Fault (Figure 2.7), southeasterly through Rollands Plains (RP on Figure 2.7) and east-northeasterly towards Crescent Head (Figure 2.7). The boundary is faulted in the west and east, but in the central part the boundary is obscured by younger volcanics and granitoids (Figure 2.7). Lennox *et al.* (1999) argued that the Bagnoo Fault and its inferred extensions, the Rollans Road Fault (RRF) and the Cowarral Fault (CWF) should be the geological boundary between the NHB and SHB (Figure 2.7). There is the continuation of the cleavages and mesoscopic folds across what is nominally the NHB-SHB boundary as defined by Roberts *et al.* (1995). It is the case that this Roberts et al. boundary reflects the region where the formations defining the dome change (stratigraphically-controlled boundary), whereas the actual structural boundary is further south nearer the

worm-derived fault. Lennox *et al.* (1999) was suggesting such a subdivision.

Major geological and structural events affected the Hastings Block in the Late Carboniferous to Early Permian, the Late Permian and in the Late Triassic. Some authors argued that these events must have been preceded by movement of the Hastings Block from a position within the fore-arc basin, possibly southeast of the Myall region, to one adjacent to an actively eroding accretionary prism (Roberts *et al.* 1993; Schmidt *et al.* 1994). Uplift in the later part of the Late Carboniferous took place throughout both the Northern Hastings Block and Southern Hastings Block prior to deposition of sediments in the Early Permian (Lennox & Roberts 1988; Roberts *et al.* 1993). Deposition took place both in the Nambucca Block as well as in the earlier formed successor basins over the HB. Slivers of forearc, including the HB, were translated northwards between faults, the NHB, and possibly the attached SHB, simultaneously being rotated 130° dextrally or 230° sinistrally (Schmidt *et al.* 1994) and juxtaposed against subduction complex rocks during the Permian. Following the major deformation, basin subsidence in the Early Triassic led to the accumulation of post-orogenic quartzose and red-bed sediments (Camden Haven Group) in the Lorne Basin (Figure 2.7c). Faulting, minor folding and the emplacement of syntectonic granitoids and rhyolitic volcanism took place in the Late Triassic, the igneous events being dated at around 226 Ma (Flood *et al.* 1993; Roberts *et al.* 1993). During this time, dextral movement on a southern extension of the Demon Fault caused minor faulting in the northeastern part of the Northern Hastings Block. Cawood *et al.* (2011), Rosenbaum *et al.* (2012), Glen & Roberts (2012) and Li *et al.* (2014) invoke large-scale 'oroclinal' folding in the Manning and Hastings area. Lennox *et al.* (2013) and Offler *et al.* (2014) showed that geological evidence for such oroclines is poor and the entire concept of the two oroclines in the SNEO seems unlikely. They indicated that Li *et al.*'s(2014) use of fabrics in the Walcha district to identify the Manning orocline axial surface trace is poorly constrained. They showed that the aeromagnetic signature for the Manning/Hastings oroclines is poor. The use of disparate serpentinites of probably

different ages to define these oroclines is also questionable as they do not form a linear belt around the NHB. The assumption that granites of the same age (~ 300 Ma) formed a linear belt and were subsequently folded during orocline formation seems unlikely because the granites commonly do not always form linear belts. In South America Phanerozoic granites are related to subduction of the Pacific plate under the continent and do form a linear belt, whereas the Precambrian granites are blocky in map view.

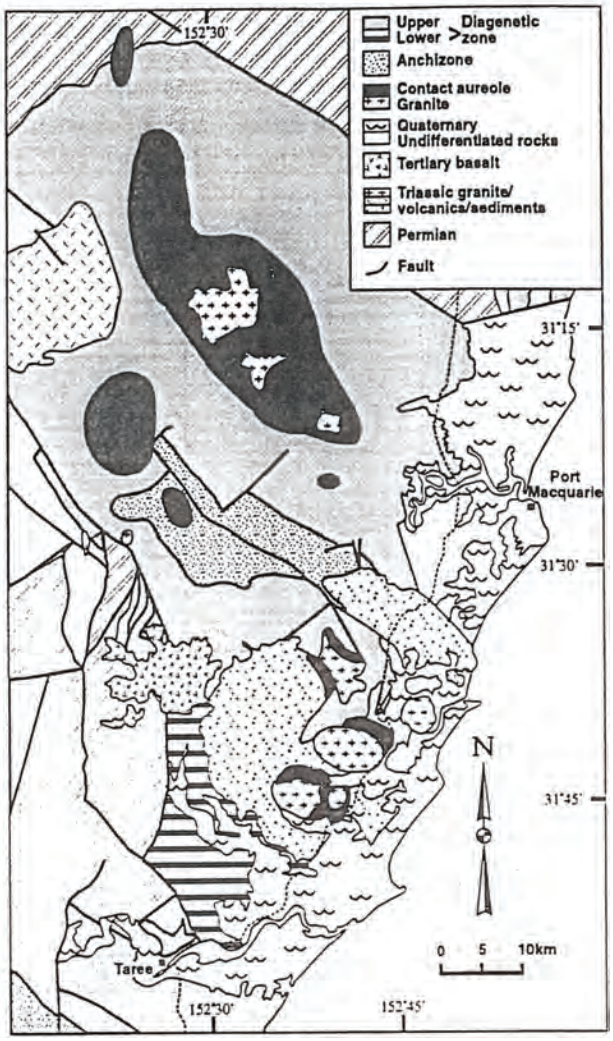

Figure 2.8: Metamorphic zones delineated in the Hastings Block (Offler *et al*. 1997).

Leitch *et al.* (1982) indicates that prehnite is widespread in Carboniferous and older rocks, pumpellyite is rare in the core of the Parrabel Dome and more common in the Devonian sequences in the southwest. Neither prehnite nor zeolites have been identified in the Early Permian strata of the HB. Offler *et al*. (1997) confirmed that mineral assemblages typical of the prehnite-pumpellyite facies occur in Devonian rocks and

zeolite facies assemblages in Carboniferous rocks.

Metamorphism in the Hastings Block (HB) is the result of burial (Leitch *et al.* 1982; Offler *et al*. 1997) and later contact metamorphism (Figure 2.8, Offler *et al*. 1997). These two metamorphic events and subsequent folding are disrupted by later faulting leading to many of the metamorphic zones being fault-bound. The contact metamorphic aureoles formed during the emplacement of Triassic granitoids in the HB (Figure 2.8, Offler *et al*. 1997).

2.3.2.1 Northern Hastings Block

The Northern Hastings Block contains the Early to Late Carboniferous rock sequences that are overlain by the Early Permian sequences. Voisey (1934, 1936) and Lindsay (1969) firstly divided the sedimentary rocks of the NHB (lower Macleay region, Figure 2.7) into six straigraphic units. They are, in ascending order, the Boonanghi Beds, the Majors Creek Formation, the Kullatine Formation, the Yessabah Limestone, the Warbro Formation and the Parrabel Beds. Lindsay (1966) proposed that the Upper Carboniferous Kullatine Formation consists of normal water-sorted shallow marine sediments in the north and fine-grained deeper water sediments in the south. These sediments contain no evidence of the action of glaciers nor do they contain evidence of floating ice (Lindsay 1966). Lindsay (1969) showed that the lowest exposed Carboniferous sedimentary rocks are turbidites and the oldest Permian rocks exposed are bioclastic limestones in the NHB. Deposition appears to be finished in the Early Permian by an orogeny (Hunter-Bowen Orogeny).

Based on the analysis of bedding recorded in the NHB as well as the overlying Permian sequences, Lennox *et al.* (1999) suggested that the NHB is characterized by a megafold the Parrabel Dome which plunges gently northwest. This analysis demonstrated that the Permian fold axes plunged less steeply than the Carboniferous fold axes, indicating that the Permian sequences were deposited on already tilted Carboniferous strata.

The NHB according to Lennox *et al*. (1999) has undergone three phases of folding namely, east-west, northwest-southeast and northeast-southwest trending. Macroscopic F_1 folds are upright, originally east-west trending, subhorizontal to gently plunging with half-wavelength from 1 to 7 km. F_2 folds are subparallel to the northwest-plunging fold axis of the Parrabel Dome (11° -> 302°, Lennox *et al*. 1999). The least well developed and spatially restricted are the third generation NE-SW folds of up to 11 km half-wavelength.

Three episodes of faulting have been recognized in the NHB (Roberts *et al*. 1993). Initially, northwest-trending faults formed with mainly sinistral strike-slip movement; followed by northeast-trending faults with dextral or sinistral strike-slip or dip-slip movement, with small displacements. Subsequently, meridional, dip-slip faults developed (Roberts *et al.* 1993). The NHB has been rotated clockwise 130° or anticlockwise 230° according to Schmidt *et al.* (1994) or 150° anticlockwise according to Klootwijk (2009).

Studies showed that cleavage was developed dominantly around the margins of the Parrabel Dome within the Permian rocks (Lennox *et al.* 1999) and that it is less well developed in the Carboniferous sequences than in the Permian sequences. The dominant cleavage in the Permian rocks trends east-west. The initial D_1 east-west trending cleavage and folding (Lennox & Roberts 1988) has been refolded by the northwest-trending fold phase, and both of these have been further modified by the northeasterly-trending fold phase. The latter fold phase is possibly associated with late stage movement on the Taylors Arm Fault System (Leitch 1978, Figure 2.5), an extension of the Demon Fault, which impinges upon the northeastern part of the NHB.

Lennox and Roberts (1988) showed that the Carboniferous palaeoslope in the NHB appears to be towards the southwest which is opposite to the same Carboniferous palaeoslope in the Tamworth Belt. This lends support to the palaeomagnetic studies in

the NHB which suggested significant rotations of the NHB (Schmidt *et al*. 1994).

2.3.2.2 Southern Hastings Block

The Southern Hastings Block, has meridional-trending, macroscopic folds overprinted by northwest-trending folds. It has suffered three episodes of faulting: (i) early meridional dip-slip faults; (ii) later northeast-striking, sinistral strike-slip or rare dip-slip faults and (iii) northwest-trending faults with both sinistral and dextral strike-slip movement (Roberts *et al*. 1993).

Devonian and Carboniferous rocks in the SHB have similar fold axis orientations but the Permian sequences are folded about axes of the same orientation as those in the NHB (Lennox *et al.* 1999). Some meridional folds have been rotated about faults, leading to the development of northeast-trending drag folds. The Bagnoo Fault is a major sinistral, strike-slip, northwest-trending fault in the SHB (Feenan 1984; Spackman 1989; Roberts *et al.* 1993). It is located west of Wauchope, cuts the Lorne Basin and is cut by the Cowarral Fault which is terminated against the Werrikimbi Volcanic complex, indicating that it is post meridional folding in the SHB and pre 226 Ma, the age of the granitoids (Figure 2.7, Flood *et al.* 1993). Triassic rocks in the Lorne Basin are folded about north-south axes (Pratt 2010, West 1990). Cleavage data obtained from the Devonian/Carboniferous and Permian sequences shows two or possible three populations (Lennox *et al.* 1999). The dominant one is an almost north-south striking cleavage developed in high strain zones adjacent to the Yarrowitch Fault, and a less common one subparallel to the northwest-trending cleavage identified in the NHB.

The SHB is structurally similar to the Tamworth Belt which is adjacent and southwest of the Peel-Manning Fault System (Figure 2.7).

2.3.3 Port Macquarie Block

The Port Macquarie Block occurs at the eastern margin of the southern New England Orogen and is situated approximately 350 km north of Sydney. To the south the Port Macquarie Block (PMB) is overlain by Triassic sedimentary and volcanic rocks of the Lorne Basin (Pratt 2010). Rocks that crop out along the coast at Port Macquarie where the best exposure of the sequences in the PMB occur, are mostly weakly metamorphosed chert, volcaniclastic sandstone and siltstone, and basalt of the Middle to Late Ordovician Watonga Formation (Och *et al.* 2007) that is cut by minor intrusions and serpentinite bodies. This formation makes up the eastern portion of the fault-bounded Port Macquarie Block of Leitch (1980). Nutman *et al.* (2013) showed that the metasedimentary blueschist and eclogite facies in the serpentinite melange in Port Macquarie Block formed at the end of the Palaeozoic, and the high-pressure metamorphic event at Port Macquarie occurred during late Palaeozoic to earliest Triassic subduction during the Hunter-Bowen Orogeny at the Gondwanan margin. The Watonga Formation is a component of the accretion-subduction complex, together with forearc basin and magmatic arc rocks further west, accreted during Devonian-Carboniferous plate convergence. Buckman *et al.* (2014) proposed that the Watonga Formation should be reserved for only the older chert and basalt components, while the Carboniferous Green Mound rocks (Figure 2.9D) be grouped with the Tablelands Complex. The Tacking Point Gabbro intruded into Watonga Formation metabasalts and cherts and is the easternmost body of its type in the NEO (Nutman *et al.* 2013; Figure 2.9B). It has a middle Devonian age of 390±7 Ma and it represents a mid-Paleozoic assemblage allochthonous to Gondwana according to Buckman *et al.* (2014) (Figure 2.9B). The mafic intrusions are members of a magmatic suite possibly emplaced during Early Permian extension that accompanied eastward relocation of convergent margin elements (Caprarelli and Leitch, 2001). The new zircon dating data from Buckman *et al.* (2014) indicating that the felsic dykes intruded the Port Macquarie serpentinite at 247±20 Ma. Subsequent tectonic movements, associated with earliest Permian extension and the Late Permian-Triassic Hunter-Bowen Orogeny, have

contributed to the disrupted character of the rocks and their present location within the accretionary complex (Och *et al*. 2003).

It is likely that metamorphism and serpentinite emplacement at Port Macquarie and in the Great Serpentinite Belt to the west occurred at different times and are unrelated (Figure 2.9 under Panthalassan Terranes, Buckman *et al*. 2014). Nutman *et al.* (2013) proposed that the emplacement of Port Macquarie serpentinite melange was related to subduction at the margin of Gondwana and/or to the juxtaposition of a Palaeopacific Ocean Permian island arc (Figure 2.9 E-F). This event caused the basement Carboniferous Tamworth Belt forearc rocks to be thrust westwards over the Permian back-arc basin (Sydney-Gunnedah-Bowen basins) (Figure 2.9E). Flood and Aitchison (1988) separated the Port Macquarie Block from the Hastings Block as a separate tectonostratigraphic unit, whereas Buckman *et al.* (2014) correlated some of the units in the Port Macquarie Block with units in the Hastings Block. They suggested a slab-rollback beneath the evolving Gamilaroi terrane and proposed that the New England orogen, involving vertical displacement, contains a large, far-travelled oceanic and island arc terrane that was emplaced over the Gondwanan margin during the latest Devonian to Early Carboniferous without large-scale ‘oroclinal’ folding and or significant sinistral faulting (Figure 2.9c).

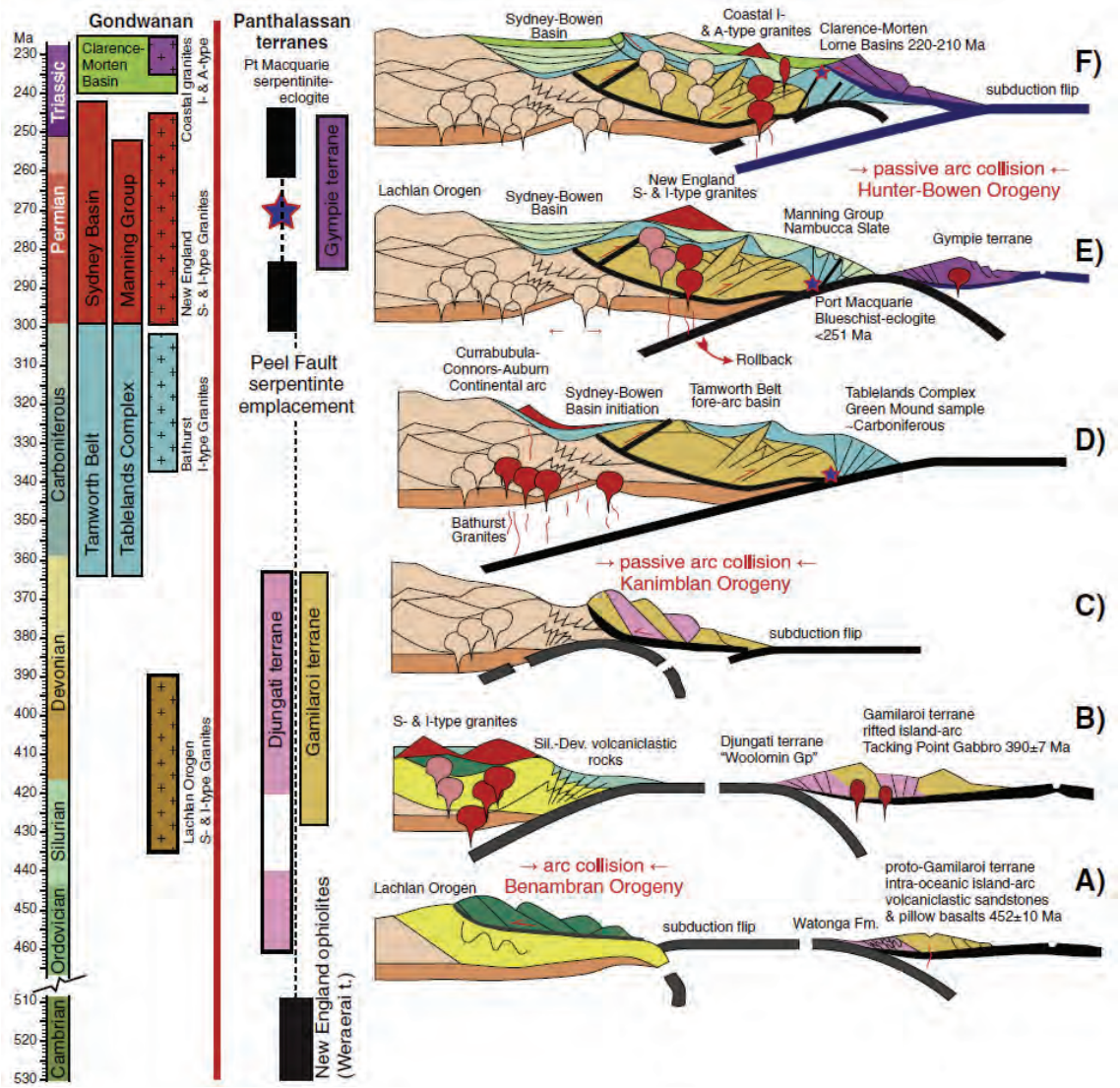

Figure 2.9: Schematic tectonic reconstruction of the eastern margin of Gondwana from the Cambrian to the Triassic highlighting the episodic nature of island arc collision events (from Buckman *et al*. 2014).

2.3.4 Tamworth Belt

The Tamworth Belt (TB) that was formerly a forearc basin is now internally imbricated and folded, and forms a generally west-verging thrust and fold belt (Offler and Murray, 2011). The southern-most part of the TB has been detached from the Tamworth Belt and translated north and rotated so that it now lies outboard of part of the Tablelands Complex as a separate block - the Hastings Block (Figure 2.10).

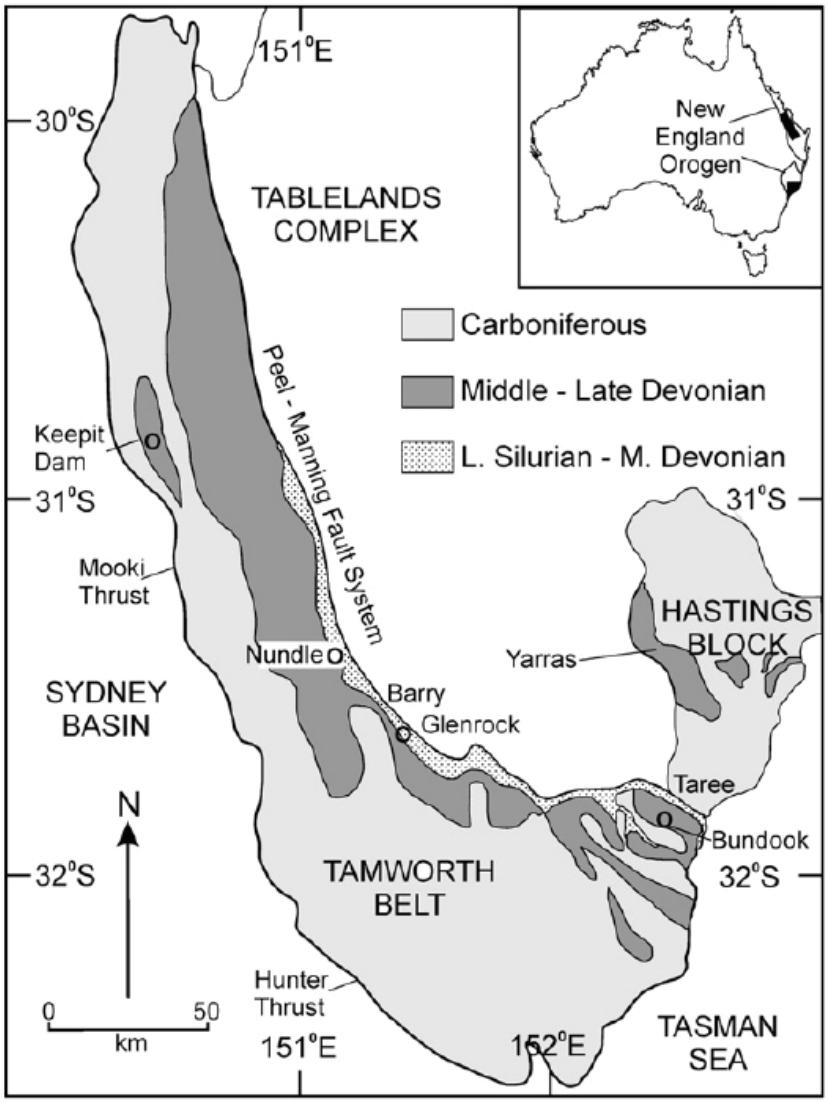

Figure 2.10: Location and age of rocks of the Tamworth Belt and Hastings Block (From Offler & Murray, 2011).

The Tamworth Belt is located between the Peel-Manning Fault System in the east and the Mooki and Hunter thrusts in the west, and consists of strata ranging in age from Late Silurian to Permian, with isolated blocks of Cambrian rocks (Cawood & Leitch, 1985) (Figures 2.10-2.12). In general, Carboniferous sediments grade from shallow- to deeper-marine from west to east, consistent with an east-facing Carboniferous arc-flank (Crook 1961; Leitch 1974). The Peel-Manning Fault System is marked by serpentinite belts.

The Tamworth Belt is made up of several separate fault-bound blocks, including the Rouchel, Gresford, Myall and Hastings Blocks in the southern Tamworth Belt (STB),

and the Rocky Creek and Werrie Synclines in northern Tamworth Belt (NTB; Figures 2.11 & 2.12). In the STB, blocks are characterised, at least in part, by the distinctive stratigraphies (Roberts *et al.* 2006). Some adjacent blocks lack any units in common (e.g. northern and southern Hastings Blocks) and hence were deposited in slightly different parts of the forearc basin. Others have different lower sequences, followed by a common succession, indicating that early in their history they received sediment in different parts of thc forearc basin, but later occupied virtually the same part of that basin (eastern and western Myall blocks; Rouchel and Gresford blocks) (Geeve *et al.* 2002). The NTB has an essentially a common early succession, but younger parts of the succession are different such as in type of volcanics, facies and sea level changes, and the location of individual volcanic centres (Geeve *et al.* 2002).

Palaeomagnetic data indicated that the blocks within the STB have been rotated between 80° and 150° sinistrally since deposition (Geeve *et al.* 2002; Klootwijk 2009) and were probably allochthonous. Emplacement of the allochthonous blocks into their present positions began during the latest Carboniferous, and was completed by the beginning of the Permian. Specifically, the Rouchel and Gresford blocks, acting as a single unit, have been rotated sinistral1y 80°, and the Western Myall block 110° (Geeve *et al.* 2002, Figure 2.11). On the other hand, given that sinistral movement is required to relocate the blocks to their present positions, Roberts and Geeve (1999) suggested that the blocks were originally part of a continuous, but segmented, forearc basin which formed an arcuate curve around a block of Lachlan Orogen basement in the Hunter region of NSW. Following the cessation of volcanism and deposition within the forearc basin, a sinistral shear movement rotated the blocks. The Hastings Blocks was rotated northwards to lie east of the Tablelands Complex, the Myall blocks northeastwards, and the Rouchel and Gresford Block moved as a single unit into a position north of the basement block in the Hunter region.

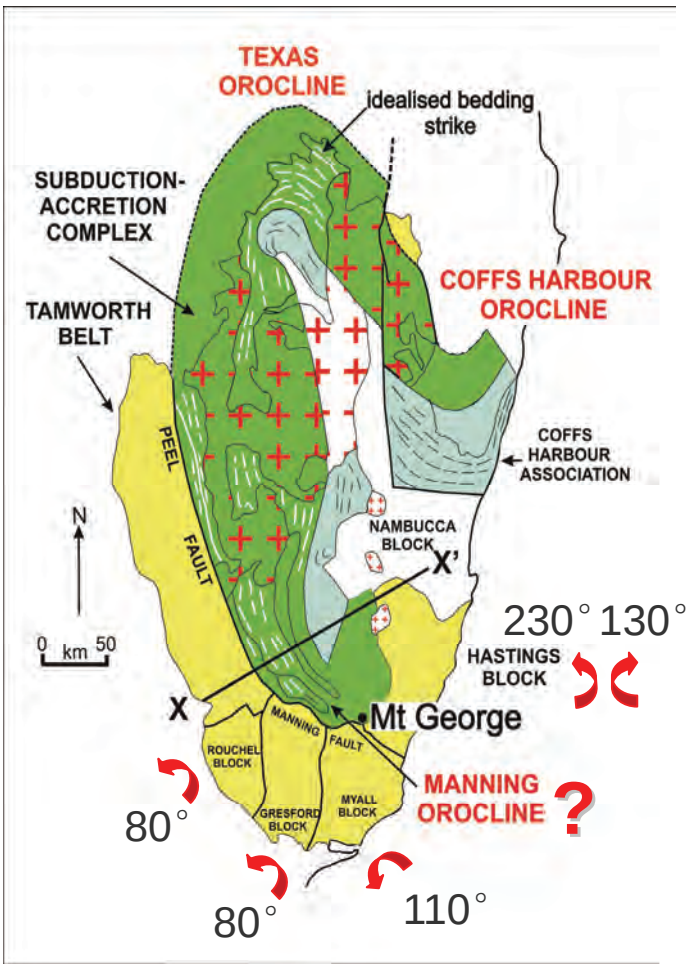

Figure 2.11: A schematic figure showing the different rotations in the Tamworth Belt (modified from Korsch and Harrington, 1987).

When the blocks are rotated back to their original position the southern Tamworth Belt forms a curvilinear feature around probable Lachlan Orogen basement in the Hunter region, with an extension to the south. The positive fold test by Geeve *et al*. (2002) and the remagnetisation in these blocks indicated that Rouchel, Gresford, Myall and Hastings blocks were rotated into their present configuration by the earliest or early Asselian, prior to folding. Glen & Beckett (1997) also indicated that the southeastern part of the Tamworth Belt was emplaced before meridional folding of Permian rocks in the footwall and before folding, the southeastern part of the Hunter Thrust had a west-northwest trend. Various forms of tectonism take place in different parts of the Tamworth Belt at different times, with diverse events taking place simultaneously in

apparently adjacent regions. The Rouchel and Gresford blocks were folded and faulted by an east-west compression in the mid to late Early Permian, prior to intrusion and hornfelsing by the Barrington Tops Granodiorite (Schmidt *et al.* 1994). No deformation of this age has been recognised elsewhere in the Tamworth Belt, but it may be linked to the loading of the Sydney Basin prior to or during deposition of the Greta Coal Measures.

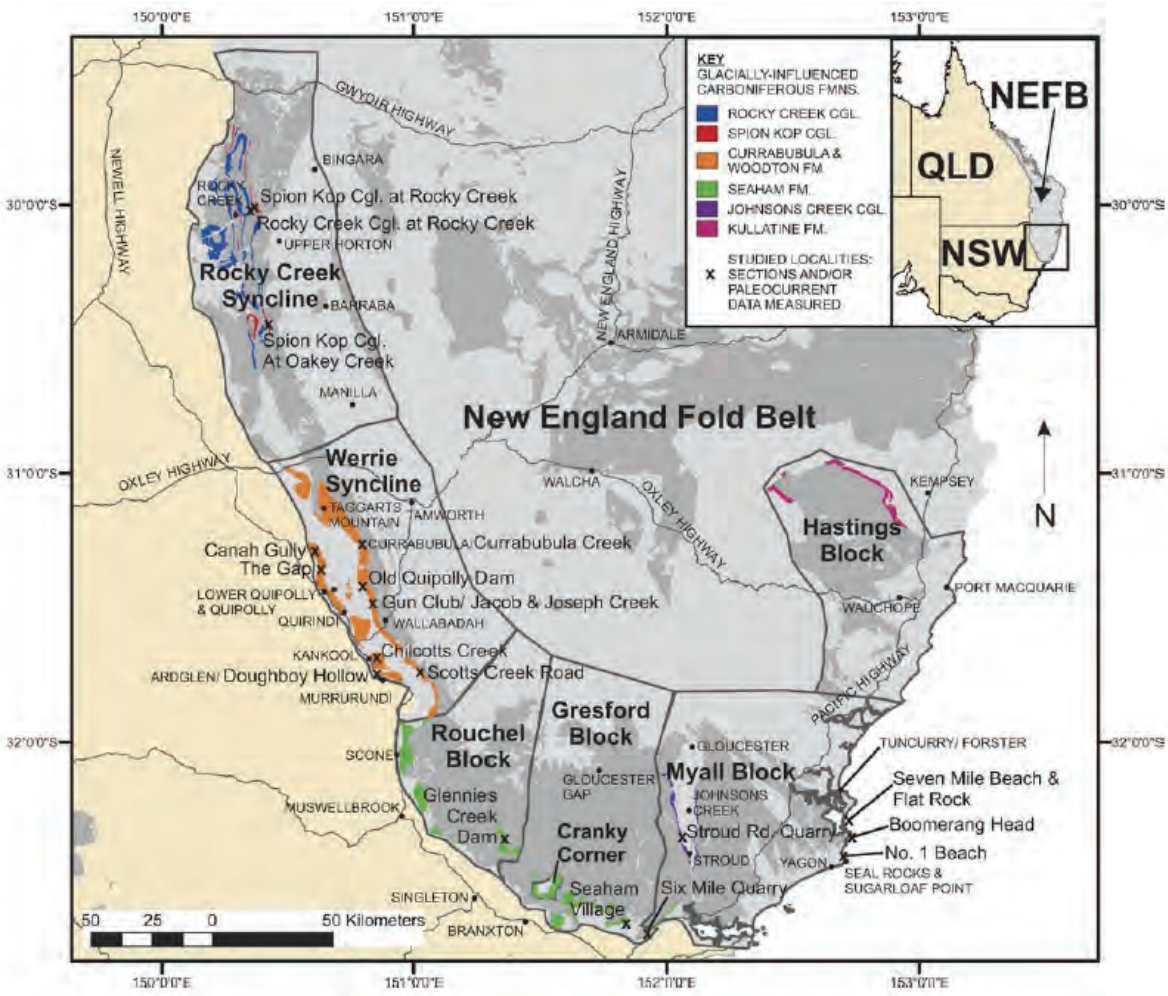

Figure 2.12: Map of Tamworth Belt (from Birgenheier *et al*. 2009)

Cawood *et al.* (2011) suggest the New England Orogen involved buckling of a pre-Permian assemblage about a vertical axis due to northward translation of the SNEO against NNEO, which was pinned relative to cratonic Gondwana. Significant differential northward displacements of the Hastings, Myall, Gresford, Rouchel, and Northern Tamworth blocks are required to reach their current configuration, which also

requires that major sinistral faults separate the Hastings Block from the Myall, Gresford and Rouchel blocks, with further faults separating these blocks from the Northern Tamworth Block. The various forearc elements (northern Tamworth, Rouchel, Gresford, Myall and Hastings) originally formed a linear to slightly curvilinear sequence prior to the orocline formation. The estimated timing of orocline formation is at ~270-265 Ma.

Major compressive events in the Nambucca block and Tablelands Complex at around the end of the Early Permian and beginning of the Late Permian roughly correspond with loading in the foreland basin and the commencement of widespread coal measure deposition, but the major east-west compression responsible for folding the entire Tamworth Belt, and the overthrusting of the foreland basin, took place in the latest Permian and earliest Triassic (Glen & Beckett, 1997).

2.4 The Hunter-Bowen Orogeny

The Hunter-Bowen Orogeny is a significant arc accretion event that affected the Australian continental margin (including the New England Orogen) during Permian to Triassic. It has two main phase: 1) the Permian accretion of the passive-marginal Devonian and Carboniferous sediments; 2) the later Permian to Triassic event resulting in arc accretion and metamorphism during a subduction event. The Hunter-Bowen Orogeny is a single but complex compressive tectonic event in the southern NEO (Collins 1991).

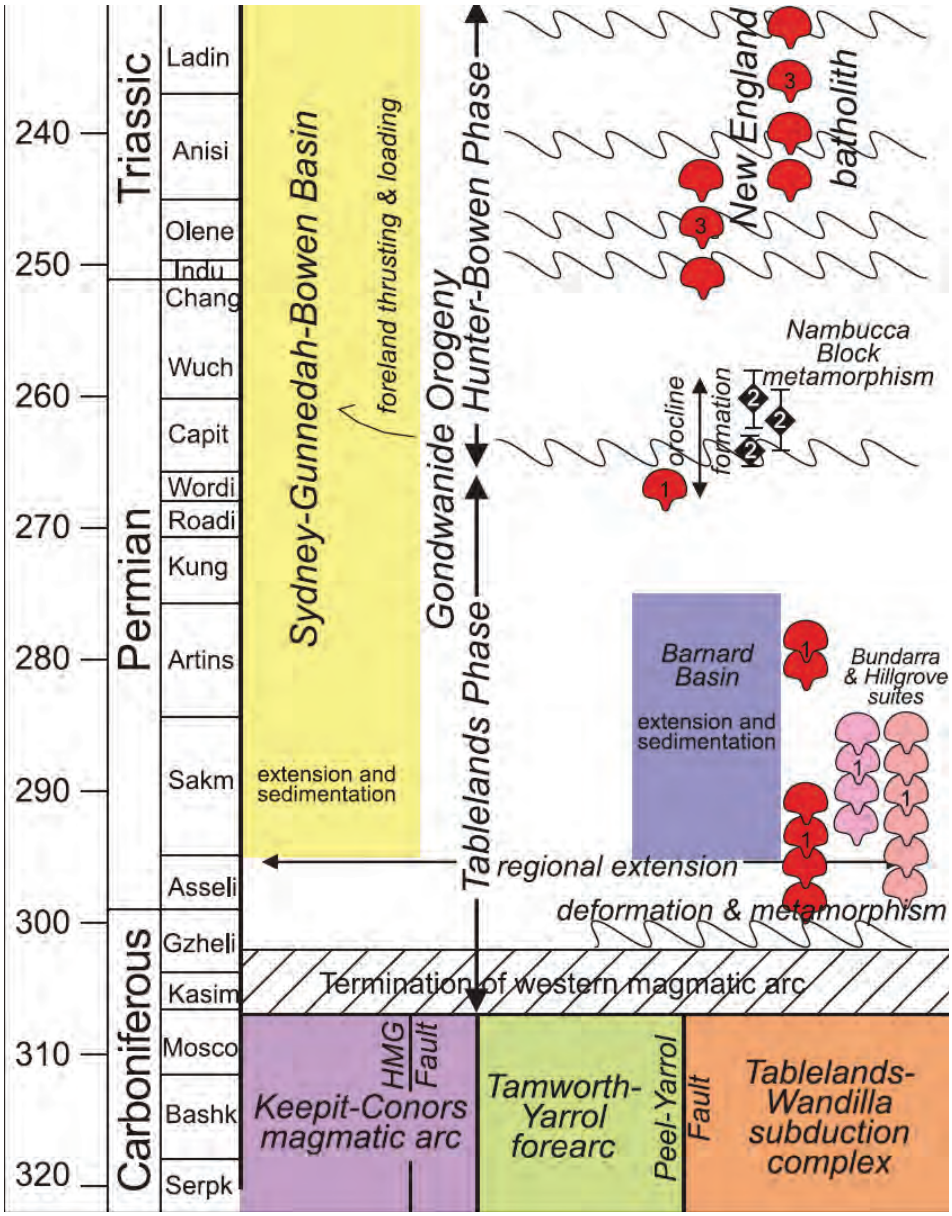

Figure 2.13: Schematic time-space diagram for the New England segment of the Terra Australis Orogen and adjoining Sydney-Gunnedah Basin. Abbreviations: Serpk – Serpukhovian; Bashk – Bashkirian; Musco – Muscovian; Kasim – Kasimovian; Gzheli – Gzhelian; Asseli – Asselian; Sakm – Sakmarian; Artins – Artinskian; Kung – Kungurian; Roadi – Roadian; Wordi – Wordian; Capit – Capitanian; Wuch – Wuchiapingian; Chang – Changhsingian; Indu – Induan; Olene – Olenekian; Anisi – Anisian; Ladin – Ladinian. Sources of data: 1, Cawood et al. (2011); 2, Offler and Foster (2008); 3, Bryant et al. (1997), Cawood et al. (2011), Shaw and Flood (2009) and Shaw et al. (2011) (From Cawood *et al*. 2011).

The contractional deformation associated with the Hunter- Bowen Orogeny in the northern NEO began at ca 265 Ma and ceased prior to ca 228 Ma (Holcombe *et al.*

1997). Whilst Cawood *et al*. (2011) has two phases of deformation, one corresponding to the Hunter (~ 265 Ma) and the other corresponding to the Bowen (~250 Ma) (Figure 2.13). All the Late Permian deformation structures in the southern NEO can be ascribed to the Hunter-Bowen Orogeny. The timing of deformation is poorly constrained. Li *et al*. (2012b) implied that it could commence at ca 256 Ma, as constrained by the timing of the end movement on the Permian Hunter-Mooki Thrust (Glen & Beckett 1997) and ceased at ca 235 Ma, as constrained by the initial development of the N–S belt of granitoids in the southern NEO.

Collins (1991) subdivided the Hunter-Bowen Orogeny in the southern NEO into four sub-events (Figure 2.14): 1) A series of meridional folds and subparallel faults (D_1) were produced by the initial east-west compression in the Late Permian (Figure 2.14a). These folds are considered to have formed above a westward propagating decollement and propagated upwards to form the Hunter Thrust; 2) Continued NE-SW compression resulting in new folds trending NW-SE in the hanging wall of the Hunter-Mooki Thrust (Figure 2.14b). F_1 folds have been rotated from meridional to northeast-southwest during thrusting; 3) The meridional faults developed during E-W compression (Figure 2.14c), and are considered to be backthrusts on the upper allochthonous plate of the Hunter Thrust. Many faults swing from north-south to the northeast-southwest at their southern limit as the thrust is approached, but never extend beyond it; 4) the Peel Fault was reactivated, resulting in the present Peel-Manning Fault System during the further E-W compression (Figure 2.14d). Fault blocks in the Tamworth Belt were rotated anticlockwise, causing sinistral translation of blocks in the Tablelands Complex. It also caused mass translation of the entire Tablelands Complex from the southeast to the northwest, possibly including the translation of the Hastings Block into its current position (Figures 2.14d and 2.15). Glen and Roberts (2012) show that the F_1 are NW-SE folds and F_2 are N-S folds which is opposite to that in Collins (1991). They argued that F_1 are overprinted by the F_2 folds near the Hunter Thrust.

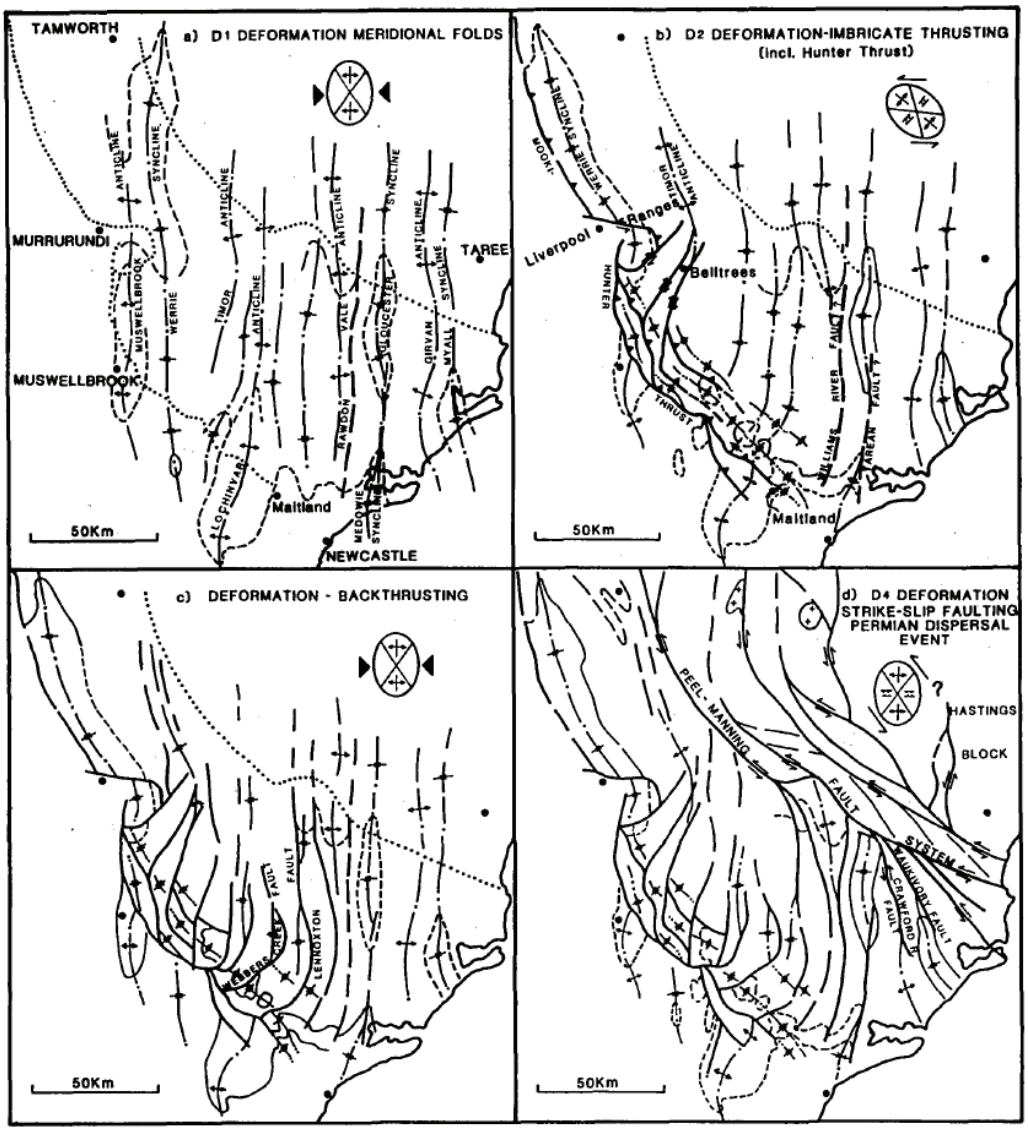

Figure 2.14: Diagram showing postulated tectonic evolution of the southern New England Fold Belt and Sydney Basin (From Collins 1991).

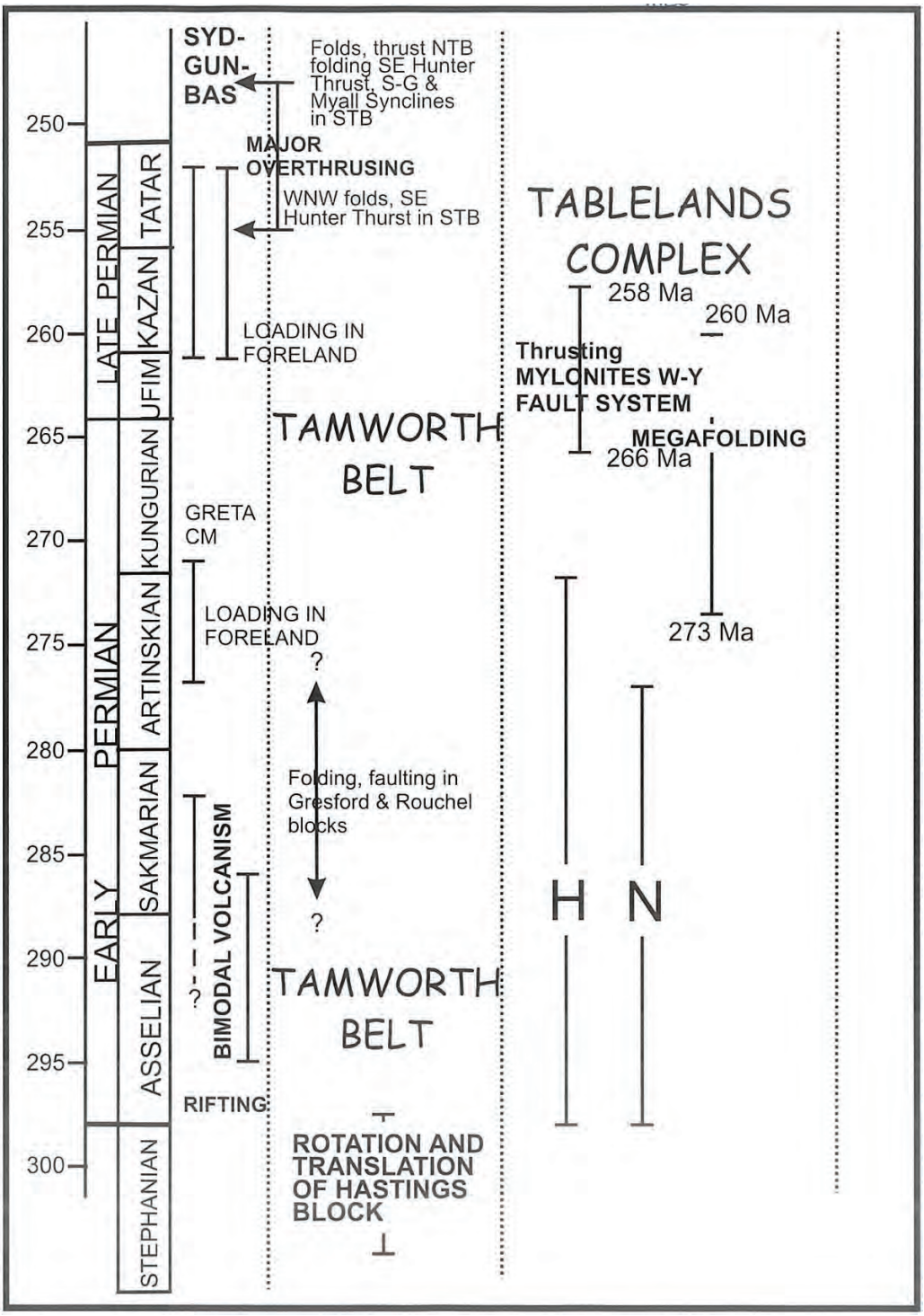

Figure 2.15: Diagram showing the tectonic events in the Tamworth Belt and those in the Nambucca Block and Hastings Block. H = Hastings Block, N = Nambucca Block (From Lennox and Offler, 2010).

Chapter 3 Folding and cleavage history in the NHB

3.1 Introduction

3.1.1 Previous work

The folding and faulting in the Northern Hastings Block can be compared with the adjacent Nambucca Block. Roberts *et al*. (1993) showed that the Northern Hastings Block had three phases of folding: (1) The initial east-west (E-W) phase; (2) which has been refolded by a northwest-trending (NW-SE) phase; and (3) these have been further modified by a northeasterly-trending (NE-SW) phase. E-W trending folds are upright, subhorizontal to gently plunging with half-wavelength from 1 to 7 km. The second NW-SE folds are subparallel to the overall fold axis of the Parrabel Dome (11° -> 302°, Lennox *et al*. 1999). The least well developed and spatially restricted are the third NE-SW folds of up to 11 km half-wavelength. In contrast, this research has identified another phase of deformation related to north-south folds and axial surface cleavage. This phase formed after E-W folding and before NW-SE folding. The orientation of folding is described using the fold axial trace orientation in this thesis.

As described in the Chapter 2.3.1, there are five fold episodes in the Nambucca Block According to Leitch (1978) (D1, E-W folds; D2, E-W; D3, ?E-W; D4, ?; D5, NNW-SSE to NW-SE folds). Johnston *et al*. (2002) confirmed that folds and cleavage formed in the Nambucca Block during D1 and D2 trend E-W. D3 cleavages varies in orientation from northwest to northeast to east–west and D4 folds has a east-northeast- trending northeast trend in the area (Figure 2.5). Shaanan *et al*. (2014) recognized four phases of folding and associated structural fabrics ($S_{1–4}$) in the Nambucca Block (E-W trending D1 folds; D2, NE-SW; D3, NNW-SSE to NW-SE; D4, NE-SW) (Table 3.1).

Overall, E-W folding and cleavage are the common early event in both the Northern Hastings Block and Nambucca Block. The Parrabel Dome in the Northern Hastings Block plunges gently northwest which would be the second event in the NHB (Table 3.1, Roberts *et al.* 1993), but the last event for Leitch (1978) or the third event for Shaanan *et al.* (2014) in the Nambucca Block. NE-SW folds are the last weak event identified in the NHB (Roberts *et al.* 1993) (Table 3.1). They coincide to the possibly the NNE-SSW trending F_3 or F_4 event (Johnston *et al.* 2002) and the NE-SW trending F_2 or F_4 (Shaanan *et al.* 2014) in the coastal exposure of the Nambucca Block. These folding event may relate to the shortening due to southward movement of the Texas-Coffs Harbour Megafold prior to its dissection by the Demon Fault under a very different stress field (NE-SW trending σ_1, Johnston *et al.* 2002).

Table 3.1: Comparison of the orientation of different fold phase between the Northern Hastings Block (NHB) and the whole of the Nambucca Block (NB).

	Northern Hastings Block		**Nambucca Block**		
Deformation	This study	Roberts *et al.* (1993)	Leitch (1978) (250-244 Ma)	Johnston *et al.* (2002)	Shaanan *et al.* (2014)
D1	E-W	E-W	E-W	E-W	E-W
D2	N-S	NW-SE	E-W	E-W (264-260 Ma)	NE-SW (275–267 Ma)
D3	NW-SE	NE-SW	?E- W	NNE-SSW	NNW-SSE to NW-SE (268–265Ma)
D4	NE-SW		?	NNE-SSW	NE-SW
D5			NNW-SSE to NW-SE		

Dating using K/Ar ages of biotite in slates and phyllites from the Nambucca Block from Leitch and McDougall (1979) implies that orogenesis started from about 255 Ma and ceased about 250 Ma (268 – 249 Ma range of K/Ar dates reported by Leitch and McDougall (1979)). All folding was accomplished in a period of about 5 Ma. Offler and Foster (2008) dated S_1 and S_2 in the slate and phyllite using $^{40}Ar/^{39}$ Ar on mica

constrained the timing between 264-260 Ma. In contrast, Shaanan *et al.* (2014) using $^{40}Ar/^{39}$ Ar on muscovite dated the second phase (S_2) at between 275–265 Ma. Re-calculation of the Offler and Foster (2008) ages for new standards gives ages which overlap the younger results reported by Shaanan *et al.* (2014).

3.2 Methodology

This study analyzed the bedding readings, cleavage data and the map pattern of the fold axes according to their orientations in the Northern Hastings Block – Nambucca Block regions. The bedding and cleavage data was obtained from rocks in the study area. Maps of the overall orientation of the bedding and the derived fold axes from these bedding readings in major subareas within the NHB were prepared. Many cleavage were measured around the margins of the Parrabel Dome (Figure 3.11). The map pattern of the orientation of the fold axes are obtained from the calculation of the bedding-cleavage intersections in the NHB and from the field measurements of mesoscopic folds. It is assumed that east-west plunging folds would have east-west oriented axial surface cleavage. Similarly folds plunging to a particular azimuth will have a (sub)parallel cleavage axial surface to the fold, if a cleavage is developed during fold development. The evidences from overprinted cleavages, bent faults, refolded folds and disrupted, cleaved fault-blocks and faults displacing cleaved and folded rock from limited exposures in the Nambucca Block and Northern Hastings Block are used to understand the order of events. This information helps to separate different deformation phases (cleavage and folds episodes) in the Northern Hastings Block and Nambucca Block.

3.3 Analysis of bedding data in the NHB

The NHB was comprehensively mapped by Lennox, Leitch, Roberts and others and about eleven honours students (Figure 3.1).

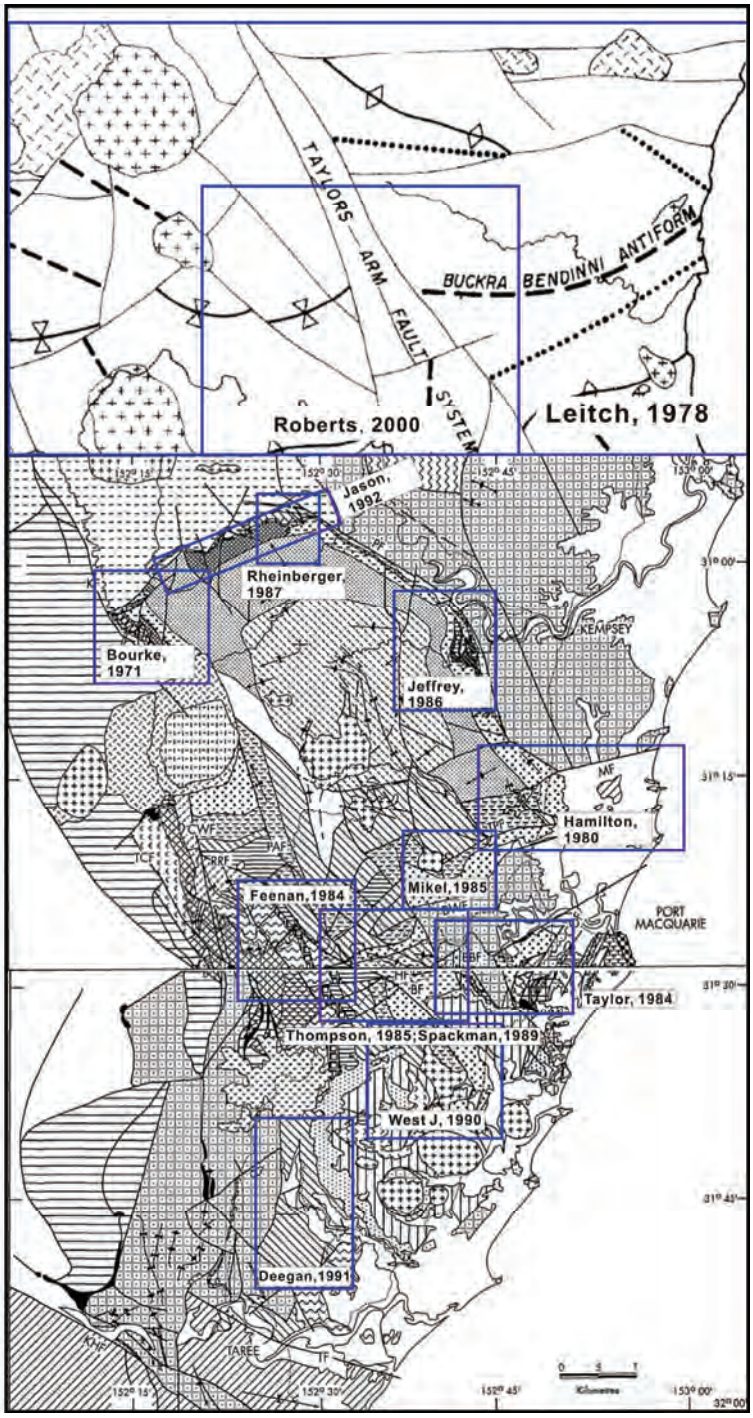

Figure 3.1: The map of areas covered by honours projects in the northern Hastings Block from which data was derived and the adjacent Nambucca Block with the majors faults and folds according to Leitch (1978).

This study analyzed over 2200 bedding readings obtained from rocks in the NHB-NB region. Maps were prepared of the overall orientation of the bedding and the derived fold axes from these bedding readings in major subareas within the NHB.

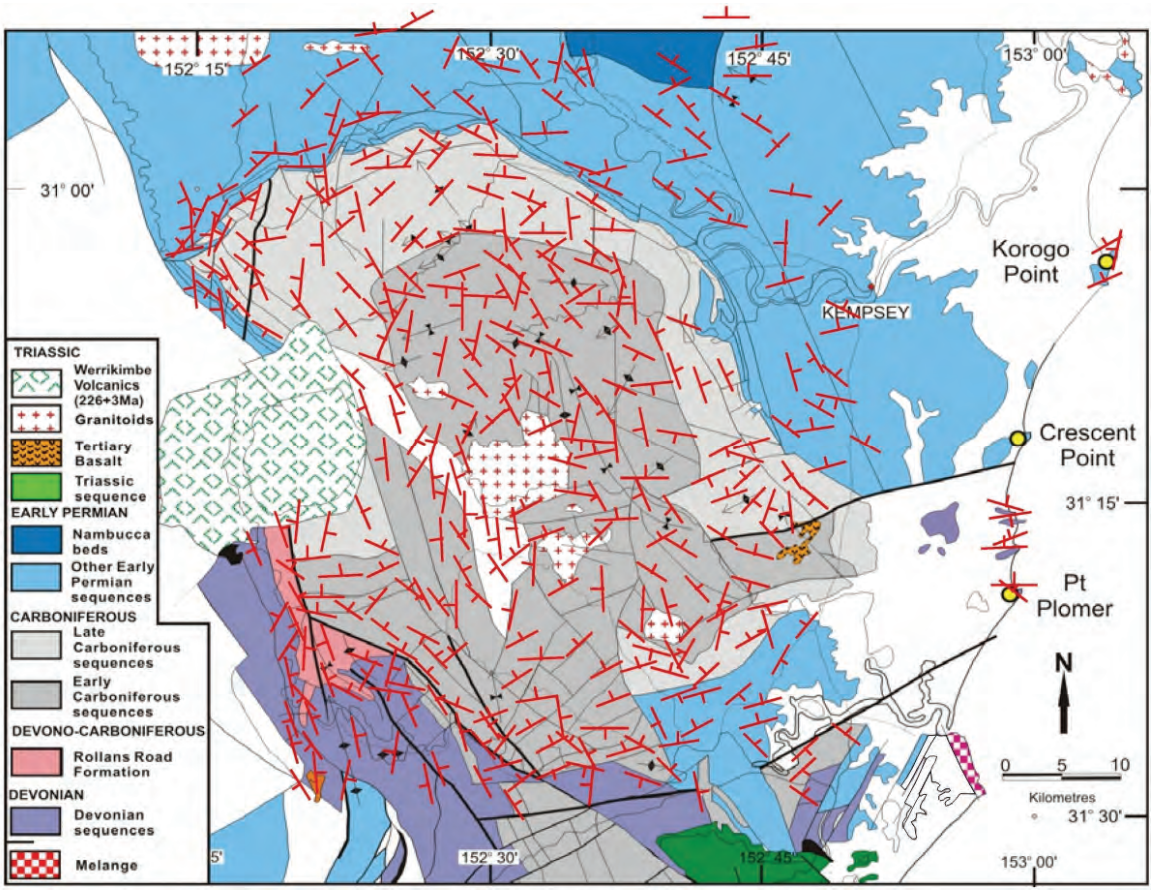

Figure 3.2: The simplified geology map with representative bedding readings in the NHB and adjoining Nambucca Block.

Form lines from a map of representative bedding readings (Figure 3.2) showing the spatial pattern of bedding across the NHB is shown in Figure 3.3. Three subareas with different spatial patterns are indentified (Figure 3.3). In Subarea 1, the bedding is likely to wrap around the gently NW-plunging, megascopic Parrabel Dome (Roberts *et al*.1993) in the NHB and consistently dips outwards from the core of the dome. The bedding data dips in different directions in the core area of the Parrabel Dome. This is likely because of the almost flat and broad crestal nature of the Parrabel Dome. The bedding data in Subarea 2 is almost all striking (N)NW-(S)SW, except for a small group in the centre of this area, striking E-W. Subarea 2, which is located on the southwestern margin of the Parrabel Dome, belongs to the SHB according to Roberts *et al*. (1995) and Lennox *et al*. (1999). In Subarea 3, most bedding is oriented E-W to ENE-WSW and dips NNW to N. A few bedding data, disrupted by the faulting, have a NW-SE

orientation.

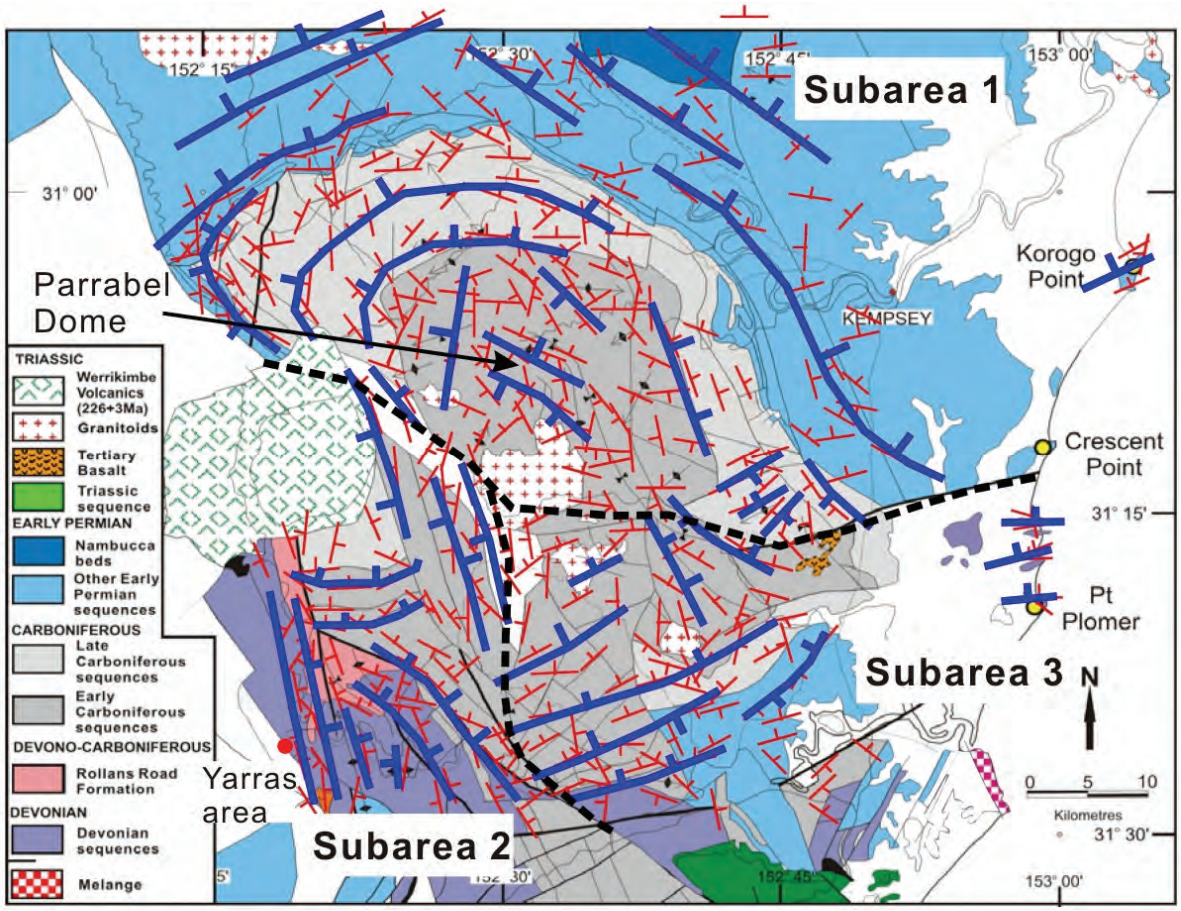

Figure 3.3: Form-lines for representative strike of bedding showing the spatial pattern of bedding across the NHB. The black dash lines divide the NHB into three subareas with different spatial patterns of bedding. The top black dashed line represents the Roberts *et al*. (1995) boundary between the NHB and SHB.

The map pattern of the form-lines for representative strike of bedding suggests there is a major boundary consistent with the Roberts *et al*. (1995) NHB-SHB boundary. The form lines near this boundary mostly conform to those expected on the southwest limb of the dome BUT the younging direction is opposite to that expected for the Parrabel Dome. Thus all bedding north of this boundary are consistent with the presence of a box-like Parrabel anticline plunging northwest. The reading south of this HB-SHB boundary are all dipping variably east, northeast or northnorthwest, contrary to that expected if the Parrabel Dome existed in this region.

Separation of the bedding data on the basis of the location around the Parrabel Dome

constituting the NHB yields fold axes for each small subarea in the NHB (Figures 3.4-3.6). These small subareas were chosen according to the Fault Blocks described in Chapter 5.6. The boundaries are normally the faults between the two fault blocks. The folding is mainly mesoscopic in scale and appears to have formed mostly before faulting in the NHB. The macroscopic folds stereographically derived from this analysis of bedding are merely representative of overall fold plunges and azimuths for each fault block and do not represent actual observed folds. The detailed derived fold axes for each fault block of the NHB are presented in the Appendix 1.

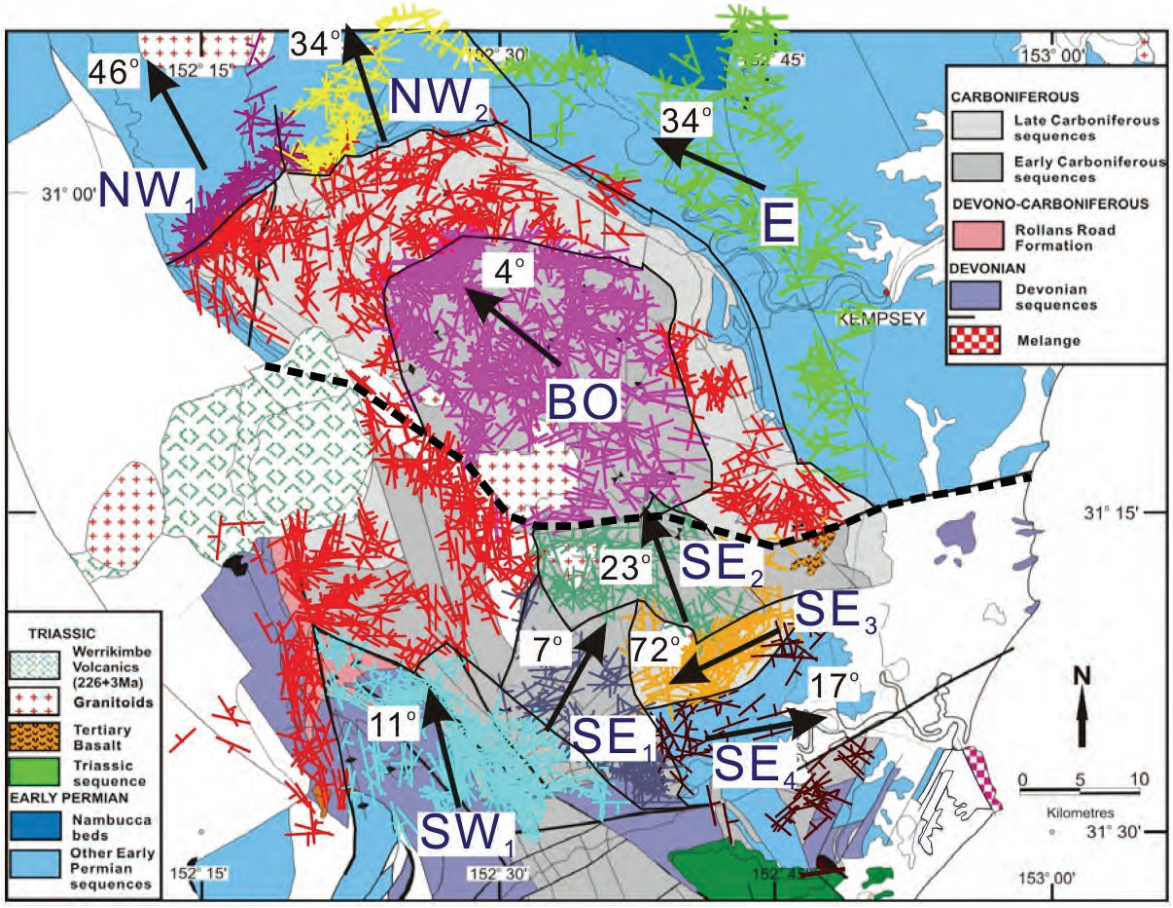

Figure 3.4: The simplified geology map with the derived fold axes from the bedding readings in each subarea in the NHB.

All the subareas north of the Roberts *et al*. (1995) boundary between the NHB-SHB are plunging either NNW or NW with those in the core of the Parrabel Dome (Subarea BO) plunging sub-horizontally NW as expected and those on the northwestern subarea (Subareas NW_1 and NW_2) plunging moderately NNW (Figure 3.4). The derived fold

axis for the Kempsey Beds northeast and east of the dome (Subarea E) is moderately plunging to the NW parallel to the core of the Parrabel Dome trend (Figure 3.4). This pattern reflects the probable re-orientation of E-W trending bedding (D1) by D3 folding (see Chapter 3.5).

The derived fold axis from the Subarea SW_1 of $11^o \rightarrow 346^o$ (Figures 3.4 and 3.5) is subparallel to the overall derived fold axis for the whole of the NHB ($5^o \rightarrow 346^o$, n = 1411, Figure 3.9) suggesting that the D3 folding event was pervasive throughout part of the SHB. The derived fold axes from the SE subareas include $7^o \rightarrow 029^o$ for Subarea SE_1, $23^o \rightarrow 340^o$ for Subarea SE_2, $72^o \rightarrow 244^o$ for Subarea SE_3 and $17^o \rightarrow 080^o$ for Subarea SE_4 (Figures 3.4 and 3.6). Subarea SE_2, located close to the core of the Parrabel Dome, shows a similar fold axis with that of the dome. Given the position of Subarea SE_2, it would have been expected that the derived fold axis would plunge to the southeast and not northwest. In contrast, the fold axes from the Subareas SE_1, SE_3 and SE_4 are very different from any of the other subareas. It may reflect the presence of a broad synform southeast of the Parrabel Dome related to the NE-SW trending D4 phase of deformation.

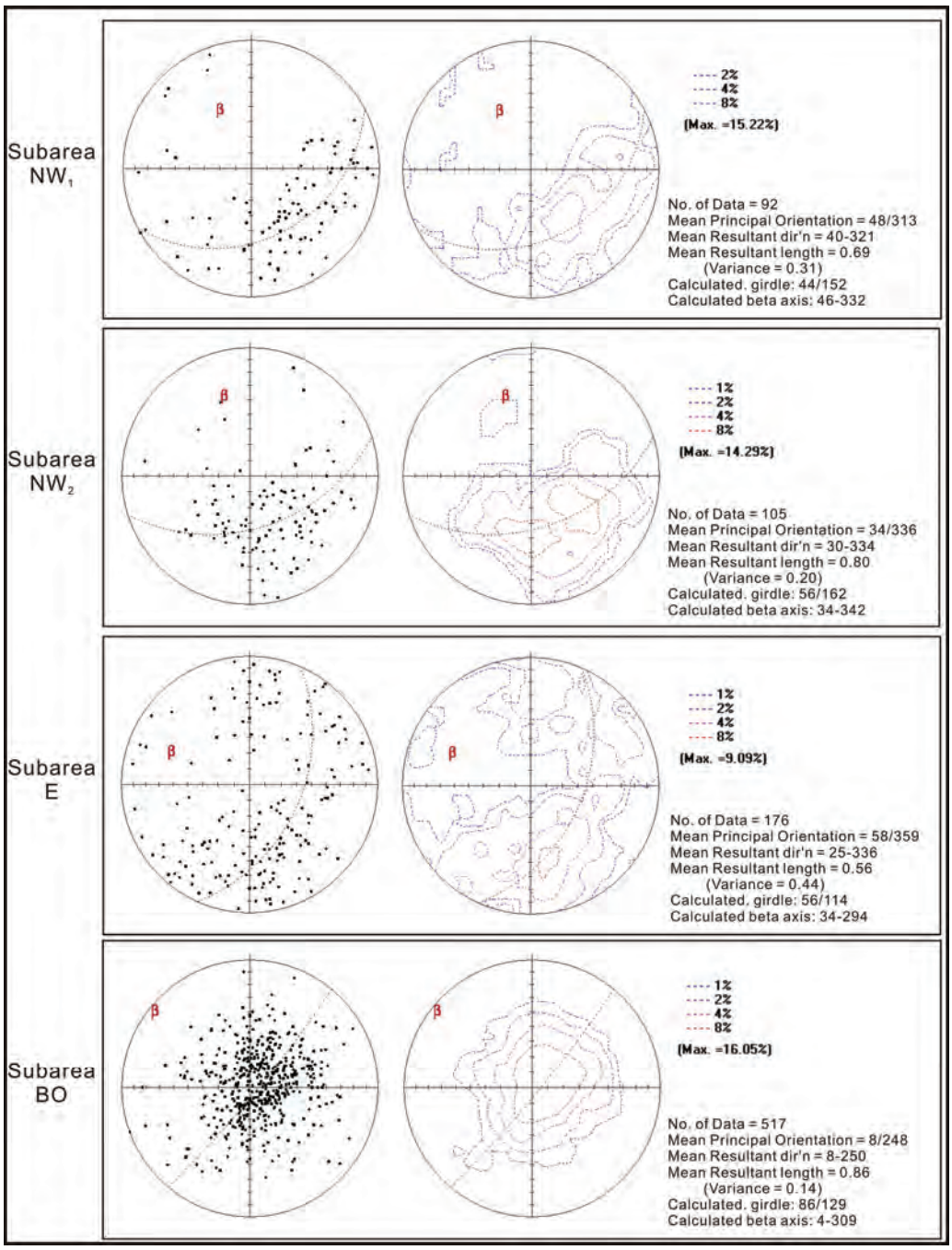

Figure 3.5: (Un)Contoured stereographic projections of poles to bedding divided according the subareas (NW_1, NW_2, E and BO) in Figure 3.4.

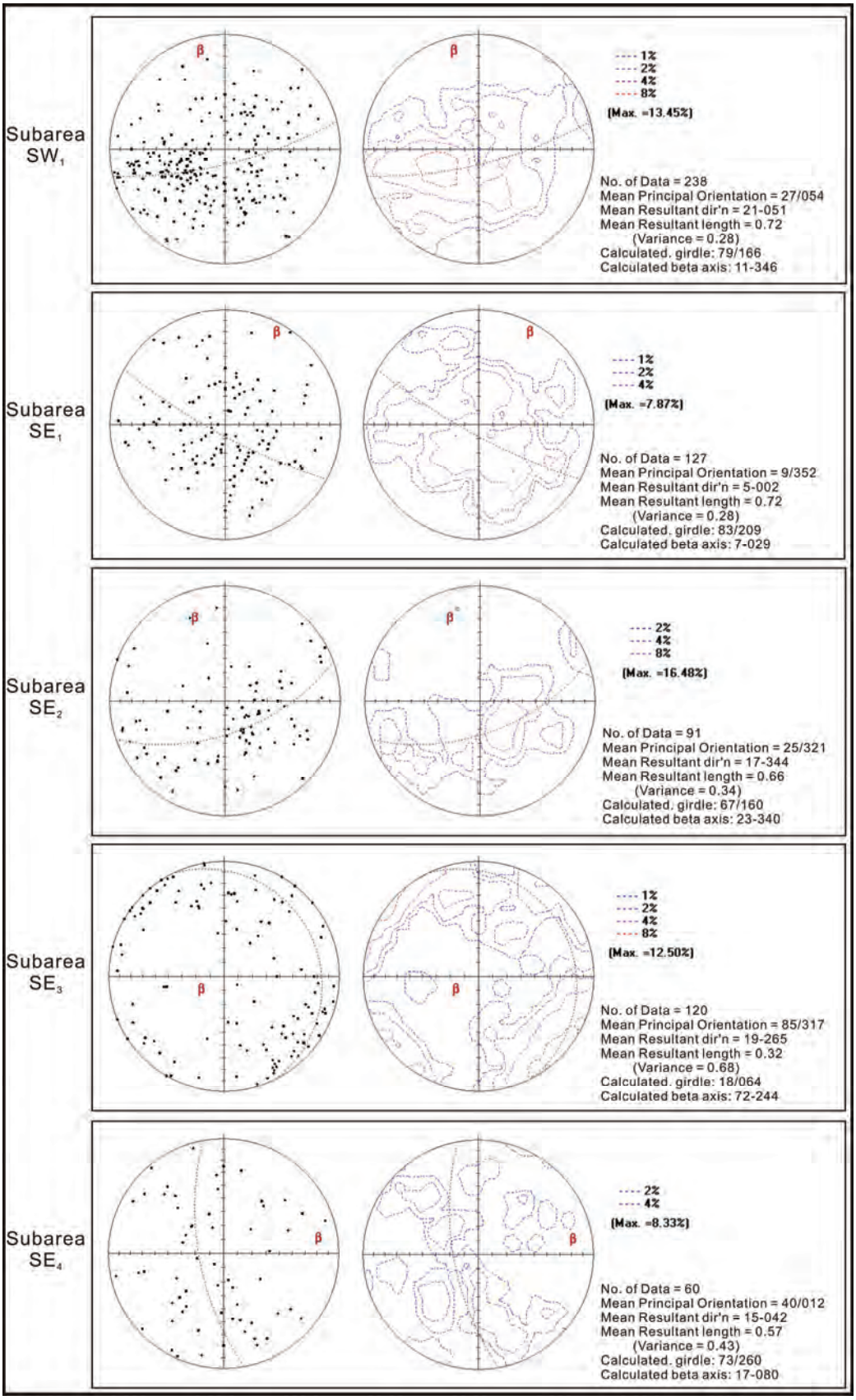

Figure 3.6: Uncontoured and contoured stereographic projections of poles to bedding divided according the subareas (SW_1 and SE_1 to SE_4) in Figure 3.4.

The pattern of derived fold axes from the larger subareas which have been generated by combining the fault blocks around the Parrabel Dome suggests that the dome has been broadly bent around a NE-SW trending fold axis (Figure 3.7 and Table 3.2). All the larger subareas in the northern part of the dome are plunging either NNW or NW. The derived fold axis from the core region of the Parrabel Dome is $1^{o} \rightarrow 312^{o}$ for the northeastern Part (NE) and $1^{o} \rightarrow 167^{o}$ for the southwestern part (SW) of the dome (Figure 3.8). This suggests a flat and broad crestal region for the dome. The D3 folding event was pervasive throughout most of the NHB and even part of the SHB (Subarea SHB, Figures 3.7 and 3.8). The derived fold axis from the larger SE subarea is $9^{o} \rightarrow 025^{o}$. It is different from any other larger subareas and may reflect the presence of a broad synform southeast of the Parrabel Dome. This derived fold axis is subparallel to the NE-SW trending D4 phase of deformation. There are macroscopic folds on the bent northeast limb of the dome and scattered mesoscopic folds consistent with this event. Shaanan *et al* (2014) observed F_2 mesoscopic recumbent folds with northeast-southwest trend at Crescent Head in Permian Kempsey Beds northeast of this subarea (Figure 3.7). Hamilton (1980) observed east-west trending bedding on the coast south of Crescent Head in Devonian Touchwood Formation (Roberts *et al*. 1995) with gently east-plunging folding (F_1). Overall, the NHB-NB region consists of a gently NW-plunging dome and a possible NNE (NE) plunging syncline (Figure 3.7).

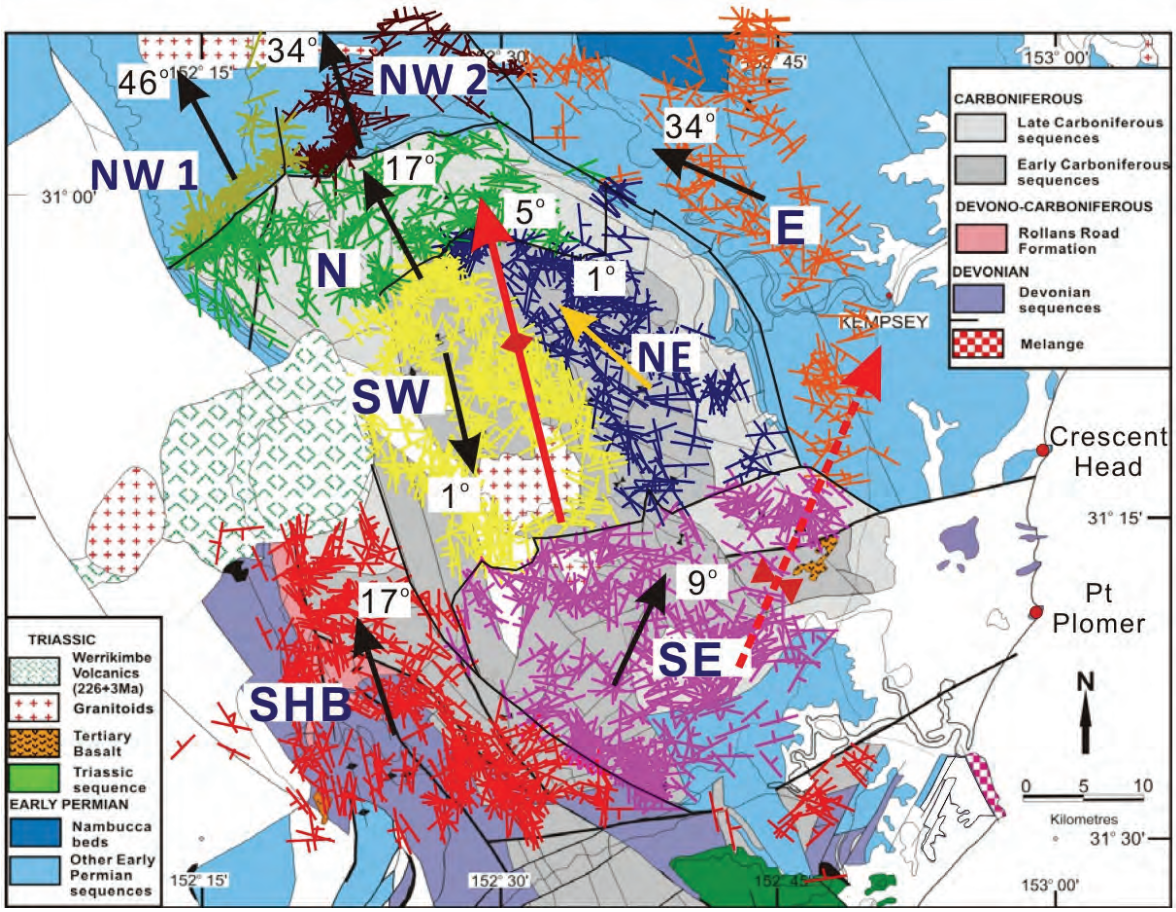

Figure 3.7: The simplified geology map with the derived fold axes (plunge and plunge azimuth) from the bedding readings in larger subareas in the NHB. NHB overall D3 fold axis trace is shown as $5^o \rightarrow 346^o$ and proposed regional syncline through Kempsey is shown by the dashed D4 fold axis trace.

Table 3.2: Fold axes and average bedding orientation from stereographic projections of poles to bedding for larger subareas.

Subarea	No. Readings	Fold Axis	Average Bedding
NW1	92	$46^o \rightarrow 332^o$	$48^o \rightarrow 313^o$
NW2	105	$34^o \rightarrow 342^o$	$34^o \rightarrow 336^o$
E	176	$34^o \rightarrow 294^o$	$58^o \rightarrow 359^o$
N	292	$17^o \rightarrow 232^o$	$20^o \rightarrow 299^o$
SW	408	$1^o \rightarrow 167^o$	$13^o \rightarrow 251^o$
NE	261	$1^o \rightarrow 312^o$	$3^o \rightarrow 241^o$
SE	450	$9^o \rightarrow 025^o$	$31^o \rightarrow 310^o$
SHB	479	$17^o \rightarrow 342^o$	$42^o \rightarrow 052^o$

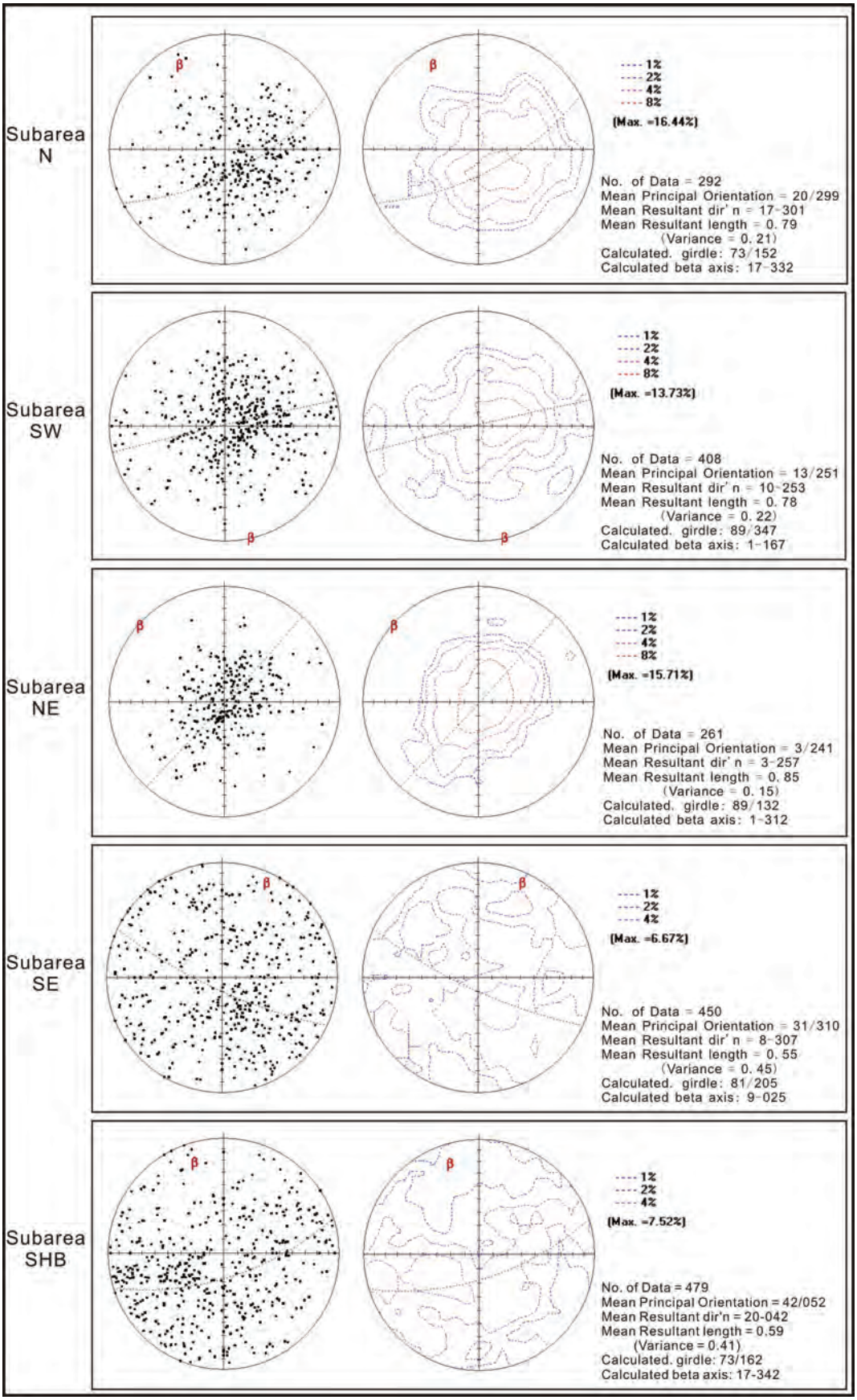

Figure 3.8: Uncontoured and contoured stereographic projections of poles to bedding divided according the larger subareas (N, SW, NE and SE) in Figure 3.7.

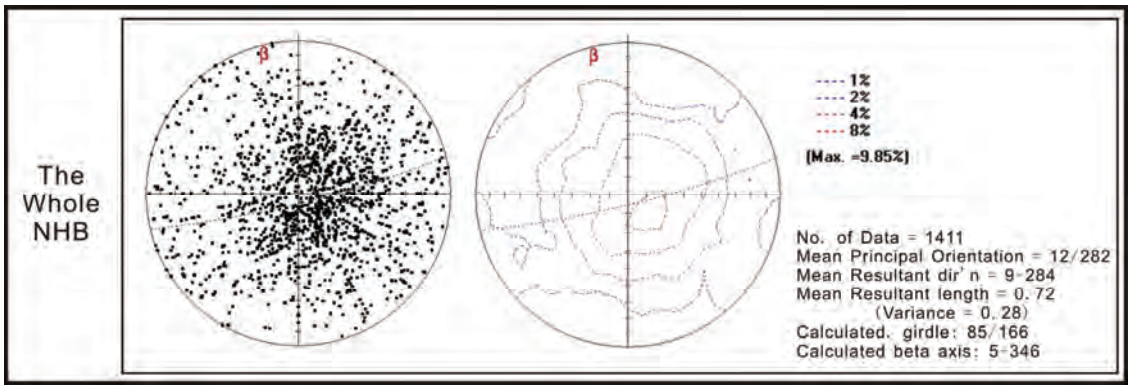

Figure 3.9: Uncontoured and contoured stereographic projections of poles to bedding in the whole NHB including the larger subareas N, SW, NE and SE in Figure 3.7.

3.4 Analysis of cleavage data in the NHB

This study analysed the cleavage data obtained from rocks in the NHB-NB regions and reveals the concentration of the cleavage measurements around the margins of the Parrabel Dome (Figure 3.11). Four cleavage populations are identified according to their orientation. All cleavages dip steeply and so there is no separation of the dip symbol according to the magnitude of the dip (Figure 3.10).

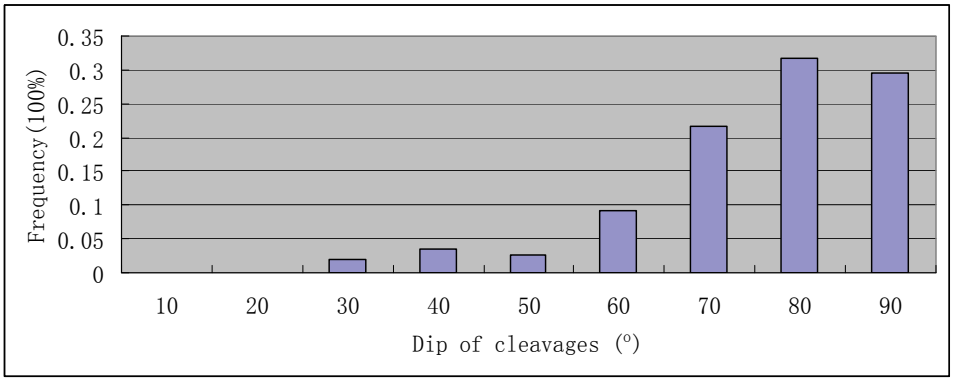

Figure 3.10: Bar chart of the dips of cleavages in the NHB showing that most cleavages are steeply dipping.

The first generation of the cleavage, $S_{1,}$ is oriented E-W, which is the common early event with the cleavage in the Nambucca Block (Figure 3.12) (Leitch 1978; Johnston *et al.* 2002; Shaanan *et al*. 2014). S_1 occurred dominantly in the Early Permian sequences on the northern and northeastern margins of the NHB, and partly in the Early Permian

sequences of the Middle Hastings Block (Figure 3.12). S_1 appears to have been passively folded around the northern margins of the Hastings Block. This supports the model that the Parrabel Dome acted as a massif during deformation of the NB as a result of the southward push of the Coffs Harbour Orocline. The Early Permian sequences of the margins on the Hastings Block are generally finer grained, mud-rich rocks. They developed a pencil to slaty type S_1 cleavage more frequently compared with the Carboniferous sequences of the Parrabel Dome which were sandier and rarely developed a cleavage.

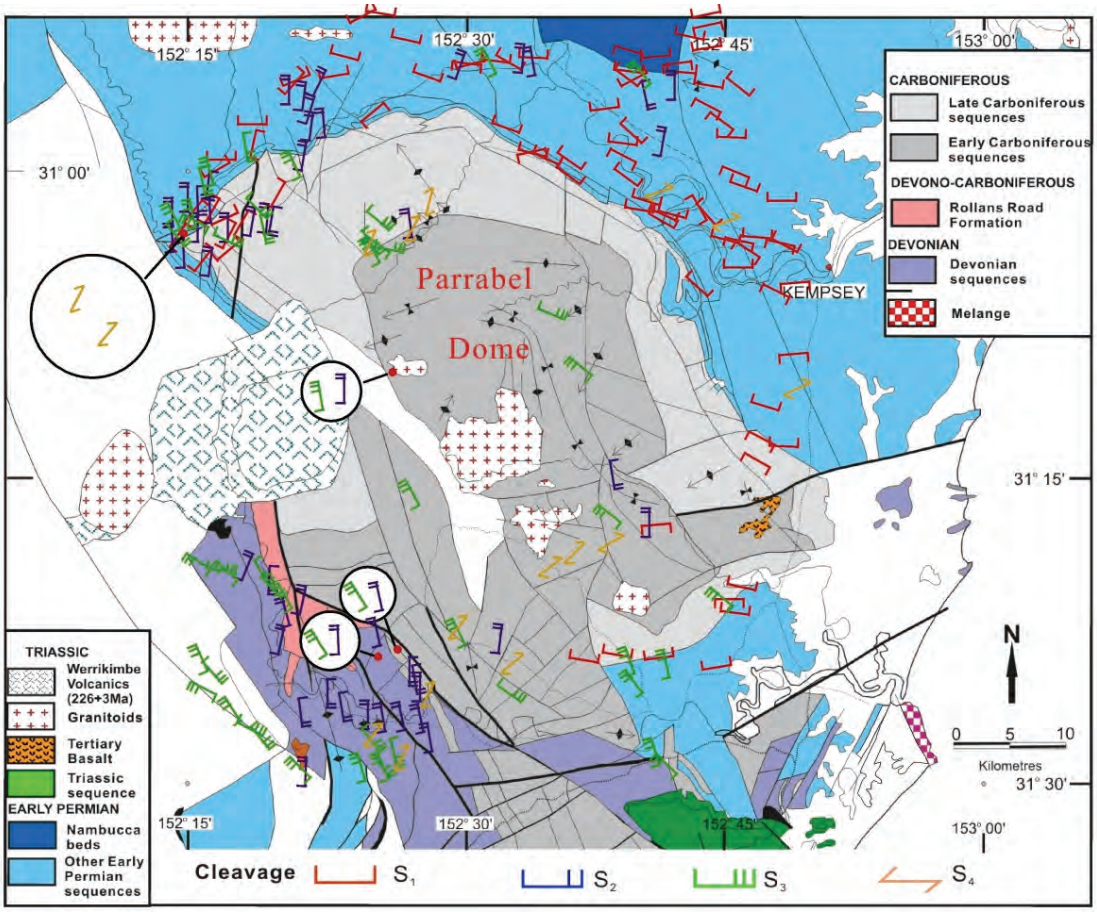

Figure 3.11: The simplified geology map with all the oriented cleavage data in the NHB. S_1 = red symbols, S_2 = purple symbol, S_3 = green symbol and S_4 = brown symbol. Note the concentration of the cleavage around the margins of the Carboniferous units (grey colour) and paucity of the reading in the core of the Parrabel Dome. The circled readings represent exposures where two cleavages were measured and it could be observed that one cleavage overprinted the other cleavage.

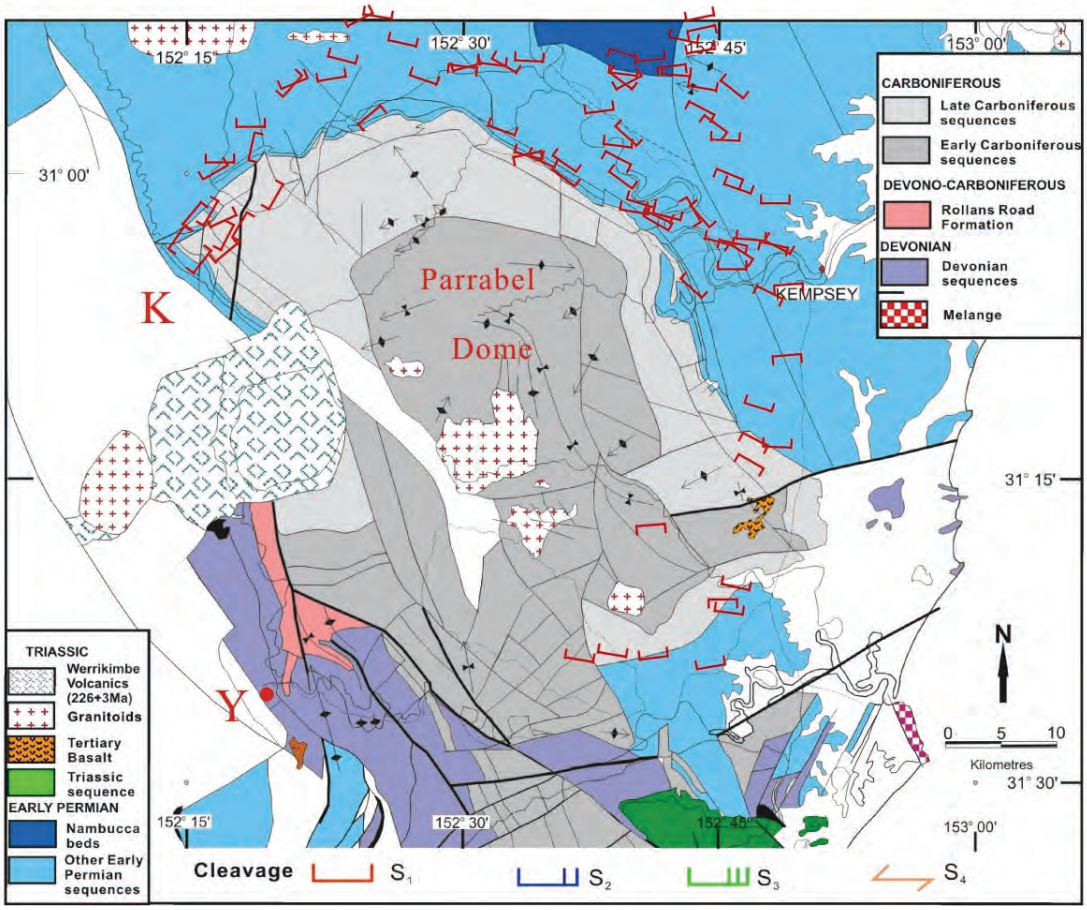

Figure 3.12: The simplified geology map with the S_1 cleavage data in the NHB. The NE-striking cleavage in the Kunderang Brook area (K) may be S_4 rather than passively rotated originally E-W trending S_1. Most S_1 data is from the Permian units wrapping around the Parrabel Dome. Y=Yarras area.

The second generation of cleavage, S_2, is oriented N-S (Figure 3.13). S_2 is dominantly located on the northwestern and southwestern margin of the Parrabel Dome (Figure 3.13). Offler pers. com. (2014) observed the N-S cleavages in the Yarras area, which he regarded as the S_1 cleavage (Figure 3.13). The prevalence of N-S striking cleavage on the western margin of the NHB may reflect increasing strain along this margin or that the rocks in these areas were more susceptible to cleavage development (i.e. more incompetent).

The S_3 cleavage striking NW-SE was located mostly on the northwestern and southwestern margin of the Parrabel Dome, and rarely in the northern middle Hastings

Block (Figure 3.14). S_2 and S_3 have been identified in the field as two generation of cleavages by Offler pers. com. (2014) in the Yarras area.

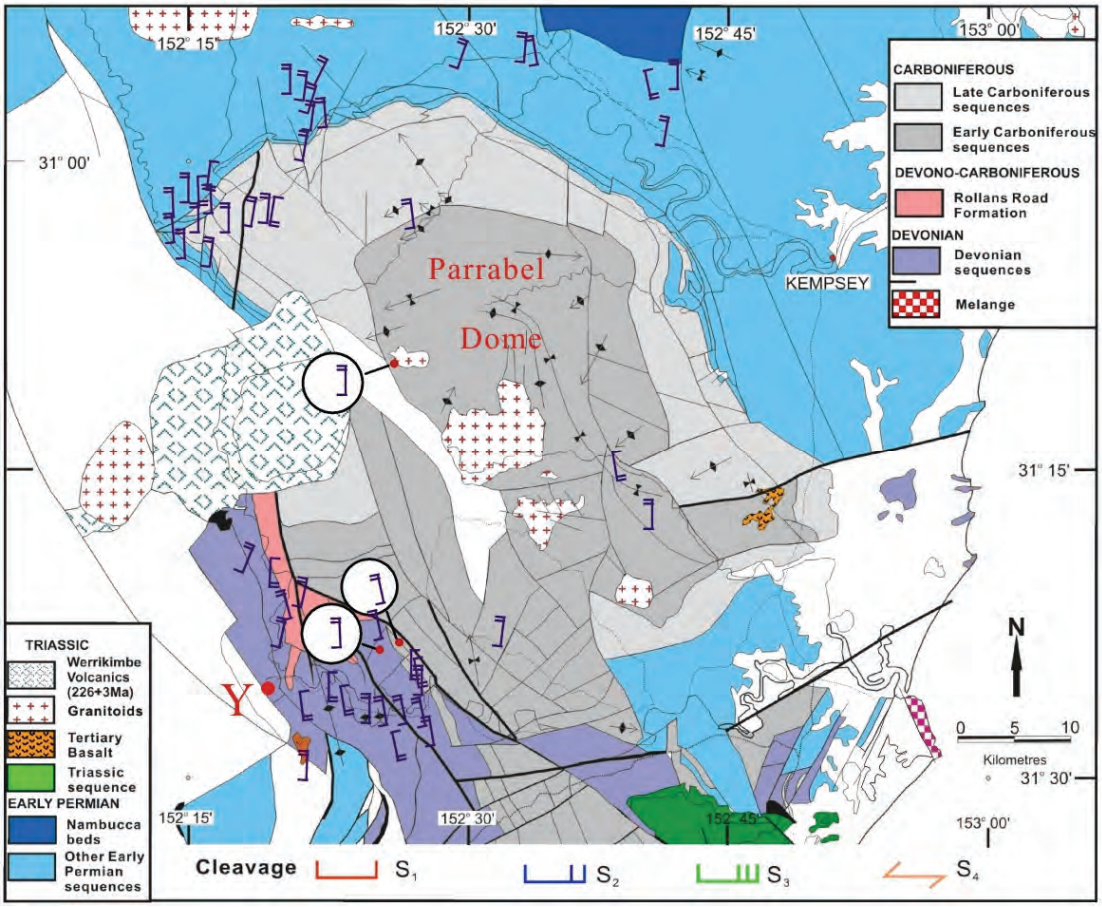

Figure 3.13: The simplified geology map with the S_2 cleavage data in the NHB. Note the concentration of the S_2 cleavage data on the northern edges of the Parrabel Dome and adjacent Permian and in the Devonian units on the southwestern margins on the Hastings Block near Yarras (Y). The circled reading represent exposures where two cleavages were measured and their order determined.

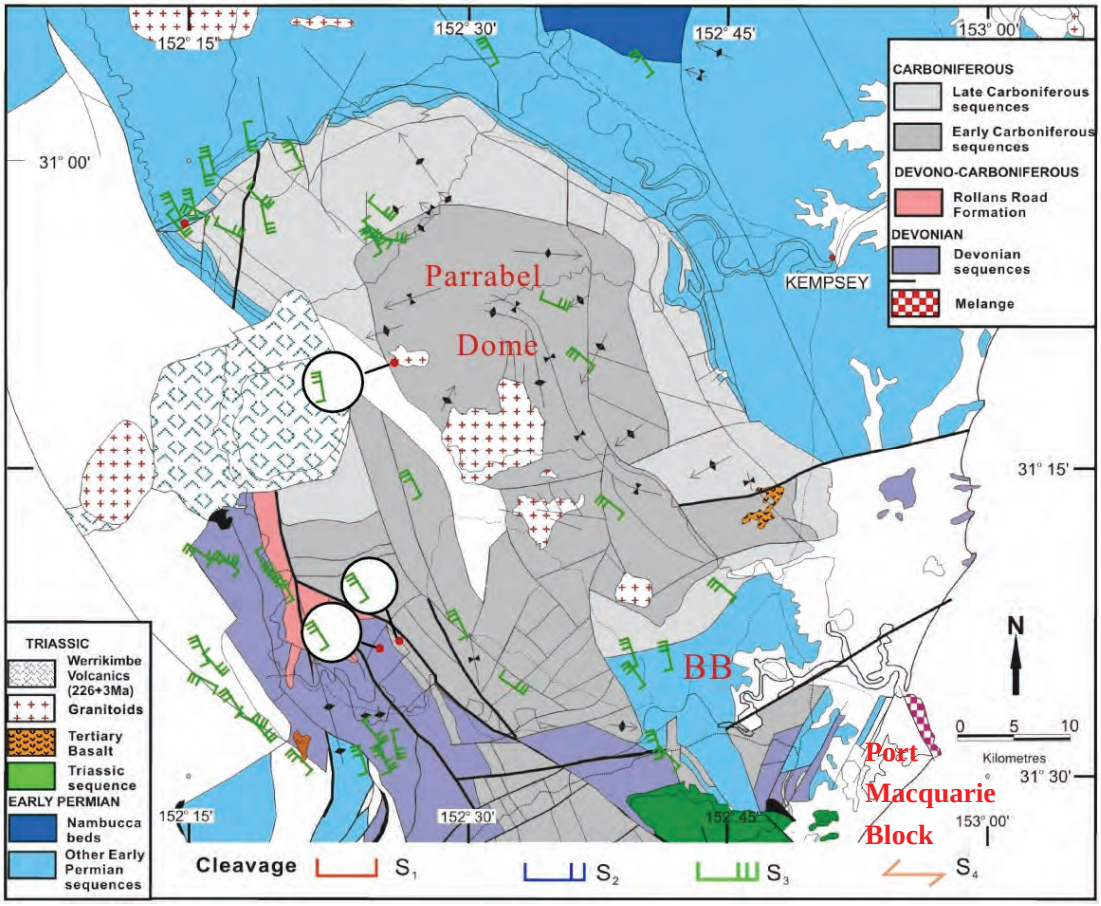

Figure 3.14: The simplified geology map with the S_3 cleavage data in the NHB. Note the concentration of readings on the northwestern margin of the Parrabel Dome and the southwestern margin of the Hastings Block like the S_2 cleavage pattern. There are a scattering of S_3 reading from the core of the Parrabel Dome and even the Permian Beechwood Beds (BB) spread between the Parrabel Dome and the Port Macquaire Block.

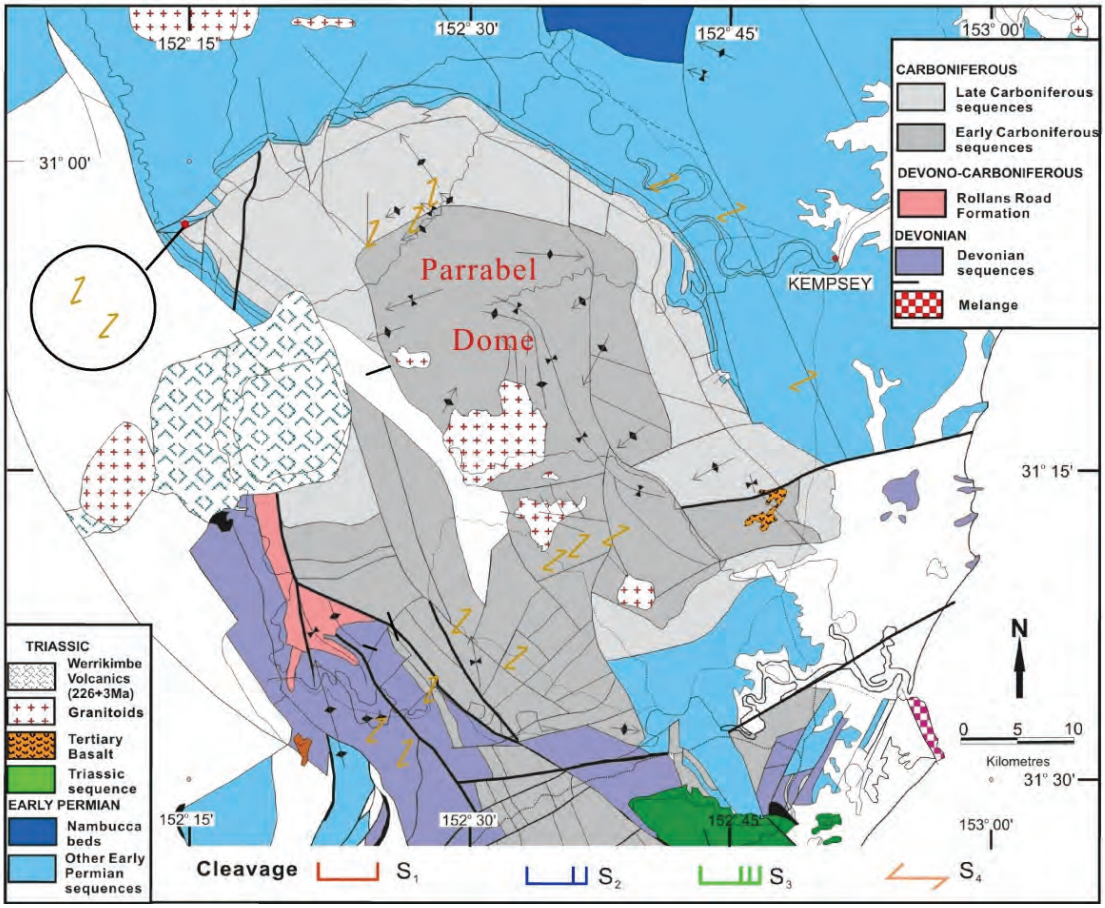

Figure 3.15: The simplified geology map with the S_4 cleavage data in the NHB. Note most S_4 reading are concentrated in a belt across the boundary between the Northern Hastings Block and Southern Hastings Block. This belt of S_4 cleavages would be oblique to the F_4 megascopic fold proposed on Figure 3.7.

S_4, the last generation of cleavages, is oriented NE-SW. It is mainly scattered across the southern margins of the Parrabel Dome (Figure 3.15). Its orientation is subparallel to the fold axes of the southwest-plunging macroscopic folds on the southeastern part of Parrabel Dome. The poor development of S_4 cleavage in these SW-plunging macroscopic folds may be due to the presence of sandier lithologies in this area compared with those further southwest where the S_4 cleavage develops.

3.5 Analysis of folding data in the NHB

This study also analyzed the map pattern of the orientation of the fold axes obtained from the calculation of the bedding-cleavage intersections in the NHB and from the field

measurements of mesoscopic fold. These are four populations of folds that are recognized according to their orientations based on both the calculated and field-observed fold axes data. These are consistent with the results from the cleavage data analysis (Figures 3.16 and 3.17). It is assumed that east-west plunging folds would have east-west oriented axial surface cleavage. Similarly folds plunging to a particular azimuth will have a (sub)parallel cleavage axial surface to the fold, if a cleavage is developed during fold development. There are many more exposures within the Permian sequences on the boundary of the NHB-NB containing cleaved rocks from which S_0/S_x intersection lineations (fold axes) can be calculated (Figure 3.11). The map pattern of calculated and observed mesoscopic folds shows a concentration of all folds within the Permian sequences compared with the Carboniferous sequences reflecting the ease of cleaving and folding more mud-rich Permian sequences (Figures 3.16 and 3.17). This study analyzed the map pattern of the orientation of the fold axes obtained from the calculation of the bedding-cleavage intersections in the NHB and from the field measurements of mesoscopic fold. These folds partially correlate with the macroscopic fold axes (1-11 km half wavelength) derived by Lennox on the map from Roberts et al. (1995). The difference in orientation of the mesoscopic (observed and derived) folds is very similar although not exactly the same as the Lennox-determined macroscopic folds. The difference reflects possible rotation of early east-west folds around the overprinting Parrabel Dome, the affects of fault movement on existing folds and the less likely but possible development of folds near faults under a common stress field.

The first generation of folds, F_1, are mostly plunging E or W, which is the same azimuth as the strike azimuth of the first generation of cleavage S_1 in the NHB (Figures 3.12 and 3.18). F_1 is believed to have formed in the same early deformation event in the adjacent Nambucca Block (Leitch 1978; Johnston *et al.* 2002; Shaanan *et al*. 2014). It is dominantly developed in the Early Permian sequences on the northern and northeastern margins of the NHB, and partly in the Early Permian sequences of the Middle Hastings Block (Figure 3.18). There are very few F_1 fold axes in the Carboniferous sequences

(Figures 3.18 and 3.19). The NE and SW-plunging fold axes in the Kunderang Brook area (labeled K on Figure 3.18) could be rotated originally E-W trending F_1 as the data were derived from the disrupted Threadneedle Fault Complex (Figure 3.19) or in the Permian Parrabel Beds north of this complex. This accords with what has been seen in the cleavage analysis and the model that the Parrabel Dome acted as a massif during deformation of the NB. As a result of the southward push of the Coffs Harbour Orocline the L_1 (= F_1) in the Permian sequence was passively rotated around the margins of NHB.

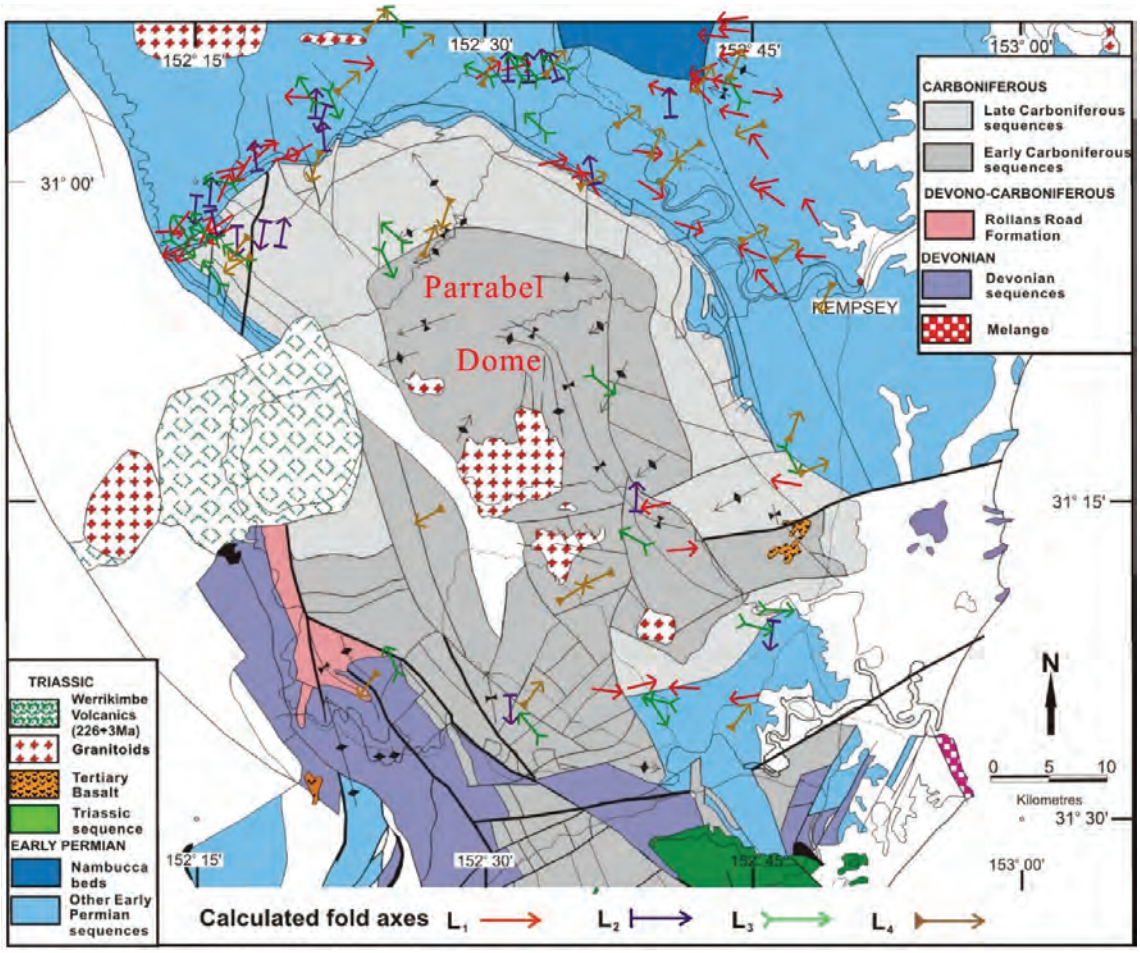

Figure 3.16: The simplified geology map with all the calculated fold axes data in the NHB (n=127). These fold axes are derived from calculating the intersection between the bedding and cleavage where both have been measured in the one exposures. These intersection lineations are labeled L_1 to L_4 on the maps and are considered to represent F_1 to F_4 folds respectively. L_1 = red symbols, L_2 = purple symbol, L_3 = green symbol and L_4 = brown symbol.

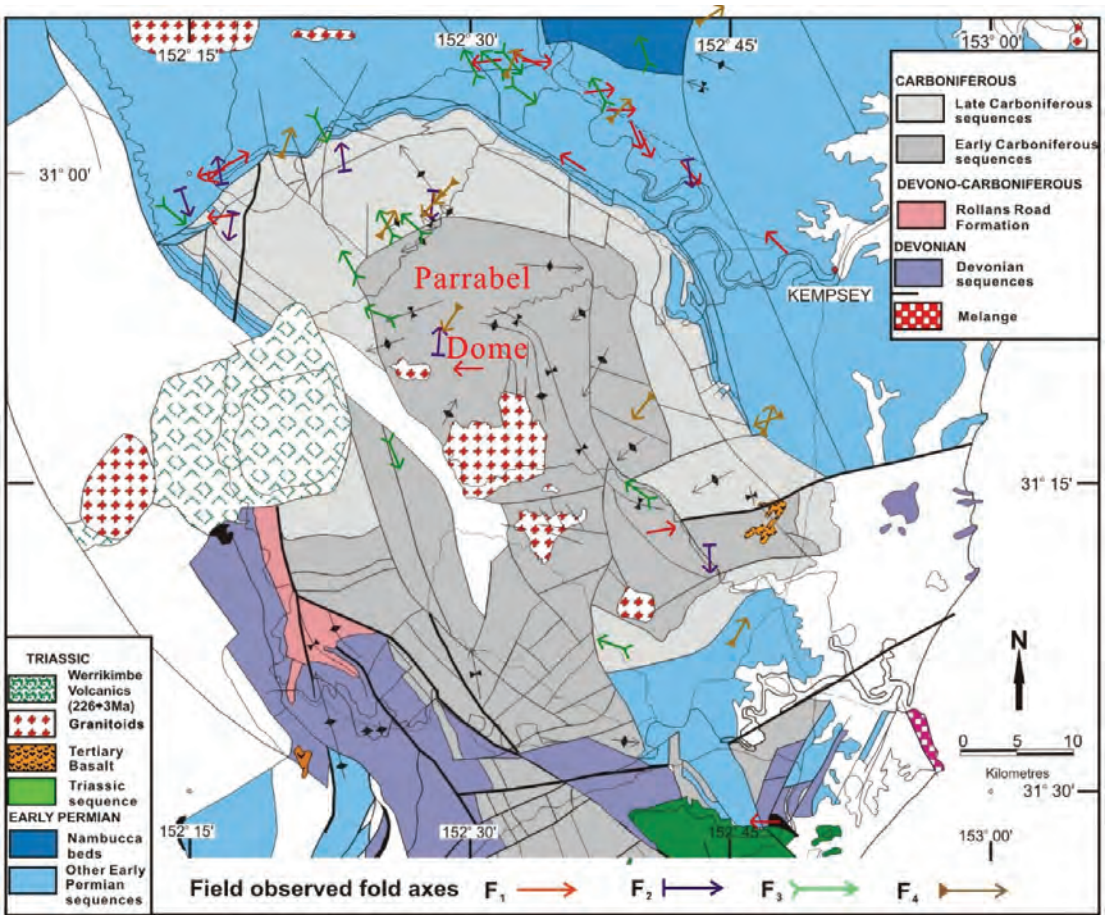

Figure 3.17: The simplified geology map with all the field-observed, mesoscopic fold axes data in the NHB (n=50). F_1 = red symbols, F_2 = purple symbol, F_3 = green symbol and F_4 = brown symbol.

It could be argued that the north-northwest or south-southwest plunging calculated folds, 5-10 km northwest of Kempsey, are not F_1 folds but F_3 folds. The north-northwest or south-southeast plunging folds which characterized the Permian sequences northwest of Kempsey are thought to represent slightly rotated former east-west oriented fold axes due to indentation of the rigid, difficult to cleave Carboniferous sequences of the Parrabel Dome. The F_1 dataset appear concentrated in the Permian sequences bordering the NHB into the Nambucca Block. This reflects the prevalence of cleaved sequences in this region of the Nambucca Block compared with the Carboniferous sequences defining the Parrabel Dome which are poorly cleaved.

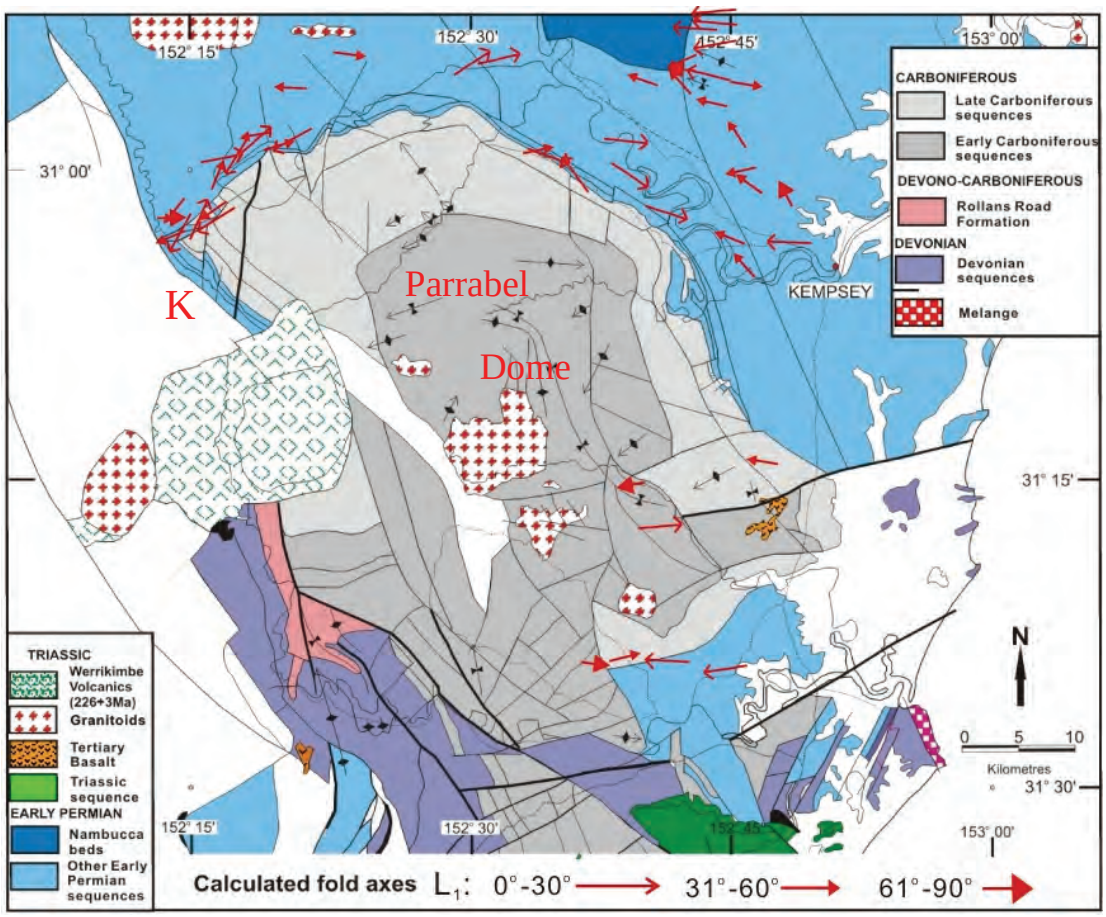

Figure 3.18: The simplified geology map with the L_1 calculated fold axis data in the NHB-Nambucca Block (n=52). The NE and SW plunging fold axis in the Kunderang Brook area (K) may be L_4 rather than the passively rotated originally E-W trending F_1. Most L_1 data is from the Permian units wrapping around the Parrabel Dome because cleavage has developed in these muddier low grade metamorphic rocks within the Nambucca Block.

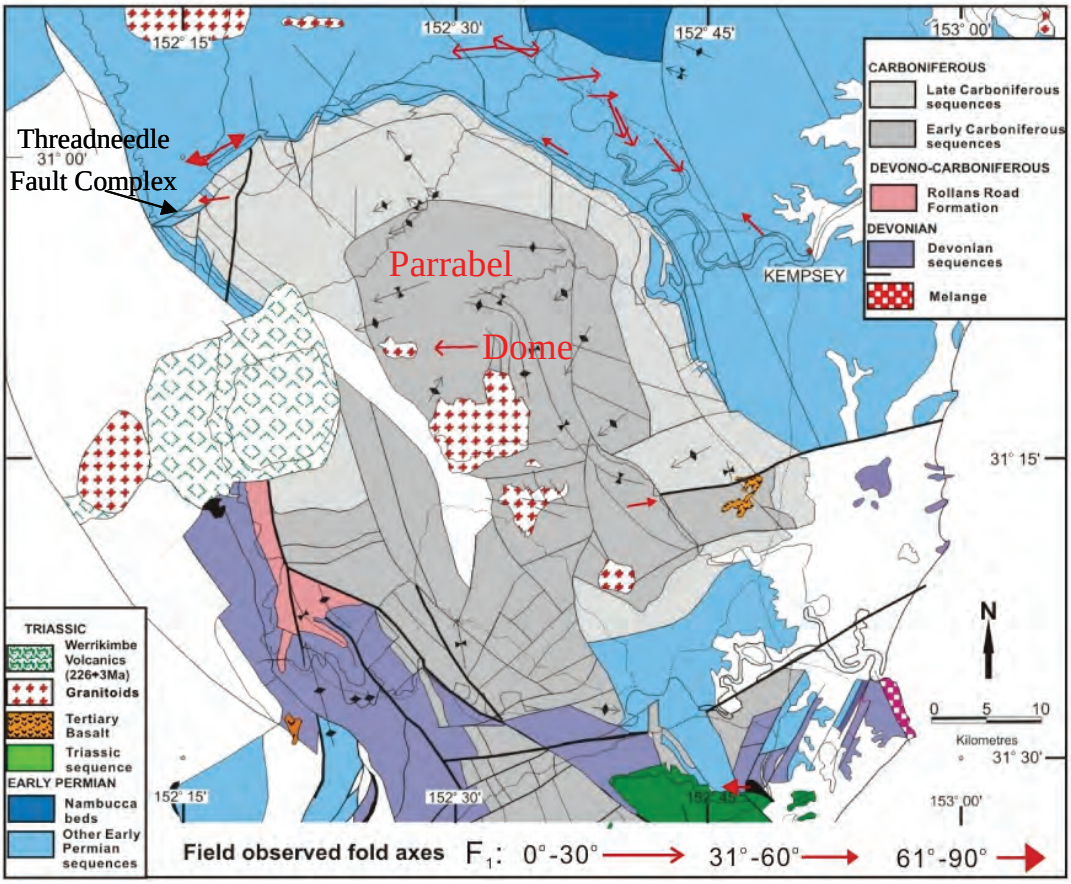

Figure 3.19: The simplified geology map with the field observed F1 fold axes data in the NHB (n=17).

The F_2 folds are the second generation of folds in the NHB, and plunge N or S (Figures 3.20 and 3.21). F_2 folds are far less prevalent than F_1 folds. F_2 folds are dominantly located on the northwestern and northern margin of the Parrabel Dome and there are very few folds in the Carboniferous sequences on the southern margin of the Parrabel Dome. The N-S oriented folds were not recognized in the previous study (Roberts *et al*. 1993). This study groups N-S folds as the second generation which is also consistent with the N-S trending cleavage S_2 in the NHB (Figure 3.13). The map pattern of F_2 folds development is concentrated in Permian units across the Hastings-Nambucca Block boundary. This is similar to the map pattern of F_1 folds. There are only rare F_2 (and F_1) folds in the Carboniferous sequences forming the core of the Parrabel Dome (Figures 3.20 and 3.21).

There are rare F_2 folds along the southwestern margin of the NHB 20 km east of Yarras (Figures 3.20 and 3.21) in contrast to the concentration of S_2 cleavages in this area (Figure 3.13). This may reflect the paucity of the N or S plunging, mesoscopic folds in these rock sequences or an inability to separate these from NW-SE plunging, mesoscopic folds.

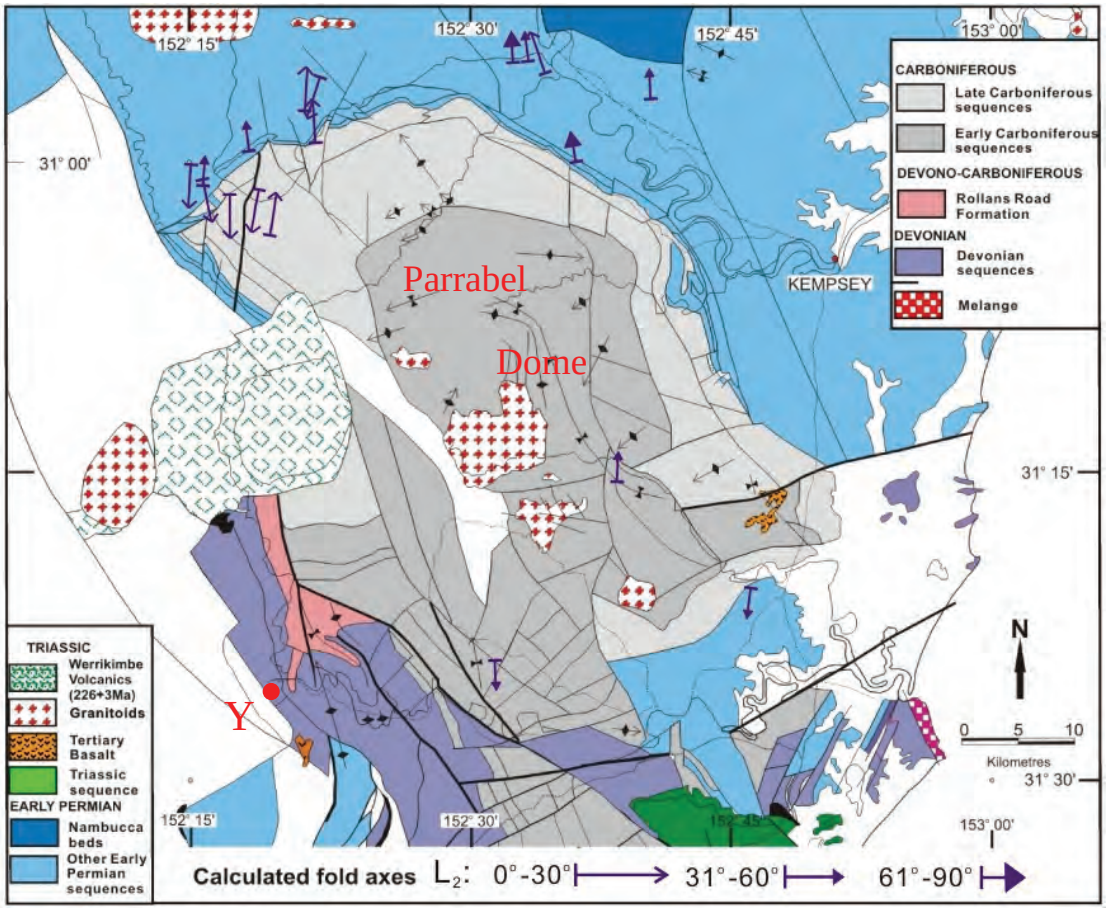

Figure 3.20: The simplified geology map with the L_2 (= F_2) calculated fold axes data in the NHB (n=19). Y = Yarras area.

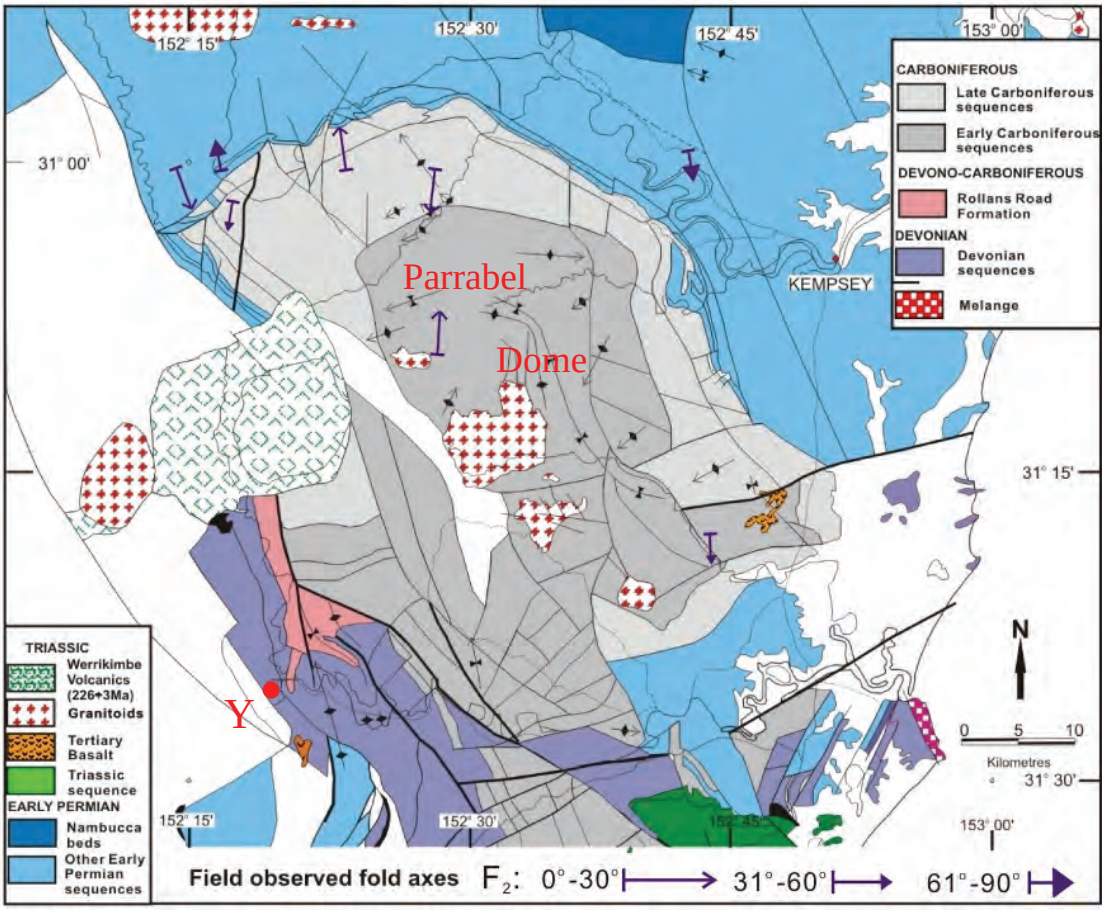

Figure 3.21: The simplified geology map with the F_2 field observed fold axes data in the NHB (n=8). Y = Yarras area.

The F_3 folds plunge NW or SE and are located mostly on the northwestern and northern margin of the Parrabel Dome, and some in the northwestern middle and southeastern middle of the Parrabel Dome (Figures 3.22 and 3.23). The Parrabel Dome is suggested as a predominantly large dome (half wavelength ~ 30km) which plunges gently northwest in the NHB (Lennox *et al.* 1999). Any mesoscopic folds related to the deformation which formed the Parrabel Dome would plunge sub-parallel to this northwest or southeast azimuth. Hence, this study suggested that the Parrabel Dome is a megafold and was formed during D3. The F_3 folds are exposed across both the Permian and Carboniferous sequences in the NHB. There are macroscopic F_3 folds shown in Figure 3.21 on the southwestern margin of the HB related to this D_3 deformation. Some of these F_3 folds in Devonian-Carboniferous rocks appear bent by northeast or southwest plunging folds (e.g. ~8km northeast of Yarras). Observed and calculated F_3

folds occur in similar concentrations and similar parts of the NHB and NB (Figures 3.22 and 3.23).

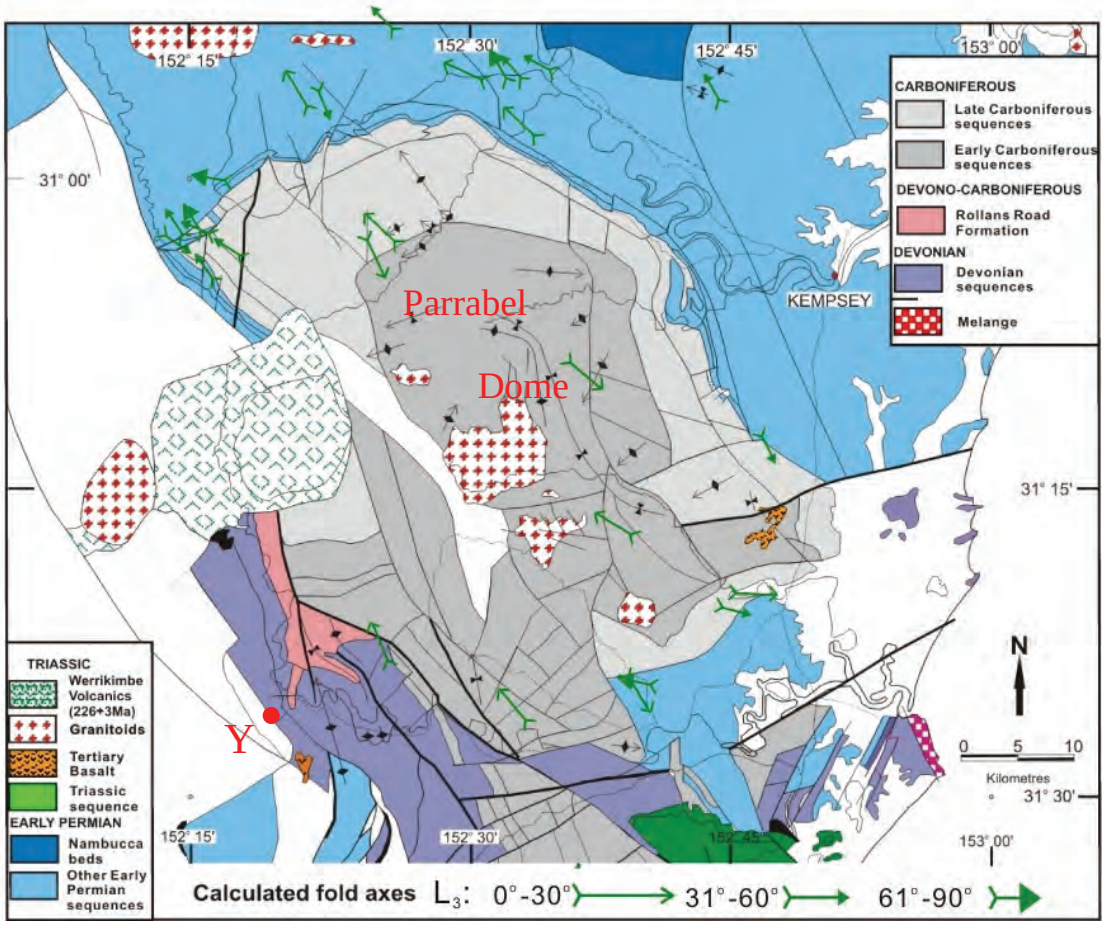

Figure 3.22: The simplified geology map with the L_3 (= F_3) calculated fold axes data in the NHB (n=27). There is a concentration of F_3 folds around the northern and northwestern margin of the Parrabel Dome. Y = Yarras.

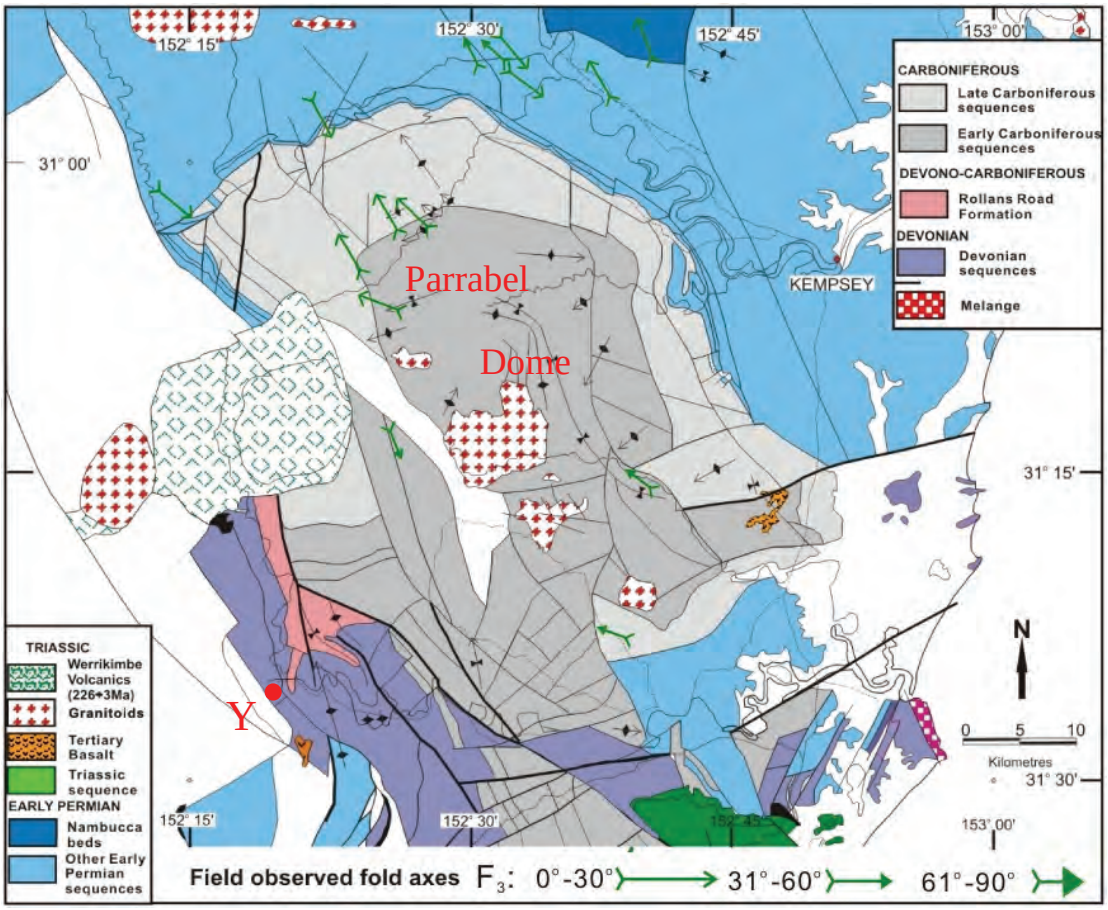

Figure 3.23: The simplified geology map with the F_3 field observed fold axes data in the NHB (n=13).

The F_4, the last generation of folds, is plunging NE or SW (Figures 3.24 and 3.25). The observed and calculated folds are scattered across the whole NHB. This pattern is somewhat consistent with the pattern of S_4 cleavage reading in the NHB (Figure 3.15) although there are more observed mesoscopic folds and calculated fold axes north and northeast of the Parrabel Dome within the Permian sequences. The calculated folds in the northwestern and north parts of the Permian bordering the Parrabel Dome may correspond to rotated F_1 folds rather than F_4 folds. These original east-west folds may have been bent around during the movement of the rigid Carboniferous sequences of the Northern Hastings Block into the Permian sequences.

The presence of two macroscopic F_4 folds antiforms plunging to the southwest (Figure 3.24 – see A and B) on the bent northeastern limb of the dome plus the bending of the

axial surface trace of the regional synform and adjacent antiform suggests refolding around these NE-SW folds.

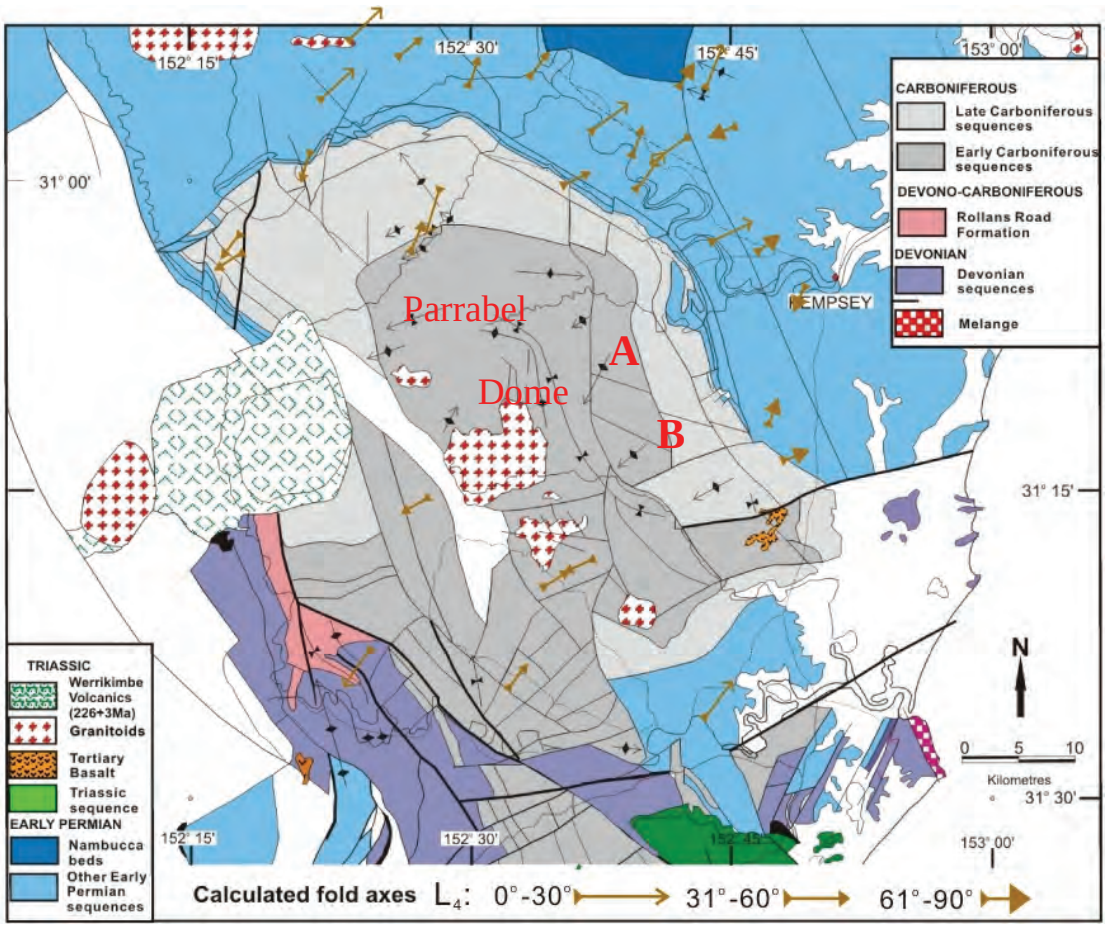

Figure 3.24: The simplified geology map with the L_4 (= F_4) calculated fold axes data in the NHB (n=29). There is a concentration of F_4 folds within the low grade Permian sequences of the Nambucca Block. This is in contrast to the areal pattern of the S_4 cleavage which is concentrated in a belt between the northern and southern Hastings Block (Figure 3.15). A and B are macroscopic F_4 folds identified by Lennox (unpubl.).

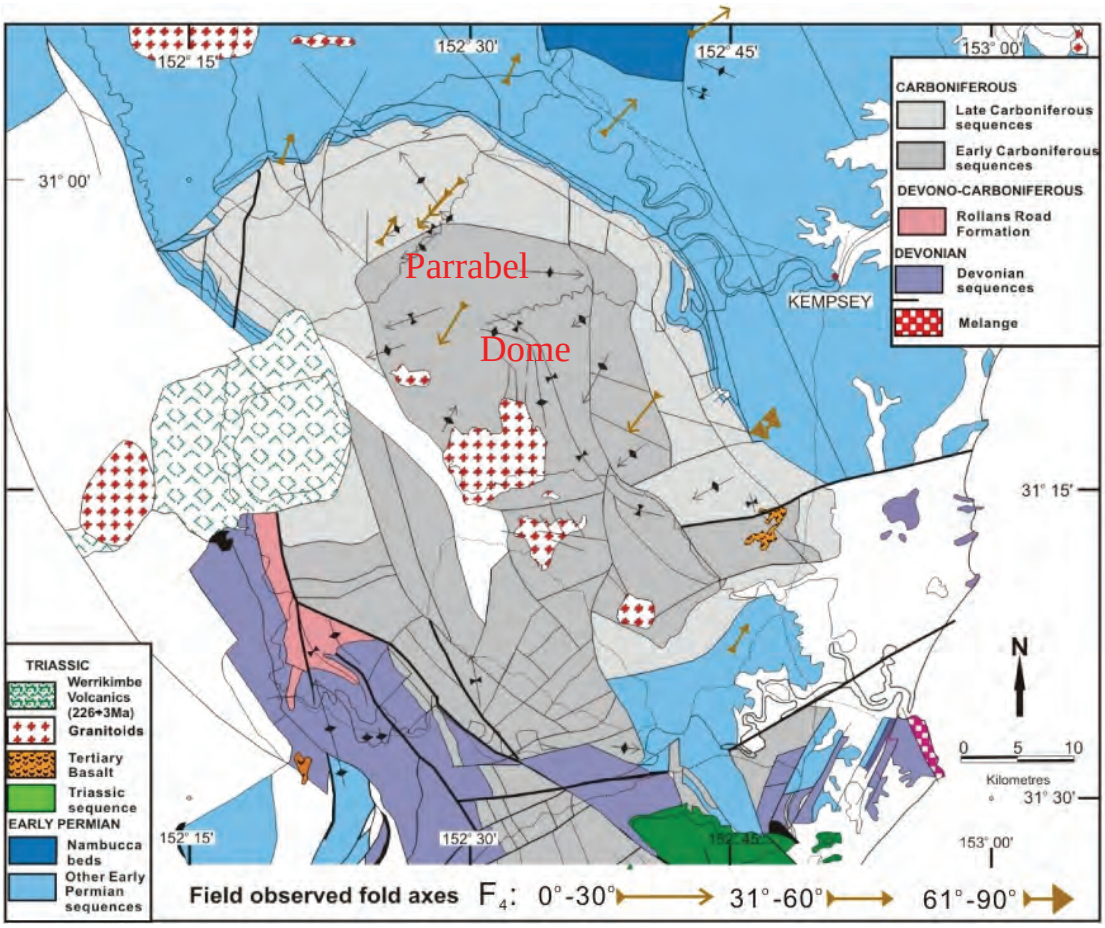

Figure 3.25: The simplified geology map with the F_4 field observed fold axes data in the NHB (n=12).

The rose diagrams of the field observed mesoscopic fold plunge azimuths and the strike of the axial surface of mesoscopic fold has been drawn (Figure 3.26) to see if there are natural breaks in orientations and/or clear differences in fold style for the different orientation groups.

The rose diagram of mesoscopic fold plunge azimuths shows five main clusters of plunge azimuths (Table 3.3) with the dominant NW-SE (130°-155°/310°-335°) clusters reflecting the Parrabel Dome forming D3 event. The second dominant cluster plunges E or W (80°-100° / 260°-280°) reflecting the D1 deformation event. The third cluster (112°-130° /292°-310°) possibly formed during D3 event and the forth (30°-40° / 210°-220°) cluster reflects the D4 event in this thesis. The last cluster of folds, orientating N-S to NNE-SSW (0°-30° / 180°-210°) reflects the D2 event in this thesis.

a) Mesoscopic fold azimuth azimuth

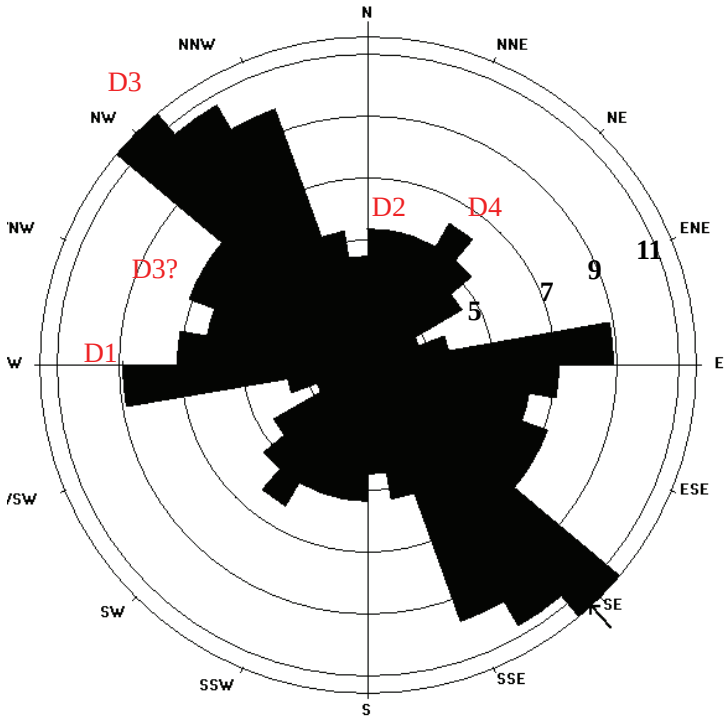

Axial (non-polar) data
No. of Data = 114
Sector angle = 10°
Scale: tick interval = 2% [2.3 data]
Maximum = 10.5% [12 data]
Mean Resultant dir'n = 137-317
[Approx. 95% Confidence interval = ±36.6°]
(valid only for unimodal data)

Mean Resultant dir'n = 137.2 - 317.2
Circ.Median = not calculated
Circ.Mean Dev.about median = not calculated
(Not calculated if too many data, or data are axial (non-polar), and too coarsely grouped
Circ. Variance = 0.32
Circular Std.Dev. = 50.68°
Circ. Dispersion = 10.56
Circ.Std Error = 0.3044
Circ.Skewness = -0.06
Circ.Kurtosis = -1.28

b) Axial surface azimuth

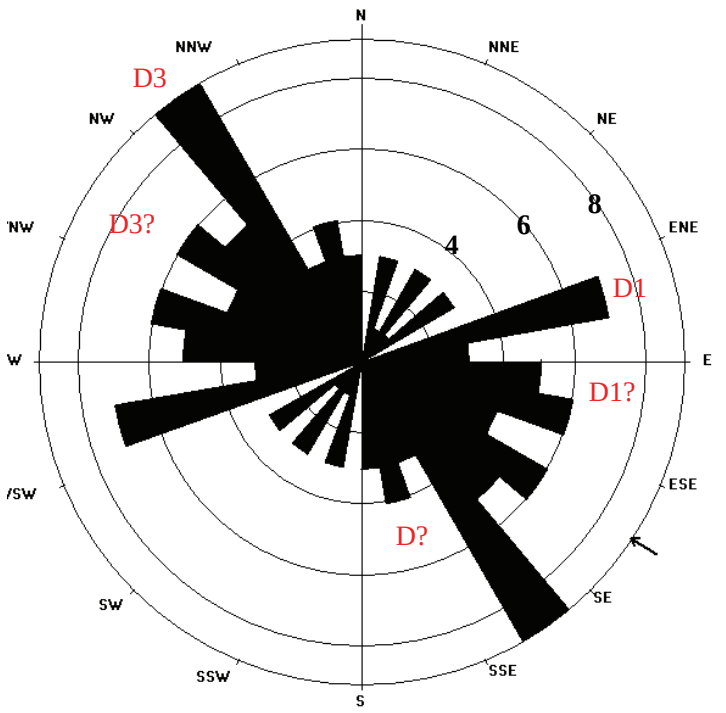

Axial (non-polar) data
No. of Data = 66
Sector angle = 10°
Scale: tick interval = 3% [2.0 data]
Maximum = 13.6% [9 data]
Mean Resultant dir'n = 123-303
[Approx. 95% Confidence interval = ±33.3°]
(valid only for unimodal data)

Mean Resultant dir'n = 123.2 - 303.2
Circ.Median = 124.0 - 304.0
Circ.Mean Dev.about median = 34.3°
Circ. Variance = 0.26
Circular Std.Dev. = 44.26°
Circ. Dispersion = 5.19
Circ.Std Error = 0.2804
Circ.Skewness = 0.34
Circ.Kurtosis = -4.33

Figure 3. 26: The rose diagram of the fold plunge azimuths (a) and (b) the rose diagram of the strike of the axial surface of mesoscopic fold with the likely deformation event in red lettering. The numbers on the circles are the number of folds of any particular orientations.

The rose diagram of the strike of the axial surface of mesoscopic fold shows similar results as the fold plunge azimuth diagram with minor difference (Table 3.3). The first cluster (140°-150°/320°-330°) reflects the dominant D3 event. The second (70°-80° / 250°-260°) and the third (100°-110° / 280°–290°) clusters may reflect the D1 deformation event in my study and the fourth cluster may reflect the D3 event.

Re-examination of the fold plunge azimuth dataset using the rose diagram suggests these five groups of common fold plunge azimuth direction which can be related to the four deformation events proposed in this thesis. The rose diagram of the strike of the axial surface to observed mesoscopic folds is similar although not the same as the rose diagram of fold plunge azimuth. The same four deformation events can be identified from this dataset (Table 3.3).

Table 3.3: Rose diagram analysis of mesoscopic folds based on the fold plunge azimuth ranges and the axial surface azimuth ranges.

Rose diagram analysis of mesoscopic fold							
Groups based on fold plunge azimuth ranges				**Groups based on axial surface azimuth ranges**			
Groups (Dominant to minor	Numbers of folds	Azimuth range	D	Groups (Dominant to minor	Numbers of folds	Azimuth range	D
1	32	130°-155°/310°-335°	D3	1	9	140°-150°/320°-330°	D3
2	16	80°-100° / 260°-280°	D1	2	7	70°-80° / 250°-260°	D1
3	7	112°-130° /292°-310°	D3?	3	6	100°-110° / 280° – 290°	D1?
4	6	30°-40° / 210°-220°	D4	4	6	120°-130° / 300° – 310°	D3?
5	5	0°-30° / 180°-210°	D2	5	4	160°-170°/-340°-350°	?

Table 3.4: Detailed fold style data for mesoscopic folds divided according to the groups identified from the rose diagram of the fold plunge azimuth.

Mesoscopic folds, NHB																
Deformation	Fold Group	Number of folds	Range of plunge azimuth	Fold interlimb angle				Half wavelenghth		Amplitude		Plunge		Fold axial plane		
				Isoclinal 0°-10°	Tight 10°-60°	Open 60°-120°	Gentle 120°-180°	Average (cm)	Range (cm)	Average (cm)	Range (cm)	Average	Range	Upright 70°-90°	Inclined 10°-70°	Recumbent 0°-10°
D3(Parrabel Dome)	1	32	130°-155°/310°-335°	3	4	6		129	2-700	48	0.5-250	28	0-72	9	2	
D1	2	16	80°-100° / 260°-280°	2	3	3		63	1.5-150	23	1.5-75	39	5-85	5	2	
D3?	3	7	112°-130° /292°-310°	1			1	27	6-50	25	4-35	35	2-85	2		
D4	4	6	30°-40° / 210°-220°		1			2	2	0.5	0.5	38	12-52		1	
D2	5	5	0°-30° / 180°-210°		2	2		118	60-200	78	20-350	33	5-72	3		2

The detailed information on the fold style, half wavelength, amplitude, plunge and fold axial surface has been given in the Table 3.4 based on the above rose diagrams analysis. As shown in Table 3.4, there are not enough mesoscopic folds in Group 3 to 5 to draw any definite conclusion regarding fold style (Table 3.4). There are limited data from Group 1 and 2 (Table 3.4) which show the variation in the fold style of folds in the same group. It is not possible to separate the four different fold generations on the basis of the style of folding.

3.6 Evidence of overprinting of structures in the Nambucca Block and NHB

A range of structures have been used to determine the order of structures in the NHB. These include overprinted cleavages, possible fold (?) - bent faults, refolded folds and cleaved rocks which have been disrupted by later faulting.

3.6.1 Evidence of overprinting of structures in the Nambucca

As outlined in Section 3.1.1 (Table 3.1), the Nambucca Block adjoining the NHB has early E-W cleavage and folds overprinted by later NW-SE structures. The presence of N-S cleavages and folds in the NHB has not been observed in NB. The late development of D_2 NE-SW structures by Shaanan *et al*. (2014) in the NB may be related to the D_4 NE-SW cleavage and folds in the NHB.

Analysis of the folding of the bedding (n = 79), probable folding of pencil cleavage to fissility (S_1) (n = 60) five kilometres either side of Station 549 (Figure 3.27) indicates early tight to elastica mesoscopic folds (F_1) have been folded around gently northwest-plunging, tight, mesoscopic folds often with faulted hinge zones (19° -> 313°, F_3) (Roberts *et al*. 1993, Lennox *et al.* 1993). This section lies within the Parrabel Beds to Kempsey Beds northeast of the Parrabel Fault on the boundary between the NHB and NB.

Roberts *et al.* (1993) identified dome and basin structures of kilometre or less scale across the crest of the Parrabel Dome consistent with superposition of what they identified as F_1 (E-W fold axial surface traces) and F_2 (NW-SE fold axial surface traces). This would not lead to regular dome and basin structures (Ramsay 1967) Type 1 where fold axes are at right angles to each other) but rather intermediate type 1 —> 2 structures. Lennox (pers. com. 2016) worked with Prof. Michel Perrin, School of Mines, Paris to model these interference structures using computer software. The plan view of these computer generated fold interference structures matches the pattern on Figure 10-13 from Ramsay's textbook consistent with type 1 → 2 structures.

3.6.2 Cleavages in the NHB

There are only a limited number of exposures where one cleavage can definitely be seen to cut another cleavage. These outcrop enable the relative order of the cleavages to be determined.

Lennox (pers com. 2015) found that, in the Station 1787, the NNE trending S_1 (207° W 86°) is overprinted by the NE trending S_2 (220° SE66^o) (Figure 3.27). The difficulty with assigning these cleavage to the proposed order of events is that this exposure has been rotated during development of the Threadneedle Fault Complex. In the Station 549, S_1 cleavages (188° E 30°, 102° S 2°, 130° SE 47°) are folded by a SE-plunging fold (Fold axis: 19°→150°) which may have formed due to drag against the Parrabel Fault (Figure

3.27, Lennox, pers. com. 2015). At Station 1413, N-S trending slaty cleavage (S_1: 000° W 63°) and NE trending spaced cleavage (S_2: 046° W 55°) associated with a WSW plunging fold (62°→255°) (Figure 3.27). It appears that the N-S cleavage is S_2 and the northeast-southwest cleavage is S_4.

Offler (pers com. 2015) found that N-S trending S_1 cleavages (348° W 70°, 358° /90° and 360° W 80°) are overprinted by the NW trending S_2 cleavages (328° W 85°, 328° /90° and 350° /90°) in the Stations By20, By22 and By33 respectively (Figure 3.27).

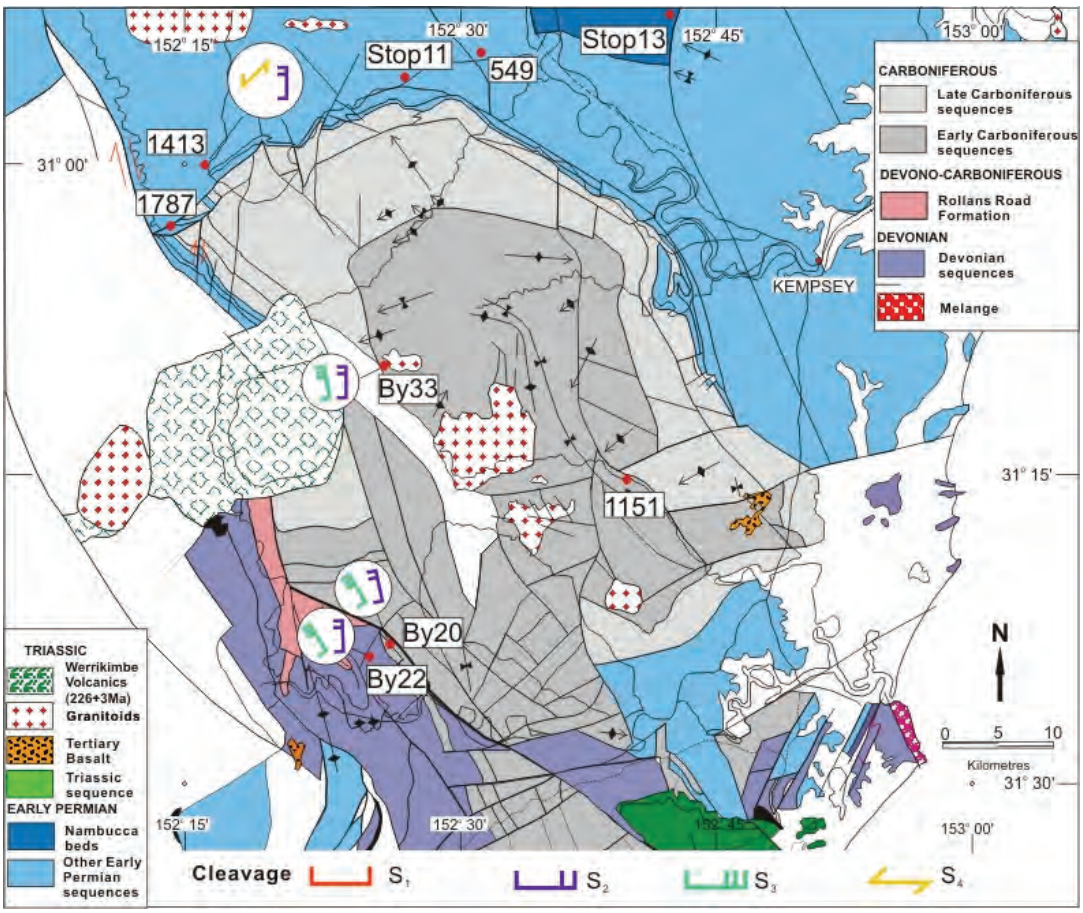

Figure 3.27: The positions of field stations which show overprinting evidence for the cleavages.

At Stop 11, there is a well developed penetrative cleavage which is refolded about northwest-trending axes in a similar manner to the folding of cleavage around the NW-trending Parrabel Dome (Lennox *et al.* 1993). At stop 13, the rocks are characterized by a single, steeply dipping, slaty cleavage (E-W striking) that has been

affected by broad late-stage (D_5) fold about a north-striking hinge surface (Figure 3.27, Leitch 1978). Further north, this slaty cleavage is deformed by at least two generations of mesoscopic folds with accompanying axial surface crenulation cleavages (Leitch 1978).

3.6.3 Folded folds in the NHB

Macroscopic folds have been constructed from measurements in the northern Hastings Block (Lennox, unpubl.) (Figure 3.28). From the map pattern of folds in the Hastings Block, it appears that some folds are apparently refolded. For example, on the southeastern part of the Parrabel Dome, the NW-SE striking Fold U is folded by a ENE-WSW striking Fold H (Figure 3.28). The NW-SE striking Fold T is folded by the NNE-SSW striking Fold F. From Figure 3.27, the NW-trending macroscopic synform through the core of the Parrabel Dome adjacent to the two Triassic plutons appears to be bent by SW-plunging macroscopic folds. This would indicate NE-SW folding overprinted NW-SE folding.

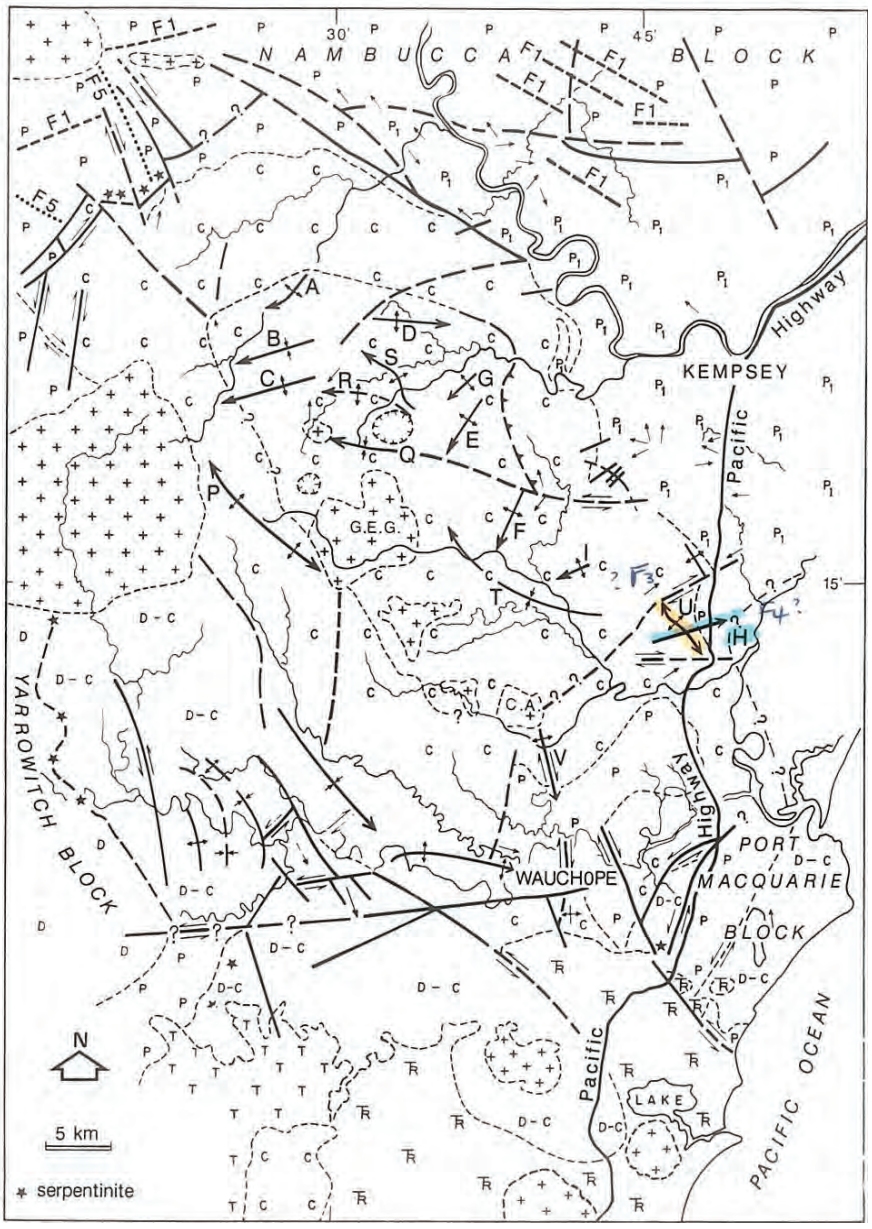

Figure 3.28: The map pattern of folds in the Hastings Block (Lennox, unpubl.).

3.6.4 Faults displacing cleaved and folded rock in the NHB

Feenan (1984) worked on the Long Flat district which is located southwest of the Parrabel Dome (Figure 3.29a). The Bagnoo fault is the major fault running through this area. Faults divided the area into several small fault-bounded blocks. From the cleavage trace in each block, we can see that these cleavage traces are apparently different in different fault blocks. The cleaved rocks were displaced by various faults in this area

(Figure 3.29), indicating that these faults are post the formation of cleavage in this region. It is usually assumed that faulting followed folding and cleavage development in the NHB. This is discussed at length in Chapter 4.

(a)

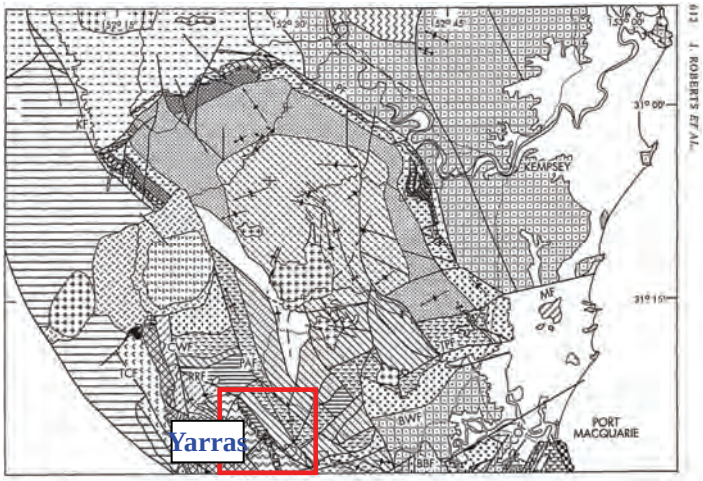

(b)

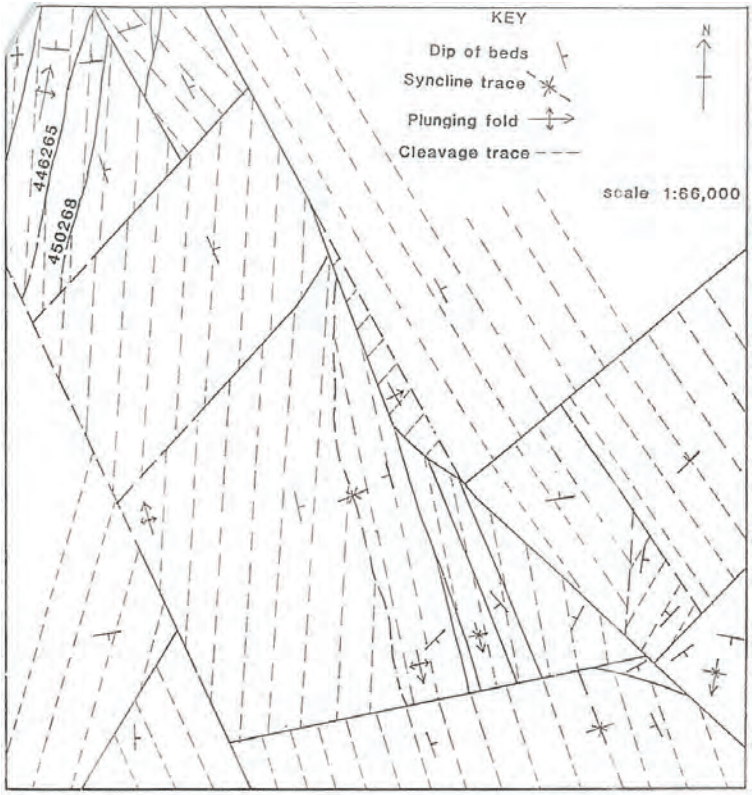

Figure 3.29: Evidence showed that faults cut the cleaved rocks. (a) Location of the area (Long Flat district). (b) Map of Long Flat district show faults apparently displacing the cleaved rocks (Feenan 1984).

3.7 Conclusions

The map pattern of representative strike of bedding suggests a major boundary consistent with the Roberts *et al*. (1995) NHB-SHB boundary. All bedding north of this boundary are consistent with the presence of a box-like Parrabel anticline plunging northwest. The readings south of this NHB-SHB boundary are contrary to that expected if the Parrabel Dome existed in this region. The derived fold axis from the major subareas suggests that the D3 folding event was pervasive throughout most of the NHB and even part of the SHB and a broad synform exists to the southeast of the Parrabel Dome related to the NE-SW trending D4 phase of deformation.

The evidence from overprinting cleavages, possible fold-bent faults, refolded folds and disrupted, already cleaved fault-blocks and faults displacing already cleaved and folded rocks has been used to determine the order of structures in the NHB. Four cleavage populations are separated according to their cross cutting relationships in the NB and NHB. The first cleavage S_1 is oriented E-W which formed and developed dominantly in the Early Permian sequences. It was passively folded around the northern margins of the more rigid Hastings Block during later deformation (Figure 3.30a). The second S_2 cleavage is oriented N-S and is dominantly located on the northwestern and southwestern margin of the Parrabel Dome (Figure 3.30b). The S_3 cleavage strikes NW-SE and is located mostly on the northwestern and southwestern margin of the Parrabel Dome, and rarely in the northern middle Hastings Block (Figure 3.30c). The last cleavages S_4 is oriented NE-SW and is poorly developed and exposures are scattered across the southern margins of the Parrabel Dome (Figure 3.30d).

Four populations of folds are recognized according to their orientations based on both the calculated and field-observed fold axes data. The first generation of folds, F_1, mostly plunge E or W and dominantly developed in the Early Permian sequences on the northern and northeastern margins of the NHB (Figure 3.31a). The F_2 folds plunge N or

S and are concentrated in Permian units across the Hastings-Nambucca Block boundary (Figure 3.31b). The F_3 folds plunge NW or SE and are located mostly on the northwestern and northern margin of the Parrabel Dome (Figure 3.31c). The gently northwest-plunging Parrabel Dome is suggested to have formed during this deformation (D3). The F_4 is the last generation of folds which plunge either NE or SW. The increased frequency of F_4 folds derived from bedding-cleavage intersections in the Permian sequences north and northeast of the Parrabel Dome reflects the more cleaved character of these sequences compared with the limited exposures of similarly derived F_4 folds from the Carboniferous sequences (Figure 3.31d).

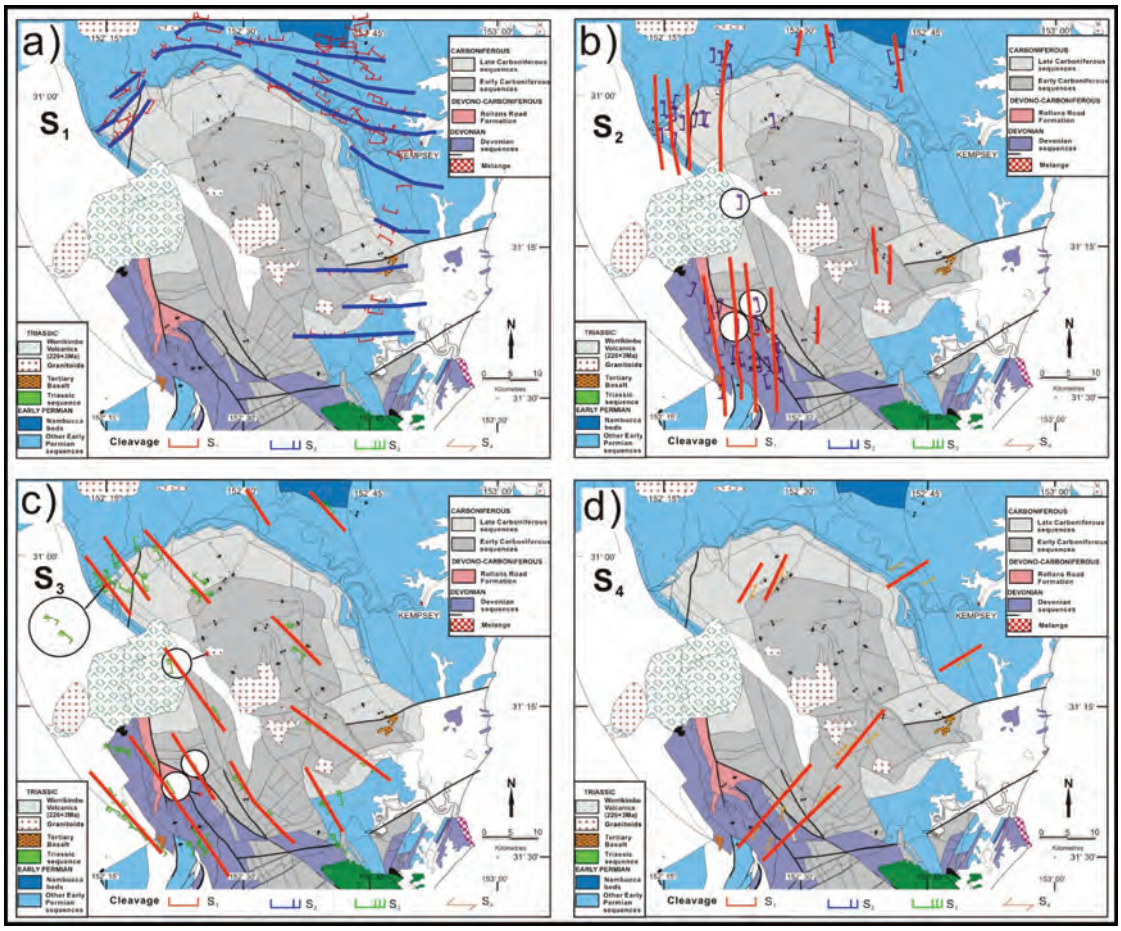

Figure 3.30: Form-lines for S_1 to S_4 showing the spatial pattern of cleavage development across the NHB and northern part of the SHB. a) S_1 appears concentrated in the Permian sequences surrounding the Parrabel Dome on three sides; b) S_2 is concentrated along mainly the western margin of the NHB and c) S_3 is concentrated along mainly the western

margin of the NHB as well; d) S_4 cleavages are poorly developed and mainly in Carboniferous sequences and to a lesser extent in Permian and Devonian rocks.

The pattern of fold populations are similar to the concentration of the cleavage populations. Specifically the map pattern of derived folds (L_1) and observed folds (F_1) (Figure 3.31a) is similar to the map parrtern of the S_1 cleavage (Figure 3.30a). The concentration of S_2 cleavage along the western margin of the NHB is similar to the L_2 and F_2 map pattern except there is a paucity of folds in the Yarras district (cf. Figure 3.30b and 3.31b). The S_3 and L_3/F_3 map patterns reflect a more even scatter of data across the whole NHB (cf. Figure 3.30c and 3.31c). The map pattern of the weakly developed S_4 cleavage is different from the better development of mesoscopic F_4 folds across the whole NHB-NB region (cf. Figure 3.30d and 3.31d).

There is a concentration of folds and cleavages within the Permian sequences compared with the Carboniferous sequences reflecting the ease of cleaving and folding the more mud-rich Permian sequences. The Permian sequences deform mainly by cleavage development and mesoscopic folding (half wavelength < 50 metres). The Parrabel Dome is much larger than any other structures in the Hastings Block (half wavelength ~ 30 km) but is comparable to late megascopic folding of similar orientation in the Nambucca Block (F_5 folds of Leitch 1978). The well developed S_1 cleavage suggesting the first deformation event adjoining the NHB was higher strain than the other cleavage forming events in this area. The prevalence of S_2 (especially) and S_3 cleavages on the western margin of the NHB may also reflect increasing strain along this margin or that the rocks in these areas were more susceptible to cleavage development.

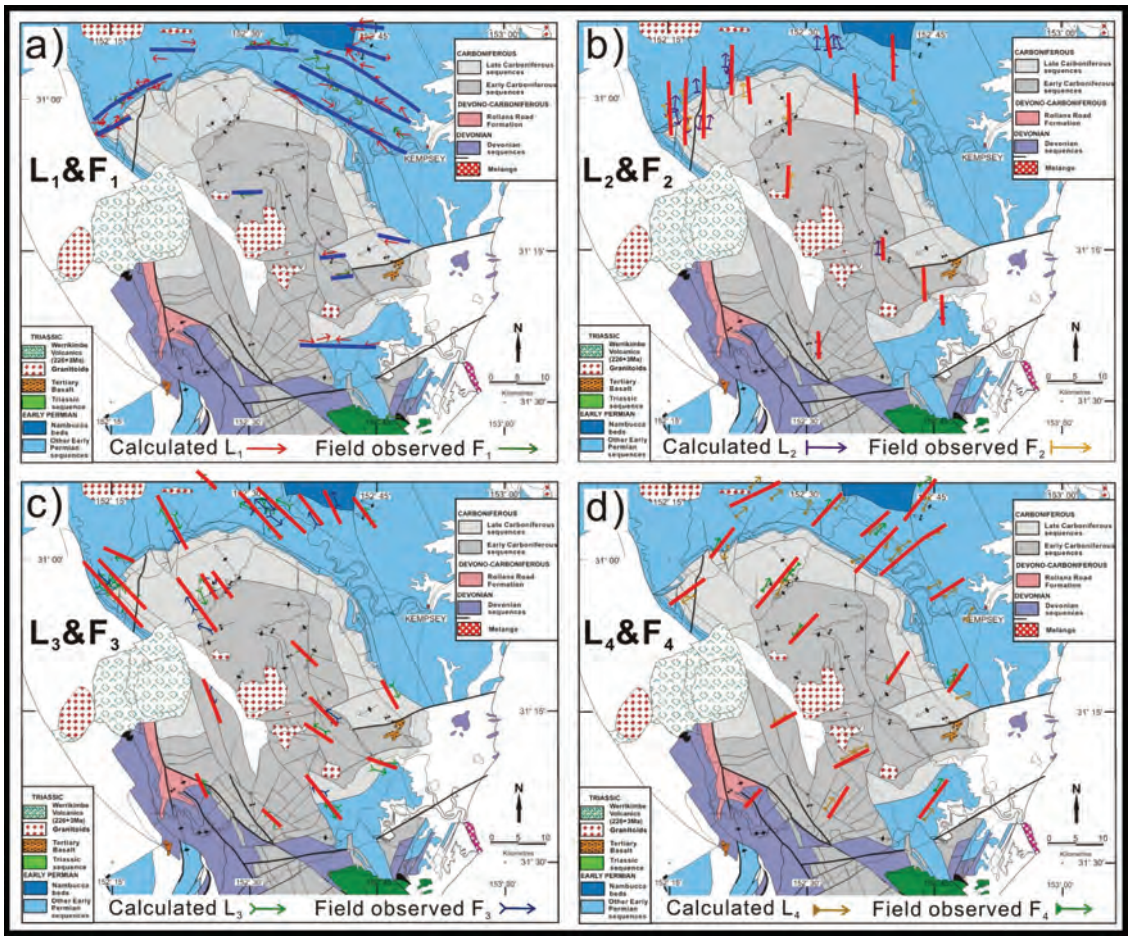

Figure 3.31: Form-lines for calculated fold axes L_1 to L_4 and the field observed fold axes F_1 to F_4 showing the spatial pattern of fold development across the NHB and northern part of the SHB. a) L_1 and F_1 are concentrated in the Permian sequences surrounding the Parrabel Dome on northern and northeastern sides; b) L_2 and F_2 are mostly concentrated in Permian units across the Hastings-Nambucca Block boundary; c) L_3 and F_3 are located mostly on the northwestern and northern margin of the Parrabel Dome and scatter across the Parrabel Dome and d) L_4 and F_4 scatter across the whole NHB.

The NHB behaved like a massif (A massive topographic and structural feature in an orogenic belt, commonly formed of rocks more rigid than those of its surroundings. Glossary of Geology, American Geological Institute 1977) after dome formation with the early cleavages in the surrounding Permian sequences wrapping around this indentor as per Figure 5.25a. There is a clear difference between the megafold model (Parrabel Dome) which some believe formed by oroclinal rotation and the indentor model which reflects a response of rocks in the adjacent Nambucca Block after Hastings Block emplacement into its current position.

Chapter 4 Fault history in the Northern Hastings Block, southern New England Orogen

4.1 Introduction

The Northern Hastings Block (NHB) is considered an along strike continuation of the fore-arc sequences in the Tamworth Belt, New England Orogen (Cawood *et al.* 2011, Figure 4.1b). Four phases of folding namely, east-west, northwest-southeast, north-south and northeast-southwest trending are recorded in the NHB. Lennox & Roberts 1988 recorded three episodes of faulting in the NHB. Roberts *et al*. (1993) show that the northwest-trending faults formed with mainly sinistral strike-slip movement followed by northeast-trending faults with dextral or sinistral strike-slip or dip-slip movement, with small displacements. Subsequently, meridional, dip-slip faults developed. Some major faults listed in the Table 1 were dealt with by previous studies in the Northern Hastings Block (Lindsay 1969; Bourke 1971; Leitch 1978 and 1980; Feenan 1984; Lennox & Roberts 1988; Spackman, 1989; Jayko *et al.* 1993; Roberts *et al.* 1993; Roberts *et al.* 1995; Lennox *et al.* 1999; Lennox and Offler 2009; Pratt 2010; Glen & Roberts, 2012; Offler pers. com. 2014). However, the exact geometry, kinematics and relationship to the regional tectonics of the majority of faults in this block are poorly understood. Some of proposed fault relationships by Roberts *et al*. (1993) are incorrect.

In this thesis, we present a detailed structural analysis of faults in the NHB with the aim of unravelling and understanding their kinematic history. It provides important data on the brittle deformation history of the Northern Hastings Block and the adjacent Nambucca Block. Further, it aids reconstruction of fault-bounded blocks and addresses questions related to the emplacement, direction and movement of the blocks within the Northern Hastings Block. Importantly, it will provide a link to the tectonics of this part of the southern New England Orogen.

4.2 Geological setting

The Hastings Block is a large, faulted-bounded block, consisting of mainly Devonian to Carboniferous rock sequences, and an Early Permian cover sedimentary sequence (Figure 4.1c). It is located east of the subduction complex (Tablelands Complex), north of the Tamworth Belt of the southern New England Orogen and south of the Nambucca Block (Figure 4.1c, Roberts *et al.* 1993). It is thought to be an along strike continuation of the fore-arc sequences in the Tamworth Belt before being translated to its current position (Cawood *et al.* 2011, Figure 4.1b). Major faults on the margins juxtapose the Hastings Block with the Early Permian successor sedimentary rocks such as the Parrabel Fault in the northeast (Figure 4.1c). Further, they juxtapose the block against the subduction complex rocks of the Yarrowitch Block (Leitch *et al*. 1990) to the west, and Devonian-Carboniferous sedimentary rocks of the Myall Block of the Tamworth Belt (Roberts & Engel 1987; Roberts *et al.* 1991) to the south (Figure 4.1c). The Port Macquarie Block is divided from the Hastings Block by the Cowarra Fault as a composite block (Leitch 1980, Figure 4.1c). Some units of the Port Macquarie Block have a close affinity with sequences in the Hastings Block (Pickett *et al.* 2009).

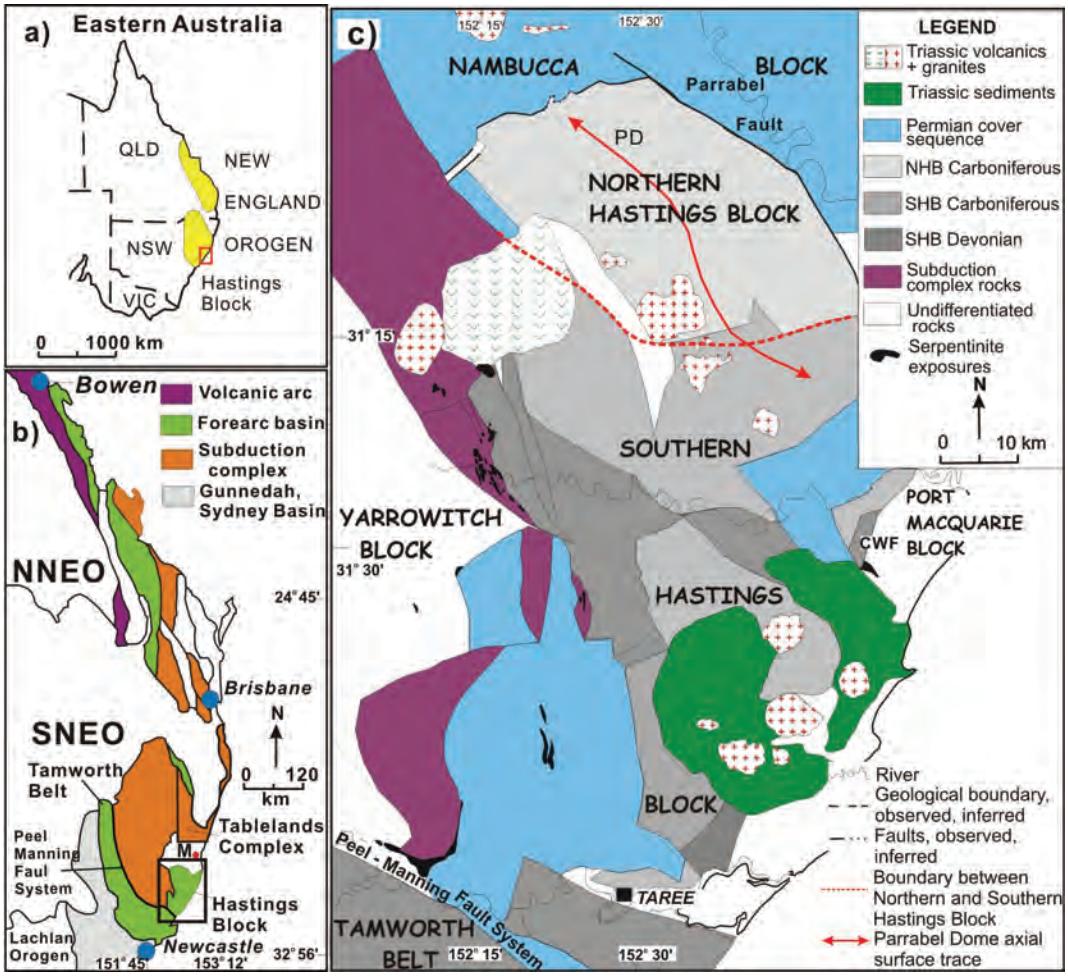

Figure 4.1: Location and tectonic setting of the Hastings Block, within eastern Australia (a), and within the southern New England Orogen (b). (c) Major tectonic units and faults within and adjacent to the Hastings Block (simplified from Roberts *et al.* 1995). CWF = Cowarra Fault.

The Hastings Block can be subdivided into the northern (NHB) and southern Hastings Block (SHB) (Figure 4.1c). They are distinguished by the differences in structural style, structural history and pre-Permian stratigraphy (Lennox & Roberts 1988; Roberts *et al.* 1993, Appendix 2). This study will focus on the NHB which is characterized by a northwesterly structural grain due to the macroscopic northwesterly-trending Parrabel Dome. It has undergone at least three, possibly four, phases of folding, namely, east-west, (? north-south), northwest-southeast and northeast-southwest trending as well as three episodes of faulting (Roberts *et al.* 1993, this thesis). Low grade metamorphism is recorded in the NHB based on the alteration patterns and reflectance studies of rocks

sampled from the measured sections (Offler *et al*. 1997). Change in the grade of metamorphism across some faults can be used to support the proposed movement history.

The Northern Hastings Block contains a sequence of Early to Late Carboniferous rocks which is disconformably overlain by Early Permian successor sedimentary rocks. Leitch (1978) showed that the D1 and D5 deformations of Nambucca Block (NB) probably affected the adjacent Northern Hastings Block. The NB is dominated by east-west trending folding, overprinting of cleavages and interference structures allowing recognition of five fold episodes. The E-W trending folds and associated cleavage developed during D1 and D2 in the Nambucca Block (260-264 Ma, Johnston *et al*. 2002; 275-265 Ma, Shaanan *et al*. 2014). The NW-SE trending folds were assigned to D5 by Leitch (1978) and D3 by Shaanan *et al*. (2014). Subsequently, faulting, dominated by NNW-striking transcurrent faults such as the Taylors Arm Fault System, replaced folding/foliation development as the major deformational mode in the Nambucca Block (Leitch 1978). The kinematic history of some major faults in the Northern Hastings Block determined from previous studies is shown in Table 4.1.

Table 4.1: Movement history, orientation and timing on some major faults in the Northern Hastings Block.

Faults ID	Fault Name	Orientation	Length (km)	Apparent movement history	Relationships to the folding and cleavages	The timing of movement and other comments	Reference
1	Kunderang Fault	147° NW-SE	33.8	Dextral strike slip	Cut cleaved rocks	Cut and displaced Early Permian Warbro Formation	Bourke, 1971
5	Threadneedle Fault Complex	50° NE-SW	13.3	Dextral strike-slip component.	Cut cleaved rocks	Cut and displaced Early Permian Yessabah Limestones	Bourke 1971
16	Parrabel Fault	122° NW-SE	21.5	Sinistral, strike-slip fault (Lennox and Offler unpubl.).	Cut cleaved rocks	Cut and displaced Eearly Permian Kempsey Beds. Containing low temperature mylonites. Post-D1 and (?) Syn-D3 (Parrabel Dome)	Lindsay 1969; Lennox and Offler unpubl.
21, 22, 23	Taylors Arm Fault System	148°-123°/106°/155°	20.3, 13 and 44.1	Right lateral displacement of up to several kilometres.	Displaced folds D1 - D5 in the Nambucca Block.	To be extensions of Demon Fault which movement started from 233 Ma (Babaahmadi and Rosenbaum, 2014).	Leitch 1978; Roberts 2000. See Appendix 4
36	Beechwood Fault	76°,39°,78° ENE-SWS	23.7	Downthrown to the southeast. Trends 045°.		Product of the final faulting episode in the area.	Mikel 1985
44	Pappinbarra fault (PAF)	130° NW-SE	34		Cut folds	West-dipping thrust, partly against early Permian strata. Truncated by the Triassic Werrikimbe Volcanics, so movement ceased pror 226 Ma.	Glen & Roberts, 2012
49	Taylors Creek Fault	146° NW-SE	35.7	Normal, sinistral, oblique-slip movement with the southeast side down relative to the northwest side (Lennox & Offler, 2009; Lennox & Offler unpubl.).		Greenschist facies assemblages on the western side and prehnite-pumpellyite facies in Devonian rocks to the east (Offler unpubl.)	Lennox & Offler, 2009; Offler , Lennox, Roberts J. unpubl. Data
52	Arizona Fault	142° NW-SE	20.2	Dip-slip fault (1~2 km). May be scissor fault as units become older on the west side of the fault to the south.	Cut the cleaved rocks	Displaced cleaved rocks. Folded D3 and refolded by D4. Move pre-Rollans Road Formation.	Feenan 1984; Figure 4.7 of Arizona Fault
56	Hastings River Fault	84° E-W	18.1 or 15 (Thompson 1985)	Sinistral strike-slip component (~2km).	Cut folds		Thompson 1985; Spackman 1989
57	Bagnoo Fault	126° NW-SE	36.2 or 25 or 57+ distance	Sinistral northwest-trending fault (Feenan 1984; Spackman, 1989; Roberts et al. 1993). Downthrown to the northeast (West, 1990; Pratt, 2010)	Cut cleaved and folded rocks	Reactivated, east-dipping, major thrust upthrown from the east (Glen & Roberts, 2012) contrary to other studies (West 1990, Pratt 2010). Post meridional folding in the SHB and pre 226 Ma (Roberts et al. 1993). Fault movement terminated pre-226 Ma (Offler pers. com. 2014)	Feenan 1984; Spackman, 1989; Roberts *et al.* 1993;West, 1990; Pratt, 2010;Glen & Roberts,2012
75	Cowarra Fault	25°/20°-60° NNE_SSE	10.6 or 8 (Taylor 1984)	Steeply, west-dipping, sinistral strike-slip fault with small displacements (Taylor 1984). Lennox & Offler (unpubl.) suggests it showed early reverse, dip-slip movement during the Hunter-Bowen Orogeny followed by late strike-slip and dip slip transcurrent movement.		Probably initiated before or during Triassic sedimentation. It must be after the greenschist facies metamorphic event in the Early Permian (~250-260Ma).	Taylor 1984; Lennox and Offler unpubl. Data.

4.3 Methodology

Each fault in the Northern Hastings Block was analysed systematically to determine the timing and extent of movement. The characteristics for each fault are presented in Appendix 3. Where there are blanks in the table a suitable answer could not be established. Figures 4.2 and 4.3 are the fault network with all faults numbered and a detailed geological map of the NHB.

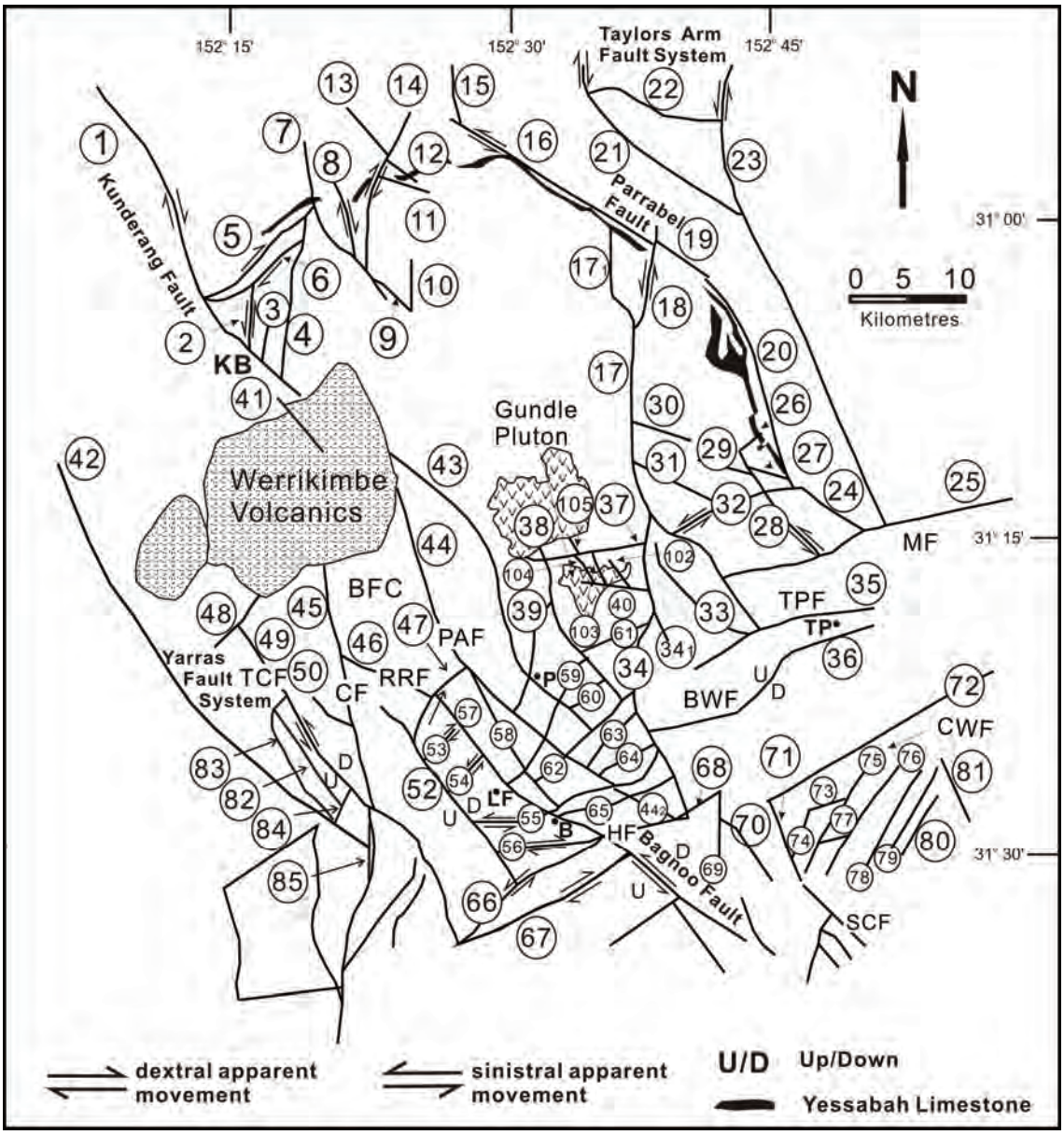

Figure 4.2: Map showing numbering of all faults in the Northern Hastings Block and part of the Southern Hastings Block. Fault locations based on Roberts *et al*. (1995). BFC =

Birdwood Fault Complex; BWF = Beechwood Fault; CWF = Cowarra Fault; CF = Cowarral Fault; HF = Hastings Fault; MF = Mingaletta Fault; PAF = Pappinbarra Fault; RRF = Rollans Road Fault; TCF = Taylors Creek Fault; TPF = Telegraph Point Fault.

In this thesis, we used conventional fault analysis to estimate the time of fault movement. The time of faulting was bracketed by determining the earliest time faulting could have begun and the latest time it could have stopped. The earliest time faulting started was established by finding the youngest rock or structure that is cut by the fault (e.g. Pappinbarra Fault (PAF) cuts the Mingaletta Formation as per Figure 4.3), whereas the latest time that faulting could have stopped was determined from the age of the oldest rock unit that intrudes, overlaps or cuts the fault (e.g. For the PAF it is the Werrikimbe Volcanics on Figure 4.3) (Bykerk-Kauffman 1987; Bykerk-Kauffman 1989). The method of determining fault timing described in the Bykerk-Kauffman (1989) is incorrect, whereas the timing described in Bykerk-Kauffman (1987) is correct. This study is based on an interpretation of the geological map of Roberts *et al.* (1995) and bedding and fault data collected by BSc (Hons) students from various universities in NSW and other authors (Paul Lennox, Robin Offler, John Roberts and Evan Leitch). No new data on the faults were collected as there is already a substantial database arising from existing studies. The cross-cutting relationships between faults are examined to determine the order of faulting (Figure 4.4, Nieto-Samaniego and Alaniz-Alvarez,1997; Tsutsumi *et al*. 2001; Van der Pluijm *et al*. 2004). Where two faults intersect in a T shape it is assumed that the fault at the top of the T formed later than the fault forming the stem of the T (Figure 4.4(1)). Faults may be overlapped by a geological unit indicating fault movement ceased prior the deposition of this unit. If a fault dies out into a particular formation, this constrains the movement on this fault to be prior to deposition of a part of this formation. If a fault is folded, it indicates folding was after all movement has ceased on the fault.

To aid discussion of the faults, all the faults are numbered (Figure 4.2). The regional structure and pattern of faulting will be discussed followed by a detailed discussion in

the morphology, fault timing and apparent fault movement (Figure 4.2).

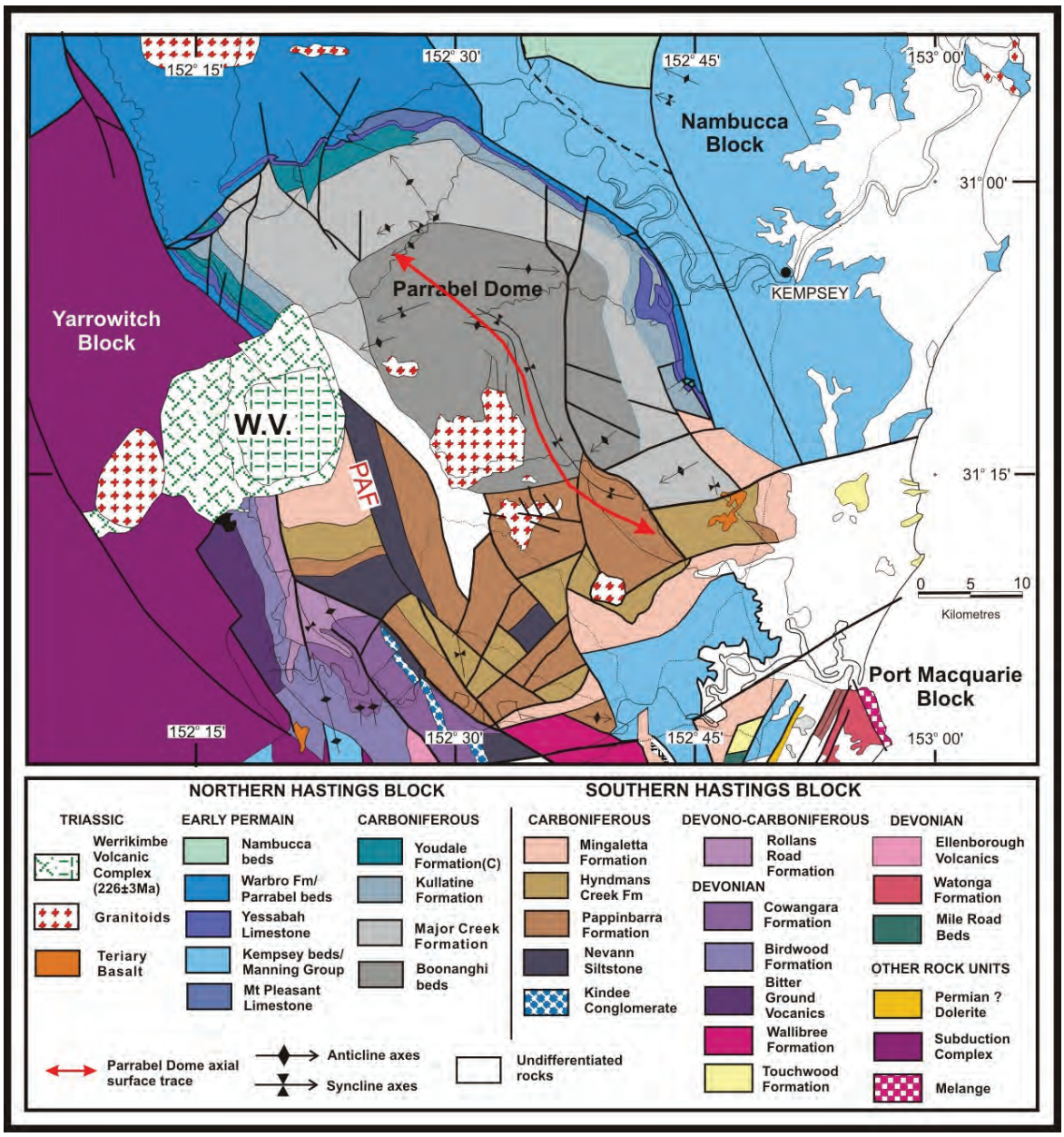

Figure 4.3: Geological map of the Northern Hastings Block and part of the Southern Hastings Block with adjoining fault blocks (Roberts *et al.* 1995). W.V. = Werrikimbe Volcanics.

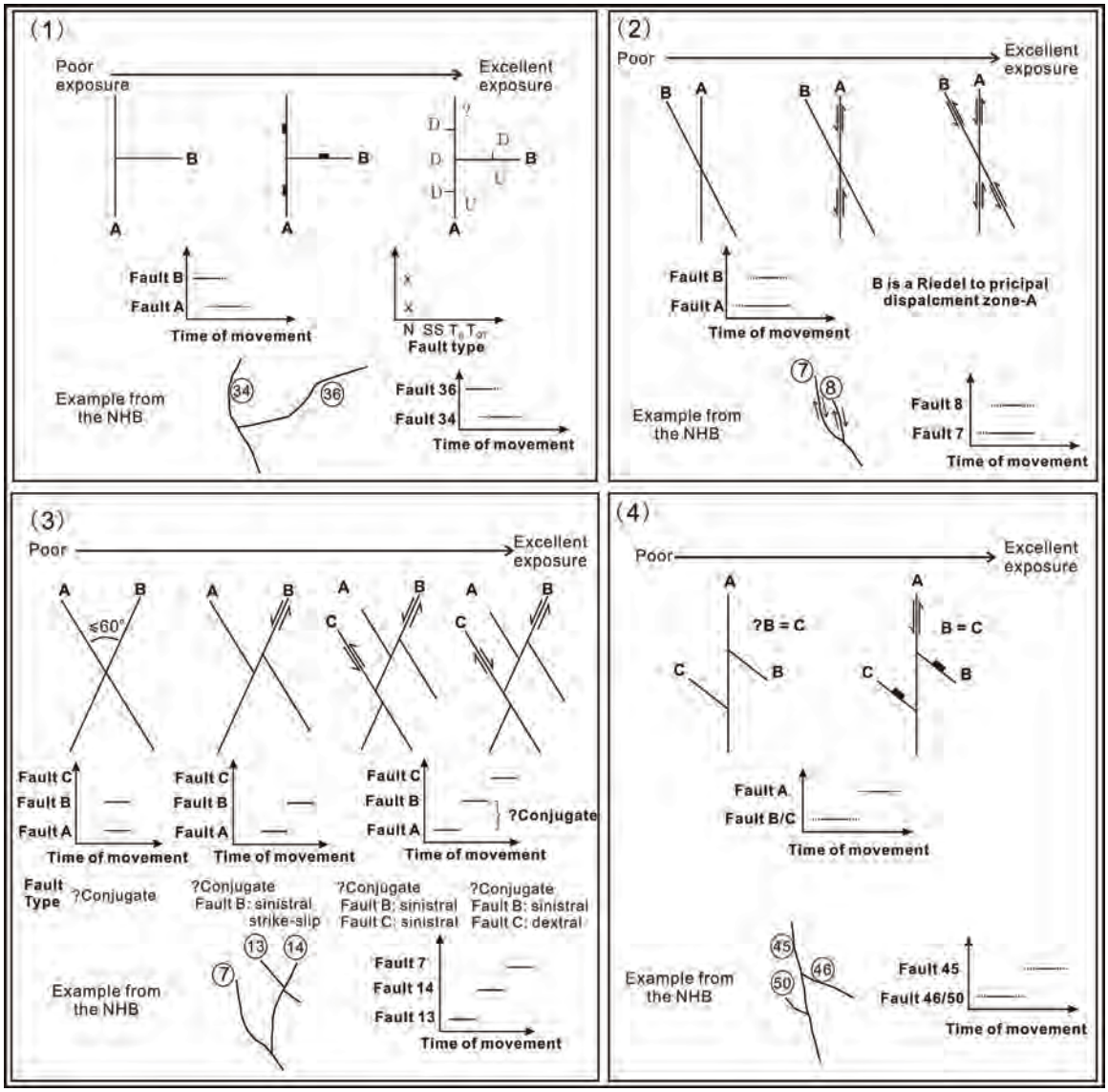

Figure 4.4: Four types of fault intersections in terms of the fault movement timing, fault types and the examples from the NHB (Nieto-Samaniego and Alaniz-Alvarez,1997; Tsutsumi *et al*. 2001; Van der Pluijm *et al*. 2004). N = normal fault; SS = strike-slip fault; T_R = thrust fault; T_{OR} = over thrust fault.

This method has a number of limitations. Only the last movement along the faults will be recorded since this will be evident by the displacement of the youngest stratigraphic unit. The estimation of the earliest and latest time of movement of each fault is constrained by the age range of the stratigraphy through which the fault passes, and the uncertainty in the position of some of the stratigraphic units in the stratigraphic column (Glen and Roberts, 2012). The actual initiation of, for example, the Pappinbarra Fault on Figure 4.5 occurs

somewhere between the bottom of the timing bar (post Mingaletta Formation) and the top of the timing bar (Late Triassic).

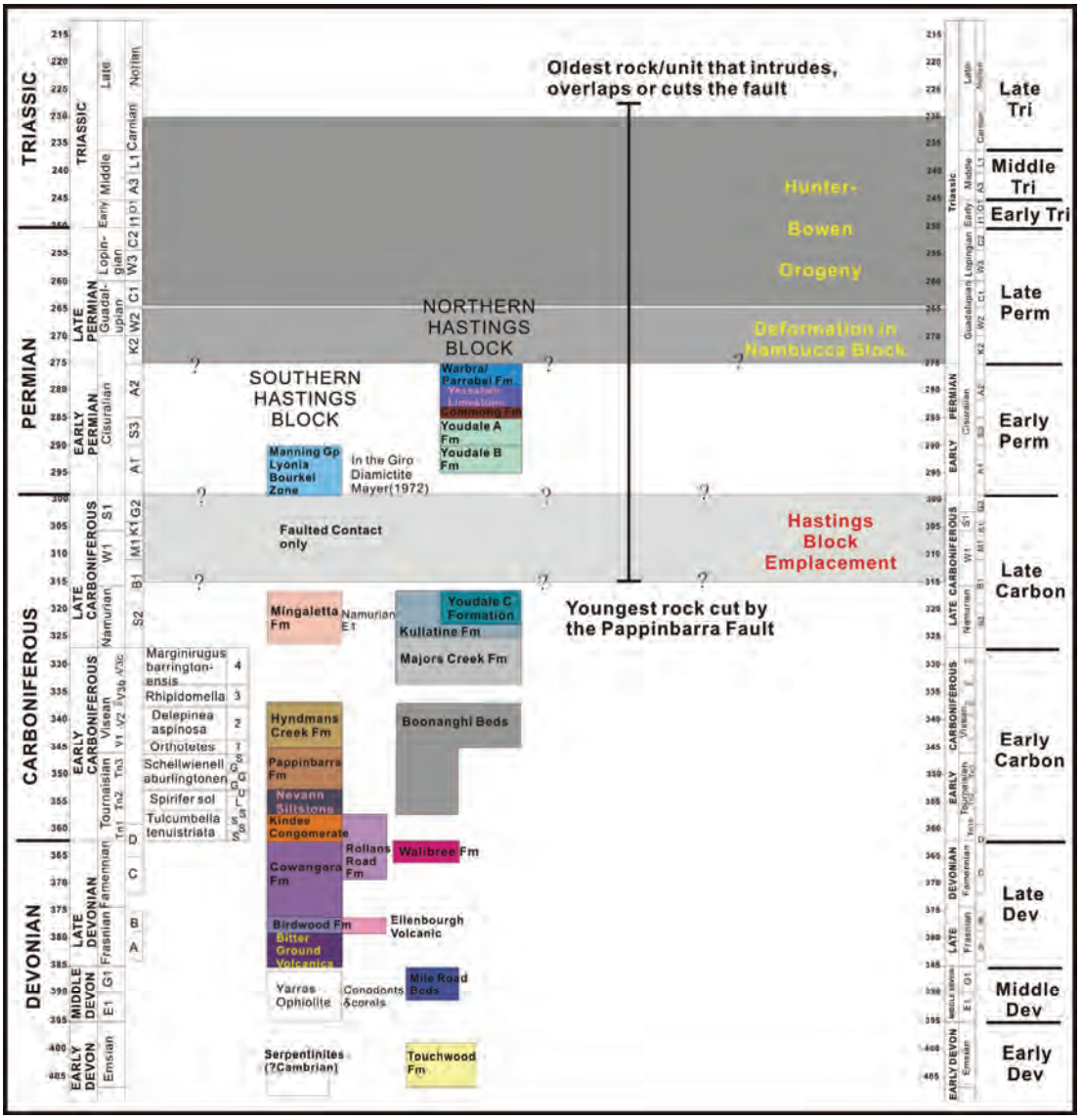

Figure 4.5: Time scale, stratigraphic columns for both the Northern and Southern Hastings Block and the movement history of the Pappinbarra Fault. The earliest time the Pappinbarra Fault could have started moving is during the Late Carboniferous (bottom of bar) as it cuts the Mingaletta Formation (Figure 4.3) and the latest time it could have stopped moving is in the Late Triassic (top of the bar) as the fault is cut by the Werrikimbe Volcanics (Figure 4.3). The timing of the Hastings Block emplacement by translational movement on suitable faults is constrained by the gap in the depositional history plus regional contraints. The time scale and stratigraphic columns are from Glen and Roberts (2012). Deformation in the Nambucca Block (and adjacent NHB) is

constrained by S_2 formation (Shaanan *et al*. 2014). The period of the Hunter-Bowen Orogeny is from Cawood *et al*. (2011). Abbreviations: A1: Asselian; A2 :Artinskian; A3: Anisian; B1: Bashkirian; C1: Capitanian; C2: Changhsingian; E1: Eifelian; G1: Givetian; G2: Gzhelian; I1: Induan; K1: Kasimovian; K2: Kungurian; L1: Ladinian; M1: Moscovian; O1: Olenskian; S1 :Steph; S2: Serpukhovian; S3: Sakmarian; W1:Westphalian; W2: Wordian; W3: Wuchiapingian.

In Appendix 3, the evidence and degree of certainty in the interpretation of apparent sense of fault movement has been tabulated. Available comments are made on the interrelationship between faults and folds/cleavages in the affected rocks. We also attempted to establish links between the timing, movement and morphology of adjacent faults. The morphology of the faults is further constrained by the dip (if it could be determined), orientation and length of each fault (Appendix 3). The orientation and length were measured from the relevant 1:25000 map for each fault in the NHB. All these data provides significant information for our interpretation of the faulting history in the NHB.

4.4 Kinematics and morphology of faults

There is a significant variation in the morphology and kinematic history of various faults in the NHB. Faults in the region trend in four main directions (NE-SW to ENE-WSW, NW-SE, N-S, E-W) and are displayed on Figure 4.6. In the following section the regional structure and pattern of major faulting will be discussed followed by a discussion of the morphology, apparent fault movement and kinematics of faults within each of the groups of faults of common strike. This discussion forms the basis for the regional structural history. It is advisable to refer back to the table in Appendix 3 for the scale, orientation and movement characteristics of each fault.

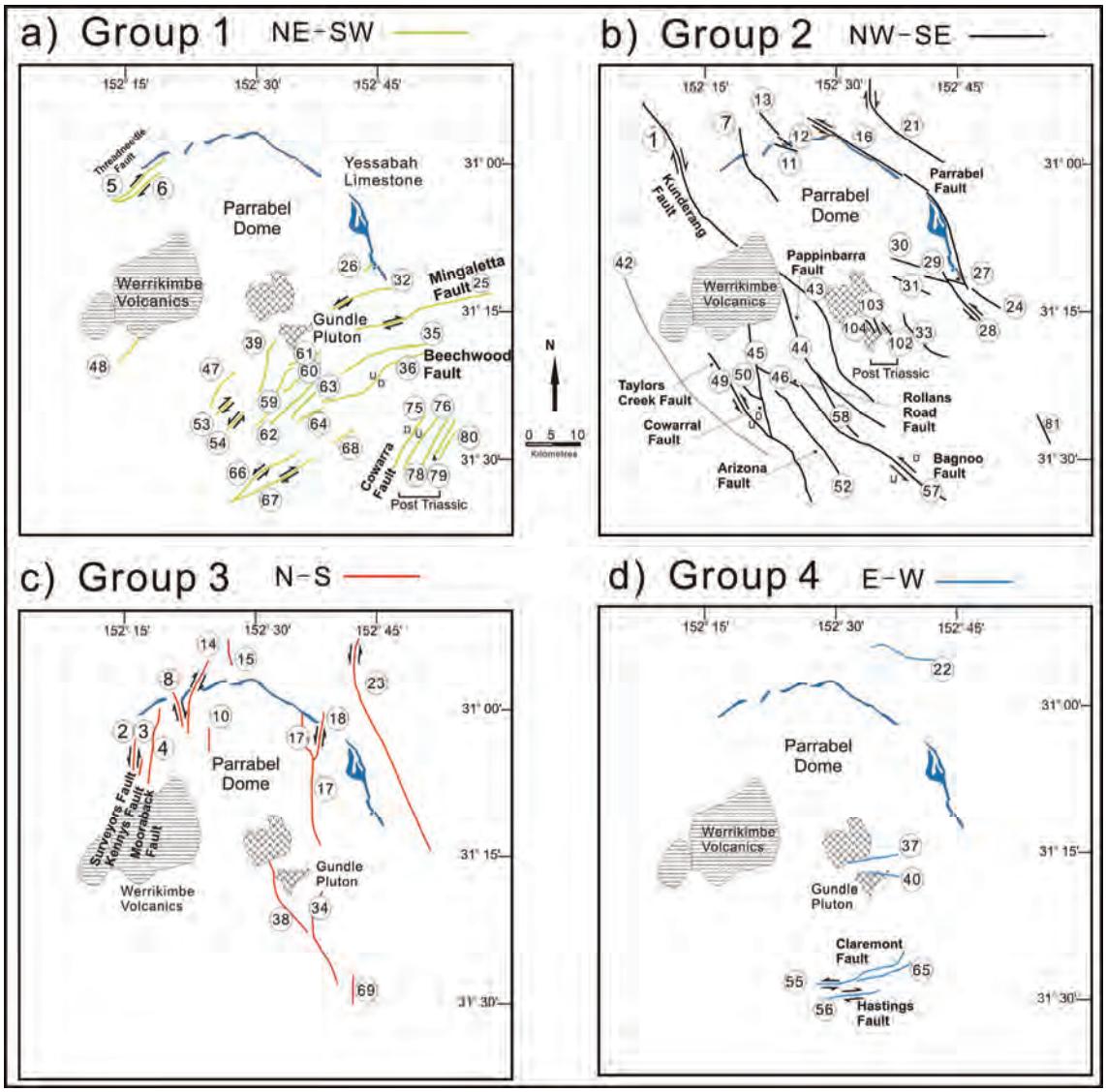

Figure 4.6: Grouping of faults with a common strike for the NHB. Group 1 faults are widely distributed south of the boundary between the NHB and SHB, whereas Group 2 faults are pervasive along the western margin of the Hastings Block, south of the Parrabel Dome in the NHB and along the northeastern margin of the NHB. Group 3 faults scatter across the NHB and Group 4 faults are mainly located on the south of the Parrabel Dome.

(1) The first fault group strikes overall NE-SW (NNE-SSW to ENE-WSW) (Figure 4.6a) and consists of faults 5-6, 25-26, 32, 35-36, 39, 47-48, 53-54, 59-64, 66-67, 75-76 and 78-80. Most of faults in this group are concentrated on the southern and southeastern margin of Parrabel Dome (Figures 4.3 and 4.6). Faults 5-6 (parts of Threadneedle Fault Complex), Fault 25 (Mingaletta Fault), Fault 36 (Beechwood Fault) and Fault 75

(Cowarra Fault) are the major faults in the group. Faults 5-6 and other small faults between them form the Threadneedle Fault Complex. Faults 5-6 are orientated at 90° to Fault 1 (Kunderang Fault). Bourke (1971) showed that the limestone between Faults 5 and 6 was dextrally displaced and rotated into its current pattern indicating the faults have a dextral, strike-slip component of movement (Figures 4.2 and 4.3). Fault 25 (Mingaletta Fault) truncates the Parrabel Fault and is cut by Fault 17 (Figure 4.2). The nature of drag folds suggests dextral strike-slip movement on the Mingaletta Fault (Hamilton 1980). Fault 36 (Beechwood Fault) is a dip-slip fault with normal movement down to the southeast (Mikel 1985). It is cut by Fault 34 (Figure 4.2). Fault 75 (Cowarra Fault) is a steeply, west-dipping, strike-slip, NNE-trending fault separating the Hastings Block from the Port Macquarie Block (Leitch 1980, Lennox & Offler unpubl.). It shows dip-slip normal movement as it juxtaposed higher grade, greenschist facies rocks in the PMB to the east against lower zeolite facies sequences in the Hastings Block to the west. Lennox & Offler (unpubl.) considered the intensively veined, sheared and brecciated Karikeree metadolerite adjacent to the Cowarra Fault showed early reverse, dip-slip movement during the Hunter-Bowen Orogeny followed by late strike-slip and dip slip transcurrent movement. Fault 32 displaced the Mingaletta Formation - Kempsey beds boundary with sinistral strike-slip consistent with post Early Permian movement (Figure 4.2). Faults 53-54 and 66-67 displace the Kindee Conglomerate in the area indicating dextral strike-slip movement on Faults 53 and 67 and sinistral strike-slip movement on Faults 54 and 66 (Figure 4.2). The apparent strike-slip offsets by these faults may alternatively reflect uplift or down-drop of blocks. NNE-trending faults (75-76 and 78-80) within the Port Macquarie Block cut the Triassic formations (Camden Haven Group and Milligans Road Formation, Pratt 2010), hence these faults should have developed post-Triassic or have been partly reactivated post-Triassic.

(2) The second fault group is orientated NW - SE and are widely scattered throughout the NHB (Figure 4.6b) and occur on the southern, southwestern, and northern margins of the Parrabel Dome (Figure 4.6b).This group consists of faults 1, 7, 9, 11-13, 16, 21,

24, 27-31, 33, 43-46, 49-50, 52, 57-58 and 102-105. Faults 1 (Kunderang Fault), 16 (Parrabel Fault), 44 (Pappinbarra Fault), 45 (Cowarral Fault), 46 (Rollans Road Fault), 49 (Taylors Creek Fault), 52 (Arizona Fault) and 57 (Bagnoo Fault) are the major faults in this group (Figure 4.6b). The drag effect of bedding cut by the Kunderang Fault (Fault 1) observed by Bourke (1971) indicates that it has undergone dextral, strike-slip movement. By contrast, Lindsay (1969) suggested dip-slip displacements of hundreds of meters based on the stratigraphic relations across this fault.

The change in orientation of both the cleavage and bedding from approximately east-west 10 kilometres east of the Parrabel Fault (Fault 16) (GR580800, Williwarrin 1: 25,000 sheet) to northeast-southwest striking adjacent to the fault (GR490780) suggests fault drag. It would indicate that post-S_1 movement was apparently sinistral, strike-slip on this fault (Lennox unpubl.). Analysis of faults near the Parrabel Fault indicate the movement was sinistral oblique-slip consistent with the essentially sinistral movement suggested by Lindsay (1969). Low temperature mylonites show deformation of quartz, minor dynamic recrystallisation and growth of new mica (Lennox & Offler unpubl.). The bending of the trace of the Parrabel Fault may reflect clockwise rotation of the northeast limb of the Parrabel dome after fault formation or more likely changes in the dip of the fault on this limb.

Fault 28 displaces the Faults 27 and 29 showing apparent sinistral, strike-slip movement (Figure 4.2). The Rollans Road Fault (46) forms the southwestern side of the Birdwood Fault Complex (Figure 4.2). This fault complex consists of faults 44-47 and bounds east-west striking sequences younging to the north which are right angles to the general north-south striking, east-younging sequences either side of the complex (Figures 4.2 and 4.3). The Rollans Road Fault (46) may be a continuation of Fault 50 which has been displaced sinistrally by the Cowarral Fault (45). The Rollans Road Fault is cut by the Cowarral Fault which in turn is cut by the Werrikimbi Volcanics. Rb-Sr dating of biotite and whole rock samples from the Werrikimbe Volcanics suggests an average age of 226±3 Ma (Flood *et al*. 1993). These cross-cutting relationships indicate the Rollans

Road Fault must have finished moving prior to 226 Ma.

The structures from the serpentinites and faults near the Fault 49 (Taylors Creek Fault) indicate normal, sinistral, oblique-slip movement with the southeast side down relative to the northwest side (Lennox & Offler, 2009; Lennox & Offler unpubl.). Metamorphic studies by Offler (unpubl.) indicate that the grade is higher on the western side with greenschist facies assemblages of possible burial origin in metadolerites within the Yarras Fault Complex and prehnite-pumpellyite facies in Devonian rocks to the east.

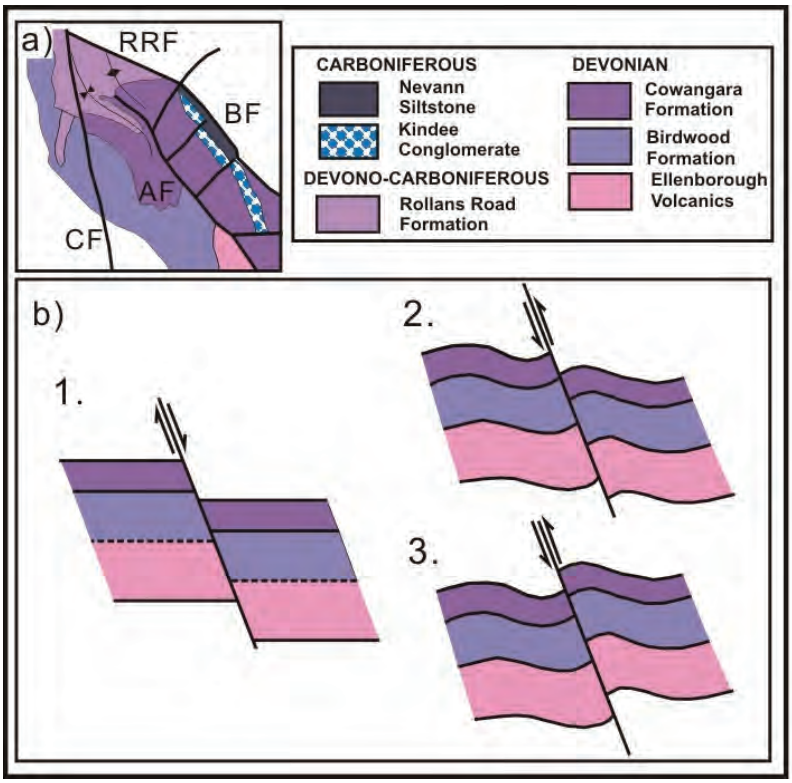

Figure 4.7: The map pattern of the Arizona Fault (AF). (a) The location of the Arizona Fault and surrounding sequences. (b) Schematic cross sections showing the formation of the Arizona Fault:- (1) it formed as a normal fault; (2) it was re-activated as a reverse fault with formation of folds either side of its northern end with small displacements; or (3) it was re-activated as a reverse fault with a larger displacement. AF = Arizona Fault; BF = Bagnoo Fault; CF = Cowarral Fault; RRF = Rollans Road Fault.

The Arizona Fault (Fault 52, Figures 4.2 and 4.7a (AF)) formed as a normal, east-side down fault before deposition of the Rollans Road Formation (Feenan 1984, Figure 4.7 b1). This fault was re-activated as a reverse fault forming folds either side of its

northern end (Figure 4.7 b2). Since it is still eastern-side down as observed, it is unlikely to have formed as far as Figure 4.7 b3. The option on Figure 4.7 b3 is canvassed as we are not sure that this fault did not reactivate in some areas (outside this map area) with the hanging wall moving such that the previous dip-slip movement was entirely eliminated. The Arizona Fault in this model would then be a thrust fault. The Arizona fault has a synform (west) and antiform (east) either side of it at its northern end (Figure 4.7a). These D3 (?) folds and the Arizona Fault appear folded by an open NE-SW trending D4 (?) fold based on the geological map of Roberts *et al*. (1995). Alternatively the AF and adjacent folds were bent during northwest-movement on the wedge-shaped block bounded by the CF/RRF-BF faults. This would be consistent with the sinistral, strike-slip movement on these faults.

The Bagnoo Fault is a major sinistral, strike-slip, northwest-trending fault indicated by the displacement of rock units on each side of the Bagnoo Fault (Feenan 1984; Spackman, 1989; Roberts *et al.* 1993). It is approximately 60 km in length. Glen & Roberts (2012) suggested the Bagnoo Fault and its inferred extensions to the north are part of a major east-dipping, thrust with northeast-over-southwest direction of movement. This is in contrast to the interpretations of Spackman (1989), Roberts *et al.* (1993) and Offler (per. com., 2014) who recorded evidence for sinistral, strike-slip movement on this fault. Field observations show the Kindee Conglomerate changes strike from N-S to NW adjacent to the Bagnoo Fault indicating drag due to the sinistral strike-slip movement on this fault (Figure 4.3). Fault movement on the Bagnoo Fault must have terminated pre-226 Ma (Rb-Sr age for Werrikimbe Volcanics; Flood *et al.* 1993). Pratt (2010) indicated that the Bagnoo Fault continues southeastwards into and cuts the Early Triassic Camden Head Claystone and Late Triassic – Early Jurassic Milligans Road Formation in the Lorne Basin where it displays a significant down throw on the northern side. Bedding is vertical adjacent to the Bagnoo fault (BF). Hence, the Bagnoo Fault movement is pre-226 Ma at its northern end, but it was still active (or was reactivated) in the Early Jurassic in the Lorne Basin. The northern part of the Pappinbarra Fault trends NNW-SSE and the

southern part NW-SE which may be due to the fault being listric and dipping variably but steeply east.

Faults 102-105 cut the Triassic Gundle Pluton according to Roberts *et al.* (1995) which constrain the timing of fault movement to be post 226 Ma (Figure 4.2). Hence, these faults ceased activity after the Late Triassic.

(3) Fault group 3 consists of faults orientated N - S. that are mostly located on the northern and northeastern margin of the Parrabel Dome (Figure 4.6c). It consists of faults 2-4, 8, 10, 14-15, 17-18, 23, 34 and 38. Fault 2 (Surveyors Fault), Fault 3 (Kennys Fault) and Fault 4 (Mooraback Fault) displace limestones along these fault showing sinistral, strike-slip movement (Bourke 1971, Roberts *et al*. 1995) (Figure 4.3). Faults 8 and 14 show dextral strike-slip based on the displacement of the Youdale C Formation and faults 12 and 13 respectively (Figure 4.2). Fault 17 appears bent by two SW-plunging folds at its southern end (Figure 4.3). Fault 18 displaces the Parrabel Fault (16), sinistrally and thus developed after the Parrabel Fault.

Faults 23 along with NW-trending Fault 21 and E-W trending Fault 22 are part of Taylors Arm Fault System (TAFS) in the Nambucca Block which are considered to be extensions of Demon Fault (see Appendix 4). This is a major transcurrent fault in the southern New England Orogen with approximately 23km of dextral strike-slip movement at its northern end (McPhie and Ferguson, 1983) and up to several kilometers on its southern end (Leitch 1978). The Demon fault was active from 233 Ma in the Triassic to Early Jurassic (or possibly during all of the Jurassic, Babaahmadi and Rosenbaum (2013)).

(4) Fault Group 4 is orientated E-W, a small group which is made up of Faults 37, 40, 55-56 and 65 that are located on the southeastern margin of the Parrabel Dome (Figure 4.6d). Faults 55 (Claremont Fault) and 56 (Hastings Fault) showed sinistral strike-slip movement and dextral strike-slip movement respectively, as they displace the Kindee Conglomerate. Faults 40 cuts the Triassic Gundle Pluton (Figure 4.2).

There are four main population shown in the rose diagram of fault strikes (Figure 4.8). They are:- the first group orientating NW-SE (130°-160°/310° -340°), the second NE-SW group (40°-60°/220°-240°), the third N-S group (0°-10°/180°-190°) and the fourth ENE-WSW group (60°-80°/240°-260°). These four main populations are almost the same as shown in the section above which separated faults according to strike. The only difference is that E-W faults proposed in my thesis are represented by ENE-WSW faults.

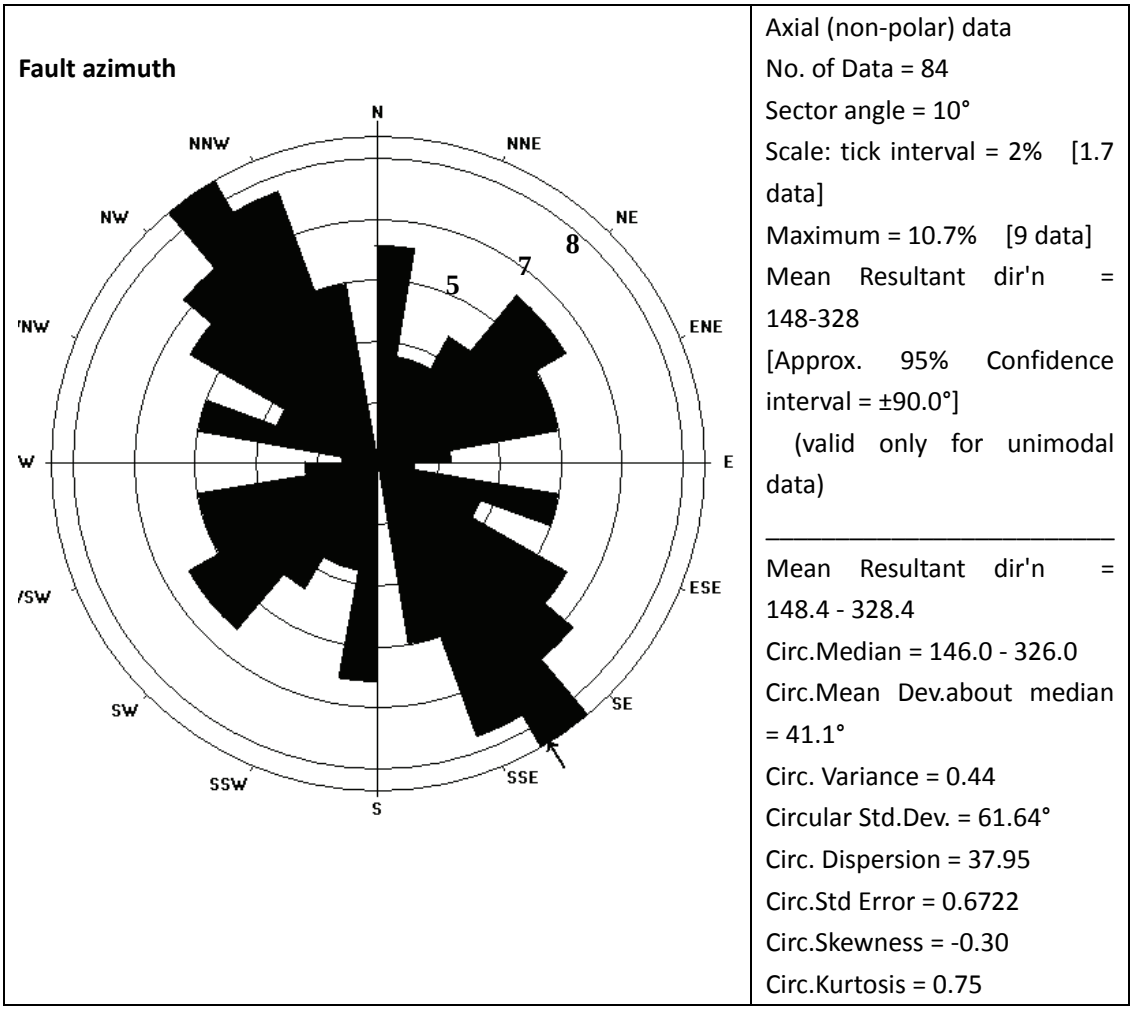

Figure 4.8: The rose diagram of the strikes of the faults. The numbers on the circles correspond to the frequency of faulting.

Faults within each group described above have the same orientation but different kinematics. This conclusion is different from Roberts *et al.* (1993) who considered all faults of one orientation had similar movement history.

4.5 Fault timing

The conventional fault analysis described in the Chapter 4.3 was used to estimate the time of movement of these faults. The evidence for the timing of earliest and latest fault movement for each fault is tabulated in a table in Appendix 3.

4.5.1 The earliest time faulting could have started

The earliest time faulting could have started was established by finding the youngest rock or structure that is cut by the fault and by examining the map pattern of cross-cutting relationships between faults. When fault activity commences at approximately the same time, they would appear to cluster on the timing diagram as shown in Figure 4.8. The earliest time of fault movement is shown by the bottom of the vertical bar. Clearly the widths of the boxes defining the earliest time of faulting varies somewhat indicating a time interval between approximately 5 (Box 1) and 30 million years (Box 4).

(1) Group 1 faults consist of faults 48, 50 and 52, which are located on the southwestern side of the Northern Hastings Block (Appendix 5 - Figure A19a). The earliest time of faulting in Group 1 is in the Late Devonian (Figure 4.9). The strike of Faults 50 and 52 is NW-SE and for Fault 48 is NE-SW (Figure 4.2).

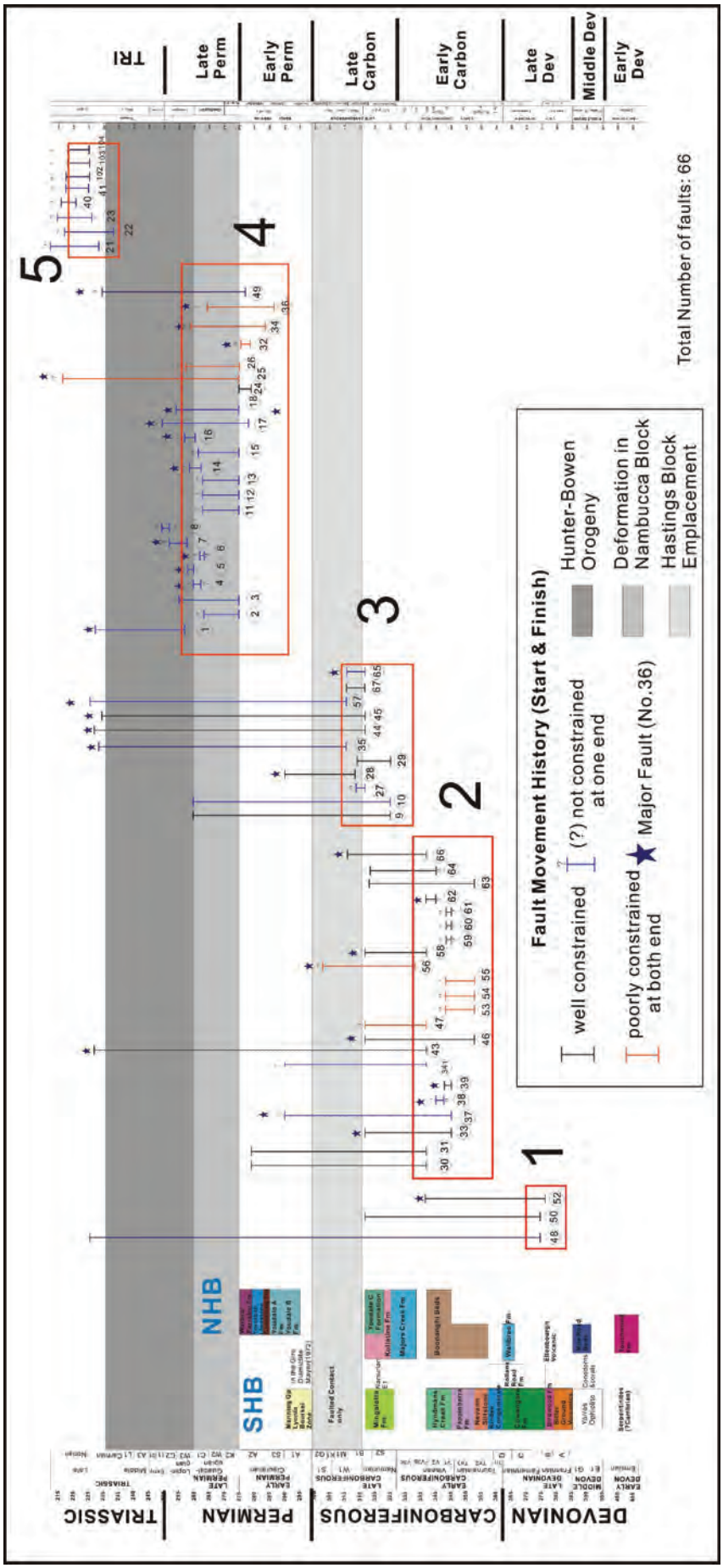
TRI
Late Perm
Early Perm
Late Carbon
Early Carbon
Late Dev
Middle Dev
Early Dev
Total Number of faults: 66
Fault Movement History (Start & Finish)
well constrained
(?) not constrained at one end
poorly constrained at both end
Major Fault (No.36)
Hunter-Bowen Orogeny
Deformation in Nambucca Block
Hastings Block Emplacement
NHB
SHB
TRIASSIC
PERMIAN
CARBONIFEROUS
DEVONIAN

Figure 4.9: Earliest time fault could have started for all major faults in the NHB. The bottom of each vertical bar represents the earliest time fault could have started and the top of each bar represents latest time fault could have stopped. Populations of faults which initiated at the same time can be identified by enclosing these in a box as shown. All faults which initiate at approximately the same time are shown within the boxes labelled 1 to 5.

(2) Group 2 faults is made up of faults 30-33, 34(1), 37-39, 43, 46-47, 53-56, 58-64, 66 and 105 (Figures 4.9 and A19b). The strike of the majority of faults in Group 2 is NE-SW and NW-SE (Figure 4.2). Faults in this group are mostly located on the southern margin of the Parrabel Dome and in the central part of Hastings Block (Appendix 5 - Figure A19b). Analysis indicated that the earliest time of movement on the faults occurred in the Early Carboniferous (Figure 4.9).

(3) Group 3 faults is composed of Fault 9-10, 27-29, 35, 44-45, 57, 65 and 67 (Figure 4.9). These faults are on the southwestern and southeastern margin of the Parrabel Dome (Appendix 5 - Figure A20a). The dominant orientation of Fault Group 3 is NW-SE. The earliest time of faulting in this group is from Visean (V3c) to Westphalian in the Late Carboniferous (Figure 4.9).

(4) Group 4 faults consists of Fault 1-8, 11-18, 24-26, 32, 34, 36 and 49 (Figure 4.9). These faults are located on the northwestern, northern and eastern part of NHB and surround the Parrabel Dome (Figure 4.9 and Appendix 5 - Figure A20b). The strike of the majority of faults in Group 4 is N-S and NW-SE. The earliest time of fault movement is during the Early Permian (Figure 4.9), but they have different senses of movement. As discussed previously, faults 2, 3, 4 and 16 (Parrabel Fault) show sinistral, strike-slip movement. Faults 1 (Kunderang Fault), 5-6 (Threadneedle Fault Complex), 8, and 14 have dextral, strike-slip movement.

(5) Group 5 faults consist of faults 21-23, 40-41 and 102-104, which crop out on the southern part of the Parrabel Dome and in the northeastern part of the NHB (Figure 4.9 and Appendix 5 - Figure A20c). The dominant orientation of Fault Group 5 is NW-SE.

The earliest movement on these faults would be in the Late Triassic (Figure 4.9). The reasons for this timing are: (1) Faults 21-23 are part of the Taylors Arm Fault System (TAFS) in the Nambucca Block which are considered to be extensions of the Demon Fault (see Appendix 4) which was active from 233 Ma in the Triassic to Early Jurassic or possibly during all of the Jurassic, (Babaahmadi and Rosenbaum, 2013). (2) Faults 40 and 102-105 cut the Triassic Gundle Pluton and Fault 41 cuts the Werrikimbe Volcanics according to Roberts *et al.* (1995) which constrain the timing of fault movement to be post 226 Ma. Faults in this group were active within the interval Late Triassic from pre-226Ma to possibly the Jurassic (Demon Fault movement) according to Babaahmadi and Rosenbaum (2013).

4.5.2 The latest time faulting could have stopped

The latest time that faulting could have stopped was determined from the age of the oldest rock unit that intrudes, overlaps or cuts the fault (e.g. Werrikimbe Volcanics and Gundle pluton in Figure 4.2) and the cross-cutting relationships between faults.

Five fault groups were identified based on the cessation of movement at different times in the NHB. The different duration times that faults ceased moving is over a period between approximately 5 (Box 4) and 30 million years (Box 2) (Figure 4.10).

(1) Fault Group 1 consists of faults 33, 38-39, 46-47, 50, 52-55 and 58-64 (Figure 4.10, Appendix 5 - Figure A21a). They are mainly located on the southern margin of the Parrabel Dome. The strikes of the majority of faults in this group are NE-SW and NW-SE. Using the conventional fault analysis to estimate the latest time faulting could have stopped, this fault group ceased movement during Early to early Late Carboniferous (Figure 4.10). This timing is before the Late Carboniferous emplacement of the NHB (Schmidt *et al.* 1994). The evidence of the timing for each fault is catalogued in the Table A2.

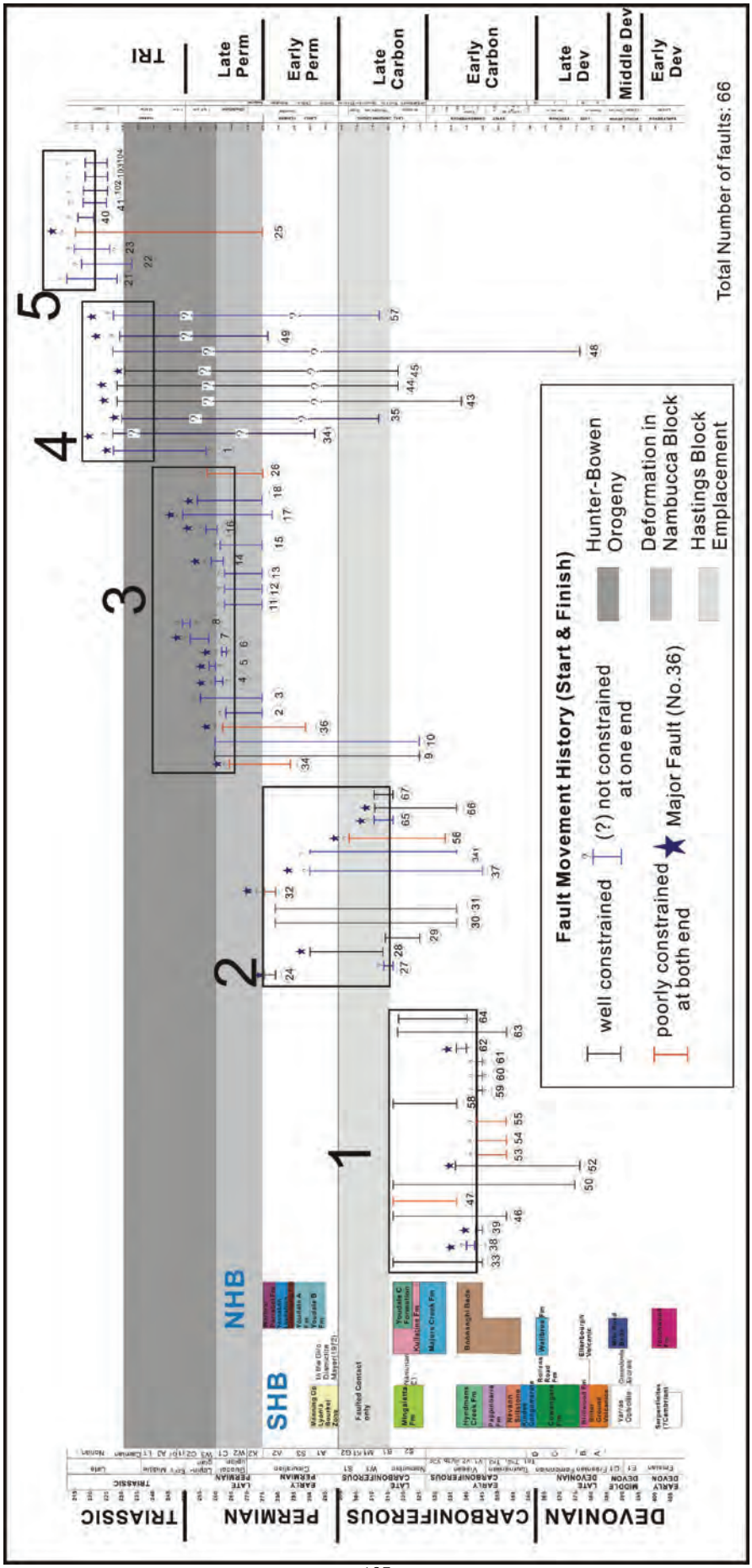
TRI
Late Perm
Early Perm
Late Carbon
Early Carbon
Late Dev
Middle Dev
Early Dev
Total Number of faults: 66
Fault Movement History (Start & Finish)
well constrained
(?) not constrained at one end
poorly constrained at both end
Major Fault (No.36)
Hunter-Bowen Orogeny
Deformation in Nambucca Block
Hastings Block Emplacement
NHB
SHB
TRIASSIC
PERMIAN
CARBONIFEROUS
DEVONIAN

Figure 4.10: Time-space diagram highlighting the cessation of fault movement. All faults which terminated (top of the vertical bar) at approximately the same time are shown within the boxes labelled 1 to 5.

(2) Fault Group 2 is made up of faults 24, 27-32, 37, 56 and 65-67. These faults are located on the southern and eastern margin of the Parrabel Dome (Figure 4.10, Appendix 5 - Figure A21b). The dominant orientations of Fault Group 3 are E-W and NW-SE. The latest time this group could have stopped moving is in the Late Carboniferous to Early Permian (Figure 4.10). This fault group was inactive during and after emplacement of the NHB and before the deformation of Nambucca Block and Hastings Block.

(3) Fault group 3 consists of faults 2-18, 26, 34 and 36, cropping out on the northwestern, northern and northeastern margin of the Parrabel Dome (Figure 4.10, Appendix 5 - Figure A22a). The strikes of the majority of faults in Group 3 are N-S, NE-SW and NW-SE. The latest time of the cessation of fault movement occurred in the Late Permian which is mostly after the time of deformation in the Nambucca Block (Figure 4.10). This indicates that the faults in this group cut mostly cleaved and or folded rocks in the NHB.

(4) The fourth group is composed of faults (faults 1, 34_1, 35, 43-45, 48-49 and 57) on the southwestern and western margin of the Parrabel Dome (Figure 4.10, Appendix 5 - Figure A22b). The dominant orientation of faults in this group is NW-SE. End of fault movement is well constrained to the Late Triassic because many of these fault are cut by the Werrikimbi Volcanics (Figure 4.10 and Appendix 5 - Figure A22b).

(5) Fault group 5 is made up of faults 21-23 (Taylors Arm Fault System), 40-41 and 102-104 (Figure 4.10 and Appendix 5 - Figure A22c). The dominant orientation of faults in this group is NW-SE. Faults 21-23 are considered to be extensions of Demon Fault that was active from 233 Ma in the Triassic to Early Jurassic (or possibly during

all of the Jurassic; Babaahmadi and Rosenbaum,2013). Faults 40 and 102-104 cut the Triassic Gundle Pluton and Fault 41 cuts the Werrikimbe Volcanics according to Roberts *et al.* (1995) which constrains the timing of fault movement to be post-226 Ma. Hence, these faults ceased moving after the Late Triassic (Figure 4.10).

4.5.3 The relationship between faulting and folding/cleavage development

The sequences in the NHB are variably cleaved and folded (Lennox and Roberts, 1988; Roberts *et al.* 1993). When analyzing the fault movement history in the NHB, the relationship between faulting and folding/cleavage development should be taken into account. Shaanan *et al.* (2014) determined that the E-W trending cleavage (S_2) in the Nambucca Block (NB) formed between 275-265 Ma. This cleavage adjacent to the NHB in the NB is S_1 and is folded around the Parrabel Dome (Roberts *et al.* 1993), hence the cleavages developed in the NHB between 275-265 Ma.

Fault groups 3-5 in the above analysis of the latest time faulting are constrained. The latest time of the fault movement for Fault Group 3 occurred in the Late Permian which is after the cleavage formation at 275-265 Ma (Figure 4.10). The cessation of fault movement for Fault Group 4 is well constrained by the Early Triassic volcanics which cut faults in this group constraining the time to be pre-226Ma (Flood *et al.* 1992) (Figure 4.10). By contrast, faults in Fault Group 5 ceased activity after the Late Triassic, because they cut the Triassic volcanics or are the extensions of the Demon Fault that formed post 233 Ma. This indicates that the movement on faults in Fault Groups 3-5 was after 275-265 Ma. Hence these faults were formed and developed after folding and cleavage development in the NHB.

Bourke (1971) studied the upper Kunderang Brook district, located on the northwestern part of the Parrabel Dome (Figures 3.3 and 4.2). The cleaved sequences are cut by the Kunderang Fault (1) and the Threadneedale Fault Complex (5, 6). Hamilton (1980) worked on the Telegraph Point District which is located on the southeast of the Parrabel Dome and north of Port Macquarie Block (Figure 3.3). He considered that faulting was

post-folding because folds are cut by faults (e.g. the Mingaletta Fault (25) and the Telegraph Point Fault (35)). Faults 7-8 and 13-16 (Group 3) cut well cleaved Early Permian sequences.

These observations are consistent with our analysis and support the post-deformation timing deduced above for the cessation of the fault movement.

The latest time of the cessation of movement deduced for Fault Groups 1 and 2, located on the southern and eastern part of the Parrabel Dome (Appendix 5 - Figure A21), is before 275 Ma (Figure 4.10) which is before the commencement of the Hunter Bowen Orogeny at 265 Ma (Cawood *et al*. 2011).

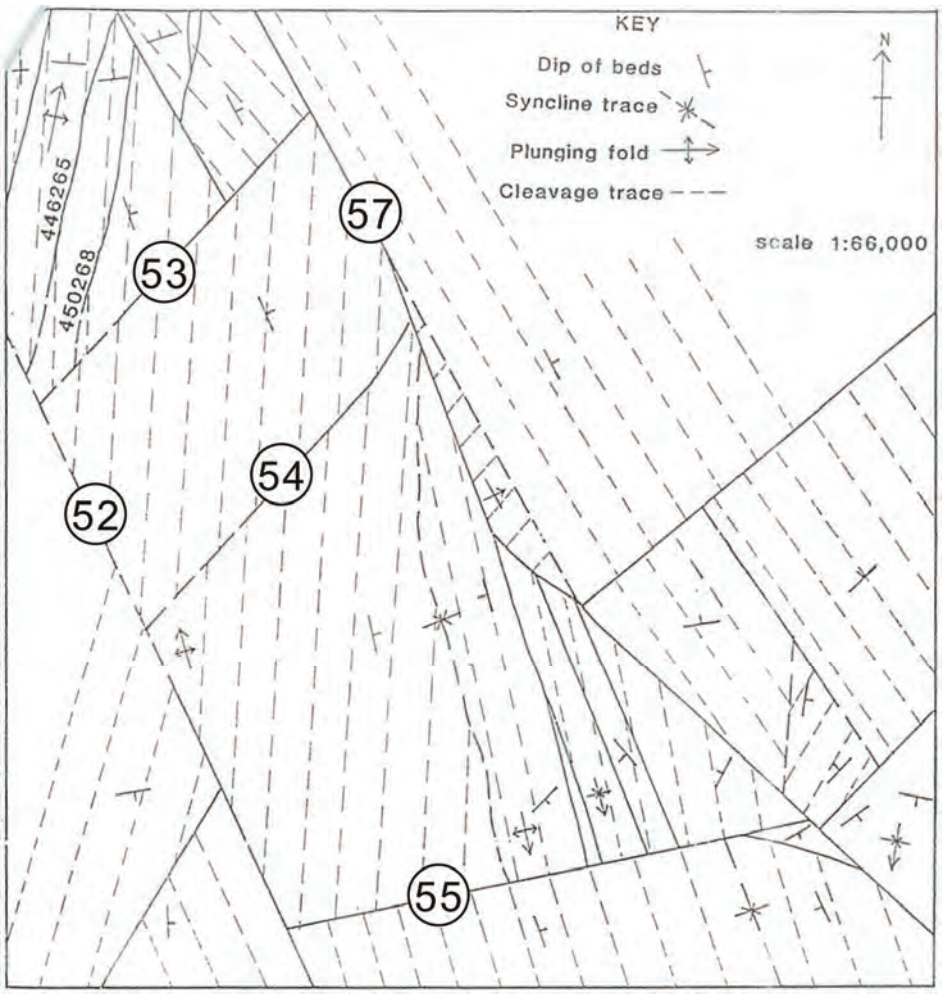

Figure 4.11: Map of Long Flat district show faults displacing the cleaved rocks (Feenan 1984). The fault numbers are as defined in this thesis. Fault 57 is the Bagnoo Fault.

Feenan (1984) carried out detailed mapping in the Long Flat district which is located on the southwest of the Parrabel Dome (Figures 3.3 and 4.11). From the cleavage trace in each blocks, it can be seen that these cleavage traces are apparently different in different fault blocks (Figure 4.11), indicating that the latest time of the cessation for these faults (Faults 52-57) is post 275-265 Ma or these faults were reactivated post 275-265 Ma. Further, in the Pappinbarra district, located on the south of the Parrabel Dome, folding was suggested to be followed by at least two episodes of faulting including Faults 44 (Pappinbarra Fault), 55, 56 (Hastings Fault) and 65 (Thompson 1985, Figure 3.3). This relationship was confirmed by Spackman (1989) in the Byabarra District, south of the Parrabel Dome, who noted that two successive faulting episodes (including Faults 44 (the Pappinbarra Fault), 55, 56 (Hastings Fault), 57 (the Bagnoo Fault), and 65-66) cut the two generations of folding in the region.

On the basis of these observations we can assume that Faults 24, 27-33, 37-39, 50, 58-64 and 67 developed post-folding/cleavage development.

4.6 Discussion

4.6.1 The earliest time faulting could have started

Five groups of faults consisting of faults which commenced moving at different times have been recognized in the Northern Hastings Block (Appendix 5 - Figures A7 and A8). The first group trends dominantly NW-SE and NE-SW and occur in the southwestern part of the Hastings Block and developed in the Late Devonian (Appendix 5 - Figure A19a). These were followed by NE-SW and NW-SE trending faults of the second group that developed from the Early Carboniferous (Appendix 5 - Figure A19b). Group 3 were initiated in the Late Carboniferous (Appendix 5 - Figure A20a), on the southwestern and southeastern margin of the Parrabel Dome. This group is predominantly orientated NW-SE. The earliest time of movement of faults in Group 4 (mainly N-S and NW-SE

orientations) was during the Early Permian (Appendix 5 - Figure A20b). This group is on the northwestern, northern and eastern part of NHB and surround the Parrabel Dome (Figure 4.9 and Appendix 5 - Figure A20b). In the final event, possible extensions of the Demon Fault in the northeastern part of the Northern Hastings Block started moving post-226 Ma and others in Group 5 cut the Triassic volcanics and granites (Appendix 5 - Figure A20c).

4.6.2 The latest time faulting could have stopped

Five groups of faults have been recognized based on the latest time faulting could have ceased movement. Fault groups 3-5 have better constraints on the cessation of fault movement. Fault Group 3 crops out on the northwestern, northern and northeastern margin of the Parrabel Dome, oriented variously N-S, NE-SW and NW-SE (Appendix 5 - Figure A22a), and stopped moving during and after the cleavages/folding development in the NHB. Fault Group 4, dominantly striking NW-SE, located on the southwestern and western margin of the Parrabel Dome (Appendix 5 - Figure A22b), are cut by the Triassic Werrikimbi Volcanics. Thus the end of fault movement is well constrained to be in the Late Triassic. Fault Group 5 (NW-SE orientation) ceased activity after the Late Triassic because they cut the Triassic volcanics or are extensions of the Demon Fault (faults 21-23, Appendix 4).

The cessation of movement for Fault Groups 1 and 2, located on the southern and eastern part of the Parrabel Dome, are poorly constrained because of the lack of the evidence of the relationship between the faulting and cleavage/folding development. Feenan (1984) showed that faults 52-55 (Group 1) and 57 (Group 4) cut cleaved country rocks. Thompson (1985) and Spackman (1989) showed that faults 55 (Group 1), 56 and 65-66 (Group 2) cut the folded rocks, thus these faults are post-folding. This is contrary to the Early to Late Carboniferous cessation of movement previously deduced. It suggests Faults 52-56 and 65-66 may have been re-activated after cleavage and fold

formation, or that they only developed in the Late Permian.

4.6.3 Faults with a common strike

Faults in the NHB are mainly oriented in four main directions (NE-SW, NW-SE, N-S and E-W). In each of the five fault groups based on timing of movement that the earliest time faults could have started moving and the latest time faults could have stopped, the faults differently oriented. Hence, it is clear that faults of one orientation did not format the same time.

The NW-SE faults were active over a long period of time. The NE-SW faults which are less common than NW-SE faults also moved over a long period of time. Similarly, the N-S and ENE-WSW faults were also active during different periods of time. It confirms that faults of similar orientation do not form and are not active at the same time. Instead they were active during different periods of time.

4.6.4 Implication of fault movement analysis

In terms of the earliest time faulting could have started, from the areal pattern, we find that faults in the Northern Hastings Block progressively commenced moving from the southwestern part to the northern part of Parrabel Dome (Figure 4.12a). Lennox & Roberts (1988) and Roberts *et al.* (1993) implied that the uplift in the latter part of the Late Carboniferous took place throughout the HB prior to deposition of sediments in the Early Permian. The Hastings Block, was translated northwards during the Late Carboniferous between major faults (Schmidt *et al.* 1994). The NHB was simultaneously rotated either 130° clockwise or 230° anticlockwise (Schmidt *et al.* 1994); and juxtaposed against subduction complex rocks. Fault Groups 1 – 2 shown in red in Figure 4.12a could start moving very early during the Devonian to late Early Carboniferous. Fault Group 3 (mainly striking NNW-SSE, shown in yellow in Figure 4.12a) may have been active during this emplacement. Fault Group 4 shown in green on

Figure 4.11a became active after the translation and emplacement of the NHB into its current position (Early Permian, Schmidt *et al.* 1994). This group could be related to the accommodation of the NHB during Texas-Coffs Harbour Orocline formation with consequent N-S shortening of the Nambucca Block and adjacent NHB (Figure 4.12).

In terms of the latest time faulting could have stopped, our fault analysis showed that faults in the NHB progressively stopped moving from the southwestern to the northwestern part of Parrabel Dome (Figure 4.12b). Fault Group 1 shown in red colour but obscured under the green colour in Figure 4.12b, located on the southwestern part of Parrabel Dome, stop moving prior to the Late Carboniferous emplacement of NHB. Fault Group 2 (shown as yellow colour but partly obscured) was terminated during the Late Carboniferous emplacement. Subsequently, the NHB was translated to its current position, and the Parrabel Dome acted as an massif. As a result of the southward push of the Coffs Harbour Orocline, deformation took place in the Nambucca Block and the boundary between the NHB and Nambucca Block. Fault Groups 3 and 4 (shown in green in Figure 4.12b), located on the eastern to northern part of Parrabel Dome stopped moving during deformation (folding and cleavage development) of the Nambucca Block and before the Triassic volcanics intrusions. This group is likely to be related to the accommodation of the NHB to the Hunter-Bowen Orogeny (Cawood *et al.* 2011). Fault Group 5 which cut the Triassic granitoids and are extensions of the Demon Fault (shown in blue in Figure 4.12b) moved from Middle Triassic to early Jurassic. The majority of faults in NHB stopped moving after 265 Ma (folding and cleavage development), indicating that the brittle failure replaced more ductile failure during Hunter-Bowen Orogen in the NHB.

Overall, some of faults on the southern part of the Parrabel Dome were active and ceased moving pre-emplacement of the HB. This may provide a clue for the position of the boundary between NHB and Southern Hastings Block (SHB). The faults on the southwestern and eastern part of the Parrabel Dome initiated and stopped moving

during Late Carboniferous emplacement. The Yarras Fault System (Taylors Creek Fault, Cowarral Fault and others) is currently on the southwestern side of the Parrabel Dome and the Parrabel Fault (and related faults) is on the eastern side of the Parrabel Dome. These two fault systems are the two major fault systems bounding the rotating NHB and are believed to be active during the emplacement. Faults on the eastern, northeastern and northern part of Parrabel Dome initiated and ceased moving after emplacement and before granitoids instrusion. These faults are related to the accommodation of the NHB due to the folding and cleavage development in the adjoining Nambucca Block. Finally, dextral movement on a southern extension of the Demon Fault occurred in the northeastern part of the NHB from the Late Triassic.

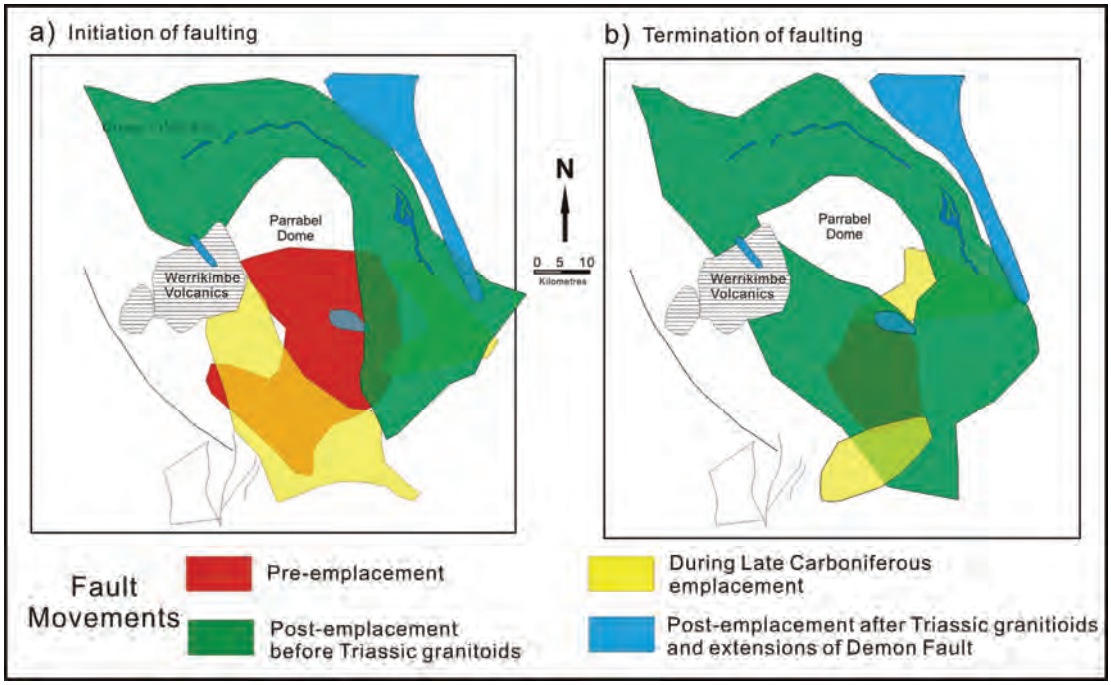

Figure 4.12: Map pattern of the fault movement (initiation and termination) for faults clustered according to whether they move prior to emplacement (red), during emplacement (yellow), post emplacement and pre-Triassic granitoids (green) and post-granitoids (blue). a) red – Group 1 and 2, yellow – Group 3, green – Group 4 and blue – Group 5; b) red – Group 1, yellow – Group 2, green – Group 3 and 4 and blue – Group 5.

4.6.5 Geological history of the Northern Hastings Block

This analysis of the fault movement history provides key information related to the

emplacement of the NHB and the probable boundary between the NHB and SHB. Initially, the NHB was probably located southeast of its current position (Schmidt *et al.* 1994). At this time, the forearc-subduction accretion complex was gently curved (Figure 4.13a and 13f, Schmidt *et al.* 1994).

During the Late Carboniferous, the NHB was transported into its current position by left lateral (sinistral) movement between the major faults prior to uplift, variable erosion and then deposition of sediments on the forearc packages in the Early Permian. The NHB was simultaneously rotated 230° anticlockwise into its current position (Figure 4.13a, Schmidt *et al.* 1994; Crowell 1985). It is possible to argue for 130° of clockwise rotation if you accept that the deformation observed along the faults (and in the serpentinite) relates to post-emplacement affects (Lennox & Offler 2009). The Parrabel Fault (and related faults) and the Yarras Fault System (Taylors Creek Fault, Yarras Mountain Trail Fault, Ralfes Creek Fault and Cowarral Fault) could be part of these two major fault systems bounding the rotating NHB. The Parrabel Fault and the faults making up the Yarras Fault System show sinistral strike-slip or oblique-slip movement (Lindsay 1969; Lennox and Offler, 2009; Lennox and Offler, unpubl.). The faults on the southwestern and eastern sides of the Parrabel Dome are thought to be related to the emplacement of NHB (Figure 4.13b – red area). During anticlockwise rotation of the NHB, faults on the western side of the block would be subjected to sinistral strike-slip movement (Figure 4.13a).

After emplacement of the Hastings Block, the forearc-subduction accretion complex was folded as a result of dextral movement on a major shear to the east of the HB producing the Texas-Coffs Harbour Orocline (Offler and Foster 2008). This caused the compression of the Nambucca Block and adjacent NHB (Figure 4.13c and 13f). The NHB is deformed in its current position, and the Parrabel Dome made up of more competent units than the NB acted as a massif. Simultaneously, as a result of the southward push of the Coffs Harbour Orocline, deformation took place in the

Nambucca Block (Figure 4.13c) and along the boundary between the NHB and Nambucca Block. Subsequently, E-W shortening associated with the Hunter-Bowen Orogeny (HBO) resulted in folding and faulting especially in the Southern Hastings Block. Faults on the eastern, northeastern and northern part of Parrabel Dome continued moving after the Late Carboniferous emplacement of the NHB and ceased moving during the accommodation of the NHB to continuing deformation in the Nambucca Block (Figure 4.13d). These faults may be associated with the Hunter-Bowen Orogeny.

Finally the emplacement of post tectonic granitoids and rhyolitic volcanism took place in the Late Triassic which cut those faults related to the emplacement of the NHB. From the Late Triassic, dextral movement on a southern extension of the Demon Fault caused limited faulting in the northeastern part of the Northern Hastings Block (Figure 4.13e).

The formation of the Hastings Block is not because of the large-scale 'oroclinal' folding in the Manning and Hastings area as suggested by Cawood *et al*. (2011); Rosenbaum *et al*. (2012); Glen & Roberts, (2012) and Li *et al*. (2014). The reasons include: (1) the serpentinites are not as continuous as required to wrap around the Hastings Block but rather form pod-like bodies near and sometimes away from the block boundary. The ages of the serpentinites and associated protoliths have not been established to be the same; (2) the NHB plunges gently NW and is not steeply plunging as expected for an orocline; (3) No hinge zone can be established for the Manning Orocline either near Mt. George (Yan *et al*. 2012; Lennox *et al*. 2013) or near Walcha (Lennox *et al*. 2014; Offler *et al*. 2014). The hinge zone near Mt.George do not define a steeply-plunging macroscopic fold as expected for an orocline; (4) Mapping by Laurie (1976) indicates that the Devonian to Carboniferous sequences south and southeast of the Mt George area are disrupted by N-S, NNE, E-W and NW-trending faults. Bedding within the fault-bound blocks south of Mt. George do not define an oroclinal structure, rather steeply-dipping, homoclinal sequences of varying orientation and uncommon N-S, NW and E-W gently plunging folds.

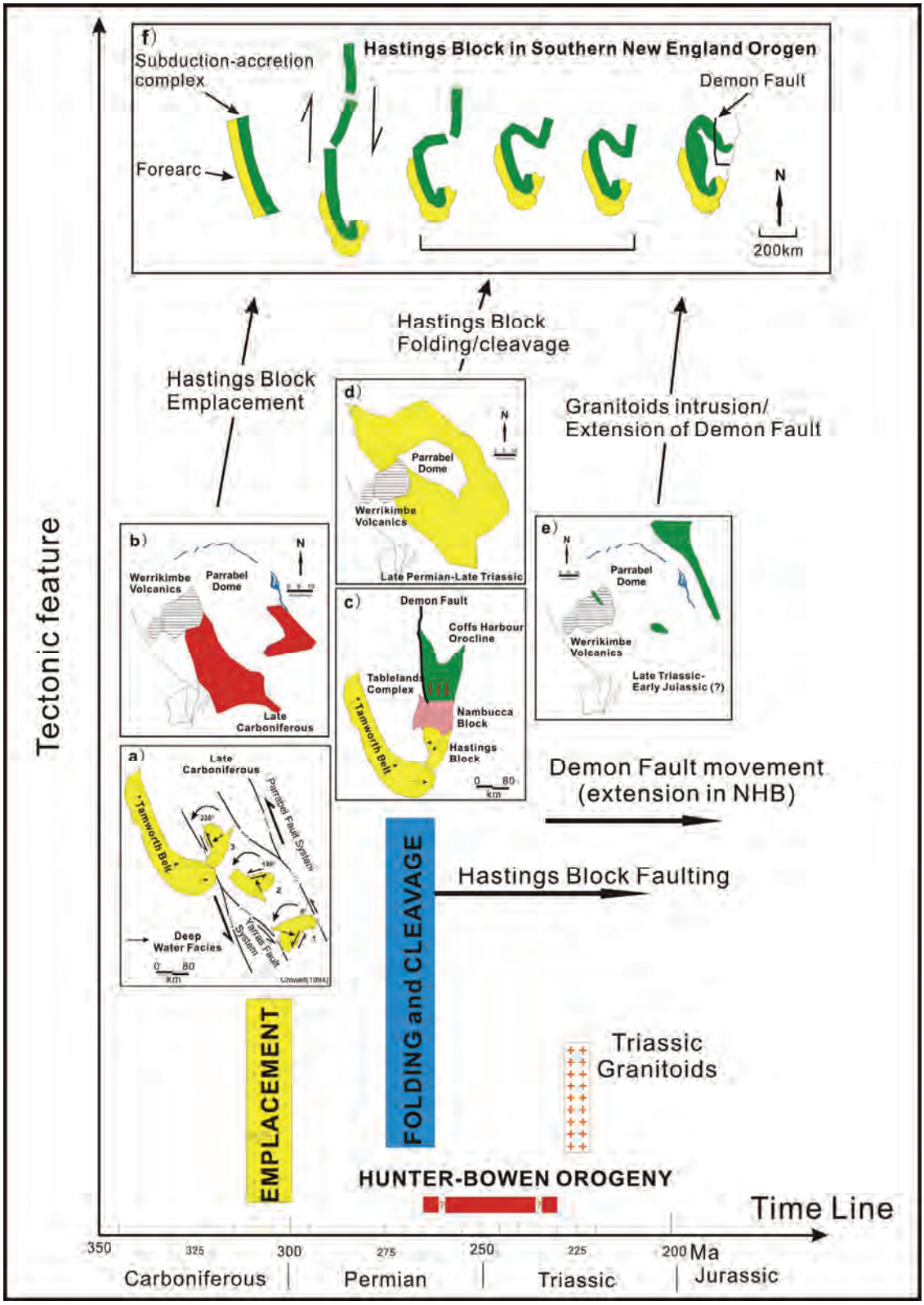

Figure 4.13: Schematic diagram of the geological history of the Northern Hastings Block showing a time line with major events in vertical or horizontal columns. (a) Sketch of the method of emplacement; (b) areas in red where faults were active during emplacement; (c) regional tectonics during folding/cleavage formation; (d) areas shown in yellow of

contemporaneous fault movement (post emplacement, pre-Triassic granitoids); and (e) areas shown in green of fault movement post granitoid intrusion. The schematic diagram (f) shows the initially gently curved forearc-subduction accretion complex being dextrally sheared after NHB emplacement to form the Texas-Coffs Harbour Orocline with compression of the Nambucca and adjacent NHB (275-265 Ma), followed by Late Triassic-Early Jurassic (?) development of the Demon Fault and its extensions such as the Taylors Arm Fault System in the Nambucca and adjoining NHB. The arrows under (c) and (e) shows the time span of the faulting in Hastings Block and the Demon Fault.

The NHB was transported northward into its current position by the sinistral strike-slip movement between the two major fault systems (the Parrabel Fault (and related faults) and the Yarras Fault System), not along one major sinistral strike-slip fault (Cawood 1982). Our model invokes the 230° anticlockwise rotation during the northward transportation of the NHB (Schmidt *et al.* 1994) and the compression of the Nambucca Block and adjacent NHB during the Hunter- Bowen Orogeny (Johnston *et al.* 2002).

Cao and Durney (1993) observed an increase in F_1 fold development towards the Peel Fault near Manilla, NSW. They considered that folding and high angle reverse motion on the Peel Fault occurred during contractional D1 deformation. Cao and Durney (1993) observed S_2 cleavage oblique to the Peel Fault increasing in intensity towards the fault. They considered cleavage development and sinistral strike-slip movement occurred at the same time. Extensions of the Peel-Manning Fault are believed by some researchers to form the western margin of the Hastings Block hence its deformation history is significant. Leitch and Lara (2000) observed F_1 N-NW plunging folds with slaty cleavage subparallel to faults and F_2 at a high angle to F_1 and producing bending of F_1 hinge trace and associated faults. They considered that F_2 folding and sinistral movement on NW to NNW striking faults occurred at the same time. It is possible that the N-S (S_2) and NW-SE (S_3) cleavage identified in the Kindee area may have formed during movement on nearby faults (Bagnoo Fault and Rollans Road Fault). Both cleavages are present throughout the Yarras to Kindee districys and do not noticeably increase in intensity near the faults. This may indicate that cleavage development was

not associated with fault movement but rather relates to imposition of a stress field across a larger region unrelated to the stress field associated with fault movement.

4.7 Conclusions

The NHB is folded and intensively faulted. Each fault in the NHB was analysed systematically to estimate the time of movement of faults (the earliest time faulting commenced and the latest time it ceased). Faults of similar orientation do not form and were not active at the same time. The majority of faults cut the folds and cleavages in the NHB and hence moved post 265 ma.

Five episodes of faulting are identified both based on the earliest time faulting could have begun and the latest time of cessation. The majority of faults in the NHB were active after folding and cleavage development. However, faults on the southwestern and eastern margin were active and ceased moving during the Late Carboniferous emplacement of the NHB. The Yarras Fault System on the southwestern side and the Parrabel Fault (and related faults) on the eastern side are believed to be the two major fault systems responsible for the (rotating) NHB during the emplacement in the Late Carboniferous. Faults on the eastern, northeastern and northern part of Parrabel Dome, (dominantly N-S, NNW-SSE and NNE-SSW orientations) started and stopped moving after emplacement and before granitoids instrusion. This movement is probably related to the accommodation of the NHB due to the folding and cleavage development in the adjoining Nambucca Block, and associated with the Hunter-Bowen Orogeny (Appendix 5 - Figures A8b and A10a). Finally, dextral movement on a southern extension of the Demon Fault caused some minor fault movement in the northeastern part of the NHB from the Late Triassic and some small faults cut the Triassic granitoids.

Chapter 5 Evidence from Fault Block Analysis for a re-interpretation of the Northern Hastings Block geology

5.1 Introduction

This study re-interprets a variety of geological data and from this we have constructed a 3D model fault-block by fault-block based on the comprehensive bedding data available from each fault block. This has highlighted shortcomings with the existing Roberts *et al.* (1995) geological map of the Northern Hastings Block. These include the variability in the orientation of bedding within some fault blocks, between adjacent fault blocks, and around significant sections of the dome. There is also incorrect positioning of some faults as they are of the wrong length or may not exist in the position proposed. A new geological map is needed in line with this fault block analysis. Standard QFL and QmFLt diagrams are used for plotting framework modes of sandstones to determine their provenance in terms of the tectonic scheme. QFL analysis of the sandstones from key formations was used to try to establish a link between fault blocks containing the same formation. The gravity and magnetic worms for the Hastings Block covered by geological map of Roberts *et al*. (1995) were used to define the dips of structures and their continuity both at depth and along strike. A different geological boundary between the NHB and SHB is proposed based on the evidence from the gravity and magnetic worms for this region.

This study proposes a series of the schematic reconstruction models with either clockwise or anti-clockwise rotation via strike-slip faulting to explain the map pattern of arrangement of fault blocks within the Northern Hastings Block (NHB). It is designed to provide a template for unravelling other comprehensively mapped, complexly folded, extensively faulted geological sequences. It will aid block reconstruction in the Tamworth Belt and provide a link to the tectonics of this part of the southern New

England Orogen. It is believed that this workflow will be widely applicable in the other areas such those undergoing hydrocarbon exploration, hard rock mining and groundwater studies.

5.2 Geological setting

The Hastings Block is a large faulted-bounded block (approximately 3000 km^2 in area), consisting of mainly Devonian to Carboniferous rock sequences, and an overlying Early Permian cover sedimentary sequence. Major faults on the margins juxtapose the Hastings Block with the Early Permian successor sediments against the Parrabel Fault in the northeast, against the subduction complex rocks of the Yarrowitch Block to the west (Leitch *et al*. 1990), and Devonian-Carboniferous sediments of the Myall Block of the Tamworth Belt (Roberts & Engel 1987; Roberts *et al.* 1991) to the south along the Manning Fault System (Figure 5.1c).

There are 20-30 major faults of 10-30 kilometre length cutting the Northern Hastings Block sequences with the majority having northwest to northnorthwest strikes. Previous honours studies and research in this area dealt with some major faults such as the Kunderang fault (Bourke 1971), Yarras Fault System (Leitch 1990; Jayko *et al.* 1993) and Parrabel Fault (Lindsay 1969). Lennox *et al.* (1999) and Roberts *et al*. (1993) address the timing and movement sense of key faults groups of common strike. Lennox and Offler (2009) used serpentinite structures (S, C, C') in major faults bounding the Hastings Block to determine the movement history and show predominant sinistral strike-slip histories for faults on the western margin of the Hastings Block. Glen & Roberts (2012) reinterpreted the Hastings Block and suggested the Parrabel Dome is a hangingwall anticline above an east-dipping thrust system represented by the Bagnoo Fault and its inferred extensions (Rollans Road Fault and Pappinbarra Fault) with a component of left-lateral movement. To aid discussion, all the faults in the NHB are numbered (Figure 5.2).

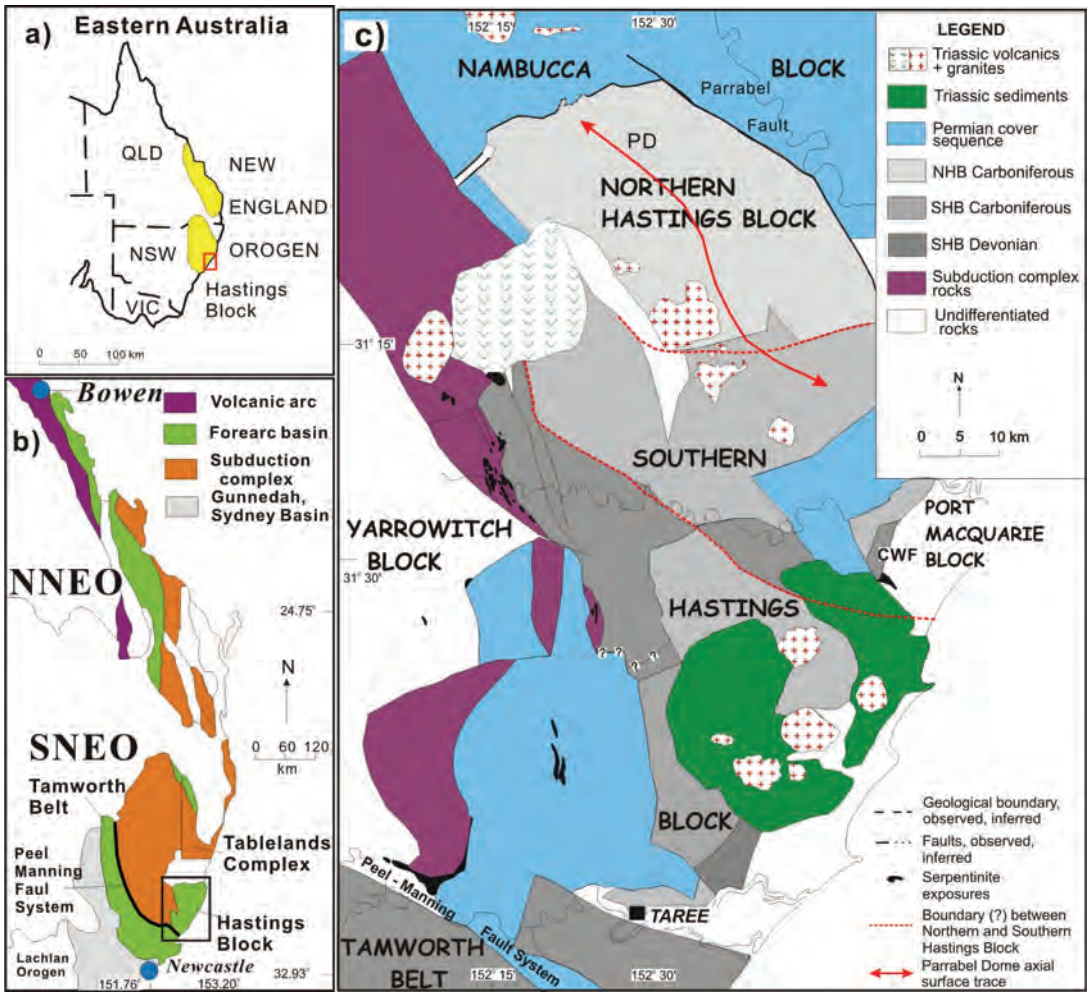

Figure 5.1: Location and tectonic setting of the Hastings Block, (a) within eastern Australia, (b) within the southern New England Orogen (NEO); NNEO = Northern NEO, SNEO = Southern NEO. (c) Major tectonic units and faults within and adjacent to the Hastings Block (simplified from Roberts *et al*. 1995). CWF = Cowarra Fault; PD = Parrabel Dome. The northern red dashed line is the NHB-SHB boundary proposed by Roberts et al. (1995) whlist the southern dashed red line is the NHB-SHB boundary suggested by Glen and Roberts (2012).

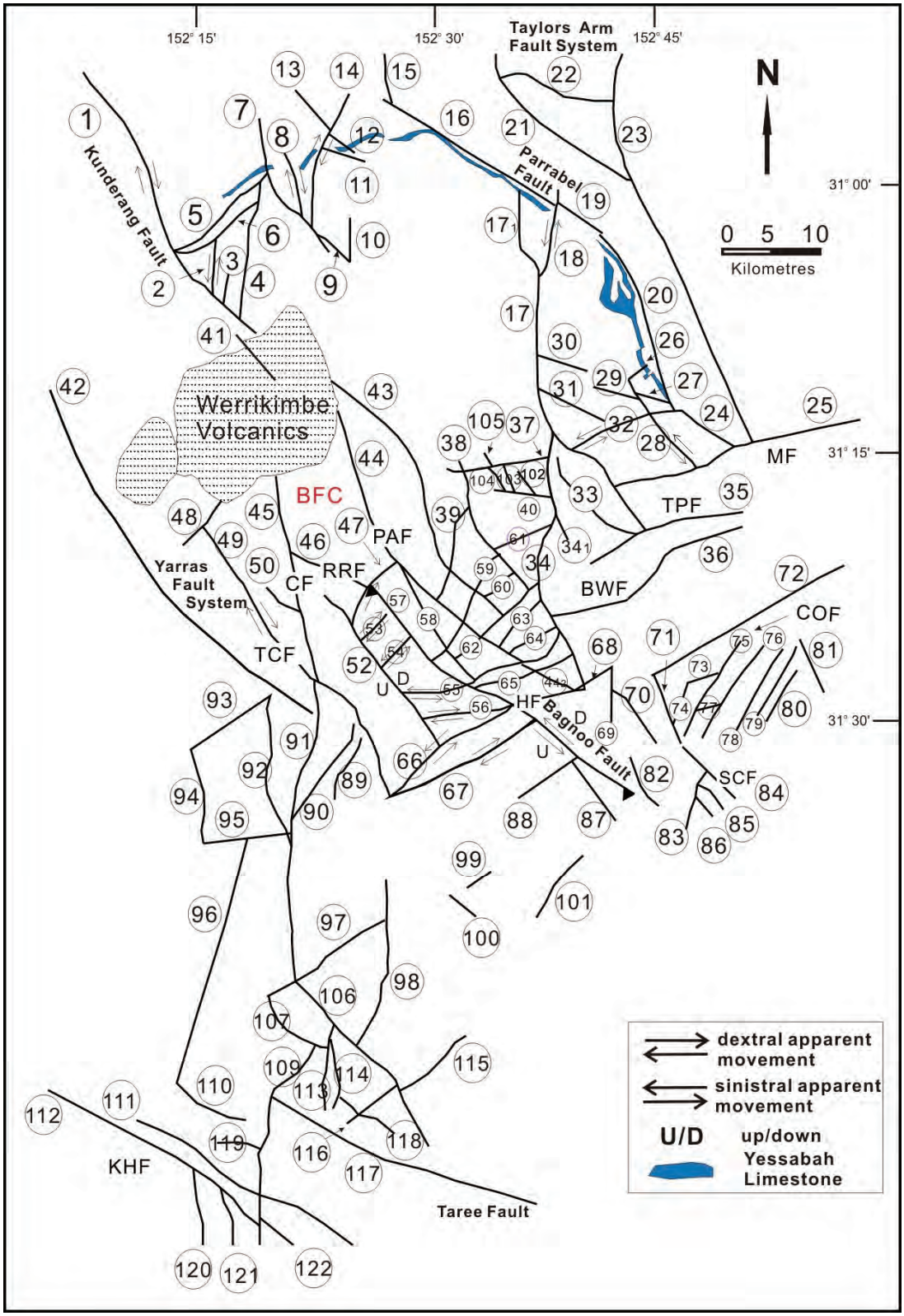

Figure 5.2: Map showing all faults in the Northern Hastings Block and part of the Southern Hastings Block based on Roberts *et al*. (1995). BFC = Birdwood Fault Complex; BWF = Beechwood Fault; COF = Cowarra Fault; CF = Cowarral Fault; HF = Hastings Fault; KHF = Khanghat Fault; MF = Mingaletta Fault; PAF = Pappinbarra Fault; RRF =

Rollans Road Fault; TCF = Taylors Creek Fault; TPF = Telegraph Point Fault; SCF = Sapling Creek Fault.

5.2.1 Fault Systems

There exists some key fault complexes such as the Bagnoo Fault and related extensions, Birdwood Fault complex, Threadneedle Fault Complex in the Kunderang Brook region, Yarras Fault Complex, Parrabel Fault and extensions and Taylors Arm Fault System in the Northern Hastings to Nambucca Blocks (Figure 5.2).

(1) The Kunderang Brook region consists of Fault 1 (Kunderang Fault), Fault 2 (Surveyors Fault), Fault 3 (Kennys Fault) and Fault 4 (Mooraback Fault) and the Threadneedle Fault Complex, located on the northwestern limb of the Parrabel Dome (Figure 5.2 – Faults 1-6). Fault 1 (Kunderang Fault) is considered to have undergone dextral strike-slip movement (Bourke, 1971). Fault 2 (Surveyors Fault), Fault 3 (Kennys Fault) and Fault 4 (Mooraback Fault) showed apparent sinistral strike-slip movement (Bourke 1971). The Threadneedle Fault Complex consists of faults 5, 6 and other small faults between them orientated overall at 90° to the Kunderang Fault (Bourke 1971). Bourke (1971) indicated that all these faults in the complex have a dextral strike-slip component of movement. Fault 2 may be a conjugate fault to the Kunderang Fault. The Threadneedle Fault Complex truncates faults 2, 3 and 4 and thus its final movement is younger than movement on these faults.

(2) The Birdwood Fault Complex consisting of faults 44-47 bounds east-west striking sequences younging to the north which are right angles to the general north-south striking, east-younging sequences either side of the complex (Figure 5.2 – see BFC). It is located on the southwestern flank of the Parrabel Dome. The Rollans Road Fault (46) forms the southern side of the Birdwood Fault Complex. The Rollans Road Fault is cut by the Cowarral Fault (45) which in turn is cut by the Werrikimbi Volcanics. These cross-cutting relationships indicate the Rollans Road Fault must have finished moving

prior to 226 Ma. Fault 44 (Pappinbarra Fault) is suggested to be a west-dipping thrust, partly against early Permian strata (Glen & Roberts, 2012), but there is no field evidence for this dip or indication that it had undergone thrust movement (Lennox *et al.* 2013).

(3) The Bagnoo Fault is a major sinistral, strike-slip, northwest-trending fault (Feenan 1984; Spackman, 1989; Roberts *et al.* 1993), approximately 60 km in length (Figure 5.2). It continues into the Lorne Basin where it displays a significant downthrow on the northern side (Pratt 2010). The bedding is vertical adjacent to the Bagnoo fault (BF) and some N-S trending faults nearby terminate faults that are parallel to the BF (Pratt, 2010). Glen & Roberts (2012) suggested the Bagnoo Fault and its inferred extensions to the north are part of a major east-dipping, thrust with northeast-over-southwest direction of movement. Previous studies (Spackman 1989; Roberts *et al* 1993) do not support the northeast-over-southwest movement suggested by Glen & Roberts (2012). The fault movement on the Bagnoo Fault (and its extension possibly as the Pappinbarra Fault) must have terminated pre-226 Ma (Rb-Sr age for Werrikimbe Volcanics, Flood *et al.* 1993). Field observations show the Kindee Conglomerate outcropping south of the Bagnoo Fault changes orientation from N-S to NW adjacent to the fault indicating sinistral strike-slip movement on this fault with dragging and reorientation of the conglomerate (Figure 5.3).

(4) The Parrabel Fault (faults 16, 19, 20 and 24) is a major siniatral, strike-slip fault in the NHB containing low temperature mylonites (Lindsay 1969; Lennox and Offler unpubl.). It may to be bent by the NE-SW oriented folds as the northern part of Parrabel Fault (16, 19 and 20) trends WNW-ESE and the southern part trends NNW-SSE (Figure 5.2). Alternatively the bending of the trace of the Parrabel Fault may reflect clockwise rotation of the northeast limb of the Parrabel dome after fault formation (Figure 5.2). Fault 17 is similarly bent by the NE-SW oriented folds at its southern end.

(5) The Yarras Fault Complex consists of the Taylors Creek Fault, Yarras Mountain Trail Fault, Ralfes Creek Fault and Cowarral Fault on the southwestern side of the Parrabel Dome (Figure 5.2). They are dominantly northerly to northwesterly striking and show strike-slip or oblique-slip movement with a small to moderate reverse component of displacement (Jayko *et al.* 1993). Lennox and Offler (2009) showed that serpentinite structures (S, C, C') in these faults display dominantly sinistral strike-slip or oblique-slip movement. The Cowarral Fault is cut by the Werrikimbi Volcanics constraining movement to be pre-226 Ma (Figure 5.2).

(6) The Taylors Arm Fault System is made up of dominantly NNW striking transcurrent faults in the Nambucca Block and the northeast margin of the NHB (including faults 21-23, Figure A17 and A18). Right lateral displacement of up to several kilometres has occurred on these faults which displaced folds D_1 - D_5 in the Nambucca Block (Leitch 1978). The Taylors Arm Fault System is considered to be an extension of the Demon Fault (Appendix 4). This fault was active from 233 Ma in the Triassic to Early Jurassic (or possibly during all of the Jurassic) according to Babaahmadi and Rosenbaum (2013). The Demon Fault is a major transcurrent fault in the New England Orogen with about 23km of dextral strike-slip movement on its northern end (McPhie and Fergusson, 1983) and up to several kilometers on its southern end (Leitch 1978).

5.3 Methodology

This study divides the Northern Hastings Block into fault blocks based on an interpretation of the geological map of Roberts *et al*. (1995) (Figure 5.3). Each fault block represents a small region bounded by faults between approximately 25 km^2 (Fault Block A) and 200 km^2 (Fault Block D) in size. Each fault block is labelled from A to K for convenience (Figure 5.3).

This study integrates the interpretation of a variety of geological data, computer modelling of fault blocks, computer visualisation of model results and restoration of

blocks using paper models.

The Northern Hastings Block was comprehensively mapped and the thousands of surface measurements of bedding, cleavage and fold characterictics provide details on the shape of the geological surfaces. This study catalogued and rectified the primary bedding data and used them to construct the bottom 3D geological surfaces of each formation within each fault block. The primary bedding data are those: (1) which represent the overall trends and strikes of the bedding surface in the area, and exclude those bedding readings which have been refolded more than once; and (2) are located at the contact between the two formations. In some cases, the bedding data that are located very close to the faults will not necessarily reflect the overall trends and strikes of bedding because of fault drag. The dips and strikes of this bedding data close to fault would be quite similar to those of the fault. These bedding data were not chosen as the primary bedding data.

The software packages Leapfrog Geothermal, Mathematica and 3D Move were used in this study as these companies kindly provided free access. The Leapfrog Geothermal software is used to visualise 3D bedding data and create 3D fault surfaces. Mathematica is used to project the field and map data and construct the 3D horizontal surfaces. 3D Move will then load in the surfaces from the output of Leapfrog and Mathematica, and use its own interpolation facilities to produce a 3D model (www.mve.com).

The QFL and QmFLt diagrams are used for plotting framework modes of sandstones to determine their provenance in terms of the tectonic scheme.The QFL analysis of the sandstones from key formations was used here to try to establish the links between fault blocks containing the same formation.

The map showing the gravity and magnetic worms for the Hastings Block covered by geological map of Roberts *et al*. (1995), are generated from the upward continuation of

the gravity and aeromagnetic data. The significant gradients in both gravity and magnetic data mirror the dips of structures and their continuity both at depth and along strike.

Restoration using paper maps along key faults will provide some key clues about the likely movement history of blocks in the Northern Hastings Block.

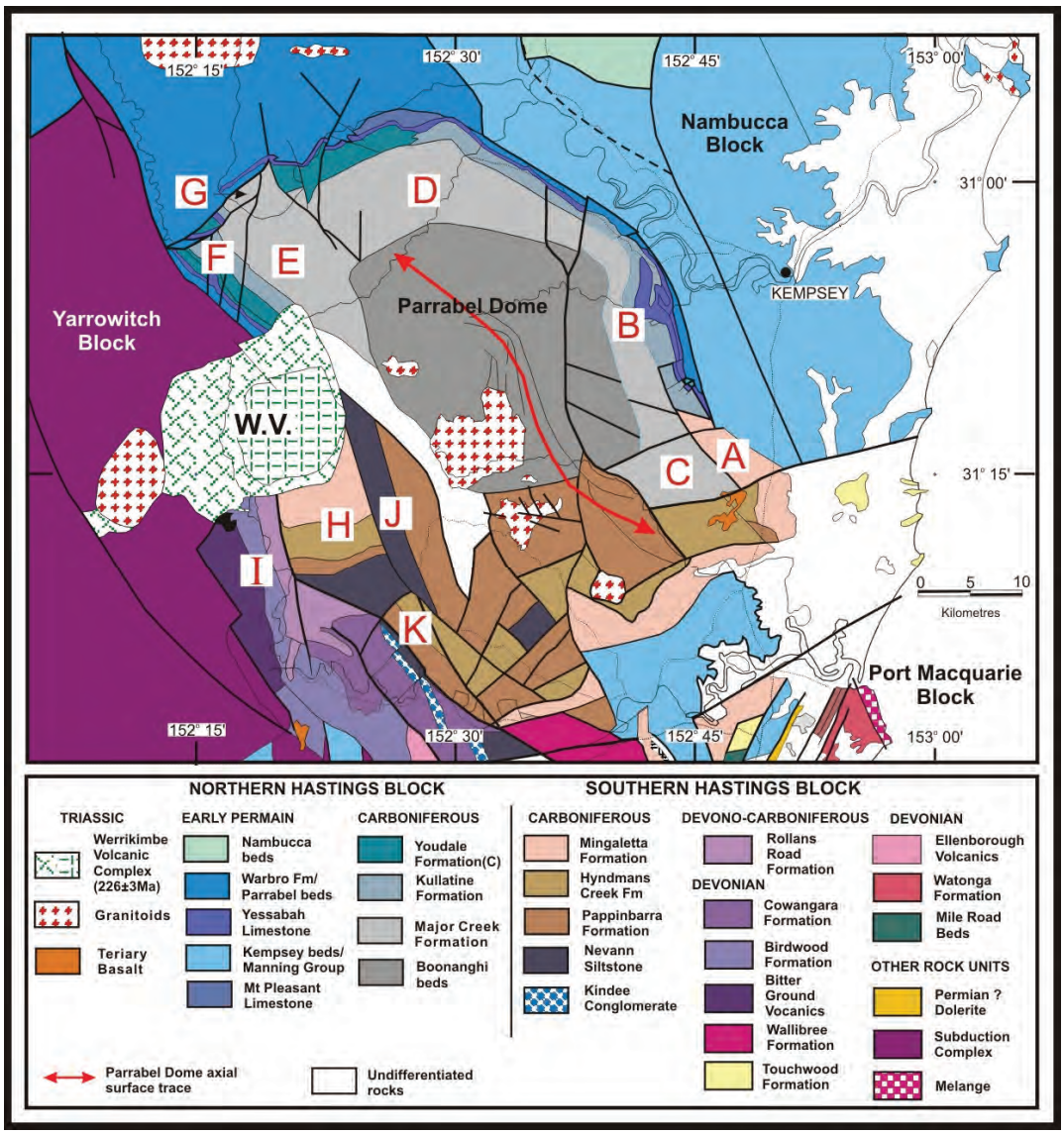

Figure 5.3: Geological map of the Northern Hastings Block with letters identifying the various fault block. W.V. = Werrikimbe Volcanics.

5.4 QFL analysis of the sandstone composition in the NHB

5.4.1 Introduction

The composition of source rocks has a great influence on the ultimate composition of sandstone. Dickinson and Suczek (1979) and Dickinson *et al*. (l983) indicate that the detrital modes of sandstone can be used to provide information about the tectonic setting of basins of deposition and associated provenances. The compositional variations among sandstones can be displayed as ternary plots on triangular diagrams. Three apices will represent recalculated proportions of key categories of grain types.

In this section, standard QFL and Q_mFL_t diagrams are used for plotting framework modes of sandstones to determine their provenance in terms of the tectonic scheme. The derivation of sandstones are mainly from provenance terranes within three fields including continental blocks, magmatic arcs and recycled orogens. Each of these three main fields is further divided into three subfields representing variants of the main provenance classes (Figure 5.4). The definition of the apices in the QFL and Q_mFL_t diagrams are explained in Table 5.1. Because of the virtual absence of polycrystalline quartz in samples from the Hastings Block, QFL diagrams are almost equivalent to Q_mFL_t diagrams in this instance.

Table 5.1: The grain parameters in QFL and Q_mFL_t (modified from Graham *et al*. (1976)).

(a)	$Q = Q_m + Q_p$	where	Q = total quartzose grains
			Q_m = monocrystalline quartz grains
			Q_p = polycrystalline aphanitic quartz grains
(b)	F = P + K	where	F = total feldspar grains
			P = plagioclase feldspar grains
			K = potassium feldspar grains
(c)	$Lt = L + Q_p$	where	L_t = total polycrystalline lithic grains + quartzose varities
			L = unstable polycrystalline lithic grains

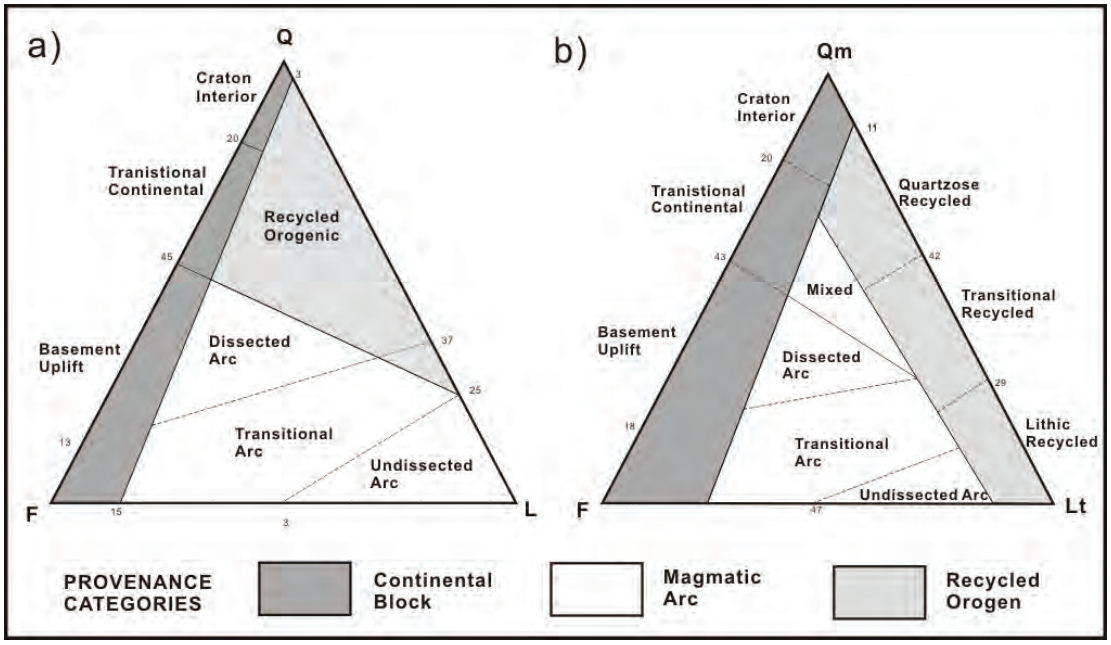

Figure 5.4: (a) QFL and (b) Q_mFL_t plots for framework modes of sandstones showing provisional subdivisions according to inferred provenance type (modified after Dickinson *et al.* (1983)).

5.4.2 Methodology

Provenance and tectonic settings of sandstones are determined by considering their QFL and QmFLt composition using provenance diagrams. Paul Lennox collected the samples and a series of undergraduate students undertook the point counts. Sandstone samples were collected from the Devonian to Permian sequences across the NHB including the Boonanghi Beds, Majors Creek Formation, Kullatine Formnation, Youdale Formation, Warbro Formation and Parrabel Beds. Six hundred points were counted in each thin section of sandstone samples. Point counts of the detrital grains were recalculated to 100. The constituent minerals of the sandstones were classified into total quartzose grains (Q), monocrystalline quartz (Q_m), total feldspar grains (F), total lithic grains (L_t) and unstable polycrystalline lithic grains (L). Composition fields are constructed onto triangular plots of QFL and QmFLt diagrams.

5.4.3 Results

Point counts of the detrital grains of the sandstones are plotted onto the triangular QFL diagrams (Figure 5.5) and the Q_mFL_t diagrams (Figure 5.6) for classification.

Figure 5.5 shows the QFL diagrams of the sandstones in the Boonanghi Beds, Majors Creek Formation, Kullatine Formnation, Youdale Formation (A, B and C), Warbro Formation and Parrabel Beds across the whole NHB. The QFL diagrams indicate that the sandstones of the NHB were derived mostly from a Magmatic Arc setting except for the Youdale A & B Formation which was mostly derived from the Recycled Orogen setting. Figure 5.5 demonstrates that the source area for the Boonanghi Beds was rich in feldspar, whereas that for the Majors Creek, Youdale, Kullatine, Warbro formations and Parrabel Beds was dominantly lithic. The sandstone in the NHB contains very low percentage quartz grains in all formations which is in agreement with Korsch (1984) for sandstones from the southern New England Orogen.

Because of the virtual absence of polycrystalline quartz, the QFL diagrams are similar to Q_mFL_t diagrams in the NHB.

Figure 5.6 displays the QmFLt diagrams of the sandstones in the Majors Creek, Kullatine, Youdale, Warbro formations and Parrabel Beds. The sandstones in the Majors Creek, Kullatine, Warbro formations and Parrabel Beds were derived mostly from the Magmatic Arc setting, whereas that in the Youdale A & B and C formations which were mostly derived from the Recycled Orogen setting. Lithics are the most dominant grain within all sandstone samples in the NHB. Overall the sandstones are quartz-poor in all formations. The feldspar content in the Youdale A & B and C formations is much less abundant compared with the other two grain composition in these Youdale formations.

Overall, the Devonian and Carboniferous sandstones from the NHB are composed of detritus derived overwhelmingly from a magmatic arc (or arcs).

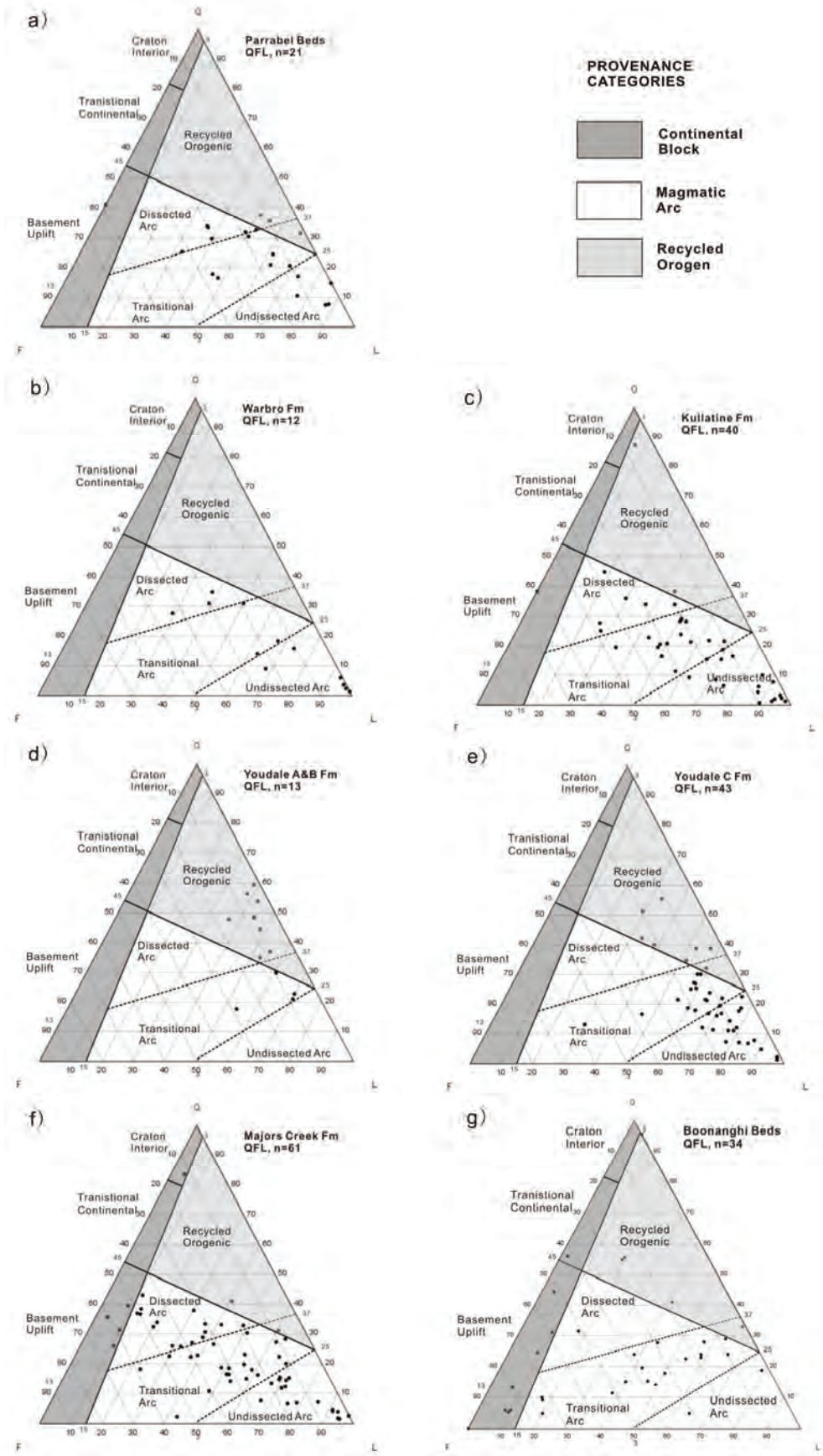

Figure 5.5: QFL diagrams for the sandstones from Devonian, Carboniferous and Permian formations in the NHB.

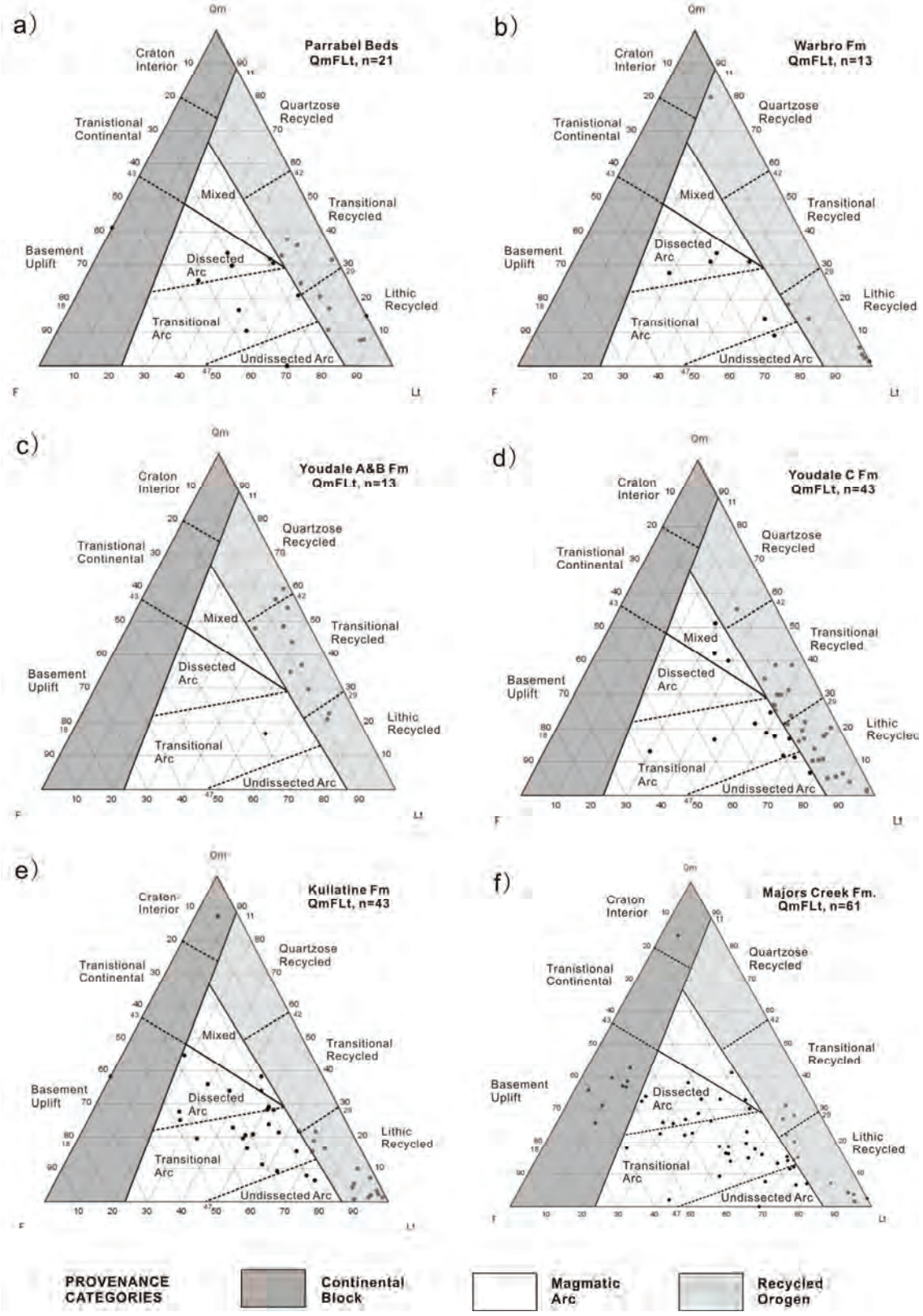

Figure 5.6: QmFLt diagrams for the sandstones from Devonian, Carboniferous and Permian formations in the NHB.

5.4.4 Discussion

5.4.4.1 Trend in provenance from Devonian to Permian

Figure 5.7 gives QFL/QmFLt mean values for Devonian to Permian formations within the largest sample populations including the Boonanghi Beds, Majors Creek Formation, Kullatine Foration, Youdale C Formation, Youdale A & B Formations, Warbro Formation and Parrabels Beds. It indicates the trend in provenance from transitional arc to recycled orogenic for Devonian to Early Permian sandstones (from the Boonanghi Beds to Youdale A & B Formations). The Early Permian sandstones of the Warbro Beds and Parrabel Beds are mainly from the transitional arc.

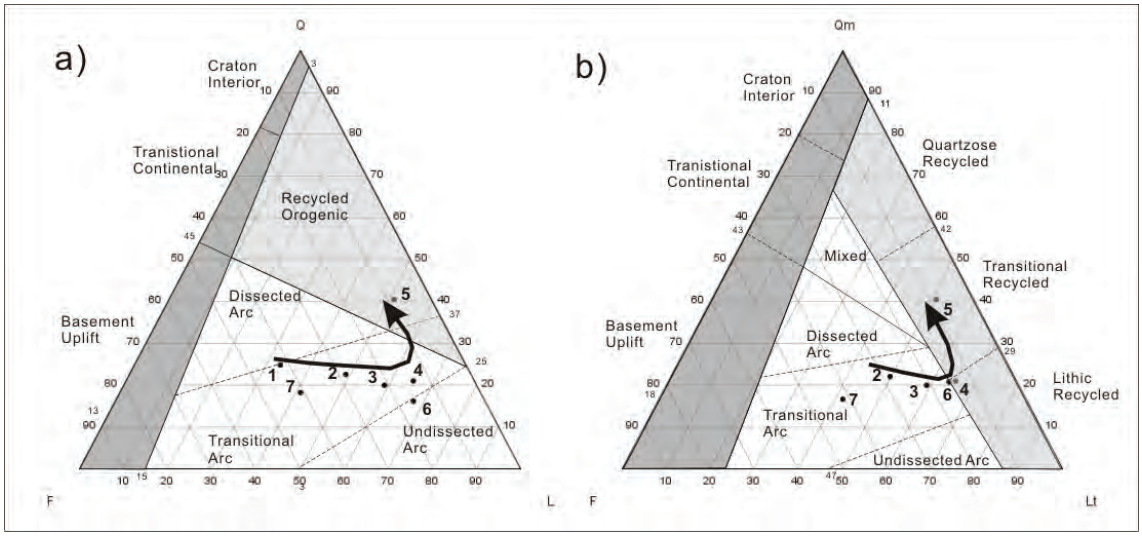

Figure 5.7: QFL and QmFLt diagrams of the mean compositions of different formations indicating the trend of provenance from transitional arc to recycled orogenic for Devonian and Carboniferous sandstones of NHB. 1– Boonanghi Beds; 2 – Majors Creek Formation; 3 – Kullatine Foration; 4 – Youdale C Formation; 5 – Youdale A and B Formations; 6 – Warbro Formation; 7 – Parrabels Beds.

Petrographic and XRD analysis by Lennox and Roberts (1988) of grains and clasts from the northern Hasting Block indicates that (1) the Boonanghi Beds were derived from a feldspathic, rhyolitic and andesitic volcanic source which was also rich in pyroxene and amphibole minerals; the latter are absent from stratigraphically higher units; (2) material

comprising the Majors Creek Formation came from an entirely volcanic source dominated by rhyodacitic ignimbrite, but with trachytic and andesitic lavas; (3) granitic, sedimentary and metamorphic clasts appear in abundance for the first time in the Carboniferous in the Kullatine and Youdale Formations. And include a characteristic micrographic granite, quartzose sandstone, quartzite, phyllite and slate; and (4) clasts similar to those in the Kullatine and Youdale Formations are presented within the Early Permian Warbro formation, Parrabel and Kempsey Beds, but the Permian units contain a greater proportion of sedimentary material.

The source of the detritus in the sandstones has changed with time. Thus in the Boonanghi and Majors Creek Formations, the main source appears to be the calc-alkaline, continental arc that existed at the time of their deposition. A minor contribution came from uplifted basement. Subsequently, mixed sources provided the detritus for the Kullatine and Youdale C Formations namely, arc and recycled orogenic (subduction complex sequences?), the former being the dominant. By the Early Permian, detritus in sandstones from Youdale A and B was received from a recycled orogenic provenance. The detritus may have been derived from accretion complex sequences in the Tablelands Complex. Contributions from the recycled orogenic source waned during the deposition of the Warbro Formation and picked up subsequently at the time the sands of the Parrabel Beds were deposited.

Korsch (1984) indicates that sandstones from the New England Orogen (NEO) are mainly derived from a volcanic arc terrane (Figure 5.8). The sandstones are mainly lithic to feldspathic types with low quartz content. From the Devonian to Permian, the detritus in the Tamworth Belt and Tablelands Complex show similar compositional evolutionary paths as they become more felsic through time. The results from our analysis in the NHB are similar with that of Korsch (1984) in the Tamworth Belt and Tablelands Complex in the NEO, both showing derivation from a volcanic arc and being quartz-poor sandstones. The major difference is that the detritus in the NHB becomes more lithic from Devonian to Early Permian.

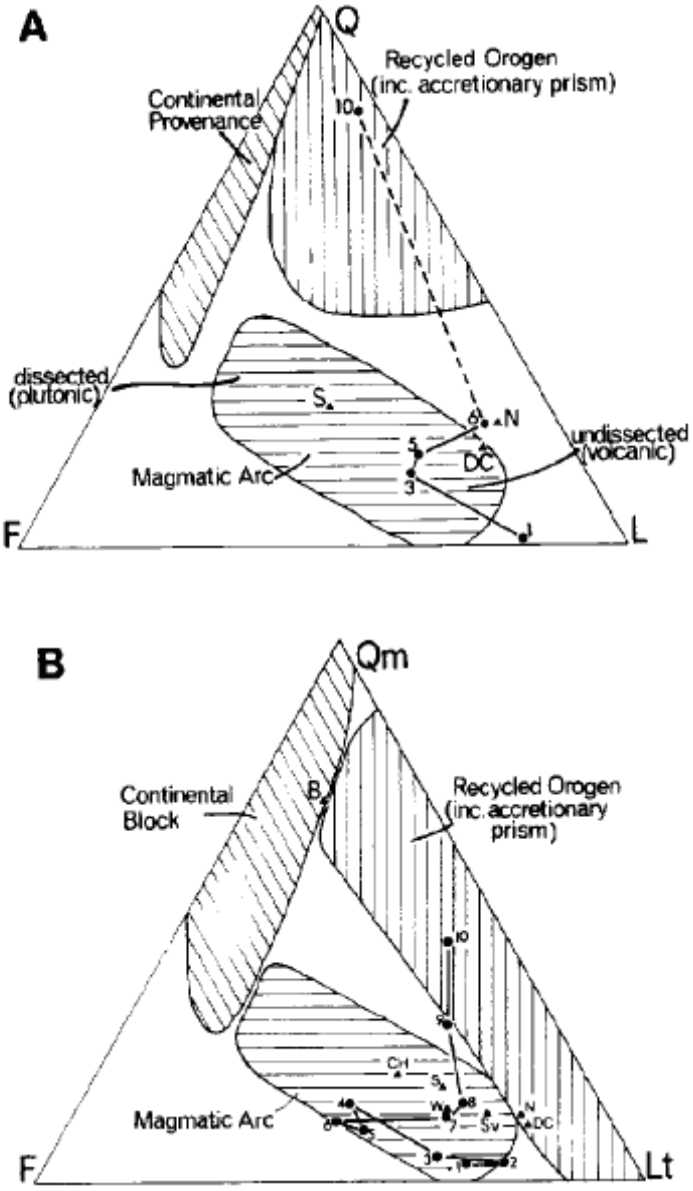

Figure 5.8: QFL and QmFLt diagrams showing data from New England Orogen and in particular the Tamworth Belt (Number 1 – Devonian Petrofacies to Number 10 - Mesozoic) (Korsch, 1984).

The Korsch (1984) trend of provenance for the Tamworth Belt is similar to the provenance trend obscured for the formations of the Hastings Block in going from feldspar – rich to more lithic – rich and then finally quartz – rich with younger units.

5.4.4.2 Composition correlations between fault blocks

If there is one formation across different fault blocks, then the QFL/QmFLt plots should

be similar. If not exactly the same, contours of the percentage of quartz, feldspar and lithic grains within these fault blocks should be comparable. In order to find the relationship between the fault blocks B, C, E and F, this study used the compositional contour maps of the percentage of different grains in the Majors Creek and Kullatine formations within these fault blocks in the NHB (Figure 5.9a). Do the compositional contour maps of the constituent minerals of sandstones in these two formations within different fault blocks have similar map pattern?

Figures 5.9b, 5.10a & 5.11b show the compositional contour maps of the percentage of Q (quartz), F (feldspar) and L (lithic) grains respectively within the sandstones of the Majors Creek Formation in Fault Blocks B to F. It seems that the compositions of sandstones in Fault Block C have a different map pattern with that shown in Fault Blocks E and F. It appears that the Fault Block C is not that closely related with Fault Block E based on the percentage of certain grains. But this result may not be true because of the limited numbers of sandstones samples in Fault Block C compared with that in Fault Blocks E and F (Table 5.2). Without an even scatter of sample sites throughout the fault blocks consisting of Majors Creek Formation, it is difficult to determine whether the composition of the sandstones is comparable. The concentration of the sample sites in same fault blocks (Fault Block D) and their absence in other fault blocks (Fault Block E and southern part of Fault Block B) makes comparisons difficult despite there being in total 61 Major Creek Formation samples (Figure 5.9, Table 5.2).

Table 5.2: Number of samples of formations in a particular fault block.

Fault Block / Formation	B	C	D	E	F	Total
Majors Creek FM	16	3	30	10	2	61
Kullatine Fm	17	0	4	0	11	32
Youdale C Fm	0	0	25	0	14	39

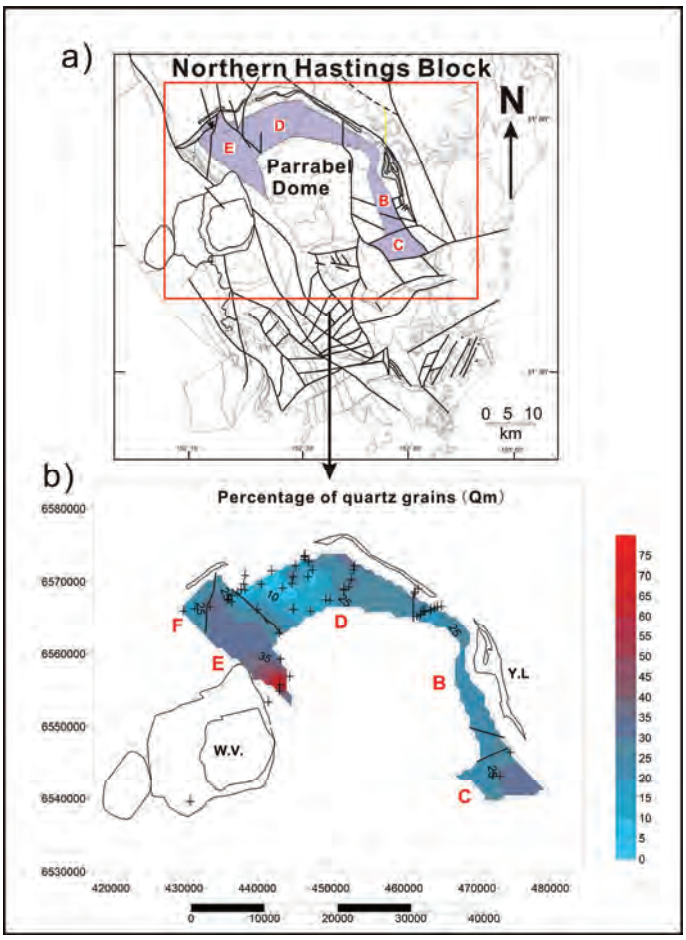

Figure 5.9: (a) The location of the Majors Creek Formation and fault blocks identifier letter in the NHB and (b) the contour map of the percentage of quartz grains in sandstones of the Majors Creek Formation between fault blocks. W.V. = Werrikimbe Volcanics; Y.L. = outcrop pattern of the Yessabah Limestone and ＋ = locality of the analyzed sample of the Majors Creek Formation.

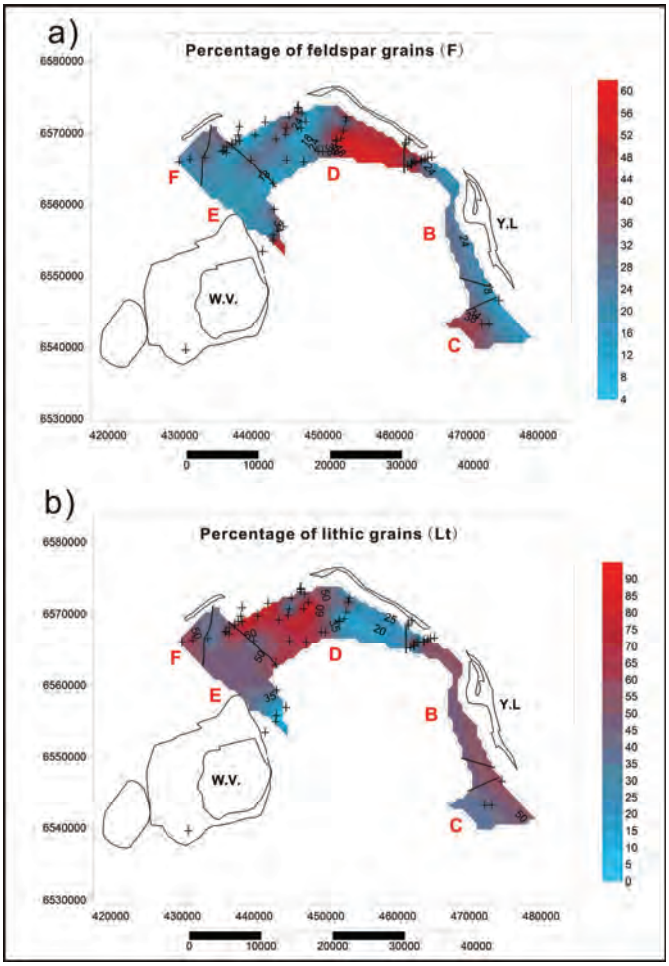

Figure 5.10: The contour map of the percentage of feldspar (a) and lithic (b) grains in sandstones of the Majors Creek Formation between fault blocks B, C, D and E. W.V. = Werrikimbe Volcanics; Y.L. = outcrop pattern of the Yessabah Limestone and ┼ = locality of the analyzed sample of the Majors Creek Fromation.

Figures 5.11b, 5.12a and 5.12b show the compositional contour maps of the percentage of the Q (quartz), F (feldspar) and L (lithic) grains in the sandstones of the Kullatine Formation in Fault Blocks B, D, E and F. Figure 5.13b, 5.14a and 5.14b show the compositional contour maps of the percentage of the Q, F and L grains in the sandstones of the Youdale C Formation in Fault Blocks D, E and F. The uneven distribution of sample sites within the Kullatine and Youdale C Formation makes it difficult to determine whether the same formation is continuous through these fault blocks as proposed from the regional mapping (Table 5.2).

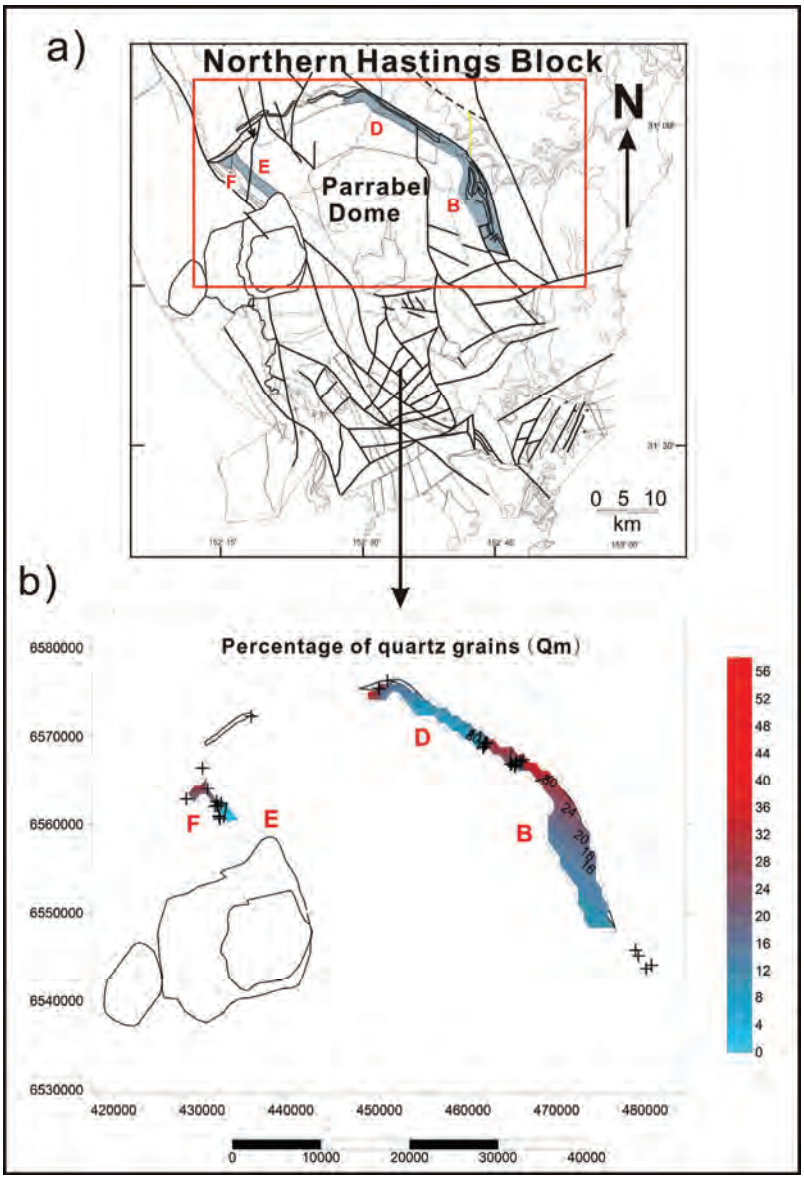

Figure 5.11: (a) The location of the Kullatine Formation and fault blocks identifier letter in the NHB and (b) the contour map of the percentage of quartz grains in the sandstones of the Kullatine Formation between the four fault blocks. W.V. = Werrikimbe Volcanics; Y.L. = outcrop pattern of the Yessabah Limestone and ＋ = locality of the analyzed sample of the Kullatine Formation.

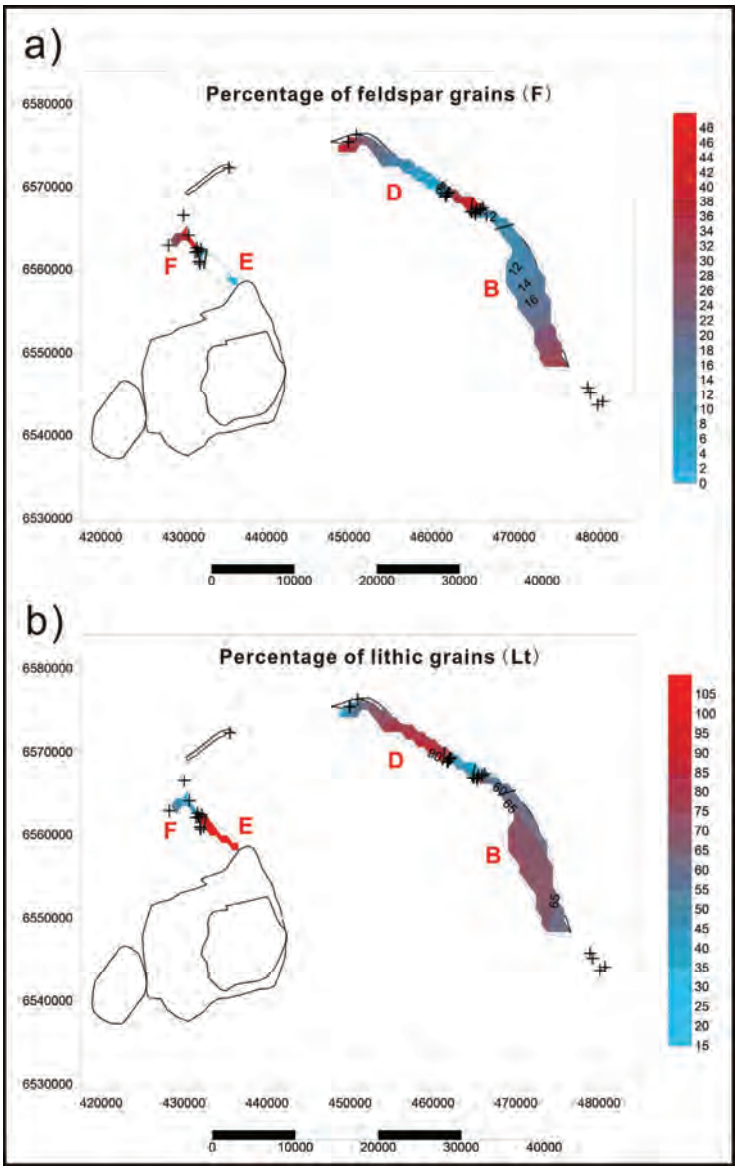

Figure 5.12: (a) The contour map of the percentage of the feldspar grains and (b) the contour map of the percentage of lithic grains in sandstones of the Kullatine Formation between the four fault blocks. W.V. = Werrikimbe Volcanics; Y.L. = outcrop pattern of the Yessabah Limestone and ＋ = locality of the analyzed sample of the Kullatine Formation.

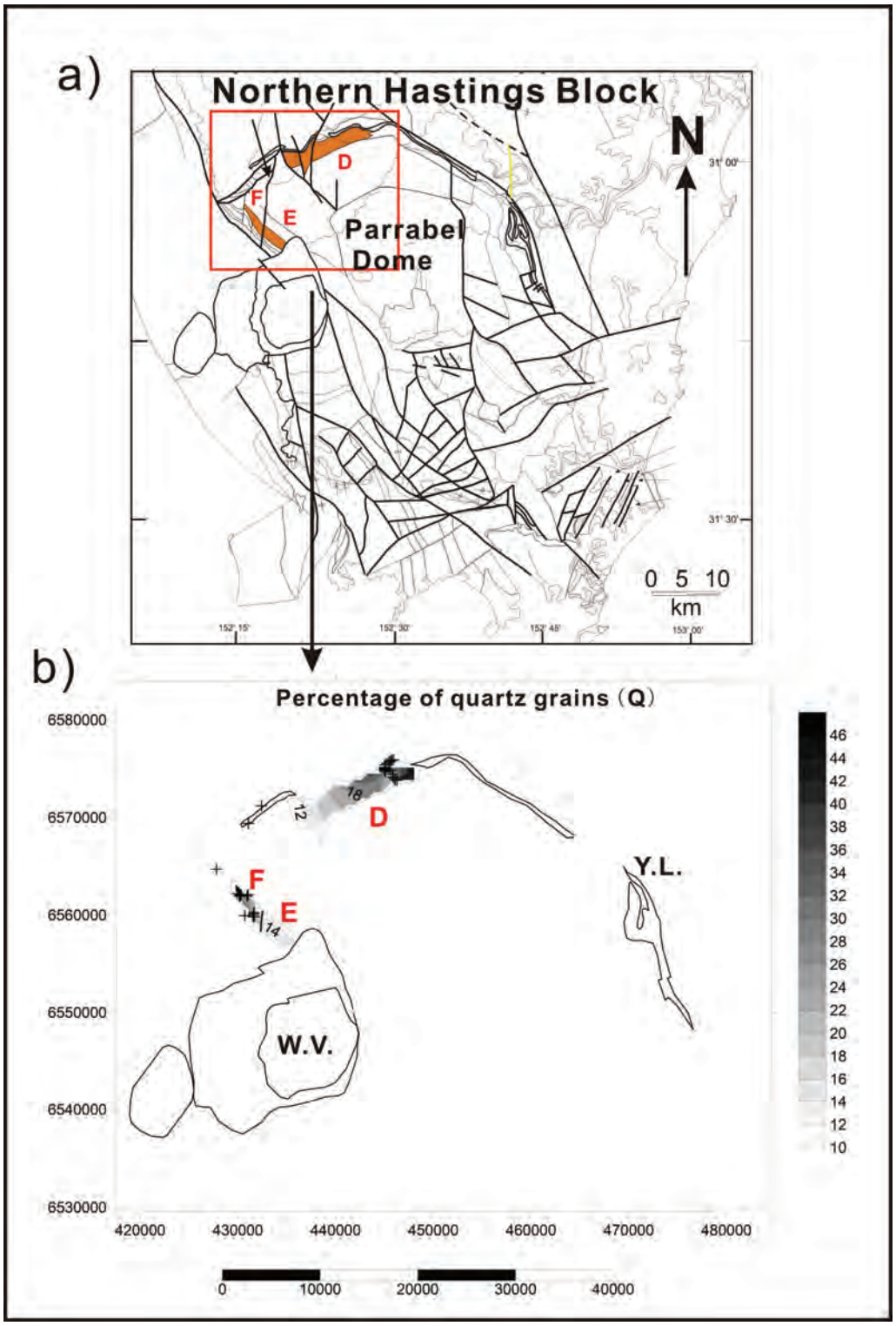

Figure 5.13: (a) The location of the Youdale C Formation and fault blocks identifier letter in the NHB and (b) the contour map of the percentage of quartz grains in the sandstones of the Youdale C Formation between the four fault blocks. W.V. = Werrikimbe Volcanics; Y.L. = outcrop pattern of the Yessabah Limestone and ＋ = locality of the analyzed sample of the Youdale C Formation.

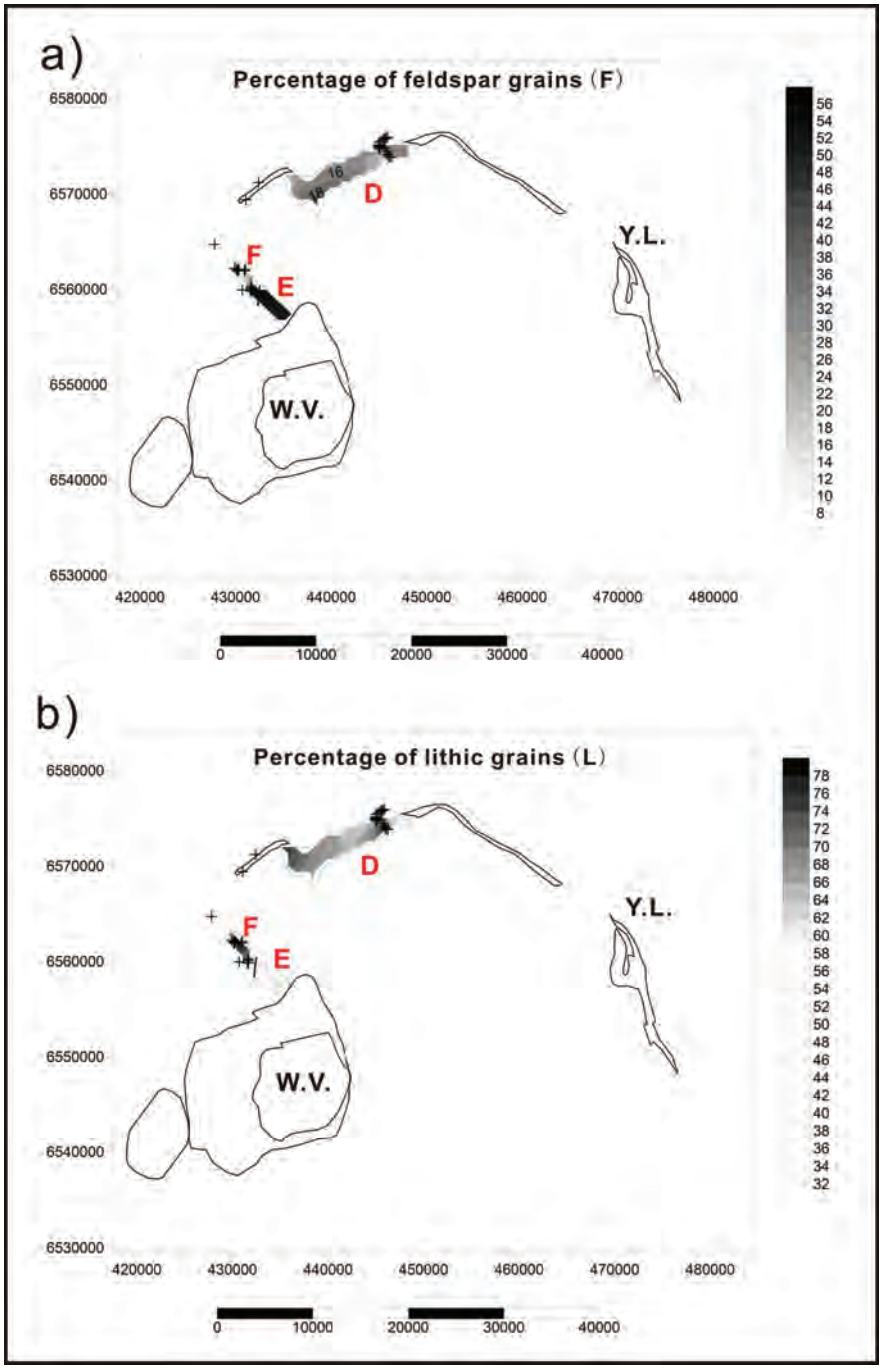

Figure 5.14: (a) The contour map of the percentage of the feldspar grains and (b) the contour map of the percentage of lithic grains in sandstones of the Youdale C Formation between the four fault blocks. W.V. = Werrikimbe Volcanics; Y.L. = outcrop pattern of the Yessabah Limestone and ＋ = locality of the analyzed sample of the Youdale C Formation.

5.4.5 Conclusions

The virtual absence of polycrystalline quartz means the QFL diagrams are very similar

to QmFLt diagrams in the NHB. These two diagrams both indicate that the Devonian and Carboniferous sandstones from the NHB were derived mostly from a Magmatic Arc setting except for the Youdale A & B Formation which was mostly derived from the Recycled Orogen provenance. It could be from the accretion-subduction complex sequences in the Tablelands Complex. Lithics are the dominant grain within all sandstone samples which invariably contain a very low percentages of quartz grains in all formations of the NHB.

The sandstones from the Devonian to Early Permian sequences (from the Boonanghi Beds to Youdale A & B Formations) indicate a provenance trend from transitional arc to recycled orogenic.

Because of the limited numbers of sandstones samples and uneven scatter of sample sites throughout the fault blocks of the same formations, it is difficult to correlate their composition between fault blocks and thus confirm that data are from the same formation.

5.5 Gravity and magnetic worms analysis in the HB

5.5.1 Introduction

Two dimensional geophysical images are frequently used to interpret the geology of an area. This involves tracing a contact or edge between bodies of contrasting density or magnetic susceptibility. Normally sharp contrasts evident in these geophysical images (edges or gradients) are assumed to result from sharp discontinuities or interfaces between contrasting rocks due to such features as faults, unconformities, or intrusive contacts (Holden *et al*. 2000).

Gravity and magnetic worms are two of these 2D geophysical images which show maximum gradients in potential field data (Archibald *et al.* 1999). They are calculated

at different upward continuation levels providing an alternative view into potential field anomalies and the geometry of the anomaly sources. They are believed to particularly useful for defining the dips of structures and their continuity both at depth and along strike (Figures 5.15 and 5.16, Archibald *et al*. 1999). Worms will be present only where there is a contrast in the petrophysical properties on either side of a fault or lithological contact. An array of upward continuation levels provides insight into the behaviour of potential field gradients at different scales and depths (i.e. small upward continuations reflect gradients near surface and large upward continuations map gradients at depth).

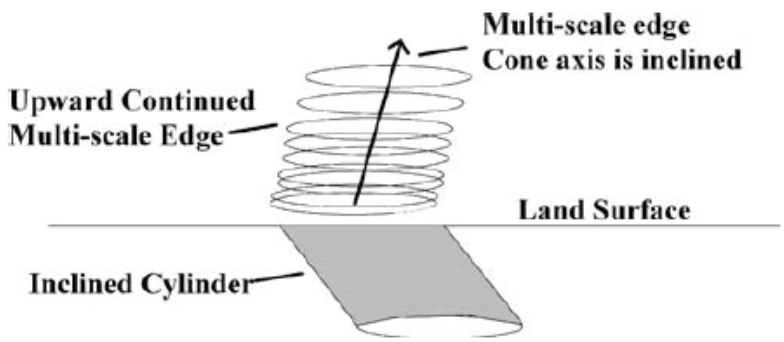

Figure 5.15: 2D visualization of synthetic multiscale edges (gravity gradients) due to an inclined cylinder; note the inclined gravity gradient sheet mirrors the dip of the cylinder and the amplitude (w) of the gradient increases with height towards a maxima (from Archibald *et al*. 1999).

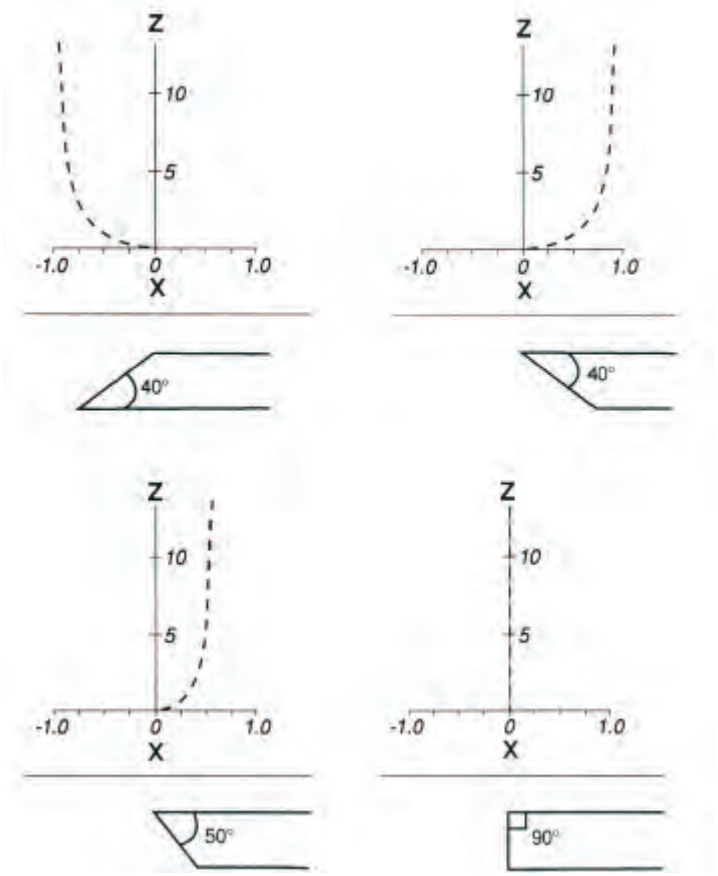

Figure 5.16: Plots of the wavelet transform maxima over synthetic fault geometries of variable dip (infinite slab model). The z-axis represents the scale of the edges (or the degree of upward continuation), whilst the x-axis is an arbitrary scale showing the position of the edges relative to the fault contact. With increasing scale, the edges move in the down-dip direction. Note that the degree of movement of the edges is also dependent on the dip angle of the fault, which allows delineation of relative dip angles (Archibald *et al*. 1999).

5.5.2 Methodology

In this study, gradients within magnetic and gravity data of the southern New England Orogen were enhanced using Intrepid WormE™software, generating multiscale edge contours at various continuation heights (Figures 5.17 and 5.18). The dataset is from NSW statewide interpretation of gravity worms (unpublished data set) provided by Dr J. Robinson of the of Geological Survey of New South Wales (2014).

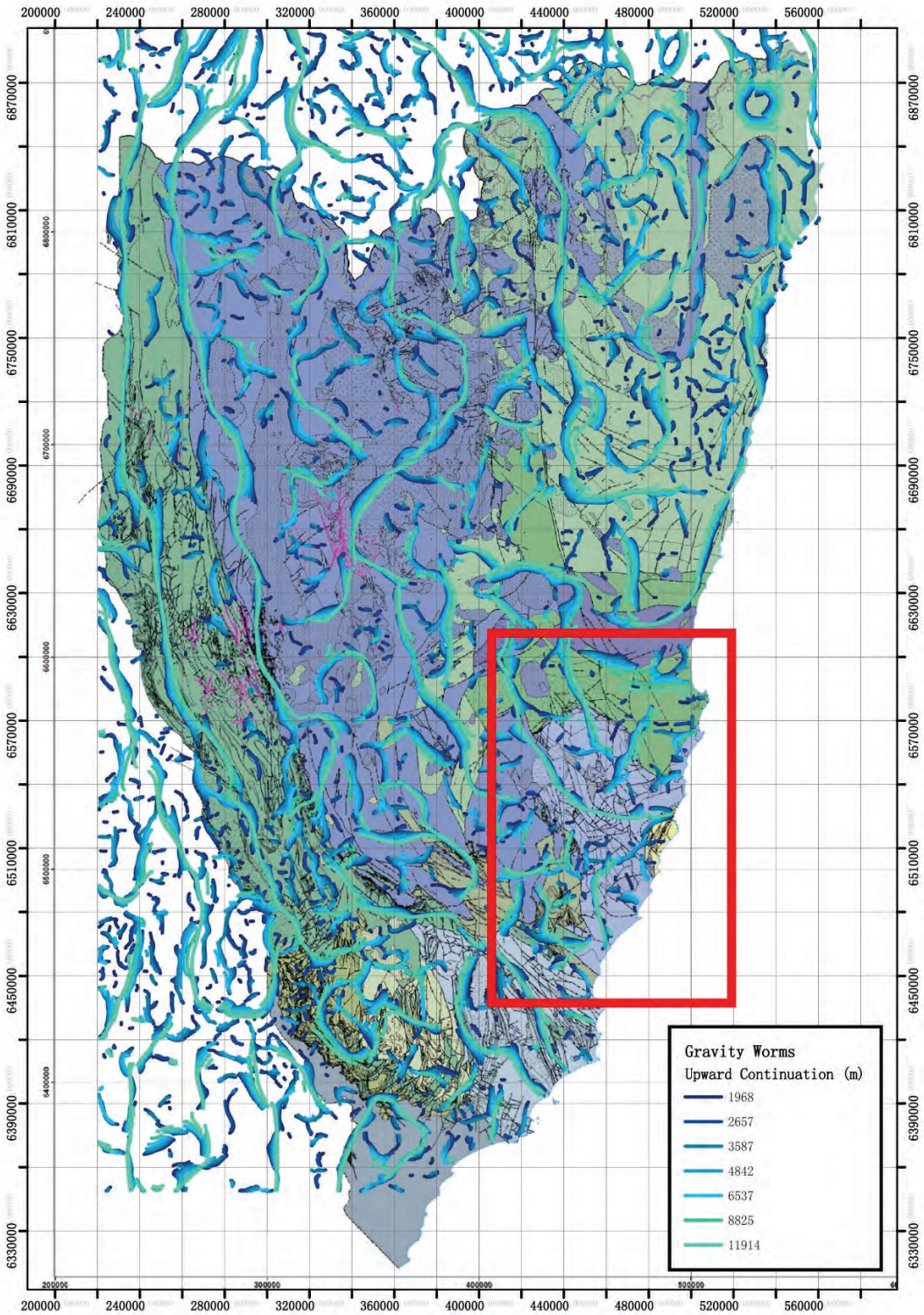

Figure 5.17: The map showing the gravity worms for the southern New England Orogen covered by geological map (dataset is from the Geological Survey of NSW). Red box highlights the study area (the Hastings Block).

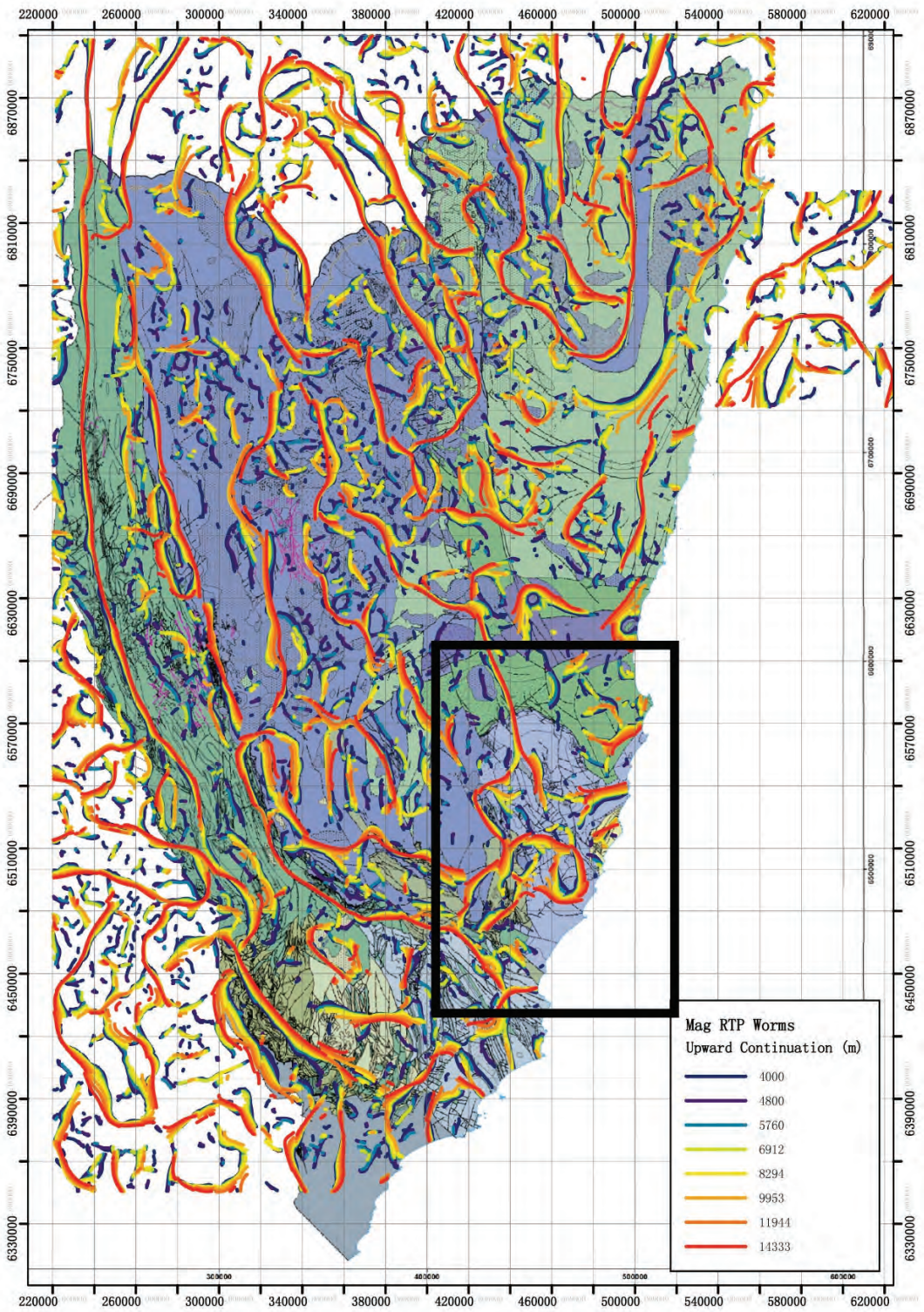

Figure 5.18: The map showing the magnetic worms for the southern New England Orogen covered by geological map (dataset is from the Geological Survey of NSW). The black box highlights the study area (the Hastings Block).

The map showing the gravity and magnetic worms for the Hastings Block covered by

geological map of Roberts *et al*. (1995), are generated from the upward continuation of the gravity and aeromagnetic data. The gravity data in the Hastings Block were processed to an upward continuation of 12 km and yield information on geological contacts that may persist into the lower crust (Figure 5.19a). Magnetic data were re-gridded upwardly to just over 14 km (Figure 5.20). Green colours are from higher levels of upward continuation and image deeper features (crustal- to lithospheric-scale structures), whereas blue colours are from lower levels of upward continuation and image shallower features. Robinson (pers. com. 2015) advised not to predict the dip of features beyond 11km, because of the unreliability in any interpretation.

Within this region, the faults can be defined by significant gradients in both gravity and magnetic data (Figures 5.19a and 5.20). The combination of crustal-scale faults, and major gradients in both gravity and magnetic data may help us to better understand the geology of the HB.

5.5.3 Results

Figure 5.19a and 5.20 are maps showing the gravity and magnetic worms for the Hastings Block covered by geological map of Roberts *et al*. (1995), generated from the upward continuation of the gravity and aeromagnetic data.

5.5.3.1 Gravity worms

The gravity worms are particularly useful to mirror related geological contact such as faults, unconformities and intrusive contacts (Archibald *et al*. 1999, Holden *et al*. 2000). They can also help to depict edges of granitic bodies where there is a major density contrast with the country rock. There are eight major upward continuing gravity worms reflecting contrasts in the properties of geological boundaries referred to as points 1 to 8 on Figure 5.19a.

Upward continuation of the gravity data at Point 1 shows the existence of a crustal-scale

east-west striking discontinuity of very closely spaced worms. This suggests a overall E – W trending, very steeply dipping (nearly vertical) geometry for a crustal-scale structure which possibly mirrors the steep dip of a fault zone or the other geological contacts (Figures 5.19a and 5.20).

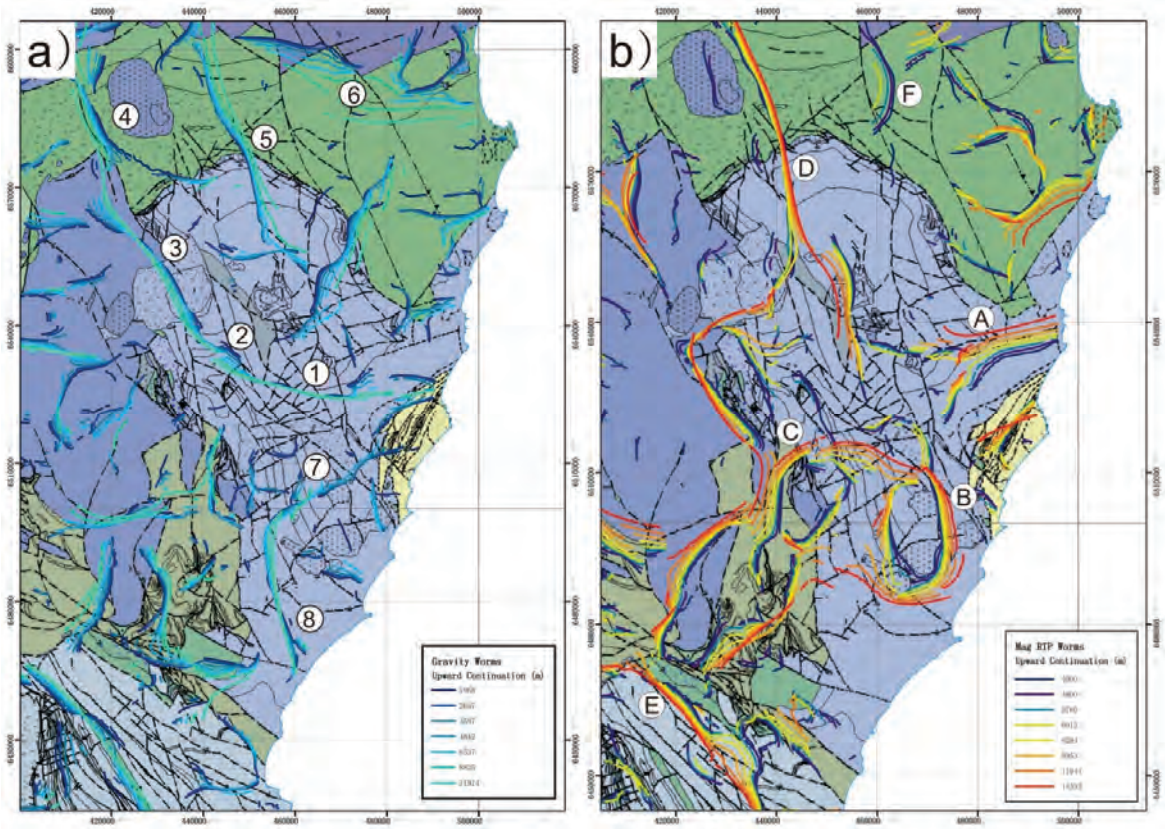

Figure 5.19: a) The map showing the gravity worms for the region covered by geological map of Roberts *et al.* (1995). The lighter green coloured worms are from higher levels of upward continuation, whereas the darker blue colours are from lower levels of upward continuation. The worms near circled number are discussed in the text. b) The map showing the magnetic worms for the region covered by geological map of Roberts *et al.* (1995). The warms colours are from higher levels of upward continuation and cooler colours are from lower levels of upward continuation. The worms near circled upper case letters are discussed in the text.

Point 2 on Figure 5.19a consists of more widely spaced worms striking NW-SE. The southwestern part of the Point 2 is a relative gravity high, around 12km; this value drops to over 2km within the northeastern part. The decreasing observed gravity gradient across the Point 2 (Figure 5.20), indicates less mass to the northeastern part of the Point 1 compared to the southwestern part. This observation suggest a overall

NW-SE trending, southwest - dipping surface (e.g. fault, geologically contrasting density rocks or igneous contact).

Point 3 on Figure 5.19a consists of tight spaced gravity worms, displaying an increasing upward continuation level from east to west. This indicates a steep northeasterly dip for this worm array and can be considered to reflect a southwesterly dip for the fault zone or other geological contrast of different density rocks (Figure 5.20).

Point 4 on Figure 5.19a shows gravity worms consistent with a discontinuity striking NW-SE. The gravity values drops from around 14 km on the western part to 2 km on the eastern part, suggesting a northeasterly to easterly-dipping worm array and hence may be interpreted to mirror the westward dip of the along strike continuation of the Kunderang Fault. This fault has apparent dextral strike-slip movement, but its dip is unknown (Bourke 1971). Similarly, Points 5 and 6 on Figure 5.19a display moderately to shallowly upward gravity continuing worms. Point 5 shows a gravity gradient from 12 km in depth on the eastern side to 2 km on the western side, suggesting that the cause of the anomaly is an overall N-S trending, moderately east-dipping geological contact. Point 6 shows an even shallower south-dipping feature of 1 km to 6 km in depth, overall E-W trending, consistent with a shallow north-dipping worm array. This would be consistent with a shallowly south-dipping geological contact (? fault). It is located near the geological boundary between the Nambucca Block and southern tip of the Coffs-Harbour Orocline. It could be the result of the southward push of the Coffs-Harbour Orocline into the Nambucca Block which then led to the northward push of the Hastings Block over a south-dipping thrust fault (Figures 5.19a and 5.20).

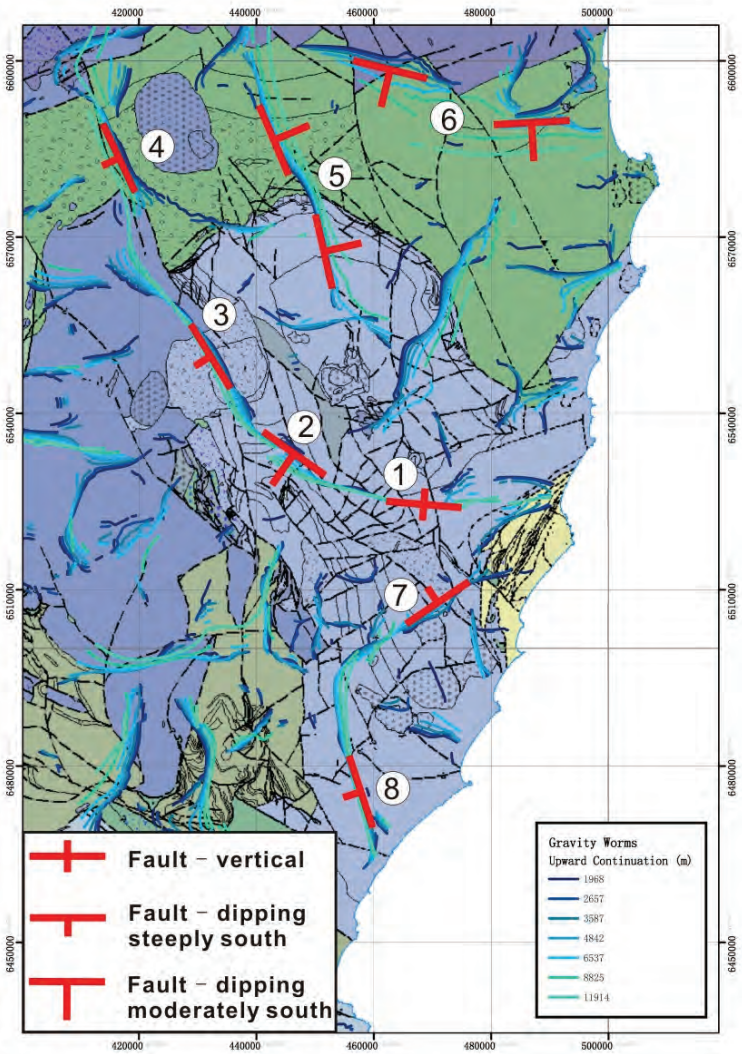

Figure 5.20: The map showing the interpreted dip of gravity worms for the region covered by geological map of Roberts *et al*. (1995).

The anomalies are deflected near Points 7 and 8 on Figure 5.19a which are located around the edges of the Lorne Basin. Gravity worms in Point 7 suggested a steeply northwest-dipping structure. Point 8 displays a steeply east-dipping worm array consistent with a steeply west-dipping fault or other geological feature. The gravity lineaments in the points 7 and 8 shows curvilinear feature which may be interpreted to represent a northeast-southwest striking fault (Point 7) similar to other NE-SW faults or less likely in part of the edge of the Lorne Basin. Point 8 lies near a north-south discontinuity which may represent a fault similar to other meridional-trending faults identified in the SHB (Figure 5.20).

5.5.3.2 Magnetic worms

Magnetic worms predominantly outline the edges of magnetic rock bodies. The major gravity (Figure 5.19a) and magnetic worms (Figure 5.19b) are approximately coincident at some points on the map. This is because some of the edges of magnetic rock bodies are considered to parallel fault structures. This can be shown by Point A in the magnetic worms (Figure 5.19b). It displays an increasing upward continuation level from south to north which indicates an almost E-W trending, steeply north-dip for this worm array. This is along strikes east of Point 1 in the gravity worms image (Figure 5.19a).

Points B shows neat curvilinear worms centered on the Triassic granites of the Lorne Basin in the Southern Hastings Block. They are interpreted to mirror the edges of magnetic rock bodies under the Lorne Basin such as the Brother Granites. Point C consists of worms extending west-northwestward from Point B plus a series of generally north-south worms which splay northwestward north of Point C and southwestward south of Point C. These generally north-south worms may mark the overall western margin of the Southern Hastings Block. The more southerly position of these worms lies under subduction-accretion rocks in the surface (Figures 5.19b and 5.21).

Point D magnetic worms are 5-10 km westward but of a similar strike to the Point 5 gravity worms (Figure 5.19a and 5.19b). Point D magnetic worms were caused by a steeply east-dipping structures. The magnetic worms at Point F are coincident with a west-dipping structure identified from the shallow gravity worms (Point 5, Figure 5.19a). This structure is a major strike-slip fault system and an extension of the Demon Fault through the Taylors Arm Fault System (Leitch 1978; Roberts *et al* 1993; McPhie and Fergussion, 1983). It is possible that the gravity worms near Point 5 are reflecting the position of a fault with a similar strike to the Taylors Arm Fault System.

Point E magnetic worms are west-northwest trending and may reflect a steeply

north-dipping magnetic discontinuity. Point E reflects in part the difference in magnetic properties between the rock sequences in the Myall and Southern Hastings blocks. The magnetic boundary is subparallel but 10-15 km south of the outcrop trace of the faulted boundary between these blocks. The Manning Fault in this area is considered to have had an early dextral strike-slip history followed by a late sinistral strike-slip history (Lennox and Offler, 2009). The steep northward-dip of the magnetic discontinuity may reflect in part this strike-slip fault system bringing together rocks of different magnetic properties on this major block boundary within the Tamworth Belt (Figures 5.19b and 5.21).

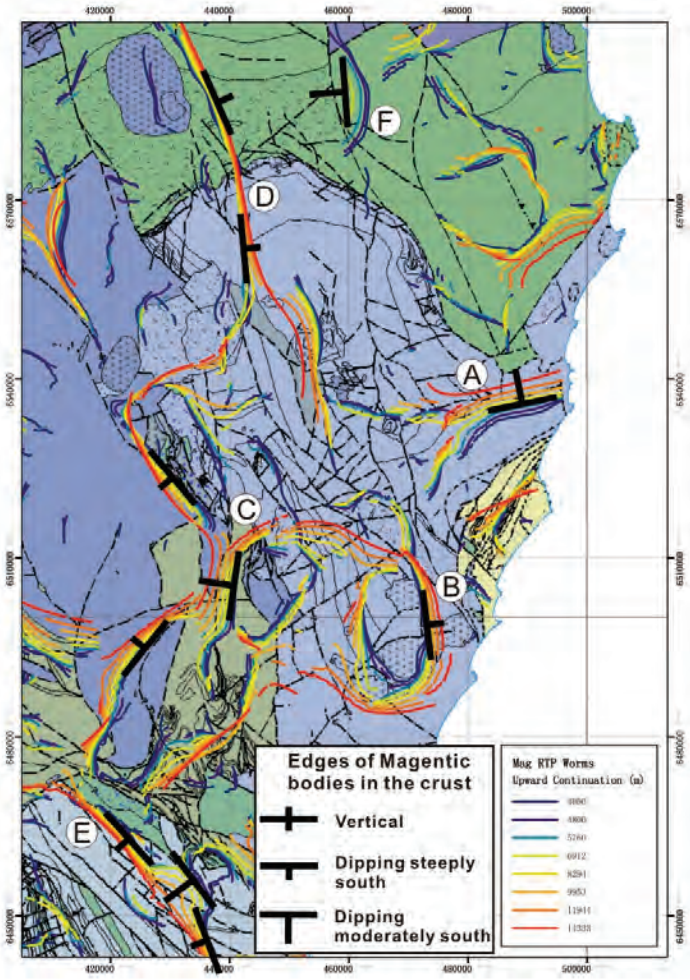

Figure 5.21: The map showing the interpreted dip of magnetic worms for the region covered by geological map of Roberts *et al*. (1995).

5.5.3.3 Boundary between the NHB and SHB

The position of an alternative boundary between NHB and SHB to that proposed by

Roberts *et al.* (1995) is uncertain (Figure 5.22 – red dashed lines). There are two suggestions for the position of the boundary. Lennox & Roberts (1988), Schmidt *et al.* (1994) and Roberts *et al*. (1995) suggested that the NHB and the SHB are separated by an arcuate line possibly related to a fault system extending from the northwestern edge of the HB near Kunderang Brook (KB on Figure 5.22), southeasterly through Rollands Plains (RP on Figure 5.22) and east-northeasterly towards Crescent Head in the position of the Mingaletta Fault (MF) (Figure 5.22 – top red dashed line). The boundary is faulted in the west and east, but in the central part the boundary is obscured by younger volcanics and granitoids (Figure 5.22). Lennox *et al*. (1999) argued that the Bagnoo Fault and its inferred extensions, the Rollans Road Fault (RRF) and the Cowarral Fault (CWF) should be the geological boundary between the NHB and SHB (Figure 5.22 – bottom red dashed line). Analysis of the bedding data and the interpretation of the stratigraphy in the Northern Hastings Block (Fault Block H, I and J) and the gravity and magnetic worms provides some clues as to the position of this geological boundary.

Points 1-4 in both the shallow gravity worms (up to 12km, Figure 5.18) and deep gravity worms images (up to 68km, Figure 5.23) indicate a large sharp linear contrasts in the middle of the Hastings Block. This large contrast strikes NW-SE at its northern part (Point 4 on Figures 5.18 and 5.23) and approximately E-W in the southern part (Point 1 on Figures 5.18 and 5.23). The worm arrays in Points 2-4 suggest a southwesterly to westerly-dipping structural feature. The observed gravity gradient across the Point 1 on Figure 5.23 suggests a very steeply north-dipping (nearly vertical) geometry for the crustal-scale structure. Figure 5.19 shows the dip of the geological structure (? fault, geologically contrasting density rocks or igneous contact) varies from almost vertical to northerly for the eastern part (near Point 1) to steeply westerly for the western part (near Point 3).

This large contrast in the dip of the gravity worms may reflects the geological boundary between the mainly Carboniferous sequences in the Northern Hastings Block and the

Devonian to Carboniferous sequences in the Southern Hastings Block. This geological boundary (Figure 5.22 – middle red dashed line) is between the one proposed by Schmidt *et al*. (1994) (Figure 5.22 – top red dashed line) and the one proposed by Lennox *et al*. (1999) (Figure 5.22 – bottom red dashed line). It extends from the northwestern edge of the HB near Kunderang Brook along the Kunderang Fault, southeasterly through the Pappinbarra Fault and the Hastings Fault and east-northeasterly towards and north of the Port Macquaire Block (Figure 5.22 – middle red dashed line). The whole boundary is faulted although some sections especially southeast of the Pappinbarra Fault are not coincident with faults on the Roberts *et al*. (1995) map. This boundary may have been disrupted during bending of the Parrabel Dome and subsequent faulting as the NHB accommodated shortening associated with deformation of the adjacent Nambucca Block. Given the continuity of the stratigraphy across this boundary it suggests there has not been too much disruption and that both the NHB and SHB were near each other during and after Late Carboniferous emplacement.

The position of this boundary will be helpful for understanding fault block reconstruction of the NHB. This will be presented in the Fault Block analysis chapter (Chapter 6).

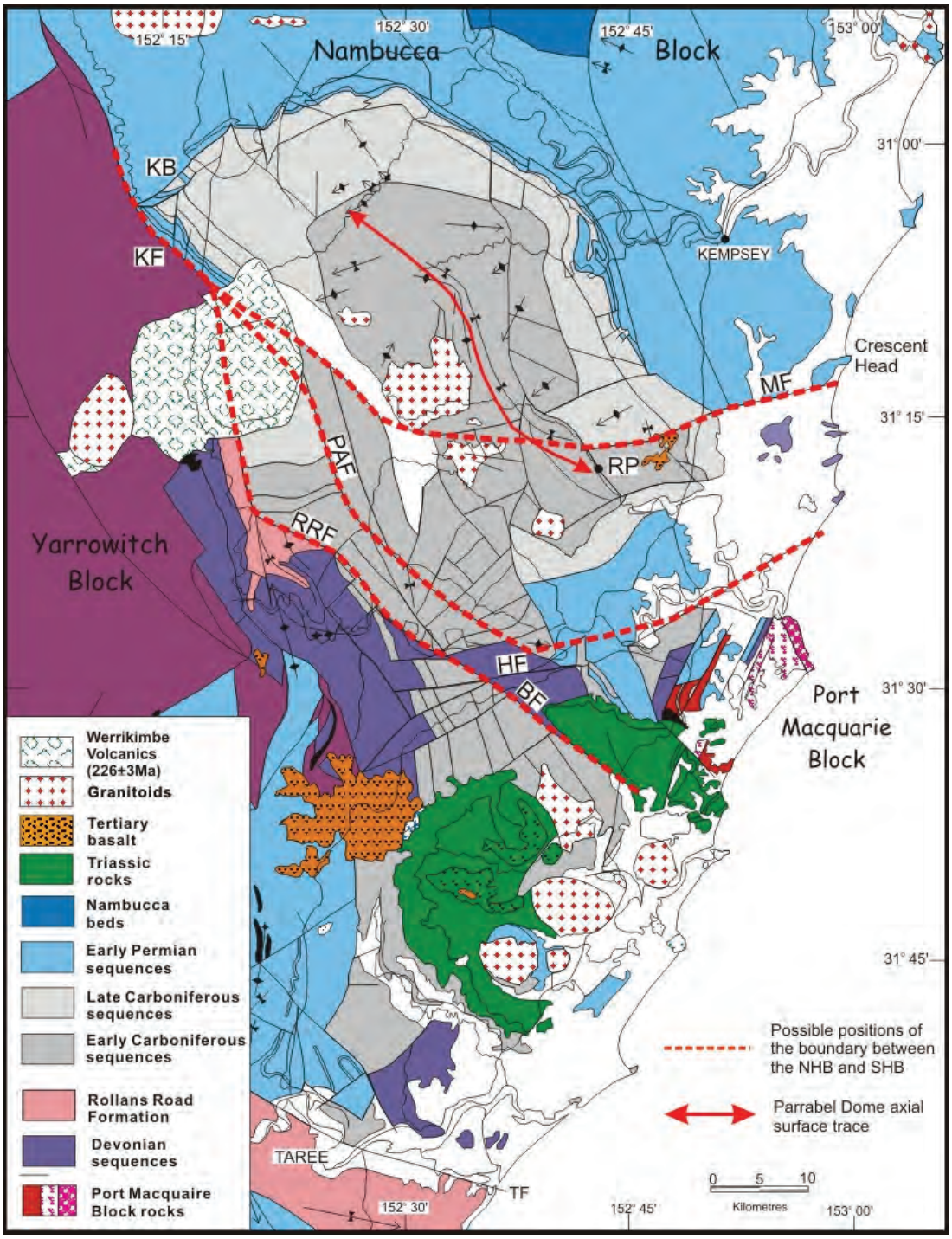

Figure 5.22: The possibilities for the position of the geological boundary between NHB and SHB as suggested in the literature (Roberts *et al*. 1995) or from this research. Abbreviations: BF = Bagnoo Fault; CWF = Cowarral Fault; HF = Hastings Fault; KB = Kunderang Brook; KF = Kunderang Fault; MF = Mingaletta Fault; PAF = Pappinbarra Fault; RP = Rollands Plains; RRF = Rollans Road Fault.

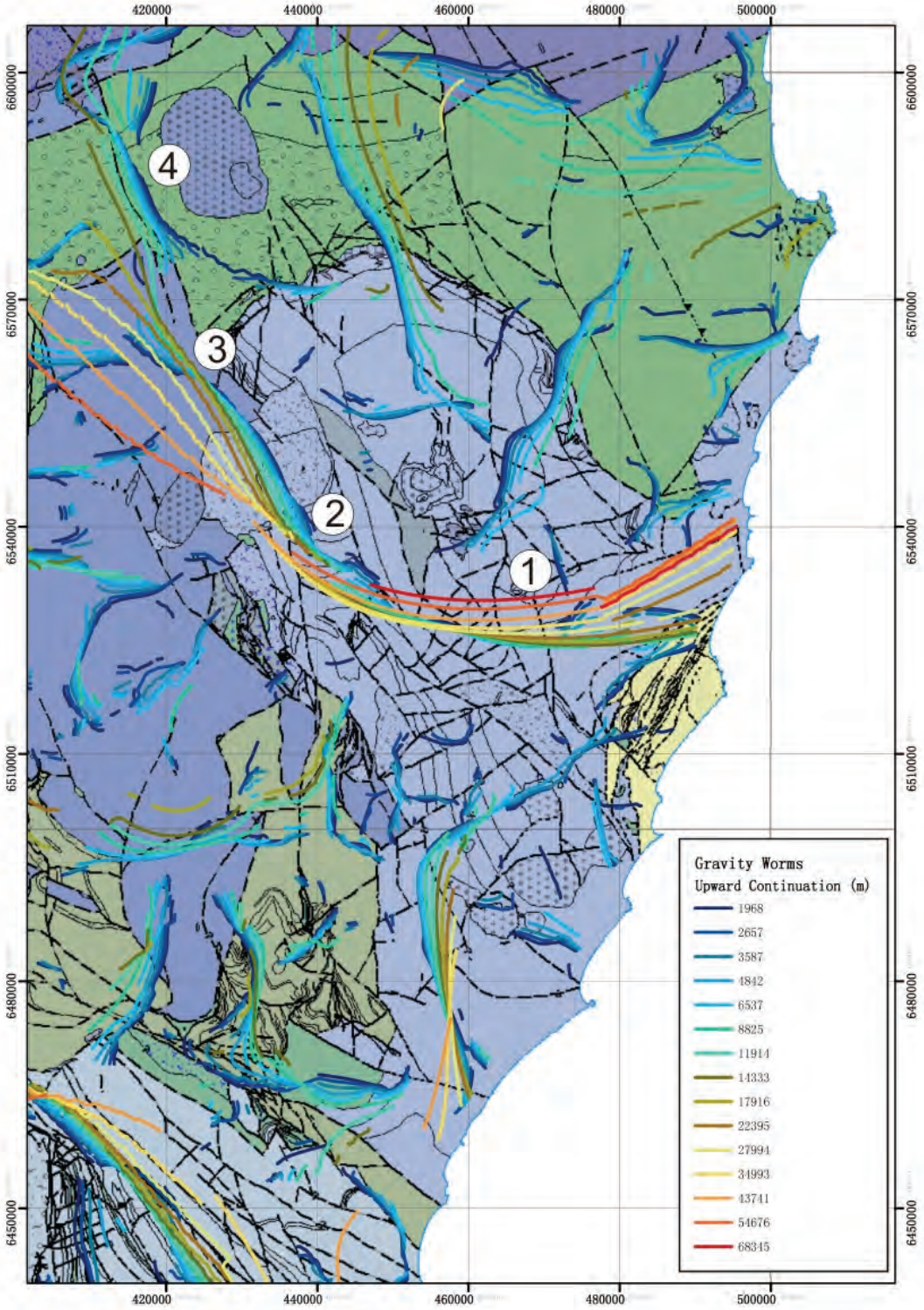

Figure 5.23: The map showing the gravity worms for the region with the upward continuation from 2 to 68 km. The numbered points are discussed in the text.

5.5.4 Conclusions

A large sharp linear contrast along the Points 1-4 in the gravity worms (Figure 5.23;

strikes ~NW-SE in its northern part and approximately E-W in the southern part) are proposed to be an alternative for the geological boundary between the NHB and SHB. It extends from the northwestern edge of the HB near Kunderang Brook along the Kunderang Fault, southeasterly through the Pappinbarra Fault and the Hastings Fault and east-northeasterly towards and north of the Port Macquaire Block (Figure 5.22). These gravity worms suggest this boundary to be southwesterly to westerly-dipping at its northern part (Points 2-4)and steeply north-dipping (nearly vertical) at its southern part (Point 1) (Figure 5.19 and 5.24).

Point 5 in the gravity worms and Point D in magnetic worms both suggest an overall N-S trending, moderately to steeply east-dipping geological boundary (Figure 5.24). The geological boundary suggested by gravity worms (Point 5) is not observed at the surface through faulting. The geological boundary suggested from the magnetic worms (Point D) may relate to the NW-elongated Carrai Granodiorite and a number of NW-striking faults between the granodiorites and the NHB. Leitch (1976) suggested faulting and granodiorite emplacement were linked. Point F in magnetic worms suggests a west-dipping, N-S trending geological boundary. This N-S boundary near Point F could be the Taylors Arm Fault System which is a major strike-slip fault system and an extension of the Demon Fault (Leitch 1987, Roberts *et al* 1993, McPhie and Fergusson, 1983).

A shallowly south-dipping geological contact was observed near the geological boundary between the Pee Dee Beds/Kempsey Beds in green in the Nambucca Block and the Nambucca Beds in purple. Johnston (1997) suggested the Nambucca Block consisted of thrust slices moving north-to-south to bring higher grade metamorphic rocks up to the surface within the core of the Nambucca Block (Figure 5.25b). The gravity worms near Point 6 would suggest a steeply south-dipping geological boundary perhaps a fault reflecting back thrusting as the Permian sequences could not accommodate shortening related to the southward push of the Coffs-Harbour Orocline

other than through faulting.

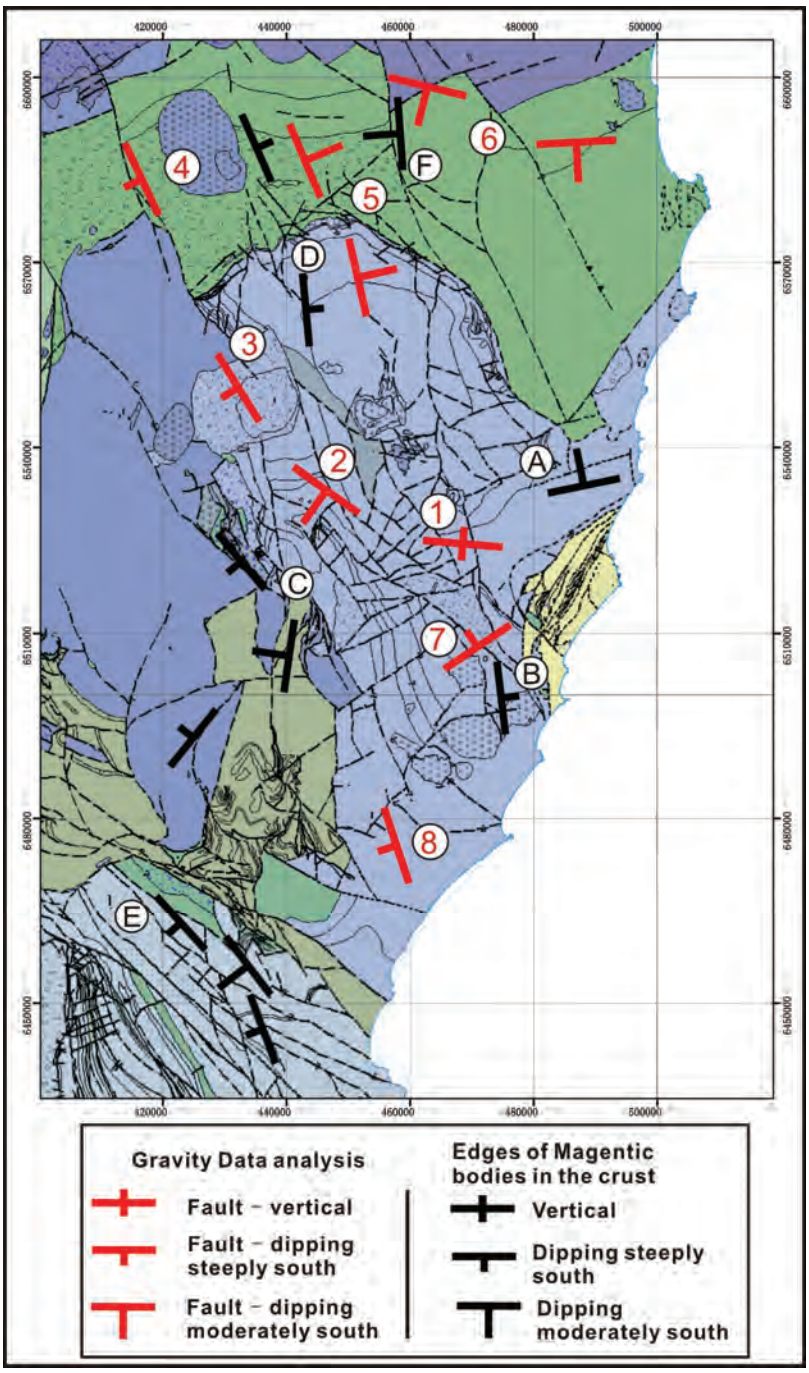

Figure 5.24: The map showing the dip of key proposed geological features from the gravity and magnetic worms analysis.

The gravity and magnetic anomalies observed near Points 7 and B outline the edge of the Triassic granites in the Lorne Basin.

The generally north-south magnetic worms near Point C (Figures 5.21 and 5.24) show

the overall western margin of the Southern Hastings Block. The Point E magnetic worms probably show the difference in the magnetic properties between the rock sequences in the Myall and southern Hastings blocks.

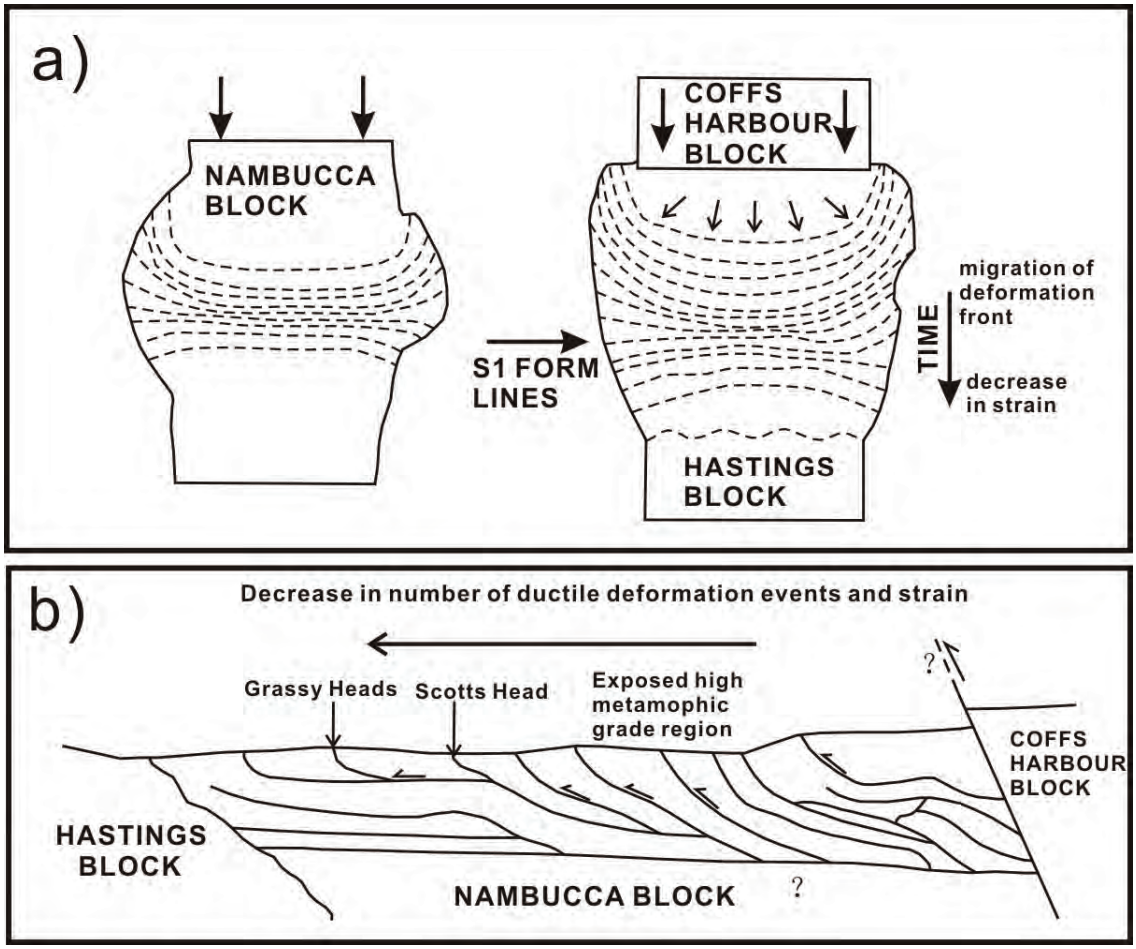

Figure 5.25: a) Experimentally derived cleavage in quartzite. The south indentation of the Coffs Harbour Block has produced similar orientation of S_1 in the NB (Tullis et al. 1973). The redrawn experiment on deformed quartzite in the laboratory on the left is thought to be an analogy for formation and then re-alignment of early formed cleavage. b) Schematic cross section indicating south directed transport and the development of listric faults after fold lock-up (Johnson 1997).

5.6 Results

5.6.1 Fault Block A

Fault block A is located on the southwestern limb of the Parrabel Dome which is a large northwesterly trending dome within the Hastings Block (see Figures 5.3 and 5.26a). Because of the presence of the macroscopic Parrabel Dome in NHB with the Boonanghi Beds in its core, the top of this formation represents the boundary between the Boonanghi Beds and Majors Creek Formation. Fault Block A is cut by Fault 28 to the southwest, Fault 32 to the north, the Mingaletta Fault to the south and the Parrabel Fault to the east (Figure 5.26b). Many stratigraphic boundaries in this block are also faults according to the Roberts *et al.* (1995) map. By defining the primary bedding data that represent the overall trends and strike of the bedding surface in the fault block A according to the method discussed above, we found that the primary bedding data close to the presumed bottom surface of the Mingaletta Formation dips to the southwest (Figure 5.26b). The bottom of the Mingaletta Formation was constructed by using Mathematica™ and 3D Move™ based on these primary bedding data (Figure 5.26c; Appendix 8 - 3).

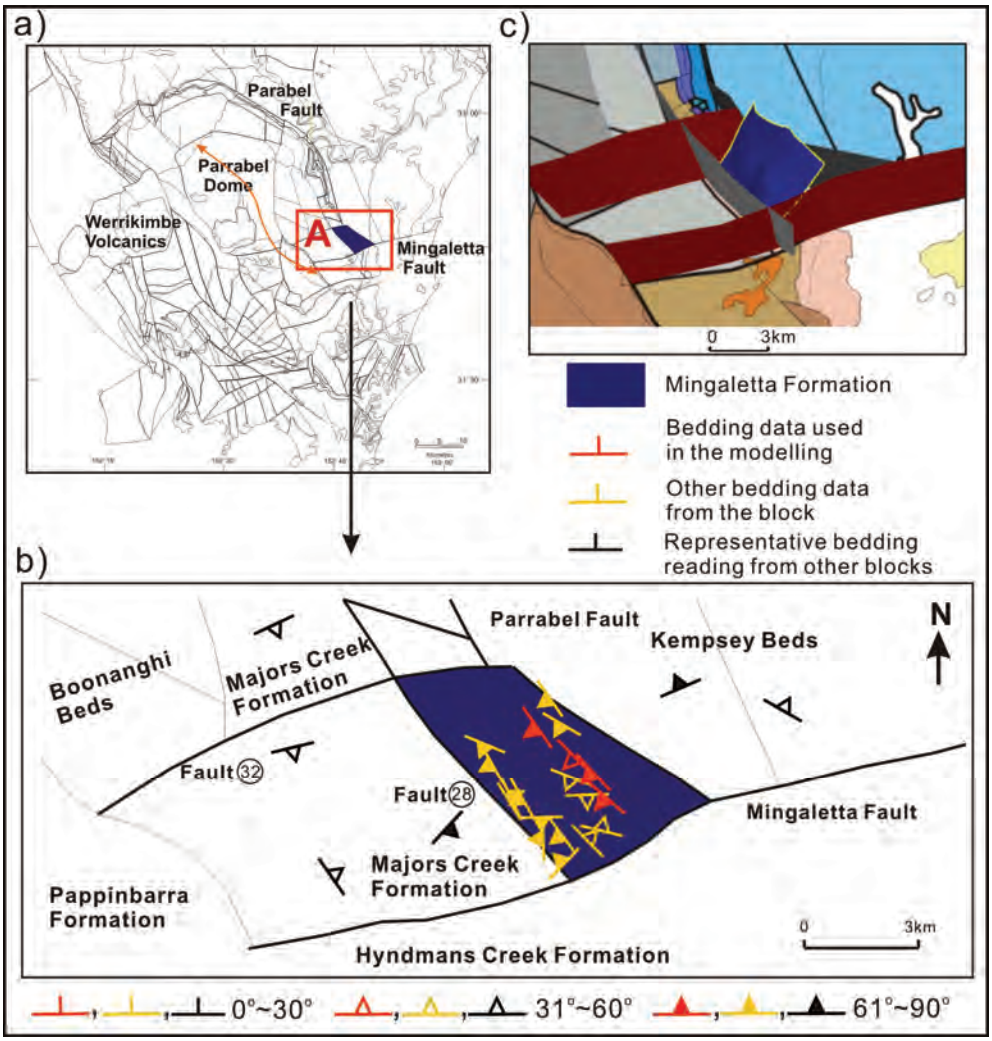

Figure 5.26: Fault Block A: a) Location of the block on the eastern limb of the Parrabel Dome; b) schematic map with observed bedding reading (red reading were used in the modelling) and c) bottom surface of the Mingaletta Formation in this block. The animated images of this bottom surface in 3D model are displayed in Appendix 8 - 3. The surrounding map units are shown in the legend for Figure 5.3 with faults shown vertical and in different coulors.

Considering that the large northwesterly trending Parrabel Dome predominates the Northern Hasting Block, the Mingaletta Formation in fault block A would be expected to dip east to southeast in line with its position within the dome and the bedding in this block should be similar with the bedding of Majors Creek Formation in Fault Block B and C (Figure 5.27c and 5.28b). Our data show that the bottom surfaces of Mingaletta Formation in fault block A of Northern Hastings Blocks dips southwest (Figure 5.26b). How did the Mingaletta Formation in fault block A change its dip direction from the

southeast to southwest? In the discussion section we are going to propose a schematic reconstruction model to account for the movements on the major faults in fault block A.

5.6.2 Fault Block B

Fault Block B is located on the eastern limb of the Parrabel Dome within the Northern Hastings Block (see Figure 5.27a). The Major Creeks Formation, the overlying Kullatine Formation and the complex folded (?) Yessabah Limestone are within Fault Block B. According to Roberts *et al.* (1995), most of the margins of the Major Creek Formation are stratigraphic boundaries except for the southeastern corner which is labelled as a fault and Fault 29 on the southern margin of this block (Figure 5.27c). The primary bedding data that are used in creating the surfaces are shown by the red dip data in Figure 5.27c. Most of the bedding data in this block dip east which is consistent with that expected for the fault block B as it is located on the eastern limb of the Parrabel Dome. The bottom surfaces of Major Creeks Formation and Kullatine Fornation in fault block B are constructed by using Mathematica™ and 3D Move™ based on these primary bedding data (Figure 5.27b; Appendix 8 - 4). This horizon dips gently east according to the primary bedding data.

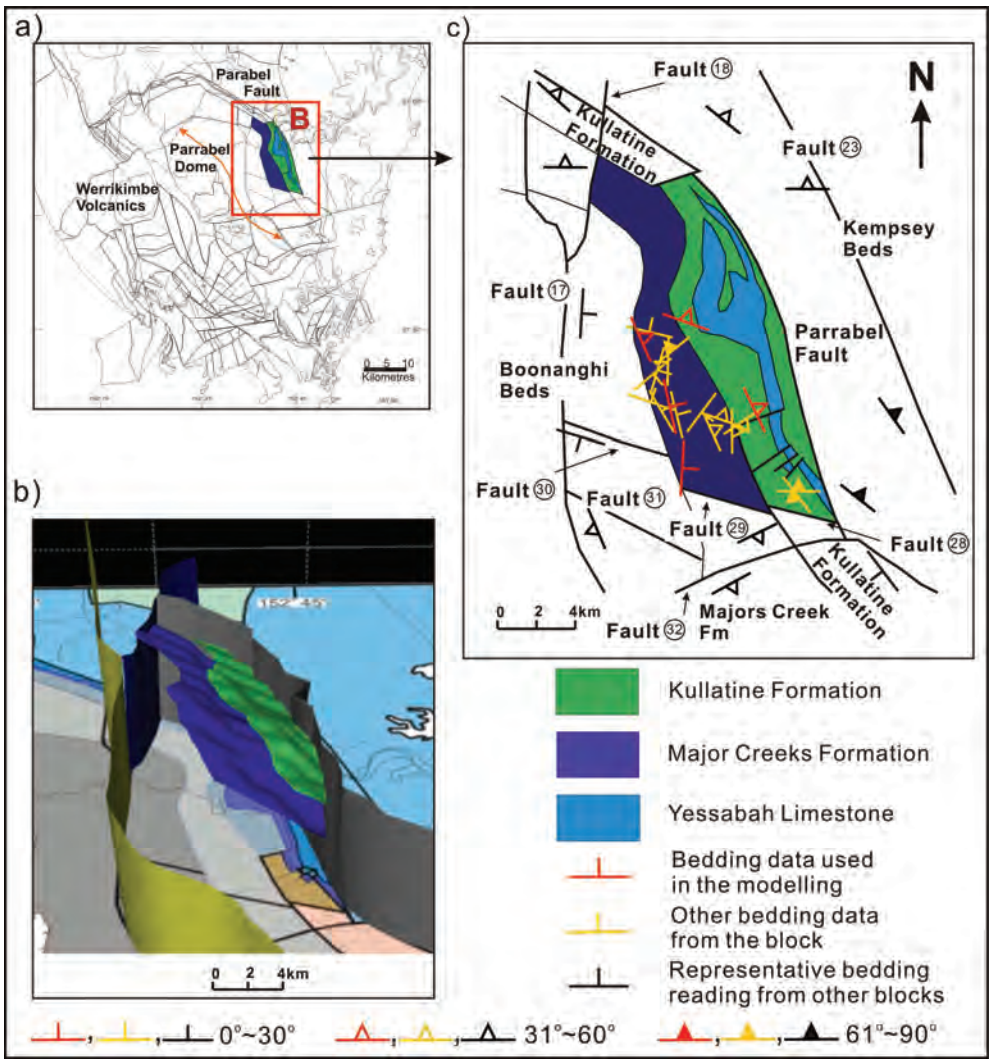

Figure 5.27: Fault block B: a) Locality map showing the position of the fault block; b) map of the bottom surfaces of the Major Creeks and Kullatine Formations in this block, the other map units are shown in the legend of Figure 5.3. The animated images of bottom surfaces in 3D model are displayed in Appendix 8 - 4; and c) schematic map with observed bedding reading.

The Yessabah Limestone in the Fault Block B has an unusual outcrop pattern. It is Permian in age and is composed essentially of limestone, sandstone and shale. It lies on the eastern limb of the Parrabel Dome, and the average dip and dip azimuth for this area is 34° to 88° (Jeffery 1986) which is consistent with other formations in Fault Block B. Bourke (1971) suggested two bands of limestone mapped in this area (Figure 5.28b), whereas Jeffery (1986) and Roberts *et al.* (1995) suggested three bands of limestone mapped which are equivalent in time and composition (Figure 5.28a). Jeffery (1986)

suggested that the repetition of this Yessabah Limestone was caused by tight, inclined isoclinal folding that plunges shallowly to the NNW and faulting in the region rather than three separate episodes of deposition. Jeffery (1986) proposed a model consisting of two phases of deformation to explain the repetition of the Yessabah Limestone. D_1 results in the formation of the Parrabel Dome with the Yessabah Limestone striking parallel to the axis of the dome and hence dipping to the northeast. D_2 caused the eastern limb of the Parrabel Dome to pivot in a clockwise rotation about a hinge point north of the Yessabah Limstone and the sequence was refolding to plunging shallowly to the NNW.

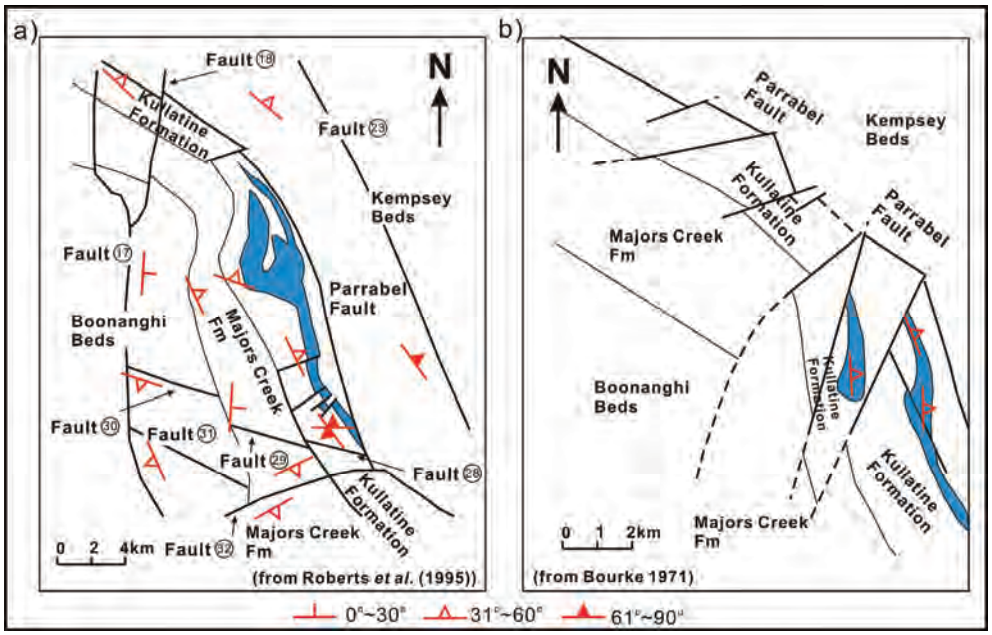

Figure 5.28: Map pattern of the Yessabah Limestone in the Fault Block B. a) Three exposures of the Yessabah limestone as interpreted by Jeffery (1986); b) two exposures of the Yessabah limestone as proposed by Bourke (1971).

5.6.3 Fault Block C

Fault Block C is located on the southeastern limb of the Parrabel Dome, southwest of Fault Block A and south of Fault Block B (Figures 5.3 and 5.29a). It is cut by Fault 17 to the west, Fault 32 to the north, Fault 28 to the east and the Mingaletta Fault to the south (Figure 5.29b). By defining the primary bedding data that represent the overall

trends and strike of the bedding surface in the Fault Block C, we found that: 1) the primary bedding data close to the northern margin of this block dips to the southsoutheast to south and 2) the primary bedding data closest to the southern margin dip to the northeast (Figure 5.29b). The horizons are constructed by using Mathematica™ and 3D Move™ based on these primary bedding data (Figure 5.29c; Appendix 8 - 3).

The Boonanghi Beds are older than the overlying Majors Creek Formation. Although clearly folded, the Majors Creek Formation in this block generally dips south suggesting it youngs in this direction. Hence, the northern margin of this block is considered to be the bottom of the formation and the southern margin is the top.

Considering that the large northwesterly trending Parrabel Dome predominates in the Northern Hasting Block, the Majors Creek Formation in Fault Block C would be expected to dip east to southeast in line with its position within the dome and the bedding in this block should be similar with the bedding of Majors Creek Formation in Fault Block B. The data shows that the presumed the bottom surfaces of Major Creek Formation in Fault Block C changes from dipping to the southeast to south (in the north of the block which represents the bottom) to the northeast (in the south of the block which represents the top). How did the Majors Creek Formation in Fault Block C change its dip direction within the block? In Figure 5.29c the bottom surfaces of the Majors Creek Formation is shown folded to explain the variations in dip direction evident in Figure 5.29b. The almost west-dipping bedding readings northwest and west of Fault Block C are similar in dip direction to many of the bedding readings in the far west of Block C and in Block A east and adjacent to this block. The dip of this bedding in fault block adjacent to Fault Block C is contrary to that expected on this northeastern to southeastern limb of the Parrabel Dome (Figure 5.29a). It is difficult to reconcile the observed bedding readings across the area shown in Figure 5.29b with its position on the northeastern margin of an extended Parrabel Dome as shown in Figure 5.29a.

Bedding dipping east or northeast would be expected. Perhaps clockwise rotation and re-orientation of the northeastern limb has disrupted the expected simple pattern of bedding in this area, compounded by extensive faulting.

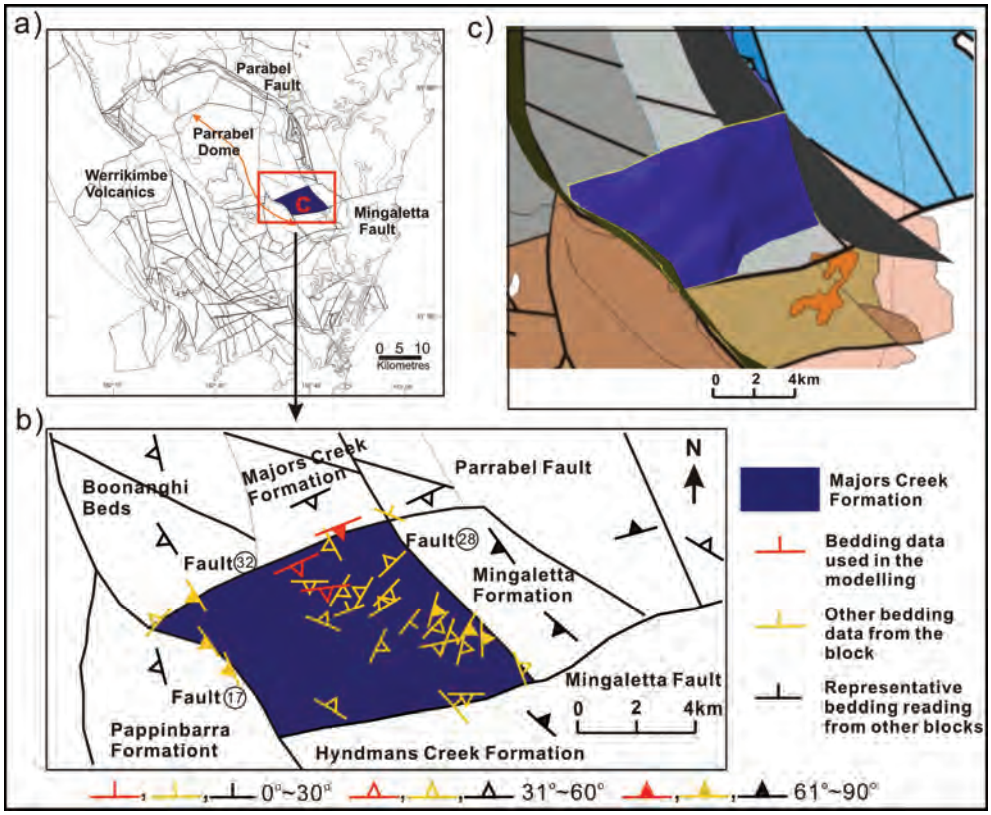

Figure 5.29: Fault Block C: a) Locality map showing the position of the fault block; b) schematic map with observed bedding reading (red reading were used in the modelling) and c) bottom surfaces of the Majors Creek Formation in this block (Appendix 8 - 3). The identity of the surrounding coloured map units are shown in the legend for Figure 5.3.

5.6.4 Fault Block D

Fault Block D is located on the northern limb of the Parrabel Dome within the Northern Hastings Block (Figure 5.30a). This fault block is cut by the Fault 7, 9 and 14 to the west, Fault 17 to the east and the Parrabel Fault to the northeast (Figure 5.30b). There are four formations in sequence within Fault Block D. They are the basal Major Creek Formation, the overlying Kullatine Formation/Youdale Formation and the top most

Warbro Formation according to Roberts *et al.* (1995). This indicates the younging direction in this fault block is from the south to the north. The Youdale Formation and the Kullatine Formation are contemporaneous according to Roberts *et al.* (1995) in Fault Block D (Figure 5.30b).

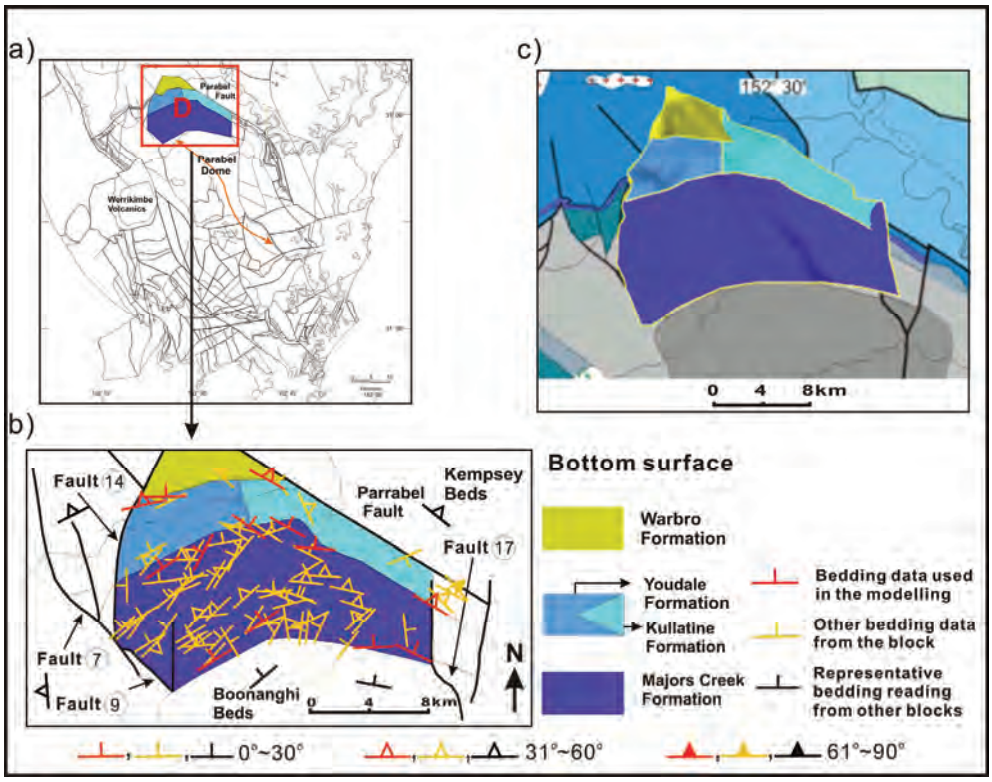

Figure 5.30: Fault Block D: a) Locality map, b) detailed map of the faulting and bedding readings within the various formations in this block. The red bedding symbols were the readings used in the generation of the computer surfaces for the formations and c) 3D model of the formations in the fault block (Appendix 8 - 5). The identity of the surrounding coloured map units are shown on the legend for Figure 5.3.

The primary bedding data that are used in creating the surfaces are shown by the red dip data in Figure 5.30b. The relevant bedding data are located close to the fault or at the geological boundary between two formations. Most of the primary bedding data dip gently northeast or northwest which is consistent with that expected for this fault block as it is located on the gently-plunging hinge region of the Parrabel Dome. Three horizons representing the basal surfaces of these four formations in Fault Block D are constructed by using Mathematica™ and 3D Move™ based on these primary bedding

data (Figure 5.30c; Appendix 8 - 5). These three horizons dip northwest to northeast according to the primary bedding data. There is an open anticline on the basal part of the Major Creek Formation and the fold axis plunges gently north which is consistent with that observed regionally F_3 (11° -> 302°, Lennox *et al*. 1999).

5.6.5 Fault Block E

Fault block E is located on the northwestern limb of the Parrabel Dome (Figures 5.3 and 5.31a). This fault block is cut by the Mooraback Fault to the northwest and Fault 7 to the northeast (Figure 5.31b). To the south of the fault block, the Triassic Werrikimbe Volcanics truncate the formations (Figure 5.31b). The Boonganhi Beds which form the basement formation in the Parrabel Dome are located on the southeastern side of the fault block (Figure 5.31b). There are five formations overlying each other in sequence in Fault Block E. They are, from the base to the top, the Major Creek Formation, Kullatine Formation, Youdale Formation (C), Yessabah Limestone and Warbro Formation.

The top of the Boonanghi Beds will represent the base of the Majors Creek Formation. The primary bedding data represent the overall dips and strikes of the bedding surface used in creating the surfaces are located close to the fault or at the geological boundary between two formations (see the red dip data in Figure 5.31b). Most of the dip data in fault block E dip southwest to west which is consistent with what is expected for the fault block E given its location on the dome. Five horizons representing the basal surfaces of the five formations in Fault Block E are then constructed by using Mathematica™ and 3D Move™ based on these primary bedding data (Figure 5.31c; Appendix 8 - 6).

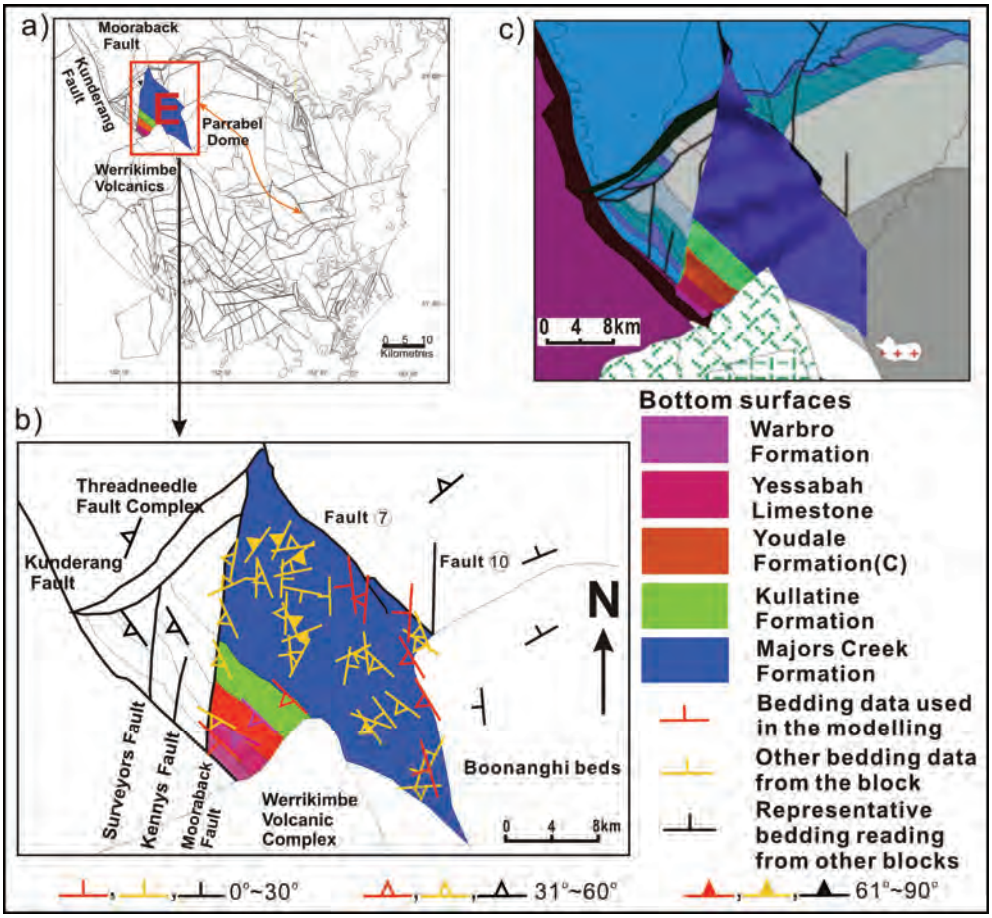

Figure 5.31: Fault Block E; a) locality map, b) detailed map of the faulting and bedding readings within the various formations, the red symbols were readings used in the generation of the surfaces and c) 3D model of the formations in the fault block (Appendix 8 - 6). The identity of the surrounding coloured map units are shown in the legend for Figure 5.3.

5.6.6 Fault Block F

Fault block F is located on the northwestern limb of the Parrabel Dome and west of Fault Block E (Figures 5.3 and 5.32a). This fault block is cut by the Mooraback Fault to the east, Kunderang Fault to the southwest and Threadneedle Fault Complex to the north (Figure 5.32b). There are five formations overlying each other in sequence in Fault Block F which is similar with that in Fault Block E. They are, from the base to the top, the Major Creek Formation, Kullatine Formation, Youdale Formation (C), Yessabah Limestone and Warbro Formation. The Surveryors Fault underwent the sinistral strike-slip movement, whereas the Kenny Fault appear to have dextral strike-slip

movement using displacement of different formations.

Most of the dip data in fault block F dip southwest to west which is consistent with what is expected for the fault block F given its location. Five horizons representing the basal surfaces of the five formations in Fault Block F are then constructed by using Mathematica™ and 3D Move™ based on the primary bedding data (Figure 5.32c).

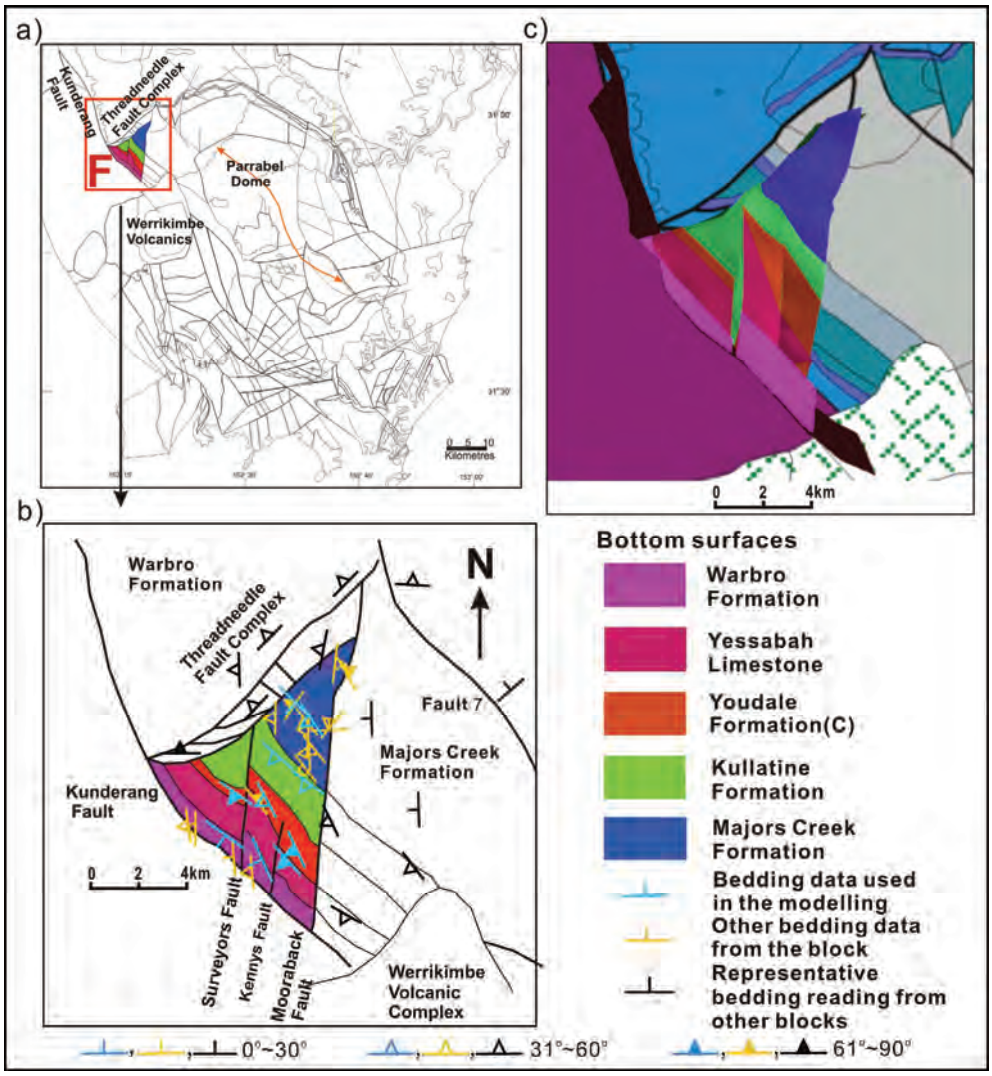

Figure 5.32: Fault Block F: a) locality map, b) detailed map of the faulting and bedding readings within the various formations, the blue symbols were readings used in the generation of the surfaces and c) 3D model of the formations in the fault block. The identity of the surrounding coloured map units are shown in the legend for Figure 5.3.

5.6.7 Fault Block G

Fault block G is located on the northwestern limb of the Parrabel Dome and north of Fault Block F (Figures 5.3 and 5.33a). This fault block is called the Threadneedle Fault Complex block. It is cut by the Mooraback Fault to the east, Fault 5 to the north, Fault 6 to the south and Kunderang Fault to the west (Figure 5.33b). There are four formations overlying each other in sequence in Threadneedle Fault Complex block. They are, from the base to the top, the Major Creek Formation, the overlying Youdale Formation, Yessabah Limestone and Warbro Formation. Bourke (1971) considered that the Threadneedle Fault Complex (faults 5, 6, T1 and T2) was not conjugate to the Kunderang Fault but rather the complex is at right angles to it. Faults 5, 6, T1 and T2 all show dextral strike-slip movements.

Most of the dip data in fault block F dip northwest to west. Given its location, we would expect to see that most data dip northwest. Why are there many west-dipping data in the fault block? A discussion of the development of this complex will be made in the Discussion section. Four horizons representing the basal surfaces of the four formations in Fault Block G are then constructed by using Mathematica™ and 3D Move™ based on the primary bedding data (Figure 5.33c).

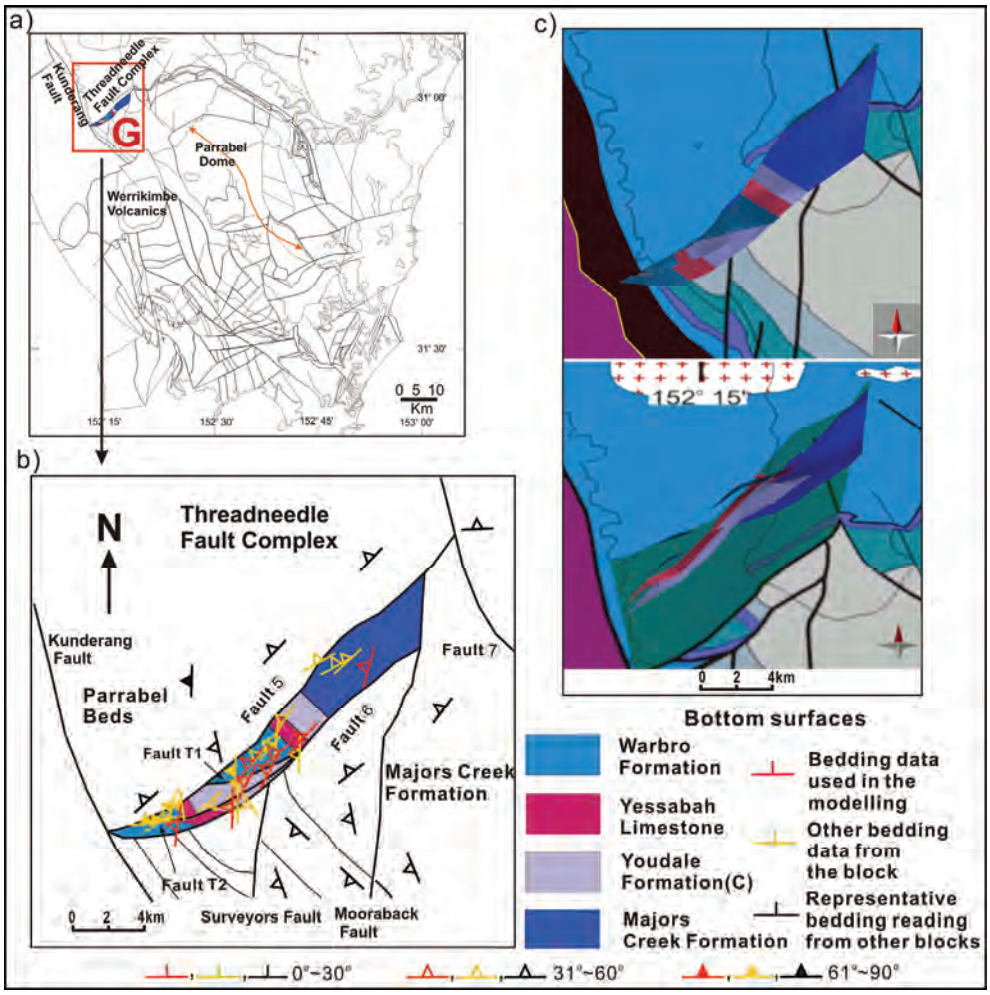

Figure 5.33: Fault Block G: a) locality map, b) detailed map of the faulting and bedding readings within the various formations, the red symbols were readings used in the generation of the surfaces and c) 3D model of the formations in the fault block with the top down and inclined top down views. The identity of surrounding coloured map units are shown in the legend for Figure 5.3.

5.6.8 Fault Block H (Birdwood Fault Complex)

Fault Block H is located on the southwestern limb of the Parrabel Dome within the Northern (?) Hastings Block (Figure 5.34a). This fault block is cut by the Pappinbarra Fault to the east, Fault 47 to the southeast, the Cowarral Fault to the west and Rollans Road Fault to the southwest (Figure 5.34b). Northwest of the fault block the Triassic Werrikimbe Volcanics truncate the formations. There are four formations overlying each other in sequence within Fault Block H. They are from base to top, the Nevann Siltstone,

the Pappinbarra Formation, the Hyndmans Creek Formation and the Mingaletta Formation according to Roberts *et al.* (1995) (Figure 5.34b). This indicates the younging direction is from south to north which is different from all the adjoining fault block which young to the east. This block may be within the Southern Hastings Block as per Figure 5.1. In some models for the Hastings Block this key boundary lies northeast of this block (Roberts *et al.* 1995; Figure 5.34) and in other models this fault block lies within the Northern Hastings Block (Lennox *et al.* 1999). Roberts *et al*. (1995) designated the formations above as belonging to the Southern Hastings Block (SHB). Glen and Roberts (2012) suggested this block was west of the Bagnoo Fault and extensions which they designated the boundary between the two blocks so that it lay in the SHB.

The primary bedding data are used in creating the surfaces which are defined in this fault block (the red dip data in Figure 5.34b). The relevant bedding data are located close to the fault or at the geological boundary between two formations. Most of the primary bedding data dip northeast to north which is different to what is expected for the Fault Block H. Since it is located on the southwestern limb of the Parrabel Dome and the beds would have been expected to dip southwest to westwards away from the dome if the area was not disrupted. The bedding in Fault Block J (adjoining and east of Fault Block F) dips west as expected for this part of the dome, whereas the bedding strike and dips in the Fault Block I (adjoining and west of Fault Block H) west of the Cowarral Fault dip northeast to east (Figures 5.3 and 5.34b).

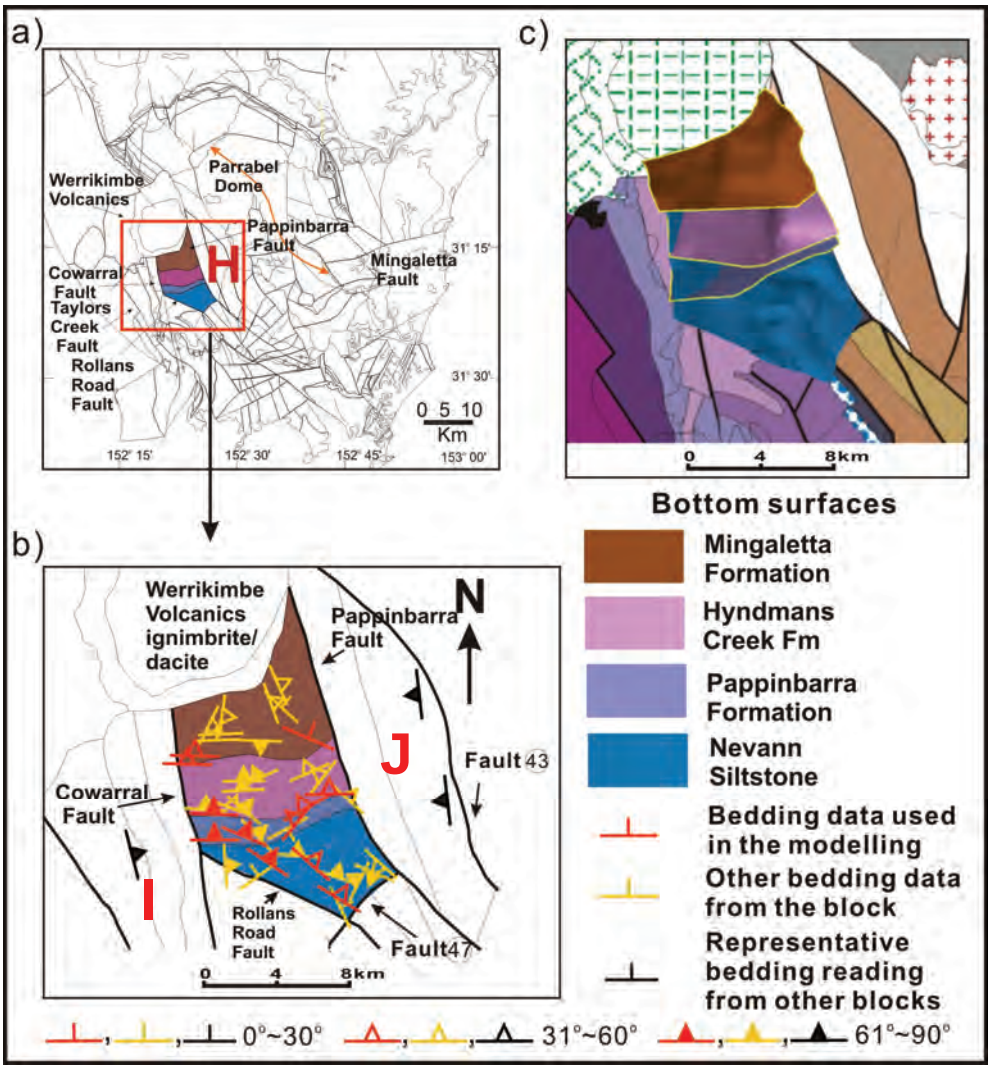

Figure 5.34: Fault Block H: a) Locality map, b) detailed map of the faulting and bedding readings within the various formations in this block, the red symbols were readings used in the generation of the computer surfaces for the formations and c) 3D model of base of the formations in the fault block (Appendix 8 – 7). The identity of surrounding coloured units are shown on the legend for Figure 3.

Four horizons representing the basal surfaces of the four formations in Fault Block H were constructed by using Mathematica™ and 3D Move™ based on these primary bedding data (Figure 5.34c; Appendix 8 - 7). The basal Nevann Siltstone dips northeast, in contrast to the overlying Pappinbarra, Hyndmans Creek and Mingaletta formations which dip north. The surfaces representing the Pappinbarra Formation and the Hyndmans Creek Formation are folded and their fold axes plunge gently north which indicates the fault block has experienced a compressional event.

5.6.9 Fault block I

Fault Block I is located on the southwestern limb of the Parrabel Dome within the Northern (?) Hastings Block (Figure 5.35a). This fault block is cut by the Taylors Creek Fault to the southwest, Fault 48 to the northwest and Cowarral Fault to east (Figure 5.35b). There are three formations in sequence within Fault Block I. They are the basal Late Devonian Bitter Ground Volcanics, the overlying Birdwood Formation and top most Rollans Road Formation. This indicates the younging direction in this fault block is from west to east.

The primary bedding data that are used in creating the surfaces are shown by the red dip data in Figure 5.35b. Most of the primary bedding data dip east which is opposite to that expected for the Fault Block I, as it is located on the southwestern limb of the Parrabel Dome and the beds would have been expected to dip southwest to westwards away from the dome. The rocks in this block are significantly older than those in Fault Block H and K. They are younging eastward whereas if there was no disruption to the sequence around the dome they may have been expected to have younged west. The difference in age and younging direction suggests major disruption to the sequences lying southwest of the Parrabel Dome perhaps consistent with the boundary between the northern and southern Hastings Block being near the Bagnoo-Rollans Road-Cowarral fault system (Figure 5.2).

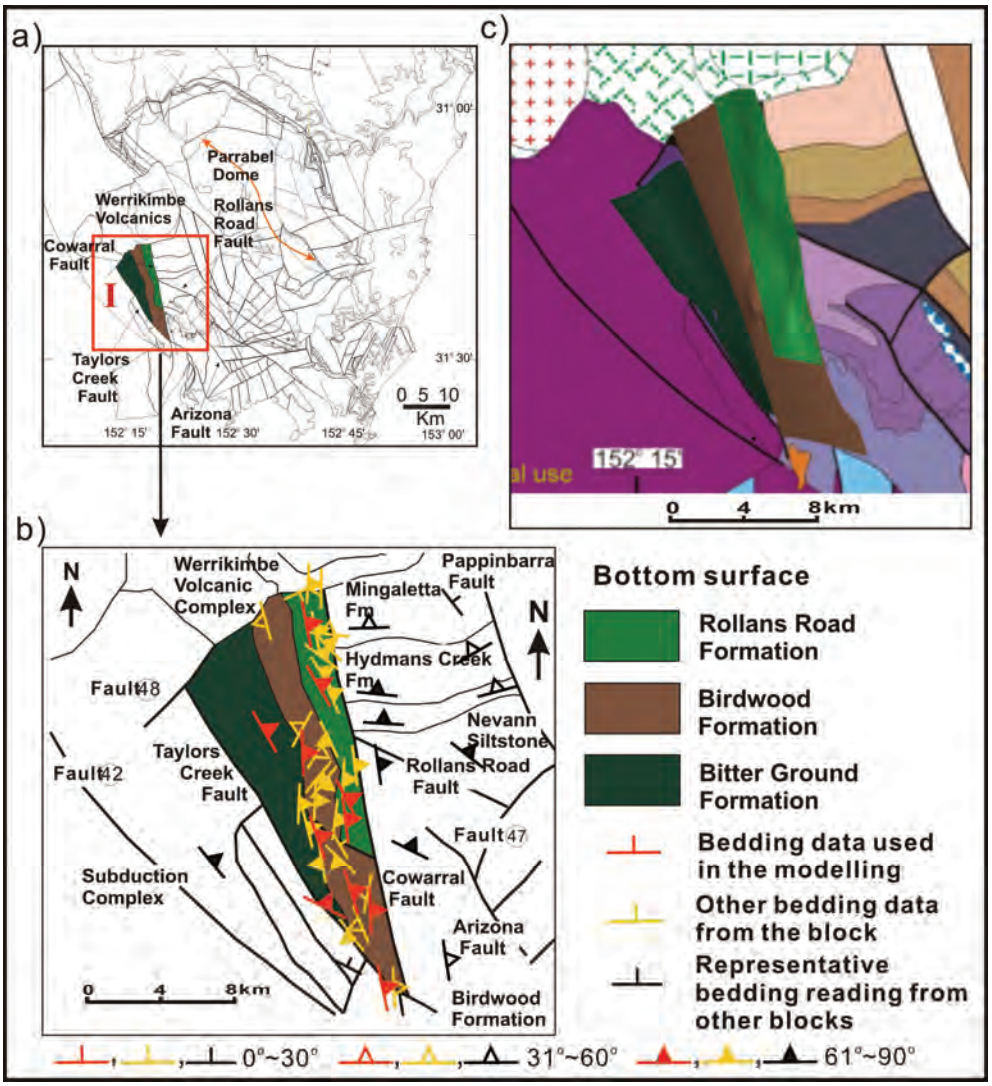

Figure 5.35: Fault Block I: a) Locality map, b) detailed map of the faulting and bedding readings within the various formations in this block, the red symbols were readings used in the generation of the computer surfaces for the formations and c) 3D model of base of the formations in the fault block. The identity of the surrounding coloured units are shown in the legend for Figure 5.3.

5.6.10 Fault block J

Fault Block J is located on the southwestern limb of the Parrabel Dome and east of Fault Block H (Figure 5.36a). This fault block is cut by the Pappinbarra Fault to the southwest, Fault 43 to the northeast and Fault 39 to the southeast (Figure 5.36b). To the northnorthwest of the fault block, the Triassic Werrikimbe Volcanics truncate the Nevann Siltstone. There are two formations in Fault Block J. They are from base to top

the Pappinbarra Formation and the Hyndmans Creek Formation according to Roberts *et al.* (1995). Leitch (pers. com. 2013) has indicated that the Hyndmans Creek Formation is in fact the Nevann Siltstone. This changes the younging direction from west younging to east younging. Roberts *et al*. (1995) designation of the unit as Hyndmans Creek Formation which would be consistent with the presence of the Parrabel Dome to the northeast of this fault block, whereas Leitch's (2013) suggestions that it is in fact the Nevann Siltstone would require a syncline between the dome and this fault block.

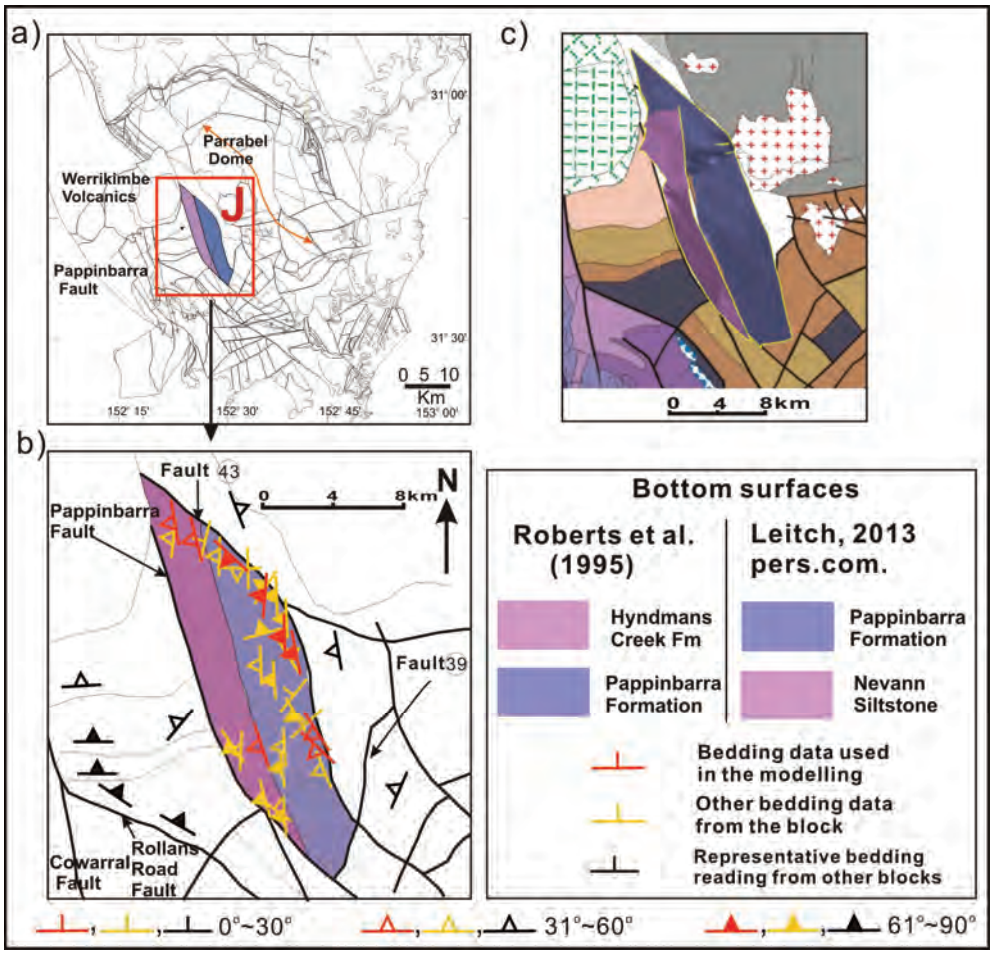

Figure 5.36: Fault Block J: a) locality map, b) detailed map of the faulting and bedding readings within the various formations, the red symbols were readings used in the generation of the surfaces and c) 3D model of the formations in the fault block. The identity of the surrounding coloured units are shown on the legend for Figure 5.3.

Most of the primary bedding data dip southwest to west which is consistent with what is expected for the Fault Block J as it is located on the southwestern limb of the Parrabel

Dome (Figure 5.36b). Two horizons representing the basal surfaces of the two formations in Fault Block J are then constructed by using Mathematica™ and 3D Move™ based on these primary bedding data (Figure 5.36c).

5.6.11 Fault Block K

Fault Block K is located on the southwestern limb of the Parrabel Dome and south of Fault Block H within the Northern (?) Hastings Block (Figure 5.37a). This fault block is cut by the Bagnoo Fault to the southwest, Fault 47 to the northwest, Fault 50 to the northeast and Fault 59 to the southeast (Figure 5.37b). There are two formations in sequence within Fault Block K. They are the basal Pappinbarra Formation and the overlying Hyndmans Creek Formation according to Roberts *et al.* (1995). This indicates the younging direction in this fault block is from the southwest to the northeast.

The primary bedding data that are used in creating the surfaces are shown by the red dip data in Figure 5.37b. Most of the primary bedding data dip northeast which is opposite to that expected for the Fault Block K, as it is located on the southwestern limb of the Parrabel Dome and the beds would have been expected to dip southwest to westwards away from the dome. Regionally fault blocks south and west of this fault block dip and young eastward consistent with this block. Fault Block H north of this fault block is unusual in striking almost east-west and dipping and younging northward. It is probably the case that many of these blocks may be part of the Southern Hastings Block. Two horizons representing the basal surfaces of these two formations in Fault Block K are constructed by using Mathematica™ and 3D Move™ based on these primary bedding data (Figure 5.37c). The basal Pappinbarra Formation dips more steeply than the overlying Hyndmans Creek Formation according to the primary bedding data.

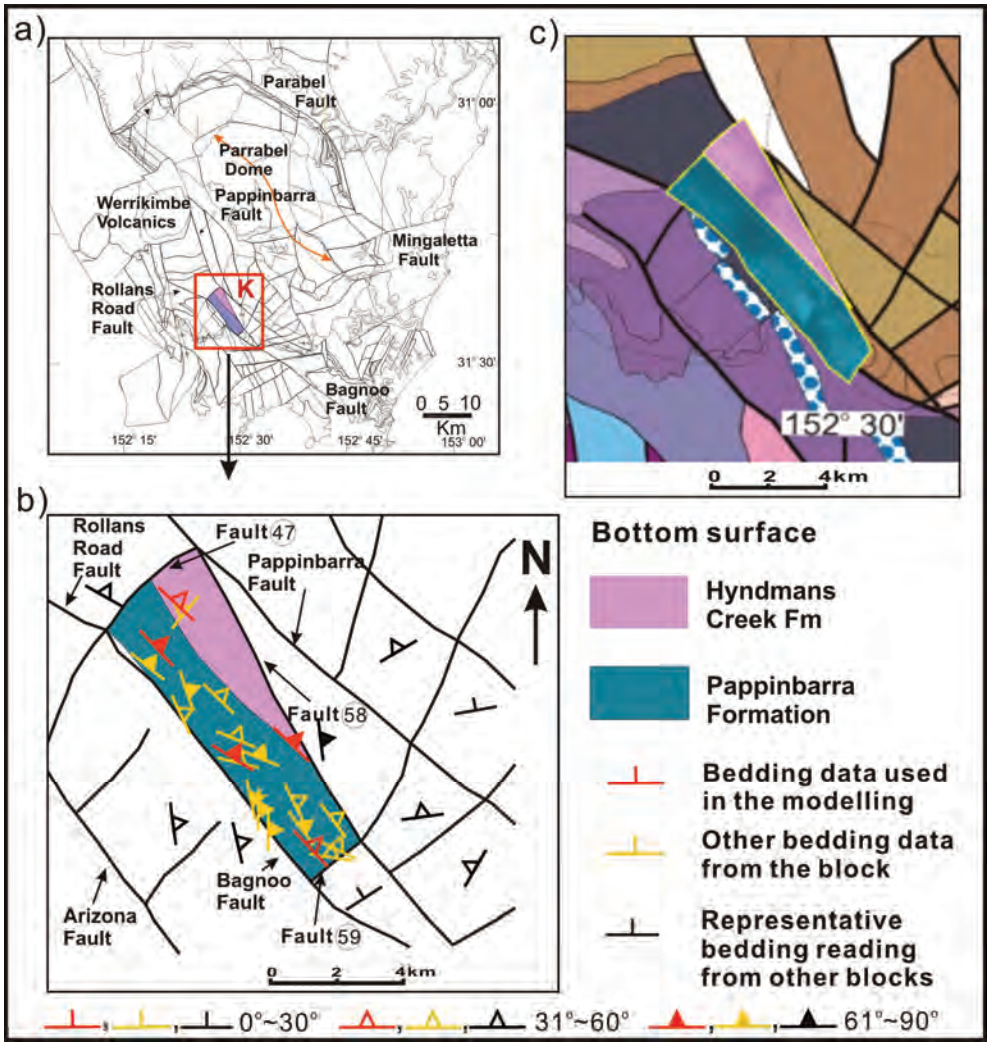

Figure 5.37: Fault Block K: a) locality map, b) detailed map of the faulting and bedding readings within the various formations in this block. The red bedding symbols were the readings used in the generation of the computer surfaces for the formations and c) 3D model of the formations in the fault block. The identity of the surrounding colour map units are shown in the legend of Figure 5.3.

5.7 Discussion

The fault-block by fault-block analysis above showed the shortcomings with the existing geological map of the NHB. These include the extreme variability in the orientation of bedding within some fault blocks, between adjacent fault blocks, and around significant sections of the dome where the dip direction is different from that expected.

5.7.1 Fault block analysis highlighted the shortcomings with the existing geological map

5.7.1.1 The reconstruction model for fault blocks A, B and C on the eastern limb of the Parrabel Dome.

Our data show that the bottom surfaces of Mingaletta Formation in Fault Block A of the NHB dips southwest, the bottom surfaces of sequences in Fault Block B dip east and that in Fault Block C dip south to southeast (Figure 5.38b). These surfaces are built based on the measured dip data. The Northern Hastings Block is characterized by a northwesterly structural grain, related to the macroscopic northwesterly-trending Parrabel Dome. The sequences in Fault Block B are consistent with what is expected in such a dome. The Mingaletta Formation in Fault Block A and the Majors Creek Formation in Fault Block C should dip east to southeast if they are part of a simple dome. How did the Mingaletta Formation in Fault Block A change its dip direction from the southeast to southwest and the Majors Creek Formation in Fault Block C from south to southeast? Here we propose a schematic reconstruction model accounting for the movements on the major faults in these fault blocks. The aim of our reconstruction is only to highlight potential mechanisms that can be tested in future studies.

The schematic reconstruction (Figure 5.38) takes into account the clockwise rotation of the limb of the dome via the strike-slip faulting as the major mechanism responsible for dip direction changes in the Mingaletta Formation in Fault Block A. The reconstruction assumes an originally gently curved limb of the dome which consists of the Youdale/Kullatine formations and contemporaneous Mingaletta Formation (Figure 5.38 c1) along strike from each other (Roberts *et al.* 1995, Figure 5.29). This originally curved structure dips to the east to southeast because of the macroscopic northwesterly-trending Parrabel Dome. We propose that in the middle of the Kullatine Formation on the limb of the dome was pinned (Figure 5.38 c1). Sinistral strike-slip on the Mingaletta Fault caused Fault Block A to rotate clockwise along with the limb of the

dome (Figure 5.38 c2). Subsequent sinistral strike-slip movement caused displacement (Fault Block B) on the Parrabel Fault. These two movements on the faults led to rotation of the bedding in fault block A into its final orientation with dips to the west. The clockwise rotation resulted in the widespread compression of the Kullatine Formation, leading to the outcrop width of the Kullatine Formation in Fault Block B being much wider than the outcrop width of this formation north of the pin point. This outcrop width may also reflect the change in dip of the Kullatine Formation along strike. The repetition of the Yessabah Limestone in the Fault Block B can also be explained in this model. The Yessabah Limestone was firstly striking parallel to the axis of the Parrabel Dome and hence dipping to the northeast. The clockwise rotation of the limb of the dome resulted in the limestone sequence being tightly folding with repetition of the unit (Jeffrey 1986).

The strike-slip movement on the faults described above may be responsible for dip direction changes of the Mingaletta Formation in Fault Block A. This clockwise rotation and re-orientation of the northeastern limb, caused the simple pattern of bedding in Fault Block C to show dip changes from the east-dipping to south-dipping.

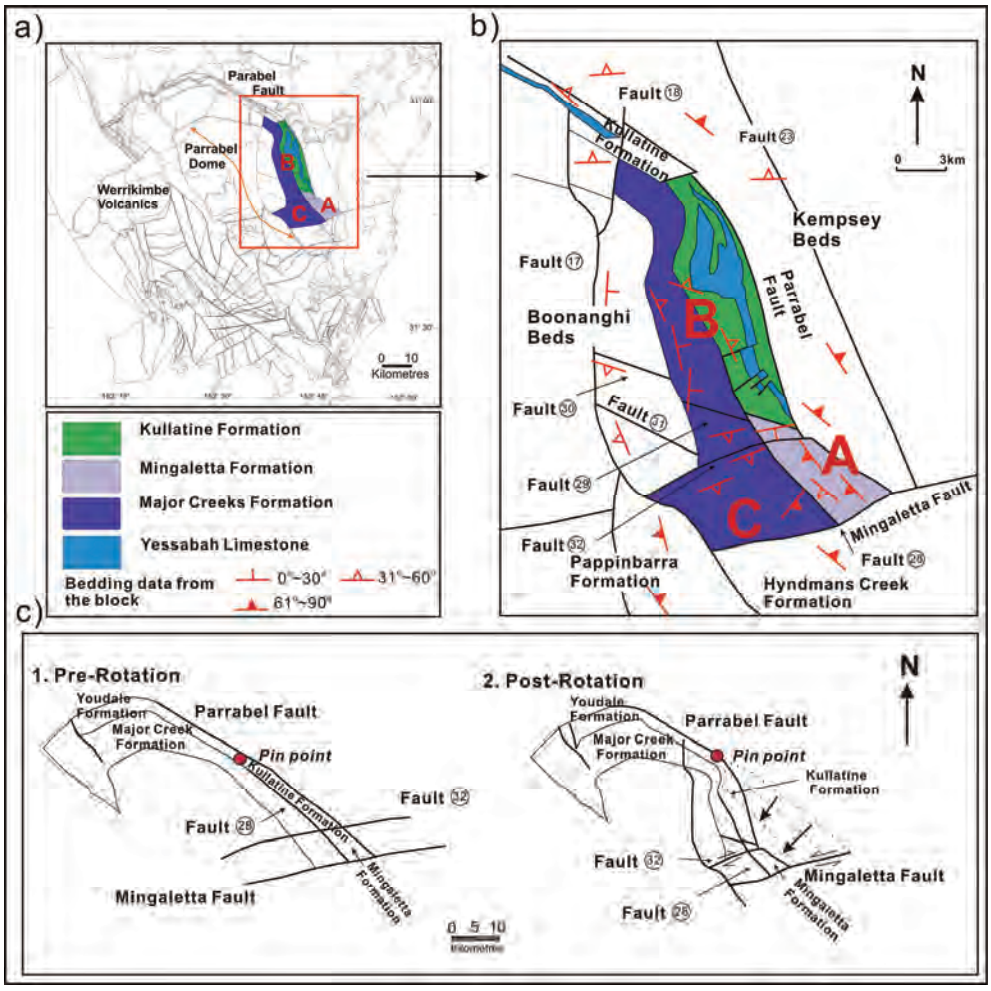

Figure 5.38: Analysis of the fault block A, B and C. a) locality map, b) detailed map of the faulting and stratigraphy within the various fault block, c) schematic diagram for a possible reconstruction model for Fault Block A between two almost east-west faults undergoing sinistral strike-slip (Mingaletta Fault) and dextral strike-slip (Fault 32) as the limb of the Parrabel Dome rotated clockwise around a pin point shown as a red dot.

5.7.1.2 Fault block analysis in the Birdwood Fault Complex, northwestern limb of the Parrabel Dome.

The Birdwood Fault Complex consists of the fault blocks H, I, J and K in NHB (Figure 5.39a). Analysis of the bedding data and stratigraphy of this area demonstrated that :

(1) There are two formations overlying each other in sequence in Fault Block J (Figure 5.36b). The re-interpreted stratigraphy means the units young to the east but dip steeply west. The dip direction is consistent with the expected dip on this part of the Parrabel

Dome but the younging direction is not consistent with the dome. Fault Block J younging is consistent with Fault Block I, but not the intervening Fault Block H. There may be a major synform between the dome and these fault blocks (I and J) or a major change in the geology.

(2) There are four formations overlying each other in Fault Block H (Figure 5.39b). They are the basal Nevann Siltstone, the overlying Pappinbarra Formation, the Hyndmans Creek Formation and the top most Mingaletta Formation. This indicates the younging direction is from the south to the north. This fault block appear rotated ninety degrees clockwise from its original position if it is considered to have originally consisted of northerly-striking bedding younging to the west or southwest. If the fault block originally younged east then it would require 90° anticlockwise rotation to fit its final orientation (Figure 5.39c).

(3) In Fault Block I, there are three formation which are, from the basal Late Devonian Bitter Ground Volcanics, the overlying Birdwood Formation and top most Rollans Road Formation (Figure 5.39b). This suggests a younging direction from west to east. These rocks are significantly older than those in Fault Block H and J and they are younging eastward whereas if there was no disruption to the sequence around the dome they may have been expected to have faced west. The difference in age and younging direction suggests major disruption to the sequences lying southwest of the Parrabel Dome perhaps consistent with the boundary between the northern and southern Hastings Block being near the Bagnoo - Rollans Road - Cowarral fault system.

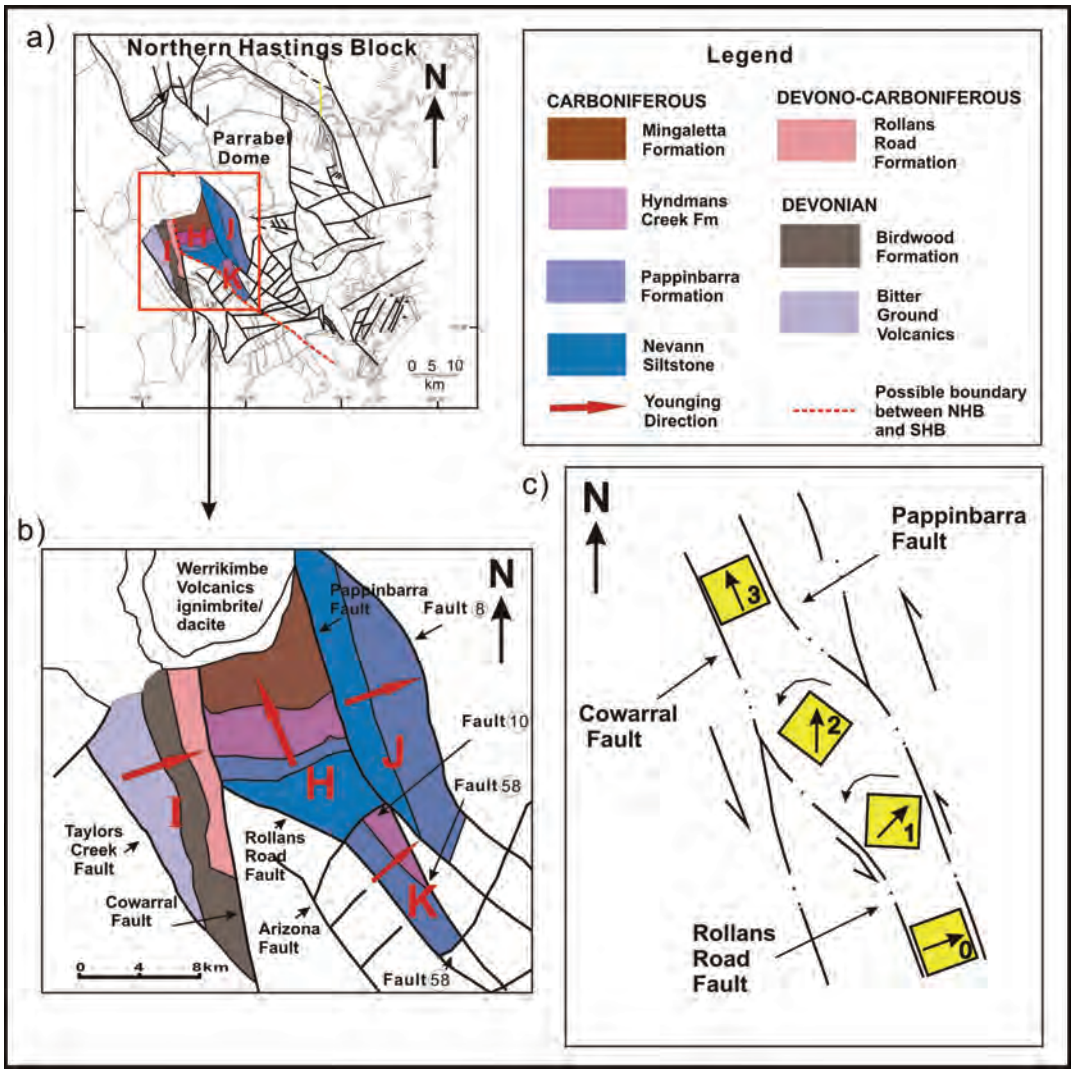

Figure 5.39: Analysis of the fault block H, I and J. a) locality map, b) detailed map of the faulting and stratigraphy within the various fault block, the red arrows are the younging direction, c) possible model of how Fault Block F was emplaced using existing bounding faults.

Fault Block H is probably rotated 90° anti-clockwise from its original position to the south if it is considered to have originally consisted of northerly-striking bedding younging to the east-northeast (Figure 5.36c). Fault Block H may have been translated into its current position by the transcurrent, sinistral movement between two bounding faults (Pappinbarra Fault and Cowarral Fault, Figure 5.39c).

5.7.1.3 Fault block analysis in the Kunderang District, northwestern limb of the Parrabel Dome

Fault Blocks E and F seem consistent with the observed macroscopic Parrabel Dome. The west to westnorthwesterly dipping beds in the Majors Creek Formation within Fault Block E probably reflect bending around the dome. Bourke (1971) argues for a Threadneedle Fault Complex (TFS) northwest and adjacent to Fault Block F to explain the change of bedding dips, the outcrops in the complex and the change in geology across to the Parrabel Beds to the northwest. This fault complex is extremely unusual given the profound changes in the geology across it. There is loss of continuity of units from fault blocks E and F to the Parrabel Beds across this complex.

Given the observed drag of bedding northwest of the TFC as shown by the red formed lines on Figure 5.40b within the Parrabel Beds, it could be argued that Fault Blocks E and F have been emplaced by sinistral movement along Fault 5. The Parrabel Beds overlie the Yessabah Limestone present in Fault Block E and are stratigraphically equivalent to the Warbro Formation which lies at the top (i.e. western margin) of Fault Block E. It is difficult to envisage bedding smoothly changing orientation from Fault Block F across the TFC into the Parrabel Beds to the northwest because of the lack of continuity of the Yessabah Limestone and Kullatine Formation across the TFC.

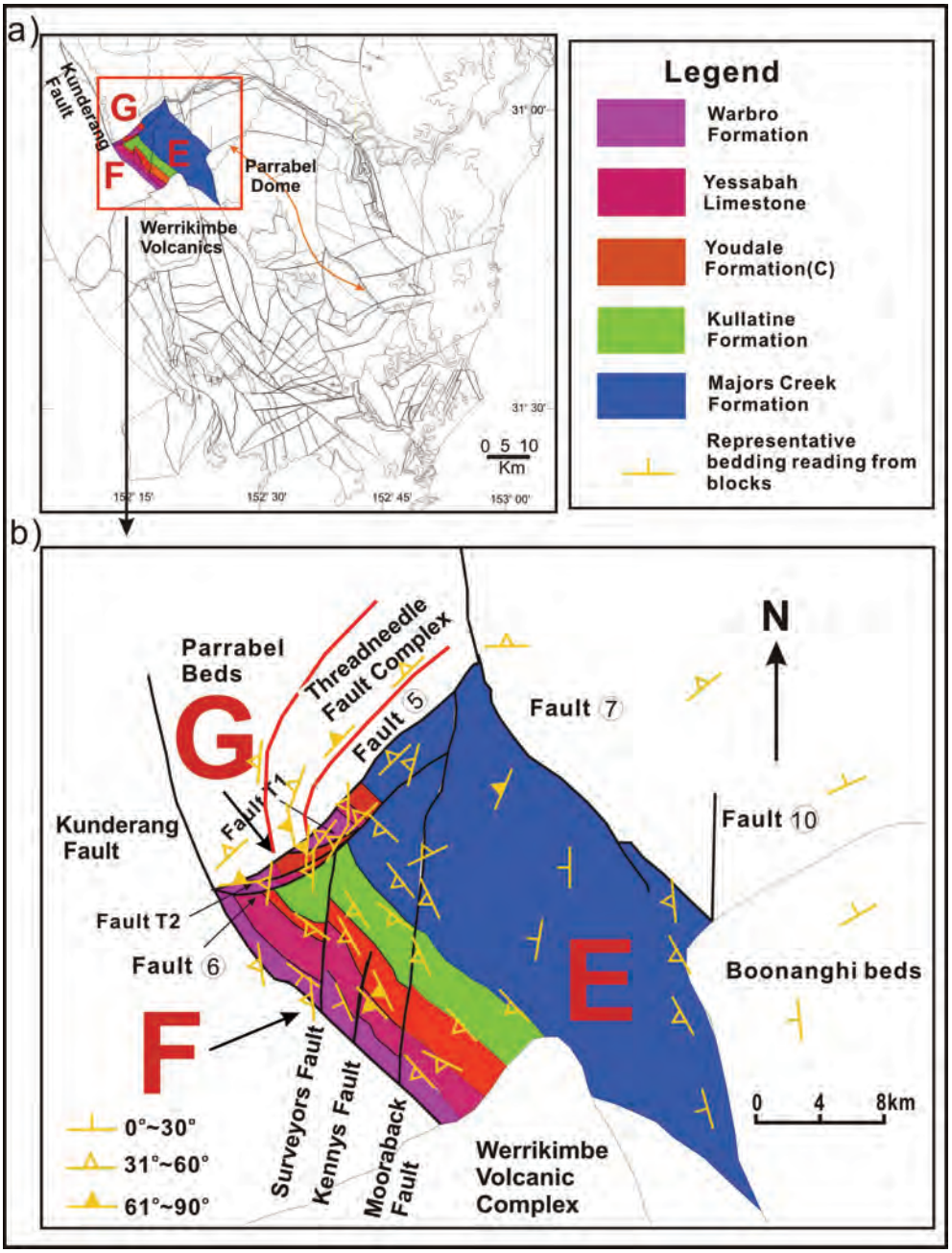

Figure 5.40: Analysis fault blocks in the Kunderang District, northwestern limb of the Parrabel Dome. a) locality map, b) detailed map of the faulting and stratigraphy within the various fault blocks. The red lines within the Parrabel Beds represent the overall strike of bedding (Lennox pers. com. 2015)

5.7.2 Implication of the fault blocks reconstruction for the entire NHB

Stratigraphic units in the NHB are similar lithologically and are time equivalent to other formations in the SHB (Figure 5.41, Glen and Roberts, 2012). Specifically, the Late

Carboniferous Mingaletta Formation in the SHB formed during the same period as the deposition of the Kullatine and Youdale C Formations in the NHB (Glen and Roberts, 2012). The sequences consisting of the Nevann Siltstone\Pappinbarra and Hyndmans Creek Formations in the SHB are the same age as that of the Boonanghi Beds in the NHB. Thus the Mingaletta Formation/Kullatine Formation/Youdale C Formation are given the same blue colour to highlight their continuity around the dome (Figure 5.42). Also shown are the younging directions based on the ages of the various formations (Figure 5.41, Glen and Roberts, 2012) (Figure 5.42). A possible alternative geological boundary between the NHB and SHB is shown as suggested by the gravity and magnetic worms analysis in the Hastings Block that extends from the Kunderang Fault, southeasterly through the Pappinbarra Fault and finally east-northeasterly towards Fault 72 (dashed black line; Figure 5.42).

The younging directions on Figure 5.42 support the existence of the Parrabel Dome in the NHB. The younging directions radiate from the center of the Parrabel Dome in the NHB except for Fault Block J in the southwestern part of the dome which is younging to the ENE. This is contrary with what we expected for a dome and shows that faulting subsequent to folding has strongly dismembered the earlier formed structures. The explanation for this could because of a tight, NW-SE trending syncline parallel to the trace of the axis of the Parrabel Dome between the Fault Block J and the Boonanghi Beds within the core of the dome. The younging direction in the SHB are mostly younging to the ENE based on the stratigraphy south of the Bagnoo Fault. The only exception is Fault Block H, which youngs to the NNW.

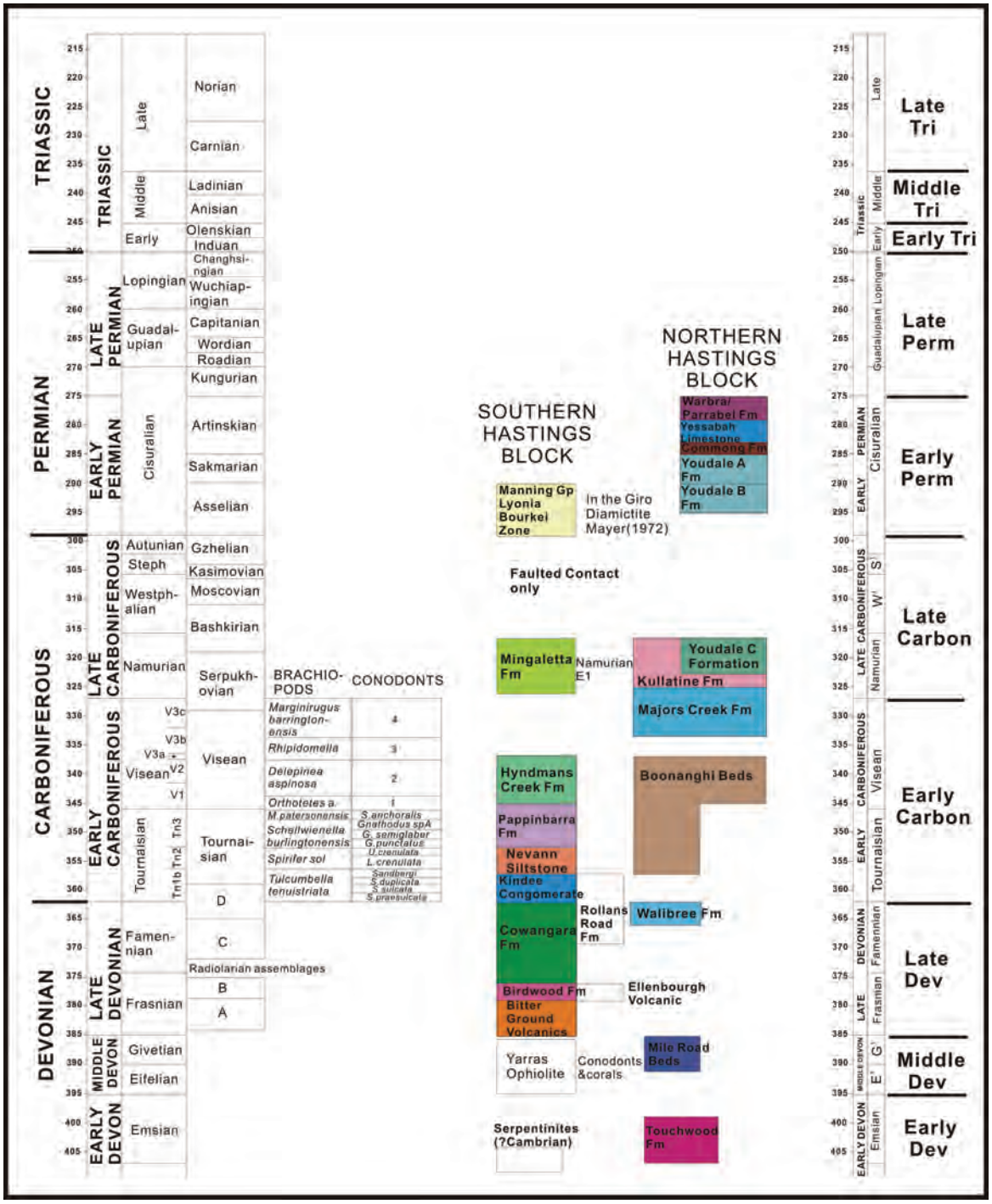

Figure 5.41: Time scale, stratigraphic columns for both the Northern and Southern Hastings Block (modified from Glen and Roberts, 2012). Abbreviations: E^1: Eifelian; G^1: Givetian; S^1 :Steph; W^1:Westphalian.

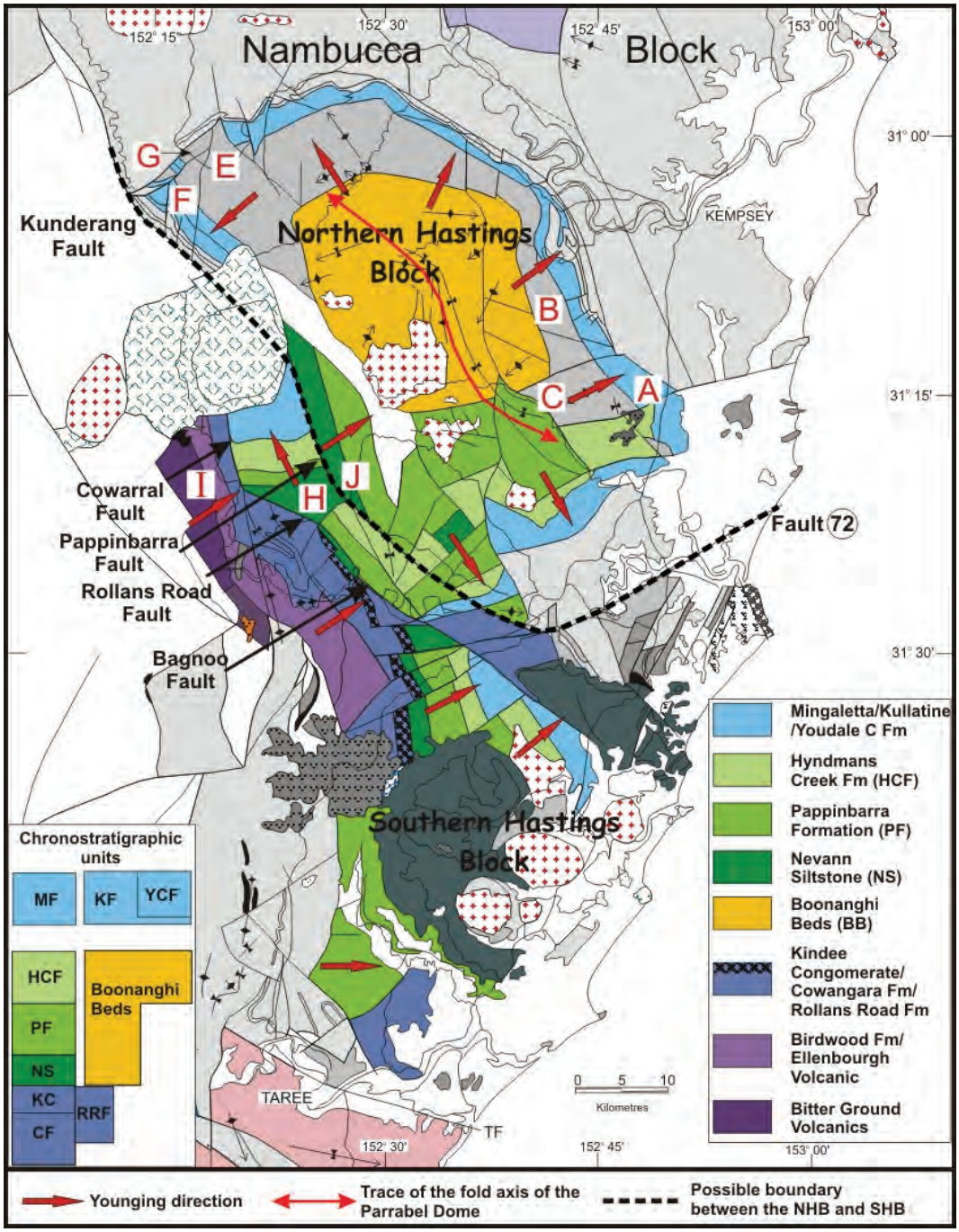

Figure 5.42: Geology of the Hastings Block highlighting the formations of the same age between the NHB and SHB. CF = Cowangara Fornmation; KC = Kindee Congomerate; KF = Kullatine Formation; MF = Mingaletta Formation; RRF = Rollans Road Formation; YCF = Youdale C Formation.

We propose here a schematic restoration of the Hastings Block taking into account fault block reconstruction models for the eastern limb of the Parrabel Dome, the rotation and translation of the Birdwood Fault Complex and the northwestern Kunderang District in

order to better understand the deformation history in the NHB (Figure 5.42). The aim of our restoration is only to highlight potential movements of fault blocks that can be tested in future studies. The steps involved for the restoration are shown in Figure 5.43 are describe below:

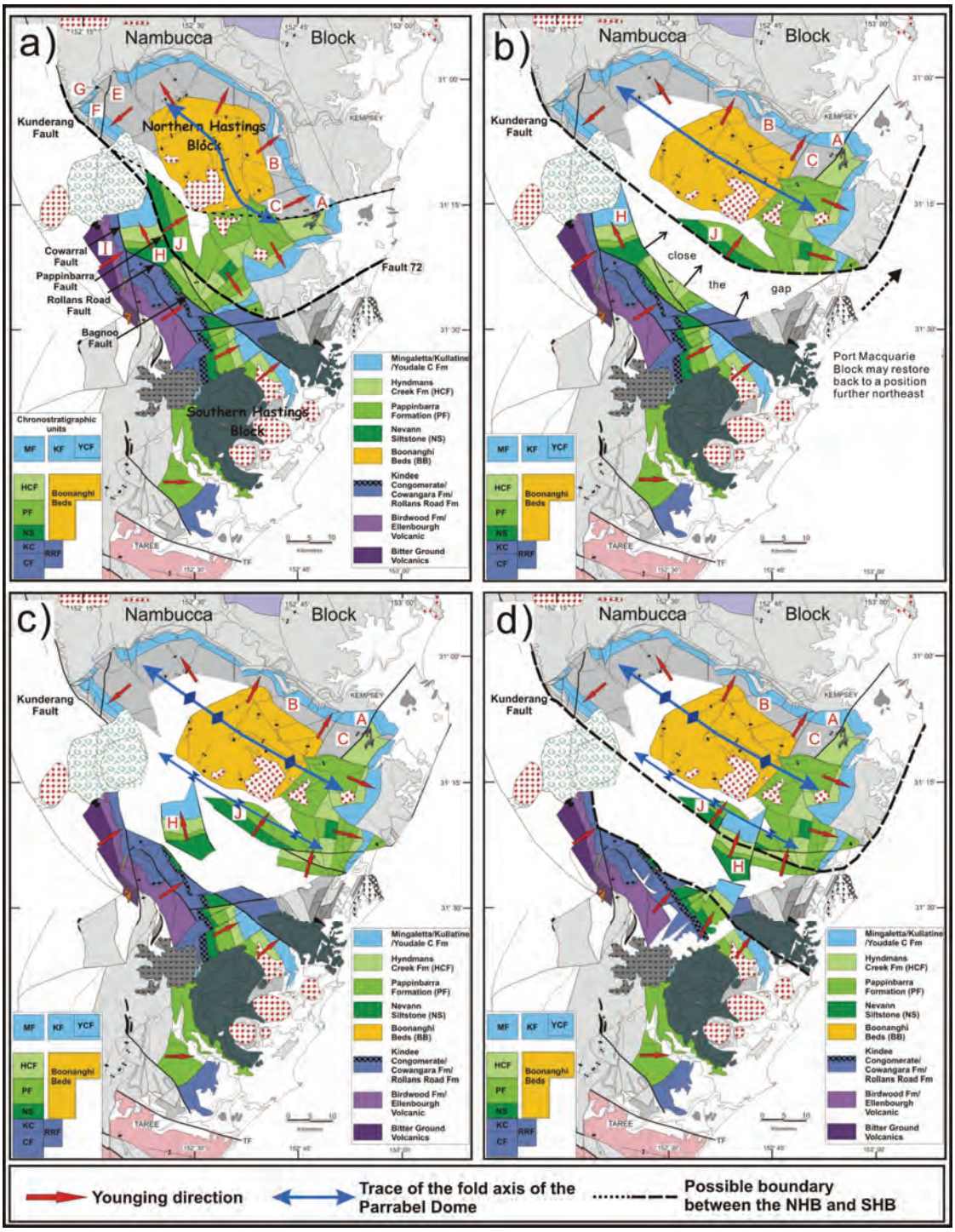

Figure 5.43: Possible restoration of the Hastings Block incorporating the above fault block analysis and reconstructions already discussed. This restoration assumes the

Parrabel Dome was originally unbent and that there may have been a macroscopic synform subparallel southwest of the dome fold axis trace. a) The current state of formations and structures in the NHB; b) The restoration of NE-limb of the Parrabel dome to ensure that the dome is unbent; c) The restoration of the Fault Block H in the SHB; d) initial state of formations and structures in the NHB.

Figure 5.43a shows the bent Parrabel Dome; position of the NHB-SHB according to Robert *et al*. (1995) (narrow dashed line) versus the proposed position suggested in this thesis (thicker dashed line).

Reconstruction

(a) The dominant, gently northwesterly/southeasterly-plunging, megascopic Parrabel Dome formed as a D_3 fold which has then been overprinted by the subsequent NE-SW trending, megascopic folding D_4 in the NHB during the Permian Hunter Orogeny. The geological boundary between the NHB and SHB is positioned from the Kunderang Fault, southeasterly through the Pappinbarra Fault and finally east-northeasterly towards Fault 72 (Figure 5.43a).

(b) The NE-limb of the Parrabel dome can be restored back to its unbent, original position via anticlockwise movement using the Kunderang-Pappinbarra–Fault 72 fault system. Fault Blocks A to C are moving back into their “original” position as discussed previously. The trace of the fold axis of the Parrabel Dome was straighten after restoring back Fault Blocks A to C. A NW-SE trending syncline parallel to the trace of the axis of the Parrabel Dome exists between the Fault Block J and the Boonanghi Beds on the southwestern limb of the dome. This unbent state of the NHB would represent the position before the NE-SW D3 macroscopic fold event (Roberts *et al*. 1993) or D4 macroscopic fold event (this thesis) during the Early Permian (Figure 5.43b).

(c) The restoration of the Fault Block H in the SHB is difficult to constrain. It is believed that Fault Block H may have been translated into its current position by the

transcurrent, sinistral movement between two major fault systems, the Cowarral-Rollans Roads-Bagnoo fault system and the Kunderang-Pappinbarra-Fault 72 fault system (Figure 5.42). During the translation from its original position to its final position, Fault Block H experienced 90° anti-clockwise rotation. The exact original position of Fault Block H is unknown. It could be to the south of its current position. For Fault Block H to have originally been north of it is current position, it would need to lie adjacent and (?) along strike from the southwest facing Fault Block F. Further, it would have had to have been rotated clockwise 90° during translation from its original position (southeast of Fault Block F) to its final position. The translation of the fault block between majors faults must have occurred during faulting after the dome formation (Figures 5.43c and 5.43d).

(d) This model is one of many possibilities for restoring Fault Block H to its original position. In this model Fault Block H has been restored into its original position, southeast of its current position. After translation and rotation, the younging direction in Fault Block H is to the NE, consistent with those in the surrounding units in the SHB (Figure 5.43d).

The disruption of the Kindee Congomerate by Faults 53-56 and 66-67 (Figure 5.43c) were removed so that the Kindee Congomerate returns to its original linear outcrop trace (Figure 5.43d). The displacement of the Kindee Congomerate along Faults 53-56 and 66-67 occurred after folding and cleavage development in the NHB (Chapter 4). The Kindee Congomerate outcrop trace is bent as shown on Figure 5.43c consistent with drag caused by sinistral strike-slip movement on the Bagnoo Fault. The bending and fault displacement of the Kindee Conglomerate has been removed in Figure 5.43d to restore it to its pre-fault position.

Alternatively, another schematic restoration model to explain the disruption of fault blocks between the NHB and SHB involves a fault network similar to those produced in

restraining fault bends along strike-slip faults (Figure 5.44).

The disruption of fault blocks between the NHB and SHB (Fault Blocks H, I and J, Figure 5.42) are suggested to have occurred under a transpressional setting during the Middle Permian Hunter Orogeny. The blocks are bound by a sinistral strike-slip fault systems consisting of the Bagnoo, Pappinbarra, Cowarral and Rollans Road faults.

A bend at which transpression occurs is called a restraining bend because, at such bends, opposing walls of the fault compress against each other (Van der Pluijm *et al.* 2004). There are two setting for restraining fault bends: double restraining bends and single bends. Double bends have bounding strike-slip faults which enter and link across them. These restraining bends commonly define positive flower structures, and strike-slip bends or 'duplexes' along strike-slip fault in plan view (Figure 5.44a). In contrast, single bends commonly have horsetail splay fault geometries in plan view, with essentially strike-slip fault-termination zones (Figure 5.44b) (Cunningham and Mann 2007).

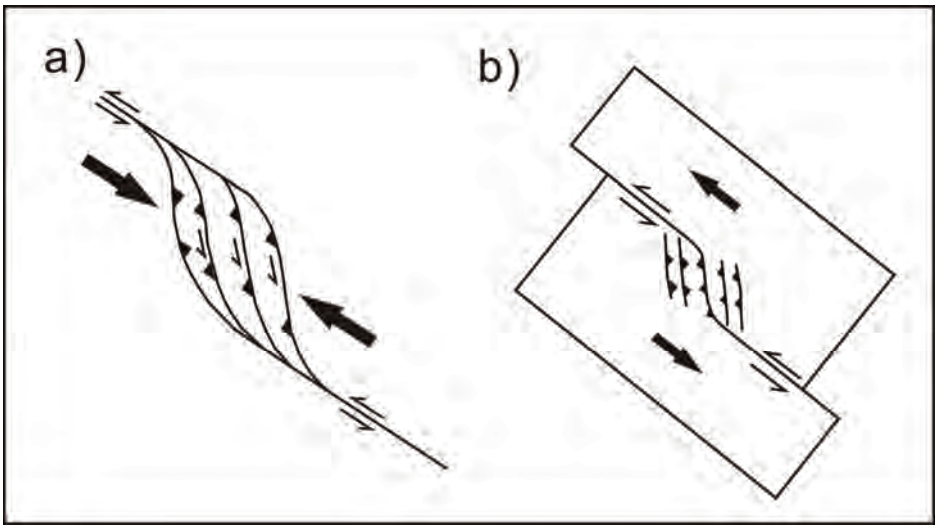

Figure 5.44: Map-view sketches of (a) strike-slip duplexes deformed along a sinistral strike-slip fault and (b) single restraining fault bends at which thrust faults have formed along the sinistral strike-slip fault (Van der Pluijm *et al.* 2004).

Double restraining bends

Flower structures develop along restraining and releasing bends on the strike-slip faults. They resemble the petals of a flower in cross section. In areas where strike-slip faults occur in converging crust, or transpression, rocks are faulted upward in a positive flower structure (Figure 5.45A). In areas of strike-slip faulting in diverging crust, or transtension, rocks drop down to form a negative flower structure (Figure 5.45B).

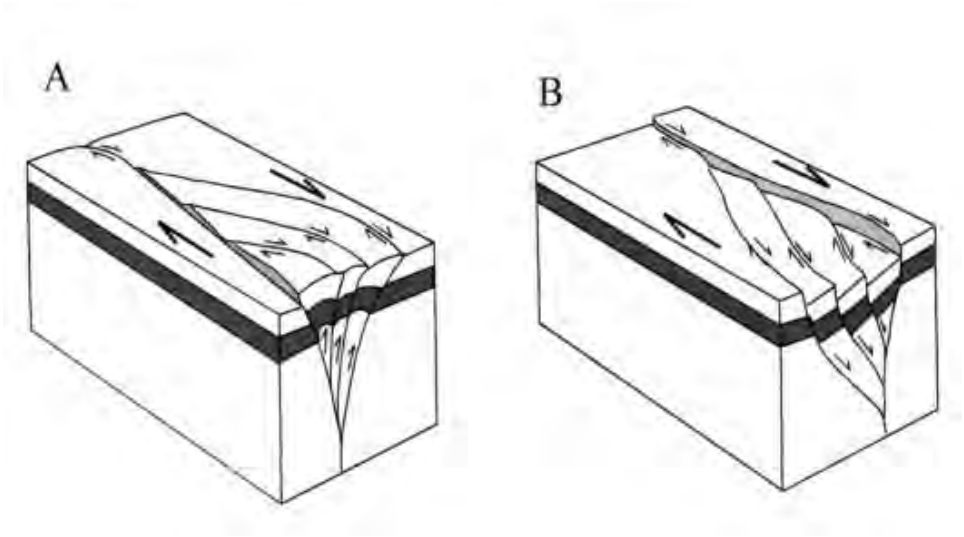

Figure 5.45: Positive (A) and negative (B) flower structures (*Source:* http://earthquake.usgs.gov/research/creep/GardeniaEE_crax.html).

In this model, the geological boundary between the NHB and SHB is suggested to be from the Kunderang Fault, southeasterly through the Fault 43 and finally towards the Bagnoo Fault (Figure 5.46). Fault Block H and J were originally part of the SHB but were affected by bounding strike-slip fault system linking the Kunderang Fault – Cowarral Fault – Rollans Road Fault and the Bagnoo Fault. Using this boundary, the NHB is compatible with the dominant, NW/SE-plunging Parrabel Dome. All the younging directions radiate from centre of the dome in the NHB. In contrast, the younging directions in the SHB are believed to have been originally all younging to the (E)NE.

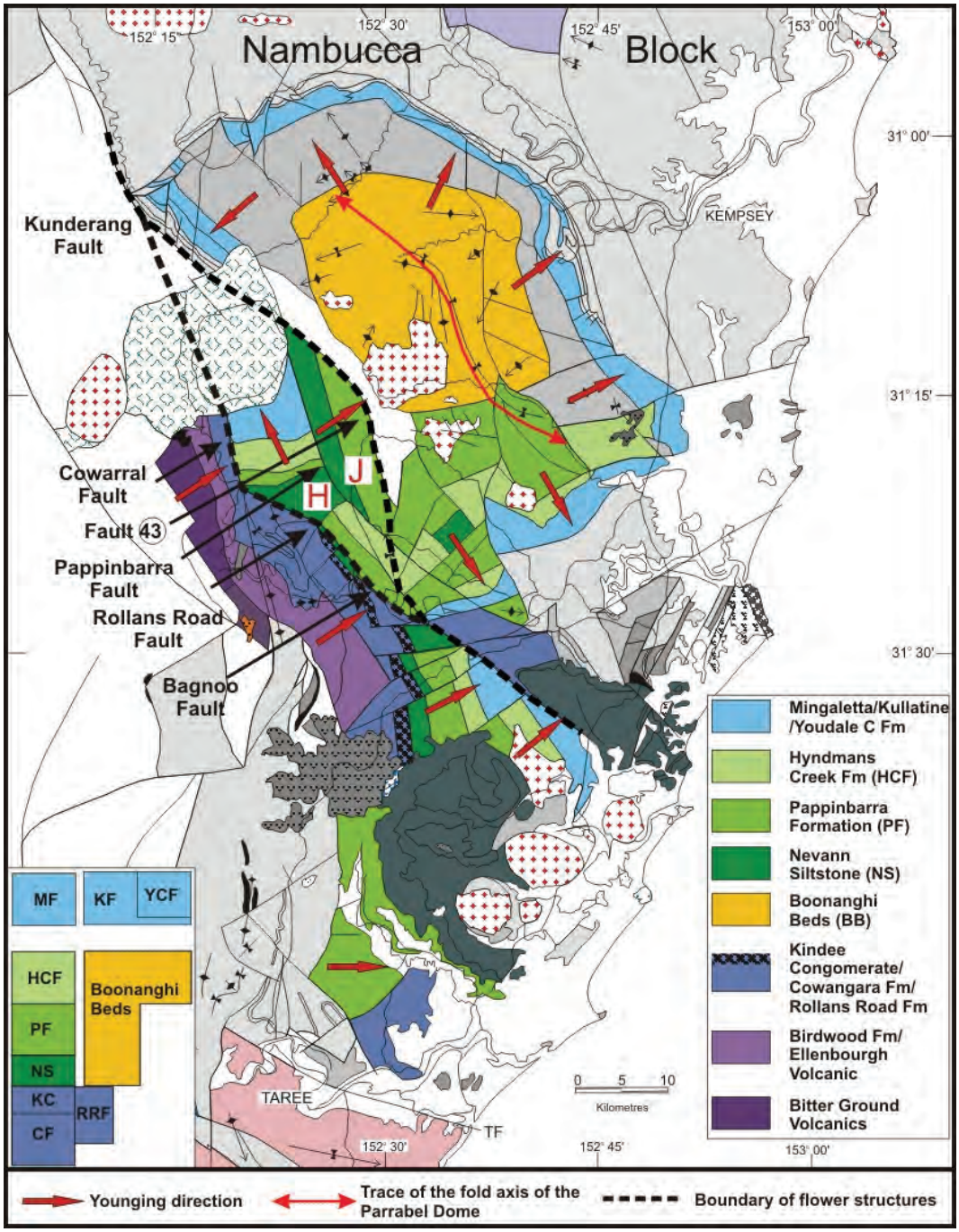

Figure 5.46: Restoration of the Hastings Block incorporating flower structures. CF = Cowangara Formation; KC = Kindee Congomerate; KF = Kullatine Formation; MF = Mingaletta Formation; RRF = Rollans Road Formation; YCF = Youdale C Formation.

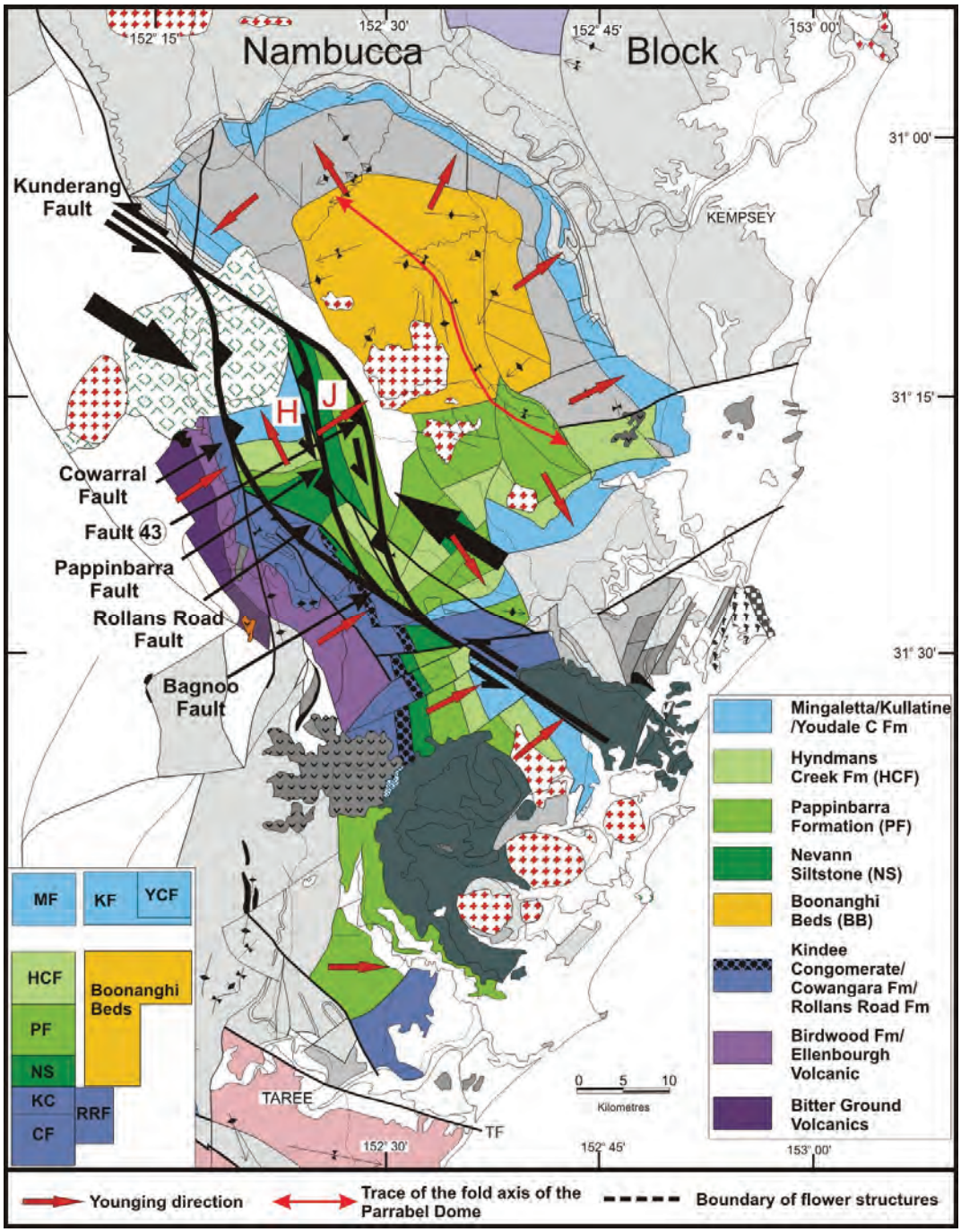

Figure 5.47: Geological map of the Hastings Block showing dip-slip and strike-slip faulting associated with a possible double restraining bends (transpressive duplexes). CF = Cowangara Fornmation; KC = Kindee Congomerate; KF = Kullatine Formation; MF = Mingaletta Formation; RRF = Rollans Road Formation; YCF = Youdale C Formation.

The flower structure (strike-slip duplexes) consists of the Kunderang Fault - Fault 43 – Bagnoo fault system (proposed geological boundary in this model) and the Cowarral – Rollans Road – Bagnoo fault system (Figure 5.47). The sinistral strike-slip movements

on these two fault systems occurred in a transpressional setting, resulting in the rocks being faulted upward in a positive flower structure and causing the disruption of the Early Carboniferous sequences (Nevann Siltstone, Pappinbarra Formation, Hyndmans Creek Formation and Mingaletta Formation). The sinistral strike-slip movements along the Cowarral – Rollans Road – Bagnoo fault system and the Pappinbarra Fault led to the translation and rotation of Fault Block H from its original position (south of its current position) to its current position shown by the Ball A in the ball bearing model (Figure 5.48a) (Hernandez-Moreno *et al*. 2014). Fault Block H experienced around 90° anticlockwise rotation during this process. Fault Block J did not experience this rotation. It is probably because of the incomplete development of the fault bounded structural wedge along the restraining bend as shown in Figure 5.48b. Fault Block J was then trapped between Pappinbarra Fault and Fault 43 and could not rotate (Figure 5.46).

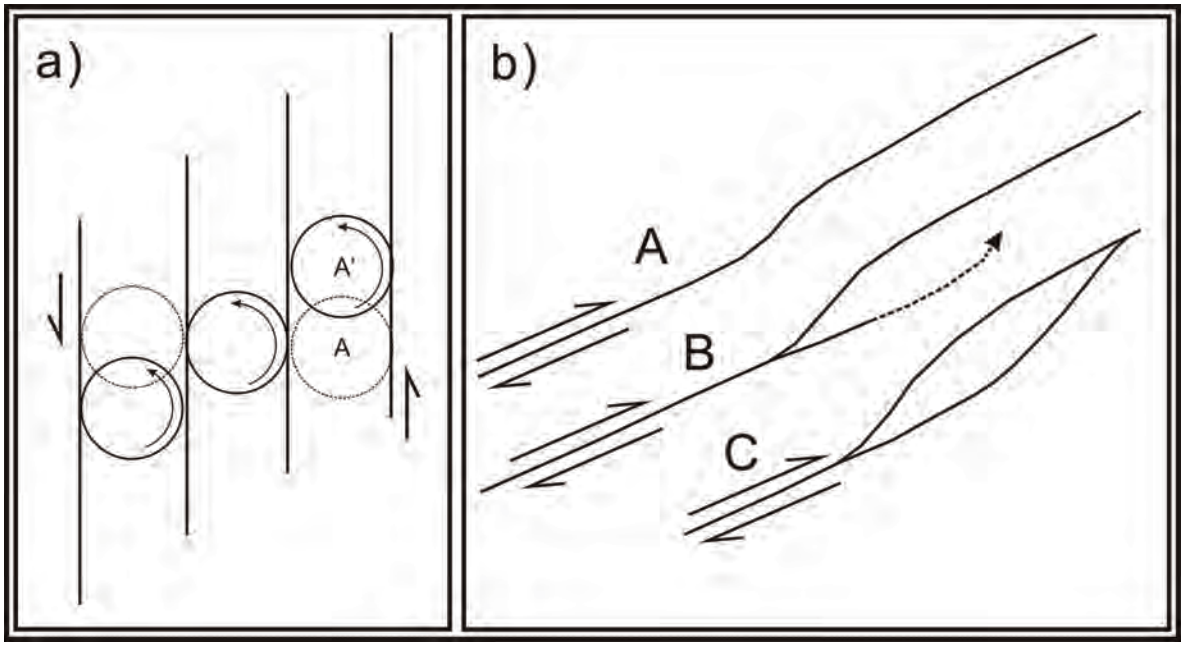

Figure 5.48: a) Ball bearing model showing the translation and rotation of the ball under sinistral strike-slip movement (Hernandez-Moreno *et al*. 2014). b) (A) to (C) the progressive development of a fault bounded structural wedge at a restraining bend of a strike-slip fault (Crowell, 1974).

Single restraining bends

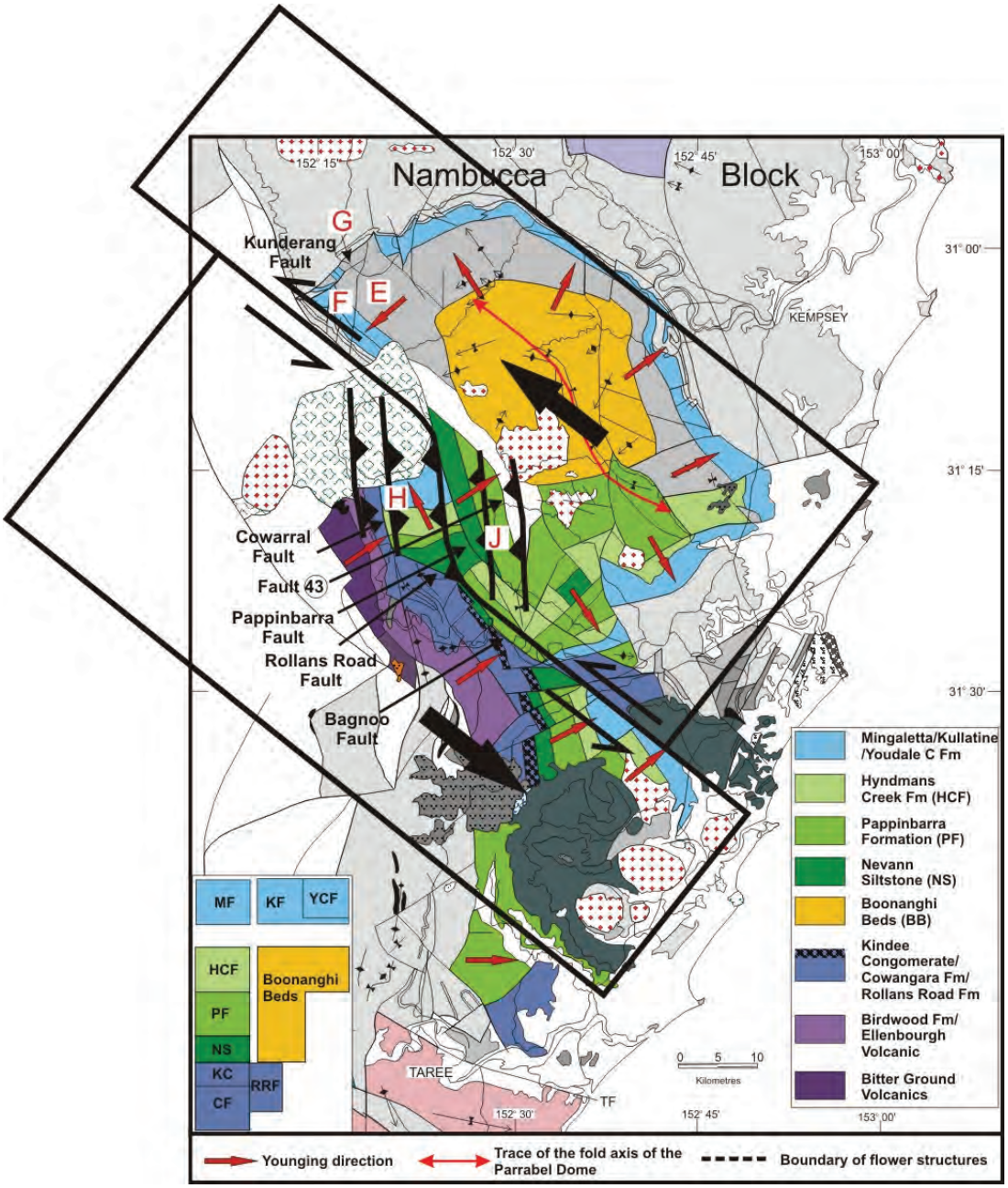

Figure 5.49: Single restraining bend model to explain the map pattern and fault blocks arrangements around the possible boundary between the Northern and Southern Hastings Block.

In this model, the single restraining bend is made of Kunderang Fault – Pappinbarra – Bagnoo faults (Figure 5.49). This fault system is bent, experiencing sinistral strike-slip movement in a transpressive setting. It is proposed that this fault system is the geological boundary between the NHB and SHB in this model. The NHB is

characterized by a dominant, gently northwesterly/southeasterly-plunging, macroscopic Parrabel Dome. A tight, NW-SE trending syncline parallel to the trace of the axis of the Parrabel Dome exists between the Fault Block J and the Boonanghi Beds. The whole NHB was moving northwestwards along the single restraining bend as a result of sinistral strike-slip movement. Fault Block G was dismembered during this process (Figure 5.49). The younging direction in the SHB is to the (E)NE except for the Fault Block H. One explanation is that Fault Block H was originally located to the northwest of its current position and was younging to SW. It was moved south during the sinistral strike-slip movement along the above fault system, uplifted between two opposed thrusts and has undergone 135° anticlockwise rotation (far left ball in Figure 5.48a, Hernandez-Moreno *et al*. 2014) (Figure 5.49).

The first model in Figure 5.43 is unconstrained. It is difficult to test this model as there are too many variables. The flower model in Figure 5.46 shows that the faults bounding blocks J and H would dip towards each other becoming steeper at depth and coalescing as in a single fault. This model can be tested via magnetic or gravity worms to find the dip of these faults. Based on the worms analysis in this thesis (Figure 5.18), this fault is not visible in the magnetic worms and partly visible in the gravity worms image. The model in Figure 5.47 suggested that faults between bounding fault (Bagnoo Fault and Kunderang Fault) show both dip-slip and strike-slip movement. Currently we found that the Bagnoo Fault shows sinistral strike-slip movement and the Kunderang Fault shows dextral (not sinitral) strike-slip movement, indicating that this model is unlikely to be correct. The model in Figure 5.49 is similar to the model in Figure 5.47. The boundary between the Block H and Block J may represent a dog-leg in this restraining bend model. The key issue is to test the dip and movement sense of faults either side of the dog-leg. We found the movement on Bagnoo Fault is consistent, but the movement on Kunderang Fault is not consistent with the model requirements.

5.8 Conclusions

This study re-interprets a variety of geological data fault-block by fault-block. The shortcomings with the existing Roberts *et al.* (1995) geological map of the Northern Hastings Block have been highlighted. These include the variability in the orientation of bedding within some fault blocks, between adjacent fault blocks, and around significant sections of the dome. Some faults are probably incorrectly positioned and will be changed in a new map of the NHB currently being prepared.

The QFL patterns for the same formation in different fault block was used to test whether it was possible to verify that the same formation was exposed in along strike outcrops. The variability in the number of samples from different fault blocks meant it was not possible to verify that it was the same formation.

A possible geological boundary between the NHB and SHB is suggested by the gravity and magnetic worms analysis in the Hastings Block that extends from the Kunderang Fault, southeasterly through the Pappinbarra Fault and finally east-northeasterly towards Fault 72 (dashed black line; Figure 5.42)

Fault Blocks A-G are located around the Parrabel Dome in the NHB. The bedding data and younging directions in these fault blocks support the existence of the Parrabel Dome which radiate from the center of the dome in the NHB except for the bedding data in Fault Block A and C that dip to the southwest and southeast to south respectively. Fault blocks H-K belongs to the SHB in this study. The younging direction in the SHB is to the ENE. The only exception is Fault Block H, which youngs to the NNW.

A schematic reconstruction of the eastern limb of the Parrabel Dome takes into account the clockwise rotation of the limb of the dome via strike-slip faulting. This is the major mechanism responsible for dip direction changes in Fault Blocks A and C. Models

involving both rotation and translation using the existing fault network are proposed. Movement in a restraining fault bend along strike-slip faults is used to explain the disruption of fault blocks between the NHB and SHB and in the northwestern Kunderang District. These models highlight the potential movements of fault blocks near the NHB-SHB boundary.

Chapter 6 Balanced and restored cross-sections across the Northern Hastings Block

6.1 Introduction

A geological cross-section is a diagram or drawing that shows features transacted by a given plane, or an actual exposure or cut that shows transected geologic features (Glossary of Geology 2005). The different types of rocks, internal structures and the geometric relationship between them are represented in cross sections. The construction of the geological cross-sections requires the application of all the knowledge of the geological (structural, stratigraphic, and cross-cutting) characteristics of the region, including the interpretation of the rocks arrangement, both in depth and on the topographic surface. The data on the surface are obtained directly from the field (direction and dip of the strata or other structures, types of contact, thickness of the stratigraphical units, lateral relationships between them).

There are numerous possible interpretations of the geology using the same data. The best model in drawing a cross section is to come up with an interpretation that is consistent with all the available data. A test of the reasonableness of a cross-section is whether it is balanced. A balanced cross section must incorporate: 1) the structures are reasonable given the geological setting of the rocks; and 2) the layers can be restored to a reasonable pre-deformation configuration with no significant gaps when the effects of the shortening by faults and folds is removed.

The 2D restoration (kinematic reconstruction) is such a fundamental test of the validity of the interpretation of the cross section. It is a technique used to progressively undeform a geological section. It begins with the present deformed state and generates an earlier undeformed (or less deformed) state. A cross section that does not restore or balance cannot be a geometrically valid representation (Gibbs 1983). The kinematic

reconstruction (2D restoration) provides insights into the geometry of earlier stages of the geological development of an area. It aids the construction of a cross section that is internally consistent, relies only on known assumptions, makes some predictions, highlights interpretation problems and highlights alternatives. It can also indicates pathways of hydrocarbon migration and constrains structural and stratigraphic histories of extensional deformation (Groshong and Richard 2006).

This chapter presents four geometrically constrained (balanced) cross sections across the Northern Hastings Block (A-B, C-D, E-F and X-Y). Cross sections A-B, C-D and E-F are oriented NE-SW over a distance of 29.5 km, 71 km and 54 km respectively. Cross section X-Y is oriented NW-SE over a distance of 74km passing through the cross sections A-B, C-D and E-F. These cross sections were constructed using known geologic relations and reprocessed thicknesses for the stratigraphy in the Northern Hastings Block. The 2D restoration (kinematic reconstruction) was then performed on the completed cross-sections following the principles of structural balance (line length balancing) (Woodward *et al.* 1989). It tests the validity of the interpretation of the cross section and provides insights into the geometry of earlier stages of the geological development and constrains structural and stratigraphic histories of extensional deformation in the NHB.

6.2 Geological setting

The Hastings Block can be subdivided into the northern (NHB) and southern Hastings Block (SHB). They are distinguished by the differences in structural style, structural history and pre-Permian stratigraphy (Lennox & Roberts 1988; Roberts *et al*. 1993, Appendix 2).

6.2.1 Stratigraphy

The Northern Hastings Block contains the Early to Late Carboniferous rock sequences

that are overlain by the Early Permian sequences. Voisey (1934, 1936) and Lindsay (1969) firstly divided the sedimentary rocks of the NHB into six stratigraphic units. They are, in ascending order, the Boonanghi Beds, the Majors Creek Formation, the Kullatine Formation, the Yessabah Limestone, the Warbro Formation and the Parrabel Beds (Figure 6.1).

The SHB consists of Devonian to Carboniferous rocks disconformably overlain by Early Permian successor sediments. The Devonian and Carboniferous rocks in the SHB associated with the three cross sections are, in ascending order, the Bitter Ground Vocanics, Birdwood Formation, Cowangara Formation, Rollans Road Formation, Kindee Conglomerate, Nevann Siltstone, Pappinbarra Formation, Hydmans Creek Formation and the Mingaletta Formation (Figure 6.1).

Stratigraphic units in the NHB are partly chronologically equal to those in the SHB (Figure 5.41, Glen and Roberts, 2012). Specifically, the Mingaletta Formation in the SHB is time equivalent to the Kullatine and Youdale (C) formations in the NHB. The time interval of deposition of the Nevann Siltstone, Pappinbarra Formation to Hyndmans Creek Formation in the SHB is same as that of the Boonanghi Beds in the NHB (Figure 5.41).

The estimated thicknesses of these Devonian to Carboniferous rock sequences, and an Early Permian cover sedimentary sequence investigated by the Lindsay (1966), Lindsay (1969), Bourke (1971), Lennox and Roberts (1988) and Roberts *et al*. (1995) are presented in the Tables 6.1 and 6.2.

Table 6.1: Estimated thickness of the Carboniferous to Permian rock sequences in the NHB and the value used in the cross sections.

Units	Lindsay (1966)	Lindsay (1969)	Bourke (1971)	Lennox *et al.* (1988)	Cross Section Thickness
Parrabel Beds		1220m	2200m	more than 2000m	2000m
Warbro Formation		1070m	637m (minimum)		1000m
Yessabah Limstone		6m in Stone Creek, 460m at Willi Willi	539m (at Moorabuck Ridge, larger than 234m)	6-460m	500m
Youdale Formation C	1775m		1775m	more than 1300m	1775m
Kullatine Formation	at least 1000m	640(Majors Creek)-1370m(Carrai clearing)	1350m (Thicker in west)	985m	1000m
Majors Creek Formation		2000m(thinner in the south)	2700m (Minimum)	2175m in the northern part, 3000+ m in the west	2300m
Boonanghi Beds		1590m		more than 500m	1590m

Table 6.2: Estimated thickness of the Devonian to Carboniferous rock sequences in the SHB and the value used in the cross sections.

Unit	Roberts *et al.* (1995)	Cross Section Thickness
Mingaletta Formation	greater than 2000 m.	2000-2500m
Hyndmans Creek Formation	2000 m.	2000m
Pappinbarra Formation	1200-1355m	1300
Nevann Siltstone	170-550m	170-550m
Kindee Conglomerate	300-1000m	300-1000m
Cowangara Formation	more than 2000 m.	2000m
Birdwood formation	1550m	1550m

6.2.2 Deformation

Three cross sections cover the NHB to the northeast and part of the SHB on the southwest.

The NHB is characterized by the macroscopic Parrabel Dome which overall plunges gently northwest. The NHB has undergone at least three phases and probably four phase of mesoscopic folding namely, east-west, northwest-southeast, north-south (?) and northeast-southwest trending (Lennox *et al*. (1999); Chapter 3.5). Three episodes of faulting have been recognized (Roberts *et al*. 1993), namely, northwest-trending faults with mainly sinistral strike-slip movement; followed by northeast-trending faults with dextral or sinistral strike-slip or dip-slip movement, with small displacements. Subsequently, meridional, dip-slip faults developed (Roberts *et al.* 1993). It is believed

that most faults in the NHB cut already cleaved and folded rocks (Chapter 4.5).

The Southern Hastings Block, in contrast, has meridional-trending, macroscopic folds overprinted by northwest-trending folds. It has suffered three episodes of faulting: (i) early meridional dip-slip faults; (ii) later northeast-striking, sinistral strike-slip or rare dip-slip faults and (iii) northwest-trending faults with both sinistral and dextral strike-slip movement (Roberts *et al*. 1993).

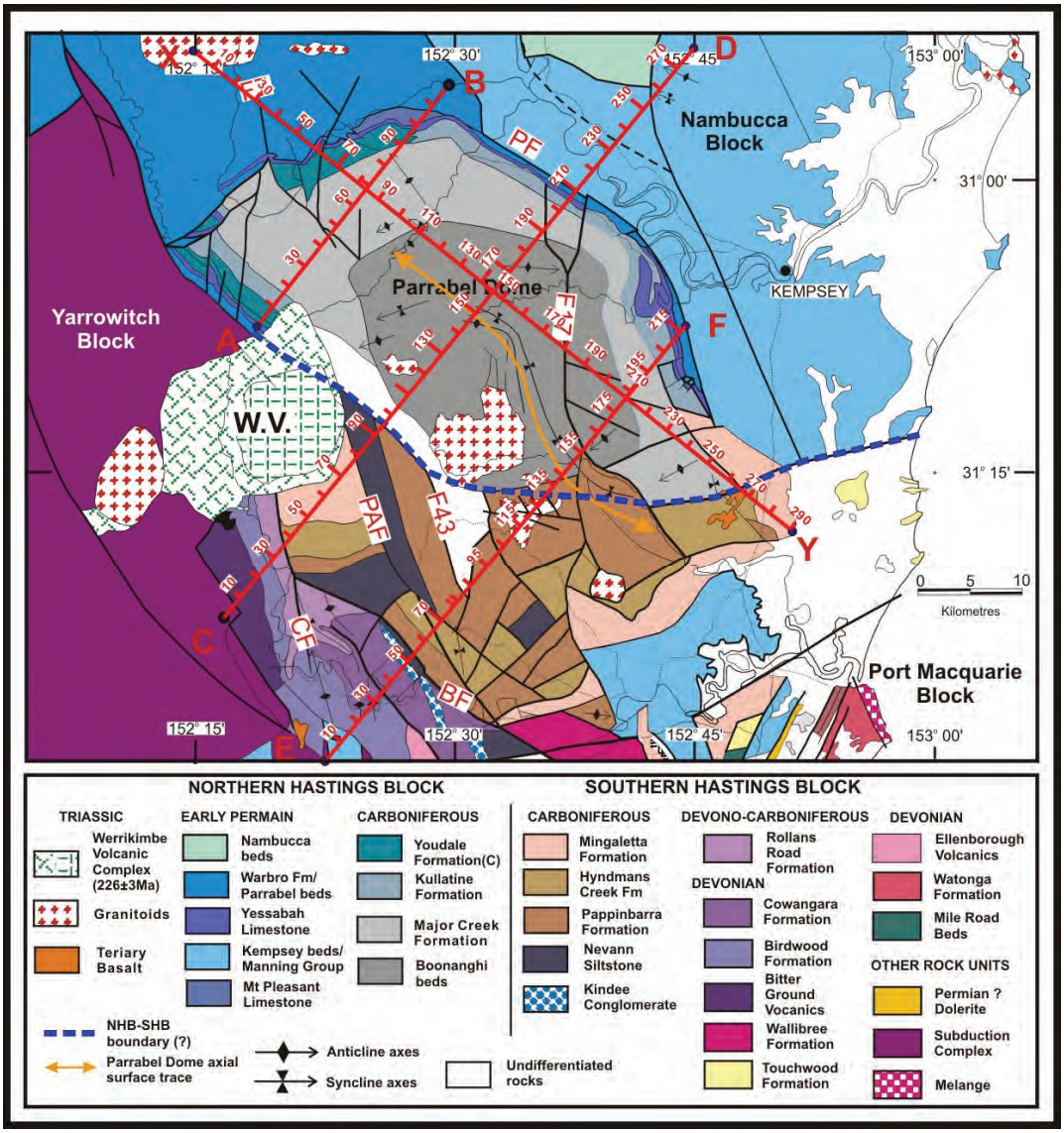

Figure 6.1: Locations of the cross sections and the geological map of the Northern Hastings Block and part of the Southern Hastings Block (Roberts *et al*. 1995). BF = Bagnoo Fault; CF = Cowarral Fault; PAF = Pappinbarra Fault; PF = Parrabel Fault; W.V. = Werrikimbe Volcanics; F17 = Fault 17; F43 = Fault 43 (Chapter 5).

6.3 Methodology

6.3.1 Construction of the balanced cross sections

Four geometrically constrained (balanced), vertical cross sections across the Northern Hastings Block (A-B, C-D, E-F and X-Y) were constructed using known geologic relations and estimated thicknesses of the stratigraphy in the Northern Hastings Block. Cross sections A-B, C-D and E-F are orientated NE-SW right angles to the dominant NW-SE structural grain of the Parrabel Dome and vertical Cross Section X-Y is orientated NW-SE parallel to the dominant NW-SE structural grain. The bedding data on the ground surface are used including the direction and dip of the strata or faults, nature of the contact, the estimated thickness of the stratigraphic units and any along strike facies changes. All bedding dips were recalculated as apparent dips. In cases where the thicknesses of the buried and eroded stratigraphic units is not known in the cross section, their thicknesses as showed in the Tables 6.1 and 6.2 as estimated by Lindsay (1969), Bourke (1971), Lennox and Roberts (1988) and Roberts *et al.* (1995) will be used. The Digital Elevation Model (DEM) of the NHB was used to constrain the top surface of the cross sections. The majority of faults in the cross sections are still shown as vertical because of the lack of data regarding their actual dip.

6.3.2 Kinematic reconstruction of the balanced cross sections

Kinematic reconstruction was performed on the completed cross-sections following the principles of structural balance (line length balancing). The purpose is to create cross sections that are internally consistent, relying only on known assumptions, make some predictions, highlight interpretation problems and highlight alternatives (Woodward *et al*. 1989). This is an iterative process and the workflow is shown in Figure 6.2 (Yan *et al*. 2014b; Yan *et al*. 2014c; Yan *et al*. 2015). 2D Move (courtesy of Midland Valley Exploration P/L) was the software used in the restoration.

Kinematic reconstruction does not provide a single valid answer. Instead a range of valid, balanced models are geologically permissible. This is due to multiple sources of uncertainty involved in constructing the starting models. The value lies in the ability to discriminate between alternative structural interpretations, their consequences and whether they are valid. This can be of great value in lowering interpretational risk (Cooper and Hill, 1997).

In detail, each section is sequentially restored back in time to its initial stage before the deposition of the Devonian to Carboniferous sequences using 2D Move. Details of the steps involved are presented below.

(1) Restoring faulted horizons.

The first step in kinematic reconstruction is to restore a formation to its initial state prior to faulting. Using the module “Move on Fault” each faulted section is restored using the “simple shear” algorithm (consistent with an extensional tectonic setting). Shear angles between 60-70 degrees were used.

(2) Unfolding restored horizons

Upon restoration of all faulting, the horizon must be geometrically restored to a regional (undeformed) elevation using the module “Unfolding” (with the simple shear or flexural slip algorithm) (Woodward *et al*. 1989). This follows the assumption that the formation top was a horizontal regional surface, and accounts for any folding and deformation that may have occurred post deposition.

Flexural-slip restoration were used to unfold the folded horizons. It consists of measuring bed lengths and straightening the lengths while preserving the thicknesses to produce the restored section. The restored section will be bound on one end by a pin line. This pin line serves as a marker from which bed lengths are measured. It must be in an area with no interbed slip and beyond the zone of deformation, usually in the

relatively undeformed foreland such as the relatively undeformed Permian in the southern Nambucca Block adjacent to the NHB.

(3) Backstripping and decompaction

After fault restoration and unfolding of each horizon, the next step is backstripping and decompacting. Decompaction is an essential step to obtain an accurate geometry of the reconstructed structures in regions with syntectonic sedimentation. As the exact compaction parameters are commonly not known for each layer, this approach decompacts the section assuming a standard compaction curve for a uniform lithology. Each point in this section is decompacted along the appropriate curve for the incremental change in its depth since the last decompaction (2D MOVE 2012 tutorials). The module “Decompaction” in 2D MOVE was used. This process displays the removal of a formation from underlying strata by moving the underlying strata upwards and tilting it.

Steps 1 to 3 are repeated for each underlying formation.

6.3.3 Assumptions

Some key assumptions are normally used to restore such sections. In this chapter they are: (1) the area of the cross-section is conserved; (2) beds are of constant or smoothly varying thickness; (3) the surface of each formation was originally horizontal at a regional elevation (prior to deformation); (4) the folding is flexural-slip in style; and (5) 2D deformation: the faulting modeled is the simplest possible consistent with the available data. The extent of strike-slip motion on the faults are not known. So it is not possible to factor into the models the extent of strike-slip motion.

During the process of structural restoration and balancing errors can be introduced. A potential source of error relevant to this study is determining shear angles used for fault restoration in MOVE. During restoration decreasing the shear angle can flatten the

horizon (vertical being 90° and horizontal being 0°). Whilst a shear angle too great can create large artificial "bumps". Hauge and Gray (1996) suggest ~70° produces the best fit for many real world faults according to their experimental data. In this study shear angles between 60-70° have been used. These match the suggested reasonable shear angles.

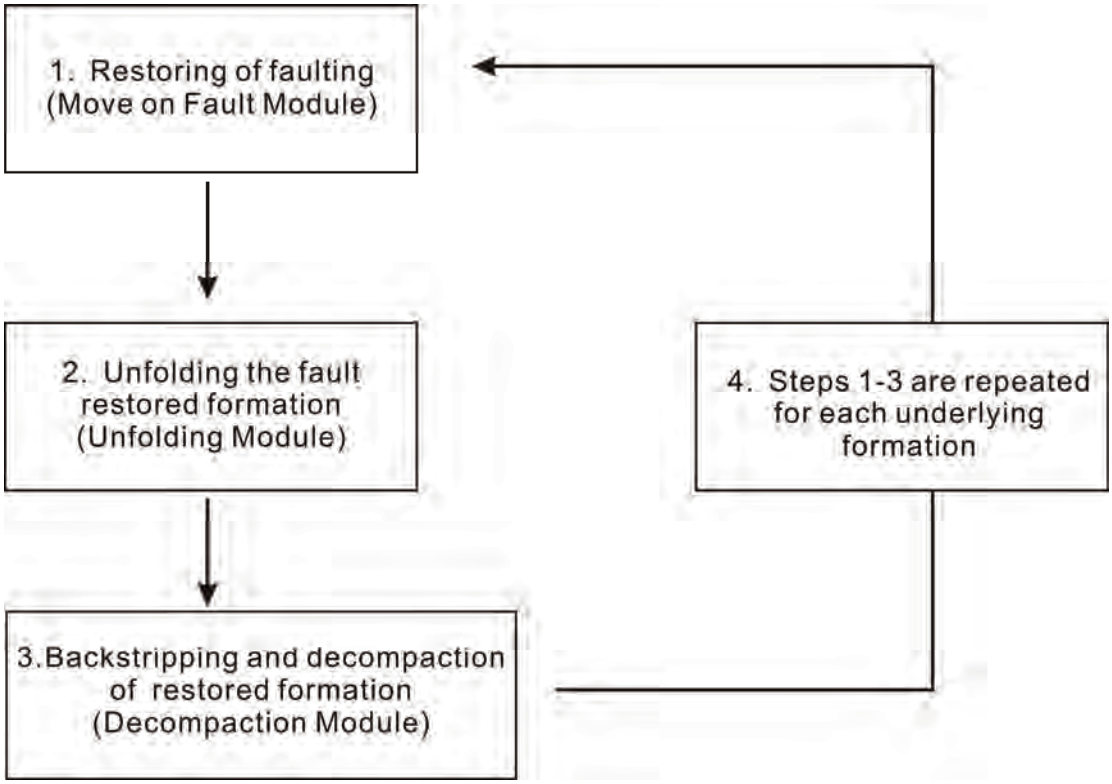

Figure 6.2: Workflow used to structurally reconstruct a model. Steps 1-3 was performed on the youngest formation then subsequently repeated for each underlying formation. This process was performed using the software Move (Midland Valley Exploration P/L).

6.4 Results and implications

6.4.1 The constructed balanced cross sections

Four geometrically constrained (balanced) cross sections across the Northern Hastings Block (A-B, C-D, E-F and X-Y) are constructed. One common major structural feature crossed by all these four cross sections is the gently northwesterly-plunging Parrabel

Dome which is the dominant feature in the NHB.

6.4.1.1 Cross Section A – B

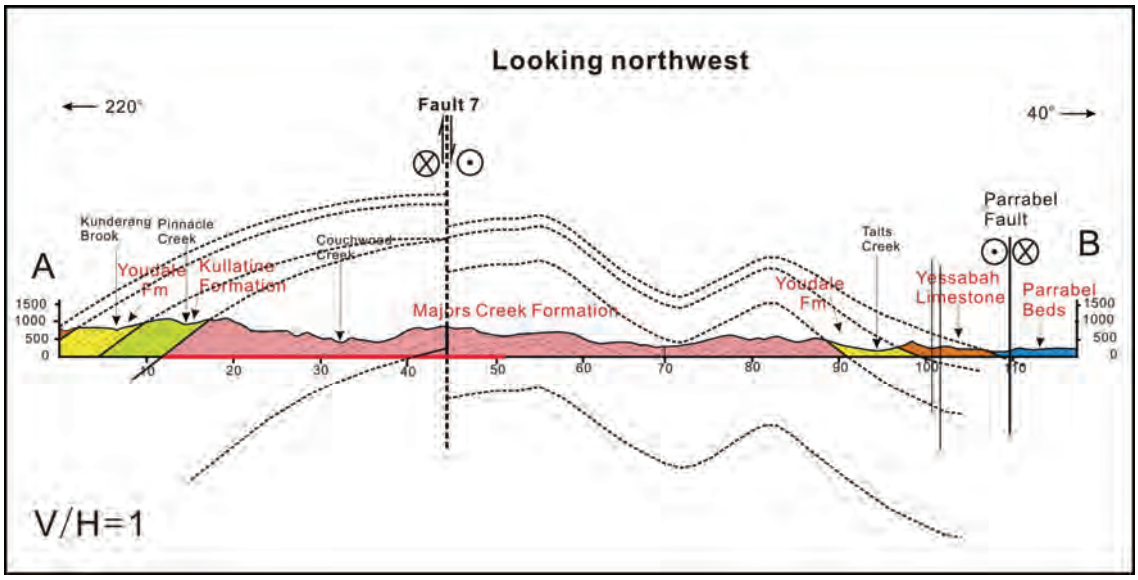

Figure 6.3: The balanced cross section A-B in the NHB prior to any restoration.

Specifically, major structural features crossed by cross section A-B in the NHB, from southwest to northeast, include: (1) the Carboniferous sequences in the Kunderang Brook area (Youdale (C), Kullatine and Major Creek formations), younging northwest and cut by Fault 7 (Stations 0-40, Figure 6.3), uplifting the rock sequences on the left side of the fault; (2) the northern part of the Parrabel Dome, mostly in the Majors Creek Formation (Stations 0-110) including the macroscopic antiform (near Station 70-90) visible on Figure 6.1; and (3) the Carboniferous to Permian sequences (Majors Creek and Youdale (C) formations, Yessabah Limestone and Parrabel Beds), younging to the east and cut by the NW-SE trending Parrabel Fault on the northeast limb of the dome (Station 90-110, Figure 6.3). Cross section A-B has been constructed assuming bed thicknesses are maintained across the section and using formation/unit thicknesses derived from Table 6.1. In this cross section the Kullatine Formation is cross cut on the western side of the cross section but not on the northeastern or eastern side of the cross section. The Kullatine Formation does not outcrop around the northwestern section of

the dome hence it has been thinned to zero thickness adjacent to Fault 7 (Figure 6.1).

6.4.1.2 Cross Section C – D

Major structural features crossed by cross section C-D, from southwest to northeast, include:- (1) the Devonian rocks sequences (Bitter Ground Vocanics, Birdwood Formation and Rollans Road Formation), younging east and steeply east-dipping (Stations 0-35 on Figure 6.4); (2) the NNW-SSE trending Cowarral Fault with uplift of Devonian rocks sequences southwest of the fault (near Station 38); (3) the Carboniferous rocks sequences in the SHB (Nevann Siltstone, Hydmans Creek Formation and Mingaletta Formation) with tight antiforms and synform and cut by small faults (Stations 37-80); (4) the NW-SE trending Pappinbarra Fault, uplifting the rock sequences on the northeast (right) (Station 80 on Figure 6.4); (5) the generally gently west-dipping Carboniferous rocks (Boonanghi Beds, Major Creek Formation Kullatine Formation) (Stations 100-180) and the shallowly dipping Permian rock sequences (Yessabah Limestone and Kempsey Beds) (Stations 200-280) in the NHB deformed by the Parrabel Dome displaying an open antiform; (6) the N-S trending Fault 17 (Station 195) and the NW-SE trending Parrabel Fault (Station 208), uplifting the rock sequence on the left side and (7) the Taylors Arms Fault System (Station 250), uplifting the Kempsey Beds on the right side of the fault (Figure 6.1).

The bent NW-trending synform near Station 150 on cross section C-D (Figure 6.1) coincides with a macroscopic, open synform in Figure 6.4. This structure lies in the crestal region of the broad Parrabel Dome with its extremely shallowly southwest-dipping beds between Stations 105 and 180.

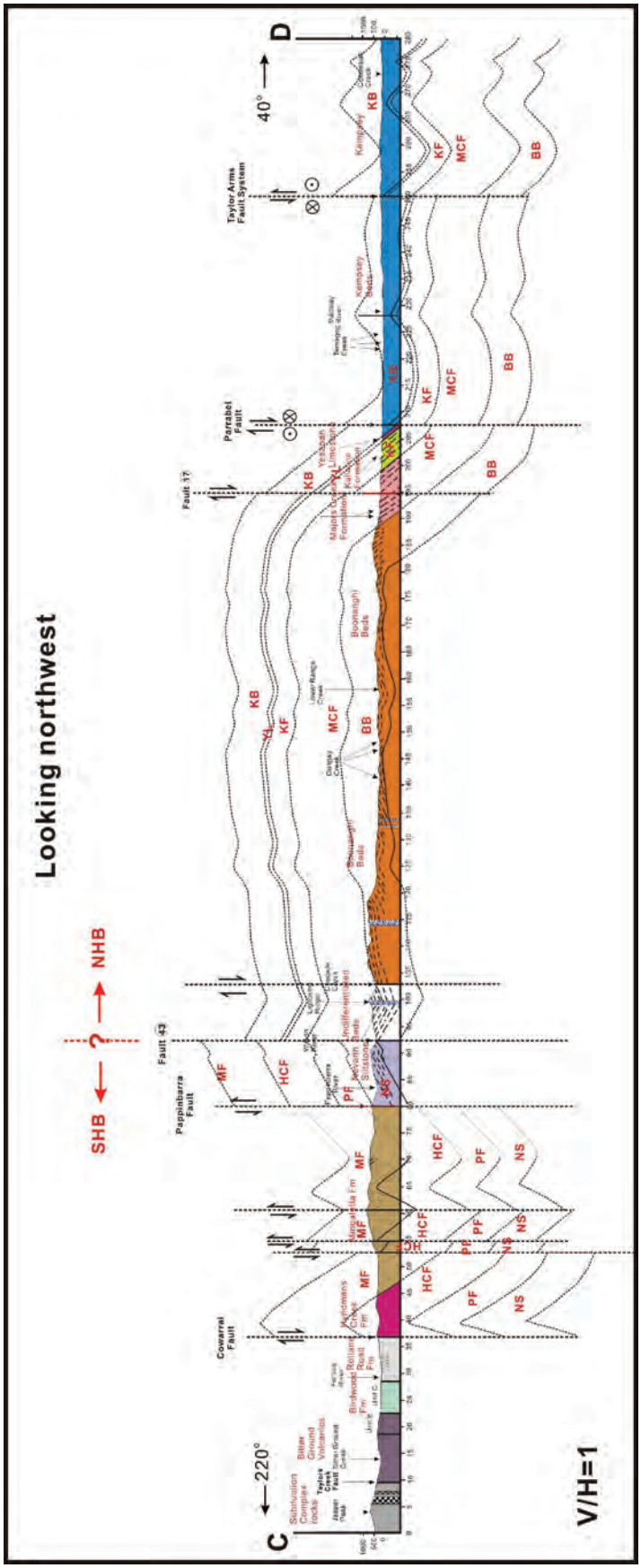

Figure 6.4: The balanced cross section C-D in the NHB prior to any restoration. Fault 43 is used as marking the boundary between the NHB and SHB as per Roberts *et al*. (1995).

6.4.1.3 Cross Section E – F

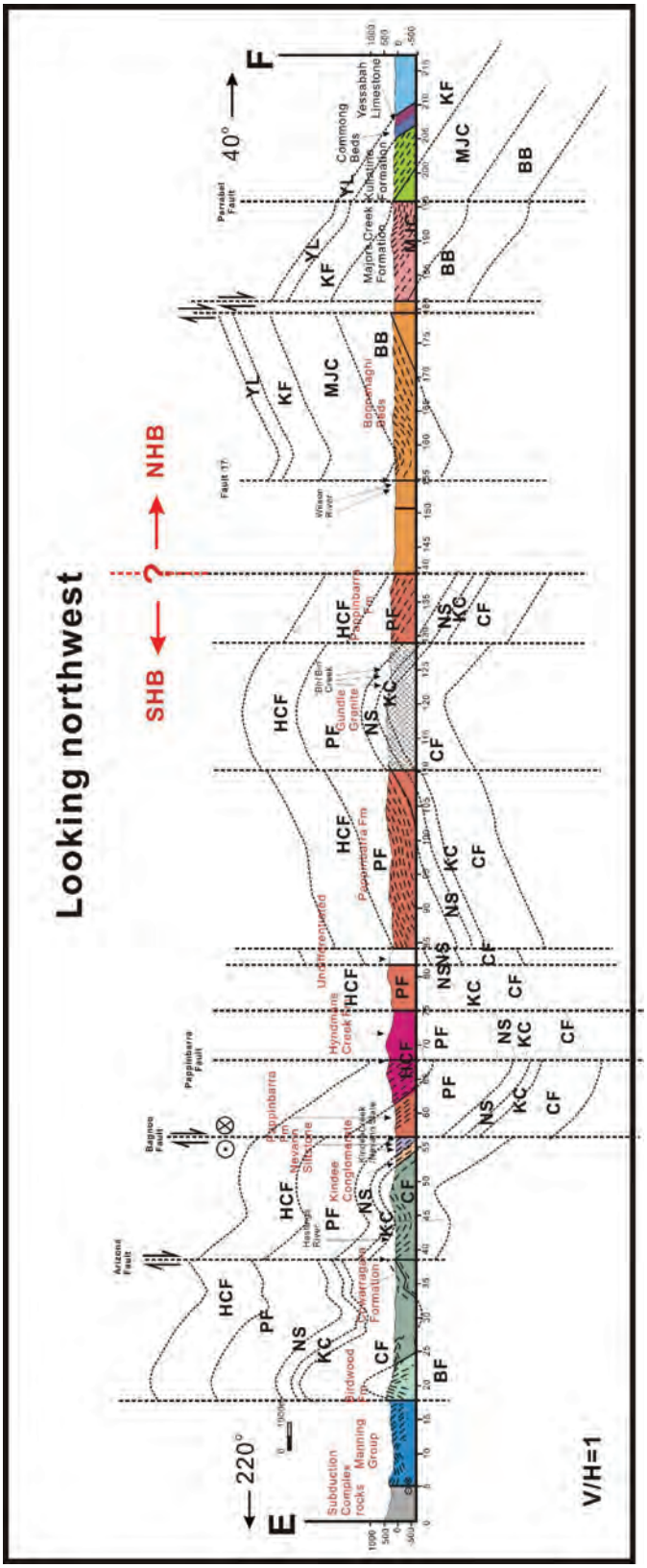

Figure 6.5: The balanced cross section E-F in the NHB prior to any restoration. The position of the boundary between the NHB and SHB is uncertain. The Roberts *et al*.

(1995) position for this boundary is shown on this section.

Major structural features crossed by cross section E-F, from southwest to northeast, include:- (1) the tightly folded Devonian rocks (Birdwood Formation and Cowangara Formation) (Station 17-38 on Figure 6.5) on the southwestern part of the Cross Section E-F and cut by the Arizona Fault (Station 38); (2) the NW-SE trending Bagnoo Fault uplifting the Carboniferous sequences on the southwestern side (Station 57); (3) the Carboniferous sequences including the Pappinbarra and Hyndmans Creek Formations in the SHB (Stations 57-140 on Figure 6.5) and the Boonanghi Beds, Majors Creek and Kullatine Formations in the NHB (Stations 140-195). The Carboniferous sequences in both blocks experience open to close folding and small displacements by faulting.

6.4.1.4 Cross Section X – Y

Major structural features crossed by cross section X-Y shown in Figure 6.6, from northwest to southeast, include:- (1) the Permian sequences (Parrabel Beds and Yessabah Limstone), younging to northwest (Station 10-60); (2) the NNW-SSE trending Fault 7 (Station 33) and NNE-SSW trending Fault 14 with uplift of Permian sequences west of faults (Station 63); (3) the Carboniferous rocks sequences in the NHB (Youdale (C) Formation, Major Creek Formation and Boonanghi Beds) (Station 60-270), deformed by the Parrabel Dome displaying an open antiform; (4) the ENE-WSW trending Fault 32 (Station 223) with small displacement, uplifting the rock sequences on the south (right); (5) the open to close antiform and synform cut by the ENE-WSW trending Mingaletta Fault (Station 268). This cross section shows that the Parrabel Dome is developed to the southeast and not merely in the northwest of the NHB.

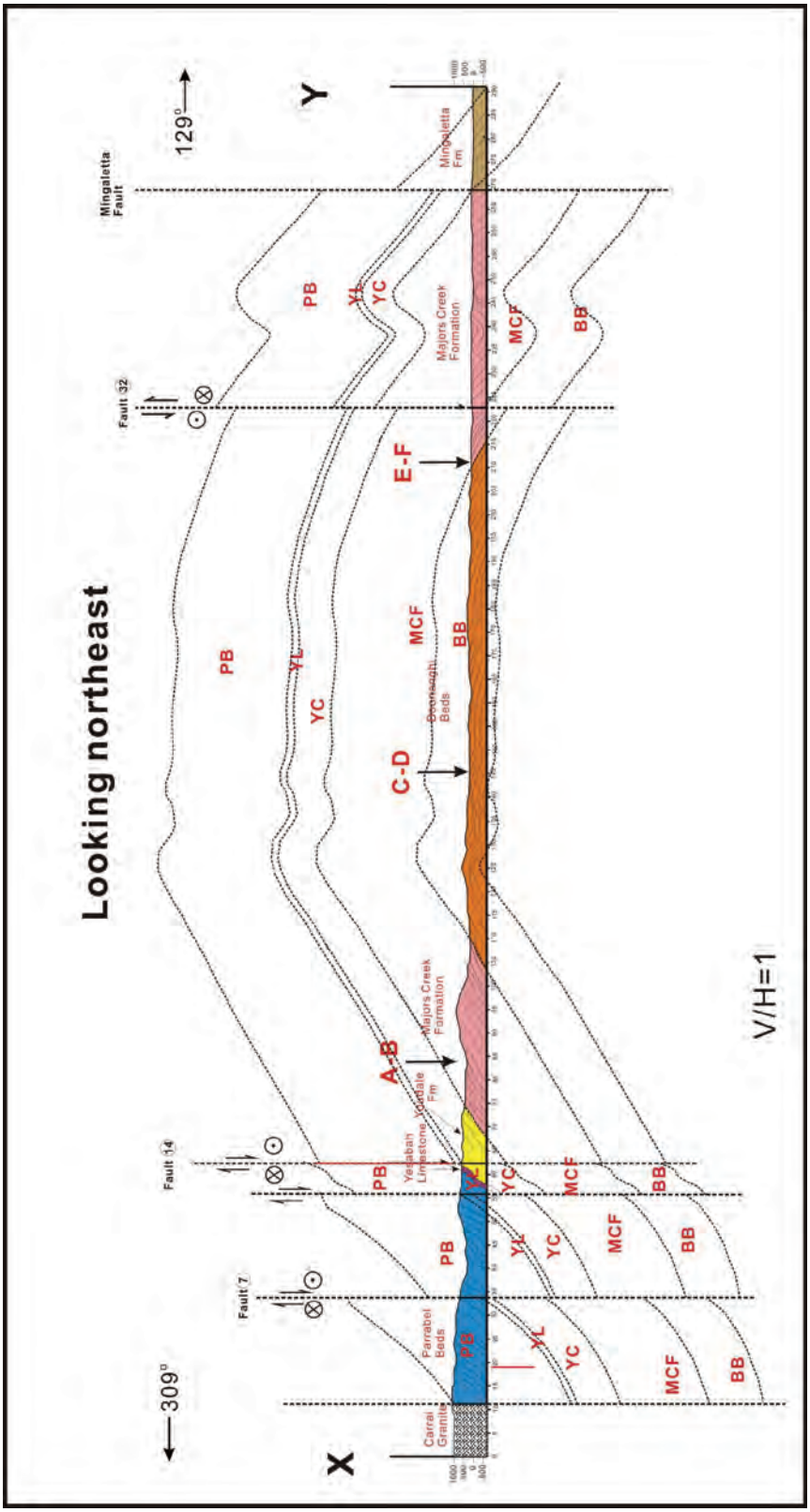

Figure 6.6: The balanced cross section X-Y in the NHB prior to any restoration.

6.4.2 Kinematic reconstruction of the balanced cross sections

Four major geological sections (A – B, C – D, E – F and X – Y) in the Northern Hastings Block were constructed and each section is sequentially restored back in time to its initial stage before the deposition of Devonian sequences using the computer section balancing software 2D Move (by Midland Valley exploration P/L).

In detail, each cross section was sequentially restored back to its initial state prior to faulting. The module "Move on Fault" on 2D Move^{TM} was used to remove the vertical displacement along each fault. The folded formations in each section was then unfolded to a regional (undeformed) elevation. Flexural-slip restoration were used to unfold the folded horizons. In this algorithm, it consists of measuring bed lengths and straightening the lengths while preserving the thicknesses to produce the restored section. After fault restoration and unfolding of each horizon, backstripping and decompaction were used to remove a formation from underlying strata and move the underlying strata upwards and tilt it. The above three steps are repeated for each underlying formation, producing the sequential restorations for each cross section.

The sequential restoration of the four sections showing the intermediate stages between the fully deformed and fully restored stages are presented in the Figures 6.7-6.10, respectively. The restoration validates any geological interpretation by allowing us to examine in detail the depositional and deformational history of the NHB. This restoration also help decipher the initial geometry of the structures, estimate the amount of shortening, and examine the general shape of the strain distribution across the NHB. The sequential restoration of the cross section A - B shows that the dome appears to be asymmetric with a slightly steeper SW-dipping limb. The macroscopic folds on this cross section are consistent with the F_3 folds (Chapter 3.5) sub-parallel to the axial surface trace of the Parrabel Dome (Figure 6.7). The southwestern margin of the cross section C-D is intensively faulted and more tightly folded (higher strain) compared with the broad flat topped dome and northeastern margin within the Nambucca Block (Figure

6.8). The Parrabel Dome is box-like in the centre of cross section C – D. Tighter small wavelength folding occur on the northeastern margin with Permian sequences in the Nambucca Block. Similarly, the southwestern margin of the cross section E-F is more intensively faulted than its northeastern counterparts (Figure 6.9). Open folds were found in this cross section indicating the open geometry of the dome as it dies out towards this southern part (Figure 6.9). Cross section X – Y, sub-parallel to the axial surface trace of the dome, shows that the dome is ~48° northwest-plunging on its northwestern margin and ~15° southeast-plunging on its southeastern margin (Figure 6.10). This is consistent with the derived fold axes from the bedding reading in subareas of the NHB (Chapter 3.3). This verified that the dome is both northwest and southeast-plunging and is plunging steeper to the northwest.

The irregular lower surfaces of the Major Creek Formation in Figure 6.7, the Boonanghi beds in Figures 6.8 – 6.10, the Nevann Siltstones in Figure 6.8 and the Cowangara Formation in Figure 6.9 are merely computer artifacts arising during processing. They are not geologically meaningful.

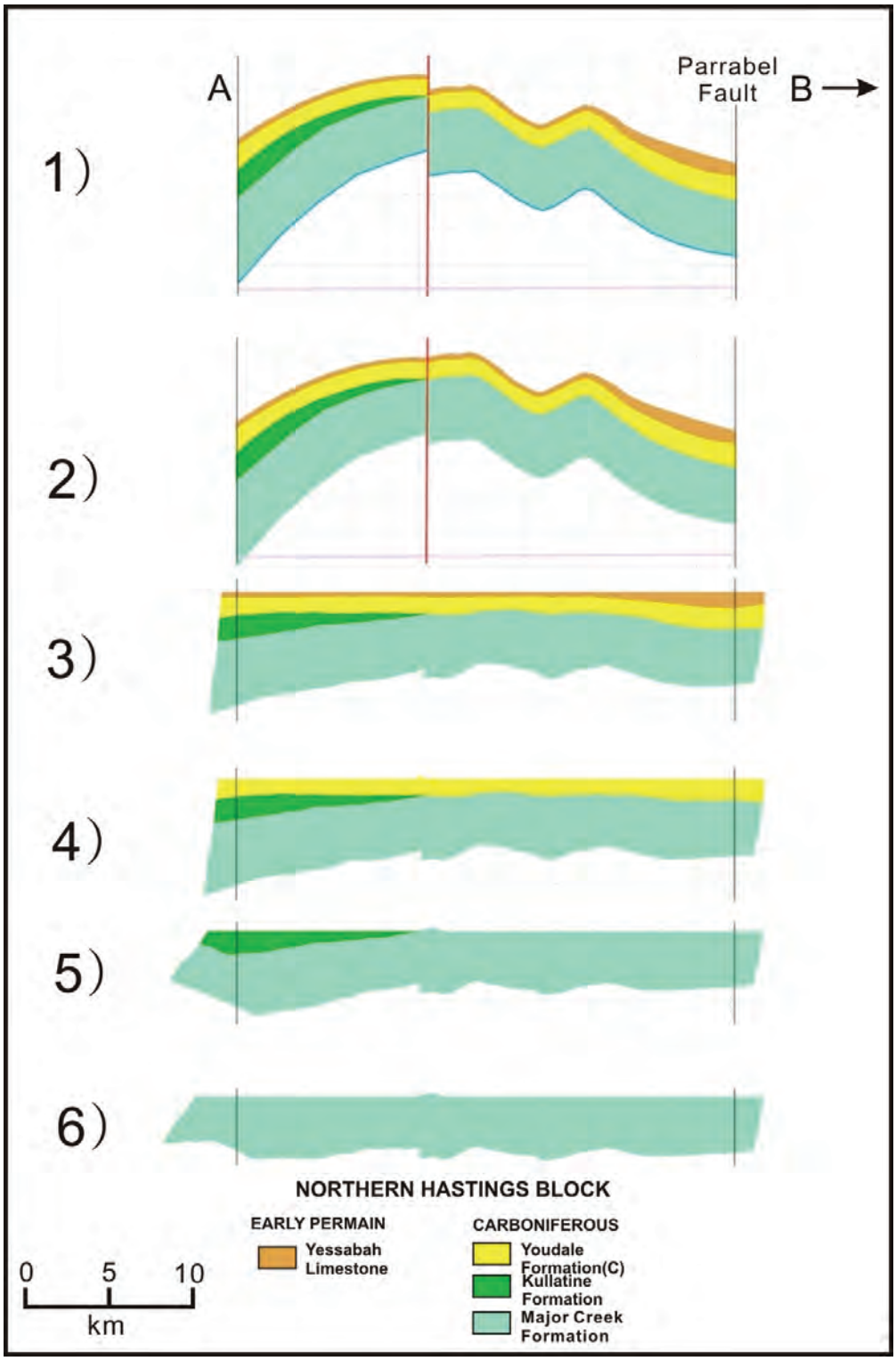

Figure 6.7: Sequential restorations of the geological Section A - B shown in Figures 6.1 and 6.3 from the margin of the Point A in the southwest to the Parrabel Fault in the northeast.

.

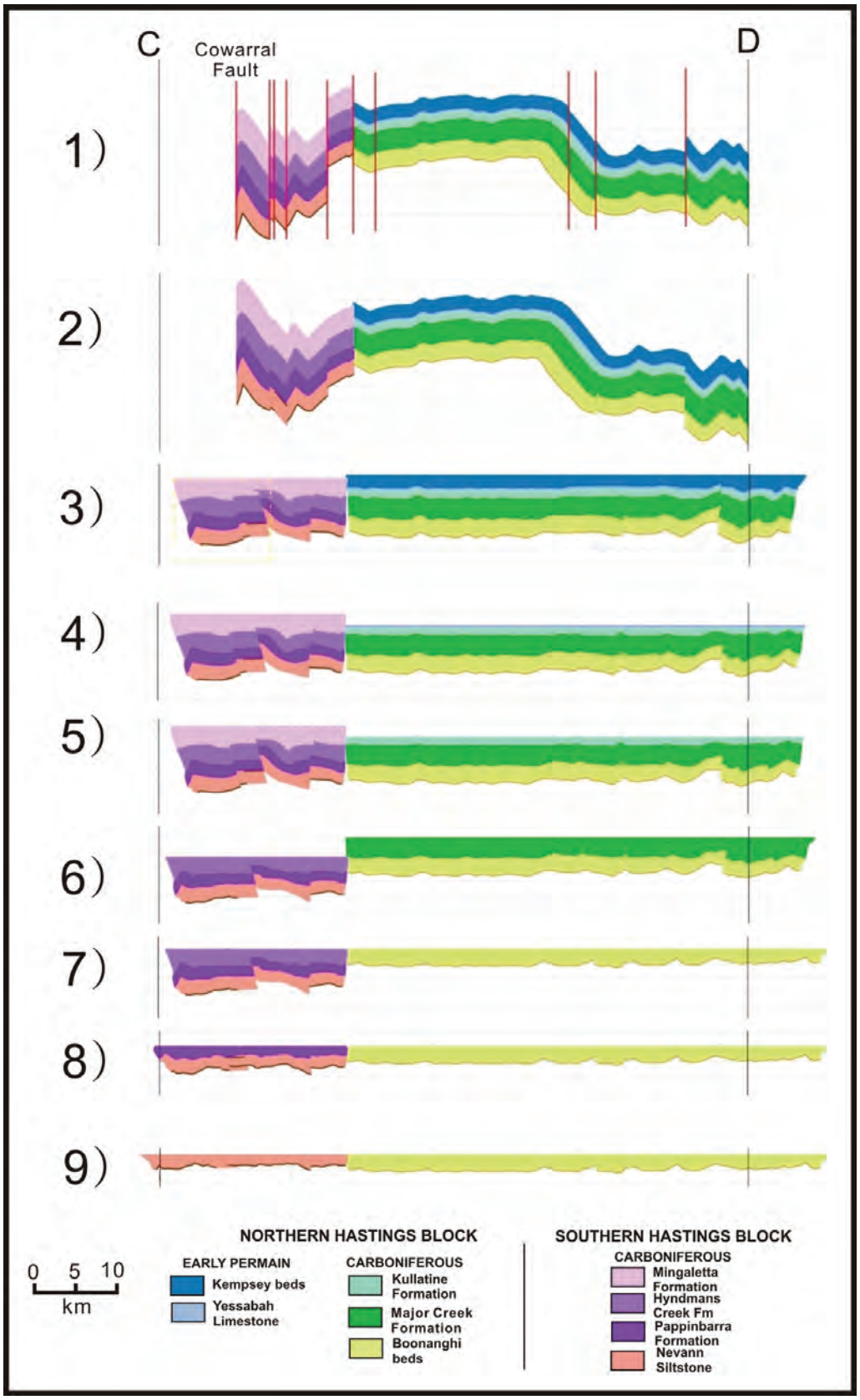

Figure 6.8: Sequential restorations of a part of the geological Section C - D in Figures 6.1 and 6.4. The southwestern end of the cross section corresponds to the Cowarral Fault.

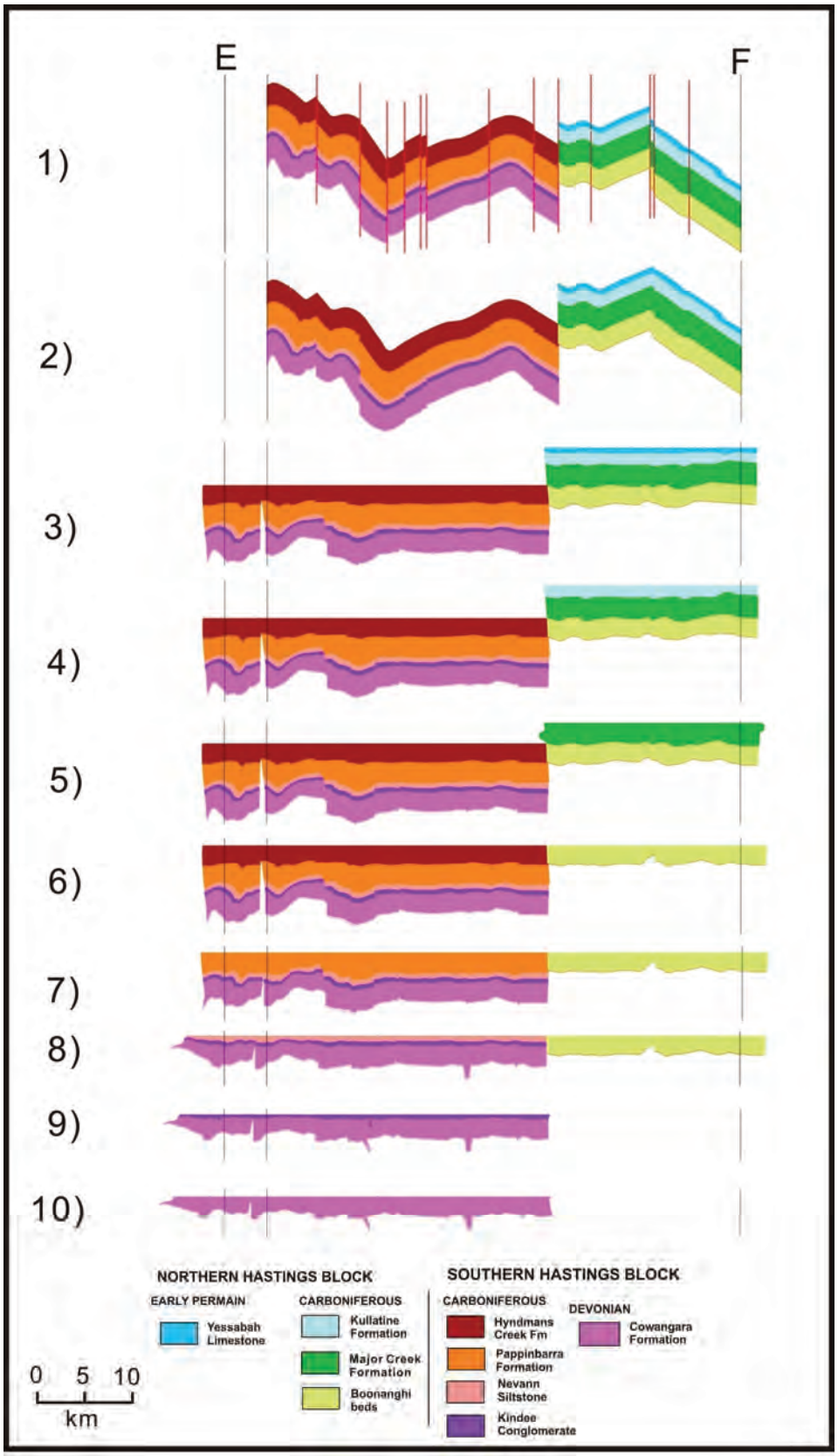

Figure 6.9: Sequential restorations of part of the geological Section E - F from the fault near Station 17 to near F (Figure 6.1). The likely geology between Station 140 and 155 has been included in this restoration.

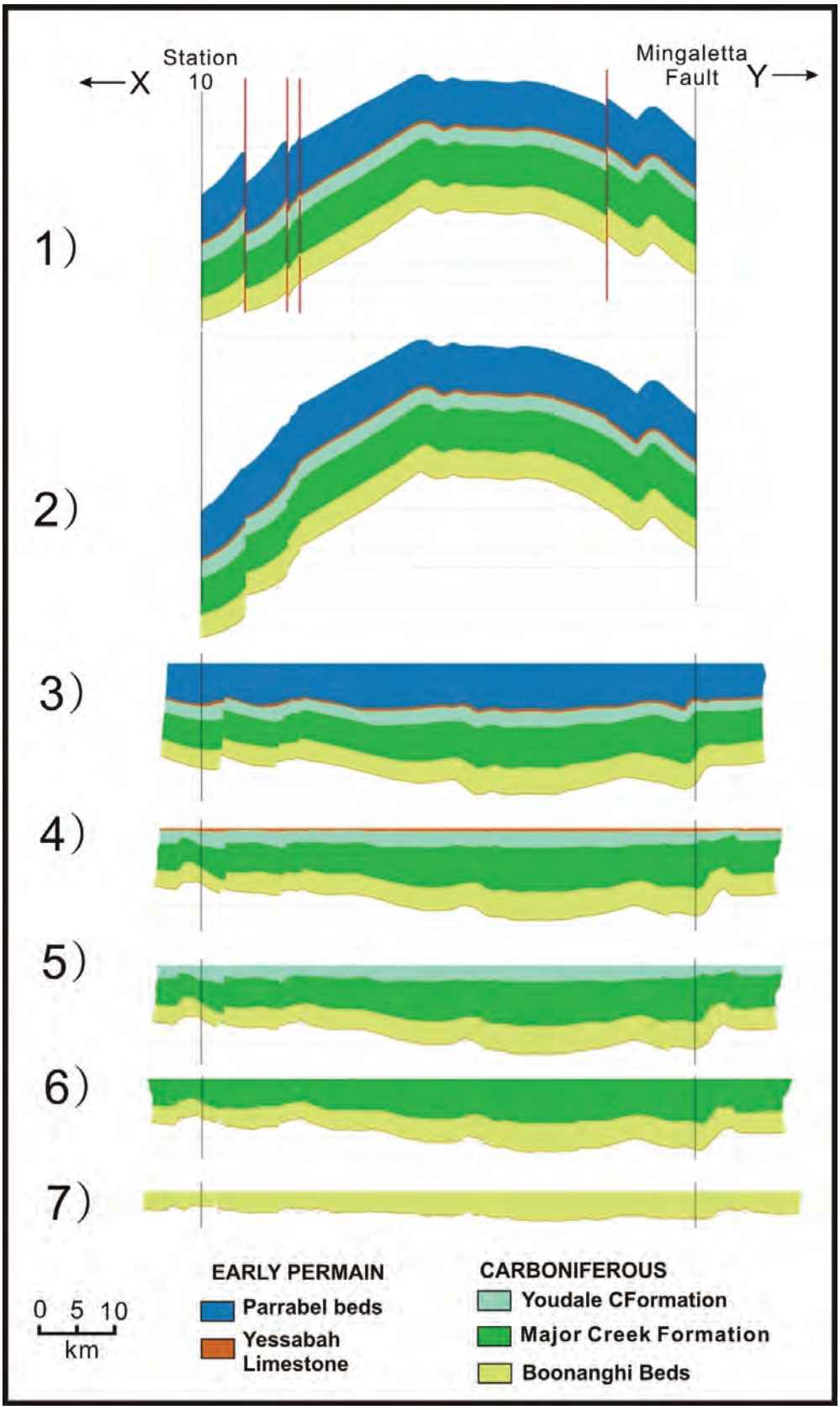

Figure 6.10: Sequential restorations of part of the geological Section X - Y from the margin of the Carrai Granite in the northwest to the Mingaletta Fault in the southeast.

The software used to restore the cross sections assumes that both sequences deform to the same degree. It is clear from field work and the development of cleavage and folds that the overlying Permian Parrabel beds and Yessabah Limestone were easily deformed with prolific cleavage development and formation of mesoscopic folds than the underlying Carboniferous (Boonanghi Beds to Youdale C). The software can not model this difference.

6.4.2.1 Shortening Estimates

The total horizontal shortening estimates for the above four geological sections are derived from cross-sections restorations and presented in Table 6.3. The difference in total length between the fully deformed and fully restored states for the cross section A-B indicates a total horizontal shortening of about 4 km or about 13% of the fully restored length of 34 km. The horizontal shortening amounts of 25% (21 km), 20% (13 km) and 25% (21 km) are obtained based on the restoration of cross sections C – D, E – F and X – Y in the NHB. The difference in shortening between cross sections is due to diffuse internal deformation. The estimated shortenings of these four cross sections support the existence of the generally NW-plunging, Parrabel Dome, which was caused by NE-SW shortening (cross sections A – B, C - D and E – F) accompanying with almost equal NW-SE shortening.

Table 6.3: Total shortening in Kilometers and shortening percentage deduced from cross-section restorations.

Cross Section	Fully deformed length (km)	Fully restored length (km)	Shortening (km)	Shortening percentage
A - B	29.5	34	4	13%
C - D	62	83	21	25%
E - F	51	64	13	20%
X - Y	63	84	21	25%

According to the classification of spaced cleavage (Davis 1984), the total horizontal shortening in the NHB suggests moderate cleavage development (4% to 25%

shortening). This is consistent with field observations of patchy, generally poor cleavage development in the sandier basal units of the NHB (see Chapter 3.4).

The results of the sequential restoration of each cross section detail a sequence of deformation that progresses from ductile deformation to finally brittle faulting. The results suggested that (1) the NHB has been undergoing continuous shortening since the beginning of the deposition of Devonian sequences and (2) the shortening of the NHB reached its maximum value after the deposition of the Early Permian sequences during the Hunter-Bowen Orogeny. It is recognized that in reality there were periods of extension related to formation of the Nambucca Basin (part of the Barnard Basin) in the Early Permian and not continuous shortening (Cawood *et al*. 2011). Approximately 8%, 19%, 14% and 17% of the shortening took place in this period for Cross Section A - B, C – D, E – F and X – Y respectively. The fold tightness may reflect the increased shortening on the southwestern side of the Cross Section C – D compared with the shortening on the northeastern side of this cross section or the difference in the competency of lithologies being folded. There was an increase in the shortening on the southwestern part during the deformation. This indicates there were probably much larger strains on the western boundary of the Hastings Block compared with the northeastern boundary as shown by more intense S_2 and to a lesser extent S_3 development on this margin (Chapter 4.6). The Parrabel Dome consists of competent sandy units which acted as a rigid massif compared with the more incompetent beds around the margins. The maximum deformation occurred on the western central part of the Hastings Block. This is compatible with field observations of intensive cleavage development along this margin of the block (see Chapter 3.4).

6.4.3 Implications

The Boonanghi beds in the NHB (centre of cross section C-D) are represented by the combined basal Nevann Siltstone, overlying Pappinbarra Formation and capping Hyndmans Creek Formation in the SHB (left of Fault 43). Any restoration will involve

moving the top of the combined package in the SHB into conformity with the top of the Boonanghi Beds in the NHB. Similarly the Kullatine Formation in cross section C-D (Figure 6.4) is the stratigraphic equivalent of the Mingaletta Formation in the SHB. In cross section C-D, it is apparent that the two formation are not the same thickness consistent with estimated thickness in the literature.

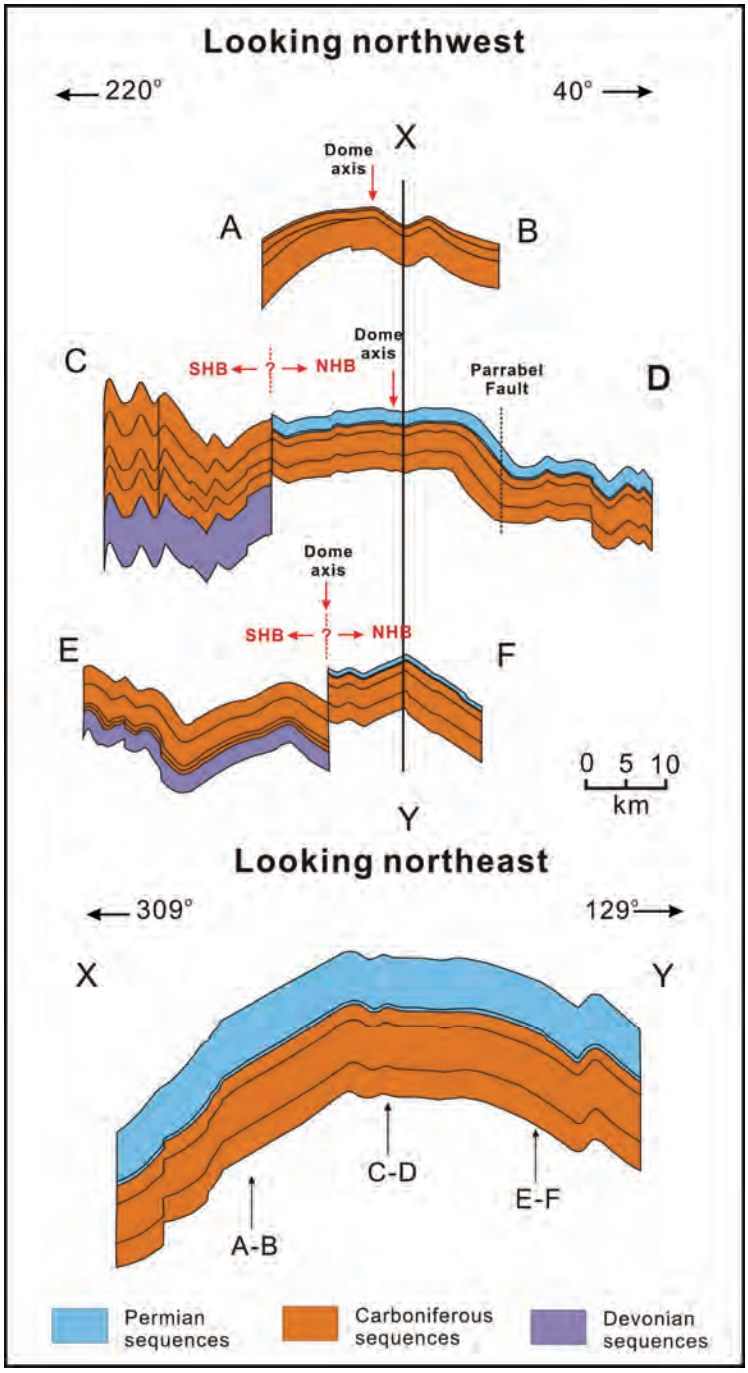

Figure 6.11: The simplified diagram of the cross sections across the NHB.

The Parrabel Dome is around 29 km in half-wavelength with 7.7 km in amplitude. The Devonian sequence exposures are absent in the northeastern part of the cross sections C-D and E-F (Figure 6.11). The tighter smaller wavelenghth folding within Carboniferous sequences on the southwestern margin of cross section C-D contrasts with the very open box-like geometry of the Parrabel Dome in the centre of cross section C-D (Figure 6.11). The Carboniferous to Permian sequences on the northeastern end of cross section C-D show an increase in the intensity of fold development is similar throughout cross section E-F (Figure 6.11). This reflects the complexity of the deformed northeastern limb of the Parrabel Dome expecially towards northeastern end (F). The cross section C-D also shows that the Hastings Block succession continues well to the north under the Nambucca Permian succession - this raises the possibility that much of the Nambucca Block is underlain by Tamworth Belt rocks that continue further north in the subsurface.

It could be envisaged that overall the dome in cross section A-B still exists in cross section C-D, but is replaced by small scale macroscopic folds in cross section E-F. Cross section X-Y indicates the dome plunges both northwest and southeast with the southeast limb plunging more gently compared with the northwest limb.

The northwestern part of the cross section X-Y supports a gently NW-plunging dome (Figure 6.11).

Glen & Roberts (2012) reinterpreted the Hastings Block and suggested the Parrabel Dome was a hangingwall anticline above an east-dipping thrust system represented by the Bagnoo Fault and its inferred extensions (Rollans Road Fault and Pappinbarra Fault) with a component of left-lateral movement (see Figure 6.5 near Station 57). The four cross sections in the NHB but especially cross section E-F indicates that this could not be the case. The reasons are: (1) The Bagnoo Fault does not show evidence for thrusting

as required by their model (Figure 6.5), rather sinistral strike-slip movement with the northeast side downthrown as observed in the field (Feenan 1984; Spackman 1989; Offler unpubl.); (2) The Parrabel Dome is seen on these cross sections as an open, upright structure with a number of smaller macroscopic folds across its crest (Figure 6.11). It's shape is not consistent with an asymmetric hanging-wall anticline above an east-dipping, listric Bagnoo Fault as proposed by Glen and Roberts (2012). In cross section E-F (Figure 6.5), there is a macroscopic synform northeast of the Bagnoo Fault and not an antiform (Stations 55-80).

6.5 Conclusions

1. The Parrabel Dome is around 29 km in half-wavelength with 7.7 km in amplitude, having gently dipping flanks and is box –like along cross section C-D.
2. None of the major faults has more than a few kilometers of vertical displacement consistent with little difference in metamorphic grade across these faults.
3. Strain is concentrated in the cleaved and folded Permian sequences and to a lesser extent the Devonian-Carboniferous sequences around margin of the Carboniferous core sequences of the dome which is especially noticeable in cross section C-D (near C) and E - F (near E).
4. The overall shape from the cross sections suggests a northwest and southeast-plunging dome which is box-like in cross section C-D and more open in cross sections A-B and E-F.
5. A macroscopic synform flanked by two macroscopic antiforms is visible in cross sections A-B and E-F near the crestal region of the Parrabel Dome (Figure 6.11).
6. The total horizontal shortening in the NHB suggests moderate cleavage development (4% to 25% shortening) consistent with field observations.
7. The maximum shortening in the NHB occurred after the deposition of the Early Permian sequences during the Hunter-(Bowen) Orogeny.

Chapter 7: 3D geological modeling of Northern Hastings Block

7.1 Introduction

One of the primary goals of computer modelling is to produce a model that is internally consistent, structurally possible, and a viable representation of the geological setting (Hoffman and Neave, 2007). 3D geological models are now used to better interpret the structural architecture and pathways of formation. For example, they can be used to solve geomechanical problems and assess or predict the extraction of natural resources, investigate geophysical problems and better understand the mechanisms that trigger earthquakes (Calcagnoa *et al*. 2008).

Software for 3D geological reconstruction has evolved considerably since its beginnings in the 1980's (Mayoraz 1993; Jessell and Valenta, 1996; Sprague and De Kemp 2005). There are now a number of mature products including (among others): 3D-Move, earthVision, Gocad, Leapfrog3D and Petrel. These applications have opened new frontiers in the Earth Sciences enabling 3 and 4 dimensional analyses of spatially complex faulted and folded geological environments (Zanchi *et al*. 2009). Despite these software developments, the process of constructing a rigorous 3D geological model from historical and new data sets remains challenging, because there are typically many gaps in the primary data sets. Information used to construct 3D geological models includes: geological field mapping records, aerial and ground based geophysical surveys, and geological well logs. When only field mapping data are available constructing a geologically feasible model requires geological insights (regional geological setting and history) and numerous model iterations before a useful 3D geological model can be built. The workflow for constructing a geological model using only maps (Figure 7.1) and bedding strike and dip measurements is outlined below (Yan *et al*. 2014a; Yan *et al*. 2014b; Yan *et al*. 2014c; Yan *et al*. 2015). The final 3D geological model is used to

explore questions relating to the emplacement, rotation and vertical movement of fault blocks within the Northern Hastings Block (NHB).

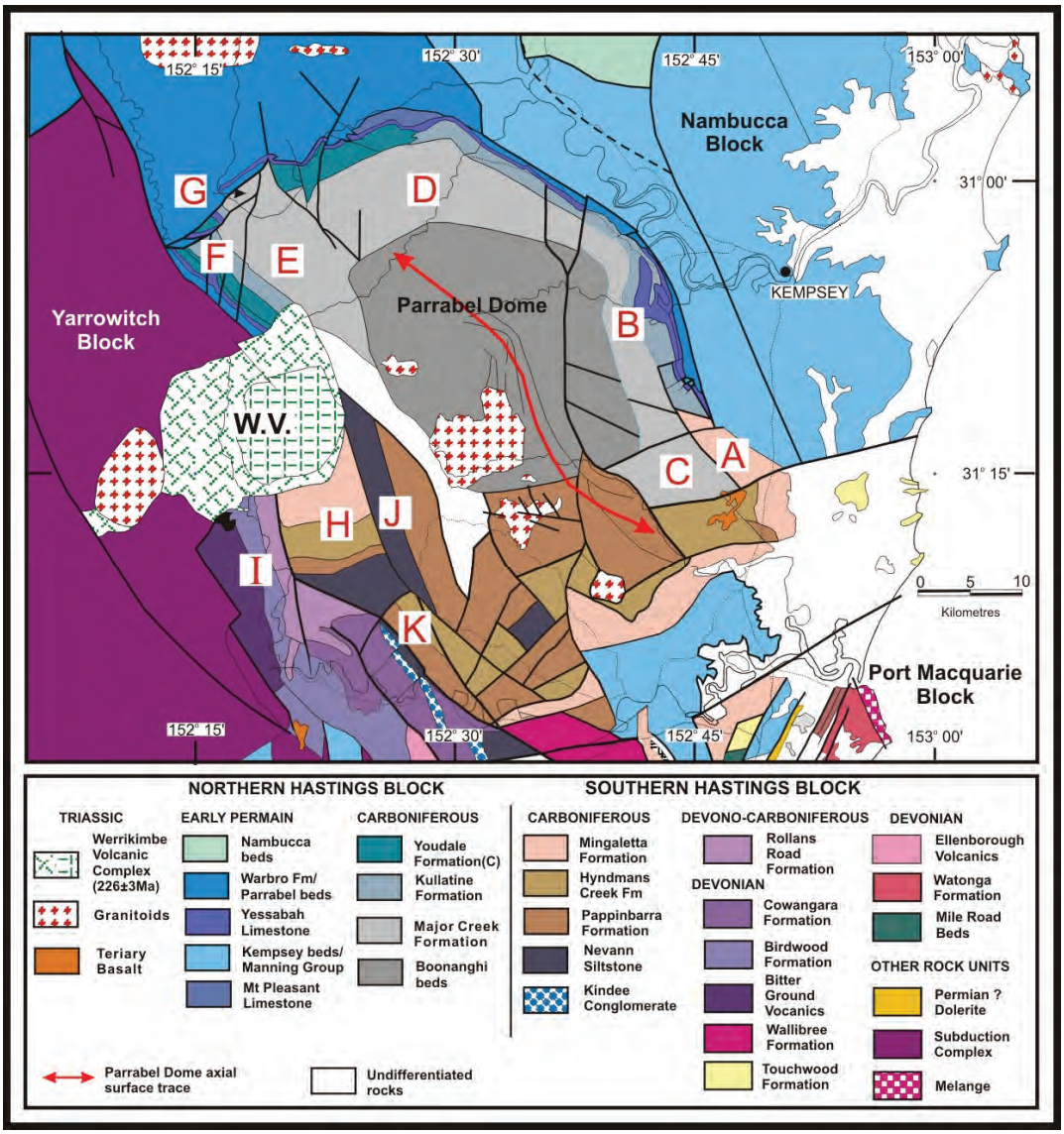

Figure 7.1: A simplified geological map of Northern Hastings Block (Roberts *et al.* 1995) with the different fault blocks labeled with upper case letters. W.V. = Werrikimbe Volcanics.

Typically structural modeling workflows start with georeferencing the data, then building the fault network, and finally generating 3D horizons which are consistent with faults and stratigraphic layering rules (Mayoraz 1993; Sprague and De Kemp 2005; Wu *et al.* 2005; Frank *et al.* 2007). These models can then be used for estimating formation

volumes, checking the feasibility of the prevailing geological conceptualization of a region, and for doing kinematic reconstructions (Jessell 2001).

A geological map consisting of exposed stratigraphic and structural boundaries, as well as structural information (bedding, faults, foliations, fold axes, lineations), is one of the most effective tools to be used in 3D reconstruction (Zanchi *et al*. 2009). These data represent spatially continuous information on the geological framework of a region, and have been traditionally used by generations of geologists to make prediction about the extension of geological structures at depth.

Faults and horizons honoring available observation data are the most important geological interfaces in 3D structural modeling. Faults partition space into regions where stratigraphic surfaces are continuous. Before interpreting the horizon-top data it is important to generate a fault tree to determine the order in which faults terminate, abut or extend across the modeling domain. In the workflow presented below, horizon construction is achieved fault-block by fault-block, from horizon data that has been gridded using inverse distance, triangulation and spline algorithms (Caumon *et al*. 2009).

This chapter demonstrates a new way of constructing 3D models of an intensively faulted and multiply folded block. It clarified the shape of the dome and compares existing cross sections across this dome with those constructed across the 3D model. Before this modeling there was no three dimensional model of the dome and this modeling demonstrated problems with the existing map of the NHB.

7.1.1 Leapfrog™ and MOVE™

Leapfrog™ and 3D MOVE™ are the two main graphic and integration software that are used in this chapter, along with ArcGIS®, Quantum GIS, System for Automated Geoscientific Analyses and Mathematica™ software for managing and analyzing the

various data set from the area.

Leapfrog

Leapfrog Geothermal is a 3-D modeling and visualization application developed by ARANZ Geo (Applied Research Associates Ltd) and GNS Science. It is based on implicit modelling methods that represent geology, structure, geophysical and reservoir data primarily gridded using radial basis functions (Alcaraz *et al*. 2011).

2D/3D Move™

2D/3D Move™ is designed by the Midland Valley Exploration Ltd to provide analysis of structural and whole earth systems using geological time as a constraint for both forward and reverse modeling. This software package provides dedicated products for digital field mapping, cross-section construction, 3D model building, kinematic restoration and validation, geomechanical modelling, fracture modelling and sediment modelling. It is a fully interactive, geometry-based, 2/3-dimensional structural modeling engine that employs algorithms that model brittle and ductile deformation while maintaining rock volume (www.mve.com). This project used 2D Move™ to perform the 2D structural restorations and forward modeling of the cross sections across the NHB. The geometric modeling of the NHB is performed within 3DMove™, which is based on surfaces composed of a triangular network of connecting data points. There is no differentiation between faults and horizons in 3DMove™ and both are treated equally as surfaces. Surfaces in 3DMove™ are commonly created using a tessellation algorithm that links nearest-neighbour data points with a triangular mesh, as opposed to draping a regularly spaced grid over the existing data cloud (www.mve.com).

7.2 Methodology

To build the model, geological map data were combined with a comprehensive field dataset that captured in greater detail both small and large scale structural details of the

Devonian, Carboniferous and Permian fore-arc or rift rocks across the Northern Hastings Block and adjacent Nambucca Block. There was no borehole data for this region. Fault and horizon surfaces were created by extrapolating to depth surface information from strike and dip field data, and the regional geological map. The structural information obtained from the geological maps included: the attitude of planar bedding, the strike and dip of faults and details on the alignment of fold axes. The 3D geological model was constructed to help visualize the NHB in three dimensions and provide insights into the geological history of the NHB.

To construct the 3D geological model the following workflow was used:

1) Data were converted into a single coordinate system, and checked for consistency with respect to the structural interpretation.
2) 2D GIS surfaces and other structural attributes were georeferenced in 3D.
3) Surface fault data were projected to depth and converted to 2D surfaces referenced in 3D space.
4) Stratigraphic horizon bottoms were generated for each fault-bound block.
5) The model feasibility was then checked using extracted cross-sections, which were validated using the field data. Where inconsistencies were discovered steps 1 to 5 were repeated.

7.3 Data Management

7.3.1 Input data for 3D modeling

Most geological models in the literature (Smallwood and Maresh 2002; Lemon and Jones 2003; Kaufmann and Martin 2008) are constrained using borehole data. In this project, however, there is no borehole data. The two primary data sets are the geological map of Northern Hastings Block (Figure 7.1) (Roberts *et al*. 1995; Leitch 1980, Honours thesis maps; 1:25000 maps constructed by Lennox of the Hastings Block and adjoining blocks) and field measurements of fault trace from the Roberts et al. (1995)

map and Honours theses. A schematic representation of the data sets and workflow used to construct the 3D geological model is presented in Figure 7.2.

To overcome the limitations of the primary data, cross-sections were generated to constrain the third dimension. These cross sections were constructed using the likely orientation of the bedding near geological boundaries and assuming literature-derived thickness data for the various units in the Northern Hastings Block.

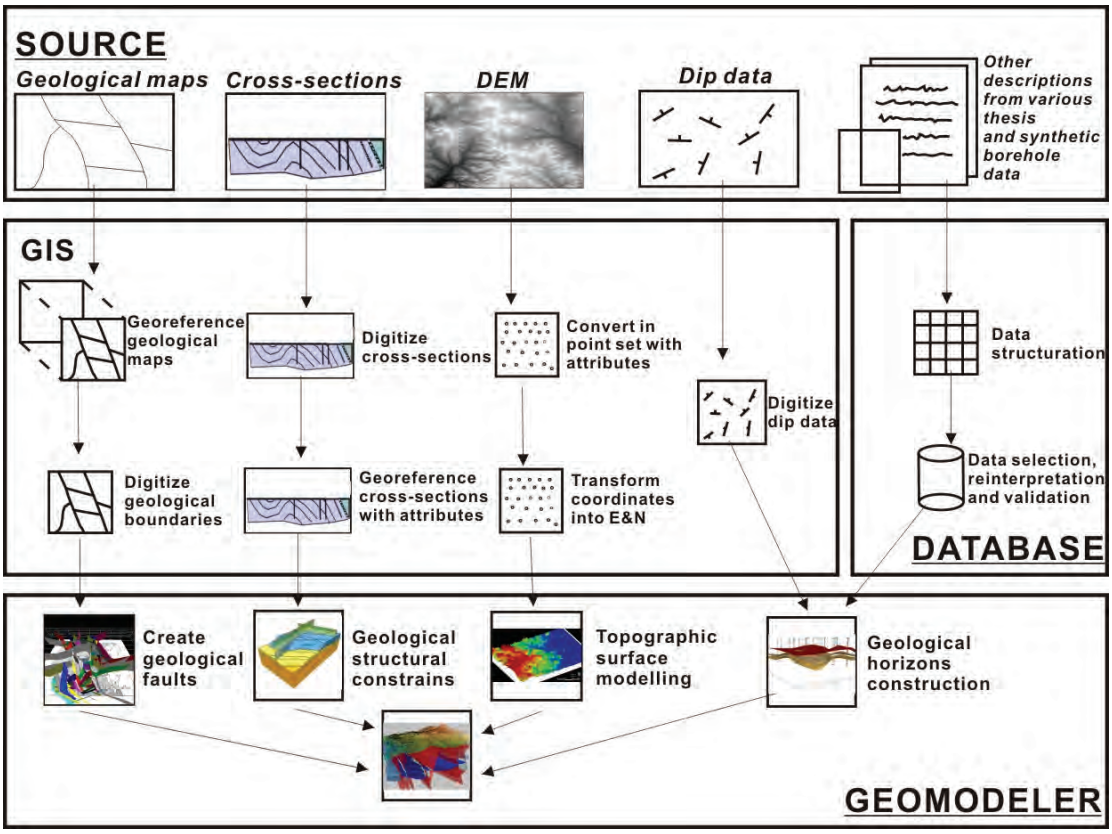

Figure 7.2: Input data and workflow used for constructing the 3D modeling of the Northern Hastings Block (modified from Kaufmann & Martin 2008).

Honours theses covering the Hastings Block and surrounding blocks were also a valuable source of geological information (Figure 7.3). Within these theses are data that usually consist of outcrop descriptions with lithological, paleontological and structural information collected during geological mapping or other fieldwork. In some cases, the descriptions from geological survey records are interpreted and their elevations are often unknown, wrong or based on topographic maps with poorly defined contours. A

DEM may be used to model the topographic surface and assign new elevations for all data. The DEM analysis includes such technique as the slope analysis, downslope distance gradient (DDG), terrain ruggedness index (TRI), vector terrain ruggedness (VTR), and multiresolution index of valley bottom flatness (MIVBF). This can greatly help improve the accuracy of the current structural interpretation and identify geological structures (Table 7.1).

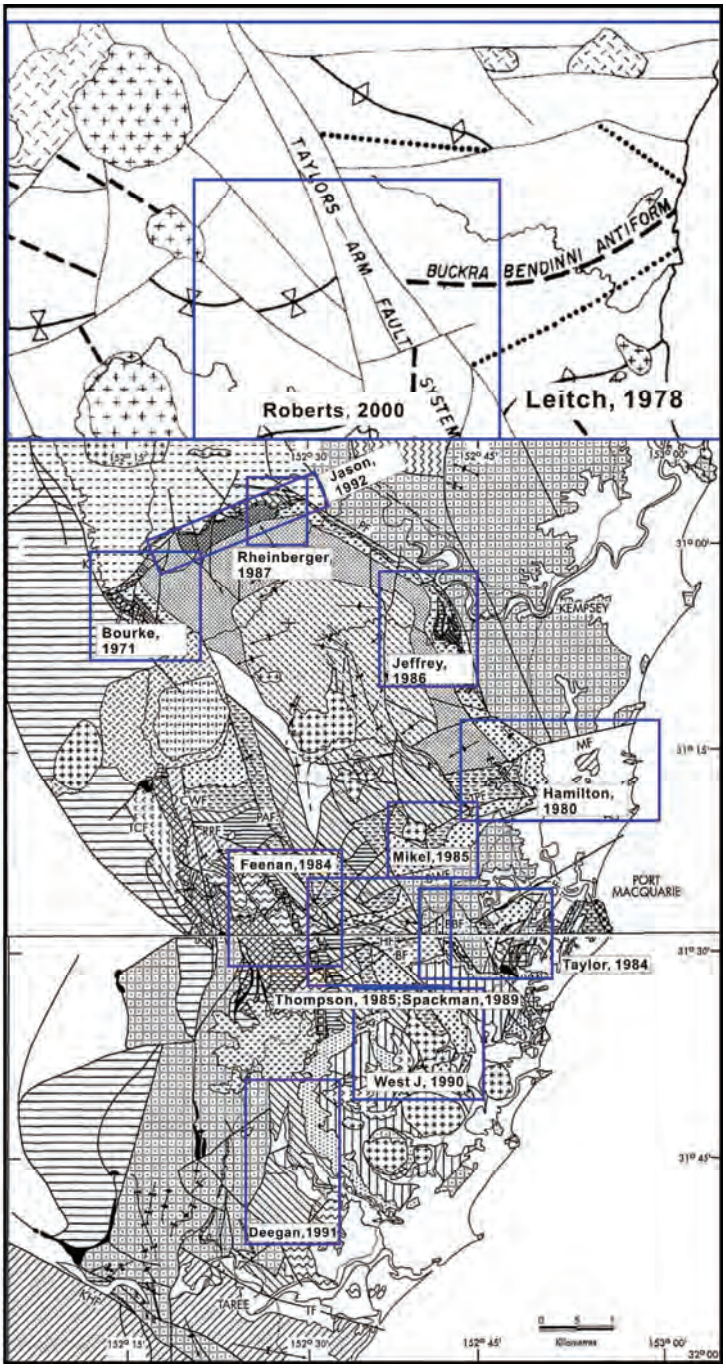

Figure 7.3: The map of areas covered by honours projects in the northern Hastings Block from which data was derived and the adjacent Nambucca Block with the major faults and

folds according to Leitch (1978).

Table 7.1: The characteristics of each DEM analysis technique

	Characteristics/ Parameter	Reference
DDG	The slope for each grid cell is portrayed by an integer value representing degrees.	SEGA-GIS-Wiki
TRI	Expresses the amount of elevation difference between adjacent cells of a digital elevation grid.	(Riley *et al.* 1999)
VTR	Measures terrain ruggedness using vector analysis to directly measure terrain heterogeneity from an elevation grid.	(Hobson 1972)
MIVBF	This index classifies degrees of valley bottom flatness. The algorithm operates at a range of scales and combines the results at different scales into a single multiresolution index.	(Gallant and Dowling, 2003)
SRI	A raster image that shows changes in elevation using light and shadows on terrains from a given angle and altitude of the sun.	support.esri.com

7.3.2 Management and 3D Visualization

Before doing the geomodelling, all the geological data need to be combined and organized into a common coordinate system. This step is called georeferencing. It is an essential step in the modeling process to choose a good coordinate system, since different maps, dip data and borehole dataset may use different projection systems. There are various tools available that can help transform the data into the coordinate system we want, such as ArcGIS, Quantum GIS and AusDatumTool. These tools contain methods to combine and overlay the data and images with minimum distortion. For example, to georeference an image, the first step is to establish at least three control

points. In order to minimize the residuals, the difference between the actual coordinates of the control points and the coordinates in final coordinate systems computed by the geographic model, the control points should be chosen as close as possible to the georeferenced points and picked on precise geographic coordinate systems to minimize errors. The larger the number of control points the better the georeferencing.

The second step in data management consists of data preparation, structure and reinterpretation. If data is not digital or is in an unstructured format, it was structured, encoded or digitized and then positioned in the spatial coordinate system of GDA 94.

7.4 Digital elevation model (DEM) and its analysis

7.4.1 Introduction

The digital Elevation Model (DEM) is a digital representation of the topographic surface expression of study area (Figure 7.4). The data are transformed from XYZ data into various formats of continuous data such as grid, contour, profile and triangulated irregular networks (TIN). Each of these formats offers advantages for certain applications, but the grid format is most widely used. DEM data has been found useful for various geological research areas such as geological analysis of morphology, geohazard, hydrologic modeling, geological mapping and potential flooding area modeling (Badura and Przybylski, 2005). Interpretation of DEM data is also used for structural interpretation particularly in terms of regional studies, because it can increase our visual ability to interpret the data (Sarapirome *et al*. 2002). Modern computer technologies have been providing better DEM software for geological analysis, which improves the agreement between the interpreted geological units with the terrain topography.

DEM data can be used for geological interpretation in terms of the morphology of an area, the rock types and in recognizing structures, at an acceptable level, particularly

when other data are not available (Ganasa *et al*. 2005; Zizioli 2008). A fine resolution DEM improves the chances of detecting faults. For this research the Geoscience Australia 1 arc-second resolution DEM product was used. Geological structural features normally appear as either linear or curvilinear features on the DEM data. Linear features usually indicate the location of faults. Curvilinear features are typically associated with underlying dome structures, caused by intrusive geological bodies (Jordan 2003).

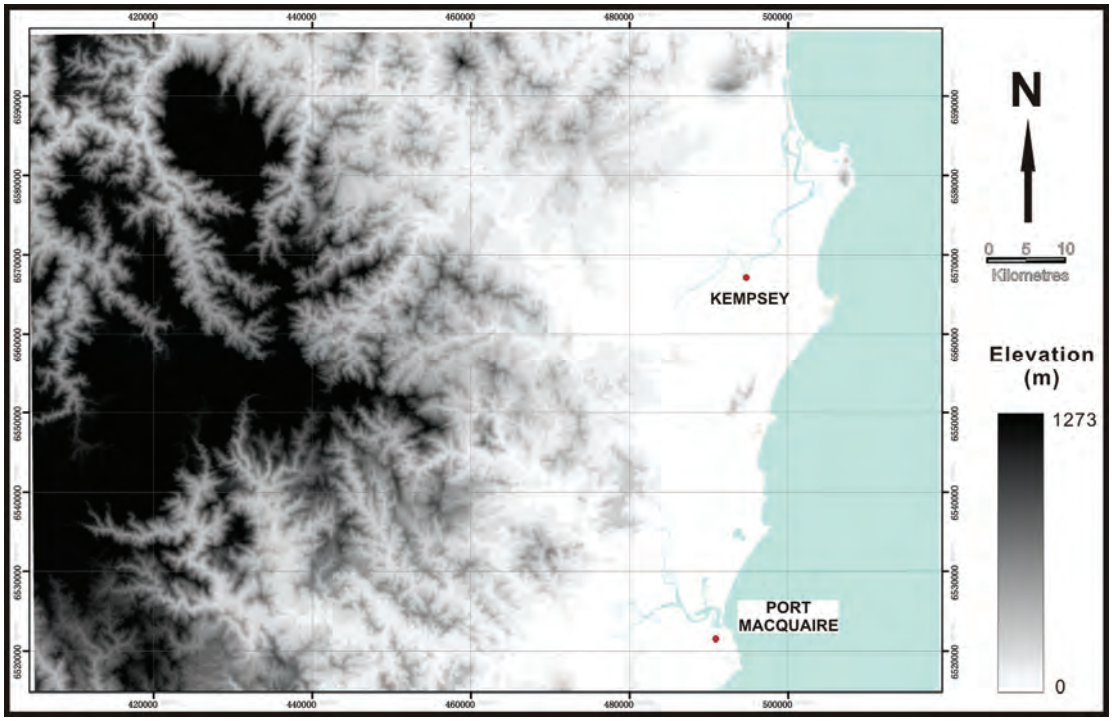

Figure 7.4: The digital elevation model (DEM) of the Northern Hastings Block (Geoscience Australia 1 arc-second resolution DEM).

Basic geometric properties that characterize the terrain surface that can be derived from the DEM are: (1) elevation; (2) properties of the gradient vector; (3) surface curvature; (4) surface-specific points and lines, such as peaks, pits, inflections, point ridges, break-lines and valley lines. These features usually relate to specific tectonic structures. For example, slope-breaks and fractures are often straightforward. Steep slopes of uniform aspect over an area may be related to faulting. Linear valleys, ridgelines and slope-breaks are morphological features commonly associated with faults. Curvilinear feature may indicates underlying dome structures (Jordan 2003)

7.4.2 Methodology

The original regional DEM was firstly extracted from the Australian continent DEM. It was converted to points that are assigned XY coordinates on the plane and the vertical coordinate Z. It is necessary to transform XYZ data into the so-called grid in order to improve the resolution the DEM. This preparatory steps can also help to remove noise and some spurious peaks in the elevation reading. The final grid can be generated and analyzed by different programs (Figures 7.4 and 7.5).

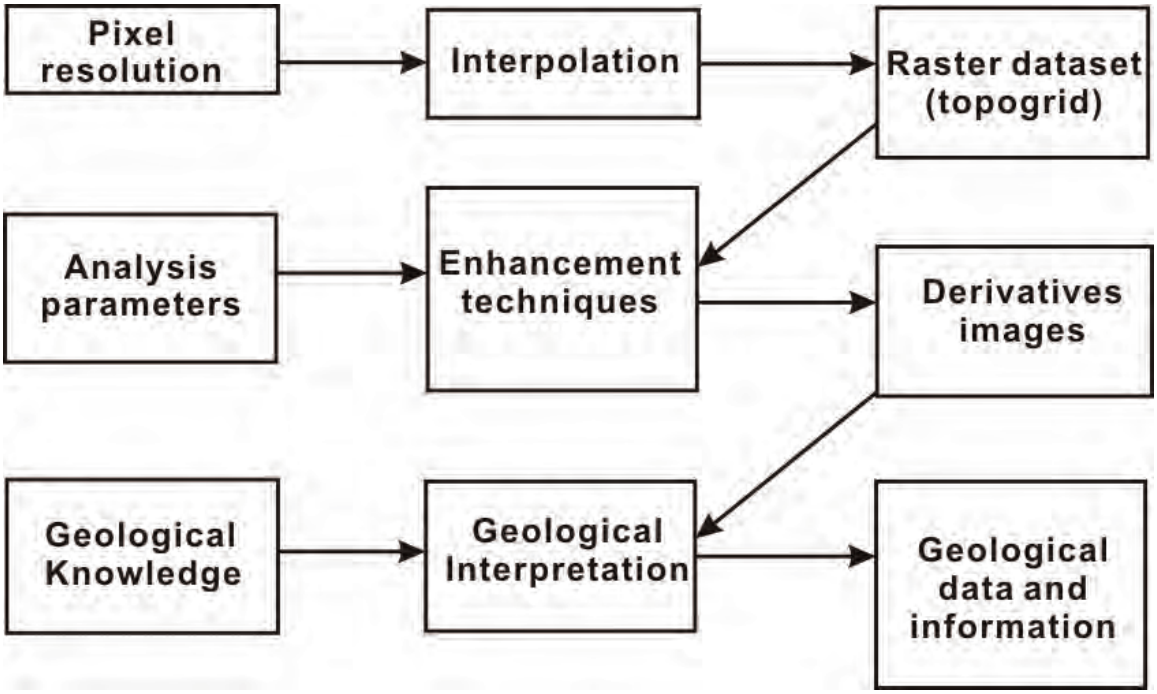

Figure 7.5: Inputs, processes, outputs to achieve better DEM images and better interpreted the geology. (modified from Sarapirome *et al*. 2002).

DEM analysis was undertaken to find geological features not indicated on the geological maps. The following steps were used: (1) image enhancement using different vertical exaggeration, shading and other parameter variation; (2) different derivatives of elevation were computed to provide an objective quantitative measure of topographic heterogeneity; (3) these enhanced image data were then used to identify lineaments and other structural features; (4) the lineaments information obtained from interpreted lineaments were plotted on an existing geological map (Figure 7.5); (5) in order to find

out whether the lineaments are faults or not, the bedding data were incorporated. The bedding trend should become parallel to the fault when it has been measured very close to the fault due to fault drag. Further, the dip of the bedding close to the fault should be quite similar to the dip of the fault if there is significant movement on the fault. The software package, System for Automated Geoscientific Analyses, was used in this section for the DEM analysis.

For lineament identification different derivatives of the DEM (DDG, TRI, VTR, MIVBT, SRI, etc) were tested (Table 7.1). Downslope distance gradient(DDG) and shaded relief images(SRI) were the most frequently used in the structural interpretation. Slope angle was calculated from each pixel of an elevation channel in DEM. Abrupt changes in slope across the landscape indicated faulting and fault scarps.

Shaded relief images show changes in elevation using light and shadows on the terrain from a given angle and altitude of the sun. In shaded relief images, it is possible to set up various illumination conditions to study the long-term evolution of landforms of the region. Interpretation can be undertaken from various oblique and vertical angle positions with various zoom options which resembles multiscale observations of an area. It is said that an oblique view is generally more useful than a vertical view because geologically-related breaks in slope can be more easily identified at lower viewing angles (Tragheim and Westhead, 1996). Vertical exaggeration of the DEM may also aid in the interpretation of subtle areas, enabling the features to be recognised more easily, and spatial relationship between them to be determined.

Digital models can also be used in analysis and verification of the existing geological maps, provided that their scanned, raster images are available. Proper software enables such raster images to be calibrated according to the coordinates of a digital elevation model, and then be superposed on a 3D shaded relief map. This image can be verified regarding the strike of structures and map units resistance to weathering contrasted with

the observed topography. This is an excellent method of verification of structural features shown on a geological map.

7.4.3 Results

The Northern Hastings Block is characterized by a northwesterly structural grain due to the macroscopic northwesterly-trending Parrabel Dome. It has undergone four phases of folding namely, east-west, north-south, northwest-southeast and northeast-southwest trending as well as three episodes of faulting (Roberts *et al.* 1993, see Chapter 3.5). Roberts *et al.* (1993) suggested northwest-trending faults formed first with mainly sinistral strike-slip movement, followed by northeast-trending faults with dextral or sinistral strike-slip or dip-slip movement; all show only minor displacement. Subsequently, meridional, dip-slip faults developed, whereas this thesis has shown there are at least four main directions of faulting and up to five groups of faults which moved at different times during the block emplacement and subsequent deformation.

To better characterize the morphology and recognize structures and different rock types of Northern Hastings Block, analysis using different derivatives of the DEM (DDG, TRI, VTR, MIVBF, SRI) was undertaken.

(1) Downslope distance gradient (DDG)

The first derivative of elevation is the downslope distance gradient (Figure 7.6). Slope angle can be calculated from each pixel of an elevation channel in DEM. The output image contains slope values which range from 0° to 90°. Abrupt changes in slope across the landscape are possible indications of active faulting and lineaments seen in slope maps and may represent where fault scarps outcrop. Using this method, we observe that there are seven areas (Figure 7.6) where the slope changes abruptly. This is shown by the red to yellow colour transition in Figure 7.6. Six areas shows the terrain lineaments

(a) are longer than 30 km, and (b) both elevation and slope angle decrease towards their ends. We suggest that their origin is attributed to fault activity or a geological boundary. One area in the northwest of the NHB shows a curvilinear feature which may indicate an underlying dome structure. This dome structure could be the Carrai Granite (Leitch 1976).

Compared with the geological map of the Northern Hastings Block, the terrain lineaments are likely to be five major faults (Parrabel Fault, Kunderang Fault, Bagnoo Fault, Cowarral Fault and Pappinbarra Fault) and a geological boundary between the Majors Creeks Formation and Kullatine Formation on the northeastern margin of the Parrabel Dome. The curvilinear feature is the edge of the intrusive Triassic Carrai Granodiorite (Leitch 1976, Figure 7.6).

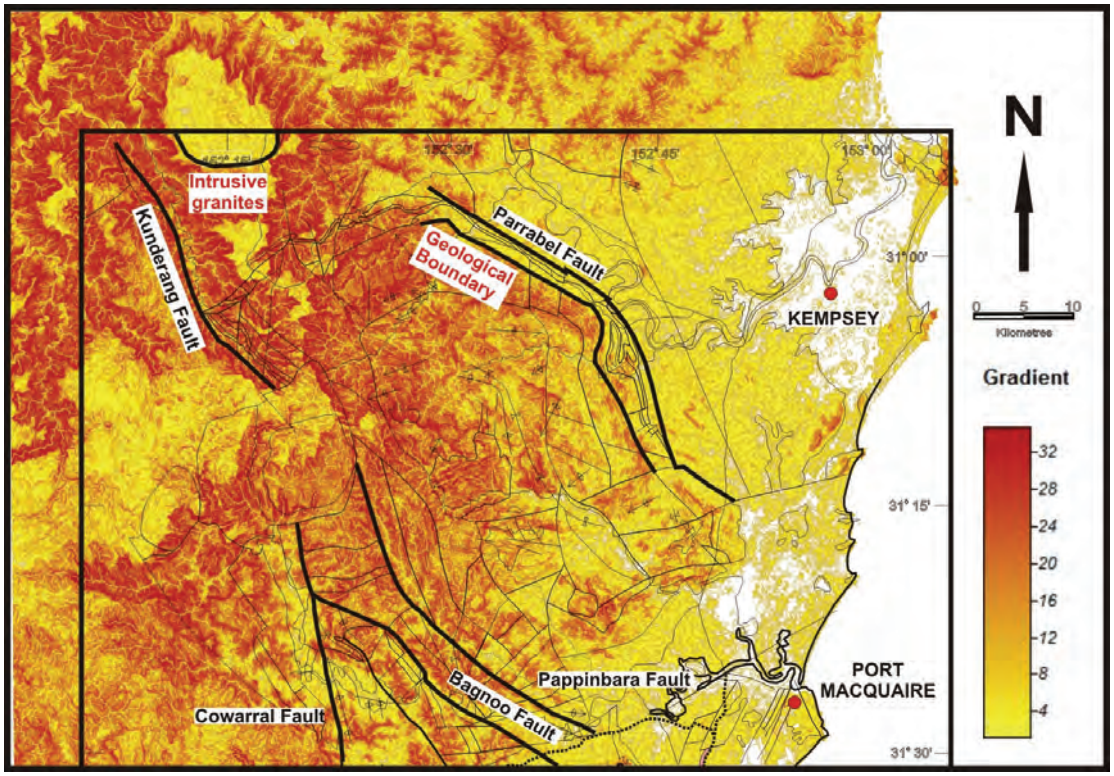

Figure 7.6: DEM analysis and interpretations of downslope distance gradient (DDG) in the Northern Hastings Block. The wireframe overlying the DDG corresponds to the geological map from Roberts *et al*. (1995) plus the main creeks, folds and roads.

(2) Shaded relief image

Shaded relief images shows changes in elevation using light and shadows on the terrain from a given angle and azimuth of the sun. A shaded relief image was created using 45° for the sun angle and 315° for the sun azimuth (Figure 7.7). This oblique view is better for geological interpretation because geologically-related breaks in slope can be more easily identified at this viewing angle. The texture and pattern of the NHB in the shaded relief images are enhanced.

From this shaded relief the structures look like a series of linear and curvilinear features. We can trace several major lineaments easily that are longer than 30km and trending NW-SE. These lineaments could be the faults because some triangular facets are displaced by these lineaments. Those structures which do not displace the triangular facets could be geological boundaries. The curvilinear feature indicates the underlying dome structure. Comparing this map with the geological map verifies the existing major faults in the NHB (Parrabel Fault, Kunderang Fault, Bagnoo Fault, Cowarral Fault, etc) and the curvilinear feature which is likely to be the Carrai Granodiorite. The data also shows that the western part of the NHB has more relief, compared with the eastern part of the NHB. The rocks in the western part of the NHB could be the harder rocks which are more difficult to erode (like the contact metamorphosed Boonanghi Beds near the Triassic Glen Esk and Gundle granites) compared with those in the eastern part (like the Kempsey Beds) (Figure 7.7).

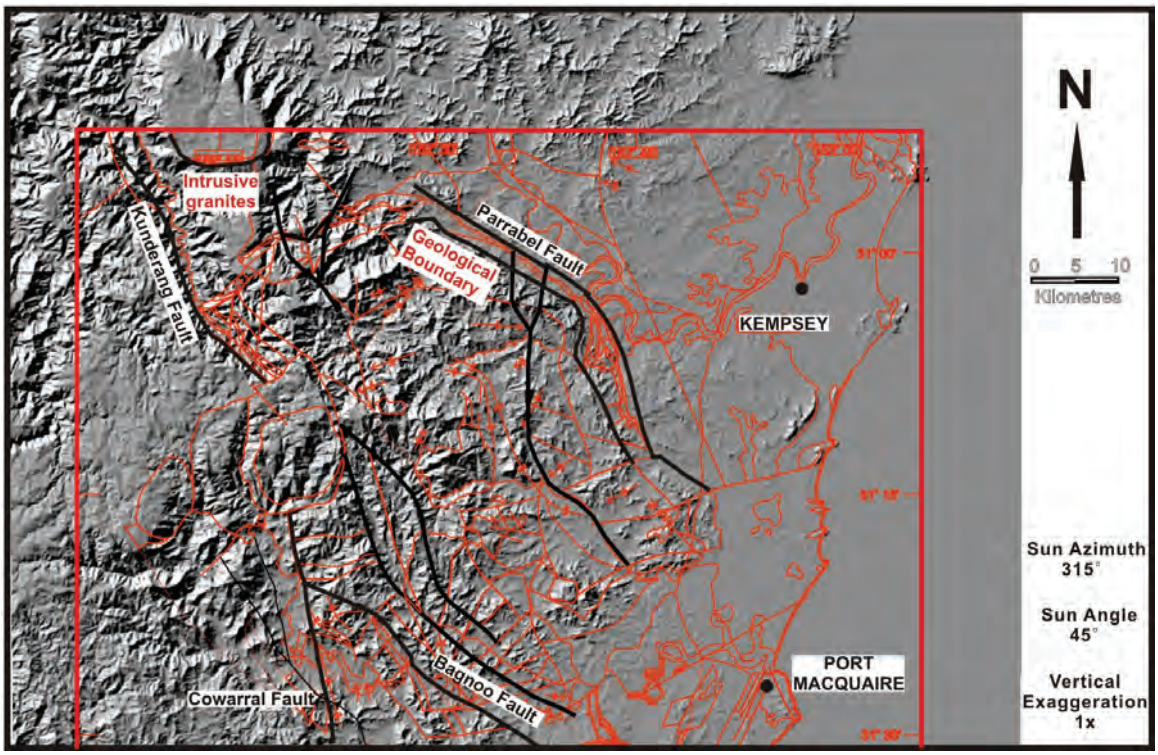

Figure 7.7: DEM analysis and interpretations of downslope distance gradient (DDG) in the Northern Hastings Block with the overlying wireframe geological map and cultural features.

(3) Multiresolution index of valley bottom flatness (MIVBF), terrain ruggedness index (TRI) and vector terrain ruggedness (VTR)

Similarly, a series of linear and curvilinear features were also identified in the MIVBF, TRI and VTR of the DEM analysis. The MIVBF classifies degrees of valley bottom flatness (Figure 7.8). The TRI express the amount of elevation difference between adjacent cells of a digital elevation grid (Figure 7.9). The VTR measures terrain ruggedness using vector analysis to directly measure terrain heterogeneity from an elevation grid (Figure 7.10). The obvious colour changes in the Figures 7.8 - 7.10 means abrupt changes in the various indices which show up as a series of linear and curvilinear features. The major faults (Parrabel Fault, Kunderang Fault, etc), the geological boundary between the Majors Creek Formation and overlying Kullatine Formation and the edge of the Carrai Granodiorite are then identified in these derivatives of the DEM. The VTR analysis indicates the Cowarral Fault appears to truncate the Bagnoo Fault indicating it moved later than the Bagnoo Fault (Figures 7.8-7.10). This is supported by mapping in this

area.

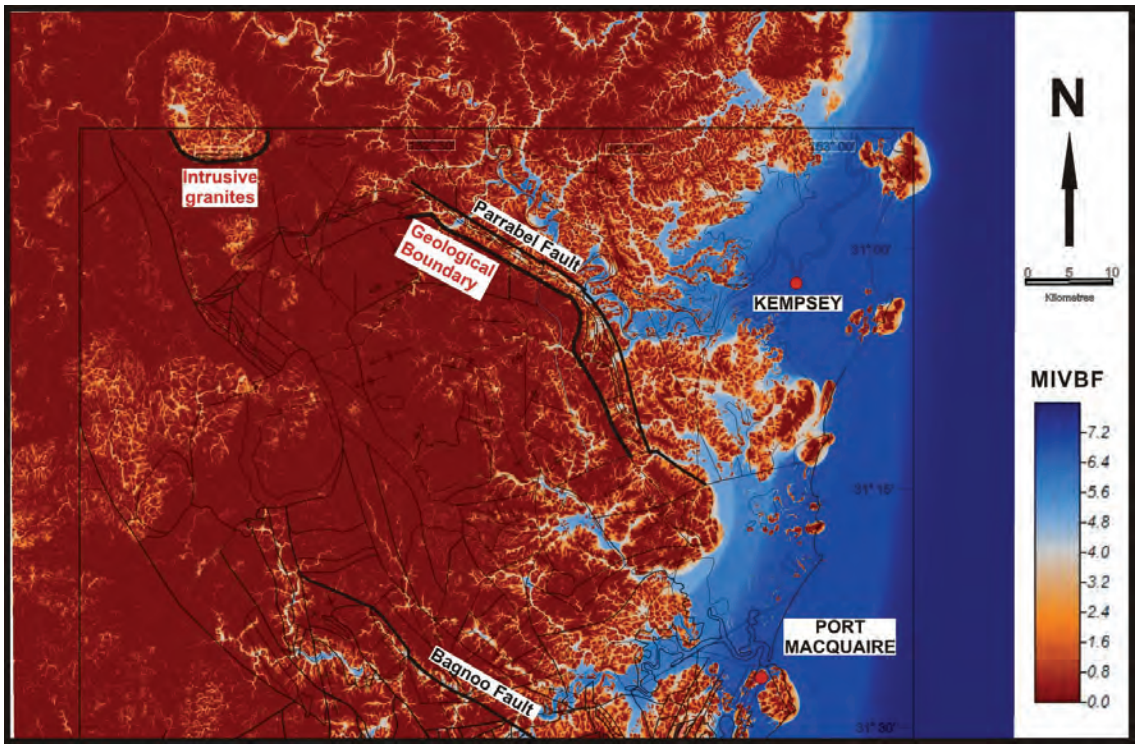

Figure 7.8: DEM analysis and interpretations of Multiresolution Index of Valley Bottom Flatness (MIVBF) in the Northern Hastings Block with the overlying simplified wireframe geological map.

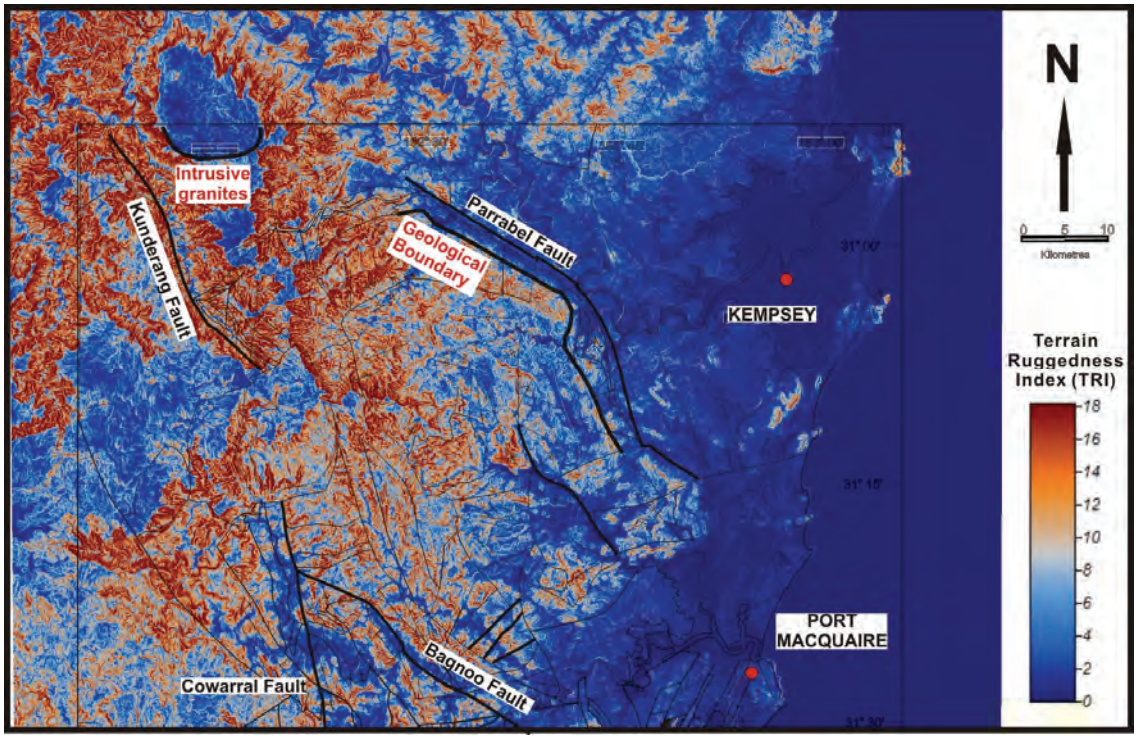

Figure 7.9: DEM analysis and interpretations of Terrain Ruggedness Index (TRI) in the Northern Hastings Block with the overlying simplified wireframe geological map.

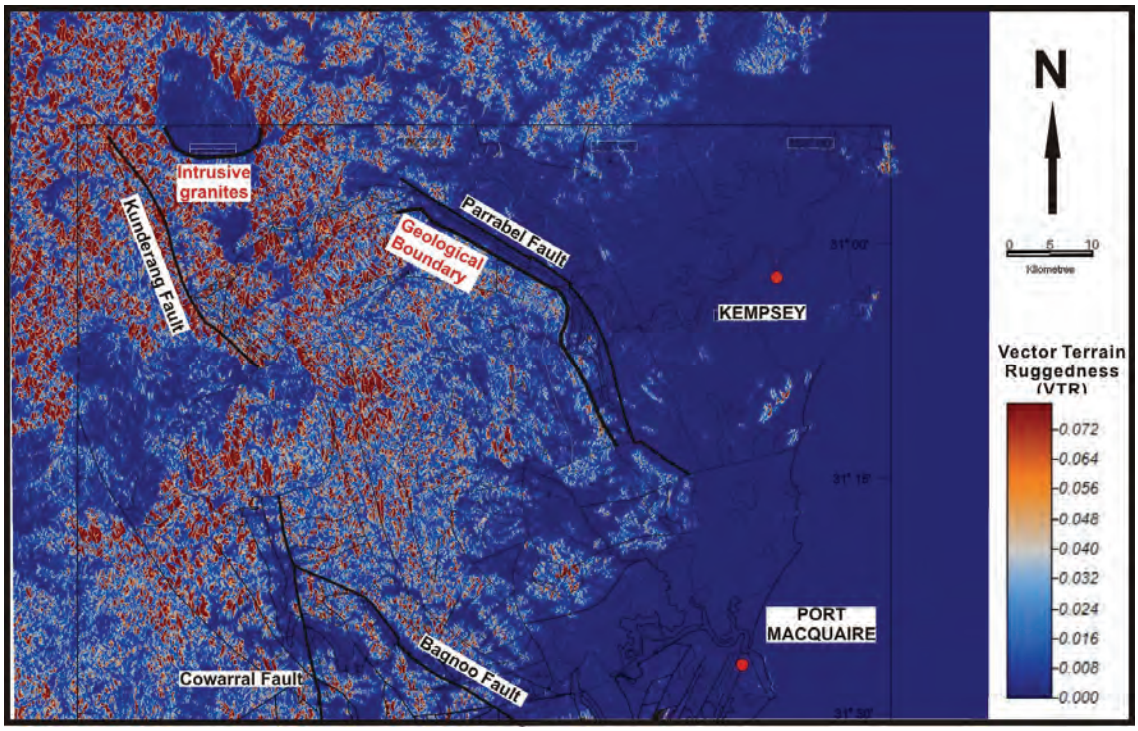

Figure 7.10: DEM analysis and interpretations of Vector Terrain Ruggedness (VTR) in the Northern Hastings Block with the overlying simplified wireframe geological map.

This analysis of DEM and their derivatives shows which major structures are detectable via this analysis. This analysis models the topographic surface, enhances the texture and pattern of the NHB and makes identifying any linear and curvilinear features easier. This analysis verified the existing structures on the geological maps. The new images verified the strike of structures and different map units which affected the topography. This analysis is a good method for the verification of cross-cutting relationships shown on a geological map such as intrusive granites and cross-cutting faults.

7.5 Fault modeling

7.5.1 Introduction

A fault is a surface or narrow zone along which one side has moved relative to the other in a direction parallel to the surface or zone (Twiss and Moores, 1992). It occurs as a

result of multiple tectonic movements and dissects the original strata, resulting in dislocation on either side of the fault. It required the use of Leapfrog™, 3D Move™, and Mathematica to be able to construct a geological model to represent the intensely folded and pervasively faulted Northern Hastings Block. This model is then used to improve our understanding of the development of the Northern Hastings Block, including the timing of fault development and fault emplacement of the block.

7.5.2 Methodology

Faults are usually observed as linear features in the field and represented as lines on geological maps and cross-sections. In three dimensional models, faults are usually irregular surfaces that are limited in lateral extent. One of the most popular techniques for modeling faults in 3D is to use geophysical data, such as 3D/2D seismic reflection data and observations from study areas. Fault surfaces can also be reasonably formed by correlating between fault lines or fault points on each cross-section.

This project applies another method to make a 3D fault model by using Leapfrog Geothermal™ and the 3D Move™. The fault surfaces are constructed within Leapfrog Geothermal™ and then imported into 3D Move™ to be combined with horizon surfaces generated in Mathematica using the scripts from the *Cystallize* geological modelling library (Kelly, 2009).

The workflow for modeling for complexly faulted areas is described below.

Step 1: Structural interpretation

Understanding the spatial organization of subsurface structures is essential for quantitative modeling of geological processes. This study incorporated all faults in the Northern Hastings Block delineated on the Roberts *et al*. (1995) map. In order to ensure the precision of the following modeling, we need to affirm the closing of each interpretation layer and check fault and contacts to be sure fault cross-cutting relations

are reasonable. In the model, each fault is individually named for operational convenience.

Specifically, it includes the following three aspects: (1) prepare digital images of Northern Hastings Block and input the digital geological map into Leapfrog Geothermal for visualization (Figure 7.1); (2) check faults and geological boundaries to be sure fault cutting relations are reasonable; (3) define faults and block boundaries by constructing the relevant lines and curves within Leapfrog Geothermal^{TM} (Figure 7.11); (4) generate the parametric surfaces using the above curves in Leapfrog Geothermal^{TM}; and (5) optimize mesh surfaces by the specification of the truncated relationship between faults (Figure 7.12).

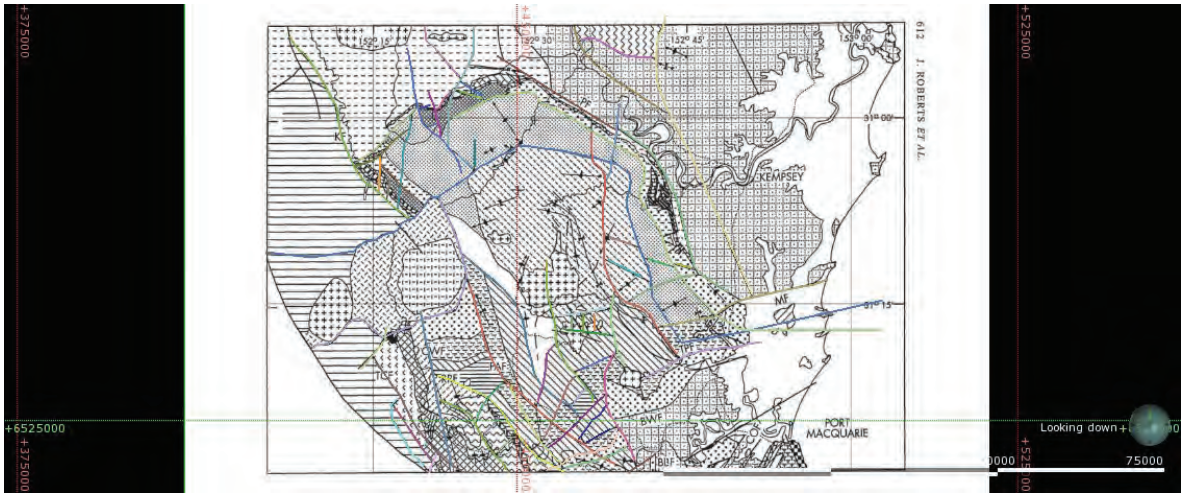

Figure 7.11: Construction of the lines and curves defining faults in the Leapfrog from the Roberts *et al*. (1995) map.

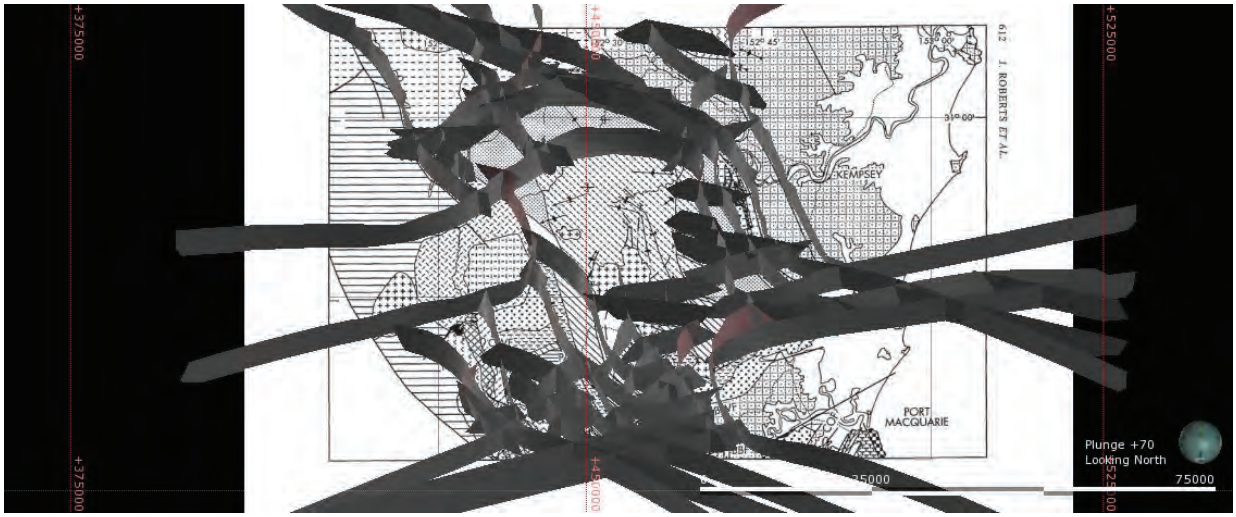

Figure 7.12: Faults mesh generation in Leapfrog from observed fault. The faults have been extended off the map area in this version.

Step 2：Preliminary fault models

In this step, fault surfaces are all vertical (Figure 7.13). This is why the model is called a preliminary fault model. The way of making a preliminary fault model is as follows: 1) output the fault meshes from Leapfrog and produce the output surface as DXF files; 2) import the DXF files into 3D Move^{TM}; 3) define the contact and dissection relationship based on geological knowledge. Also, cut off the unnecessary part of any intersecting faults; and 4) extend the range of any faults in order to eliminate the sawtooth edge of surfaces (Figure 7.14).

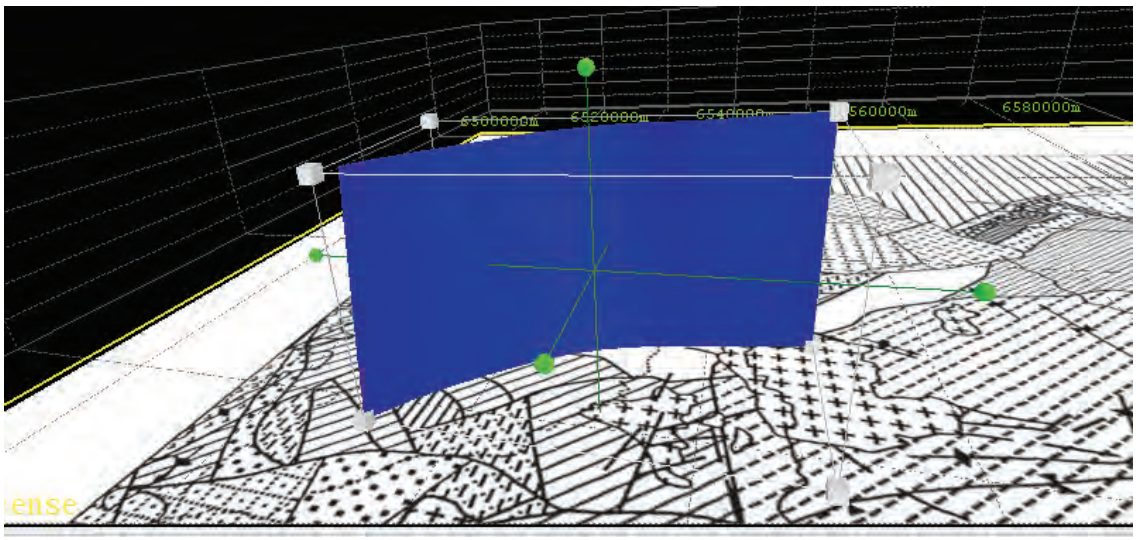

Figure 7.13: This single fault surface was vertical in this preliminary model. This is view is looking southwest across the southern end of the Parrabel Dome.

Step 3: Fault model editing

Modelling of real fault in three dimensions requires a consideration of several parameters, including fault surface geometry, variable displacement along the fault, movement direction (ie. dip, strike or oblique slip), and the angle and direction of shear by which the hanging wall deforms following movement over a fault surface. All of these parameters interact to control the deformation of crust and its geometry following movement over an underlying fault. Part of this information can be obtained from published papers and any honours or postgraduate theses. The faults in the preliminary fault model are all vertical.

7.5.3 Results

Understanding the spatial organization of subsurface structures is essential for quantitative modeling of geological processes. 3D subsurface modeling is generally not an end, but a means of improving data interpretation through visualization and comparison of data with each other and with the model being created. The preliminary fault model (Figure 7.14) divides the Northern Hastings Block into regions, to help determine how faults terminate with each other and to aid the fault history analysis in

the NHB (Chapter 5) including fault interrelationships, movement timing and orientations.

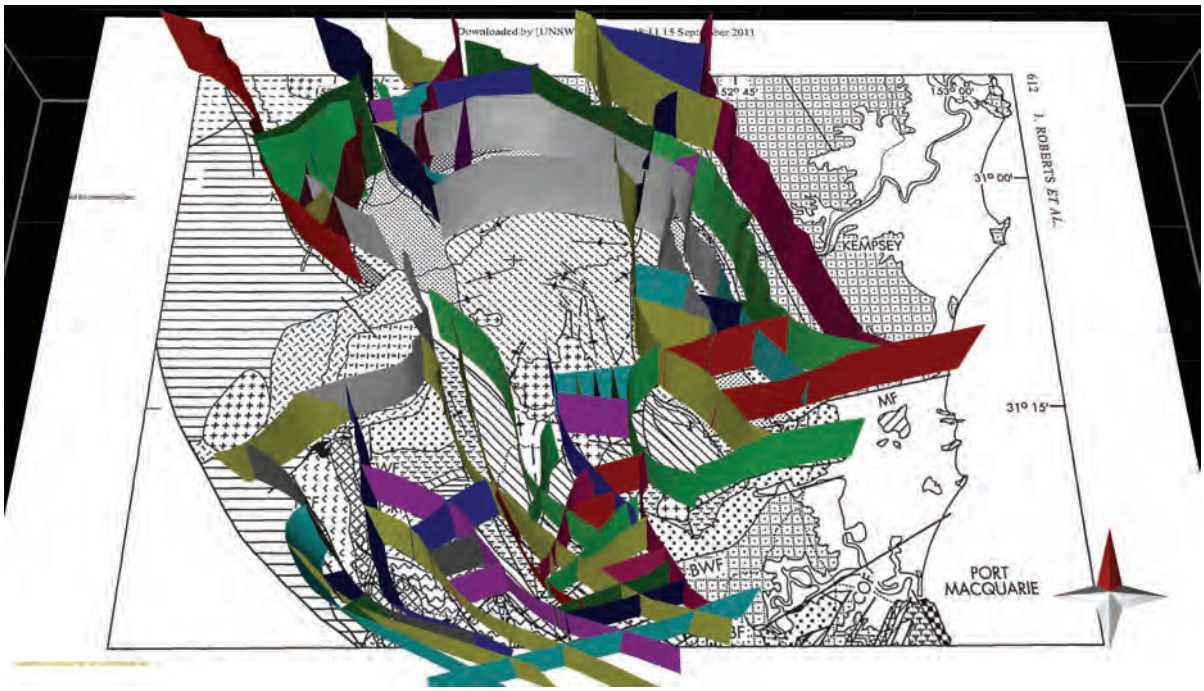

Figure 7.14: Preliminary fault model of the NHB in which all faults are shown coloured and assumed vertical based on the existing geological map of Roberts *et al*. (1995). The grey surfaces are formation boundaries such as the top of the Boonanghi Beds in the northern margins of the dome shown as vertical in this version.

7.6 Horizon construction

7.6.1 Introduction

A horizon is a bedding surface where there is a marked change in the lithology within a sequence of sedimentary or volcanic rocks. In some cases, it can also be a distinctive layer or thin bed with a characteristic lithology or fossil content within a sequence (Rey, 2008).

Horizon construction is generally achieved in two steps. First, the fault surfaces are built to partition the domain of the study into fault blocks. Then, the stratigraphic horizons are created fault block by fault block, from horizon data using various surface building methods. In the Northern Hastings Block we have abundant field measurements

(bedding measurements) arising from work by Lennox and others and about eleven honours theses data (Figure 7.3). This thesis integrates all these data into the geological model. An original aspect of this thesis is the scale of modelling undertaken, particularly with respect to the number of faults incorporated into the model.

7.6.2 Methodology

Mathematica™ and 3D MOVE™ are used to create the horizons in the complexly folded and faulted NHB without any borehole data. There are only a limited number of such examples in the literature (Berra *et al*. 2008; Zanchi *et al.* 2009).

Mathematica™ is a computational software program used in the scientific, engineering, mathematical and computing fields (www.wolfram.com). In this project, we have a large number of surface measurements in the Northern Hastings Block. If the surface measurements of bedding were shown in every fault block, the data set would be quite sparse in some blocks and quite dense in other blocks. These bedding measurements are irregularly distributed in space, because of the difficulties of accessing this forested and relatively rugged environment, and therefore the data set needed to be extended to control the gridding of sparse fault and horizon information. Mathematica™ provides a single environment to edit and sort the data, grid the sparse data, interpolate surfaces and then view the 3D conceptual geological model (Kelly, 2009; Kelly & Giambastiani, 2009).

Kelly (2009) developed a complete 3D geological modelling environment in Mathematica called *Crystallize*. Within this package are all the required algorithms for projecting strike and dip data, and interpolating irregularly spaced data onto regular grids.

To enable clean intersections of fault and horizons surfaces the data need to be interpolated onto regular grids, and these grids need to extend over the x,y, and z domains. Mathematica™ does not have the built in functionality for interpolating irregularly spaced point data onto a regular grid. In Kelly (2009) and Kelly &

Giambastiani (2009) two new algorithms are described called NearestNeighbourGrid2D and InverseDistanceGrid2D and these were used to interpolate the data onto the regularly spaced grids. These grids were then exported from Mathematica and imported to 3DMove^{TM}, using ASCII formatted files.

In 3D Move^{TM}, the surfaces generated in Leapfrog3D and Mathematica were regridded to produce a consistent set of grids. Several gridding artifacts arose at the intersections of the faults and horizons, and using the editing tools in MOVE the surfaces were edited to produce clean intersections between surfaces.

The following is an explanation of the main steps in the defining of horizons.

Step 1: Assign the data to fault block

The first step in the process is to assign a letter to each fault block within the whole Northern Hastings Block. There are a number of key geological units within the NHB including the Boonanghi Beds, Majors Creek Formation (Pappinbarra Formation), Kullatine/Mingaletta Formation and Commong Fm/Yesabah-Warbro Fm and others. The top of the Boonanghi Beds and the base of all other formations are used to model the geology of the NHB. The horizon building is completed fault block by fault block. The identification of fault blocks represents the order in which the horizon construction was undertaken. This fault block order has been defined by the capital lettering showing fault blocks in Figure 7.15. One surface was constructed in every fault block to represent the bottom of depositional sequence present in that fault block. All overlying surfaces used to represent the stratigraphic sequence were constrained by the base surface.

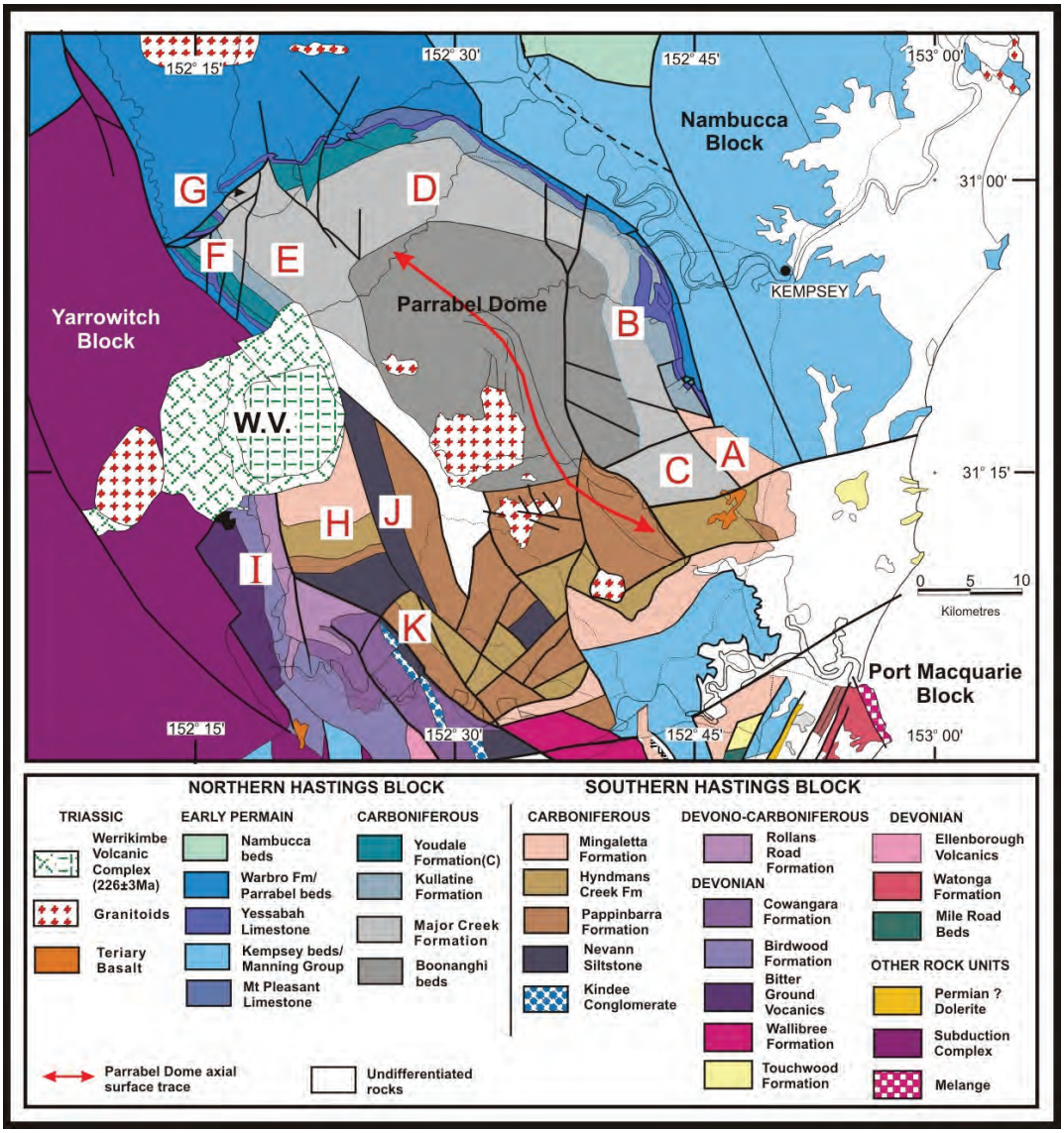

Figure 7.15: Geological map of the Northern Hastings Block with letters identifying the various key fault block. W.V = Werrikimbe Volcanics.

Step 2: Define the primary bedding data within the fault block. In selected fault blocks, the upper surface of geological structures with the dip and dip azimuth of bedding (or fault orientation) are recorded. The structures can be geological boundaries, the bottom or tops of formations, or fault surfaces. In the case of the Hastings Block this is invariably bedding data from near the fault block edges. These data sets provide details on the shape of the geological surfaces, in this case bedding that define the volume of the geological elements of interest, which is used to create the horizons of interest. Azimuth values range from 0 to 360, north is 0, east is 90. Inclination values range from 0 to 90, where 0 is horizontal and 90 is vertically down.

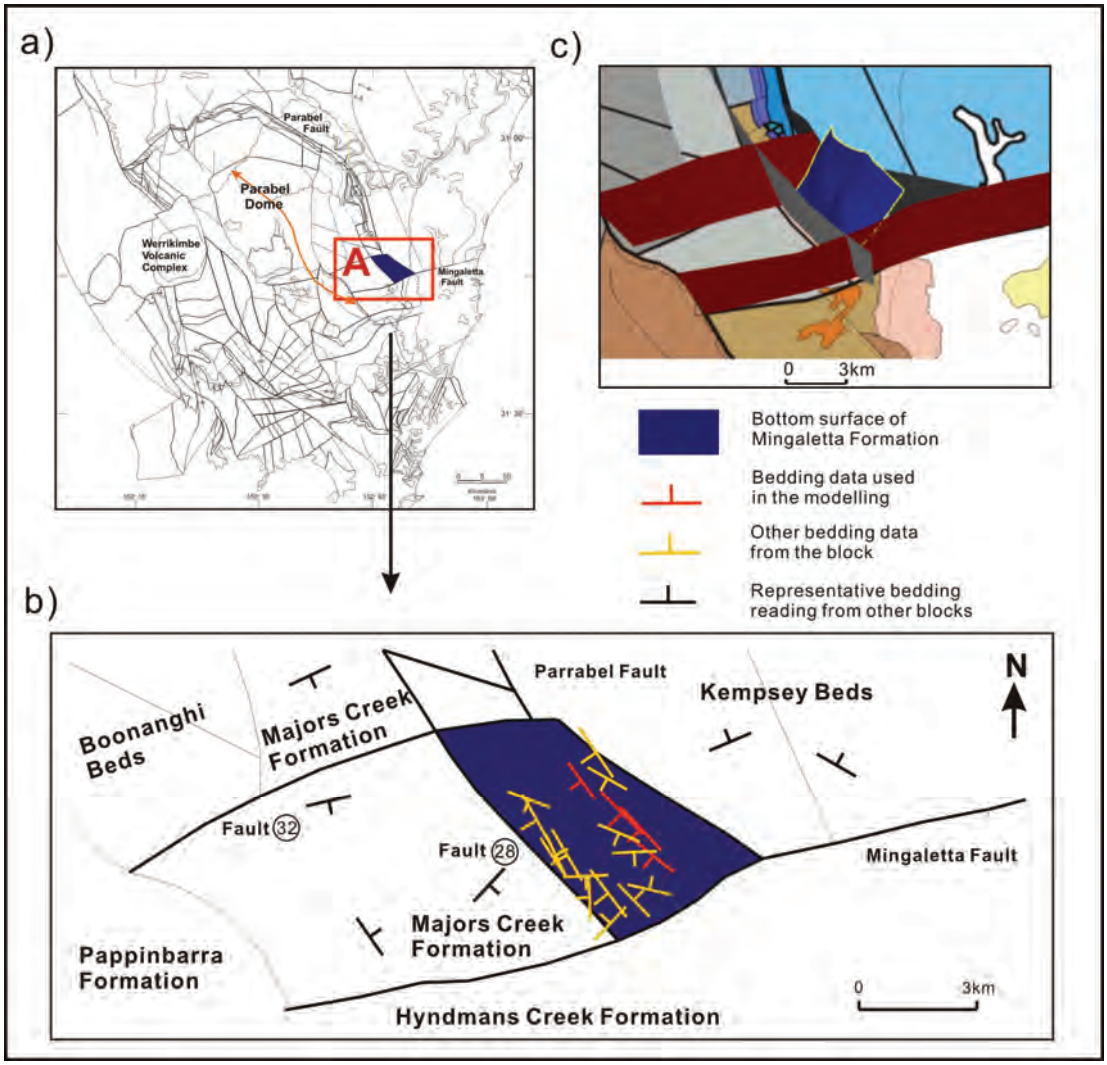

Figure 7.16: The process of horizon construction in Fault Block A. a) Location of the block on the eastern limb of the Parrabel Dome; b) schematic map with observed bedding reading (red reading were used in the modelling) and c) bottom surfaces of the Mingaletta Formation in this block.

The key point is to isolate bedding data that provide the information on the bottom/top of the formation within a fault block. Here we call these bedding data the primary bedding data. These bedding data have two basic features that can be used to help identify the data set we need: (1) these bedding data represent the overall trends and strikes of the bedding surface in the area. They are not bedding which has been refolded. (2) These bedding data are located at the contact between two formations. In some cases, the bedding data located very close to the faults do not reflect the regional trends, because the beds have been affected by fault drag. The dips and strikes of these bedding data may be quite similar in orientation to the fault, and dissimilar to other bedding

orientation readings within the same formation. These fault affected bedding data were excluded from the data used to generate the horizon surfaces. A set of primary bedding data from the Mingaletta Formation found in the Fault Block A is shown in Fig. 7.16b.

Step 3: Construct the geological surface. The third step is to create the horizon representing the bottom of the Mingaletta Formation within Mathematica™ using the primary bedding data (Figure 7.16b). These bedding data sets provide sparse details on the shape of the geological surfaces that define the volume of the geological elements of interest. The set approach for building horizons is:

(1) Define the dimensions of the region.
Three dimensional geological models are built using a combination of 2D and 3D grids. In this project the horizontal surfaces are constructed fault block by fault block. When building each horizontal surface, the minimum and maximum parameters for the X, Y and Z co-ordinates for the work space are set up.

(2) Projection of field and map data. Starting at the measurement point (x_0,y_0,z_0), the n-th point (x_n,y_n,z_n) projected along the linear line in the down-dip direction is calculated using the trigonometric equations (Kelly, 2009; Kelly & Giambastiani, 2009):

$x_n = x_0 + \text{Cos[inclination] Sin[azimuth] } n\ s,$ equation 1

$y_n = y_0 + \text{Cos[inclination] Cos[azimuth] } n\ s,$ equation 2

$z_n = z_0 - \text{Sin[inclination] } n\ s,$ equation 3

where s is the size of the interval between each point. A set of points is projected both up and down dip from the field or digitized data location. These data points are projected beyond the domain of interest in order to control the shape of the grids to be calculated. These calculations are done using the Mathematica algorithm called GeoPointProjectLine described in detail in Kelly (2009) and Kelly and Giambastiani (2009).

Figure 7.17 is a 3D plot of the projected data after the equations above have been applied to each geological structural datasets within Mathematica™. (See Appendix 7: The script of the geological structural model in MathematicaTM using two algorithms (the NearestNeighbourGrid2D and InverseDistanceGrid2D) from Kelly (2009) and Kelly & Giambastiani (2009))

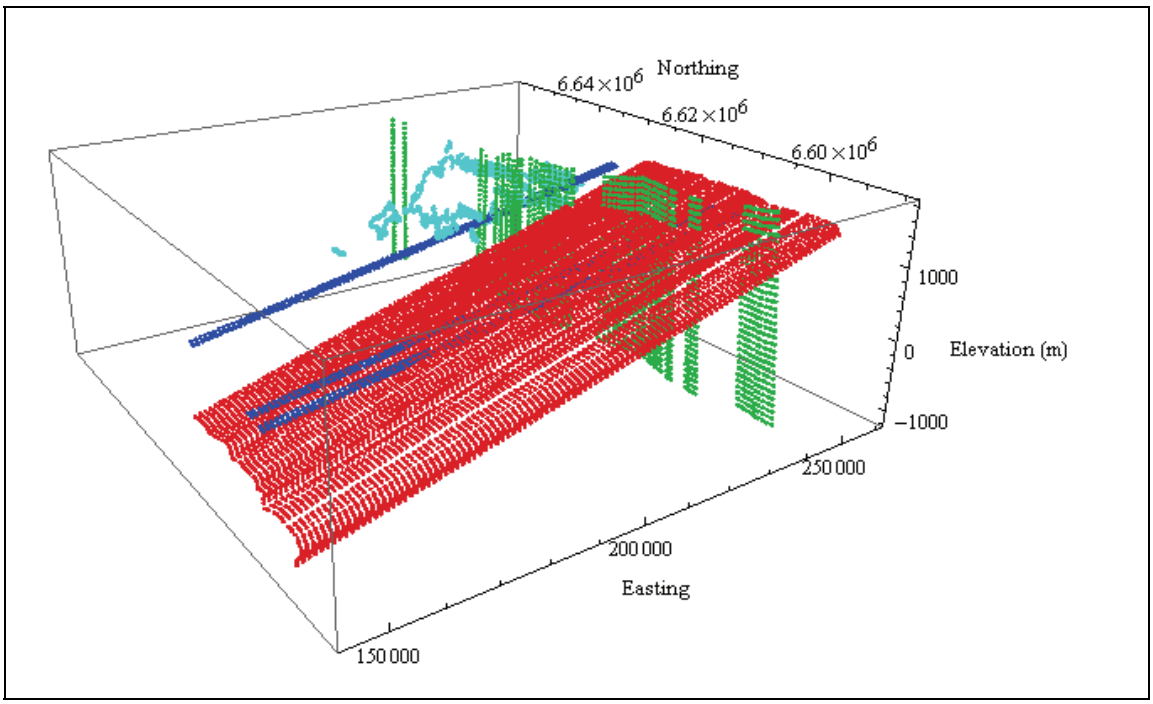

Figure 7.17: An example set of extended horizon points (blue and red) and fault data (green) (Kelly, 2009; Kelly & Giambastiani, 2009).

(3) Grid the projected data. Each projected data set can now be gridded using the functions NearestNeighbourGrid2D and InverseDistanceGrid2D (Kelly, 2009). An example set of interpolated surfaces calculated using the data shown in Figure 7.17 are presented in Figure 7.18.

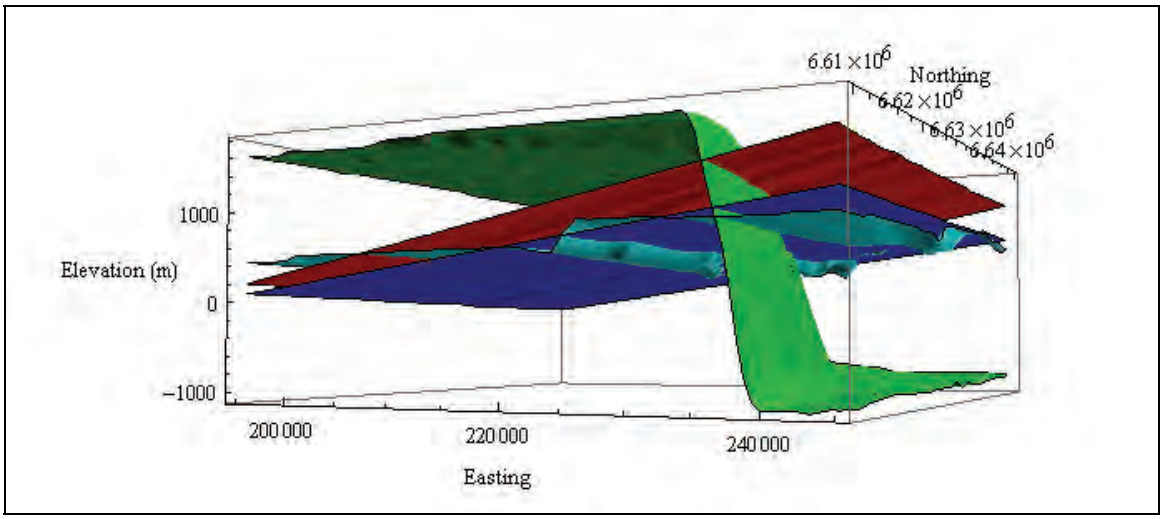

Figure 7.18: Example of the gridding of the projected data (modified from Kelly 2009, Kelly & Giambastiani, 2009).

(4) Import the horizons into MOVE^{TM}. Surfaces generated in step 3 were exported as ASCII files that define the coordinates of surface regular grid points (X,Y,Z). In 3D MoveTM, the "Create surface from points" toolbox was used to generate surfaces from the imported ASCII files. Horizon construction was then refined in each fault block, using the surface intersection tools in 3D MoveTM. One example of the bedding surface being cut by block-bounding faults can be seen in Figure 7.16c where southeast-striking bedding is truncated against the Mingaletta Fault on the southeast side of the block.

Step 4: Construction of the top surface of the Boonanghi Beds is different from the method outlined above. It makes use of the field-based cross sections across the Northern Hastings Block. Four field-based cross sections (A-B, C-D, E-F and X-Y) are presented in Chapter 6 (Figures 6.3 – 6.6). Cross sections A-B, C-D and E-F are oriented NE-SW and are right angles to the Parrabel Dome axial surface trace. Cross section X-Y is oriented NW-SE passing through the cross sections A-B, C-D and E-F. These four cross sections can be used to create the top surface of the Boonanghi Beds within the 3D Move^{TM}, which also perfectly demonstrate the general shape of the Parrabel Dome.

(1) Import the geological map of the NHB and the cross sections A-B, C-D, E-F and X-Y into the 3D Move™ at precise position (Figure 7.19).

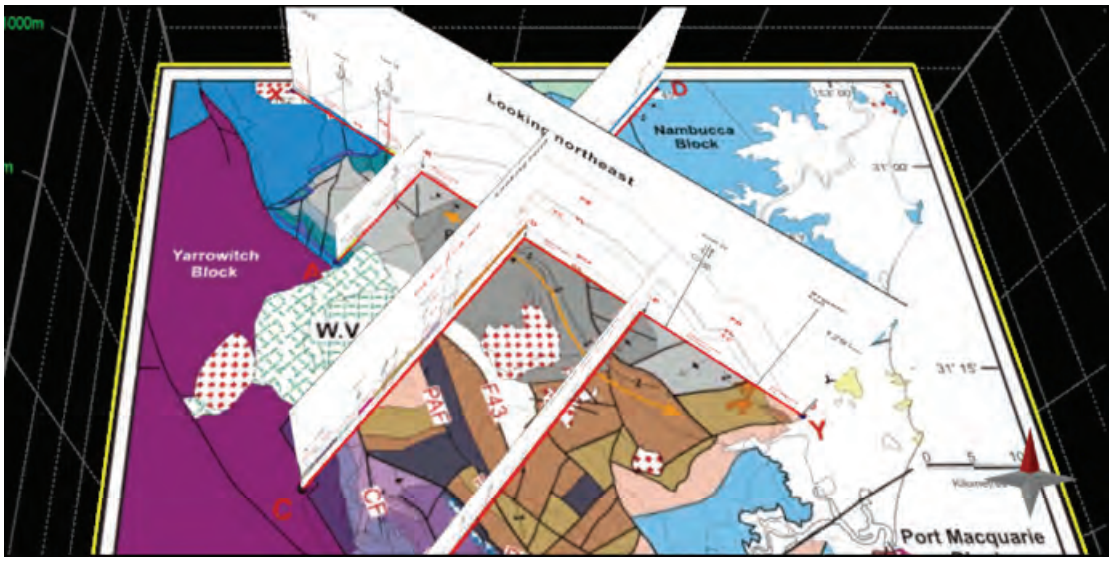

Figure 7.19: Geological map of the NHB and the position of the four cross sections.

(2) Digitize the top of the Boonanghi Beds as lines on each cross sections.

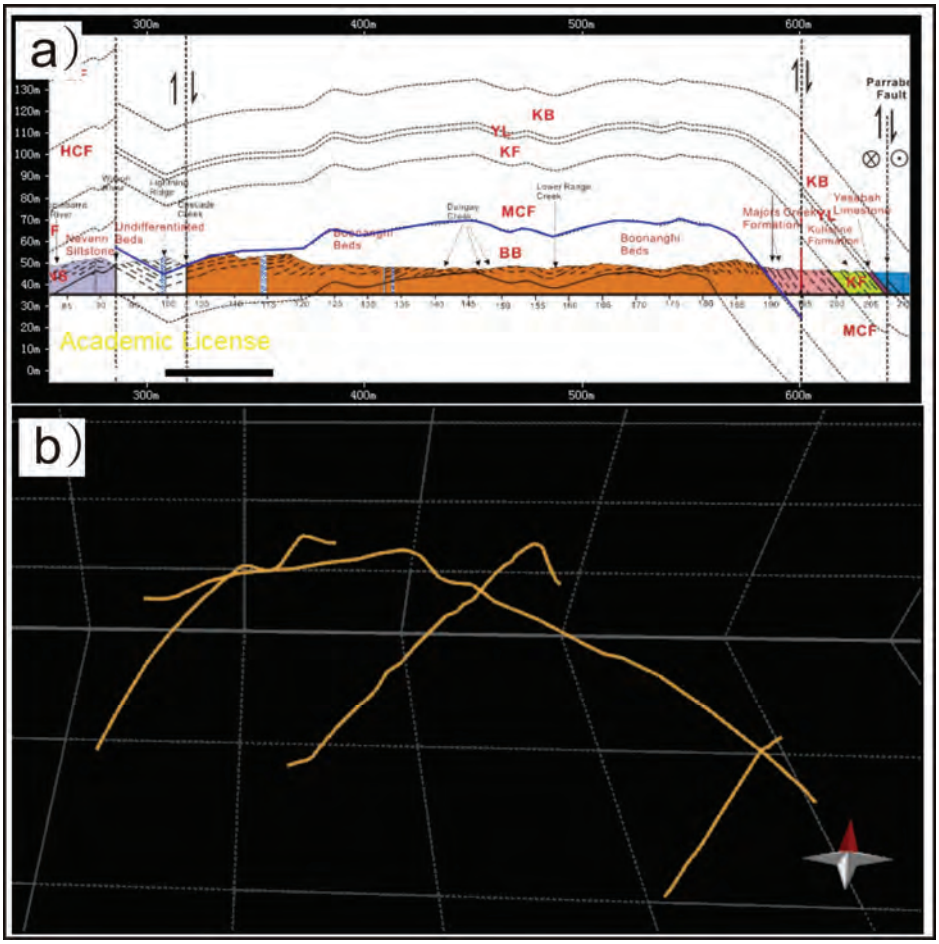

Figure 7.20: a) Example of the digitizing of the top Boonanghi Beds as line on cross section C-D (the blue line). b) The 3D visualization the lines representing the top Boonanghi Beds on each cross section.

(3) Create the top surface of the Boonanghi Beds from lines in each section within the 3D Move™ using the module "Inverse Distance Weight".

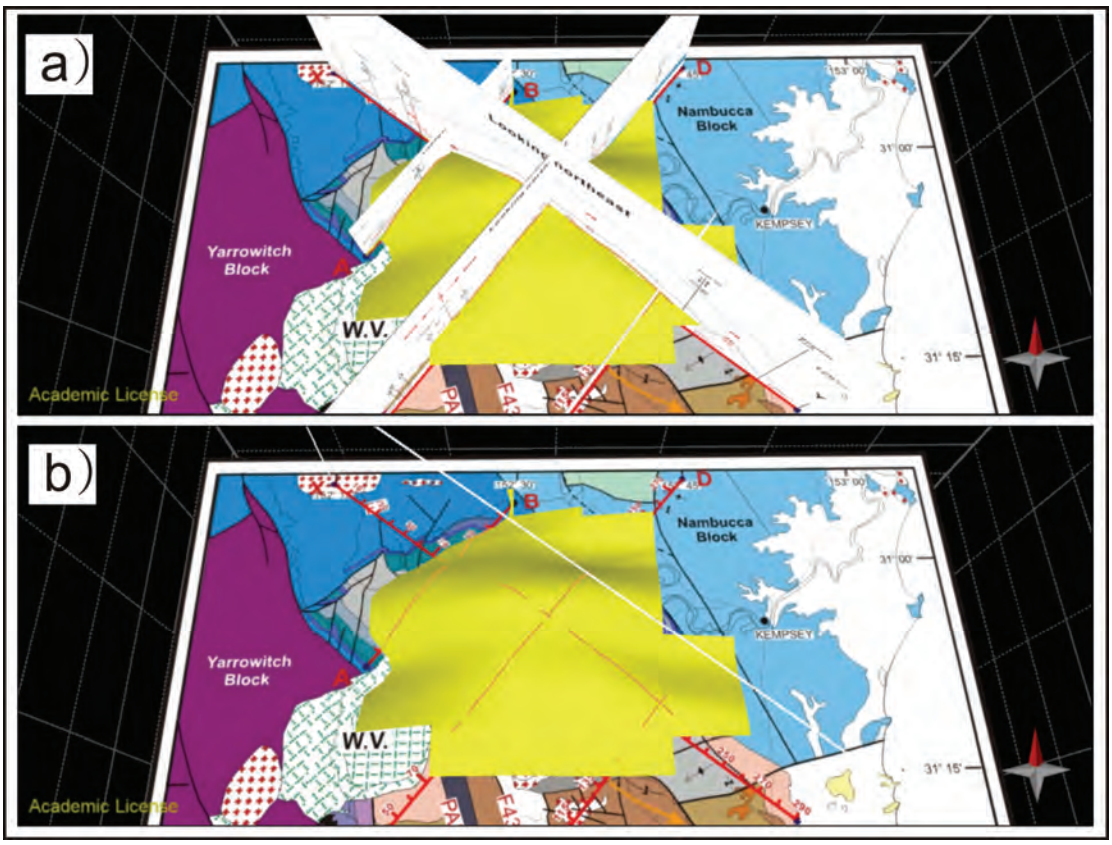

Figure 7.21: a) The 3D visualization of the top Boonanghi Beds within each cross section. b) The 3D visualization of the top Boonanghi Beds with the cross sections removed (Appendix 8 - 2).

7.6.3 Results

Figure 7.22 shows the result of the horizons construction that represent the bottom surfaces of depositional sequences in each fault block. Combined with a preliminary fault model, Figure 7.22 shows us a gross picture of the Northern Hastings Block which can help us control gross rock volumes and connectivity of adjacent formations and provides clues to characterize strain and the spatial trends. This information is widely used in the Chapter 5 (Fault Block Analysis) for a re-interpretation of the NHB geology. It aids the fault block reconstruction and helps address questions related to the

emplacement, direction and movement of fault blocks within the Northern Hastings Block.

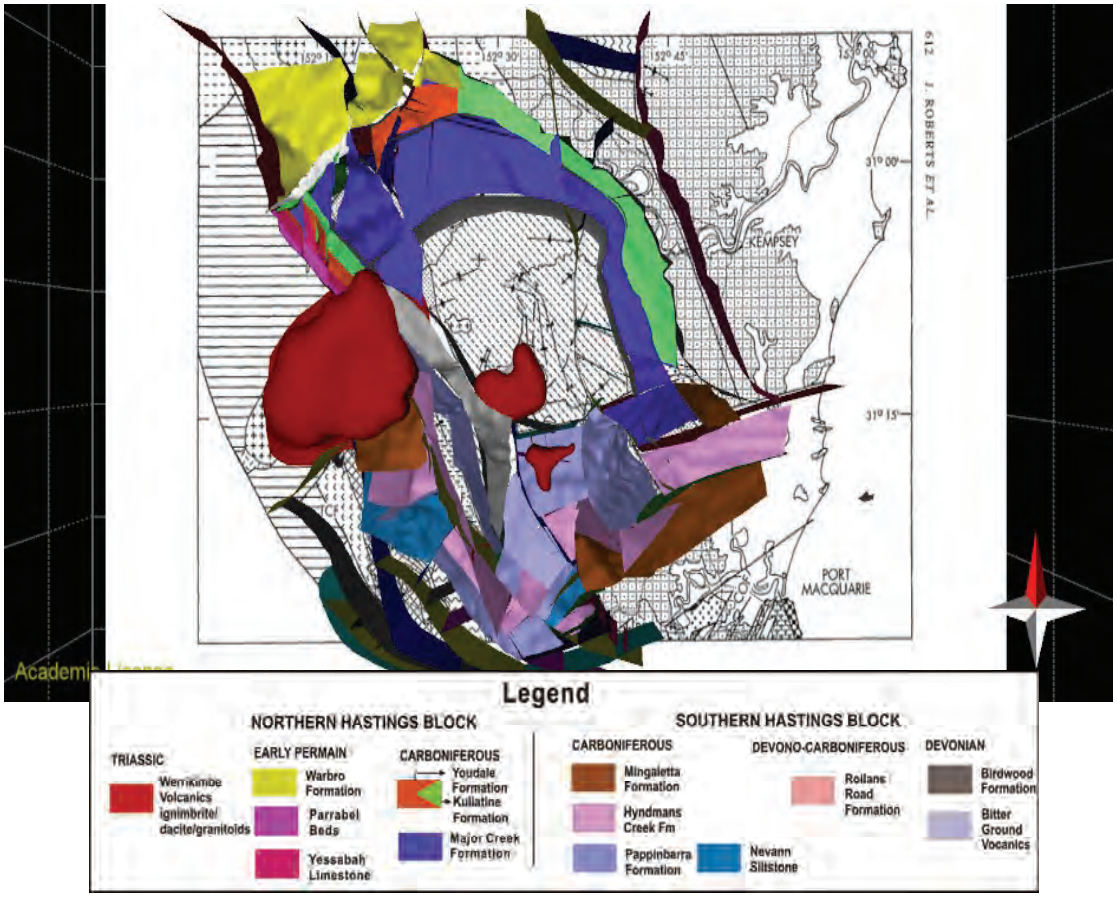

Figure 7.22: Horizons construction of the Northern Hastings Block with the preliminary fault models. The animated images of 3D models of the NHB are displayed in Appendix 8 - 1.

7.6.4 Discussion

7.6.4.1 Fold in the horizon construction

The horizons representing the bottom of the formations are created within the program Mathematica^{TM} using the primary bedding data (Figure 7.23b). These bedding data sets provide sparse details on the shape of the geological surfaces that define the volume of the geological elements of interest.

In some cases, mesoscopic folds can be constructed during formation construction. See

the folds in the Hydmans Creek Formation and Nevann Siltstone in Figure 7.23c. There are two main reasons for this situation.

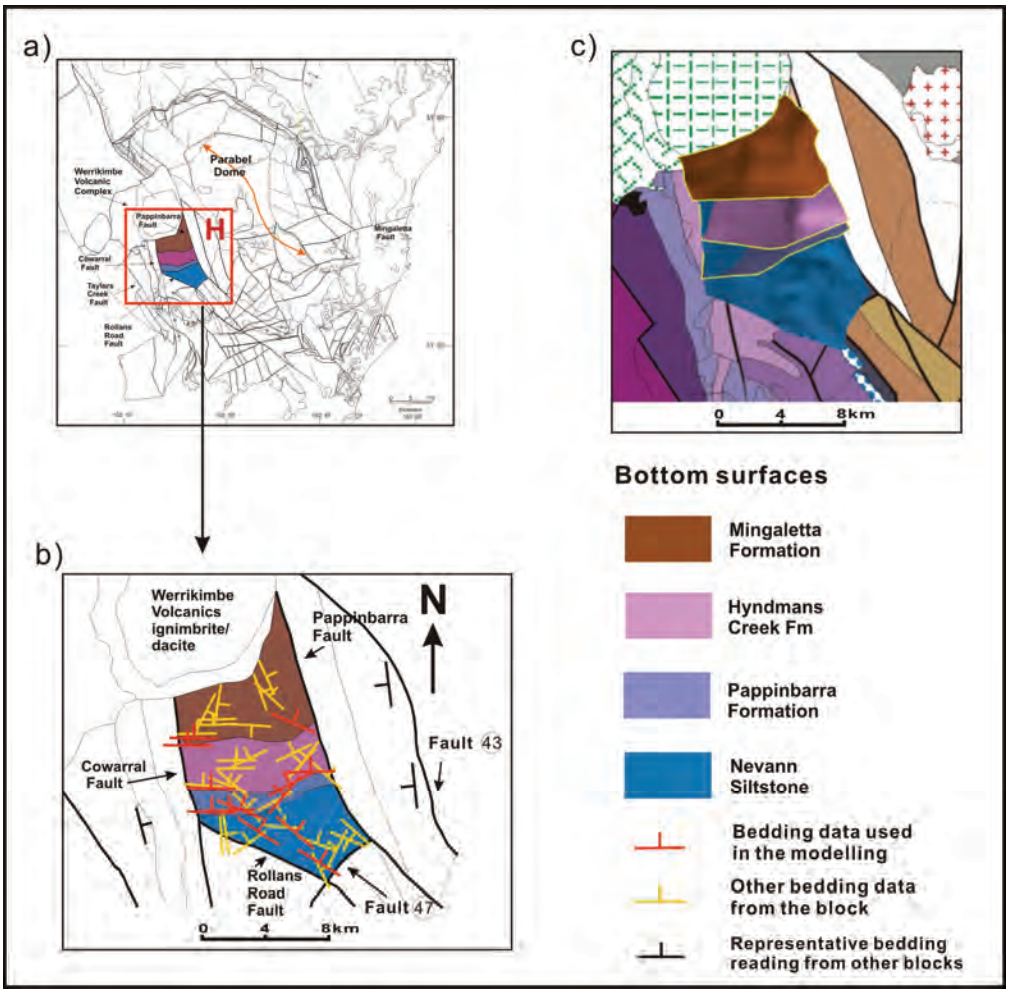

Figure 7.23: Fault Block H: a) Locality map, b) detailed map of the faulting and bedding readings within the various formations in this block, the red symbols were readings used in the generation of the computer surfaces for the formations and c) 3D model of the formations in this fault block.

(1) The primary bedding data in Fault Block H represent the overall dips and strikes of the bedding surface and show whether there is a possible folding of the formations. All the bedding readings within the Hyndmans Creek Formation were plotted as poles on an equal area, Schmidt stereographic net. Calculation show that the fold axis is 51°→305°. The bedding symbols (yellow and red) in the Figure 7.24b were the primary bedding readings. When using the primary bedding data shown in red and yellow symbols within the Hyndmans Creek Formation to construct the shape of this formation, a fold is

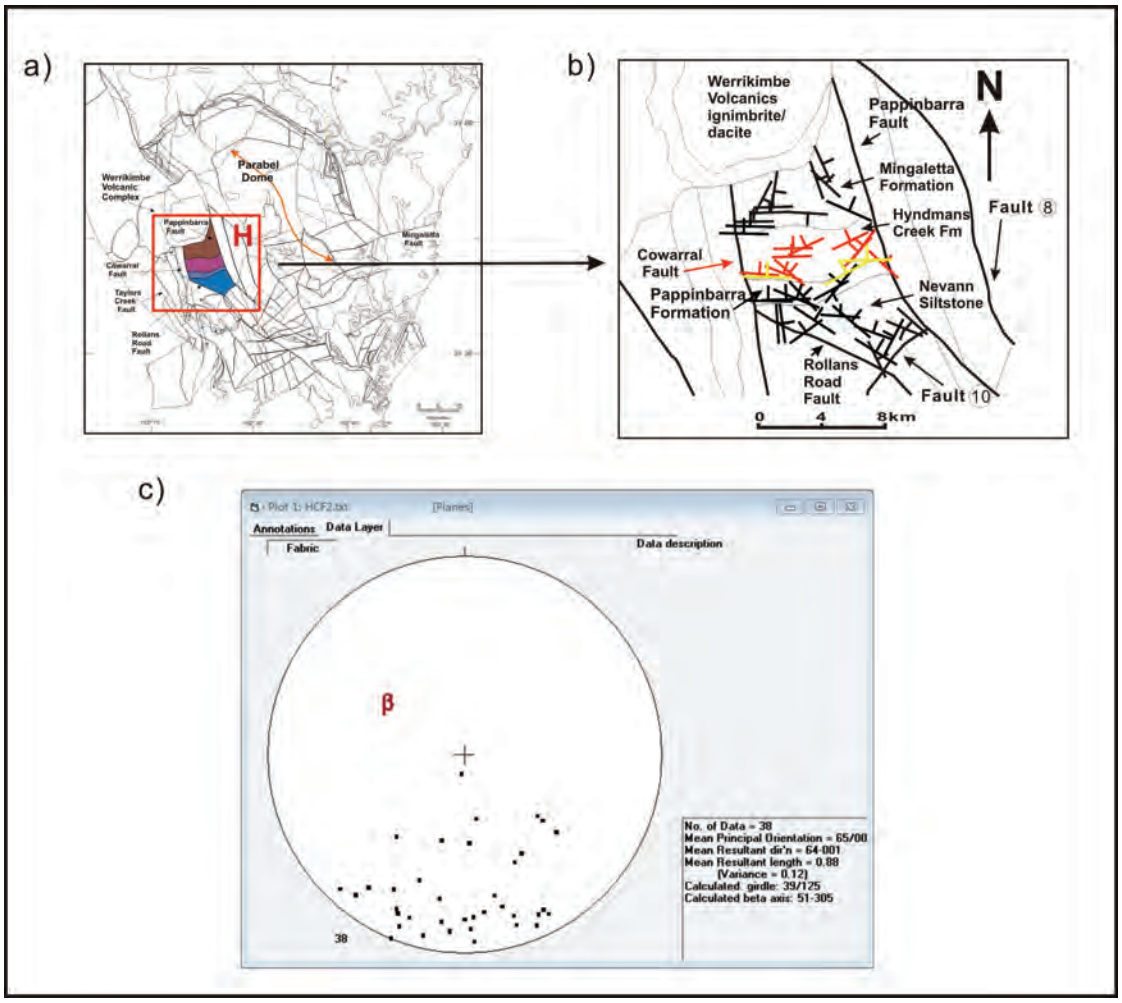

Figure 7.24: Maps and stereographic projection for fault block H: a) Locality map, b) detailed map of the faulting and bedding readings within the various formations in this block, the yellow symbols were readings used in the generation of the computer surfaces for the formations and c) Stereographic projection of the poles to bedding data in the Hyndmans Creek Formation within Fault Block H.

(2) Another possible reason for the generation of artificial folds in the computer-generated surface would be the height difference between two primary bedding data combined with miniscule difference in the azimuth and inclination. This may cause fold generation during construction of the formation surfaces. Take the Nevann Siltstone in Fault Block H as an example.

Table 7.2: Primary bedding data in the Nevann Siltstone of Fault Block H.

Number	Easting	Northing	Elevation	Inclination	Azimuth
1106	441305	6531889	532.8280029	65	30
1096	445105	6529889	157.50939941	60	30
1818	437405	6533089	135.27549744	74	24
1107	443605	6531789	574.63964844	59	35

There are four primary bedding readings defined in the Nevann Siltstone of Fault Block H (Table 7.2). These four primary bedding data have very similar azimuths and inclinations, but significant differences in elevation. When projecting these primary bedding data along the linear line in the down dip direction using the trigonometric equations ($x_n = x_0$ + Cos[inclination] Sin[azimuth] n s, $y_n = y_0$ + Cos[inclination] Cos[azimuth] n s, $z_n = z_0$ - Sin[inclination]), the small difference in the elevation combined with azimuth and inclination could cause a large difference along the projected line in the down-dip direction (Figure 7.25). When projected data set are gridded using the Inverse Distance Functions in Mathematica, the fold appears on the surface (Figure 7.26).

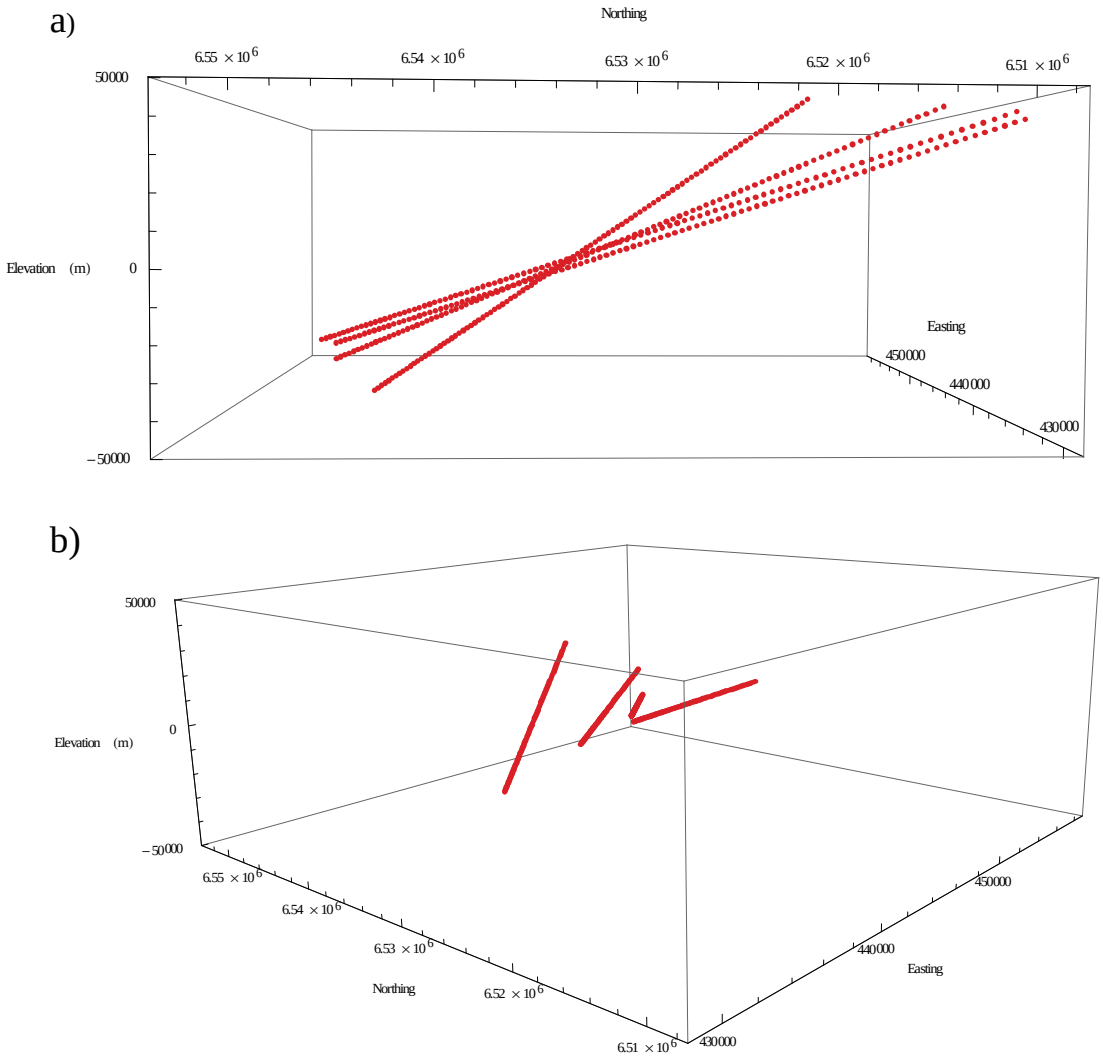

Figure 7.25: A set of points representing the dip of bedding of the Nevann Siltstone projecting into space. a) figure looking north; b) figure looking northeast suggesting that there is fold when none exists because of slighter differences in elevation and dip direction for data from the Nevann Siltstone.

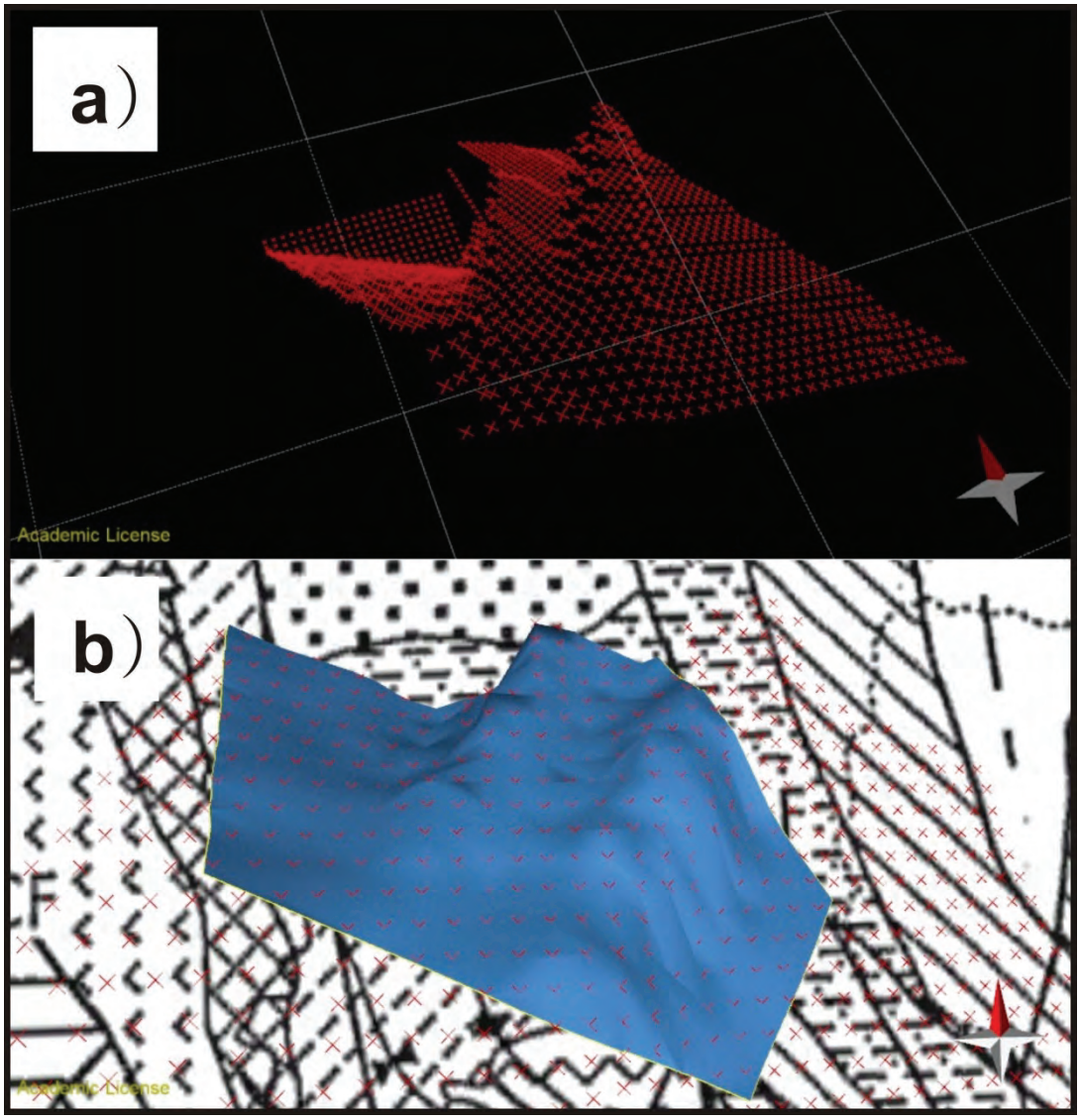

Figure 7.26: 3D model of the surfaces of the Nevann Siltstone in the fault block. a) the red points were create using the InverseDistanceGrid2D function in Mathematica™ (looking NNW and down); b) view of the bottom surface of the Nevann Siltstone gridded in 3D Move™ (looking N and down).

7.7 Virtual Cross sections

7.7.1 Introduction

Virtual cross-sections are built in the 3D Move™ in this project slicing the constructed 3D geological model of the NHB and representing all the surface data in the 3D models including the mapped locations, measurements of bedding data, the DEM and the

formation thicknesses. Such cross-sections highlight inconsistencies with the present fault and horizon interpretation. The aim of this section is to develop a 3D geological model that is consistent with the field mapping data and known geological processes through the comparison between the two types of cross sections and their interpretation.

7.7.2 Methods

The 3D models in this project were created mainly with 3D Move™ and Mathematica™. The faults in virtual cross sections and fieldwork-based cross sections are all assumed to be vertical because of the lack of relevant information. Faults are all located in the correct position, because they are built and corrected according to the Roberts *et al*. (1995) geological map. This section will focus on horizon correction to ensure they are consistent with the field mapping data.

The main steps in this process includes:

Step 1: Prepare cross sections from the existing fieldwork.

Four fieldwork-based cross sections across the Northern Hastings Block (A-B, C-D, E-F and X-Y) were presented in the Chapter 6 (Figures 6.3 – 6.6). Cross sections A-B, C-D and E-F are oriented NE-SW right angles to the Parrabel Dome axial surface trace. Cross section X-Y is oriented NW-SE through the cross sections A-B, C-D and E-F. These cross sections were constructed using known geologic relations and observed or literature-derived thicknesses for the stratigraphy in the Northern Hastings Block.

For detailed geological analysis of these cross sections seen was Chapter 6.

Step 2: Construct the virtual cross-sections.

Four virtual cross-sections sharing the same positions as cross sections A-B, C-D, E-F and X-Y were constructed in the 3D Move™ across the 3D geological models of the NHB. The module “Slice 3D” was used to create these virtual cross-sections. The orientation and end points of virtual cross-sections are set up according to the position

of the corresponding fieldwork-based cross sections.

Step 3: Comparison between field-based and virtual cross section and interpretation.

Each horizon in the virtual cross sections are compared with that in the field-based cross section. Where there are differences between the two types of cross sections, the corresponding horizon will be selected for the further modification. Normally, four types of differences were observed including differences in elevations, gaps, redundant surfaces, and wrong shapes.

The differences in elevation, any gaps and any redundant surfaces can be easily fixed within the 3D Move^{TM} program using the modules “Transform”, “Extend” and “Split”. If the horizon surfaces are the wrong shapes reinterpretation and reconstruction will be needed to fix the problem. The new primary bedding data used to create the horizon surfaces will be identified (Section 7.6.2) until a reasonable horizon surface is constructed that is consistent with the field mapping data and known geological processes.

7.7.3 Results

Using the methods described above, some correspondence between the virtual cross sections and field-based cross sections can be achieved. The virtual cross sections then became the skeleton for a validated 3D model.

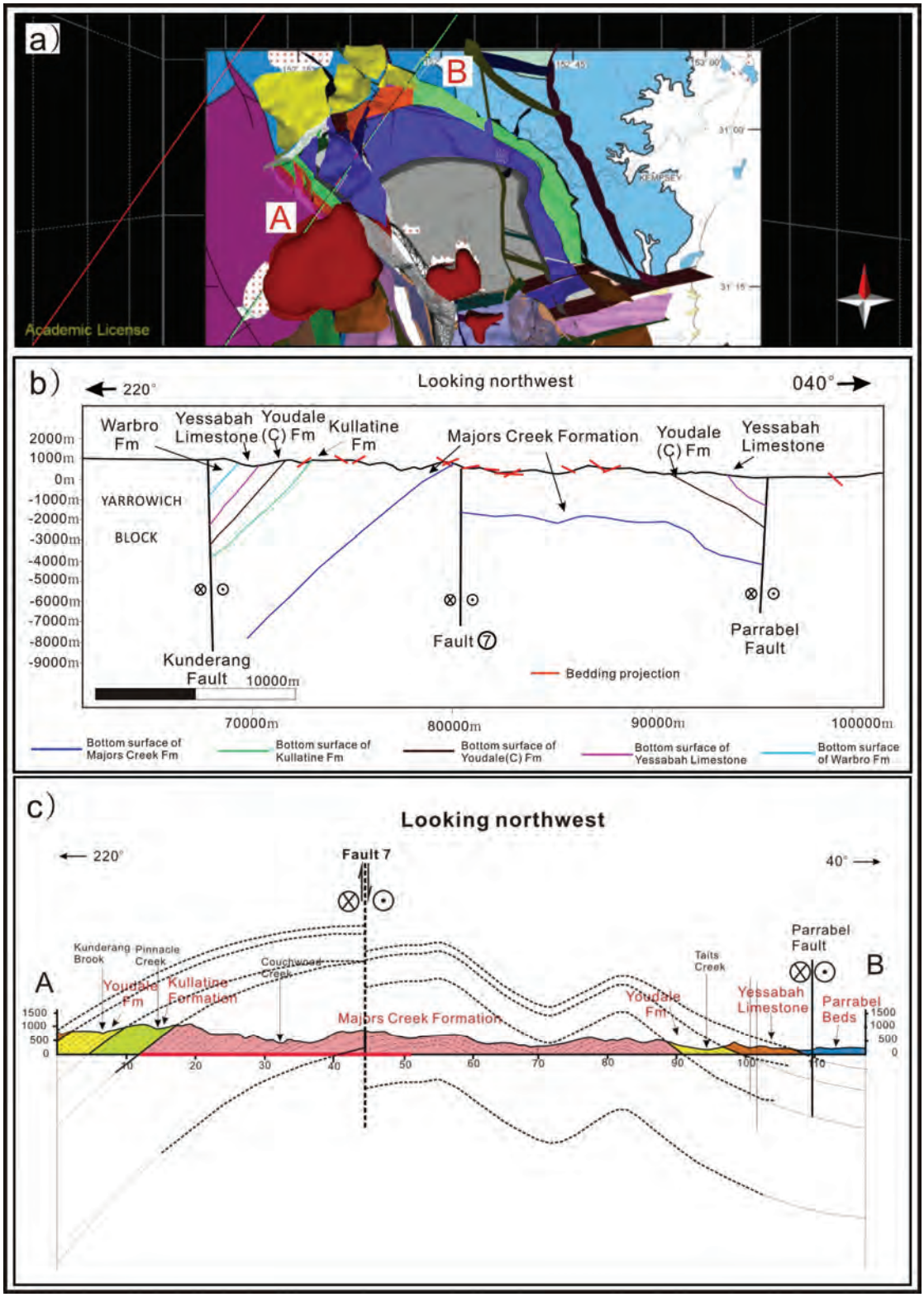

Figure 7.27: The virtual cross-section A-B extracted from the 3D geological model and the field-based cross sections across the northern section of the Parrabel Dome. a) Map showing the location of virtual cross-section A-B in the NHB; b) the detailed structural features of this virtual cross-section. c) The detailed structural features of the field-based cross section. Two vertical lines in Yesabah Limestone are two small faults.

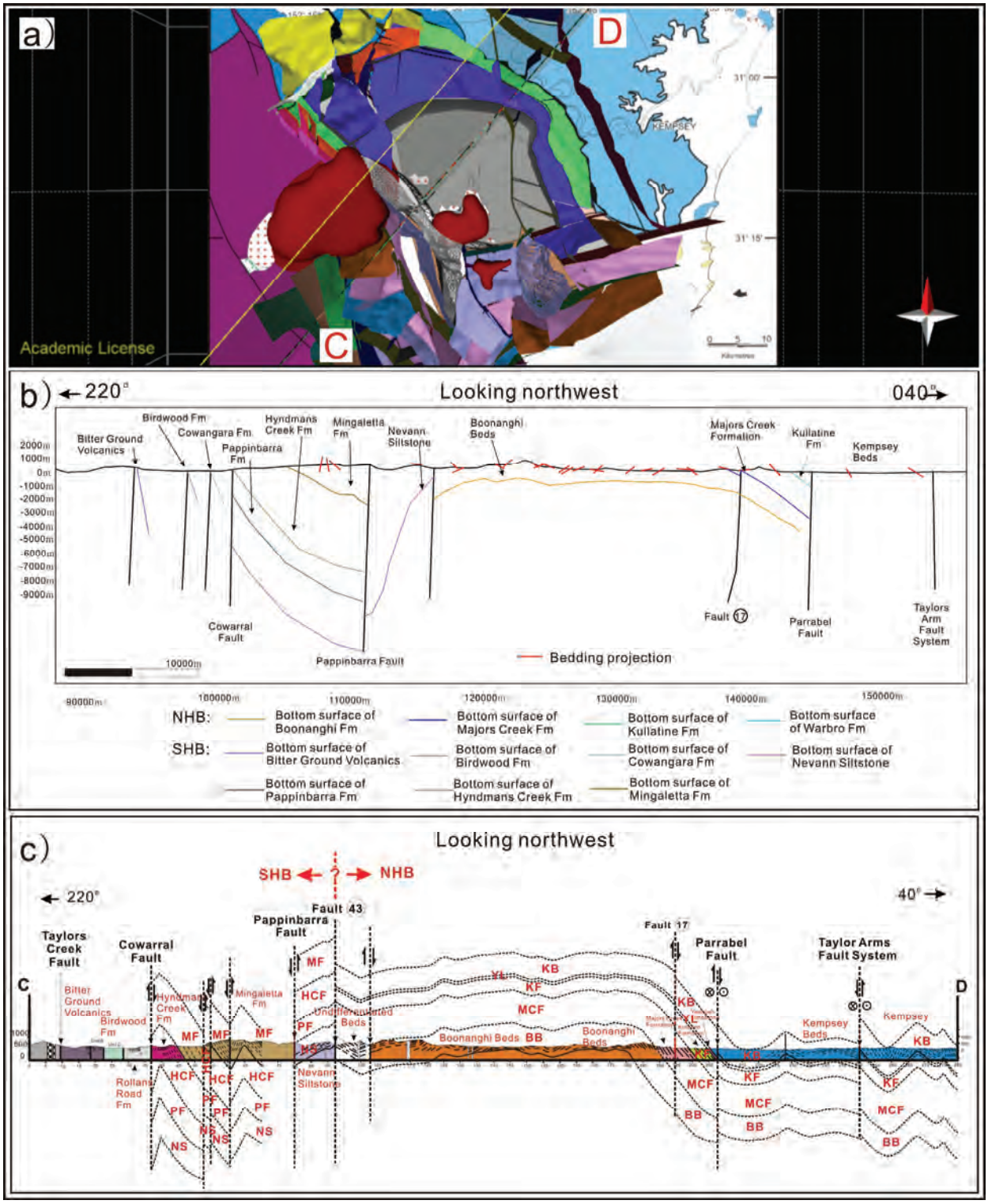

Figure 7.28: The virtual cross-section C-D extracted from the 3D geological model and the field-based cross sections across the northern section of the Parrabel Dome. a) Map of the location of the virtual cross-section C-D in the NHB; b) the detailed structural features of this virtual cross-section and c) the detailed structural features of the field-based cross section.

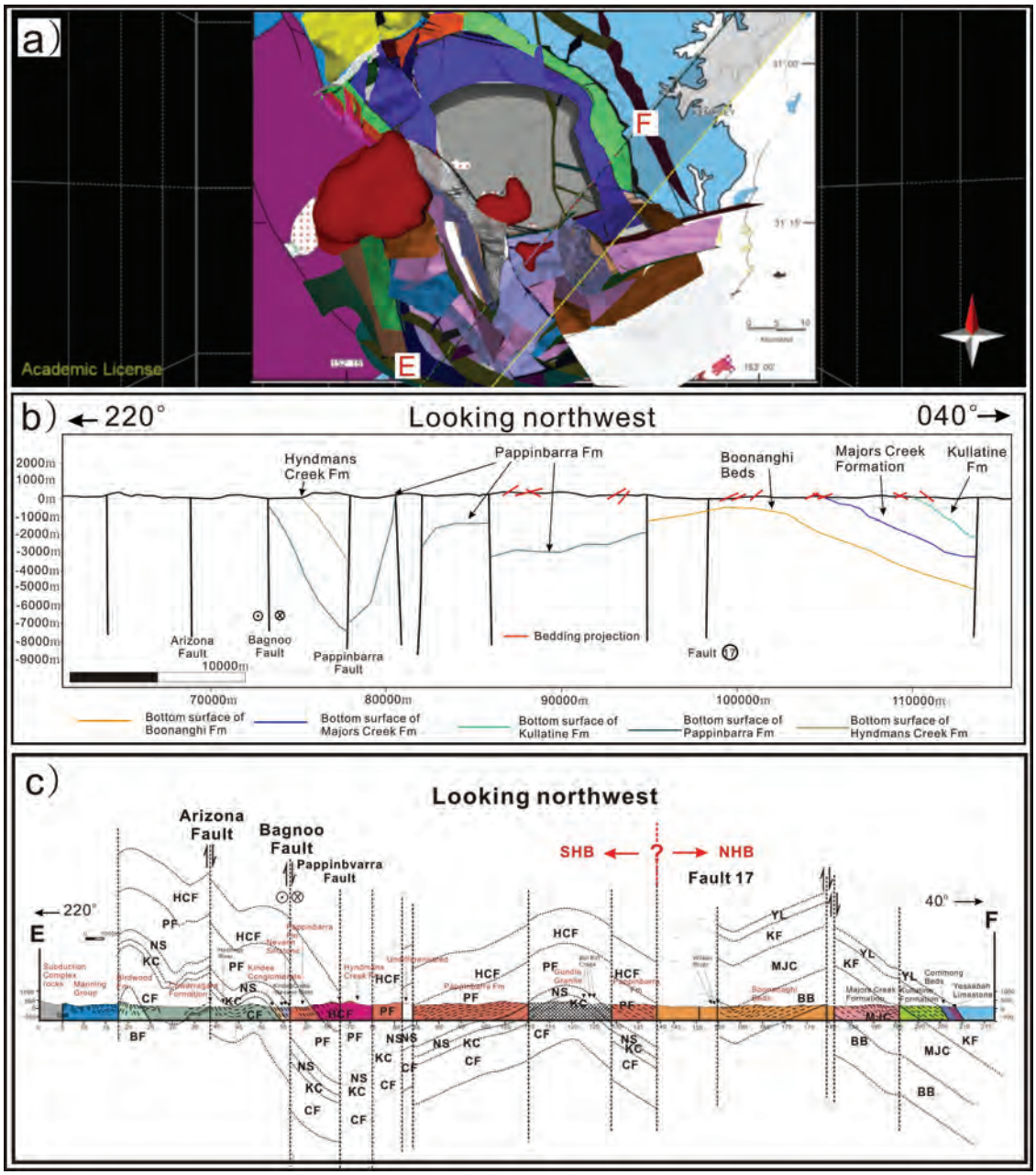

Figure 7.29: The virtual cross-section E-F extracted from the 3D geological model and the field-based cross sections across the northern section of the Parrabel Dome. a) Map of the location of the virtual cross-section E-F in the NHB; b) the key structural features of this virtual cross-section and c) the detailed structural features of the field-based cross section.

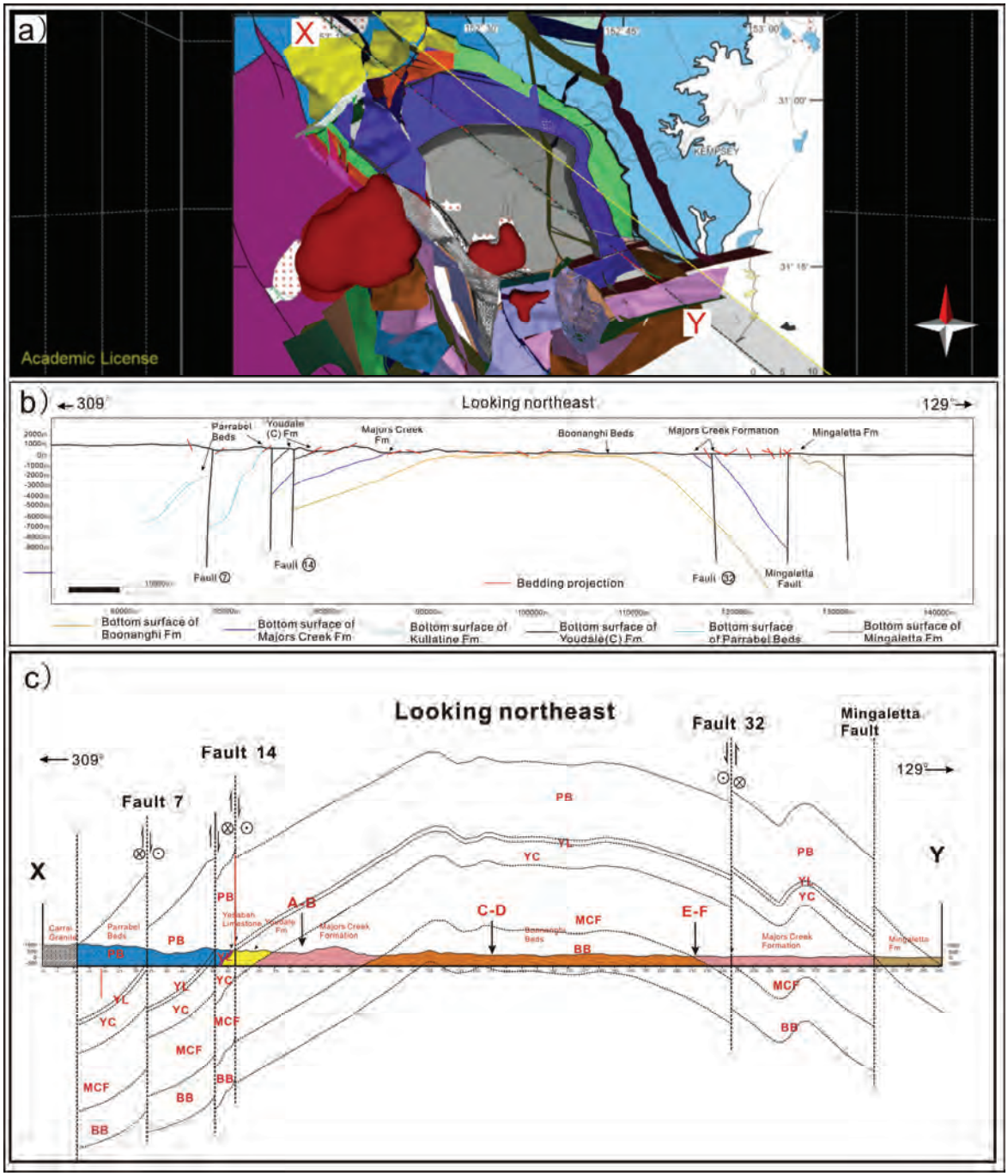

Figure 7.30: The virtual cross-section X-Y extracted from the 3D geological model and the field-based cross sections across the northern section of the Parrabel Dome. a) Map of the location of the virtual cross-section X-Y in the NHB; b) the detailed structural features of this virtual cross-section and c) the detailed structural features of the field-based cross section.

Figures 7.27 - 7.30 show the results of four corrected virtual cross sections in the NHB. In these virtual cross sections, the DEM, bedding measurements on the surface, vertical

faults and the interpreted bottom horizons of key formations are presented. The gaps and redundant surfaces have been removed. The incorrectly positioned and differences in the shape of the horizons have been fixed compared with the field-based cross sections (Figures 6.3-6.6) using the method described. However, some folds (e.g. (folded) bottom surface of the Majors Creek Formation between Fault 7 and the Parrabel Fault in Figure 7.27b, formation surfaces between the Cowarral and Pappinbarra Fault in Figure 7.28b and between Fault 32 and Mingaletta Fault in Figure 7.30b) extremely difficult to construct in virtual cross sections using the methods described in Section 7.6.2. This is because the primary bedding used in computer modelling are usually selected close to the boundary or fault. This results in the folds which are parallel to the geological boundary (or faults) being captured in the modeling. However, any folds at right angles to the boundary/faults are difficult to resolve in the modelling.

At present, these virtual cross sections show similarities with the field-based cross sections. As seen on these virtual cross sections, the bottom surfaces of each formation are consistent with their bedding measurement on the ground surface. These virtual cross section confirm the vertical displacements along some major faults (e.g. Fault 7 on Figure 7.27) and display a northwest and southeast-plunging dome which is box-like in cross section C-D and more open in cross sections A-B and E-F.

7.7.4 Conclusions

Comparisons between the cross-sections extracted from the 3D models (Figures 7.27 - 7.30) and those from the existing fieldwork (Figures 6.3-6.6) provide better constraints on the validity of the 3D models. It increases the accuracy of modeling and makes the 3D models consistent with the field mapping data and known geological processes which occurred in this area.

7.8 Conclusion

This chapter outlined the workflow for constructing a 3D model from a comprehensive field dataset on the Permo-Carboniferous rift and fore-arc rocks across the Northern Hastings Block. Leapfrog™, 3D MOVE™ and Mathematica™ were used along with ArcGIS®, Quantum GIS and System for Automated Geoscientific Analyses for managing and analyzing the various data sets. The various data sets include the comprehensive bedding data, the existing geological maps of the NHB, the cross sections across the NHB plus digital elevation model (DEM) and the valuable geological information from Honours theses, geological survey records and other published papers on this block.

The DEM models the topographic surface and assigns new elevation parameter for all data. Its analysis helps to verify elements of the current structural interpretation (such as regional faults) and identified other geological structures such as intrusive contacts and differences in the weatherability of the NHB.

Preliminary fault models and horizons between the faults were constructed. This new workflow is designed to unravel a comprehensively mapped, complexly folded, extensively faulted geological sequence where there are no well-log data. It is believed that this workflow is widely applicable in the oil, gas, mining, and groundwater sectors. The preliminary fault model (Figure 7.14) divides the Northern Hastings Block into regions, to help determine how faults terminate against other faults and to aid the fault history analysis in the NHB (Chapter 4) including fault interrelationships, movement timing and orientations. Combining with the horizons construction and the DEM, the 3D structural models of the NHB shows a gross picture of the Northern Hastings Block which can help us constrain the relative timing of fault development and provide a basis for test fault emplacement of the overall block in any future work.

This 3D geological structural model used in the Chapter 5 (Fault Block Analysis for a re-interpretation of the NHB geology) and Chapter 6 (Kinematic reconstruction along a 2D traverse of the NHB). In Chapter 5, this model aided the block reconstruction and helped address questions related to the emplacement, direction and movement of fault blocks within the Northern Hastings Block. In Chapter 6, the comparison between the cross-sections constructed from this 3D model and those from the existing fieldwork provide better constraints on the validity of the 3D model and the kinematic restoration helps to explain the existing geological history.

In summary, this chapter demonstrates a new way of constructing 3D models of an extensively faulted and multiply folded block. It clarified the shape of the dome and compared existing cross sections across this dome with those constructed across the 3D model. Before this modeling there was no three dimensional model of the dome and this modeling demonstrated problems with the existing map of the NHB. Model construction showed that the original map from Roberts et al. (1995) consists of some faults which are clearly not in the correct position, that the dome does plunge gently southeast as well as northwest and that it is possible to determine the amount of shortening across the dome.

Chapter 8 Conclusions

8.1 Summary

The Northern Hastings Block is comprehensively mapped, complexly folded and extensively faulted.

Overprinting cleavages, possible fold-bent faults, refolded folds and disrupted, fault-blocks showing folded and cleaved rocks and faults displacing cleaved and folded rocks have been used to determine the order of structures in the NHB. Four cleavage populations are recognised according to their cross cutting relationships in the NB and NHB. They are E-W striking S_1 (NB/NHB), N-S striking S_2 (NHB), NW-SE (NB/NHB) striking S_3 and finally NE-SW striking S_4 cleavages (NB/NHB). Four generations of folds are recognized according to their orientations and the limited evidence of refolding. These folds are derived from the calculated bedding-cleavage intersection lineations and, observed mesoscopic and macroscopic fold axes data obtained in the field. The first generation folds, F_1, plunge approximately east or west, and are re-oriented during the formation of the D3 Parrabel Dome. F_2 folds plunge north or south and F_3 folds plunge northwest or southeast. The last generation of folds, F_4, plunge northeast or southwest.

There are more mesoscopic, observed folds and cleavages within the Permian sequences compared with the Carboniferous sequences probably reflecting the ease of cleaving and folding the more mud-rich Permian sequences. The prevalence of S_2 (especially) and S_3 cleavages on the western margin of the NHB may also reflect increasing strain along this margin. In summary, increase in strain towards the Yarras Fault System has been well documented and is manifested by increase in development of cleavage and tightness of folds (Jayko *et al*. 1993).

Fault history analysis provided important information on the morphology, apparent fault

movement, fault timing and regional structure in the NHB. Faults of similar orientation in the NHB do not form and were not active at the same time. The majority of faults cut the folds and cleavages in the NHB. Five episodes of faulting are identified. Faults on the southwestern and eastern margin were active and ceased moving during the Late Carboniferous emplacement of the NHB. The Yarras Fault System on the southwestern side and the Parrabel Fault (and related faults) on the eastern side are believed to be the two major fault systems responsible for transporting and rotating the NHB in the Late Carboniferous.

Faults on the eastern, northeastern and northern part of Parrabel Dome, (dominantly N-S, NNW-SSE and NNE-SSW orientations) started and stopped moving after Late Carboniferous emplacement of the HB and before Triassic granitoids instrusion. This fault movement is related to the accommodation of the NHB due to the Hunter-Bowen Orogeny (Figures A20b and A22a). Most fault movement was after folding and cleavage formation and was predominantly northwest-southeast striking.

Finally, limited dextral movement on the extensions of the Taylors Arm Fault System caused some minor displacement in the northeastern part of the NHB during the Late Triassic. Some small faults cut the Triassic granitoids indicating tectonic activity continued post Triassic.

The variability in the orientation of bedding within some fault blocks, between adjacent fault blocks, and around significant sections of the dome were analyzed in the NHB. This analysis highlights the shortcomings particularly on the southeastern and southwestern section of the Parrabel Dome with the existing Roberts *et al.* (1995) geological map. It is likely that some re-interpretation of the geology and repositioning of some faults will provide a better geology map (Lennox, Leitch and Offler, in prep. 2015). It appears that the region south of the Roberts et al. (1995) NHB-SHB boundary has been extensively deformed by faulting, although there is still gross apparent

stratigraphic continuity despite this faulting.

Bedding data and younging directions in fault blocks B and D-G around the Parrabel Dome support the existence of the dome. The bedding data in Fault Block A and C dips to the southwest and southeast to south respectively, unlike that expected in this section of the dome. The younging direction in the SHB are mostly younging to the ENE. The only exception is Fault Block H, which youngs to the NNW. A schematic reconstruction of the eastern limb of the Parrabel Dome that has undergone clockwise rotation via strike-slip faulting, is proposed to explain the dip direction changes in Fault Blocks A and C.

Models involving either the rotation and translation or a fault network produced in a restraining fault-bend along strike-slip faults is used to explain the disruption of fault blocks between the NHB and SHB. The reorientation of Fault Block H suggests it either was originally northnorthwest or southeast of its current position. It has been rotated and translated within a possible restraining bend as the NHB moved post-D3 folding northwest along a deep seated fault which may represent the interface between the NHB and SHB. It appears that the stratigraphic and structural boundary between the NHB and SHB is difficult to delineate because the fault blocks are shuffled (? rotated, translated and tilted) in this area.

Gravity and magnetic worm analysis enabled the overall dip of deep-seated structures and their continuity (geological boundary, faults, unconformities or intrusive contacts) that was not previously available. It provides evidence for major faults possibly located in the basement beneath the Hastings Block or along its margins. A possible different geological boundary between the NHB and SHB than that suggested by Roberts et al. (1995) is suggested by the gravity and magnetic worms analysis in the Hastings Block that extends from the Kunderang Fault, southeasterly through the Pappinbarra Fault and finally east-northeasterly towards Fault 72 (dashed black line; Figure 5.42). This

boundary is south of that proposed by Roberts *et al*. (1995) and may indicate that there is no definite break between the block but rather a diffuse zone of fault disruption.

The QFL analyses of Carboniferous sandstones in the NHB indicates the source for these sandstones changed with time. In the Boonanghi beds and Majors Creek Formations, the main source appears to be a calc-alkaline, continental arc that existed at the time of their deposition. A minor contribution came from uplifted basement. Subsequently, mixed sources provided the detritus for the overlying Kullatine and Youdale C Formations namely, arc and recycled orogenic (accretion-subduction complex sequences?), the former being the dominant. By the Early Permian, detritus in sandstones from Youdale A and B was received from a recycled orogenic provenance. The detritus may have been derived from accretion-subduction complex sequences in the Tablelands Complex.

Four geometrically constrained (balanced) cross sections across the Northern Hastings Block (A-B, C-D, E-F and X-Y) based on field data are presented which have been 2D restored following the principles of structural balance (line length balancing).

The overall shape from the cross sections suggests a northwest and southeast-plunging Parrabel Dome (29 km in half-wavelength with 7.7 km in amplitude) which is box-like in cross section C-D and more open in cross sections A-B and E-F. None of the major faults in the cross sections has more than a few kilometers of vertical displacement. Higher strain is concentrated in the Permian sequences transitional to the Nambucca Block and more particularly the Devonian-Carboniferous sequences around the southwestern margin of the dome around Yarras. This is especially noticeable in cross section C-D (near C) and E-F (near E). A macroscopic synform flanked by two macroscopic antiforms is visible in cross sections A-B and E-F near the crestal region of the Parrabel Dome. The total horizontal shortening (4% to 25% shortening) suggests only moderate cleavage development could occur consistent with field observations.

The maximum shortening in the NHB occurred after the deposition of the Early Permian sequences during the Hunter-Bowen Orogeny.

To show a gross shape of the Northern Hastings Block, provide better constraints on the relative timing of fault development and test various tectonic models to explain the formation of the NHB, a 3D structural model was created from the comprehensive field dataset on the Devonian to Carboniferous fore-arc rocks across the block. This 3D model incorporates the different DEM models for this region, the extensive fault network, horizon construction and virtual cross-sections. This 3D Model clarified the shape of the dome and compared the existing cross sections across this dome with those constructed across the 3D model (Chapter 6). Before this modelling there was no three dimensional model of the dome and this modelling demonstrated problems with the existing map of the NHB. Model construction showed that the map from Roberts et al.(1995) contains some faults which are clearly not in the correct position, that the dome does plunge gently southeast as well as northwest and that it is possible to determine the amount of shortening across the dome (Chapter 5).

The DEM analysis verified elements of the current structural interpretation (such as regional faults) and identified other geological structures such as intrusive contacts and differences in the weatherability of the NHB. Preliminary fault models divided the Northern Hastings Block into regions, which helped determine fault interrelationships, movement timing and orientations analysis (Chapter 4). Along with formation surface modeling, the 3D structural models has aided fault block reconstruction and provided information on the direction and movement of fault blocks (Chapter 5).

8.2 Geological history

This study involved the re-analysis of the comprehensively mapped, complexly folded, extensively faulted Northern Hastings Block. It provided evidence regarding the key brittle and ductile events in its deformation history.

8.2.1 NHB – NB

Initially, the NHB is believed to have been an along strike continuation of the fore-arc sequences in the Tamworth Belt (Schmidt *et al*. 1994; Cawood *et al*. 2011) and located southeast of its current position (Schmidt *et al*. 1994). At this time, the forearc-subduction accretion complex was gently curved (Figures 8.1a, Schmidt *et al*. 1994).

During the Late Carboniferous, the NHB was translated to its current position by anticlockwise (230°) movement between major faults prior to uplift, variable erosion and then deposition of the Permian sediments on the forearc packages in the Early Permian. (Figure 8.1a, Schmidt *et al*, 1994; Crowell 1985). The Parrabel Fault (and related faults) and the Yarras Fault System (Taylors Creek Fault, Yarras Mountain Trail Fault, Ralfes Creek Fault and Cowarral Fault) could be part of these two major fault systems bounding the rotating NHB. The Parrabel Fault and the faults making up the Yarras Fault System show sinistral strike-slip or oblique-slip movement (Lindsay 1969; Lennox and Offler, 2009). The faults on the southwestern and eastern sides of the Parrabel Dome are thought to be related to the emplacement of NHB (Figure 8.1b – red area). During anticlockwise rotation of the NHB, faults on the western side of the block would be subjected to sinistral strike-slip movement (Figure 8.1a) consistent with movement determined by Lennox and Offler (2009).

After emplacement, the forearc-subduction accretion complex (Tablelands Complex) was folded as a result of dextral movement on a major shear to the east of the HB producing the Texas-Coffs Harbour Orocline (Offler & Foster 2008). This resulted in the compression of the Nambucca Block and adjacent NHB (Figures 8.1c) producing E-W trending S_1. At this time the NHB made up of more competent units than the NB, acted as a massif. Subsequently, E-W shortening associated with the Hunter-Bowen Orogeny (HBO) resulted in folding and faulting especially in the Southern Hastings Block. Another three phases of variably developed cleavages (N-S orientation S_2,

NW-SE S_3 and the final NE-SW striking S_4) and three generations of macroscopic and mesoscopic folds (N or S plunging F_2, NW or SE-plunging F_3 and the NE or SW-plunging F_4) developed during this period (Figure 8.1d). The northwest and southeast-plunging Parrabel Dome formed during D3 deformation event. The subsequent NE-plunging macroscopic F_4 deformed the Parrabel Dome. All these folded and cleaved rocks in the NHB were then cut and disrupted by the subsequent faulting resulting in major changes in bedding orientation of some formations around the dome and the disruption of fault blocks between the NHB and SHB and in the northwestern Kunderang District. The sinistral strike-slip movement along a new geology boundary (solid red line in Figure 8.1e) revealed by the gravity and magnetic worms analysis led to the northwestwards translation of the whole NHB and clockwise rotation of the southern and southeastern limb of the dome (Figure 8.1e). Faults on the eastern, northeastern and northern part of Parrabel Dome continued moving after the Late Carboniferous emplacement of the NHB and ceased moving during the accommodation of the NHB to continuing deformation in the Nambucca Block (Figure 8.1f, yellow area). They cut the folded and cleaved rocks in the NHB and may be associated with the Hunter-Bowen Orogeny.

Finally the emplacement of post tectonic granitoids and rhyolitic volcanism took place in the Late Triassic cutting those faults related to the emplacement of the NHB. The Werrikimbe Volcanics and associated rocks welded the Yarrowitch Block (accretion-subduction complex) to the forearc rocks of the Hastings Block. From the Late Triassic, limited dextral movement on extensions of the Taylors Arm Fault System caused limited faulting in the northeastern part of the Northern Hastings Block (Figure 8.1g-green area).

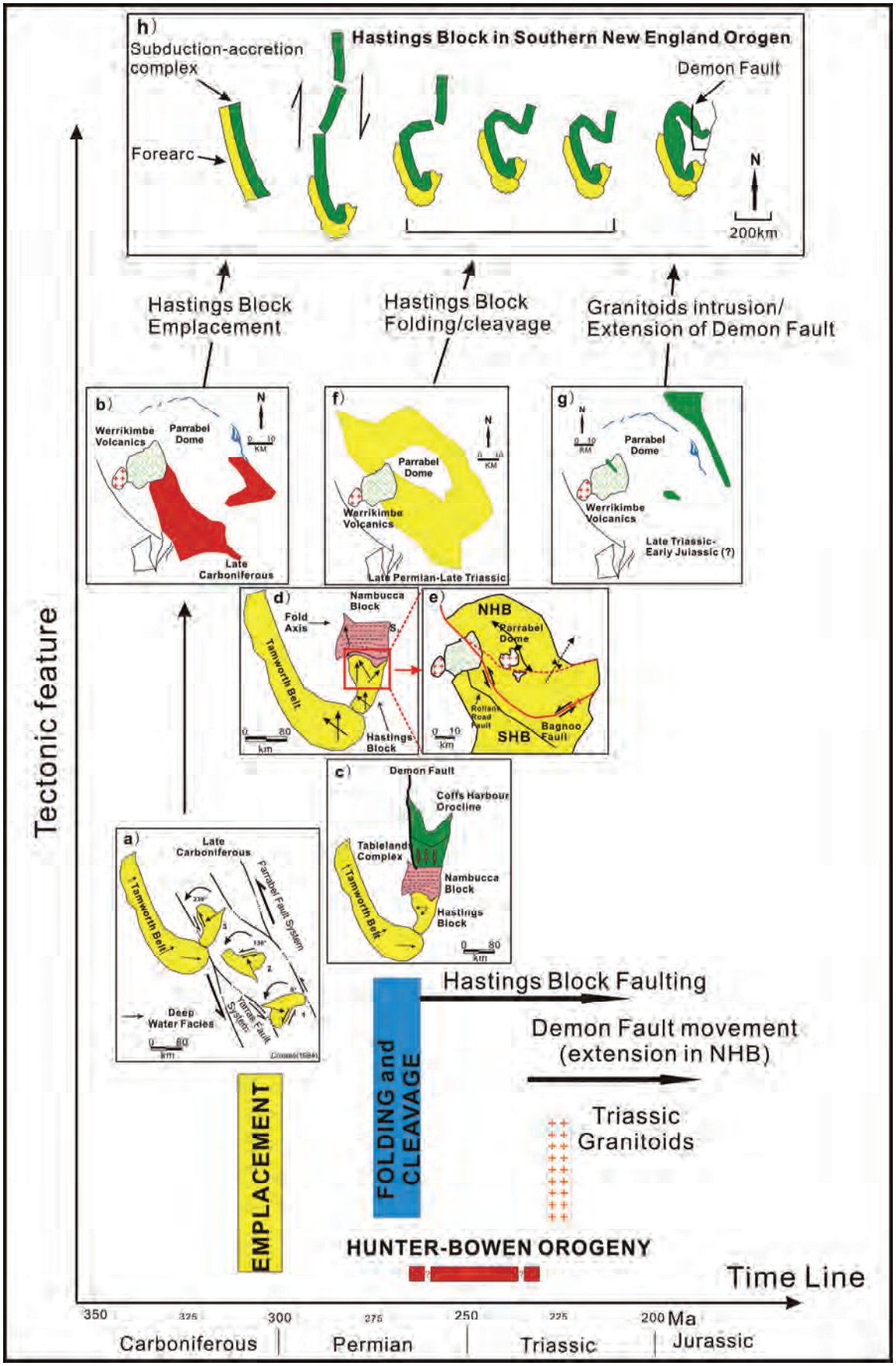

Figure 8.1: Schematic diagram of geological history of the Northern Hastings Block

showing a time line with major events in vertical or horizontal columns. (a) Sketches of the method of emplacement (Crowell 1985; Hernandez-Moreno *et al*. 2014); (b) areas shown in red where faults were active during the Late Carboniferous emplacement; (c) regional tectonics during folding/cleavage formation as the Coffs Harbour Orocline moved south compressing the NB; (d) different fold phase among NHB, SHB and TB; (e) the sinistral strike-slip movement along a new geology boundary led to the translation and clockwise rotation of the Parrabel dome; (f) areas shown in yellow of contemporaneous fault movement after cleavage and fold formation; and (g) areas shown in green of fault movement post-Triassic granitoids intrusion. The schematic diagram (h) shows the initially gently curved forearc-subduction accretion complex being dextrally sheared after NHB emplacement to form the Texas-Coffs Harbour Orocline with compression of the Nambucca and adjacent NHB (275-265 Ma, Shaanan *et al*. 2014), followed by Late Triassic-Early Jurassic (?) development of the Demon Fault and its extensions (Leitch 1978; Babaahmadi and Rosenbaum 2013) such as the Taylors Arm Fault System in the Nambucca and adjoining NHB. The black arrows under (c) shows the time span of the faulting in Hastings Block and the Demon Fault.

8.2.2 Relationship to surrounding blocks

After emplacement of the Hastings Block and development by rifting of the overlying Nambucca Basin, this NHB-NB region was subjected to north-south shortening (Figure 8.1d), followed by east-west to northeast-southwest shortening with Parrabel Dome formation (Figure 8.1e). In the SHB and southern Tamworth Belt (TB), there is no evidence for east-west structures (Table 8.1). Collins (1991) proposed early N-S folds being refolded around NW-SE folds, whereas Glen and Roberts (2012) proposed the opposite order of events (Figure 8.1d). It is considered that Glen and Roberts (2012) are correct so the stress field generating folds in the NHB was different from that in the southern Tamworth Belt reflecting their slightly different positions inboard of the likely subduction zone to the east.

The Parrabel anticline must have been refolded by a macroscopic NE-plunging syncline whose folding axis trace passes through Kempsey Township to cause it to be doubly plunging as observed. After dome formation continued shortening caused by squeezing

of the Nambucca Block could not be accommodated by further folding in the NHB, so extensive faulting occurred throughout the block but expecially in the boundary zone between the NHB and SHB.

The northeast limb of the dome was rotated clockwise with dismemberment of the southeast-plunging part of the dome. The fault blocks between the dome and rocks further south were disrupted during apparent clockwise, northwest-movement of the NHB around a series of different faults undergoing sinistral strike-slip forming a single curved, concave-south fault system (Figure 8.1e – solid red line). The SHB south of this curved fault system is relatively simple structurally with east-dipping and younging Devonian-Carboniferous sequences showing NW-SE folds overprinting N-S megascopic folds (Figure 8.1d, Table 8.1).

Table 8.1: Comparison of the orientation of different fold phase among the NHB, SHB, NB and Tamworth Belt using data in this thesis and the literature.

Deformation	**Nambucca Block**		**NHB**	**SHB**	**Tamworth Belt**	
	Leitch *et al.* (1978)	Shaanan *et al.* (2014)	This thesis	Roberts *et al.* (1993)	Collins (1991)	Glen and Roberts (2012)
D1	E-W	E-W	E-W	—	—	—
D2	E-W	NE-SW	N-S	N-S	N-S	NW-SE
D3	?E- W	NNW-SSE to NW-SE	NW-SE	NW-SE	NW-SE	N-S
D4	?	NE-SW	NE-SW	—	—	—
D5	NNW-SSE to NW-SE	—	—	—	—	—

The NHB was only slightly affected by post Triassic (to ?Jurassic) movement on extensions of the Taylors Arm Fault System which is connected further north to the Demon Fault (Appendix 4).

The Port Macquarie Block on the south eastern side of the NHB-SHB boundary consists of western parts similar to the Hastings Block and eastern parts consisting of Ordovician

cherts (Watonga Formation) and subduction-accretion rocks which are outboard relative to similar rocks elsewhere in the Tableland Complex. The northnortheast-southsouthwest structural grain of the Hastings Block - like western section of the Port Macquarie Block may represent the SE-limb of the F_4 megascopic syncline observed in the NHB.

The formation of the Hastings Block is not because of large-scale 'oroclinal' folding in the Manning and Hastings area as suggested by Cawood et al. (2011); Rosenbaum et al. (2012); Glen & Roberts, (2012) and Li et al. (2014). The reasons include: (1) the serpentinites are not as continuous as required to wrap around the Hastings Block but rather form pod-like bodies near and sometimes away from the block boundary. The ages of the serpentinites and associated protoliths have not been established to be the same; (2) the NHB plunges gently NW and is not steeply plunging as expected for an orocline; (3) No hinge zone can be established for the Manning Orocline either near Mt. George (Yan et al. 2012; Lennox et al. 2013) or near Walcha (Lennox et al. 2014; Offler et al. 2014). The hinge zone near Mt.George do not define a steeply-plunging macroscopic fold as expected for an orocline; (4) Mapping by Laurie (1976) indicates that the Devonian to Carboniferous sequences south and southeast of the Mt George area are disrupted by N-S, NNE, E-W and NW-trending faults. Bedding within the fault-bound blocks south of Mt. George do not define an oroclinal structure, rather steeply-dipping, homoclinal sequences of varying orientation and uncommon N-S, NW and E-W gently plunging folds.

8.3 Limitations of this study

When using the fault analysis to estimate the time of fault movement, only the last movement along the faults will be recorded since this will be evident by the displacement of the youngest stratigraphic unit. The estimation of the earliest and latest time of movement of each fault is constrained by the age range of the stratigraphy through which the fault passes. More fieldwork should be undertaken to better

characterize the fault history. Unfortunately good exposures of faults in the NHB are very rare (Lennox pers.com.2015).

References

ADAMS C. J., KORSCH R. J. & GRIFFIN W. L. 2013. Provenance comparisons between the Nambucca Block, Eastern Australia and the Torlesse Composite Terrane, New Zealand: connections and implications from detrital zircon age patterns. *Australian Journal of Earth Sciences* **60**, 241-253.

AITCHISON J. C., FLOOD P. G. & SPILLER F. C. P. 1992. Tectonic setting and paleoenvironment of terranes in the southern New England orogen, eastern Australia as constrained by radiolarian biostratigraphy. *Palaeogeography, Palaeo-climatology, Palaeoecology* **94**, 31–54.

AITCHISON J. C. & IRELAND T. R. 1995. Age profile of ophiolitic rocks across the Late Palaeozoic New England Orogen, New South Wales: Implications for tectonic models. *Australian Journal of Earth Sciences* **42**, 11-23.

ALCARAZ S., LANE R., SPRAGG K., MILICICH S., SEPULVEDA F. & BIGNALL1 G. 2011. 3D geological modelling using Leapfrog Geothermal software. Proceedings, Thirty-Sixth Workshop on Geothermal Reservoir Engineering. Stanford University, Stanford, California.

ARCHIBALD N. J., GOW P. & BOSCHETTI F. 1999. Multiscale edge analysis of potential field data. *Exploration Geophysics* **30**, 38-44.

ASTHANA D. L. & LEITCH E. C. 1985. Petroi Metabasalt: Alkaline within-plate mafic rocks from the Nambucca Slate Belt, northeastern New South Wales. *Australian Journal of Earth Sciences* **32**, 261-277.

BABAAHMADI A. & ROSENBAUM G. 2013. Kinematics of the Demon Fault: Implications for Mesozoic strike-slip faulting in eastern Australia. *Australian Journal of Earth Sciences* **60**, 255-269.

BADURA J. & PRZYBYLSKI B. 2005. Application of digital elevation models to geological and geomorphological studies—some examples. *Przeglad Geologiczny* **53**, 977-983.

BERRA F., SALVI F., ZANCHI A., AVARO A., BONAVERA M. & STERLACCHINI S. 2008. 3D reconstruction from surface data in complex geological settings: the example of a thrust stack in the Mesozoic cover of the Southern Alps (Italy). *GeoInformatica* 1-15.

BIRGENHEIER L. P., FIELDING C. R., RYGEL M. C., FRANK T. D. & ROBERTS J. 2009. Evidence for Dynamic Climate Change on Sub-106-Year Scales from the Late Paleozoic Glacial Record, Tamworth Belt, New South Wales, Australia. *Journal of Sedimentary Research* **79**, 56-82.

BOURKE D. J. 1971. The structural and stratigraphic study of the upper Kunderang Brook District. BSc Hons Thesis (unpubl.), University of New England, Armidale.

BRYANT C. J., COSCA M. A. & ARCULUS R. J. 1997. $^{40}Ar/^{39}Ar$ ages of the Clarence River Supersuite intrusions from the northern portions of the New England Orogen. *Special Publication of Geological Society Australia* **19**, 242-253.

BUCKMAN S., NUTMAN A. P., AITCHISON J. C., PARKER J., BEMBRICK S., LINE T., HIDAKA H. & KAMIICHI T. 2014. The Watonga Formation and Tacking Point Gabbro, Port Macquarie, Australia: Insights into crustal growth mechanisms on the eastern margin of Gondwana. *Gondwana Research.* **28**, 133-151.

BYKERK-KAUFFMAN A. 1987. Lab exercise on analysis of tectonostratigraphic terranes : instructions and data. Department of Geosciences, University of Arizona.

BYKERK-KAUFFMAN A. 1989. A hands-on approach to teaching the terrane concept in historical geology. *Journal of Geological Education* **37**, 83-89.

CALCAGNOA P., CHILÈS J. P., COURRIOUXA G. & GUILLENA A. 2008. Geological modelling from field data and geological knowledge Part I. Modelling method coupling 3D potential-field interpolation and geological rules. *Physics of the Earth and Planetary Interiors* **171**, 147–157.

CAPRARELLI G. & LEITCH E. C. 2001. Geochemical evidence from Lower Permian volcanic rocks of northeast New South Wales for asthenospheric upwelling following slab breakoff. *Australian Journal of Earth Sciences* **48**, 151-166.

CAUMON G., COLLON-DROUAILLET P., LE CARLIER DE VESLUD C., VISEUR S. & SAUSSE J. 2009. Surface-Based 3D Modeling of Geological Structures. *Mathematical Geosciences* **41**, 927–945.

CAWOOD P. A. 1982. Structural relations in the subduction complex of the Paleozoic New England Fold Belt, eastern Australia. *Journal of Geology* **90**, 381-392.

CAWOOD P. A. & LEITCH E. C. 1985. Accretion and dispersal tectonics of the southern New England Fold Belt, Eastern Australia. In HOWELL D. G. ed. Tectonostratigraphic Terranes of the Circum-Pacific Region. pp. 481-492. Circum Pacific Council for Energy and Mineral Resources. Earth Science Series.

CAWOOD P. A. & LEITCH E. C. 2006. Unravelling the New England Orocline and implications for end Paleozoic to early Mesozoic orogenesis along the Pacific margin of Gondwana. *Geological Society of America Abstracts with Programs, Speciality Meeting* **2**, 78.

CAWOOD P. A., PISAREVSKY S. A. & LEITCH E. C. 2011. Unraveling the New England orocline, east Gondwana accretionary margin. *Tectonics* **30**, 1-15.

COLLINS W. J. 1991. A reassessment of the 'Hunter-Bowen Orogeny': Tectonic implications for the southern New England fold belt. *Australian Journal of Earth Sciences* **38**, 409-423.

COOPER G. T. & HILL K. C. 1997. Cross-section balancing and thermochronological analysis of the Mesozoic development of the eastern Otway Basin. *The APPEA Journal* **37**, 390-414.

CROOK K. A. W. 1961. Stratigraphy of the Tamworth Group (Lower and Middle Devonian), Tamworth-Nundle District, NSW. *Journal and Proceedings of the Royal Society of New South Wales* **94**, 173-188.

CROWELL J. C. 1974. Origin of Late Cenozoic basins in Southern California. In DICKINSON W. R. ed. Tectonic and Sedimentation: Society of Economic Paleontologists and Mineralogists, Special publication 22. pp. 190-204.

CROWELL J. C. 1985. The recognition of transform terrane dispersion within mobile belts. *Tectonostratigrahic Terranes of the Circum-Pacific Region, Earth Science Series* **1**, 51-61.

CUNNINGHAM W. D. & MANN P. 2007. Tectonics of Strike-Slip Restraining and Releasing Bends. *Geological Society, London, Special Publications,* **290**, 1–12. DOI: 10.1144/SP290.1.

DAVIS G. H. 1984. Structural Geology of Rocks and Regions. New York: Wiley. 492pp.

DEEGAN C. M. 1991. Geology of the Lansdowne Area, southern part of the Hastings Block. BSc Hons Thesis (unpubl.), University of Sydney, Sydney.

DICKINSON W. R., BEARD L. S., BRAKENRIDGE G. R., ERJAVEC J. L., FERGUSON R. C., INMAN K. F., KNEPP R. A., LINDBERG F. A. & RYBERG P. T. 1983. Provenance of North American Phanerozoic sandstones in relation to tectonic setting. *Geological Society of America Bulletin* **94**, 222-235.

DICKINSON W. R. & SUCZEK C. A. 1979. Plate tectonics and sandstone compositions. *AAPG Bulletin* **63**, 2164-2182.

DIRKS P. H. G. M., HAND M., COLLINS W. J. & OFFLER R. 1992. Structural-metamorphic evolution of the Tia Complex, New England fold belt; thermal overprint of the an accretion-subduction complex in a compressional back-arc setting. *Journal of Structural Geology* **14**, 669-688.

FEENAN J. P. 1984. Stratigraphy and structure of the Long Flat District, west of Wauchope, NSW BSc Hons Thesis (unpubl.), University of Sydney, Sydney, New South Wales, Australia.

FERGUSSON C. L. 1988. Tectonostratigraphic terranes in the central Coffs Harbour Block, northeastern New South Wales. In KLEEMAN J. D. ed. New England Orogen -- Tectonics and Metallogenesis,. pp. 42-48. Armidale.: Department of Geology and Geophysics, University of New England.

FLOOD P. G. & AITCHISON J. C. 1988. Tectonostratigraphic terranes of the southern part of the New England Orogen. In KLEEMAN J. D. ed. New England Orogen — Tectonics and Metallogenesis. pp. 7-10. Armidale: University of New England.

FLOOD P. G. & FERGUSSON C. L. 1982. Tectono-stratigraphic units and structure of the Texas-Coffs Harbour region. In FLOOD P. G. & RUNNEGAR B. eds. New England Geology,. pp. 71-78. Armidale: University of New England.

FLOOD R. H., LEITCH E. C. & SHAW S. E. 1993. The Werrikimbe Volcanics: a Late Triassic caldera in southeastern New England, NSW. *Centre for Isotope Studies Research Report* **1991-92**, 117-121. CSIRO.

FRANK T., TERTOIS A. L. & MALLET J. L. 2007. 3D-reconstruction of complex geological interfaces from irregularly distributed and noisy point data. *Computers & Geosciences* **33**, 932-943.

GALLANT J. C. & DOWLING T. I. 2003. A multiresolution index of valley bottom flatness for mapping depositional areas. *Water Resources Research* **39**, 1347.

GANASA A., PAVLIDESB S. & KARASTATHIS V. 2005. DEM-based morphometry of range-front escarpments in Attica, central Greece, and its relation to fault slip rates. *Geomorphology* **65**, 301–319.

GEEVE R. J., SCHMIDT P. W. & ROBERTS J. 2002. Paleomagnetic results indicate pre-Permian counter-clockwise rotation of the southern Tamworth Belt, southern New England Orogen, Australia. *Journal of Geophysical Research* **107**, 10.1029/2000jb000037.

GIBBS A. D. 1983. Balanced cross-section construction from seismic sections in areas of extensional tectonics. *Journal of Structural Geology* **5**, 153–160. doi:10.1016/0191-8141(83)90040-8.

GLEN R. A. 2005. The Tasmanides of eastern Australia. In VAUGHAN A. P. M., LEAT P. T. & PANKHURST R. J. eds. Terrane Processes at the Margins of Gondwana. pp. 23–96. London: Geological Society,Special Publication **246**.

GLEN R. A. & BECKETT J. 1997. Structure and tectonics along the inner edge of a foreland basin: the Hunter Coalfield in the northern Sydney Basin, New South Wales. *Australian Journal of Earth Sciences* **44**, 853-877.

GLEN R. A. & ROBERTS J. 2012. Formation of Oroclines in the New England Orogen, Eastern Australia. *Journal of the Virtual Explorer* **43**, Paper 3, http://dx.doi.org/10.3809/jvirtex.2012.00305.

GRAHAM S. A., INGERSOLL R. V. & DICKINSON W. R. 1976. Common provenance for lithic grains in Carboniferous sandstones from Ouachita Mountains and Black Warrior Basin. *Journal of*

Sedimentary Research **46**, 620-632.

GROSHONG J. & RICHARD H. 2006. 3-D Structural Geology. Springer, Berlin.

HAMILTON D. S. 1980. Stratigraphy and Sedimentology of the Carboniferous Rocks in the Telegraph Point District, NSW. BSc Hons Thesis (unpubl.), University of Sydney, Sydney, New South Wales, Australia.

HAUGE T. & GRAY G. 1996. A critique of techniques for modelling normal-fault and rollover geometries. *Geological Society, London, Special Publications* **99**, 89-97.

HERNANDEZ-MORENO C., SPERANZA F. & CHIARA A. D. 2014. Understanding kinematics of intra-arc transcurrent deformation: Paleomagnetic evidence from the Liquiñe-Ofqui fault zone (Chile, 38–41°S). *Tectonics* **33**, 1964–1988, doi:10.1002/ 2014TC003622.

HOBSON R. D. 1972. Surface roughness in topography: quantitative approach. *Spatial analysis in geomorphology* 225-245.

HOFFMAN K. S. & NEAVE J. W. 2007. The fused fault block approach to fault network modelling. *Geological Society, London, Special Publications* **292**, 75-87.

HOLCOMBE R. J., STEPHENS C. J., FIELDING C. R., GUST D A., LITTLE T. A., SLIWA R., KASSAN J., MCPHIE J. & EWART A. 1997. Tectonic evolution of the northern New England Fold Belt: the Permian–Triassic Hunter–Bowen event. In FLOOD P. G. & ASHLEY P. M. eds. Tectonics and metallogenesis of the New England Orogen. pp. 52–65. Geological Society of Australia Special Publication **19**.

HOLDEN D. J., J. A. N., BOSCHETTI F. & JESSELL M. W. 2000. Inferring Geological Structures Using Wavelet-Based Multiscale Edge Analysis and Forward Models. *Exploration Geophysics* **31**, 67-71.

HOY D., ROSENBAUM G., WORMALD R. & SHAANAN U. 2014. Geology and geochronology of the Emu Creek Block (northern New South Wales, Australia) and implications for oroclinal bending in the New England Orogen. *Australian Journal of Earth Sciences* **61**, 1109-1124.

JASON R. 1992. An investigation of the rocks underlying the Permian Yessabah Limestone, North-East NSW. BSc Hons Thesis (unpubl.), University of Technology, Sydney.

JAYKO A. S., BLAKE M. C., AITCHISON J. & AITCHISON J. 1993. Structural uplift of ophiolitic slivers along major faults of the New England orogen. In FLOOD P. G. & AITCHISON J. C. eds. New England Orogen, eastern Australia. pp. 163-179. Armidale: Department of Geology and Geophysics, University of New England, Armidale.

JEFFREY S. 1986. Geology of the Yessabah area, Kempsey. BSc Hons Thesis (unpubl.), University of New South Wales, Sydney.

JESSELL M. W. 2001. Three-dimensional geological modelling of potential-field data. *Computers & Geosciences* **27**, 455-465.

JESSELL M. W. & VALENTA R. K. 1996. Structural geophysics: integrated structural and geophysical modelling. *Computer Methods in the Geosciences* **15**, 303-324.

JOHNSTON A. 1997. Structural analysis of Early Permian meta-sediments on wave cut platforms, Nambucca Block, NSW. Tectonic implications. BSc Hons Thesis (unpubl.), University of Newcastle, Newcastle.

JOHNSTON A. J., OFFLER R. & LIU S. 2002. Structural fabric evidence for indentation tectonics in the Nambucca Block, southern New England Fold Belt, New South Wales. *Australian Journal of Earth Sciences* **49**, 407-421.

JORDAN G. 2003. Morphometric analysis and tectnoic interpretation of digital terrain data: a case

study. *Earth Surface Processes and Landforms* **28**, 807–822.

KAUFMANN O. & MARTIN T. 2008. 3D geological modelling from boreholes, cross-sections and geological maps, application over former natural gas storages in coal mines. *Computers & Geosciences* **34**, 278–290.

KELLY B. F. J. 2009. Catchment Scale 3D Geological Models from Sparse Data Sets. International Mathematica User Conference. Champaign, Illinois, USA.

KELLY B. F. J. & GIAMBASTIANI B. M. S. 2009. Functional Programming Algorithms for Constructing 3D Geological Models. In LEES B. G. & LAFFAN S. W. eds. 10th International Conference on GeoComputation. The University of New South Wales, Sydney.

KINNY P. D. 1982. Geology of the Willi Willi - Carrai area, NSW with particular reference to its thermal metamorphic history. BSc Hons Thesis (unpubl.), University of Sydney, Sydney, New South Wales, Australia.

KLOOTWIJK C. 2009. Sedimentary basins of eastern Australia: paleomagnetic constraints on geodynamic evolution in a global context. *Australian Journal of Earth Sciences* **56**, 273-308.

KORSCH R. 1984. Sandstone compositions from the New England Orogen, eastern Australia: implications for tectonic setting. *Journal of Sedimentary Research* **54**, 192-211.

KORSCH R. J. 1977. A framework for the Palaeozoic geology of the southern part of the New England Geosyncline. *Journal of the Geological Society of Australia* **25**, 339-355.

KORSCH R. J. 1981. Deformation history of the Coffs Harbour Block. *Journal and Proceedings of the Royal Society of New South Wales* **114**, 17-22.

KORSCH R. J. & HARRINGTON H. J. 1987. Oroclinal bending, fragmentation and deformation of terranes in the New England Orogen, eastern Australia. **19**, 129-139.

KORSCH R. J., JOHNSTONE D. W. & WAKE-DYSTER K. D. 1997. Crustal architecture of the New England Orogen based on deep seismic reflection profiling. In Tectonics and Metallogenesis of the New England Orogen. *Geological Society of Australia Special Publication* **19**, 29-51.

KORSCH R. J., WAKE-DYSTER K. D. & JOHNSTONE D. W. 1993. The Gunnedah Basin-New England Orogen deep seismic reflection profile: Implications for New England tectonics. In FLOOD P. G. & AITCHISON J. C. eds. New England Orogen, eastern Australia. pp. 85-100. Armidale: University of New England.

LAURIE J. R. 1976. The Geology of the Kimbriki Area. BSc Hons Thesis (unpubl.), University of Newcastle, Newcastle.

LEITCH E., MILLIGAN I., PRICE G., FLOOD P. & RUNNEGAR B. 1982. Thermal metamorphism and mineralization in the northern part of the Hastings Block. *New England Geology* 345-350.

LEITCH E. C. 1972. The geology development of the Bellinger-Macleay region, northeastern New South Wales. Ph.D. thesis, University of New England (unpublished).

LEITCH E. C. 1974. The geological development of the southern part of the New England Fold Belt. *Journal of the Geological Society of Australia* **21**, 133-156.

LEITCH E. C. 1975. Plate tectonic interpretation of the Paleozoic history of the New England Fold Belt. *Geological Society of America Bulletin* **86**, 141-154.

LEITCH E. C. 1976. Emplacement of an epizonal pluton by vertical block elevation. *Geological Magazine* **113**, 553-560.

LEITCH E. C. 1978. Structural succession in a late Paleozoic slate belt and its tectonic significance. *Tectonophysics* **47**, 311-323.

LEITCH E. C. 1980. Rock units, structure and metamorphism of the Port Macquarie Block, eastern New England Fold Belt. *Proceedings of the Linnean Society of New South Wales* **104**, 273-292.

LEITCH E. C. 1988. The Barnard Basin and the Early Permian development of the southern part of the New England Belt. In KLEEMAN J. D. ed. New England Orogen -- Tectonics and Metallogenesis. pp. 61-67. Armidale: Department of Geology and Geophysics, University of New England.

LEITCH E. C. & MACDOUGALL I. 1979. The age of orogeneris in the Nambucca slate Belt: A K-Ar study of Low grade regional metamorphic rocks. *Journal Geological Society of Australia* **26**, 111-119.

LEITCH E. C., WATANABE T., IWASAKI M., ISHIGA H., ISUZUMI S., HONMA H. & KAWACHI Y. 1990. Terranes of the southern part of the New England Fold Belt—a critical review. In WILET T. J., HOWELL D. G. & WONG F. L. eds. Terrane analysis of China and the Pacific rim. pp. 95-101. Circum-Pacific Council for Energy and Mineral Resources.

LEMON A. M. & JONES N. L. 2003. Building solid models from boreholes and user-defined cross-sections. *Computers and Geosciences* **29**, 547-555.

LENNOX P. G. & FLOOD P. G. 1997. Age and structural characterisation of the Texas megafold, southern New England Orogen, eastern Australia. In ASHLEY P. M. & FLOOD P. G. eds. Tectonics and Metallogenesis of the New England Orogen pp. 161–177. Geological Society of Australia Special Publication **19**.

LENNOX P. G., LEITCH E. C. & OFFLER R. 1993 Geologcal relationship between major crustal units of southern New England Fold Belt. Field Guidebook. Sydney Consortium of Geology and Geophysics (SUCOGG) and SGTSG. 37pp.

LENNOX P. G. & OFFLER R. 2009. Kinematic history of serpentinites in the faulted margins of the Hastings Block, New England Orogen, eastern Australia. *Australian Journal of Earth Sciences* **56**, 621-638.

LENNOX P. G. & OFFLER R. 2010. Emplacement and deformation recorded in the Hastings Block-constraints from serpentinite bodies and structures within and adjacent to the block. New England Orogen 2010 Conference Proceedings. pp. 213-217. University of New England.

LENNOX P. G., OFFLER R. & YAN J. 2013. Discussion of Glen R.A. and Roberts J. 2012: Formation of oroclines in the New England Orogen, Eastern Australia. *Journal of the Virtual Explorer* **44**, (paper 3).

LENNOX P. G., OFFLER R. & YAN J. 2014. Why the Manning and Hastings (Nambucca) oroclines do not exist. *Geological Society of Australia Abstracts* **110**, 01DPB-02.

LENNOX P. G. & ROBERTS J. 1988. The Hastings Block: A key to the tectonic development of the New England Orogen. In KLEEMAN J. D. ed. New England Orogen: Tectonics and Metallogenesis,. pp. 68-77. Armidale: Department of Geology and Geophysics, University of New England, Armidale.

LENNOX P. G., ROBERTS J. & OFFLER R. 1999. Structural analysis of the Hastings Block. In FLOOD P. G. ed. New England Orogen, eastern Australia. pp. 115–124. Armidale: University of New England, Armidale.

LI P. & ROSENBAUM G. 2014. Does the Manning Orocline exist? New structural evidence from the inner hinge of the Manning Orocline (eastern Australia). *Gondwana Research* **25**,

1599-1613.

LI P., ROSENBAUM G. & DONCHAK P. J. T. 2012a. Structural evolution of the Texas Orocline, eastern Australia. *Gondwana Research* **22**, 279-289.

LI P., ROSENBAUM G. & RUBATTO D. 2012b. Triassic asymmetric subduction rollback in the southern New England Orogen (eastern Australia): the end of the Hunter-Bowen Orogeny. *Australian Journal of Earth Sciences* **59**, 965-981.

LI P., ROSENBAUM G. & VASCONCELOS P. 2014. Chronological constraints on the Permian geodynamic evolution of eastern Australia. *Tectonophysics* **617**, 20-30.

LI P., ROSENBAUM G., YANG J. H. & HOY D. 2015. Australian-derived detrital zircons in the Permian-Triassic Gympie terrane (eastern Australia): Evidence for an autochthonous origin. *Tectonics* **34**, 858-874.

LINDSAY J. F. 1966. Carboniferous subaqueous mass-movement in the Manning-Macleay Basin, Kempsey, New South Wales. *Journal of Sedimentary Petrology* **36**, 719-732.

LINDSAY J. F. 1969. Stratigraphy and structure of the Palaeozoic sediments of the Lower Macleay region, northeastern New South Wales. *Journal and Proceedings of The Royal Society of New South Wales* **102**, 41- 55.

LUCAS K. G. 1960. The Texas area. *Journal of the Geological Society of Australia* **7**, 229-235.

MAYORAZ R. 1993. Modélisation et visualisation infographiques tridimensionelle de structures et propriétés géologiques. Ph.D. Thesis, École polytechnique Fédérale de Lausanne (EPFL), Switzerland.

MCPHIE J. & FERGUSSON C. L. 1983. Dextral movement on the Demon Fault, northeastern New South Wales: a reassessment (Australia). *Journal & Proceedings Royal Society of New South Wales* **116**, 123–127.

MIKEL M. 1985. The Mount Cairncross silicic porphyry complex and associated rocks. BSc Hons Thesis (unpubl.), University of Sydney, Sydney.

MILLIGAN I. M. 1975. The Geology of the Gundle and Glen Esk Plutons, Upper Wilson River district, NSW. BSc Hons Thesis, University of Sydney, Sydney.

MOCHALES T., ROSENBAUM G., SPERANZA F. & PISAREVSKY S. A. 2014. Unraveling the geometry of the New England oroclines (eastern Australia): Constraints from magnetic fabrics. *Tectonics* **33**, 2261-2282.

MURRAY C. G., FERGUSSON C. L., FLOOD P. G., WHITAKER W. G. & KORSCH R. J. 1987. Plate tectonic model for the Carboniferous evolution of the New England Fold Belt. *Australian Journal of Earth Sciences* **34**, 213-236.

NIETO-SAMANIEGO A. F. & ALANIZ-ALVAREZ S. A. 1997. Origin and tectonic interpretation of multiple fault patterns. *Tectonophysics* **270**, 197-206.

NUTMAN A. P., BUCKMAN S., HIDAKA H., KAMIICHI, T., BELOUSOVA E. & AITCHISON J. 2013. Middle Carboniferous-Early Triassic eclogite–blueschist blocks within a serpentinite mélange at Port Macquarie, eastern Australia: Implications for the evolution of Gondwana's eastern margin. *Gondwana Research* **24**, 1038-1050.

OCH D. J., LEITCH E. C., CAPRARELLI G. & WATANABE T. 2003. Blueschist and eclogite in tectonic melange, Port Macquarie, New South Wales, Australia. *Mineralogical Magazine* **67**, 609-624.

OCH D. J., PERCIVAL I. G. & LEITCH E. C. 2007. Ordovician conodonts from the Watonga Formation, Port Macquarie, northeast New South Wales. *Proceedings of the Linnean Society of New*

South Wales **128**, 209-216.

OFFLER R. 2005. Metamorphism in the southern New England Fold Belt - an overview. SGGMP Conference, Pt. Macquarie, NSW. *Geological Society of Australia Abstract* **76**, 100-104.

OFFLER R. & BRIME C. 1994. Characterisation of the low grade metamorphism in the Nambucca Block (NSW, Australia). *Revisita Geologica de Chile Special issue on low grade metamorphism* **21**, 285-293.

OFFLER R. & FOSTER D. A. 2008. Timing and development of oroclines in the southern New England Orogen, New South Wales. *Australian Journal of Earth Sciences* **55**, 331-340.

OFFLER R., LENNOX P. G., PHILLIPS G. & YAN J. 2014. Comment on: "Does the Manning Orocline exist? New structural evidence from the inner hinge of the Manning Orocline (eastern Australia)" by Li and Rosenbaum (2013). *Gondwana Research* **27**, 1686-1688.

OFFLER R. & MURRAY C. 2011. Devonian volcanics in the New England Orogen: tectonic setting and polarity. *Gondwana Research* **19**, 706-715.

OFFLER R., ROBERTS J., LENNOX P. & GIBSON J. 1997. Metamorphism in Palaeozoic forearc basin sequences, southern New England Fold Belt, N.S.W., Australia. *Proceedings of the 30th International Geological Congress* **17**, 241-250.

PHILLIPS G., HAND M. & OFFLER R. 2010. P-T-X controls on phase stability and composition in LT-MP metabasite rocks - a thermodynamic evaluation. *Journal of Metamorphic Geology.* Doi:10.1111/j.1525-1314.2010.00874.x.

PICKETT J. W., OCH D. J. & LEITCH E. C. 2009. Devonian marine invertebrate fossils from the Port Macquarie Block, New South Wales. *Proceedings of the Linnean Society of New South Wales* **130**, 193-217.

PRATT G. W. 2010. A revised Triassic stratigraphy for the Lorne basin, NSW. *Quarterly Notes of the Geological Survey of NSW* **134**, 1-35.

RAMSAY J. G. 1967. Folding and fracturing of rocks. McGraw-Hill Book Company, Sydney.

REY J. 2008. Stratigraphy: Foundations and Perspectives. In REY J. & GALEOTTI S. eds. Stratigraphy: Terminology and Practice. pp. 10.

RHEINBERGER G. 1987. Geology of the Willi Willi area, Kempsey. BSc Hons Thesis (unpubl.), University of New South Wales, Sydney.

RILEY S. J., DEGLORIA S. D. & ELLIOT R. 1999. A terrain ruggedness index that quantifies topographic heterogeneity. *Intermountain Journal of Sciences* **5**, 23-27.

ROBERTS J. & ENGEL B. A. 1987. Depositional and tectonic history of the southern New England Orogen. *Australian Journal of Earth Sciences* **34**, 1-20.

ROBERTS J., ENGEL B. A. & CHAPMAN J. 1991. Geology of the Camberwell, Dungog and Bulahdelah 1:100 000 sheets (9133, 9233 and 9333). *Geological Survey of New South Wales, Explanatory Notes* Geological Survey of New South Wales.

ROBERTS J. & GEEVE R. 1999. Allochthonous forearc blocks and their influence on an orogenic timetable for the Southern New England Orogen. In FLOOD P. G. ed. New England Orogen, eastern Australia. pp. 105–114. Armidale: University of New England.

ROBERTS J., LEITCH E. C., LENNOX P. G. & OFFLER R. 1995. Devonian - Carboniferous stratigraphy of the southern Hastings Block, New England Orogen, eastern Australia. *Australian Journal of Earth Sciences* **42**, 609-633.

ROBERTS J., LENNOX P. G. & OFFLER R. 1993. The geological development of the Hastings Terrane: Displaced fore-arc fragments of the Tamworth Belt. In FLOOD P. G. & AITCHISON J. C.

eds. New England Orogen, eastern Australia. pp. 231–242. Armidale: Department of Geology and Geophysics, University of New England, Armidale.

ROBERTS J., OFFLER R. & FANNING M. 2006. Carboniferous to Lower Permian stratigraphy of the southern Tamworth Belt, southern New England Orogen, Australia. *Australian Journal of Earth Sciences* **53**, 249-284.

ROBERTS J. J. 2000. Structural evolution of the Taylors Arm Fault System and mesothermal Sb mineralization, Nambucca Block, NSW. BSc Hons Thesis (unpubl.), University of Newcastle, Newcastle.

ROSENBAUM G. 2010. A subduction model for the formation of the New England oroclines. Australian Earth Sciences Convention (AESC). Brisbane: Geological Society of Australian, Earth systems: change, sustainability, vulnerability. Abstracts **98**.

ROSENBAUM G., LI P. & RUBATTO D. 2012. The contorted New England Orogen (eastern Australia): New evidence from U-Pb geochronology of early Permian granitoids. *Tectonics* **31**, doi: 10.1029/2011TC002960.

ROSENBAUM G., UYSAL I. & BABAAHMADI A. 2015. The Red Rock Fault zone (northeast New South Wales): kinematics, timing of deformation and relationships to the New England oroclines. *Australian Journal of Earth Sciences* **62**, 409-423.

SARAPIROME S., SURINKUM A. & SAKSUTTHIPONG P. 2002. Application of DEM Data to Geological Interpretation: Thong Pha Phum Area, Thailand. 23rd Asian Conference on Remote Sensing. Kathmandu, Nepal.

SCHEIBNER E. 1973. A plate tectonic model of the Paleozoic tectonic history of New South Wales. *Journal of the Geological Society of Australia* **20**, 405-426.

SCHMIDT P. W., AUBOURG C., LENNOX P. G. & ROBERTS J. 1994. Palaeomagnetism and tectonic rotation of the Hastings Terrane, eastern Australia. *Australian Journal of Earth Sciences* **41**, 547-560.

SHAANAN U., ROSENBAUM G., LI P. & VASCONCELOS P. 2014. Structural evolution of the early Permian Nambucca Block (New England Orogen, eastern Australia) and implications for oroclinal bending,. *Tectonics* **33**, 1-19.

SHAANAN U., ROSENBAUM G. & WORMALD R. 2015. Provenance of the Early Permian Nambucca block (eastern Australia) and implications for the role of trench retreat in accretionary orogens. *Geological Society of America Bulletin* **127**, 1052-1063.

SHAW S. E. & FLOOD R. H. 2009. Zircon Hf isotopic evidence for mixing of crustal and silicic mantle‐derived magmas in a zoned granite pluton, eastern Australia. *Journal of Petrology* **50**, 147–168.

SHAW S. E., FLOOD R. H. & PEARSON N. J. 2011. The New England Batholith eastern Australia: Evidence of silicic magma mixing from zircon ^{176}Hf/^{177}Hf ratios. *Lithos* **126**, 115–126.

SMALLWOOD J. R. & MARESH J. 2002. The properties, morphology and distribution of igneous sills: modelling, borehole data and 3D seismic from the Faroe-Shetland area. *Geological Society, London, Special Publications* **197**, 271-306.

SPACKMAN J. 1989. Structure and Stratigraphy of the Byabarra district. BSc Hons Thesis (unpubl.), University of New South Wales, Sydney.

SPRAGUE K. B. & DE KEMP E. A. 2005. Interpretive tools for 3-D structural geological modelling part II: surface design from sparse spatial data. *GeoInformatica* **9**, 5-32.

TAYLOR M. A. 1984. Geology of the Middle Devonian to Early Triassic of the Wauchope district,

NSW. BSc Hons Thesis (unpubl.), University of Sydney Sydney.

THOMPSON G. A. 1985. The structure and stratigraphy if the Pappinbarra district, west of Wauchope, NSW. BSc Hons Thesis (unpubl.), University of Sydney, Sydney.

TRAGHEIM D. & WESTHEAD K. 1996. Seeing the lie of the land: digital photogrammetry aids geological mapping. *Mapping Awareness* **10**, 7-34.

TSUTSUMI H., YEATS R. S. & HUFTILE G. J. 2001. Late Cenozoic tectonics of the northern Los Angeles fault system, California. *GSA bulletin* **113**, 454-468.

TWISS R. J. & MOORES E. M. 1992. Structural Geology. W. H. Freeman, New York.

VAN DER PLUIJM B. A., MARSHAK S. & ALLMENDINGER R. W. 2004 Earth structure: an introduction to structural geology and tectonics. WW Norton New York.

VOISEY A. H. 1934. A preliminary account of the geology of the middle North Coast district of New South Wales. *Journal and Proceedings of the Linnean Society of New South Wales* **59**, 333-347.

VOISEY A. H. 1936. The Upper Palaeozoic rocks around Yessabah, near Kempsey, New South Wales. *Journal and Proceedings of the Linnean Society of New South Wales* **70**, 183-204.

WELLMAN P. 1990. A tectonic interpretation of the gravity and magnetic anomalies in southern Queensland. *Australia Bureau Mineral Resources, Geology and Geophysic Bulletin* **232**, 21-34.

WEST J. 1990. A geological investigation of the Kew area, NSW. BSc Hons Thesis (unpubl.), University of New South Wales, Sydney.

WOODWARD N. B., BOYER S. E. & SUPPE J. 1989. Balanced Geological Cross-Sections: An Essential Technique in Geological Research and Exploration,. American Geophysical Union, Washington, D.C. doi: 10.1002/9781118667354.

WU Q., XU H. & ZOU X. 2005. An effective method for 3D geological modeling with multi-source data integration. *Computers & Geosciences* **31**, 35-43.

YAN J., LENNOX P., KELLY B. & OFFLER R. 2014a. Kinematic reconstruction of the Hastings Block, Southern New England Orogen. In FRASER G., FORSTER M. & MCCLUSKY S. eds. Biennial Conference of the Specialist Group for Tectonics and Structural Geology, Snowies. Geological Society of Australia Abstracts **109**, 93.

YAN J., LENNOX P., KELLY B. & OFFLER R. 2014b. Kinematic reconstruction of the Hastings Block, Southern New England Orogen, Australia. In ELGER K., HAUG Ø. T. & RITTER M. C. eds. Proceedings of GeoMod2014-Modelling in Geosciences: Programme and Extended Abstracts. pp. 153-158. Potsdam: GFZ German Research Centre for Geosciences.

YAN J., LENNOX P., KELLY B. & OFFLER R. 2014c. Kinematic reconstruction of the Hastings Block, Southern New England Orogen. *Geological Society of Australia Abstracts* **110**, 01DPB2-03. Australian Earth Sciences Convention 2014. Newcastle, NSW.

YAN J., LENNOX P., KELLY B. & OFFLER R. 2015. Kinematic reconstruction of the Hastings Block, Southern New England Orogen, Australia. ASEG-PESA 2015. pp. 1-4. Perth.

YAN J., LENNOX P. & OFFLER R. 2012. Does the Manning Orocline exist? 34th International Geological Congress, Brisbane.

ZANCHI A., FRANCESCA S., STEFANO Z., SIMONE S. & GRAZIANO G. 2009. 3D reconstruction of complex geological bodies: Examples from the Alps. *Computers & Geosciences* **35**, 49-69.

ZIZIOLI D. 2008. DEM-based morphotectonics analysis of Western Ligurian Alps. *Scientifica Acta* **2**, 44 – 47.

Appendices

Appendix 1: Analysis of uncontoured and contoured stereographic projections of poles to bedding within individual fault blocks in the NHB.

Fault Block A – The bedding dips predominantly steeply southwest ($76^{o} \rightarrow 218^{o}$). This is the opposite for bedding that expected in the Parrabel Dome in this position.

Fault Block B –The overall derived fold axis is $8^{o} \rightarrow 356^{o}$. It includes a population of poles on the westside of the plot which indicate a gently east-dipping derived fold in this area. This fold probably reflects the overall tight folding bending of the bedding in Block B proposed by Jeffery (1986).

Fault Block C – The scattering of bedding poles in five population reflects the observed mesoscopic folding in this block. This includes tight NE-plunging folds, tight NNE or SSW plunging folds and a population defining a plane dipping steeply almost westward. These NE or NNE-plunging folds may reflect F_4 folding in the dome.

The poles to bedding plots in Fault Block D and Fault Block E are consistent with their position in the dome.

Fault Block F – The derived fold axis is not as expected because the population of poles on the western side of the plot represent poles from Majors Creek Formation and should probably better be assigned to Block E. If the dominant population of poles is used then a derived fold axis plunging moderately to the WSW would be expected (? $50^{o} \rightarrow 250^{o}$) reflecting the bending observed from Bourke's (1971) map of this district.

Fault Block G –This is within bedding data in the Threadneedle Fault Complex which is a fault-bound area which consists of smaller slivers of different units variously oriented with respect to the bounding faults (Bourke 1971). The derived fold axis does not represent anything meaningful because of the disrupted character of the fault slivers in this subarea.

Fault Block H – This is bedding data from the Birdwood Fault Complex, a fault-bound section of dominantly east-west bedding which shows evidence from the field data of being mesoscopically folded. The derived fold axis 56 ^{o} → 046 ^{o} is parallel to the F_4 folds across the NHB. The average bedding 62 ^{o} → 008 ^{o} faithfully reflects the overall bedding orientation in this block.

Fault Block I – The derived fold axis 52° → 160° in these Devonian-Carboniferous rocks and is parallel to the D3 folding which indicates that despite being nominally in the SHB it contains evidence of the Parrabel Dome forming event.

Fault Block J – The derived fold axis is very similar to the D3 folding and the low plunge reflects the almost flat section of the Parrabel Dome in this block.

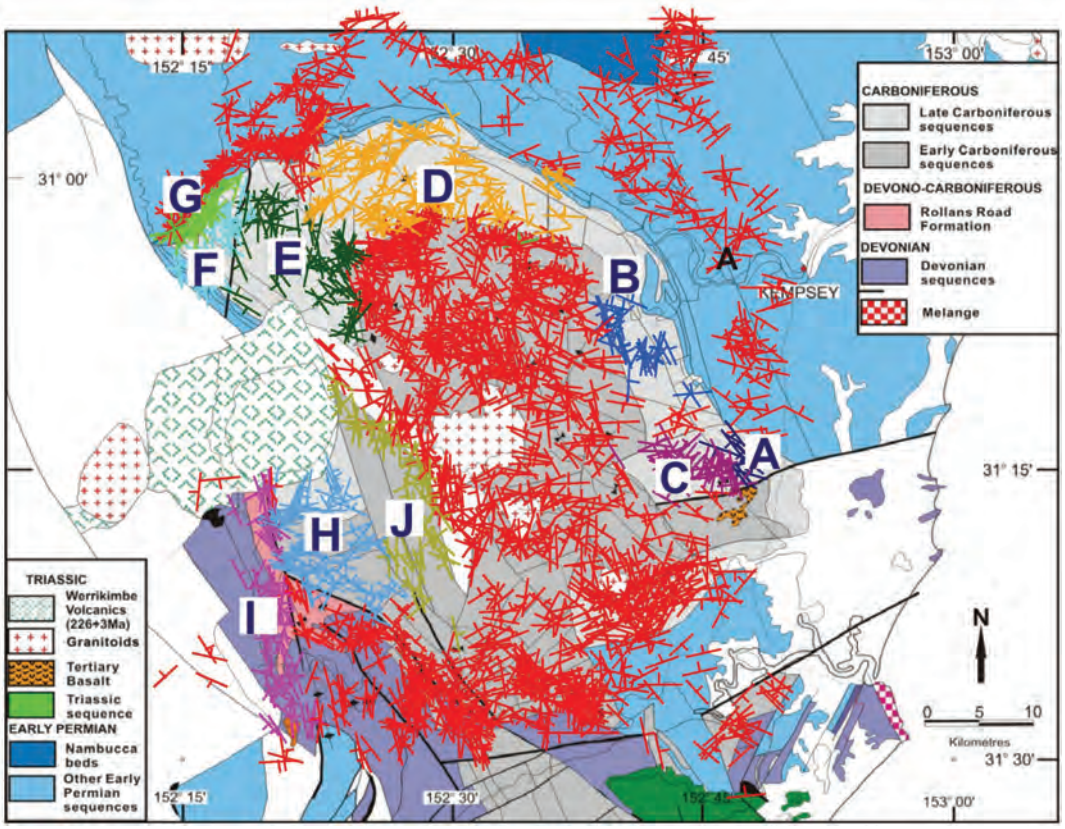

Figure A1: The simplified geology map with the bedding readings within fault blocks A-J in the NHB. The extensive bedding database and the scale of this map means many bedding symbols are overlapping. Clearer maps showing all bedding symbols are provided in Figures A6 to A16 below.

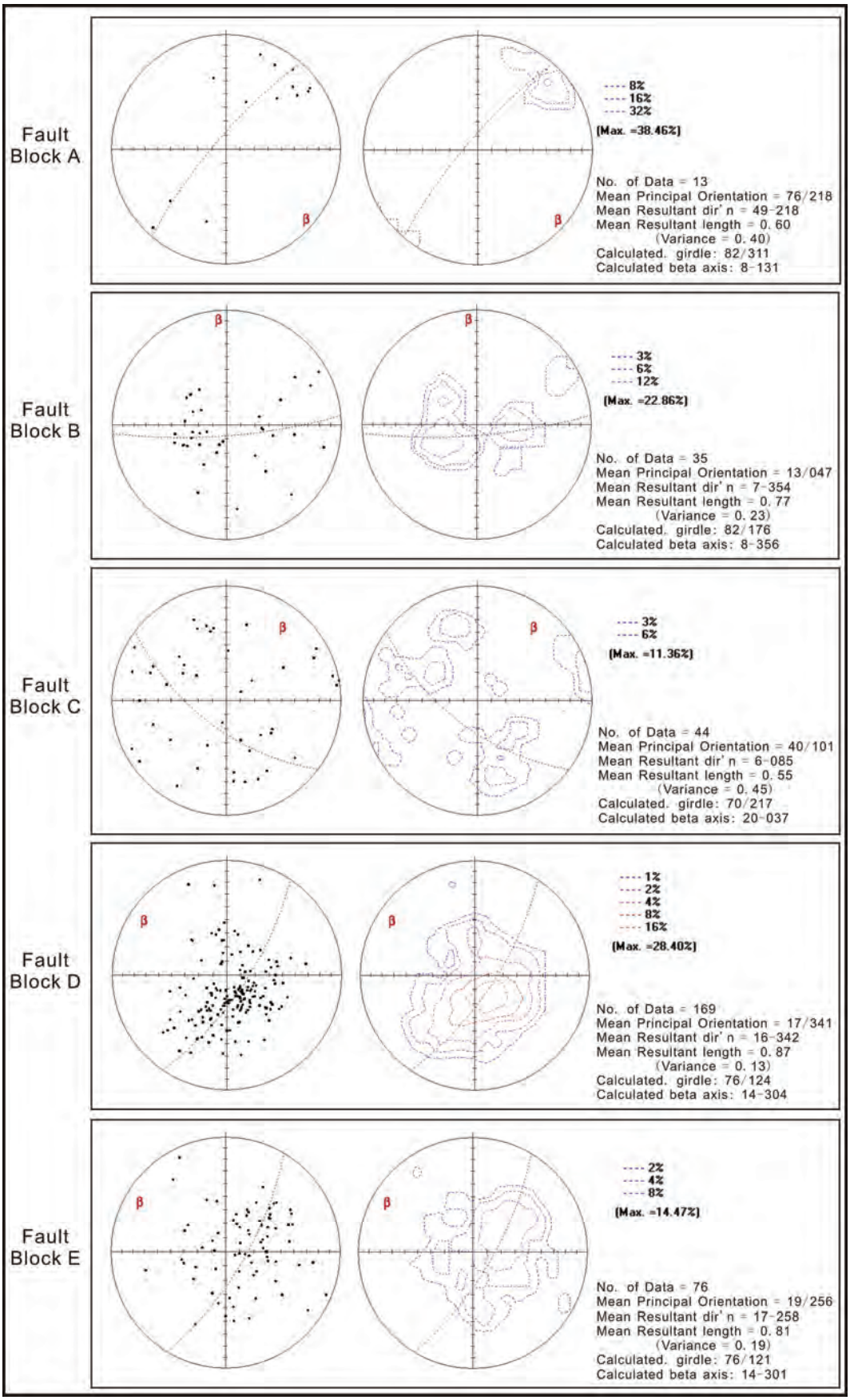

Figure A2: Uncontoured and contoured stereographic projections of poles to bedding divided according the fault blocks A-E in Figure A1.

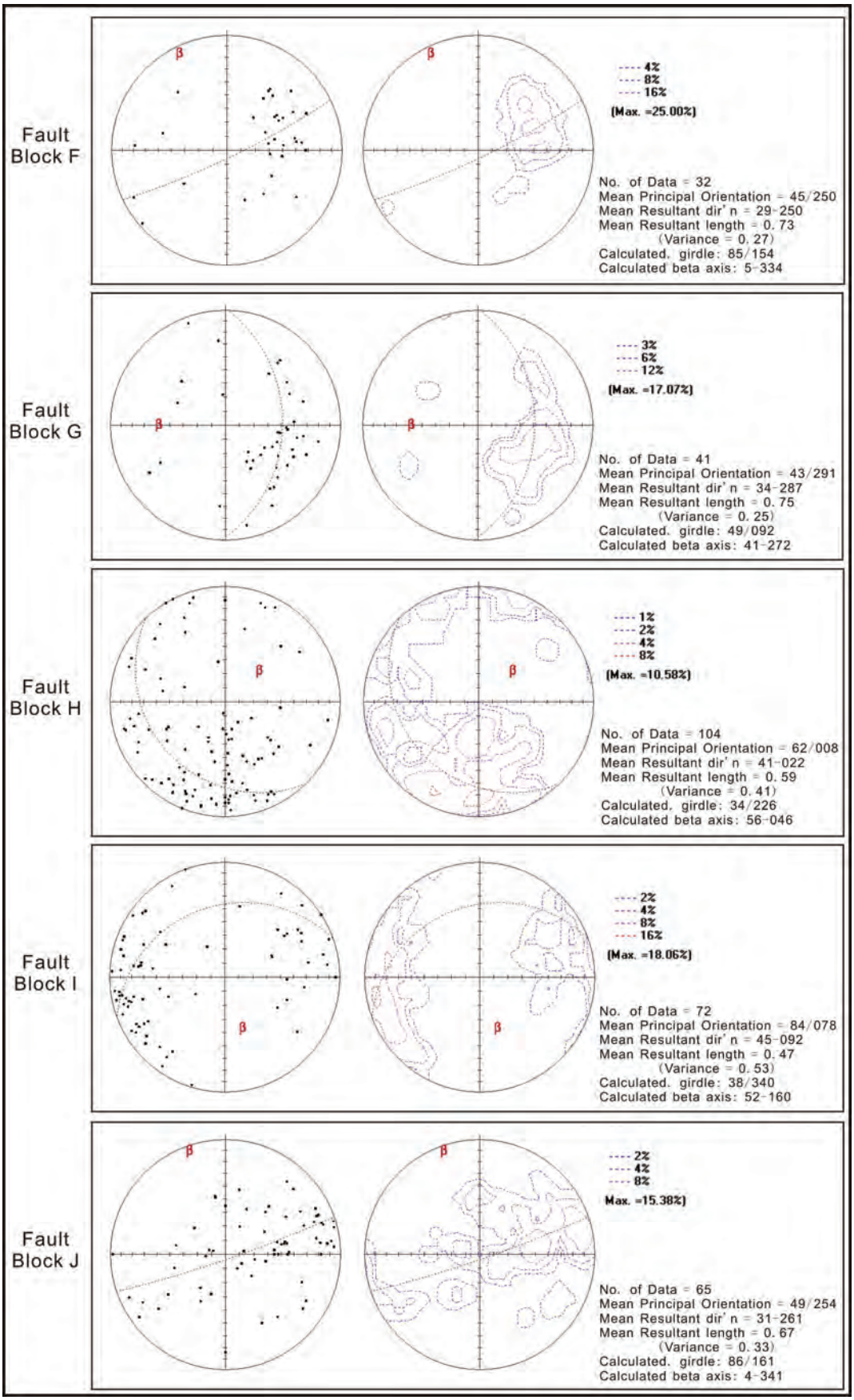

Figure A3: Uncontoured and contoured stereographic projections of poles to bedding divided according the fault blocks F-J in Figure A1.

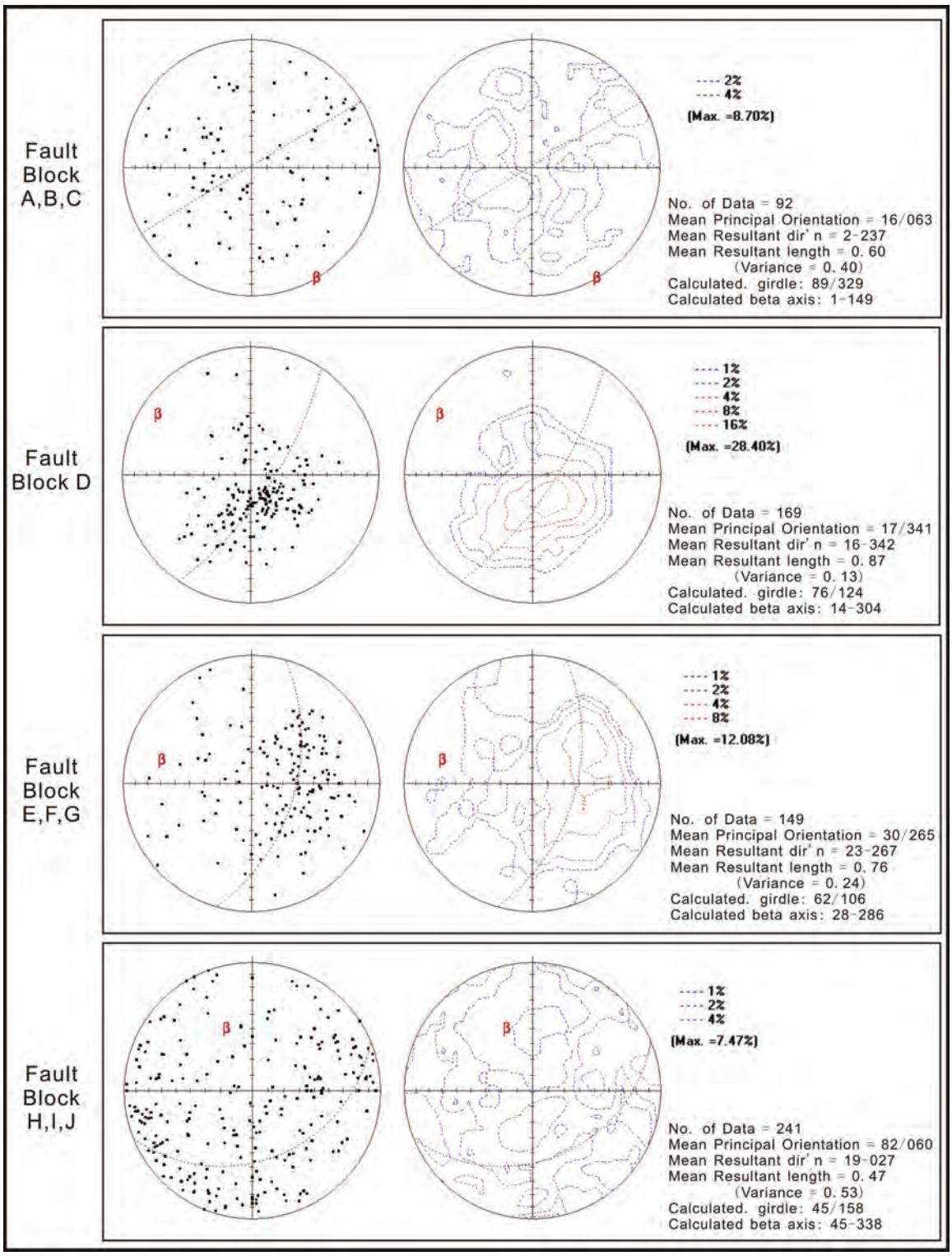

Figure A4: Uncontoured and contoured stereographic projections of poles to bedding divided according the fault blocks groups in Figure A1.

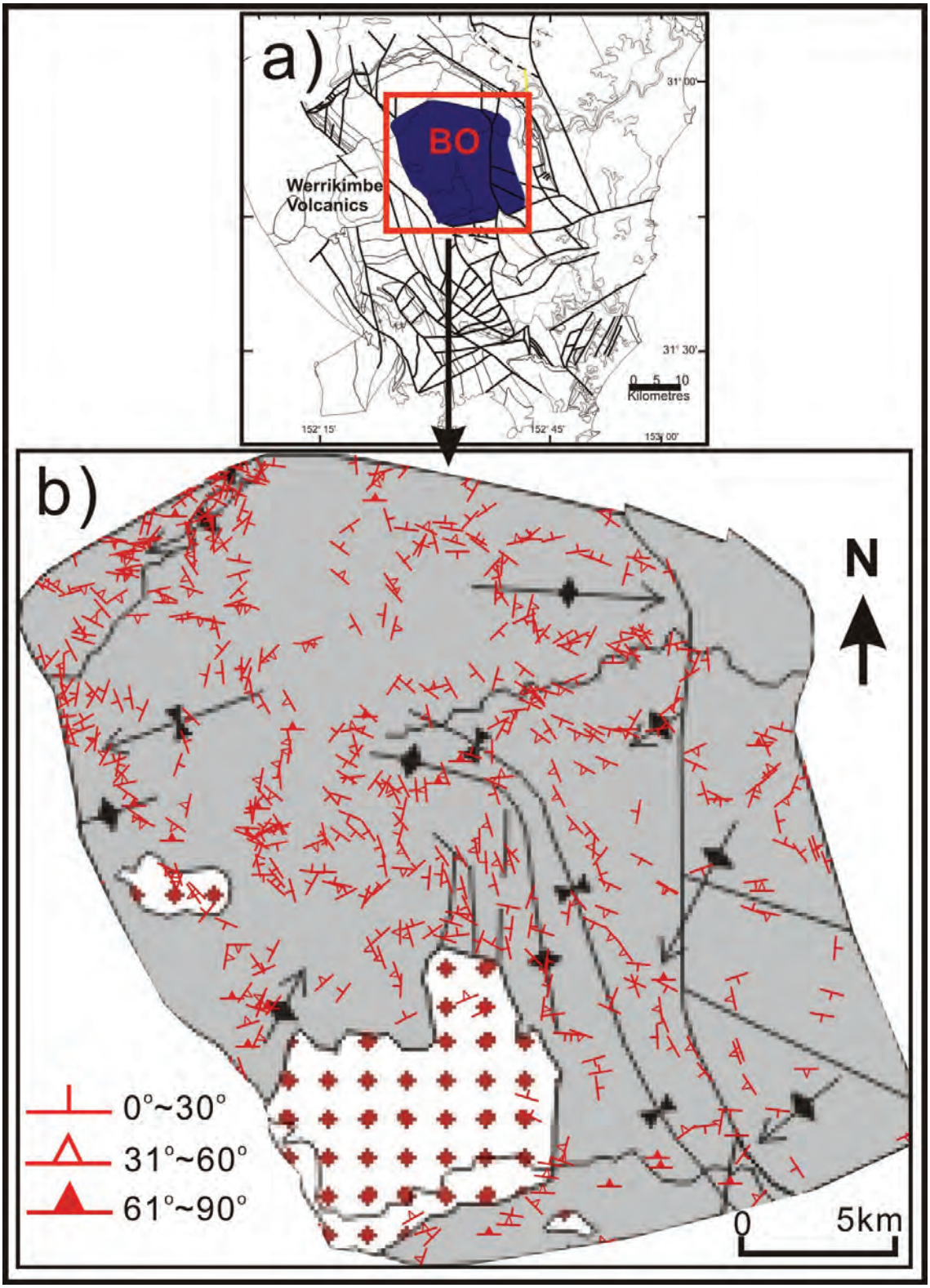

Figure A5: Enlarged subarea BO in Figure 3.6 to better show the bedding symbols pattern in the Early Carboniferous Boonanghi Beds: a) location of the Subarea BO in the NHB; b) bedding readings with the strike and dip information within the subarea. Notice the pattern suggests domes and basins indicating fold interference between ? D1 (east-west) and D3 (northwest-southeast) macroscopic folds (Chapter 3).

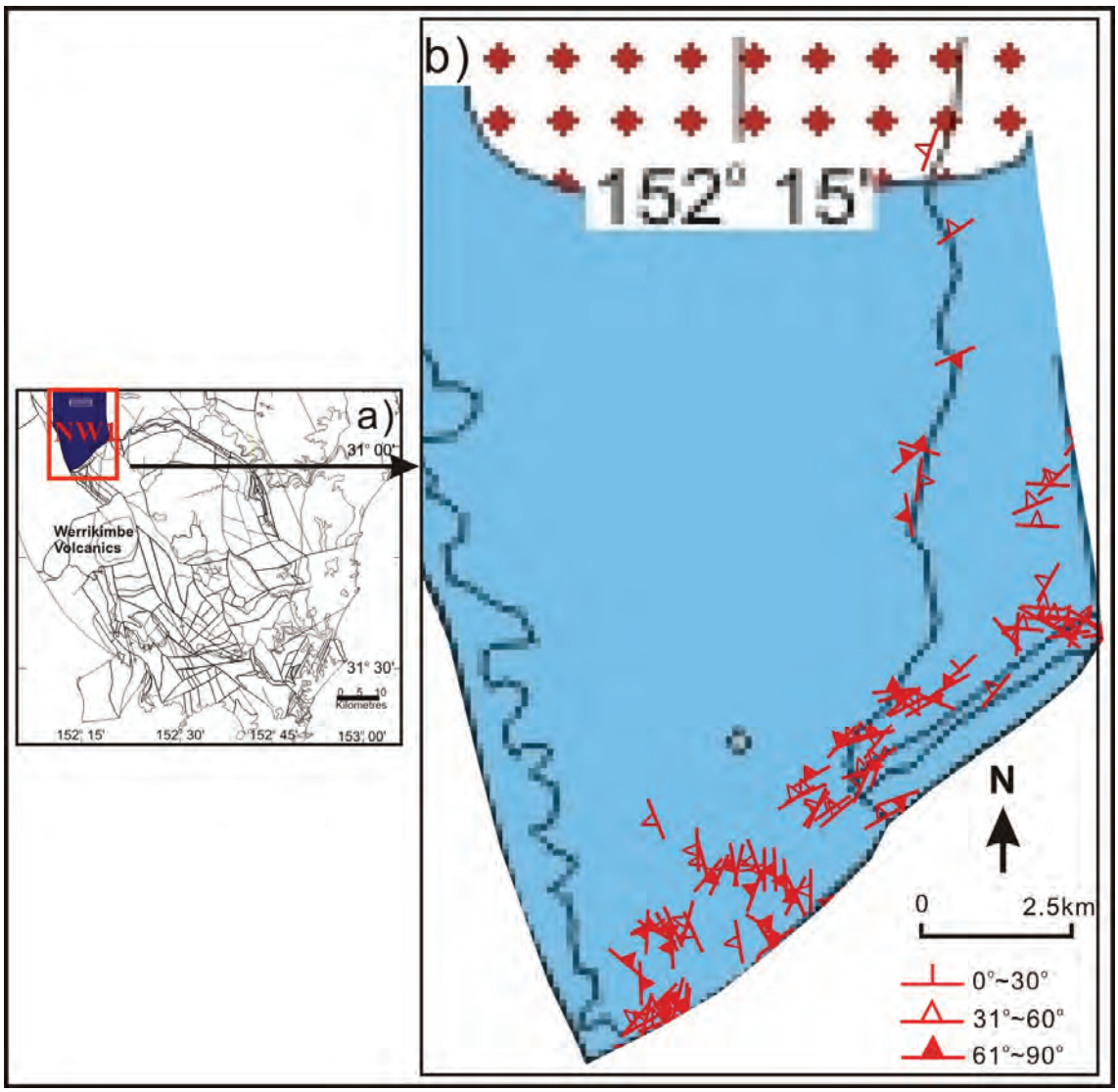

Figure A6: Subarea NW1 consisting mainly of Permian Parrabel Beds adjacent to the Threadneedle Fault Complex in Figure 3.6: a) location of the Subarea NW1 in the NHB; b) bedding readings with the strike and dip information within the subarea. Most readings are consistent with its position on the Parrabel Dome.

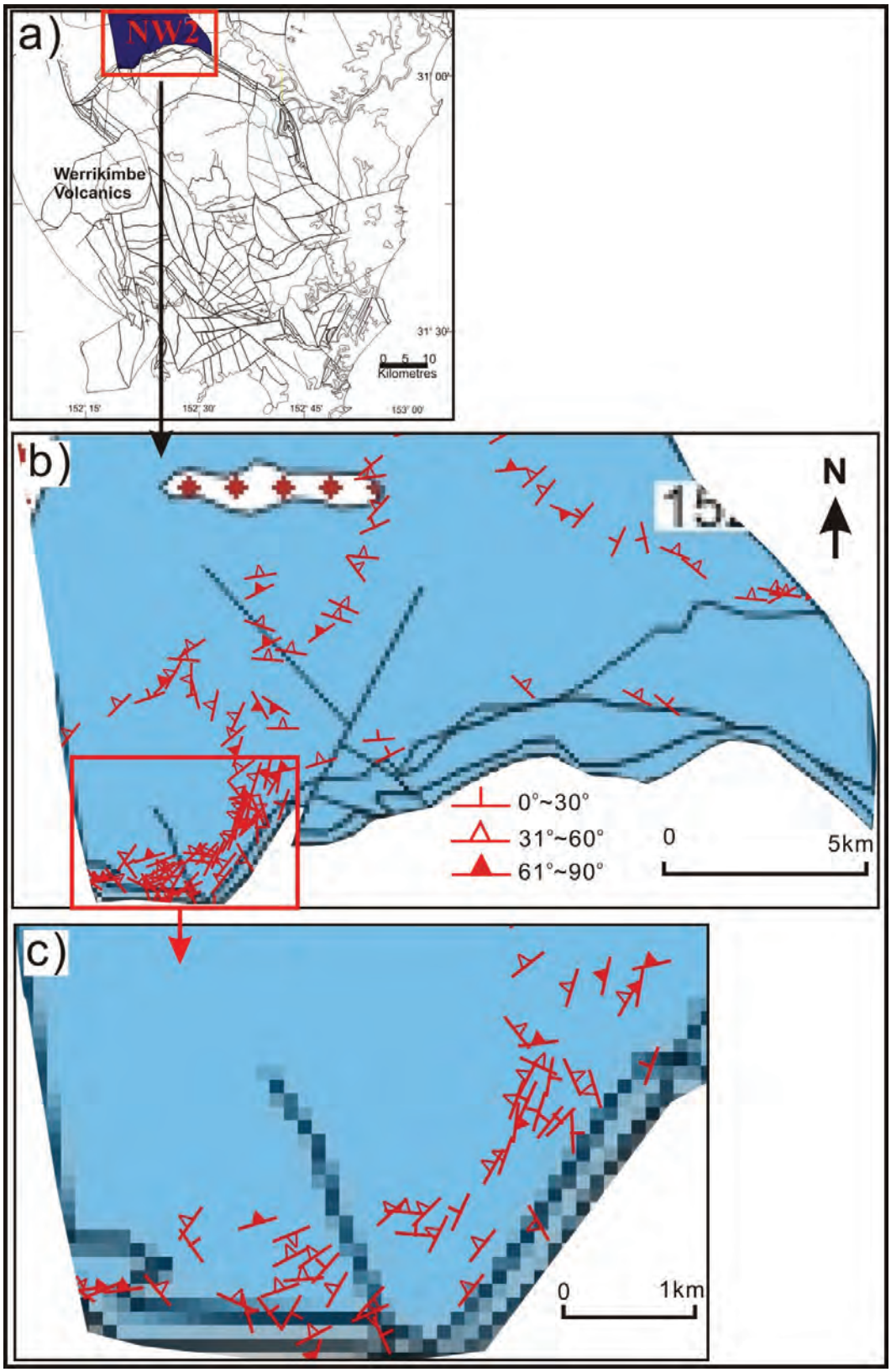

Figure A7: Subarea NW2 in Permian Warbro Formation or Parrabel Beds from Figure 3.6: a) location of the Subarea NW2 in the NHB; b) bedding readings with the strike and dip information within the subarea. Grossly the bedding pattern is consistent with this blocks position on the Parrabel Dome.

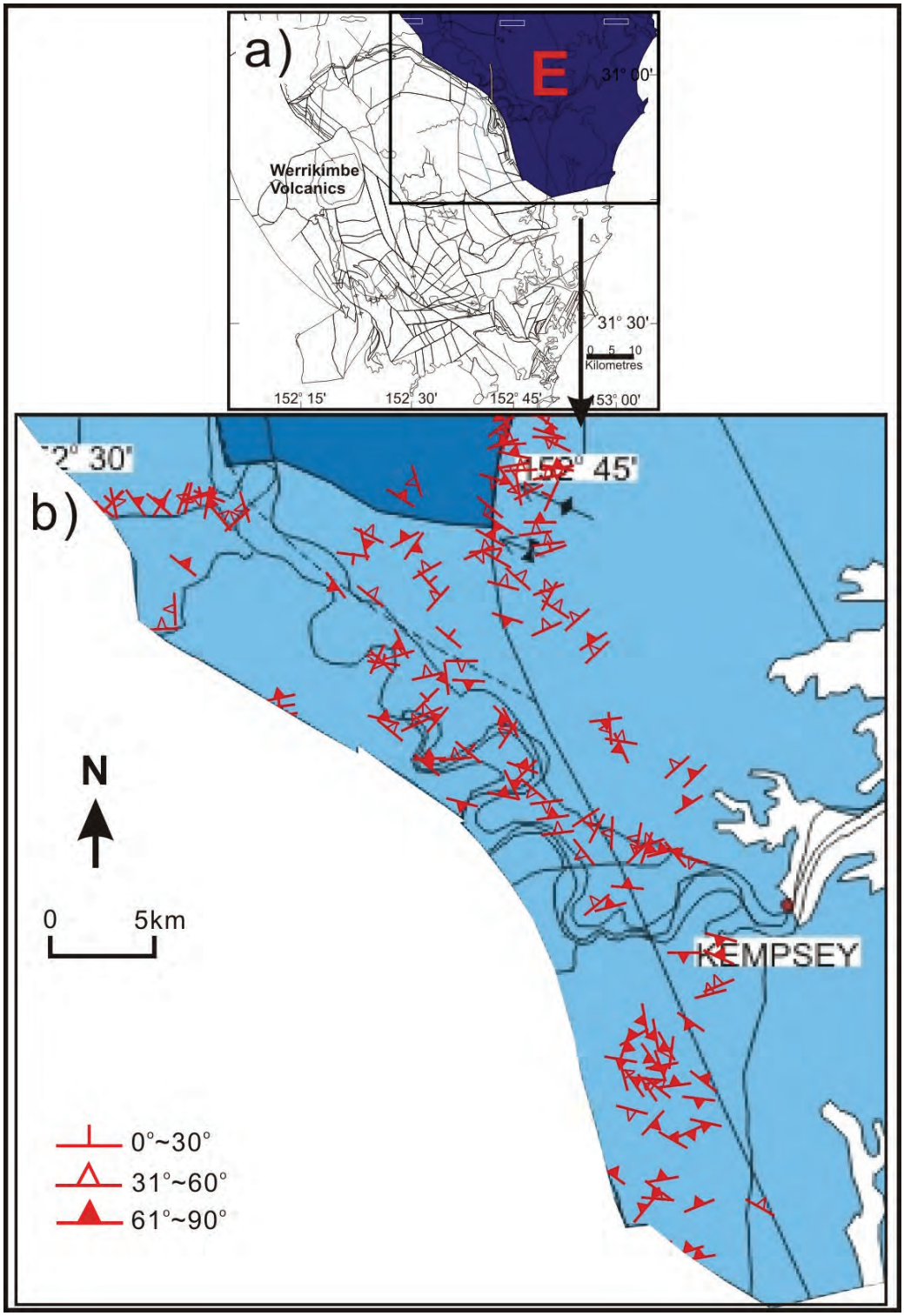

Figure A8: Subarea E within the Kempsey Beds (light blue) and Nambucca Beds (dark blue) on Figure 3.6: a) location of the Subarea E in the NHB; b) bedding readings with the strike and dip information within the subarea. The gross pattern is consistent with the Parrabel Dome but there is some significant bending of the bedding indicating apparent wrapping of initially east-west trending D1 structures around the D3 megafold.

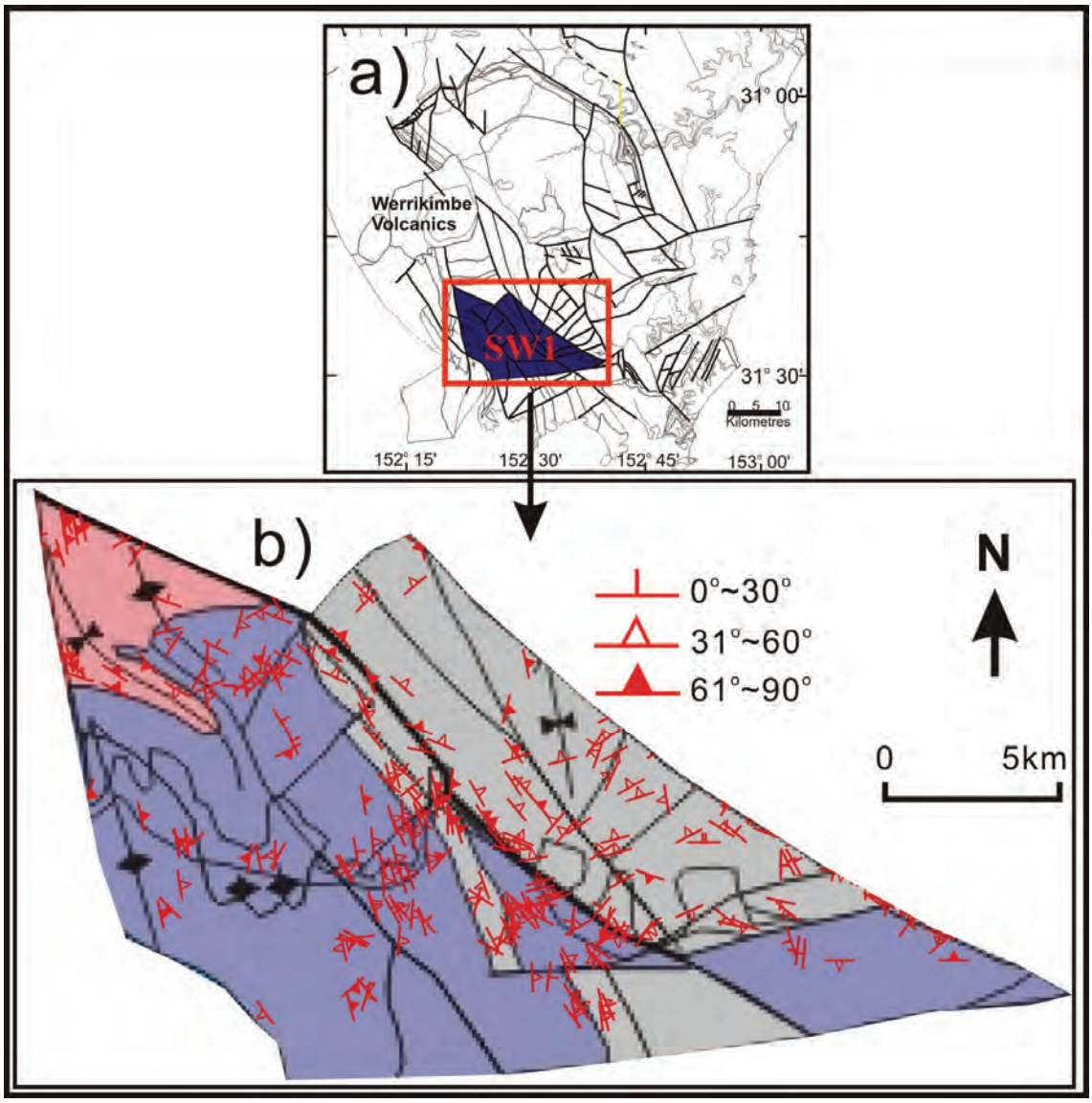

Figure A9: Subarea SW1 within mainly Devonian (purple) – Devono-Carboniferous (pink) and Early Carboniferous (light grey) sequences on Figure 3.6: a) location of the Subarea SW1 in the NHB; b) bedding readings with the strike and dip information within the subarea. Most bedding readings are broadly consistent with the Roberts et al. (1995) as shown underneath although there are some bedding readings oriented oblique to the fault block boundaries in the center of the map. There is extensive fault disruption in this region bordering the Yarras Fault complex and the bedding orientations reflect this disruption.

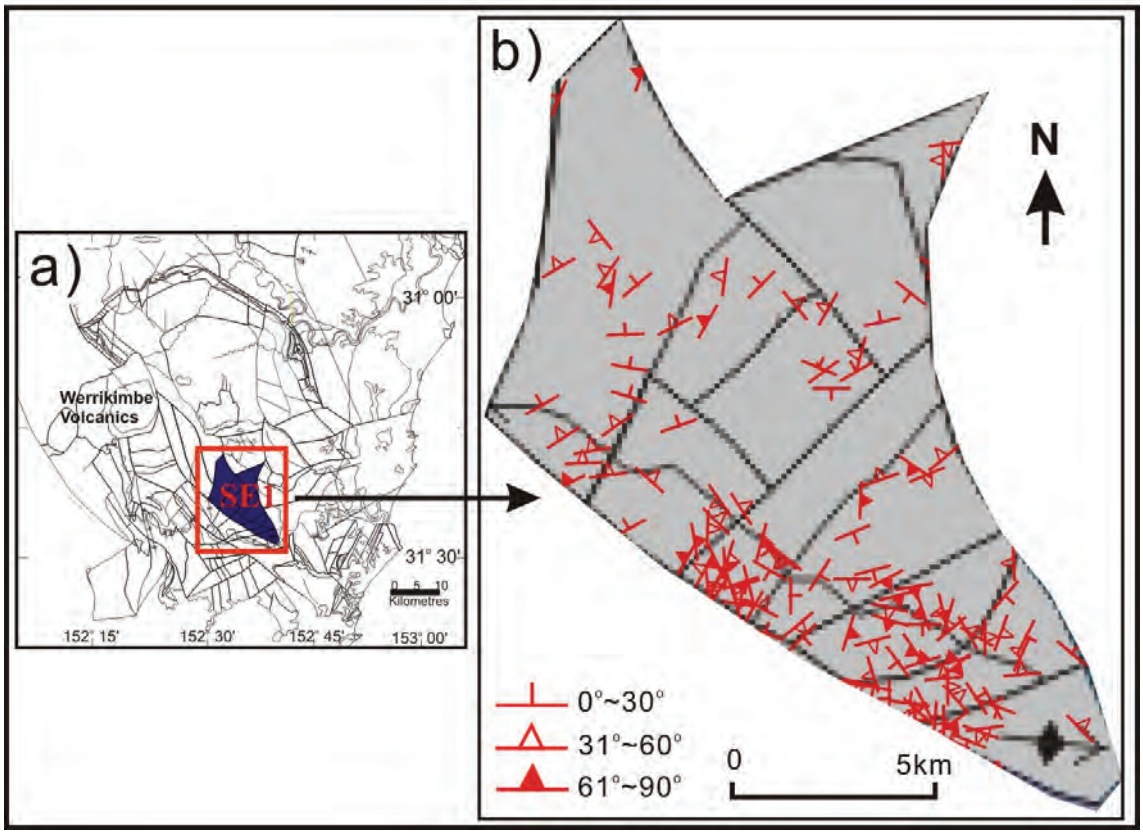

Figure A10: Subarea SE1 within the Early Carboniferous sequences on the southern margins of the Parrabel Dome onFigure 3.6: a) location of the Subarea SE1 in the NHB; b) bedding readings with the strike and dip information within the subarea. The bedding is not consistent with the position on the dome as it should dip away form the dome if the dome was undeformed. The bedding pattern reflects major changes due to ? synform megafold development (NE-SW, D4) on this part of the dome and ? fault block disruption after folding as the HB accommodated squeezing from the HBO.

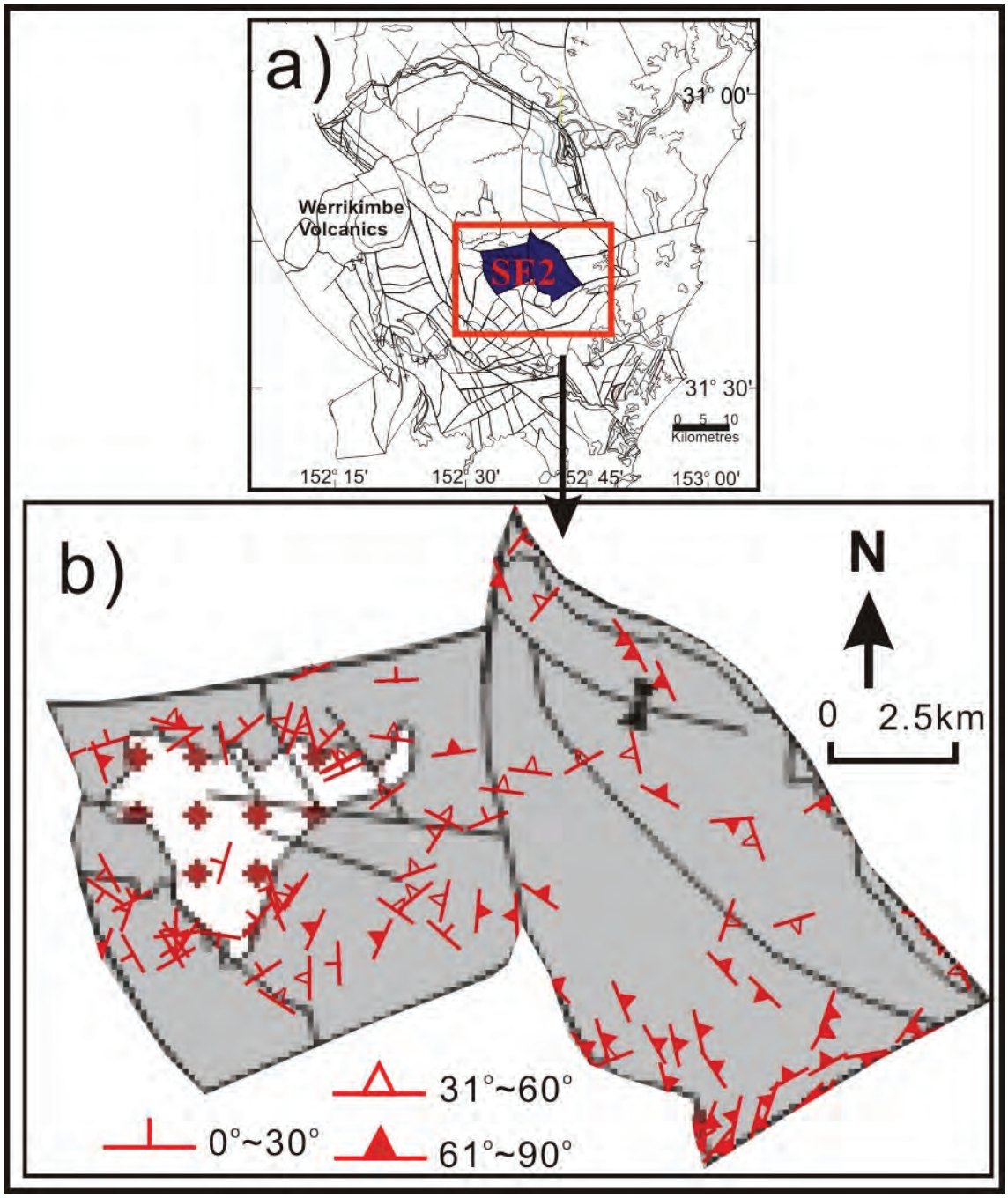

Figure A11: Subarea SE2 within Early Carboniferous sequences southeast of the Parrabel Dome on Figure 3.6: a) location of the Subarea SE2 in the NHB; b) bedding readings with the strike and dip information within the subarea. There appears to be a number of dome and basin strcutres with the Triassic Gundle Granite filling one dome. Some bedding appears to be re-oriented into parallelism with the faults such as along the southeastern margin of this block.

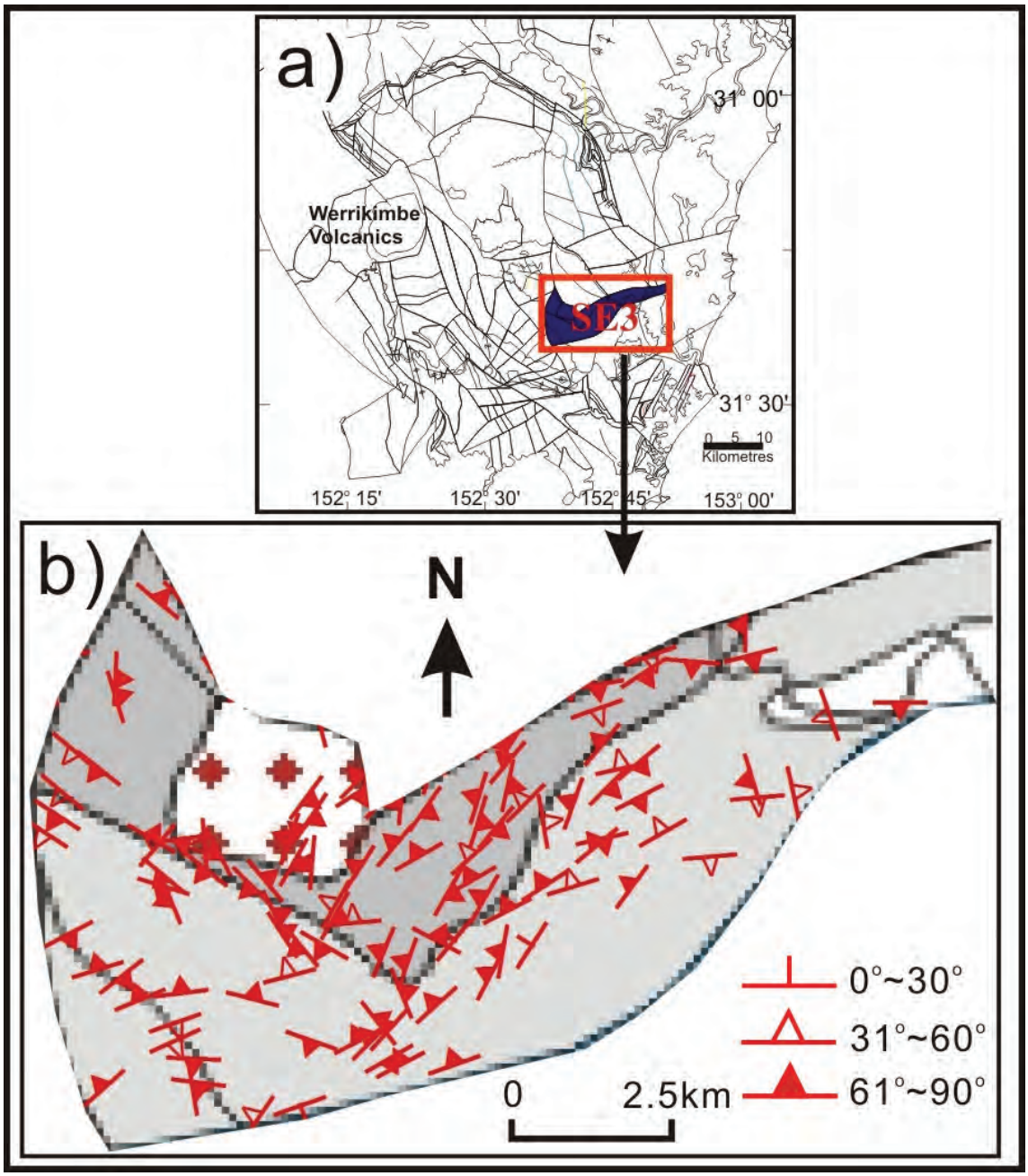

Figure A12: Subarea SE3 within Early Carboniferous sequences on Figure 3.6: a) Location of the Subarea SE3 in the NHB; b) bedding readings with the strike and dip information within the subarea.

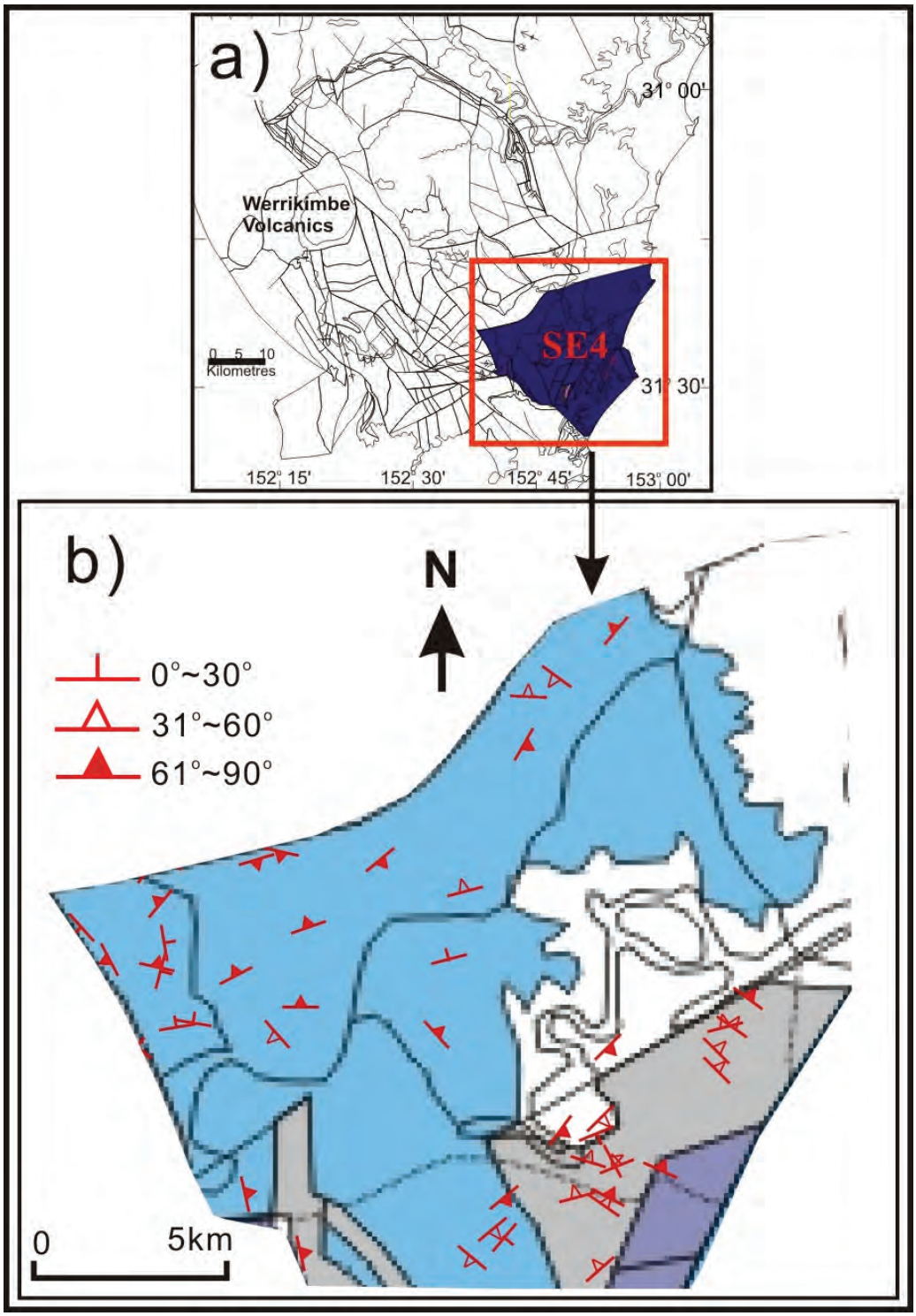

Figure A13: Subarea SE4 within Early Permian Beechwood Beds (light blue), Carboniferous Mingaletta Formation (grey) and Devonian Touchwood Formation (purple) on the boundary with the Port Macquarie Block (white in the southeastern corner) from Figure 3.6: a) location of the Subarea SE4 in the NHB; b) bedding readings with the strike and dip information within the subarea. The Beechwood Beds strike mainly northeast-southwest and dip northwest consistent with the megasynform to the northwest of this block.

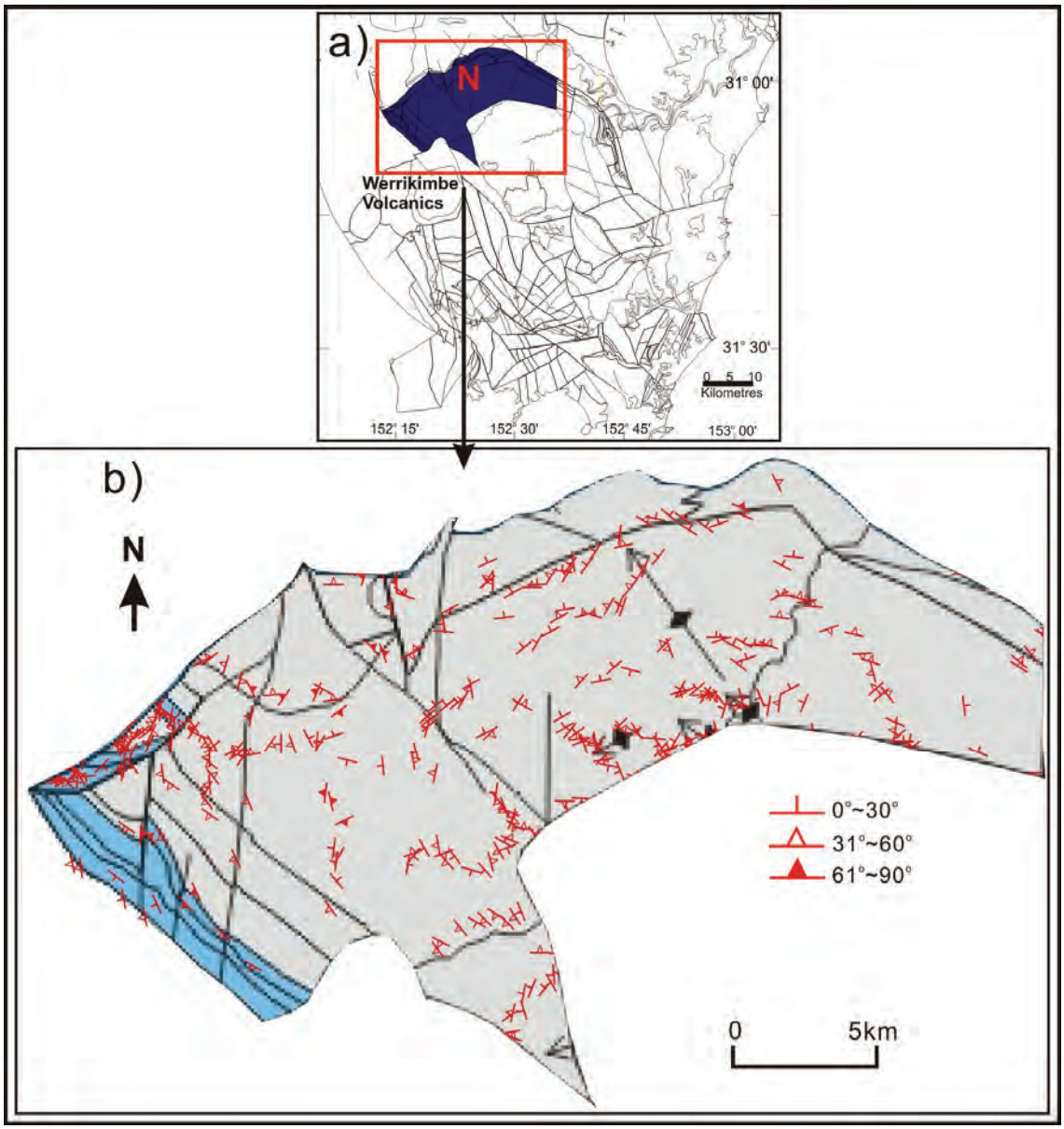

Figure A14: Subarea N mainly within Carboniferous Majors Creek Formation and overlying Kullatine Formation/Youdale C (grey) and overlying Permian Yesabah Limestone/Warbro Formation (NW light blue) from Figure 3.9: a) location of the Subarea N in the NHB; b) bedding readings with the strike and dip information within the subarea. The northwest margin of the Parrabel Dome is well defined by these bedding readings. The dome is rather box-like with two axial surfaces; one in the northwest plunging more northwest and the other in the northeast plunging more northerly.

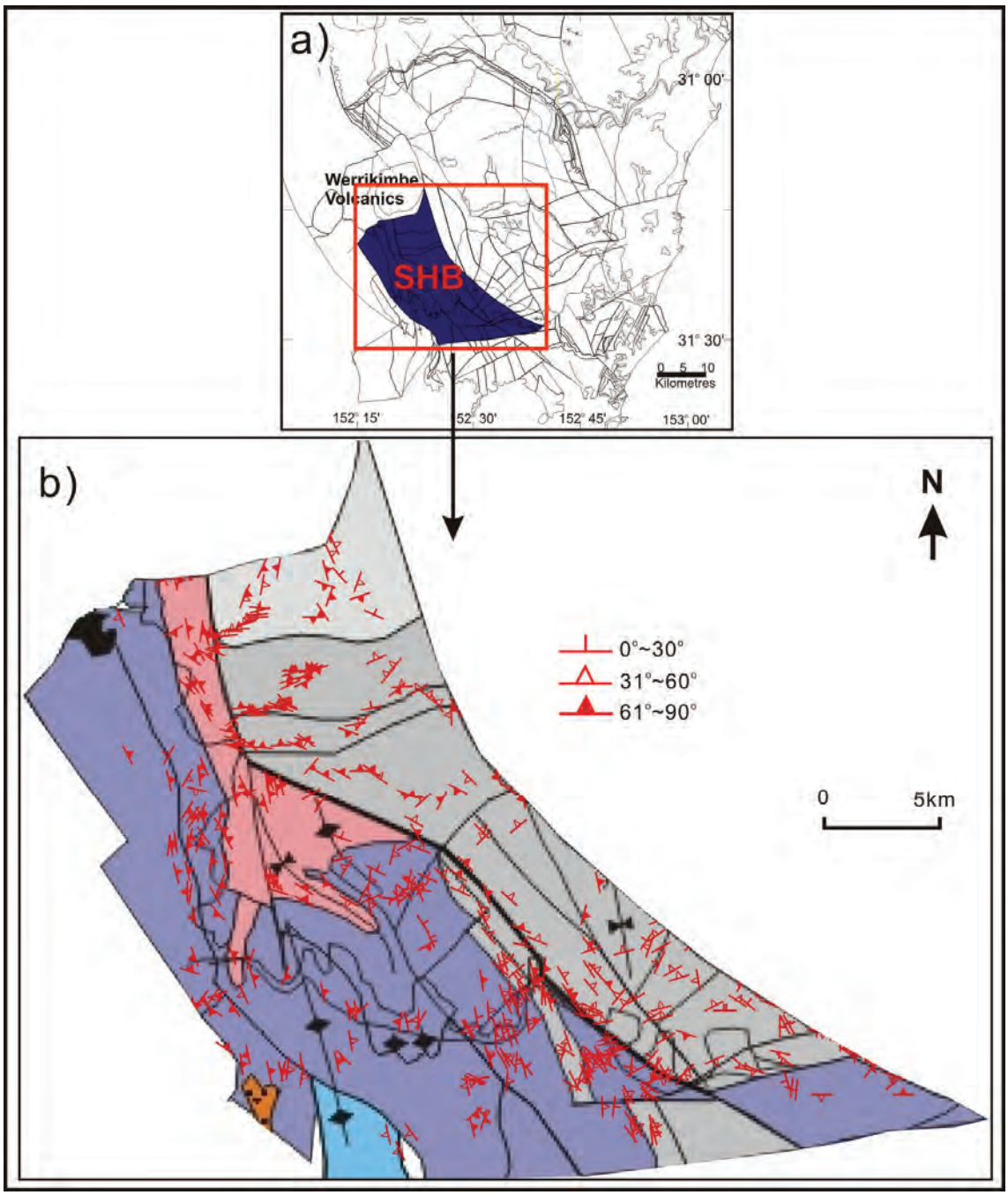

Figure A15: Subarea SHB on the western margin of the block with the Yarras complex west of this block from Figure 3.9: a) location of the Subarea SHB; b) bedding readings with the strike and dip information within the subarea. This subarea consists of Devonian sequences (purple), Devono-Carboniferous (pink) and Early Carboniferous (dark grey) and Later Carboniferous Mingaletta Formation (light grey). This subarea has been affected by fault movement along the major Bagnoo-Rollans Road fault shown as a heavy black line on this map. The visible megascopic folding in this subarea may be related to the same stress field which caused movement along the faults.

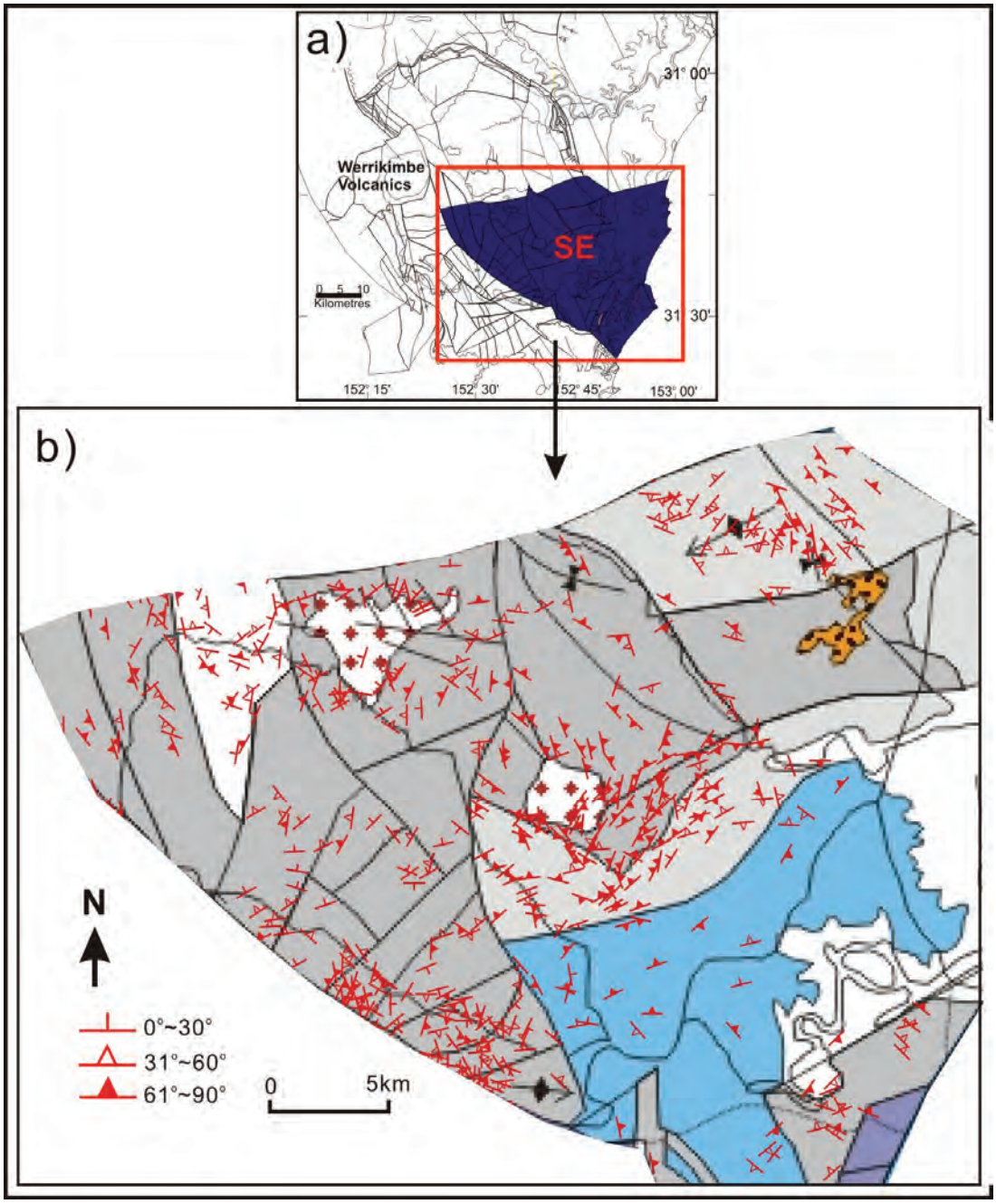

Figure A16: Subarea SE within Permian (blue), Early Carboniferous (dark grey) and Late Carboniferous (light grey) and undifferentiated rocks (white section with bedding in the northwest corner of the map) from Figure 3.9: a) location of the Subarea SE; b) bedding readings with the strike and dip information within the subarea. The square-shaped Cairncross granite seems to intrude a dome within the early Carboniferous, whilst the irregular shaped Gundle Granite seems to fit within a less well defined dome. This subarea lies on the margins of the Parrabel Dome but within the hinge-zone of the northeast-plunging, D4 synform which passes through Kempsey township. The bedding reflects the influence of the dome and this synform.

Appendix 2: Table A1: The key differences between the NHB and SHB using structural style, structural history and pre-Permian stratigraphy. The boundary between the blocks is taken from the Roberts et al. (1995) map, although it is now clear this is not as clear cut from research discussed in this thesis. The dominant faulting pattern is derived from Roberts *et al.* (1993). It is clear from this thesis that not all NW-SE faults formed at the same time as proposed by Roberts *et al.* (1993).

	Northern Hastings Block	Southern Hastings Block
Folding events	4	2
	D_1: E-W, D_2: N-S, D_3: NW-SE, D_4: NE-SW	D_1: N-S, D_2: NW-SE
Major Structural grain	Northwesterly trending	North-south trending
Dominant Faulting (F_x)	F_a: NW-SE, F_b: NE-SW, F_c: N-S to NNW-SSE	NW-SE, N-S
Pre-Permian stratigraphy	Early to Late Carboniferous	Middle Devonian to Late Carboniferous
Age of deformation	Nambucca Block (275-265 Ma). (Shaanan *et al*. 2014)	Same as that in Tamworth Belt (prior to 269 Ma). (Roberts *et al*. 1993)

Appendix 3: Table A2 – Characteristics of faulting in the NHB from analysis of the literature, unpublished studies by Lennox and Offler and the various honours theses completed in the area. The timing evidence is based on the time scale in Glen and Roberts (2012). Major faults are shown in bold print.

Fault	Earliest time faulting could have started		Cessation of faulting		Apparent sense of movement	Evidence	Relationships to the folding and cleavages	Orientation (°)	Length (km)	Description	Comment
	Time	Evidence	Time	Evidence			NB=Nambucca				
1 Kunderang Fault	Kungurian, Glen & Roberts(2012) Fig.2	the youngest rock cut by fault is Warbro Fm/Parrabel Beds	Triassic	cut by Triassic Granitoids	dextral strike slip	Drag effect of bedding cut by the fault	cut F5 and F1 in the NB, NE cleavage	147	33.8		Bourke, 1971
2 Surveyors Fault	Kungurian, Glen & Roberts(2012) Fig.2	the youngest rock cut by fault is Warbro Fm/Parrabel Beds		cut by 1 & 6	sinistral movement	fault displace Youdale Fm	cut NE cleavage	7	5.9		
3 Kennys Fault	Kungurian, Glen & Roberts(2012) Fig.2	the youngest rock cut by fault is Warbro Fm/Parrabel Beds		cut by 1			cut NE cleavage	9	3.4		
4 Mooraback Fault	Kungurian, Glen & Roberts(2012) Fig.2	the youngest rock cut by fault is Warbro Fm/Parrabel Beds		cut by 1 & 5	sinistral movement	fault displace Youdale Fm	cut cleavage	7	14.7		Mikel 1985
5 Threadneedle Fault	Kungurian, Glen & Roberts(2012) Fig.2	the youngest rock cut by fault is Warbro Fm/Parrabel Beds		cut by 1 & 7	dextral strike-slip movement	dextrally displaced the Limestone	cut F5 in the NB and NW cleavage	50	13.3		Bourke, 1971
6	Kungurian, Glen & Roberts(2012) Fig.2	the youngest rock cut by fault is Warbro Fm/Parrabel Beds		cut by 1 & 4	dextral strike-slip movement	dextrally displaced the Limestone	cut NE cleavage	59	10.9		Bourke, 1971
7	Kungurian, Glen & Roberts(2012) Fig.2	the youngest rock cut by fault is Warbro Fm/Parrabel Beds		7 is after fault 8 as it cuts fault 8			cut NE and E-W cleavage	134-171	16.5		
8	Kungurian, Glen & Roberts(2012) Fig.2	the youngest rock cut by fault is Warbro Fm/Parrabel Beds		cut by 7	dextral movement	fault displaces Youdale Fm	cut F1 in the NB and NE cleavage	166	7.1		
9	Namurian,Serpukhovian, Glen & Roberts(2012) Fig.2	the youngest rock cut by fault is Major creek Fm	Kungurian, Glen & Roberts(2012)	cut by 7			cut NE fold	134	4.6		
10	Namurian,Serpukhovian, Glen & Roberts(2012) Fig.2	the youngest rock cut by fault is Major creek Fm					cut NE fold and NW cleavage?	1	4.6		
11	Kungurian, Glen & Roberts(2012) Fig.2	the youngest rock cut by fault is Warbro Fm	Kungurian	cut by 14			cut cleavage	108	4.8		
12	Kungurian, Glen & Roberts(2012) Fig.2	the youngest rock cut by fault is Warbro Fm/Parrabel Beds		cut by 14			cut cleavage	127	3.2		
13	Kungurian, Glen & Roberts(2012) Fig.2	the youngest rock cut by fault is Warbro Fm/Parrabel Beds		cut by 14			cut F1 and NE	140	5.8		
14	Kungurian, Glen & Roberts(2012) Fig.2	the youngest rock cut by fault is Warbro Fm/Parrabel Beds		cut by 7	dextral movement, assuming faults 12 and 13 were once one fault 430m	fault displace 12 & 13	cut F5 and NE and NW cleavage	3–28	14.7		
15	Kungurian, Glen & Roberts(2012) Fig.2	the youngest rock cut by fault is Warbro Fm/Parrabel Beds		cut by 16			cut F1 and NW CLE	170	5.2		
16 Parrabel Fault	Kungurian, Glen & Roberts(2012) Fig.2	the youngest rock cut by fault is Warbro Fm/Parrabel Beds/Kempsey Beds		cut by 18	dextral strike-slip movement	stratigraphic separation along the fault	cut F1 and NW cleavage	122	21.5		Lindsay 1969; Offler and Lennox unpubl. data
17	Artinskian,Glen & Roberts(2012) Fig.2	the youngest rock cut by fault is Yesabah Limestone		cut by 35			Cut NE, NW and EW fold and NE cleavage	1,136,1, 140	41.2		
18	Kungurian, Glen & Roberts(2012) Fig.2	the youngest rock cut by fault is Warbro Fm/Parrabel Beds		cut by 17?????	sinistral movement	fault displace 16 & 19	Cut EW fold and NW cleavage	10	9.3		
19	Kungurian, Glen & Roberts(2012) Fig.2	the youngest rock cut by fault is Warbro Fm/Parrabel Beds		cut by 18			cut NW and EW cleavage	125	5.7		
20	Kungurian, Glen & Roberts(2012) Fig.2	the youngest rock cut by fault is Warbro Fm/Parrabel Beds		cut by 32			cut NW and EW cleavage	144-166	20.3		
21	post 233 Ma	extensions of Demon Fault		cut by 23			cut F1 and NW and EW cleavage	148-123	20.3	extensions of Demon Fault	Leitch 1978; Roberts *et al*. 1993

Fault	Earliest time faulting could have started		Cessation of faulting		Apparent sense of movement	Evidence	Relationships to the folding and cleavages	Orientation (°)	Length (km)	Description	Comment
	Time	Evidence	Time	Evidence			NB=Nambucca				
22	post 233 Ma	extensions of Demon Fault:		cut by 21 & 23			cut NW fold and NW cleavage	106	13	extensions of Demon Fault	Leitch 1978; Roberts *et al*. 1993
23 Taylors Arm Fault system	post D2 prior to NE-trending Faults(prior to 230-220ma)	extensions of Demon Fault		cut by 25	3-5km dexitral movement		cut F1 in the NB and NW and EW cleavage	155	44.1/>30km	extensions of Demon Fault	Leitch 1978; Roberts *et al*. 1993
24	Sakmarian,Early Permian, G&R(2012) Fig.2	the youngest rock cut by fault is Kempsey beds		cut by 25				124	7		
25 Mingaletta Fault	Sakmarian,Early Permian, G&R(2012) Fig.2	the youngest rock cut by fault is Kempsey Beds		cut by 17	dextral strike-slip movement	The nature of drag folds suggested it	cut NW Folding and NW cleavage	77	27.3		Hamilton 1980
26	Kungurian, Glen & Roberts(2012) Fig.2	the youngest rock cut by fault is Warbro Fm		intersected by 28			cut EW cleavage	53	2.5		
27	Namurian, Bashkirian, G&R(2012) Fig.2	the youngest rock cut by fault is Mingaletta Fm		cut by 28 & 20				106	3.8		
28	Namurian, Bashkirian, G&R(2012) Fig.2	the youngest rock cut by fault is Mingaletta Fm	Sakmarian,Early Permian, G&R(2012) Fig.2	cut by 25	sinistral movement	fault displace 27 & 29		139	12.2		
29	Namurian,Serpukhovian, Glen & Roberts(2012) Fig.2	the youngest rock cut by fault is Major creek Fm	Namurian Bashkirian, G&R(2012) Fig.2	cut by 28				105	5.1		
30	Visean V3b G&R(2012) Fig.2	the youngest rock cut by fault is Boonanghi beds	Namurian, Bashkirian,Glen & Roberts(2012) Fig.2	cut by 17				108	5.8		
31	Visean V3b G&R(2012) Fig.2	the youngest rock cut by fault is Boonanghi beds	Namurian, Bashkirian,Glen & Roberts(2012) Fig.2	cut by 17				116	8		
32	Sakmarian, G&R(2012) Fig.2	the youngest rock cut by fault is Kempsey Beds		cut by 17 and displaces 20	sinistral movement	fault displaces 20 & 24, and displaced the Mingaletta - Kempsey beds boundary		71			
33	Visean V1 G&R(2012) Fig.2	the youngest rock cut by fault is Pappinbarra Fm	Namurian, Bashkirian	cut by 35				139	12.4		
34	Sakmarian,Early Permian, G&R(2012) Fig.2	the youngest rock cut by fault is Beechwood beds	second episode	cut by 17			cut NW folding and NE and NW cleavage	170	12		
34(1) Mortons Creek Fault	Visean V3b G&R(2012) Fig.2	the youngest rock cut by fault is Hydmans Creek Fm	second episode	cut by 34 and Triassic Granitoids		Werrikimbi Volcanic complex 226 +/- 3 Ma, Flood et al. 1992	cut the cleavage				
35 Telegraph Point Fault	Namurian Bashkirian, G&R(2012) Fig.2	the youngest rock cut by fault is Mingaletta Fm	Fault cut by Cairncross Granite	cut by Triassic Granitoids		as above	cut the cleavage	71	17.6		
36 Beechwood Fault	Sakmarian,Early Permian, G&R(2012) Fig.2	the youngest rock cut by fault is Beechwood beds last in the Mt cairncross area	final episode	cut by 34	??unclear vertical or strike-slip displacement/downthrown to SE		cut NW cleavage	76,39,78/20-80	23.7/21+		M.Mikel 1985

Fault	Earliest time faulting could have started		Cessation of faulting		Apparent sense of movement	Evidence	Relationships to the folding and cleavages	Orientation (°)	Length (km)	Description	Comment
	Time	Evidence	Time	Evidence			NB=Nambucca				
37	Visean V1 G&R(2012) Fig.2	the youngest rock cut by fault is Pappinbarra Fm	west end-overlaine byTriassicGrannitoids, east - older than fault 34	cut by 34 and Triassic/Jurassic Grannitoids				82	11.5		
38	Visean V3b G&R(2012) Fig.2	the youngest rock cut by fault is Hydmans Creek Fm		cut by 62				153	16.4		
39	Visean V1 G&R(2012) Fig.2	the youngest rock cut by fault is Pappinbarra Fm	north end-cut by 38,Visean V3b, south - cut by 44,Namurian Bashkirian, G&R(2012) Fig.2	cut by 38 & 44				20	10.6		
40	Triassic	the youngest rock cut by fault is Triassic Grannitoids		cut by 34			cut cleavage	98	6.6		
41	Late Triassic(~226Ma)	the youngest rock cut by fault is Werrikimbe Volcanics which is 226 Ma =+/- ?? (Sshmidt et al.1994)	younger than Late Triassic				cut cleavage	140	6.2		
42 Rafles Creek Fault	Late Triassic(~226Ma)	the youngest rock cut by fault is Werrikimbe Volcanics which is 226 Ma =+/- ?? (Sshmidt et al.1994)		cut by 85			cut NW cleavage	145	45.1		
43	Glen & Roberts(2012) Fig.2, Visean V3b	the youngest rock cut by fault is HCF and be the boundary of Nevann siltstone and HCF	Late Triassic(~226Ma)	cut by Werrikimbe Volcanics which is 226 Ma (Flood et al. 1993)			cut NW fold and NW cleavage	131/168/130	32.1	147.9	
44 Pappinbarra Fault	Namurian Bashkirian, G&R(2012) Fig.2	the youngest rock cut by fault is Mingaletta Fm	Late Triassic(~226Ma)	cut by Werrikimbe Volcanics			cut NW fold and NNW cleavage	130	34		
45 Cowarral Fault	Namurian Bashkirian	the youngest rock cut by fault is Mingaletta Fm	Late Triassic(~226Ma)	cut by Werrikimbe Volcanics and 49			cut NW fold	169	21.9		M.Mikel 1985
46 Rollans Road Fault	Glen & Roberts(2012) Fig.2; Tournasian, Tn3	be the boundary of Nevann Siltstone and Rollans Road Fm	Namurian Bashkirian	cut by 45			cut NW fold and NNW cleavage	114	9.1		
47	Glen & Roberts(2012) Fig.2, Visean V3b	be the boundary of Nevann Siltstone,Pappin FM and HCF	Namurian Bashkirian, G&R(2012) Fig.2	cut by 44 and 52			cut NE and NNW cleavage	38	3.3		
48	Famennian see Aitchison et al. 1992	the youngest rock cut by fault is subduction complex	Triassic	cut by Werrikimbe Volcanics			cut cleavage	45	7		
49 Taylors Creek Fault	Sakmar,Early Permian, G&R(2012) Fig.2	the youngest rock cut by fault is Beechwood beds	Triassic??	cut by 48	Sinistral strike-slip movement or oblique, down dip, dextral strike-slip movement	dragging of the serpentinites along this fault suggested sinistral. But shear joints close to fault record dextral.	cut NW fold and NW cleavage	146	35.7		Lennox *et al.* 2009; Offler , Lennox, Roberts J.J. unpunl. Data
50	Frasnian B (Aitchison et al. 1992)	the youngest rock cut by fault is Rollans Road Formation	Namurian Bashkirian	it was cut by 45				120	4.8		

Fault	Earliest time faulting could have started		Cessation of faulting		Apparent sense of movement	Evidence	Relationships to the folding and cleavages	Orientation (°)	Length (km)	Description	Comment
	Time	Evidence	Time	Evidence			NB=Nambucca				
52 Arizona Fault	Frasnian B, G&R(2012) Fig.2 before folding	the youngest rock cut by fault is Cowangara Fm	Nth end-overlaine by Rollans Rd Fm (end Famennian C), south - older than fault 66, Visean V3b G&R(2012) Fig.2	it was cut by 66, and it cut the cleavages	dip-slip movement(1000 (min.) - ~ 2000m)/downthrown to NE, dip-slip 1~2km (Feenan1984)	appears to be bent by folding post-fault formation	appears to be bent by NW folding and cut the N-S cleavage	142	20.2	before folding event	J.P.Feenan 1984
53	Tournaisian Tn3, G&R(2012) Fig.2	the youngest rock cut by fault is Nevann Siltstone	Pre-Fault 52	cut by 52	dextral movement 500m	fault displaced Kindee Conglomerat	cut the N-S cleavage	46	4.2		
54	Tournasian Tn3, G&R(2012) Fig.2	the youngest rock cut by fault is Nevann Siltstone		cut by 52 and 57	sinistral movement 580m	fault displace Kindee Conglomerat e	cut NW cleavage	45	4.6		
55 ?? Claremont Fault	Latest Namurian, G&R(2012) Fig.2	the youngest rock cut by fault is Mingaletta Fm		terminated by 52 (west) and 57 in the east	Strike-slip fault 0~1800m/1.9km sinistral ss partly downthrown to SW 2100m	fault displace Kindee Conglomerat e	cut NW fold	70	18.9/17	faults 55, 59, 57 are dominantly steep to vertical with eroded crush zones.	J.P.Feenan 1984
56 Hastings Fault	Visean V3b G&R(2012) Fig.2	the youngest rock cut by fault is Hydmans Creek Fm		cut by 52	sinistral strike slip (displacement in W 1700m and 2000m in the east) /dextral 1.8km thonerv sinistral 2.1km (Spackman 1989) dextral movement 1.8km	fault displaces Kindee Conglomerat e	cut NW fold	84	18.1/15 km/55+		Thompson 1985; Spackman 1989
57 Bagnoo Fault	Namurian Bashkirian	the youngest rock cut by fault is Mingaletta Fm	Triassic from map with Grants Head Fm	Fault appears to die out into the Triassic Grants Head Formation. This suggests movement must have stopped during the deposition of the Grants Head Formation	dip-slip sinistral movement/sinistral (Feenan 1984), dip slip 1-2km downthrown to NE(Spackman 1989)	displacement of rock units on each side of the Bagnoo fault	cut NW fold and NNW CLE	126	36.2/25 km /57+ distance		Feenan 1984; Spackman, 1989; Roberts *et al.* 1993;West, 1990; Pratt, 2010;Glen & Roberts,2012
58	Visean V3b G&R(2012) Fig.2	the youngest rock cut by fault is Hydmans Creek Fm	Namurian Bashkirian, G&R(2012) Fig.2	cut by 55 &44				152	14.4		
59 Warrawillah Fault	Visean V3b G&R(2012) Fig.2	the youngest rock cut by fault is Hydmans Creek Fm		cut by 38 & 57	dip-slip of substantial displacement (several thousand metres) /Strike-slip fault 0~1800m			34	13.8		J.P.Feenan 1984
60	Visean V3b G&R(2012) Fig.2	the youngest rock cut by fault is Hydmans Creek Fm		cut by 38 & 43				49	4.5		
61	Visean V3b G&R(2012) Fig.2	the youngest rock cut by fault is Hydmans Creek Fm		cut by 38 & 34				68	6.8		

Fault	Earliest time faulting could have started		Cessation of faulting		Apparent sense of movement	Evidence	Relationships to the folding and cleavages	Orientation (°)	Length (km)	Description	Comment
	Time	Evidence	Time	Evidence			NB=Nambucca				
62	Visean V3b G&R(2012) Fig.2	the youngest rock cut by fault is Hydmans Creek Fm		cut by 58 & 34				47	12.1		
63	Visean V1 G&R(2012) Fig.2	the youngest rock cut by fault is Pappinbarra Fm	Namurian Bashkirian	cut by 44 & 34				40	7.2		
64	Visean V3b G&R(2012) Fig.2	the youngest rock cut by fault is Hydmans Creek Fm	Namurian Bashkirian	cut by 44 & 34				62	5.9		
65	Namurian Bashkirian	the youngest rock cut by fault is Mingaletta Fm		cut by 57 & 34			cut NW fold	75	11.3		
66 Thone River Fault	Visean V3b G&R(2012) Fig.2	the youngest rock cut by fault is Hydmans Creek Fm		cut by 57(east end) and 49 (west end)	Strike-slip fault 0~750m	fault displace Kindee Conglomerate.		43-65	16.4		
67	Namurian Bashkirian, G&R(2012) Fig.2	the youngest rock cut by fault is Mingaletta Fm		cut by 57(east) and 49(west)	dextral movement 2.5km	fault displace Kindee Conglomerate.	cut NW fold	62	17.5		
68	Sakmar,Early Permian, G&R(2012) Fig.2	the youngest rock cut by fault is Beechwood beds		cut by 44				58	4.4		
69 Broken Bago Fault	Sakmar,Early Permian, G&R(2012) Fig.2	the youngest rock cut by fault is Beechwood beds						1	5.6/5km	NE-block down	Taylor 1984
70	Sakmar,Early Permian, G&R(2012) Fig.2	the youngest rock cut by fault is Beechwood beds	Triassic	cut by Laourieton conglomerate				143	8.4		
71	Sakmar,Early Permian, G&R(2012) Fig.2	the youngest rock cut by fault is Beechwood beds	Triassic	cut by Laourieton conglomerate				162	7.8		
72	Sakmar,Early Permian, G&R(2012) Fig.2	the youngest rock cut by fault is Beechwood beds						60	22		
73	Namurian Bashkirian	the youngest rock cut by fault is Mingaletta Fm	Sakmar,Early Permian, G&R(2012) Fig.2	cut by 75				72	3.6		
74 Sancroix Fault	Namurian Bashkirian	the youngest rock cut by fault is Mingaletta Fm	Sakmar,Early Permian, G&R(2012) Fig.2	cut by 71	sinistral strike slip/dip angles at sancrox quarry is 70~45o	separates the Mingaletta fm form the sepencers quarry Fm. Diaplace the Mingaletta Fm		19	4.8	dip north-west with 70-45 dip angale	M.A.Taylor 1984
75 Cowarra Fault		the youngest rock cut by fault is Triassic formations	post Triassic	cut by the serpentinite	sinistral strike slip(small displacements)			25/20-60	10.6/8	steep dip	Taylor 1984; Offler and Lennox unpubl. Data. Pratt 2010
76 Innes Estate Fault	initiated during Triassic sedimentation	the youngest rock cut by fault is Beechwood beds	post Triassic	cut the Triassic formations (Camden Haven Group and Milligans Road				31/15-40	11.9/12		Pratt 2010
77	initiated during Triassic sedimentation	the youngest rock cut by fault is Triassic formations		cut by 75 & 76				70	2.5		Pratt 2010
78 Lake Innes Fault	initiated during Triassic sedimentation	the youngest rock cut by fault is Triassic formations			large, uneatablished SS movements			25	9.2/13		Pratt 2010
79	initiated during Triassic sedimentation	the youngest rock cut by fault is Triassic formations			bound allachthonous touchwood Fm (ditto)			30/20	8.5/15		Pratt 2010

Fault	Earliest time faulting could have started		Cessation of faulting		Apparent sense of movement	Evidence	Relationships to the folding and cleavages	Orientation (°)	Length (km)	Description	Comment
	Time	Evidence	Time	Evidence			NB=Nambucca				
80	initiated during Triassic sedimentation	the youngest rock cut by fault is Triassic formations			cleaved prehnite-pumpellyite(ditto)			27			
81		the youngest rock cut by fault is Melange						156	6.1		
82 old highway Yarras mountain trail fault	Late Devonian	the youngest rock cut by fault is subduction complex		cut by 84 and 85				125	10.6		
83	Late Devonian	the youngest rock cut by fault is subduction complex		cut by 49 and 84				124	13.6		
84	Late Carboniferous	the youngest rock cut by fault is subduction complex		cut by 49 and 42				25	3.5		
85	Late Devonian	the youngest rock cut by fault is subduction complex		cut by 45				3	6		
102	Triassic	the youngest rock cut by fault is the Triassic Gundle Pluton		cut by 40 & 37				146	3.4		
103	Triassic	the youngest rock cut by fault is the Triassic Gundle Pluton		cut by 40 & 37				156	3.4		
104	Triassic	the youngest rock cut by fault is the Triassic Gundle Pluton		cut by 40 & 37				158	2.8		
105	Visean V3b G&R(2012) Fig.2	the youngest rock cut by fault is Boonanghi beds		cut by Triassic/Jurassic Granitoids				146	2.4		

Appendix 4: Review of the movement history on the Taylors Arm Fault System.

From Leitch's (1972) map of the faults cross-cutting the whole of the Nambucca Block, it is possible to determine the order of faulting (see Table 1). There are four main populations of faults:-(1) almost E-W striking; (2) N-S to NNW-SSE striking (Taylors Arm Fault System); (3) ENE-WSW striking and (4) NW-SE striking (Figure A17). Analysis of the map pattern of faulting provides evidence as to the relative timing of the fault movement. It appears NW-SE striking faults formed first, followed by E-W striking faults and then there was an early period of ENE-WSW striking faults. The Taylors Arm Fault System (NS to NNW-SSE striking) then displaced all the other faults except for a small number of ENE-WSW striking faults (Table 1).

From displacement of the boundary between the Pee Dee Beds and Kempsey (or Parrabel) Beds from Leitch's (1972) Nambucca Block geology map, the western-most fault of the TAFS (Nulla Nulla Fault, along strike extension of Fault 21) has 15km of apparent dextral displacement (Figure A17). The Mungay Creek Fault (along strike extension of Fault 23) has 13km of apparent sinistral displacement (Figure A17). The Taylors Arm Fault which is the eastern-most fault of the TAFS has ~ 6 km of apparent dextral displacement (Figure A17).

Roberts (2000) mapped an area north of the Hastings Block across a part of the TAFS. He considered the east-west faults were thrust faults and that the over 30km long Taylors Arm Fault (eastern most fault in TAFS) had 3-5 km of dextral movement prior to the NE-trending faults (pre 230-220 Ma) (Table 1). Roberts (2000) proposed that the western most fault of the TAFS which he called the over 30km long Nulla Nulla Fault (equivalent to along strike extensions of Fault 21) had 3-5 km of apparent dextral movement again before NE-trending faults. The NNW-SSE striking Burrapine Fault which lies between the converging Taylors Arm and Nulla Nulla Faults 20 km north of the Hastings Block has dip slip and 3-5 km of apparent dextral movement according to

Roberts (2000).

Table A3: Fault characteristic within the Taylors Arm Fault System.

	Leitch (1972)	Roberts (2000)
Fault sets (strike)	E-W	E-W
	N-S to NNW-SSE	NNW-SSE (TAF,NNF and BF)
	ENE-WSW	N-S to NNE (MCF)
	NW-SE	NE-SW
Fault Timing (Early to Late)	1. NW-SE	1. E-W thrust
	2. E-W	2. NNW-SSE (TAF,NNF and BF)(pre 230-220 Ma)
	3. ENE-WSW (majority)	Demon fault dextral movement, pre 230 Ma
	4. N-S to NNW-SSE	3. NE-SW destral then sinistral movement (mineralisation)
	5. ENE-WSW (minor)	4. E-W normal fault
Conclusion (Early to Late)	1. NW-SE	Early Faulting
	2. E-W	*Based on Leitch (1972) only*
	3. ENE-WSW	
	4. N-S to NNW-SSE (TAF,NNF and BF)	Later Faulting
Relative time of fault movement	1. NW-SE ——? ——? ——	
	2. E-W ——? ——? ——	
	3. ENE-WSW ——? ——? —— ——? ——?	
	4. N-S to NNW-SSE (TAF,NNF and BF) ——? ——? ——	
	⟶ Time of movement	
Absolute time of fault movement	TAF,NNF and BD are all pre-230-220 Ma (Triassic granites intruded across other NW-trending faults in the Nambucca Block, Leitch 1976)	
	Demon Fault – post Triassic granite as faults cuts it.	
Fault Names	TAF = Taylors Arm Fault = eastern-most NNW-striking faults of TAFS	
	NNF = Nulla Nulla Fault = Western-most NNW-striking fault of TAFS = Fault 21	
	BF = Burrapine Fault = NNW-trending fault between converging TAF and NNF	
	MCF = Mungay Creek Fault = N-S to NNE trending fault, extension of Fault 23	

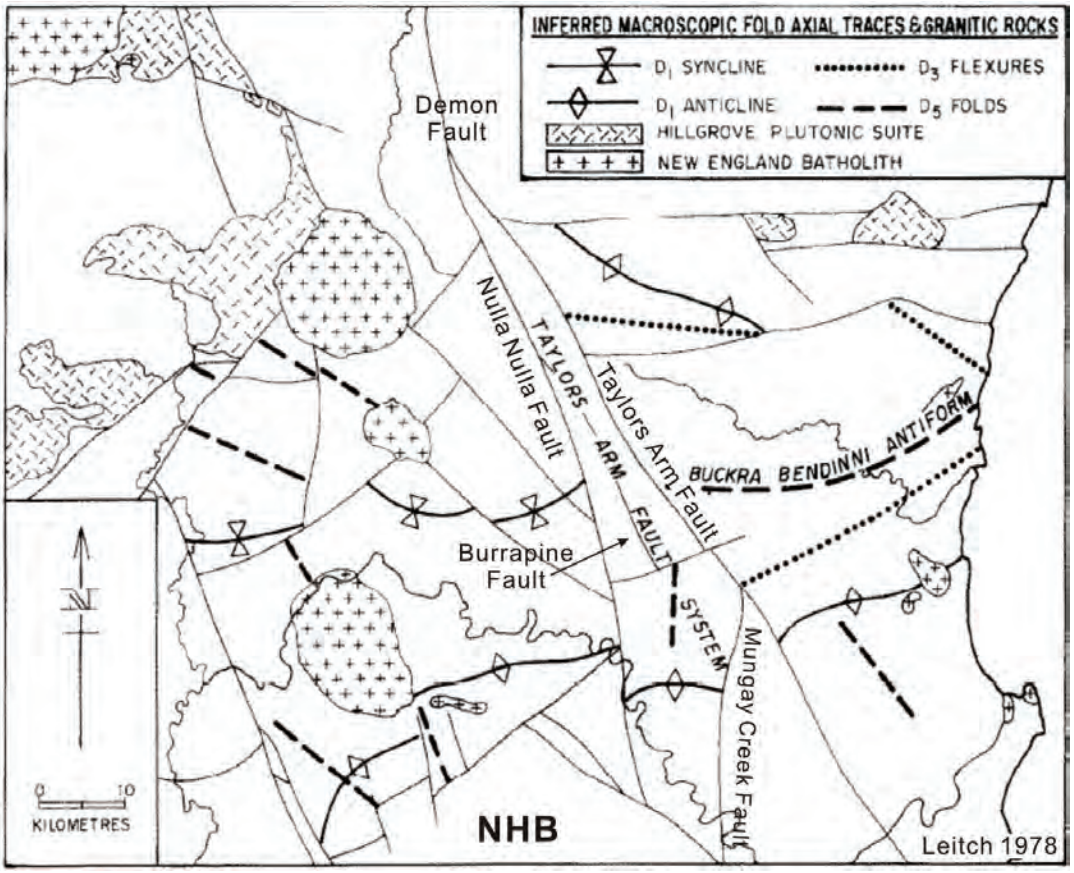

Figure A17: Leitch's (1978) fault and macroscopic fold map for the Nambucca Block with the key faults affecting the NHB labeled. NHB = Northern Hastings Block.

The major NNW-SSE trending, Demon-Taylors Arm Fault (TAF, NNF) System, Kunderang Fault (and the Pappinbarra Fault and Bagnoo Fault) and the fault affecting the eastern margin of the Carrai Granodiorite extensions are shown on Figure A18 from Leitch (1976). All these faults except the Pappinbarra fault, Bagnoo fault and Mungay Creek Fault are shown as undergoing dextral strike-slip movement. As shown above most are considered to have developed prior to Triassic granites intrusion except for the Demon Fault. The Demon Fault and its along strike continuation as the TAFS is considered to have approximately 23km of dextral strike-slip movement at its northern end (McPhie and Ferguson, 1983) and up to several kilometers on its southern end (Leitch 1978).

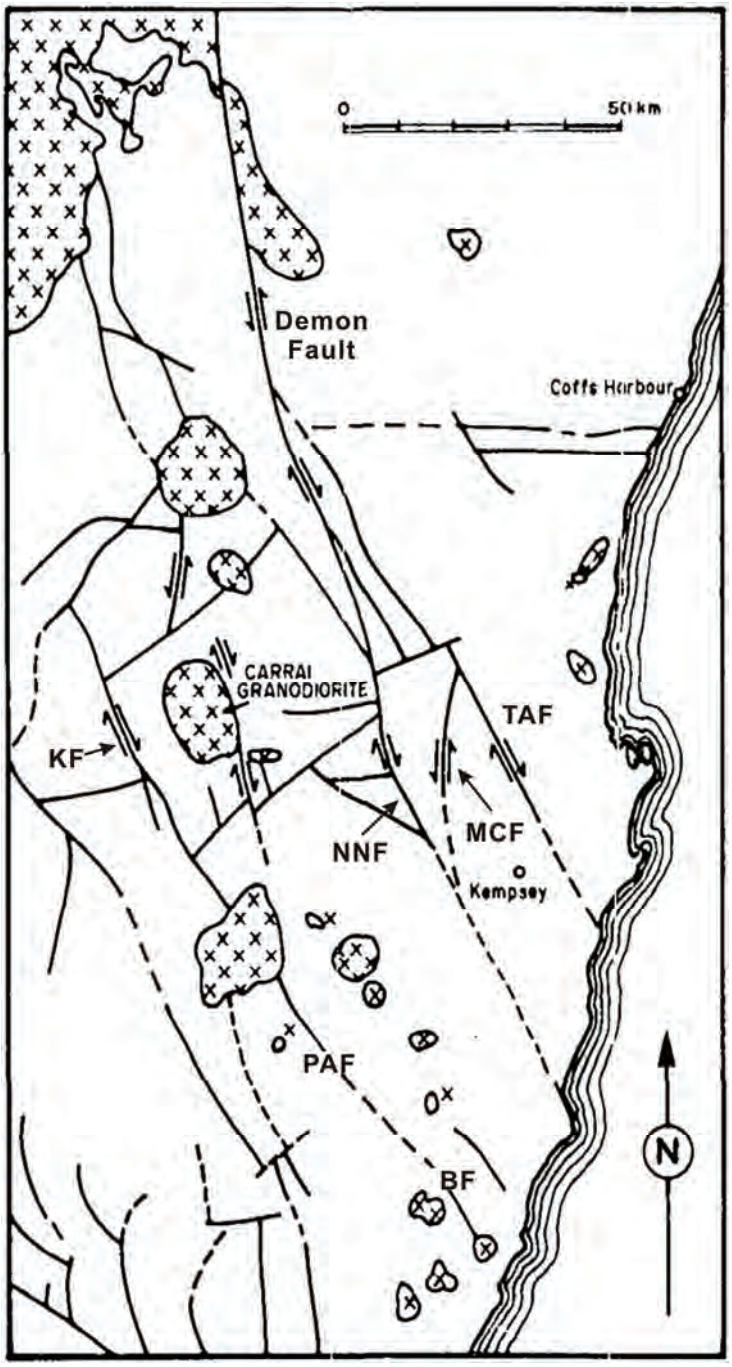

Figure A18: Leitch's (1976) map of key NNW-SSE trending faults across the Hastings Block (south), Nambucca Block and southern end of the Coffs Harbour megafold. BF = Bagnoo Fault; KF = Kunderang Fault; MCF = Mungay Creek Fault; NNF = Nulla Nulla Fault; TAF = Taylors Arm Fault.

Appendix 5: The map pattern of fault movement within the NHB. The earliest time when faulting wasdetermined to have started and the latest time faulting finished.

Faulting commenced:

Figure A19: The map pattern of faults whose earliest time of movement was in a) the Late Devonian – Group 1 and b) the Early Carboniferous – Group 2.

Figure A20: The map pattern of faults whose earliest time of movement was in a) the Late Carboniferous – Group 3 and b) the Permian – Group 4 and c) the Late Triassic – Group 5.

Faulting ceased:

Figure A21: The map pattern of faults which were determined to have finished moving in a) the Early Carboniferous – Group 1 and b) the Late Carboniferous – Group 2.

Figure A22: The map pattern of faults which were determined to have finished moving in a) the Permian – Group 3 and b) pre-Late Triassic – Group 4. and c) post-Late Triassic – Group 5.

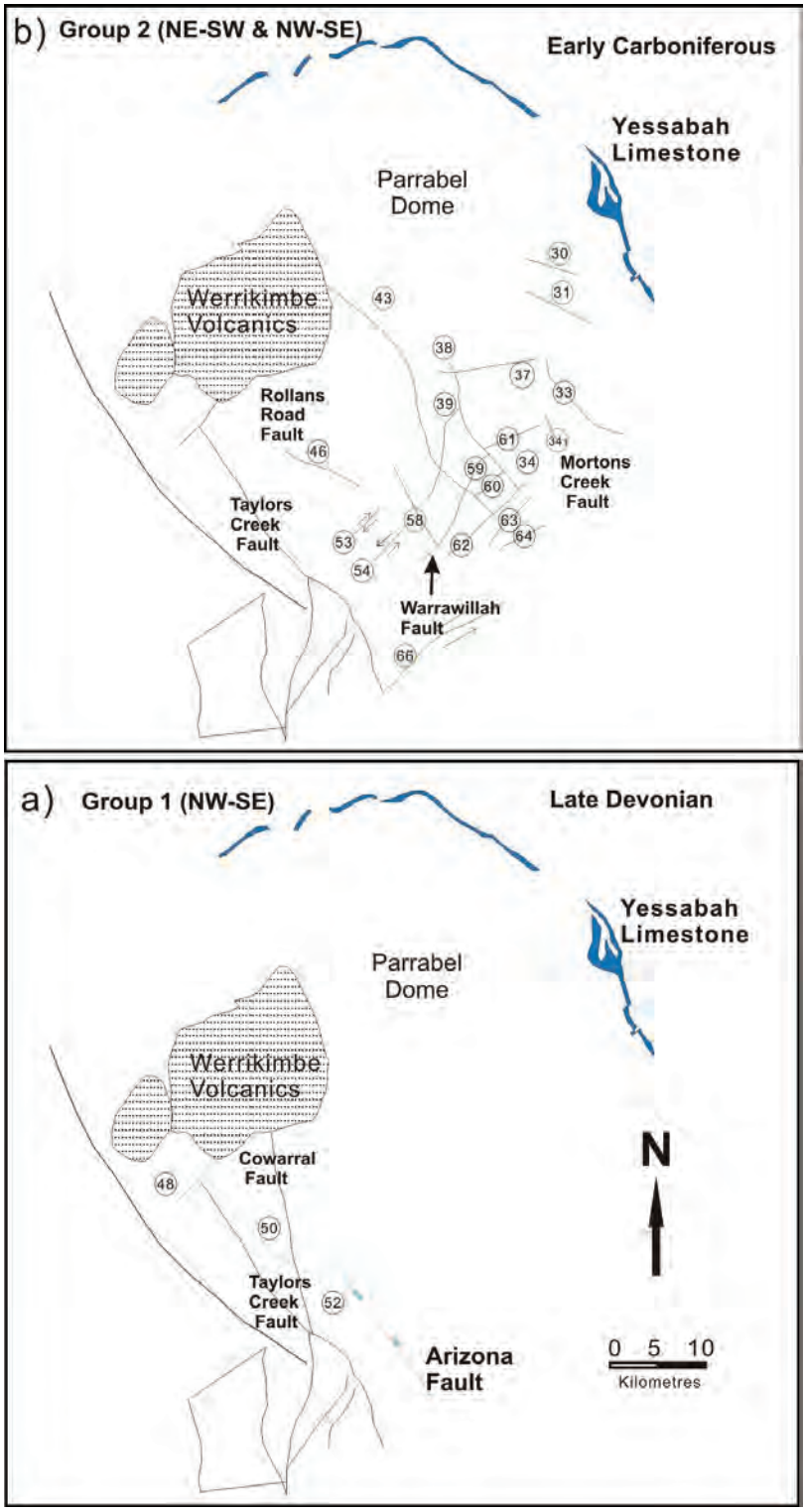

Figure A19: The map pattern of faults whose earliest time of movement was in a) the Late Devonian – Group 1 and b) the Early Carboniferous – Group 2.

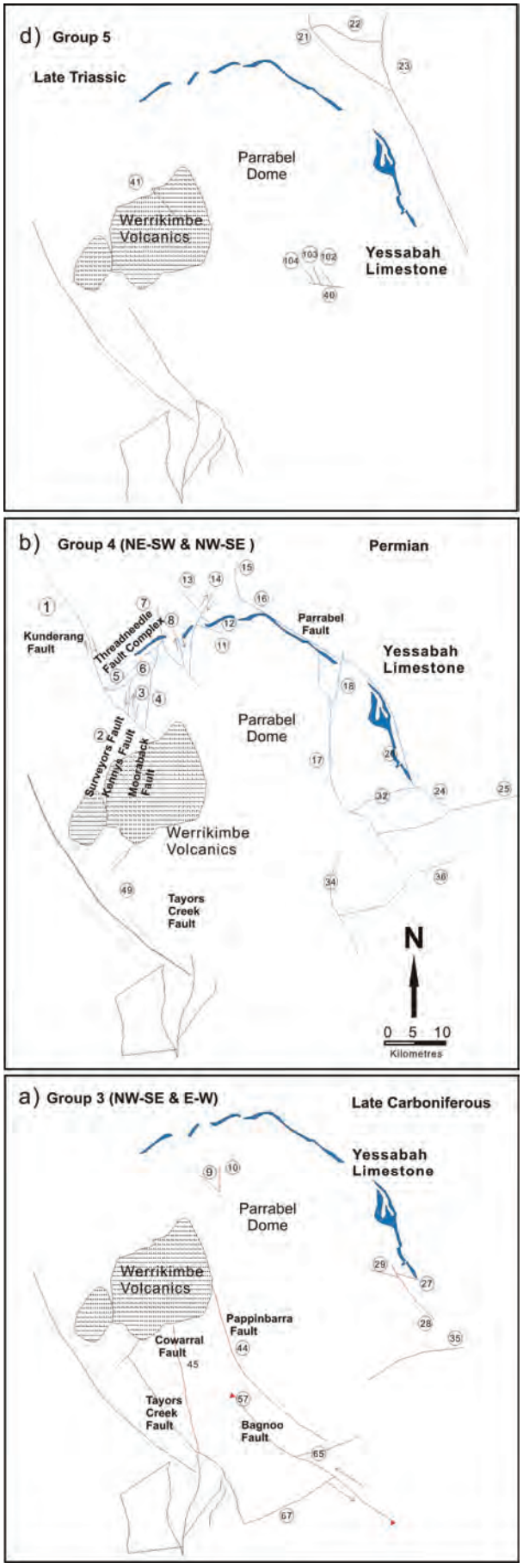

Figure A20: The map pattern of faults whose earliest time of movement was in a) the

Late Carboniferous – Group 3; b) the Permian – Group 4 and c) the Late Triassic – Group 5.

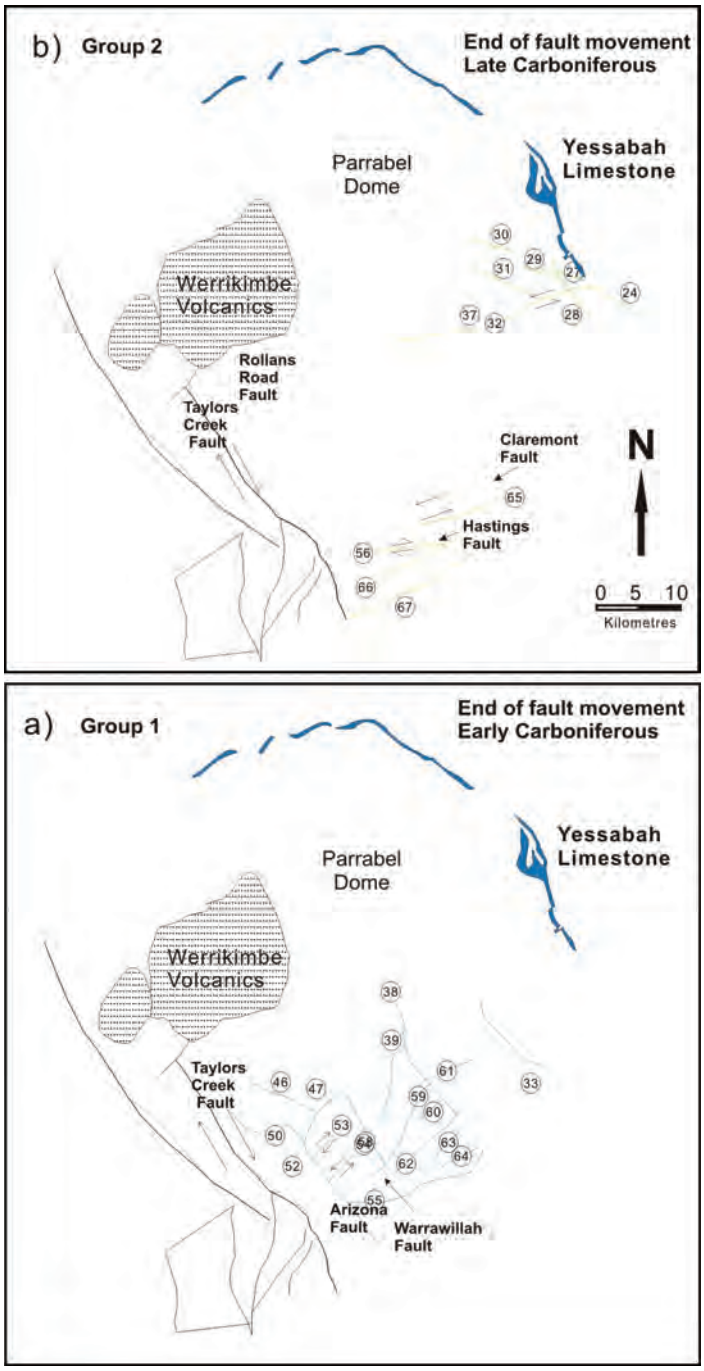

Figure A21: The map pattern of faults which were determined to have ceased moving in a) the Early Carboniferous – Group 1 and b) the Late Carboniferous – Group 2.

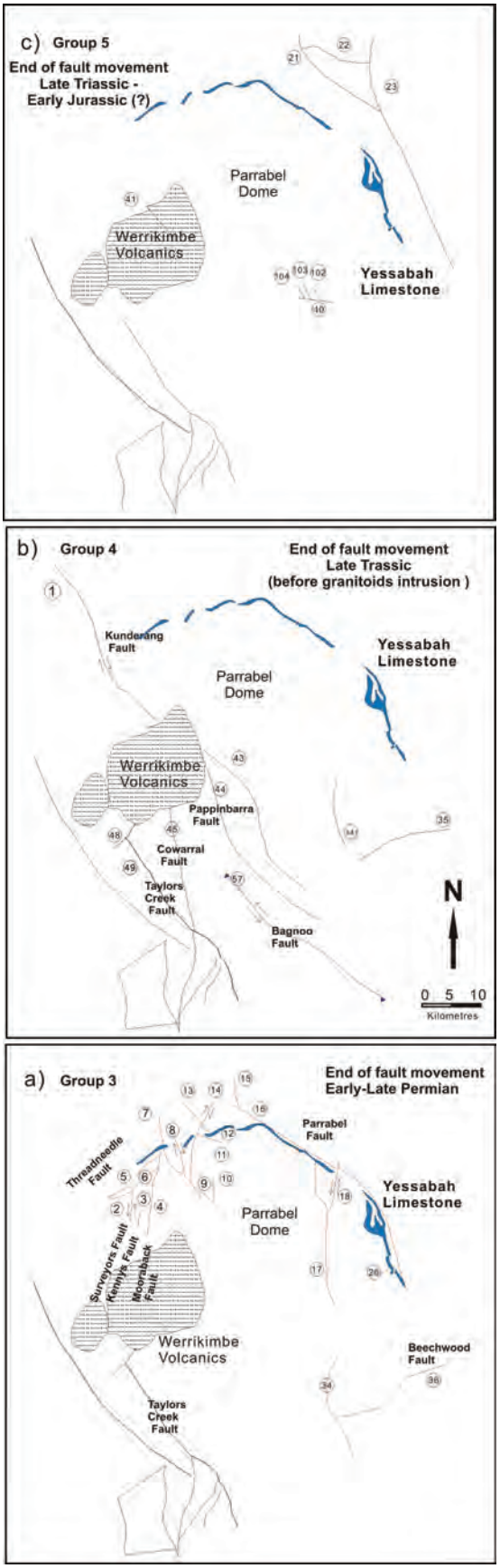

Figure A22: The map pattern of faults which were determined to have ceased moving in a) the Permian – Group 3; b) pre-Late Triassic – Group 4. and c) post-Late Triassic – Group 5.

Appendix 6: Fault initiation and termination - Formations-cut-by-the fault.

This method uses the age of the formations that the fault cuts. The timing was constrained by the youngest and oldest rock/unit which are cut by the major faults (Figure A23).

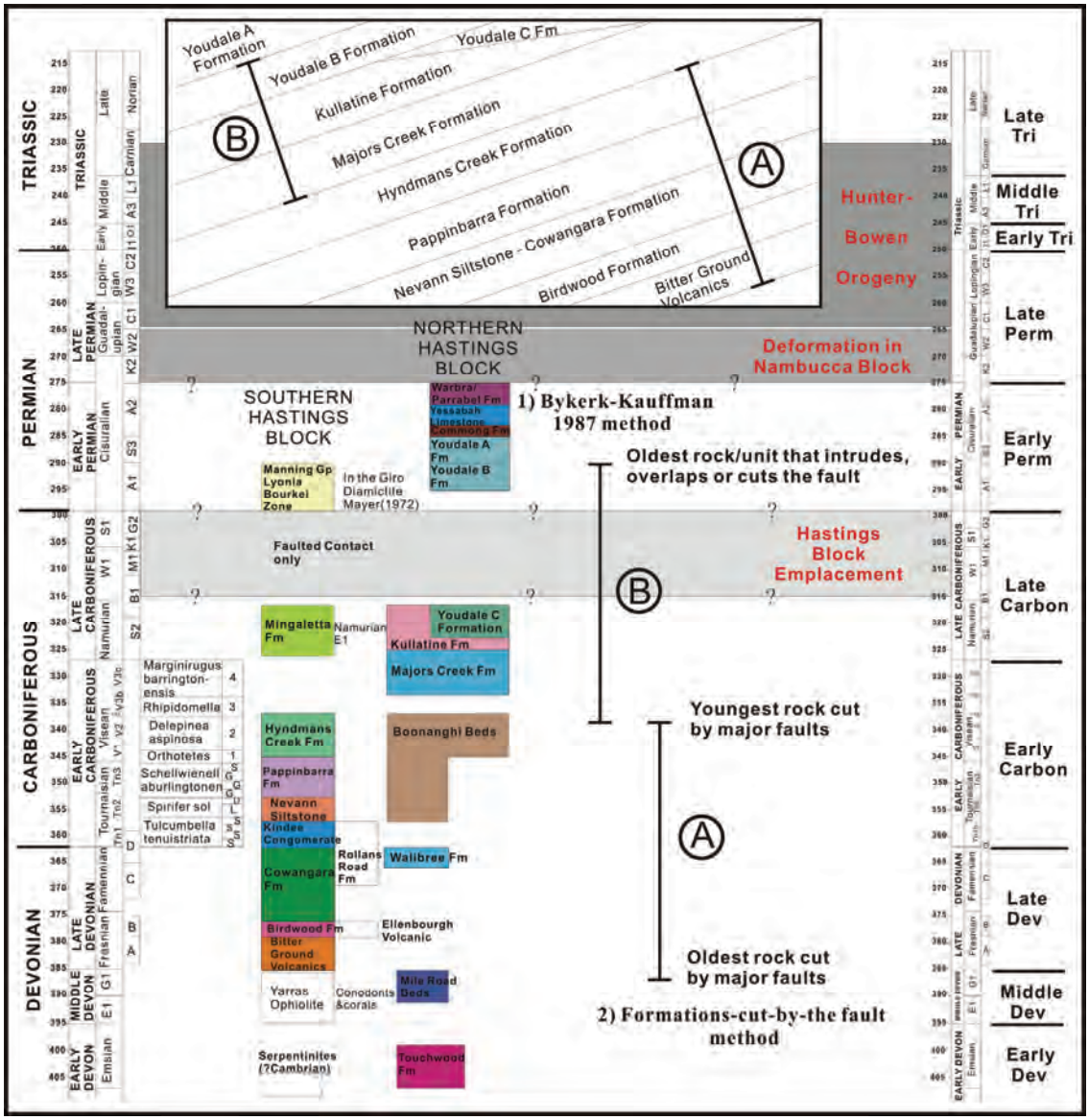

Figure A23: A map, time scale and stratigraphic columns showing faults A and B and their movement history. Fault A movement history has been determined by the formation that is cut-by-the-fault-method. This fault may have initiated during the Late Devonian (bottom of bar) and terminated in the late Early Carboniferous (top of the bar). Fault B has been analyzed using the Bykerk-Kauffman (1987) method which indicates fault initiation in the late Early Carboniferous and fault termination in the Early Permian. Abbreviations: A1: Asselian; A2 :Artinskian; A3: Anisian; B1: Bashkirian; C1:

Capitanian; C2: Changhsingian; E1: Eifelian; G1: Givetian; G2: Gzhelian; I1: Induan; K1: Kasimovian; K2: Kungurian; L1: Ladinian; M1: Moscovian; O1: Olenskian; S1 :Steph; S2: Serpukhovian; S3: Sakmarian; W1:Westphalian; W2: Wordian; W3: Wuchiapingian. Hastings Block emplacement by translational movement on faults timing is constrained by the depositional history. The time scale and stratigraphic columns are from Glens and Roberts (2012). Deformation in the Nambucca Block is constrained by S2 formation (Shaanan *et al*. 2014). The period of the Hunter-Bowen Orogeny is from Cawood *et al*. (2011).

6.1 Initiation of faulting

Five fault groups have been recognized in this analysis (Figure A24) that initiated over periods of approximately 10 million years (Group 2 & 3) and 20 million years (Group 5).

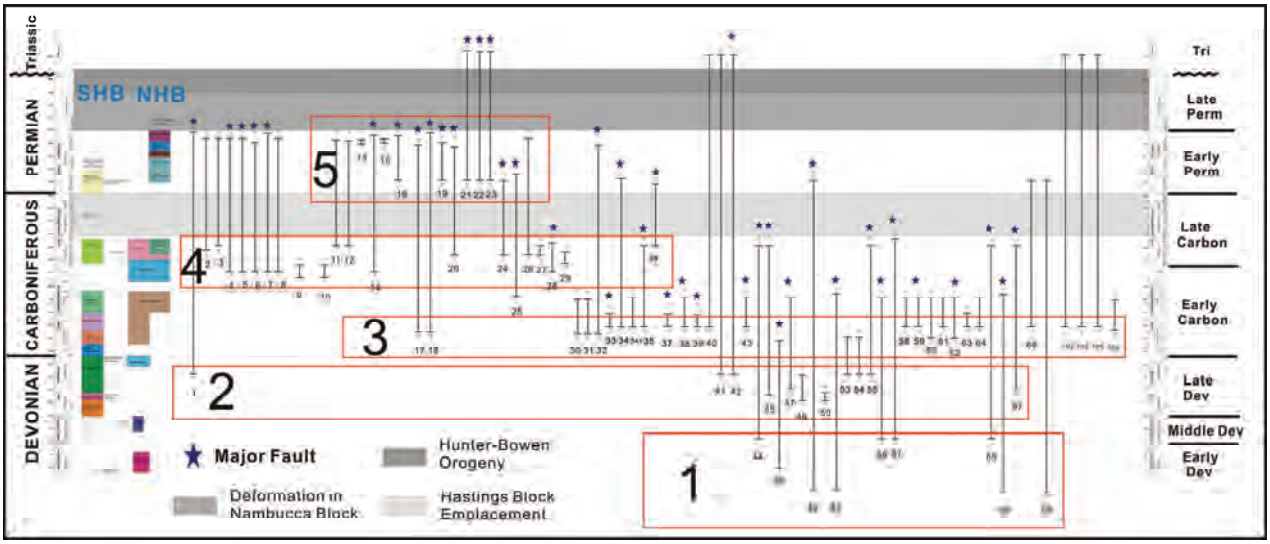

Figure A24: Timing of fault initiation based on the formation cut-by- the fault method. The question mark at each end of the vertical bar reflects the fact that the exact position of the fault movement termination is not discernible. The termination occurred somewhere within the time internal during which one formation was formed. It is impossible to know whether this time was early, middle or late within a formation.

(1) The first fault group consists of Faults 44, 46, 52, 56-57, 65-66 and 69 (Figures A24 & A25a), which are located on the southwestern part of Parrabel Dome. The timing of

this fault group is poorly constrained because they cut sequences varying in age from Early to Middle Devonian (Figure A24).

(2) Fault Group 2 is made up of Fault 1, 41, 45, 47, 48, 50, 53-55 and 67 (Figure A24). These faults spread along the western margin of the Hastings Block (Figure A25b) and vary in strike between ENE-WSW in the south and more northerly in the north. The timing of fault initiation suggested by this method is constrained to be in the Late Devonian (Figure A24).

(3) Faults 17-18, 30-35, 37-40, 43, 58-64, 68 and 102-105 make up Fault group 3 (Figure A24). They are located on the southwestern and southern margin of the Parrabel Dome (Figure A25c). The timing of fault initiation suggested by this method is constrained to be in the Late Devonian (Figure A24) fault initiation in the Early Carboniferous (Figure A24).

(4) The fourth group is composed of Fault 2-14, 20, 24, 26-29 and 36 (Figure A24) that are situated on the northwestern and southeastern margin of the Parrabel Dome (Figure 14a). Fault initiation is from Early to Late Carboniferous (Figure A24).

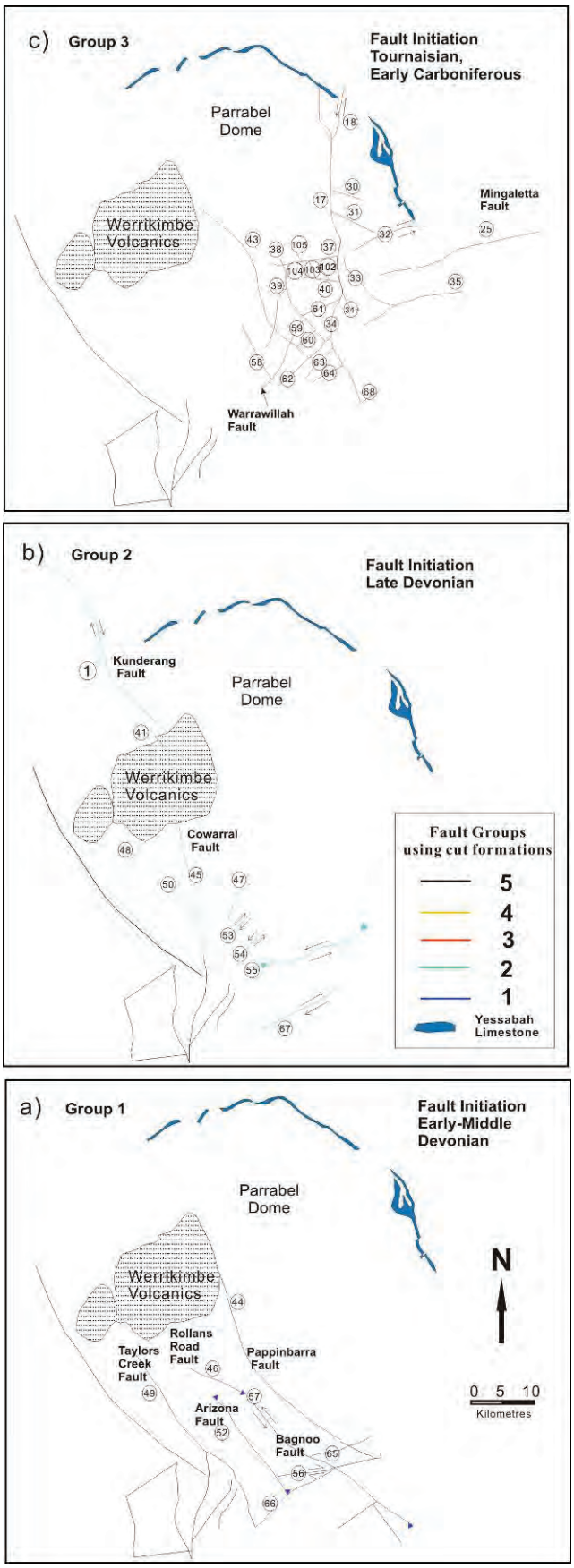

Figure A25: The initiation of movement for fault groups 1-3 according to formations cut-by-the fault method.

(5) This fifth group consists of Faults 13, 15-16, 19 and 21-23 (Figure A26), that are located on the northern and northeastern margin of the Parrabel Dome (Figure A26b). They initiated during the Early Permian (Figure A24).

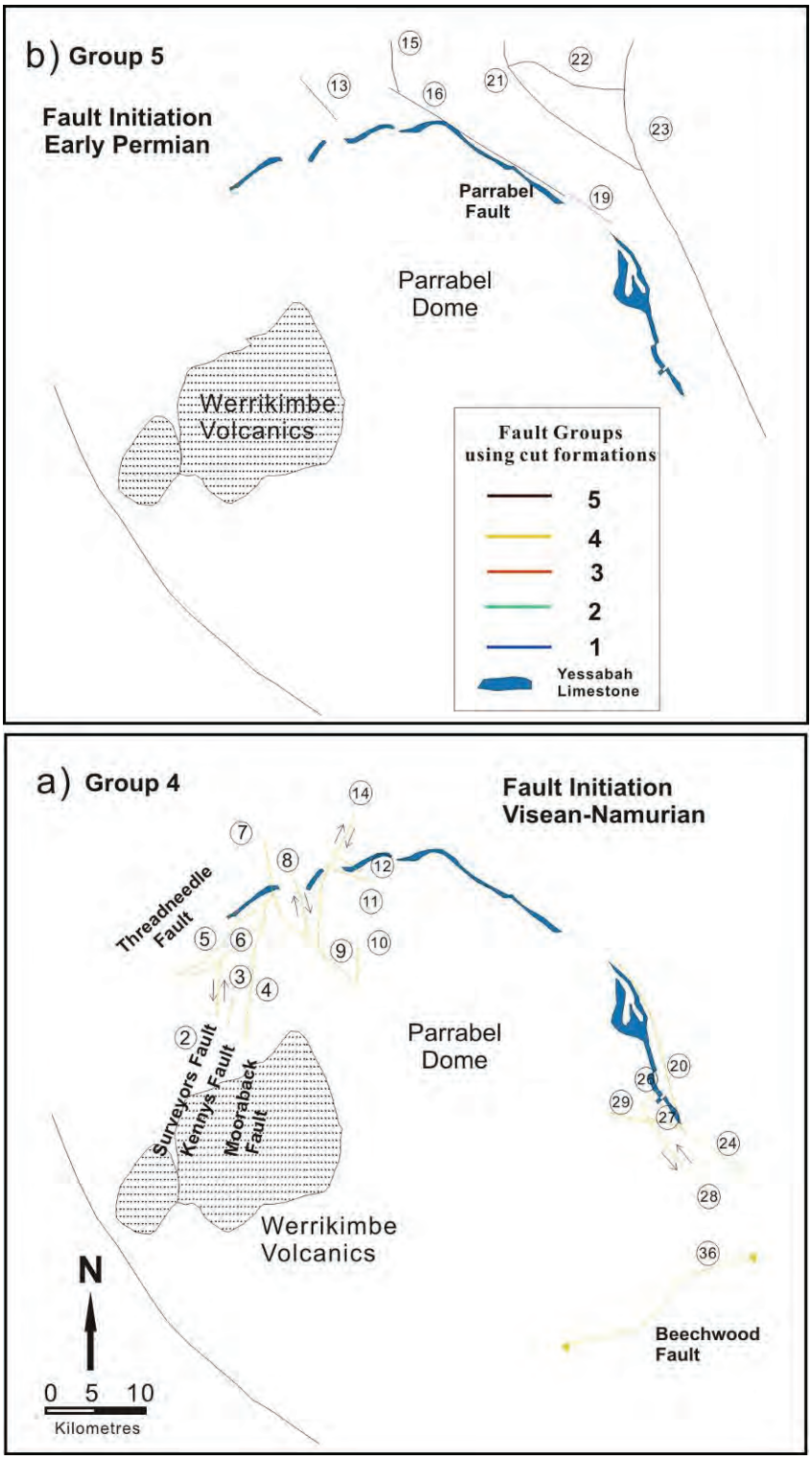

Figure A26: Map pattern of faults in Groups 4 and5 according to formations cut-by-the fault method.

6.2 Overview of initiation of movement

There are five fault groups recognized that have initiated at different times, namely (1) the southwestern Group 1 from the Early to Middle Devonian (Figure A25a); (2) the western Group 2 in the Late Devonian (Figure A25b); (3) the central and southeast Group 3, in the Early Carboniferous (Figure A25c); (4) the northwest and southeast Group 4 from the, Early - Late Carboniferous (Figure A26a); and (5) Group 5 during the Early Permian (Figure A26b).

6.3 Termination of faulting

Six fault groups were recognized to have finished moving over periods of approximately 5 million years (Group 3 - 5) and up to 15 million years (Group 1) (Figure A27).

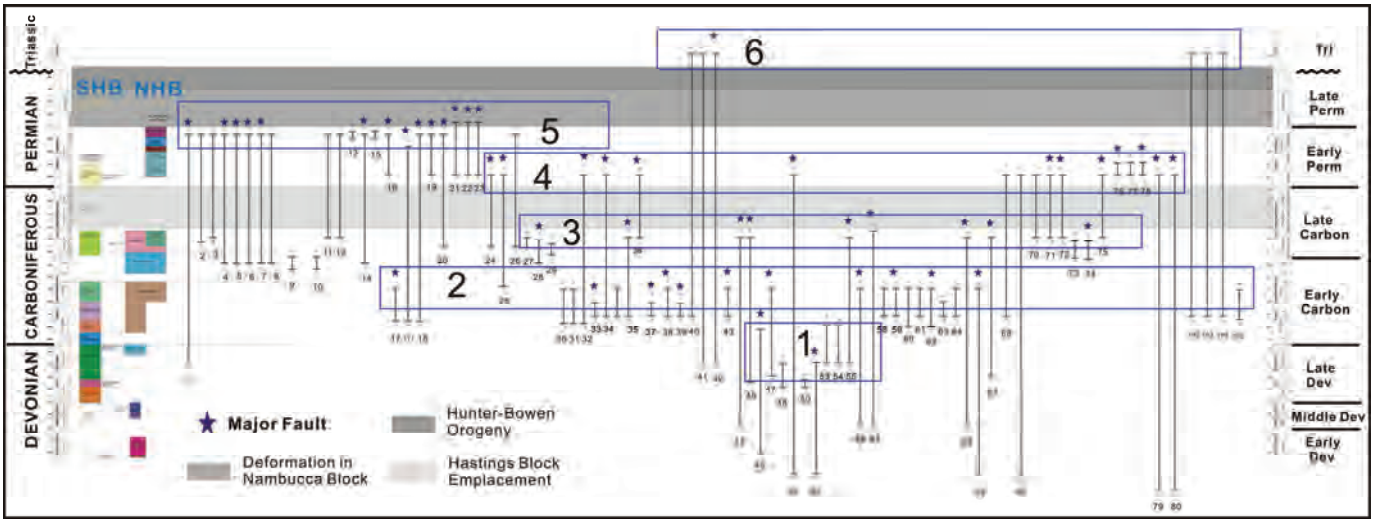

Figure A27: The fault groups according to the time of cessation of fault movement using formation cut-by-the fault method. The question mark at each end of the vertical bar reflects the fact that the exact position of the fault movement termination is not discernible. The termination occurred somewhere within the time internal during which one formation was formed. It is impossible to know whether this time was early, middle or late within a formation.

(1) Fault Group 1 consists of Faults 46, 48, 50 and 52-54 (Figures A27 & A28a), which are located on the southernwestern margin of the Parrabel Dome. The faults in this group stopped moving from the Late Devonian to Early Carboniferous (Figure A27).

(2) Fault Group 2 is made up of Faults 30, 31, 33, 34_1, 37-39, 43 47, 56, 58-64, 66 and 105 (Figure A27). These faults spread along the southeastern and eastern margin of the Parrabel Dome (Figure A28b). The timing of last fault movement is constrained to be in the late Early Carboniferous (Figure A27).

(3) Fault Group 3 is made up of faults 27-29, 35, 44-45, 55, 57, 65 and 67 (Figure A27). They are located on the southern and eastern margin of the Parrabel Dome (Figure A28c). The timing of fault termination is early Late Carboniferous (Figure A27).

(4) The fourth group is composed of faults 24-25, 34, 36, 49, 68-69 and 75 (Figure A27). These faults are situated on the southeastern margin of the Parrabel Dome (Figure A29a). The faults in this group stopped moving in the Early Permian (Figure A27).

(5) Faults 1-8, 11-20, 26 and 32 make up Group 5 (Figure A27), that are located on the northern, northeastern and northwestern margin of the Parrabel Dome (Figure A29b). They stopped moving during the Early to Late Permian (Figure A27).

(6) Fault Group 6 consists of Faults 21-23, 40-42 and 102-104 (Figures A27 & A29c), which are mainly located on the southern part of Parrabel Dome and in the northeast of NHB. The faults in this group ceased moving in the Late Triassic (Figure A27).

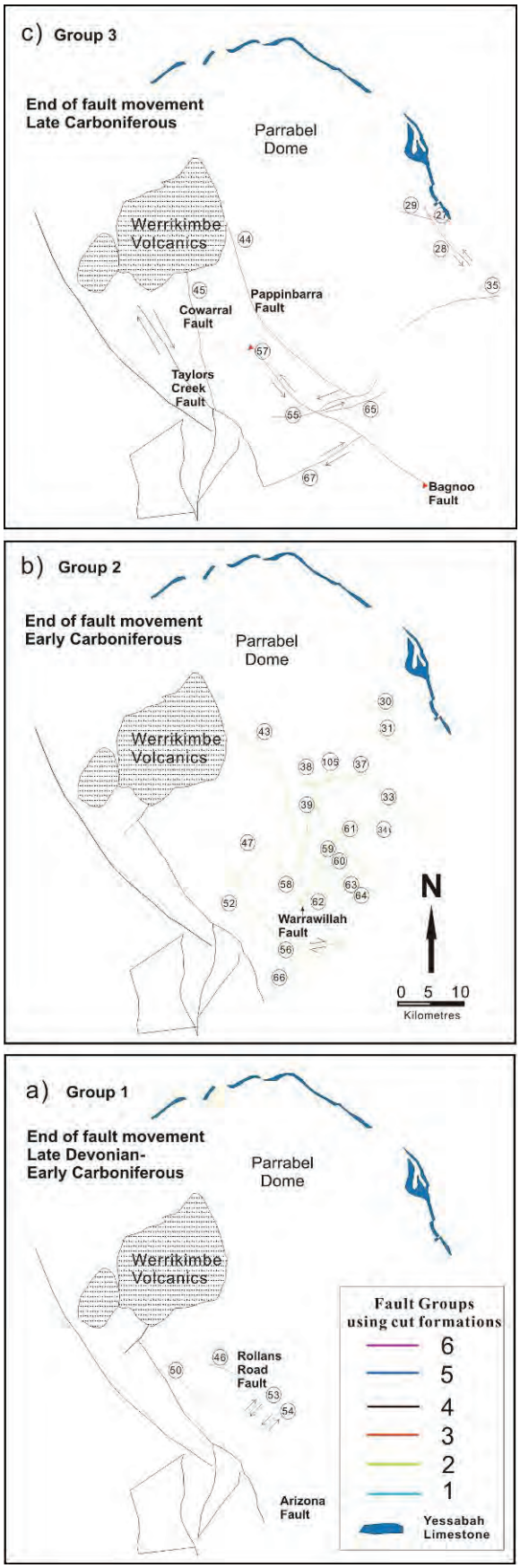

Figure A28: Pattern of fault groups 1-3 (end of fault movement) according to formations cut-by-the fault method.

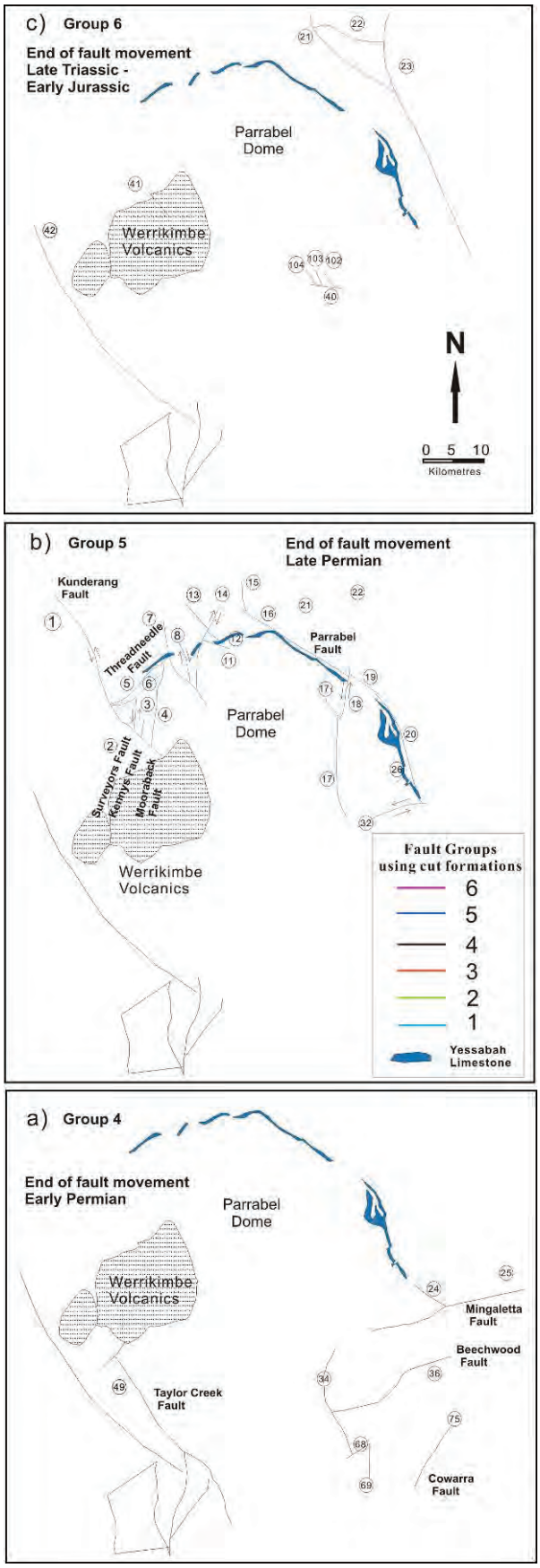

Figure A29: The map pattern of fault groups 4-6 (end of fault movement) according to formations cut-by-the fault method.

6.4 Overview of termination of movement

Six fault groups that finished moving at the same time have been recognized by this method. They are: (1) the southern Group 1 from the Late Devonian to Early Carboniferous (Figure A28a); (2) the southeastern and eastern Group 2 in the Early Carboniferous (Figure A28b); (3) the southern and eastern Group 3, in the Late Carboniferous (Figure A28c); (4) the southeastern Group 4 in the Early Permian (Figure A29a); (5) the northern, northeastern and northwestern Group 5 during the Early to Late Permian and finally (Figure A29b); (6) Group 6 in the southern part of the dome stopped moving in the Late Triassic (Figure A29c).

Appendix 7: The script of the geological structural model in Mathematica™ using two algorithms (the NearestNeighbourGrid2D and InverseDistanceGrid2D) from Kelly (2009) and Kelly & Giambastiani (2009).

```
SetDirectory[NotebookDirectory[]];
xmin=435203;xmax=452325;xspace=100;
ymin=6525460;ymax=6549567;yspace=100;
zmin=0;zmax=1200;zspace=5;
grid2D=Flatten[Table[{x,y},{x,xmin,xmax,xspace},{y,ymin,ymax,yspace}],1];
Dimensions[grid2D]

ListPlot[grid2D,AxesOrigin    {xmin,ymin},PlotStyle    PointSize[0.008],
AspectRatio    1,
AxesLabel    {"Easting","Northing"},ImageSize      {350,350}]

InverseDistanceGrid2D[datain_,k_,p_,gridin_]:=
  Module[{nfunction,xyz,xy,z,d,zestimate,zgrid,zfunction},
    nfunction=Nearest[datain[[All,{1,2}]]    datain[[All]]];
    xyz=Map[nfunction[{#,#},k]&,gridin];
    xy=xyz[[All,All,{1,2}]];
    z=xyz[[All,All,3]];
d=Table[EuclideanDistance[gridin[[i]],xy[[i,j]]],{i,Length[gridin]},{j,Length[xy[[1]]]}];
    zestimate=
      Table[If[d[[i,1]]    0.,
          z[[i,1]],Mean[Table[ z[[i,j]]/d[[i,j]]^p/(1/d[[i,j]]^p),{j,Length[d[[i]] ]}]]]
        ,{i,Length[d]}];
    zgrid=Table[{gridin[[i,1]],gridin[[i,2]],zestimate[[i]]},{i,Length[gridin]}];
```

```
    zfunction=Interpolation[zgrid,Method    "Spline",InterpolationOrder    1];
    Return[zfunction]]

bottomsurface=Drop[Import["BottomSurface2.csv"],1];
ListPointPlot3D[{bottomsurface[[All,{2,3,4}]]},PlotRange    {{xmin,xmax},{ymin,ymax},{zmin,z
max}},PlotStyle    {Directive[Darker[Red,0.1],PointSize[0.012]],Directive[Blue,PointSize[0.012]],
Directive[Darker[Green,0.1],PointSize[0.012]],Directive[Darker[Cyan,0.1],PointSize[0.007]]},
AxesLabel    {"Easting","Northing","Elevation (m)"},ViewPoint      {-1.0,-1.5,0.75},ImageSize
{500,400}]

GeoPointProjectLine[geodatain_,stepin_,countin_]:=
  Module[{step,projectdown,projectup,projectiontable},
    projectdown =Flatten[N[Table[{
            geodatain[[i,2]]+(Cos[geodatain[[i,5]] °]*Sin[geodatain[[i,6]] °]) stepin n,
            geodatain[[i,3]]+(Cos[geodatain[[i,5]] °]*Cos[geodatain[[i,6]] °]) stepin n,
            geodatain[[i,4]]-Sin[geodatain[[i,5]] °] stepin n},
          {i,Length[geodatain]},{n,0,countin}]],1];
    projectup=Flatten[N[Table[{
            geodatain[[i,2]]-(Cos[geodatain[[i,5]] °]*Sin[geodatain[[i,6]] °]) stepin n,
            geodatain[[i,3]]-(Cos[geodatain[[i,5]] °]*Cos[geodatain[[i,6]] °]) stepin n,
            geodatain[[i,4]]+Sin[geodatain[[i,5]] °] stepin n},
          {i,Length[geodatain]},{n,0,countin}]],1];
    projectiontable=Join[projectup,projectdown];
    Return[projectiontable]]

step=1000;count=50;
linesbottomsurface =GeoPointProjectLine[bottomsurface,step,count];

ListPointPlot3D[{linesbottomsurface },

PlotRange    {{xmin,xmax},{ymin,ymax}},PlotStyle    {Directive[Darker[Red,0.1],PointSize[0.006]
],Directive[Blue,PointSize[0.006]],Directive[Darker[Green,0.3],PointSize[0.006]],Directive[Darker[
Cyan,0.1],PointSize[0.006]]},
AxesLabel    {"Easting","Northing","Elevation (m)"},
ViewPoint      {-1.0,-1.5,0.75},ImageSize      {500,450}]

ksearch=3;power=2;
grid2Dc=Partition[Flatten[Table[{x,y},{x,xmin,xmax,1000},{y,ymin,ymax,1000}]],2];
fPermian=InverseDistanceGrid2D[linesbottomsurface,ksearch,power,grid2Dc];

Plot3D[{fPermian[x,y]},{x,xmin,xmax},{y,ymin,ymax},

PlotStyle    {Darker[Red,0.1],Blue,Darker[Green,0.3],Darker[Cyan,0.1]},PlotPoints    50,Mesh    No
ne,
```

```
AxesLabel {"Easting","Northing","Elevation (m)"},
ViewPoint {1,-2,-0.1}, ImageSize
{500,300},Lighting {{"Directional",GrayLevel[0.95],{220000,6620000,5000}},{"Directional",Gr
ayLevel[0.8],{350000,6630000,-500}},{"Directional",GrayLevel[0.8],{210000,6660000,-5000}}}]

plane1data = Table [ {x,y,fPermian[x,y]},{x, xmin,xmax, 500}, {y, ymin,ymax,500 }]

ListPointPlot3D[plane1data]
header = {"Xloc", "Yloc", "Elevation"};
exportdata = Partition[Flatten[Append[header, plane1data]],3];
Export["J4_b1_horizon.csv",exportdata]
```

Appendix 8: List of the gif files of the fault blocks and the whole NHB in 3D structural models (attached CD).

1. Gif file of the whole NHB in 3D models.
2. Gif file of the Parrabel Dome in 3D models.
3. Gif file of bottom surfaces of formations in Fault Blocks A and C in 3D models.
4. Gif file of bottom surfaces of formations in Fault Block B in 3D models.
5. Gif file of bottom surfaces of formations in Fault Block D in 3D models.
6. Gif file of bottom surfaces of formations in Fault Block E in 3D models.
7. Gif file of bottom surfaces of formations in Fault Block H in 3D models.